The role of mesenchymal stem cells and osteocytes in subchondral bone changes in hip osteoarthritis

Dragos Constantin Ilas

Submitted in accordance with the requirements for the degree of
Doctor of Philosophy

The University of Leeds
Faculty of Medicine and Health

May 2019

The candidate confirms that the work submitted is his own, except where work which has formed part of jointly authored publications has been included. The contribution of the candidate and the other authors to this work has been explicitly indicated below. The candidate confirms that appropriate credit has been given within the thesis where reference has been made to the work of others.

Jointly-authored publications:

1. **The simultaneous analysis of mesenchymal stem cells and early osteocytes accumulation in osteoarthritic femoral head sclerotic bone (Chapter 3 and 4)**

   Dragos C. Ilas, Sarah M. Churchman, Thomas Baboolal, Peter V. Giannoudis, Joseph Aderinto, Dennis McGonagle and Elena Jones

   Rheumatology (Oxford, England), Accepted 16th March 2019, In press

   Work attributed to Dragos C. Ilas: study conception and design, manuscript preparation and final draft, performing the experiments, acquisition, analysis and interpretation of data, composition of figures, response to reviewers and revisions following peer review.

   Work attributed to others: study conception and design (E.J, D.M); sample collection (P.V.G, J.A), analysis and interpretation of data (E.J, D.M, T.B, S.M.C), manuscript preparation and final draft (E.J, D.M, T.B), response to reviewers and revisions following peer review (EJ).

2. **Bone marrow–harvesting technique influences functional heterogeneity of mesenchymal stem/stromal cells and cartilage regeneration (Chapter 5)**

   Kavitha Sivasubramaniyan, Dragos C. Ilas, Abhishek Harichandan, Pieter K. Bos, Diego L. Santos, Peter de Zwart, Wendy J.L.M. Koevoet, Heather Owston, Hans-Jörg Bühring, Elena Jones, and Gerjo J.V.M. van Osch

   The American Journal of Sports Medicine, Volume 46, Issue 14, December 2018, pages 3521-3531

   Work attributed to Dragos C. Ilas: Figure 5 right panels as well as Supplementary Figure 1E and analysis of the corresponding data, discussion of results and final manuscript.

Work attributed to others: Study design and first draft of the manuscript (AH, KS, GJVMO), final version of the manuscript and overall study direction (EJ, HJB and GJVMO), data collection, analysis and interpretation as follows: Supplementary Figure 1A-D (AH), establishing the bone marrow harvesting methods and samples collection (PKB, PZ), Figure 6 (DLS), Figure 2 (WJLMK), data for Figure 5, right panels (HO).

Acknowledgements

I would firstly like to thank my supervisors, Dr. Elena Jones and Prof. Dennis McGonagle, for the continuous support and guidance throughout this project. Their doors have always been open and I am indebted for their encouragement in times of hardship, and confidence in me. I am also thankful for their inspiration, enthusiasm and consistent motivation during my studies.

I would also like to thank Dr. Sarah Churchman who worked actively during my first year to provide me with excellent molecular biology skills essential for completing this thesis. Sincere thanks also go to Dr. Thomas Baboolal and Dr. Rich Cuthbert for their persistent mentorship and sharing of invaluable knowledge and experience in the laboratory.

I thank Dr. Adam Davidson and Ms. Liz Straszynski for their expert technical assistance during cell sorting experiments as well as Mr. Mike Shires for sharing his histological expertise so willingly. My gratitude extends to the clinical teams at Chapel Allerton Hospital and Leeds General Infirmary, particularly to Mr. Joseph Aderinto and Prof. Peter V. Giannoudis, for their generosity in providing me with patient samples. Without their contribution this project would not have been possible.

Last but not the least, my heartfelt thanks go to my family, especially to my wife Nicolette for providing me with unfailing support, continuous encouragement throughout my years of studies and for her stoicism during difficult times. My sincere gratitude also goes to my parents and to my brother and his family for supporting me spiritually throughout writing this thesis and my life in general.

Abstract

Osteoarthritis (OA) is a disease of the whole joint, and subchondral bone changes are a universal OA feature. The cellular mechanisms of subchondral bone sclerosis in late OA joints implicate altered osteoblast and osteoclast activities, however the roles of the most abundant bone cells, the osteocytes, and their immature progenitors, the mesenchymal stem cells (MSCs) are not understood. The cell fraction characterised by the $CD45^-$ $CD271^+$ phenotype represents a reservoir of native bone-resident MSCs in humans, however it consists of topographically different subsets, whose relative contributions to bone formation in OA remain unclear. The aim of this study was to investigate gene expression profiles and topographical features of osteocytes, MSCs and their subsets in femoral head OA bone.

Compared to healthy cancellous bone, $CD45^-CD271^+$ MSCs resident in OA bone were more abundant (3.4-fold, $p<0.05$) and had significantly ($p<0.05$) higher expression of osteogenic genes, such as runt related transcription factor 2 (*RUNX2*, 7-fold) and osteonectin (*SPARC*, 5-fold) indicating their osteogenic commitment. Furthermore, chondrogenic genes were significantly ($p<0.05$) decreased (*SOX9*, 5-fold and UDP-glucose 6-dehydrogenase, *UGDH*, 14-fold). The native OA osteocytes transcriptional profile was consistent with their early, embedding stage of development, evidenced by significantly ($p<0.01$) higher levels of podoplanin (*E11*, 9-fold) and matrix metalloproteinase-14 (*MMP14*, 4-fold) compared to healthy bone osteocytes. Active bone formation in OA was evident as an accumulation and co-localisation of $CD271^+$ MSCs and immature $E11^+$ osteocytes in areas of bone sclerosis. Additionally, transcriptional and immunohistochemical analysis demonstrated that both MSCs and osteocytes in OA-affected bone favoured bone formation by elevated expression of the osteoclastogenesis inhibitor osteoprotegerin.

To define osteogenically-committed MSC subset, CD56 was chosen as a candidate molecule. Dual immunofluorescence confirmed co-localisation of CD271 and CD56 at the bone surface. $CD271^+CD56^+$ cells were significantly more abundant in OA bone compared to healthy bone (8-fold, $p<0.0001$) and also accumulated in OA sclerotic areas, having the unique topography in proximity to active bone formation sites. The $CD271^+CD56^+$ MSC subset displayed significantly ($p<0.01$) over 100-fold higher expression of osteogenesis- and chondrogenesis-related genes, including osteopontin

(*SPP1*), osteocalcin (*BGLAP*) and *SOX9,* compared to a donor-matched $CD271^{+}CD146^{+}$ subset, whilst the predominant $CD271^{+}CD146^{-}CD56^{-}$ subset represented a transcriptionally 'intermediate' MSC population with the highest levels of stromal-derived factor 1 (*CXCL12*) transcript. While all three subsets were multipotential, their native gene expression traits were lost after *in vitro* culture.

This study implicates native bone-resident MSCs in subchondral bone sclerosis in late-stage hip OA. It defines the $CD271^{+}CD56^{+}$ osteogenically-committed MSC subset that has bone-lining topography and therefore the closest proximity to bone formation sites. Novel MSC subsets may represent future therapeutic targets for OA and other bone associated pathologies.

Table of Contents

List of Figures

List of Tables

List of Abbreviations

ACI – Autologous chondrocyte implantation

ACTA2 – Actin, alpha 2, smooth muscle, aorta

ALP – Alkaline phosphatase

BGLAP – Bone gamma-carboxyglutamate (gla) protein (osteocalcin)

BMI – Body mass index

BML – Bone marrow lesion

BMP – bone morphogenetic protein

BMP – Bone morphogenic protein

BMU – Basic multicellular units

CDH11 – Cadherin 11

cDNA – Complementary deoxyribonucleic acid

CFU-F – Colony forming unit – fibroblast

COL1A1 – Collagen 1 type 1

COL2A1 – Collagen, type II, alpha 1

CTSK – Cathepsin K

CXCL12 – Chemokine (C-X-C motif) ligand 12

DKK1 – Dickkopf 1

DMEM – Dulbecco's Modified Eagle Medium

DMEM – Dulbecco's Modified Eagle Medium

DMP1 – Dentin matrix related protein 1

DMSO – Dimethyl sulfoxide

DNA – Deoxyribonucleic acid

E11 – Podoplanin

ECM – Extracellular matrix

EDTA – Ethylenediaminetetraacetic acid

FABP4 – Fatty acid binding protein

FACS – Fluorescence activated cell sorting

FCS – Foetal calf serum

FGF – Fibroblast growth factor

FGF23 – Fibroblast growth factor-23

FSC – Forward scatter

FZD – Frizzled

GATA2 – GATA binding protein 2

HCl – Hydrochloric acid

HLC – Haematopoietic lineage cell

HPRT1 – Hypoxanthine Phosphoribosyltransferase 1

IGF-1 – Insulin-like growth factor 1

ISCT – International Society for Cellular Therapy

LCN – Lacuno-canalicular network

LNGFR – Low-affinity nerve growth factor receptor

LRP5/6 – Low density lipoprotein related protein 5/6

M-CAM – Melanoma cell – adhesion molecule (CD146)

M-CSF – Macrophage colony stimulating factor

MCAM – Melanoma cell adhesion molecule

MEPE – Matrix extracellular phosphoglycoprotein

MMP14 – Matrix metalloproteinase 14

MNC – Mononuclear cell

MRI – Magnetic Resonance Imaging

MSC – Mesenchymal stem cell

NCAM – Neural cell adhesion molecule

NS – Non-Sclerotic

OA – Osteoarthritis

OMD – Osteomodulin

OPG – Osteoprotegerin

OPN – Osteopontin

P – Passage

P/S – Penyl/Strep

PBS – Phosphate buffered saline

PD – Population doublings

PD – Population doubling

PFA – Paraformaldehyde

PHEX – Phosphate-regulating neutral endopeptidase, X-linked

PPARG – Peroxisome proliferator-activated receptor gamma

qPCR – Quantitative polymerase chain reaction

RANKL – Receptor activator of nuclear factor κB ligand

RNA – Ribonucleic acid

S – Sclerotic

SOST – Sclerostin

SOX9 – SRY (sex determining region Y)-box 9

SP7 – Osterix

SPARC – Osteonectin

SPP1 – Osteopontin

SSC – Side scatter

TBS – Tris buffer saline

TGF-b – Transforming growth factor b

TLDA – TaqMan Low Density Array

TNFRSF11B – Osteoprotegerin

TNFSF11 – Receptor activator of NF-KB ligand

TRAP – Tartrate resistant alkaline phosphatase

Chapter 1 General introduction

1.1 Osteoarthritis

1.1.1 Osteoarthritis: an introduction

Osteoarthritis (OA) is the most common degenerative joint disease and represents one of the leading cause of pain and disability and is a major public health problem (WHO Scientific Group, 2003). The growing age of the population in developed and developing countries, as well as increased risk factors for OA, particularly obesity and a sedentary lifestyle may lead to a substantial increase in the number of people living with hip or knee OA over the coming decades (De Angelis and Chen, 2013).

Osteoarthritis is considered the planet's oldest known disease, with evidence recovered from burial grounds around the world showing arthritic disease in 50-70 million year dinosaurs as well as skeletal changes in Neanderthal man (100,000 – 35,000 B.C.) (Wells, 1973; Buchanan et al., 2003). But despite its widespread occurrence in ancient skeletons and early reference by Hippocrates (460-375 B.C.), it was only in the 18th century that clinicians formally recognised OA as a malady (Buchanan et al., 2003). The delay was in part due to the few obvious physical signs but also because of the confusion in nomenclature, OA being initially grouped together with rheumatoid arthritis until the 19th century. Today there are clear criteria established for the clinical appearance or rheumatic conditions, although more research must be undertaken for a clear understanding of their pathogenesis.

Osteoarthritis affects many diarthrodial joints (Figure 1.1) and is characterised by cell stress and extracellular matrix degradation initiated by micro- and macro-injury which subsequently activates a maladaptive tissue repair (Kraus et al., 2015; Martel-Pelletier et al., 2016). Given its continuous and evolving complexity, several definitions are widely used to describe OA. This condition manifests first on a molecular level as abnormal joint tissue metabolism followed by anatomic, and/or physiologic derangements, characterized by articular cartilage degradation, bone remodelling, osteophyte formation, joint inflammation and loss of normal joint function (Kraus et al., 2015). Clinically OA is characterized by joint pain, swelling and stiffness that leads to activity limitations, participation restrictions, sleep interruption, fatigue and depression or anxious mood, and ultimately loss of independence and reduced quality of life.

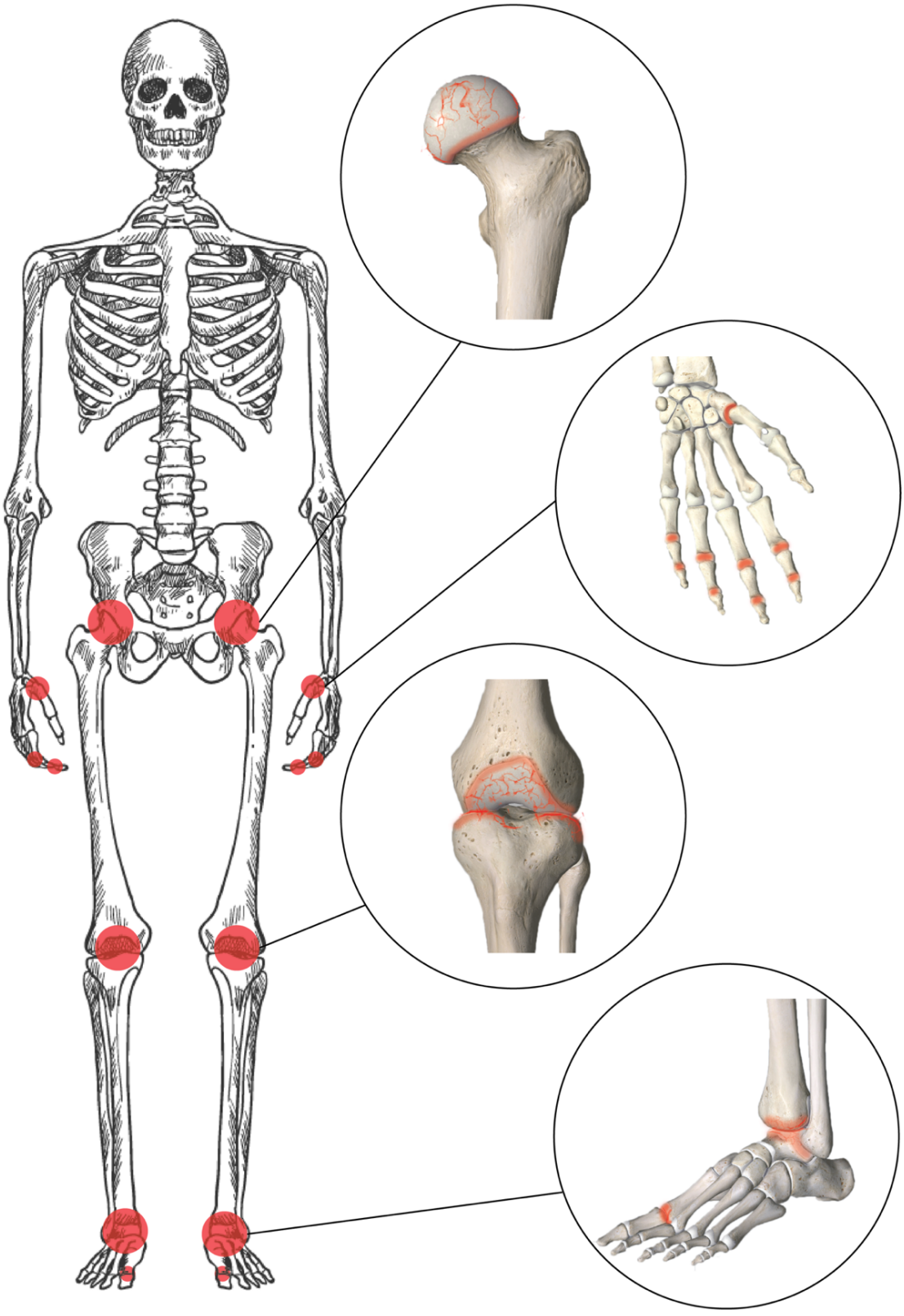

Figure 1.1. Common joints affected by OA. *Any joint can be affected by OA but the disease occurs most commonly in joints that have experienced repetitive stress or injury, with the highest prevalence in hip, knee and ankle. Other small joints like small joints of the fingers and the bases of the thumb and big toe can also be affected.*

1.1.2 Epidemiology and risk factors

Epidemiological studies have been used to describe the distribution of OA in the population and to examine risk factors for its occurrence and progression. But the incidence and prevalence of OA, depending on the definition used and it can be described pathologically, radiographically, or clinically. Due to the various definitions of OA that are used, the reported prevalence and incidence rates vary across studies, however an estimated 8.75 million people aged 45 years and over (33%) in the UK have sought treatment for osteoarthritis (60% female, 40% male) (Arthritis Research UK, 2013).

Osteoarthritis is undisputedly a complex disease with a multifactorial pathogenesis. The risk factors commonly associated with the initiation and progression of OA can be divided into person-level risk factors, those that act at the level of individual susceptibility, and joint-level factors, those that alter the biomechanical stability of individual joints (Palazzo et al., 2016) (Figure 1.2). Person-level risk factors include increasing age, gender, obesity and genetic factors while the predominant joint-level factors are joint injury, repetitive joint use through occupation or leisure and joint malalignment (Palazzo et al., 2016; Martel-Pelletier et al., 2016).

Risk of developing OA increases with age. A third of women and almost a quarter of men between 45 and 64 have sought treatment for OA, this rises to almost half of people aged 75 and over (Arthritis Research UK, 2013). Sex differences in the development, prevalence, and incidence of hip and knee OA have long been known, with females generally at a higher risk (Srikanth et al., 2005). However, it is important to note that females had more severe radiographic knee OA than males, while no significant differences were found between sexes in the severity of hip and hand OA (Srikanth et al., 2005). The high prevalence in women may be associated with various factors, including genetics, women more often reported a family history of OA than men (49% vs. 37%) (Van Tunen et al., 2018). Furthermore, anatomical differences and body composition have also been reported to account for the aforementioned increase in prevalence amongst women, gender-specific hormones, such as estrogen, being known to influence the incidence and severity of OA (Boyan et al., 2013). While prior to menopause, the OA incidence was shown to be similar in women and men, after menopause, however, the prevalence is much greater in females than age-matched males (Nevitt and Felson, 1996). In addition, some studies revealed sex-related difference in cartilage matrix composition, women shown to have a thinner and more reduced volume of cartilage in the knee than men (Maleki-Fischbach and Jordan, 2010).

Obesity and high body mass index are important risk factors for OA. Obesity is associated with the incidence and progression of OA of both weight-bearing and non-weight-bearing joints (Lementowski and Zelicof, 2008). Increased joint loading leads to changes in body composition with detrimental effects related to low grade' chronic inflammation (Wluka et al., 2013). Behavioural factors may also play a role in OA development, such as diminished physical activity and subsequent loss of protective muscle strength. According to data from the Framingham Study, a community study of OA, among women with a baseline body mass index (BMI) greater than or equal to 25, weight loss was associated with a significantly lower risk of knee OA (Felson et al., 1997). Estimations based on data from the same study indicate that weight reduction by 5 kg over a 10 year period decreased the risk of developing knee OA by 50% (Felson et al., 1992; Christensen et al., 2006).

A hereditary component of OA development has long been recognized, with several genes shown to be directly associated with OA (Valdes and Spector, 2010) and many more have been determined to be associated with contributing factors, such as excessive inflammation and obesity (Valdes and Spector, 2011). Genetic factors account for 60% of hand and hip OA and 40% of knee OA (Martel-Pelletier et al., 2016). Many genes could play a role in the disease onset and so could provide targets for future pharmacological treatments (e.g., genes encoded for vitamin D receptor, insulin-like growth factor 1, type 2 collagen, growth differentiation factor 5) (Palotie et al., 1989; Chapman et al., 2008; Evangelou et al., 2009). Genetic studies aim to identify which genetic variants at which genetic locations (loci) influence the risk of disease. The past decade has seen a number of contributions to the genetic influence in OA in the form of genome-wide association studies (GWAS). Genes such as *GDF5*, *ASPN*, *FRZB* and *PTGS2* have been identified in these studies. One of the most powerful GWAS performed on OA was published in 2012 called arcOGEN and involved the analysis of over 7400 OA cases, 80% of whom had undergone total joint replacement (arcOGEN Consortium et al., 2012). This study identified 11 loci associated with OA susceptibility of OA and highlighted key biological pathways through which OA genetic susceptibility is operating, such as skeletogenesis or development and differentiation of osteoblasts and chondrocytes (Reynard and Loughlin, 2013). In another recent study on 199 target genes, it was revealed that only two variants (in the COL11A1 and VEGF genes) reached the significance level after adjustment for multiple tests (Rodriguez-Fontenla et al., 2014).

Trauma or surgical repair of traumatic injuries involving the articular cartilage, ligaments, or menisci (knee) can result in alterations of joint biomechanics and accelerate OA. For example in individuals who have sustained significant joint injuries, the risk of post-traumatic OA ranges from about 20% to more than 50% (Anderson et al., 2011). Joint deformations are also known to be a contributing factor for OA development. Valgus malalignment at the knee has been shown to increase the incidence and risk of radiographic progression of knee osteoarthritis involving the lateral compartment (Felson et al., 2013). While these causes are common occurrence in knee, mechanical load or abnormal stresses cause almost all disease in hip OA (Felson, 2013). Abnormalities in the shape of the hip bones, such as hip dysplasia and femoroacetabular impingement, are central to OA pathogenesis of this joint (Martel-Pelletier et al., 2016) and were shown to represent major risk factors predisposing to later-life hip OA (Felson, 2013).

However, joint damage may occur even in the absence of obvious trauma, such as prolonged small injuries, especially in individuals whose occupation or lifestyle involves frequent squatting, stair-climbing, or kneeling. Other life style associated factors may also be play a part in OA development, such as smoking. Interestingly, some studies indicated that smoking may have contradictory effects on OA, with an inverse relationship observed between smoking and OA (Hui et al., 2011). However, while the effects mediated through the nicotine sensitive acetylcholine receptor may help prevent disease, similar receptors on neuronal cells may, when excited, induce musculoskeletal pain (Felson and Zhang, 2015) indirectly affecting the disease.

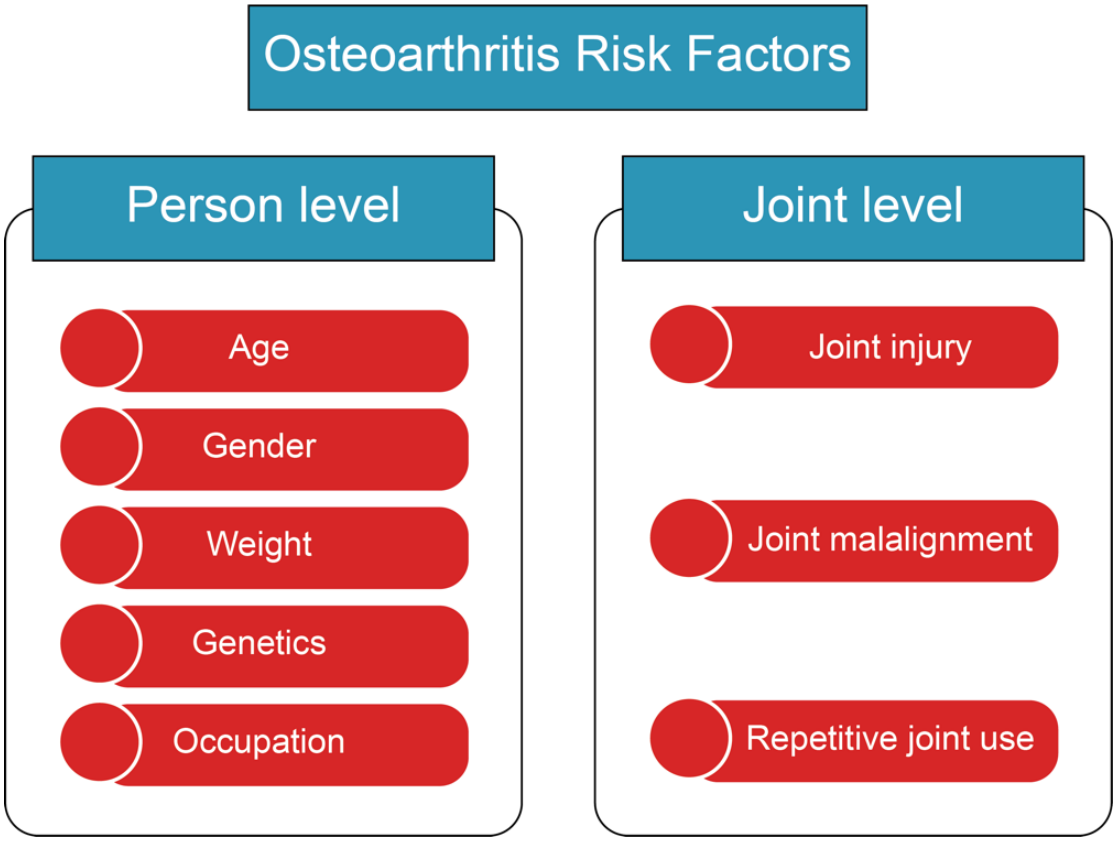

Figure 1.2. Risk factors for OA development. *OA is a multifactorial disease and the interactions between systemic factors that act on the person level and the local factors that act at the joint level play an important role in the development and prognosis of OA.*

1.1.3 Classification and pathogenesis

Historically OA has been classified as 'primary' and 'secondary' (Table 1.1). Primary OA is usually of unknown aetiology, where the disease onset may be initiated by no apparent factor (idiopathic) while secondary OA occurs when the triggering factor was apparent, such as trauma or congenital deformity (Altman et al., 1986). However, most patients cannot fit easily into these proposed OA subgroups due to the complexity of the influencing factors and intra-articular distribution of the disease. Various classifications have been proposed depending on the main underlying pathophysiological mechanisms, clinically relevant patient characteristics, stage of the disease, involved joints and degree of inflammation.

A more comprehensive classification suggests its onset may be initiated at different anatomical locations, such as cartilage, ligaments, meniscus, synovium or bone (McGonagle et al., 2010). The historical view of OA places cartilage and chondrocyte behaviour in a central position in the OA disease process. As noted in Table 1.1, articular cartilage can be damaged by normal wear and tear (primary OA) or following pathological insults, such as injury or trauma (secondary OA). Osteoarthritic cartilage is characterised by initial degenerative changes in the extracellular matrix leading to softening of the cartilage, fibrillation of the superficial layers, fissuring and reduced cartilage thickness, all of which become more pronounced with time, leading to complete cartilage destruction, eventually leaving the underlying subchondral bone completely exposed (Pritzker et al., 2006). A central role in these pathological features is played by the deviant behaviour of resident chondrocytes. In an attempt to initiate repair caused by pathological stimulation, chondrocytes compensate by increasing synthesis of matrix molecules (collagen, proteoglycans and hyaluronate) and proliferate forming clusters in the deeper layers of the cartilage, therefore being able to maintain the integrity of the articular cartilage at the early stages of disease (Goldring and Goldring, 2007). However, as the disease progresses this increase in anabolic and catabolic activity leads to chondrocytes senescence and failure to maintain homeostasis between synthesis and degradation of the extracellular matrix component (Loeser, 2009). As the proteoglycans and then the collagen network breakdown, cartilage integrity is disrupted (Goldring and Goldring, 2010).

However, alternative routes have also been described to lead to OA. For example, the idea of OA originating in bone, also known as osteogenic OA (McGonagle et al., 2010), has been long proposed by the early studies of Radin and Paul, who suggested that the

pathogenesis of OA could be attributed to a primary alteration in periarticular bone (Radin et al., 1970). According to this hypothesis, the pathogenesis of OA was initiated by an increase in the thickness, volume and stiffness in the subchondral bone which in turn shifted the weight-bearing burden to the overlying articular cartilage resulting in alterations in chondrocyte function and cartilage matrix deterioration (Goldring, 2012). In support to this theory, work in the early 1990s by Dieppe *et al.* provided evidence that changes in bone turnover assessed scintigraphically preceded detectable radiographic changes (McCrae et al., 1992; Dieppe et al., 1993). More importantly, these scintigraphic bone changes may be responsible for the pain associated with the disease and were predictive of the progression of anatomical changes in OA, such as the subsequent development of osteophytes and subchondral bone sclerosis.

Despite being a multifactorial and complex disease, the pathological changes observed in OA joints show common features that affect the entire joint structure leading to pain, deformity and complete loss of function. As mentioned, defining OA has long been centred on the wear and tear concept which was commonly associated with changes in the articular cartilage. However, this idea has evolved and OA is now considered a disease of the whole joint, including alterations in articular cartilage, subchondral bone, ligaments, capsule and synovial membrane (Loeser et al., 2012).

Table 1.1. Classification of subsets of OA, *adapted from* (Altman, 1991)

I. Primary (idiopathic)

A. Localized

1. Hands: nodal (Heberden's and Bouchard's nodes), nonnodal (erosive IP arthritis), S-MC, S-T
2. Feet: hallux valgus, hallux rigidus, hammer/cockup toes, talo-navicular joint
3. Knee:
    a. Medial compartment
    b. Lateral compartment
    c. Patellofemoral compartment
4. Hip:
    a. Eccentric (superior)
    b. Concentric (axial, medial)
    c. Diffuse (coxae senilis)
5. Spine (cervical and lumbar)
    a. Apophyseal
    b. Intervertebral (disc)
    c. Spondylosis (osteophytes)
    d. Ligamentous (hyperostosis [Forestier's disease, or DISH])
6. Other joints: shoulder, temporomandibular, sacroiliac, ankle, wrist, acromioclavicular

B. Generalized (includes 3 or more areas listed above)

1. Small (peripheral) and spine
2. Large (central) and spine
3. Mixed (peripheral and central) and spine

II. Secondary

A. Post-traumatic

B. Congenital or developmental diseases

1. Localized
    a. Hip diseases: LCPD, DDH, SCFE, shallow acetabulum
    b. Mechanical and local factors: obesity, leg length inequality, extreme valgus/varus deformity, hypermobility syndromes, scoliosis
2. Generalized
    a. Bone dysplasias: epiphyseal dysplasia, spondylo-apophyseal dysplasia
    b. Metabolic diseases: hemochromatosis, ochronosis, Gaucher's disease, hemoglobinopathy

C. Calcium deposition disease

1. Calcium pyrophosphate deposition disease
2. Apatite arthropathy
3. Destructive arthropathy (shoulder, knee)

D. Other bone and joint disorders: avascular necrosis, rheumatoid arthritis, gouty arthritis, septic arthritis, Paget's disease, osteopetrosis, osteochondritis

E. Other diseases

1. Endocrine diseases: diabetes mellitus, acromegaly, hypothyroidism, hyperparathyroidism
2. Neuropathic arthropathy (Charcot joints)
3. Miscellaneous: frostbite

Legend: DDH – Developmental Dysplasia of the Hip; DISH – Diffuse idiopathic skeletal hyperostosis; IP – Interphalangeal; LCPD – Legg–Calvé–Perthes Disease; SCFE – Slipped Capital Femoral Epiphysis; S-MC – Scapho-metacarpal; S-T – Scapho-trapezial

1.1.5 Therapies

Currently, there is no cure for this debilitating condition and most of the treatments focus on reducing symptoms and improving the functional status, with joint replacement as the ultimate consequence and current surgical treatment for OA. According to the Osteoarthritis Research Society International (OARSI), the mainstay of OA treatments involves a combination of physical measures, drug therapy, and surgery (Zhang et al., 2008; Zhang, Ouyang, Crispin R Dass, et al., 2016) as outlined in Figure 1.3. These lines of treatments described in the following sections are also in line with other international guidelines, such as European League Against Rheumatism (EULAR) in Europe, American College of Rheumatology (ACR in United States) and National Institute for Health and Care Excellence (NICE) in the UK.

As first-line management of mild to moderate OA, non-surgical treatment of OA is recommended including land-based exercise, weight management and strengthening with water-based exercise, self-management and education (Zhang et al., 2008). Pharmacological interventions are also used in combination as a treatment option aimed mainly at relieving pain and reduce inflammation. The most common pharmacological agents used for OA treatment are acetaminophen, non-steroidal anti-inflammatory drugs (NSAIDs), opioid analgesics, serotonin-norepinephrine reuptake inhibitors (SNRIs), and intra-articular injections (Martel-Pelletier et al., 2016). However, these traditional OA therapeutic agents are limited to control the symptoms and so far, none can reverse the damage in the OA joint and have modest benefits on pain and function, leaving the surgical interventions as final options to restore joint function.

The therapeutic approaches described in the following paragraphs involve surgical and cellular-based procedures that were shown to be limited to younger subjects with isolated chondral defects and do not work for generalised OA. A common surgical technique is the microfracture at sites of focal full-thickness defects. This technique is usually adopted at early stages and it involves drilling holes in the subchondral plate at the chondral defect site which in turn triggers the migration of bone marrow (BM) cells to the articular surface through stimulation of inflammatory response (Steadman et al., 1999). The technique is inexpensive and easy to do and is the most widely used regenerative approach with the purpose to provide an enriched environment for tissue regeneration. However, the resultant tissue is inferior fibrocartilage containing type I collagen or hybrid repair cartilage tissue, not the normal hyaline cartilage (type II collagen) (Mollon et al., 2013).

Furthermore, the observed subchondral bone overgrowth (25%–49%) might limit durability and the long-term outcome of the microfracture (Mithoefer et al., 2009).

Since these procedures have drawbacks, tissue engineering has led to the development of more advanced regenerative techniques. Autologous chondrocyte implantation (ACI) used for focal cartilage damage involves the transplantation of chondrocytes that are harvested from non-weight-bearing cartilage from the patient (Brittberg, 2008). However, this technique has some concerns as well since it causes not only donor site morbidity but also chondrocyte dedifferentiation in the transplanted site leading to the expression of type I collagen rather than type II collagen that may result in fibrocartilage rather than the desired hyaline-like cartilage (Jakobsen et al., 2005).

Other therapeutic approaches include mosaicplasty, a procedure similar to the ACI technique that involves the use of autologous osteochondral grafts; the use of other sources of cells, growth factors, and implantation of cells into three-dimensional scaffolds or matrices that support growth, differentiation, and maintenance of a chondrogenic phenotype are also increasingly used in therapy (Mollon et al., 2013). However, the results are disappointingly minimal and only offer short-term benefits and no evidence exists that the above techniques modify the development of OA. Furthermore, the majority of cellular therapies have a major drawback regarding their cost. The isolation, expansion and production of advanced medicinal products for cellular therapies are labour intensive, costly and require facilities that are GMP certified.

Joint replacement is well established for advanced OA of the knee and hip joints and is considered in cases of advanced disease with severe pain and functional limitations where other treatment options have failed (Dieppe and Lohmander, 2005). In the UK, according to NICE total hip replacement surgeries are only recommended for people with end-stage arthritis, if they have 10-year revision rates of 5% or lower (NICE, 2014). The main concern in the long-term outcome of total hip and knee replacements is survival of the prosthesis however, a recent study showed that over half of hip replacements last 25 years (Evans et al., 2019). The prosthesis may fail for various reasons, but the most common is aseptic loosening caused by osteolysis when polyethene wear debris trigger an inflammatory response leading to bone erosion (Katz, 2006). Furthermore, a small minority of joint arthroplasties may become infected. While the incidence is only 1% of total hip replacements (Engesæter et al., 2011), periprosthetic infections represent a challenging and serious complication with unpredictable responses to the standard of care (Tande and Patel, 2014).

Emergent therapy for advanced OA is knee joint distraction (KJD) which is associated with cartilage regeneration (Van Valburg et al., 2000; van der Woude et al., 2016). Spontaneous cartilage regeneration also occurs in advanced OA following wedge osteotomies (Koshino et al., 2003). The basis for joint regeneration in such advanced disease is incompletely understood but is likely to involve endogenous joint repair mechanisms. The unsatisfactory effects associated with the traditional OA drugs warrant continuous research into novel approaches, such as biologics and gene therapeutic interventions. Gene therapy enables the spatiotemporal control and persistent synthesis of gene products at target sites. While this approach holds great potential and prospects with several preclinical studies already confirming its safety and efficacy, only few clinical trials have been conducted and no gene products have been approved for OA treatment (Zhang, Ouyang, Crispin R. Dass, et al., 2016).

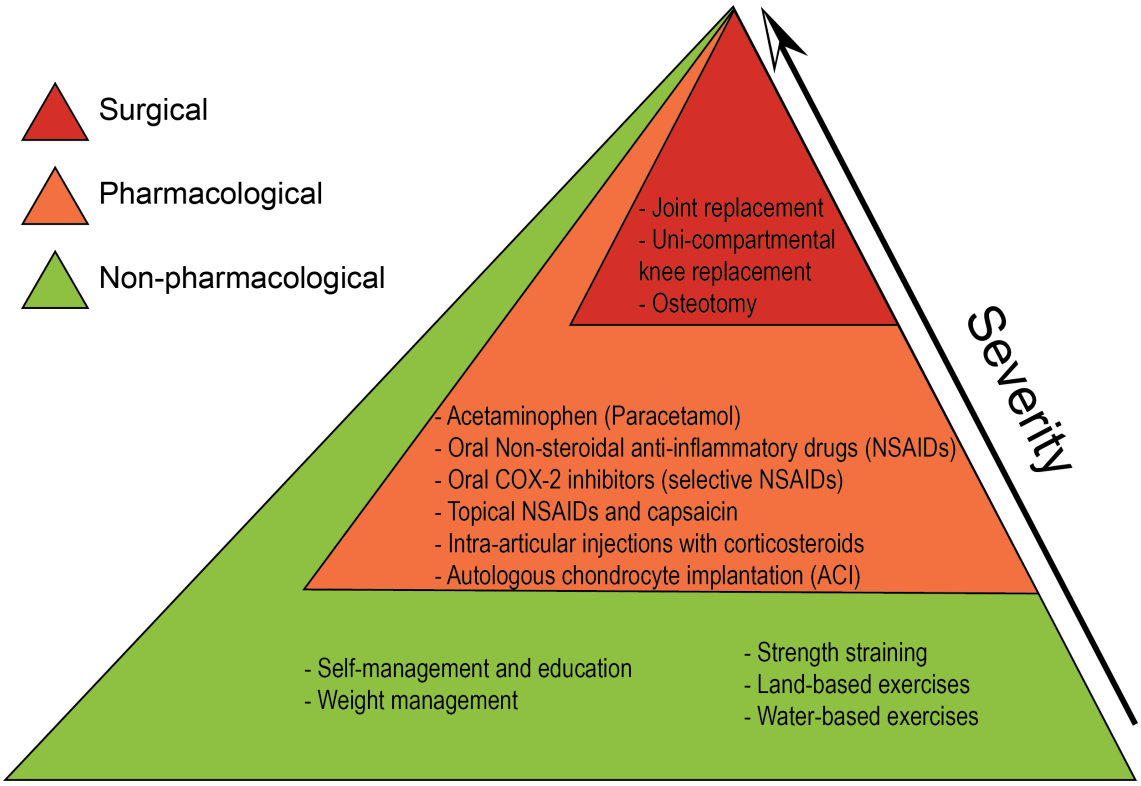

Figure 1.3. The OA treatment pyramid. *Non-surgical interventions are commonly recommended as a first-line treatment comprising of education, exercise and weight control with the addition of pharmacological and surgical interventions when needed as a second and third line of treatment. Adapted from* (Roos and Juhl, 2012)

1.1.6 Pathophysiology of OA

For a better understanding of OA disease mechanisms, it is important to describe the complex structures of the joint. Human joints join adjacent bones to form functional units that are uniquely adapted to permit constrained joint motion. Depending on the degree of motion, joint can be classified into immovable, or synarthroses, such as the distal tibiofibular joint and the skull bones; slightly movable, or amphiarthrosis, representing joints with a restricted degree of motion, such as the vertebrae; and freely movable, or diarthroses/ diarthrodial joints. Archetypal examples of diarthrodial joints are the knee, hip, and small joints of the fingers, comprising of numerous components that work in a synchronised manner to facilitate movement of the body. These components are structured into distinct elements including the two articulating bones stabilised by the tendons, ligaments, and menisci (in knee joints); the articular cartilage covering the adjacent bone surfaces to allow smooth movement with minimal friction, the synovial lining of the joint cavity that secrete synovial fluid for lubrication and nourishing of the joint (Smith, 2011).

1.1.6.1 Osteochondral unit

An important component of joints commonly affected by OA is the osteochondral unit (Goldring and Goldring, 2016a). This unit is a complex structure represented by the articular cartilage, the subchondral bone beneath the cartilage which is separated by a thin layer of calcified cartilage that persists after growth plate closure (Figure 1.4). The importance of osteochondral unit stems in its unique capability of transferring loads during weight-bearing and joint motion. Although the biomechanical coupling within the osteochondral unit is well established, their biochemical interaction is still unclear. The permeability of calcified cartilage and subchondral bone plates may allow crossover communication as evident from studies showing connecting channels between subchondral bone and cartilage (Pan et al., 2009). This is particularly important for advanced OA in which the osteochondral junction is breached thus allowing an enhanced molecular and cellular communication between these two separate entities.

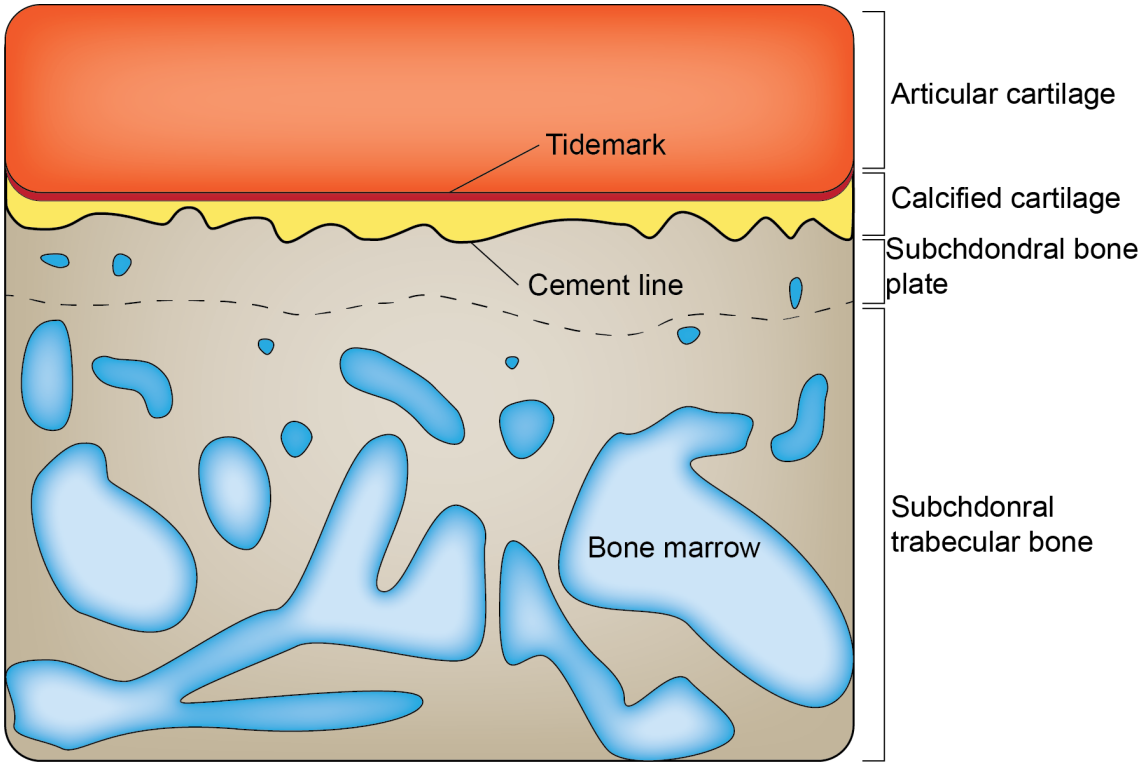

Figure 1.4. The structure of osteochondral unit in normal human joint. *The osteochondral unit comprises of the articular cartilage separated by the subchondral bone by calcified cartilage and a tidemark. The subchondral bone is composed by a cortical subchondral plate underlying the calcified cartilage (marked by the dotted line) and trabecular bone.*

1.1.6.2 Subchondral bone

The subchondral bone represents the bony components lying deep to articular cartilage separated by a zone of calcified cartilage (Li et al., 2013). As illustrated in Figure 1.4, the calcified cartilage is separated by the overlying articular cartilage by the so-called tidemark and the underlying subchondral bone by a cement line (Goldring, 2012). Although the subchondral bone is not clearly defined, it resembles a thin, dome-like structure, composed of the subchondral bone plate and the subchondral trabecular bone underneath (Burr, 2004) (Figure 1.4). The subchondral bone plate is a thin mineralised cortical bone layer lying immediately underneath the calcified cartilage (Milz and Putz, 1994). Arising from the subchondral bone plate is a network of subchondral trabecular bone, together with the deeper trabecular structure acting as a buttress, providing important shock absorbing and supportive functions to the joint (Madry et al., 2010). The distinction between the subchondral bone plate and subchondral trabecular bone is not always clear but differences in their mechanical properties and ability to adapt to mechanical load have been previously documented (Choi et al., 1990; Burr, 2004).

Moreover, relative to the subchondral bone plate, subchondral trabecular bone is more porous and metabolically active, containing blood vessels, sensory nerves, and BM (Suri and Walsh, 2012).

1.1.6.3 Pathological changes in OA osteochondral unit

The pathophysiology of OA is complex and multifactorial, with numerous genetic, biological, and biomechanical components (Glyn-Jones et al., 2015). While the disease process may be initiated at a single-tissue level, due to the intimate physiological and functional association of joint tissues, OA eventually affects the whole joint (Loeser et al., 2012). Alteration in the composition or structure of any of the individual components results in 'joint failure' characterised by disruption of joint integrity and loss of function (Goldring and Goldring, 2016b), a classic description of OA pathology. The structural changes of the individual joint tissues can occur either spontaneously following trauma or injury, or can evolve over time mediated by cellular or microenvironmental factors that contribute together to alterations in the composition, structure and material properties of the joint tissues.

The articular cartilage undergoes changes in its conformation and structure, starting with softening and surface fibrillation, ulceration and deep fissures as the disease progresses. Cartilage degradation, specifically involving alterations in the collagen and aggrecan content, is central to OA pathology. Studies showed important roles played by Adamalysin with Thrombospondin Motifs 5 (ADAMTS-5) in aggrecan degradation and the collagenolytic matrix metalloproteinase MMP-13 in collagen degradation (Troeberg and Nagase, 2012). Ultimately these deleterious processes lead to complete loss of articular cartilage thereby exposing the calcified cartilage and subchondral bone (Martel-Pelletier et al., 2016) (Figure 1.5). Furthermore, subchondral bone eburnation and sclerosis occurs (Figure 1.5) together with the development of subchondral bone cysts and osteophytes (Suri and Walsh, 2012).

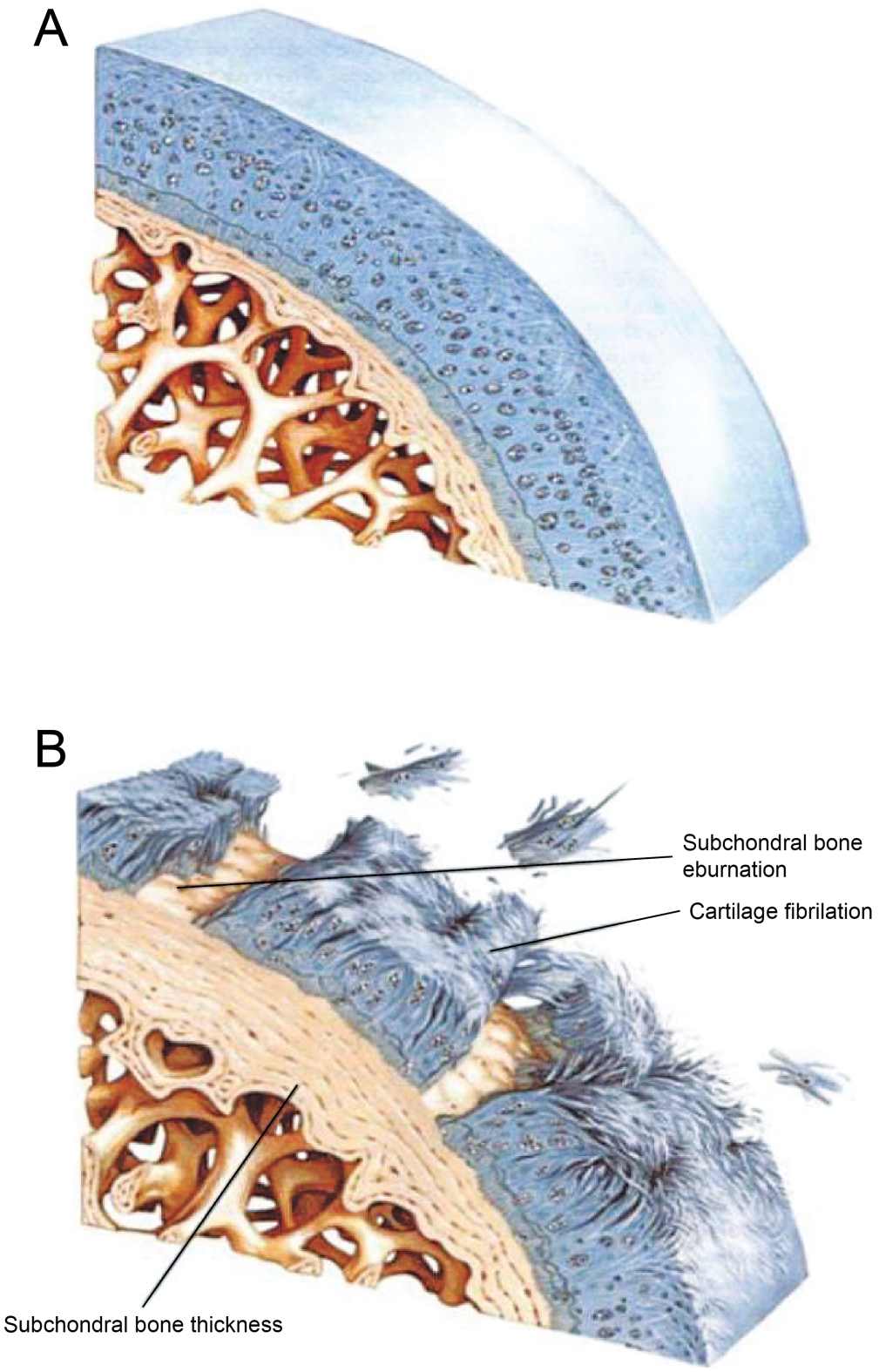

Figure 1.5. Structure of the normal (A) and pathophysiological changes in OA osteochondral unit (B). *During OA progression the entire joint structure is ultimately affected, including the articular cartilage and subchondral bone. Fibrillation and progressive loss of cartilage expose the subchondral bone which consequently increases its volume and becomes sclerotic. Image modified from* (Netter et al., 2005).

1.1.7 Bone-related changes in OA

Although the pathological process can initially target a single tissue with further progress to encompass the whole joint including articular cartilage and bone, as mentioned before and reviewed in detail by published literature (Martel-Pelletier et al., 2016), the work in this thesis is focused on bone associated OA pathology, which therefore will be described in more detail below.

1.1.7.1 Subchondral bone

Subchondral bone is believed to play a pivotal role in OA pathogenesis, pronounced changes being a common sight in the structure and composition of periarticular bone, i.e. both the subchondral plate and trabecular bone in OA (Weinans et al., 2012). However, as mentioned in Section 1.1.4, it is still unclear whether these alterations act as a trigger or a secondary consequence to cartilage degeneration (Madry et al., 2010). Subchondral bone commonly associated with OA involve microarchitectural alterations, including an increase in the number of trabeculae and bone volume consequently leading to a decrease of trabecular separation and BM spacing (Lajeunesse et al., 2003; Burr and Gallant, 2012). Hypomineralisation of subchondral bone succeeding as a consequence of abnormal local high bone turnover and densification of the subchondral plate associated with a complete loss of cartilage (Bettica et al., 2002; Burr and Gallant, 2012). Other histopathological changes that have been reported in the subchondral bone, include microdamage, vascularisation of osteochondral junction and bone marrow lesions (BMLs) (Burr and Radin, 2003; Walsh et al., 2010; Campbell et al., 2016).

1.1.7.2 Bone marrow lesions

Bone marrow lesions have been consistently documented to play a fundamental role in development of OA and are considered to represent an important risk factor for structural deterioration (Felson et al., 2003; Kazakia et al., 2013). BMLs were first described as an ill-defined high signal on magnetic resonance imaging (MRI) with increased signal intensity using fluid sensitive magnetic resonance sequences (Wilson et al., 1988). Histological evaluation at these sites revealed the presence of fat cell necrosis and localized marrow fibrosis associated with microfractures of the trabecular bone at various stages of healing (Leydet-Quilici et al., 2010). The lesions lack well defined margins, may fluctuate in size within a short time and are associated with the progression of increased vascularity, articular cartilage loss and fluctuation of pain in knee OA (Xu et al., 2012).

The BMLs have received increased attention lately due to their 'almost exclusive' association with cartilage degradation and alteration of the articular surface in OA (Bowes et al., 2016). BMLs were also shown to be associated with abnormal trabeculae on histopathology (Zanetti et al., 2000), subchondral bone cysts (Carrino et al., 2006) possibly developed in pre-existing BML regions. The presence of BMLs in OA correlates overall with the severity of joint pain and with progression of OA cartilage and bone changes (Taljanovic et al., 2008). Their association with pain has been recently evidenced by an elegant study by Kuttapitiya *et al*. using extensive histological and gene expression analysis of bone areas with BMLs (Kuttapitiya et al., 2017). In this study it was demonstrated that BMLs areas are characterised by a high metabolic activity and their transcriptional profile showed increased expression of multiple genes associated with pain sensitivity as well as genes associated with bone remodelling activity (Kuttapitiya et al., 2017).

Furthermore, work by the Leeds group showed that in hip OA, BML areas were associated with topographic and numerical disturbances of bone resident mesenchymal stem cells (MSCs) (Campbell et al., 2016). This study also reported functional *in vitro* alterations of these cells which may point to a role of MSCs in the abnormal bone phenotype in OA.

1.1.7.3 Bone sclerosis

There is agreement in the findings of most studies that the subchondral bone thickness and trabecular bone volume in OA increases (Fazzalari and Parkinson, 1997; Lajeunesse et al., 1999) and this may be accounted by the subchondral bone sclerosis observed in the late stages of the disease. Subchondral bone sclerosis is defined as an increase in bone mass and density, and is a common radiographical feature of advanced disease stages (Burr and Gallant, 2012). A marked characteristic of subchondral bone sclerosis is the formation of new bone tissue that has lower mineralization (L.G. Cox et al., 2012) and consequently alterations in the strength and stiffness of the bone tissue.

1.1.7.4 Subchondral bone cysts

The cavitary lesions in the subchondral bone, commonly described as 'intra-osseous lesions', 'pseudo-cysts' or 'geodes', are a common feature of advanced OA, especially at sites of great cartilage loss (Li et al., 2013). Subchondral bone cysts are composed of fibroconnective tissue that may initially contain fluid but ossify in later disease stages. Despite a continuous focus on these OA lesions over many decades, the exact aetiology

and pathogenesis of subchondral bone cysts are still not clear (Li et al., 2013). Some observations suggested that bone cysts in OA tend to develop at sites of pre-existing BMLs (Carrino et al., 2006) which have led to the concept that they are generated directly within the subchondral bone (Martel-Pelletier et al., 2016). It was proposed that bone damage and necrosis initiate the process of osteoclast-mediated bone resorption that leads to cyst formation (Crema et al., 2010). Evidence also showed that patients with subchondral bone cysts had greater disease severity and pain, and a higher risk of joint replacement than donors with BML alone (Tanamas et al., 2010). More studies showed that areas of subchondral bone cysts in OA are also accompanied by activated osteoblasts and osteoclasts (Havdrup et al., 1976; Sabokbar et al., 2000). This indicates an association of these bone cells with a high bone turnover, however the exact cellular mechanisms involved are still unclear.

1.1.7.5 Osteophytes

Similar to subchondral bone cysts, osteophytes are also very common alterations in OA described as "fibrocartilage-capped bony outgrowths" (van der Kraan and van den Berg, 2007). Osteophyte formation is an integral component of OA pathogenesis and are usually observed at the joint margins (Martel-Pelletier et al., 2016).

Osteophytes can form early in the development of OA and can be observed prior to joint space narrowing, potentially arising as an attempt to stabilize the joint rather than contribute to the progression of joint pathology (van der Kraan and van den Berg, 2007). In support to this idea, studies shown that osteophytes removal increased joint instability in some OA animal models (Pottenger et al., 1990) and no association was found between osteophyte size and OA progression in humans (Felson et al., 2005). While marginal osteophytes are common in patients with OA, the appearance of osteophytic outgrowths in the central portions of the articular space of both hip and knee OA have also been documented (Varich et al., 1993; McCauley et al., 2001). While less common, these central osteophytes were found to be in a temporal relationship with the marginal outgrowths and furthermore, associated with the severity of cartilage damage (Varich et al., 1993; McCauley et al., 2001).

Although the histological features of this tissue pathology has been thoroughly investigated and its importance clearly stated (Lajeunesse et al., 2003), there is a lack of information pertinent to the cellular mechanisms behind these tissue alterations. Histological appearance of damaged tissue is a mere reflection of skewed cellular and molecular mechanisms and evidence pertaining these drivers is still insufficient.

1.1.8 Hip OA

The hip joint is the second most common site for OA (after knee) with around 11% (2.46 million) of people in England affected (Aresti et al., 2016). It carries a heavy burden of disease having a high prevalence amongst elderly population with an estimated 25% of lifetime risk of symptomatic OA in people who live to the age of 85 (Murphy et al., 2010). However, research in hip OA is fairly scant compared to knee OA focused research, possibly owing to the reported higher prevalence of knee OA (Neogi and Zhang, 2013) as well as ease of imaging and accessibility for various clinical interventions (Gold et al., 2015).

As for OA in general, there is no single cause for hip OA. Several risk factors are linked to the development of hip OA including age, gender, genetics, obesity, and local joint risk factors, such as cartilage matrix composition and structure, and mechanical stress (Martel-Pelletier et al., 2016). However, the aetiology of primary hip OA remains unknown. In addition to these generic risk factors, it was shown that long-term exposure to sports among men, especially when combined with heavy workloads, increased the risk of hip OA (Vingård et al., 1993). Furthermore, some studies provided more evidence that heavy workloads and musculoskeletal injuries were specifically associated with an increased predilection for hip OA (Juhakoski et al., 2008) while others indicated obesity as another influencing factor (Lievense et al., 2002), body weight having been shown to be a predictor of OA incidence not only in hand and knee, but also in the hip (Oliveria et al., 1999).

The arcOGEN GWAS study provided clear evidence that hip OA at the molecular genetic level is different than knee OA and it that the risk of OA is not uniform between these two skeletal sites (arcOGEN Consortium et al., 2012). This may confirm that hip OA has a different pathophysiology than knee OA, having been shown that some of the hip OA associated polymorphisms were not necessarily associated with knee OA and vice-versa. For example, results from arcOGEN study revealed that single nucleotide polymorphisms (SNPs) specifically associated with hip OA were located on *ASTN2* the *CHST11* genes as well as in between the *FILIP1* and *SENP6* genes and between the *KLHDC5* and *PTHLH* genes respectively (arcOGEN Consortium et al., 2012; Warner et al., 2016). Some of these genes, including *PTHLH* are known to be linked to bone development and osteogenesis (Minina et al., 2002).

1.1.9 Pathogenesis of hip OA

The cellular and molecular changes in hip OA may be a result of altered biomechanical loading on the hip joint and share common features with all other OA-affected joints (Aresti et al., 2016). It is commonly believed that biomechanical alterations caused by risk factors acting at the person level and/or joint level, initiate the driving force of OA pathogenesis. This imply an acceleration of the subchondral bone turnover and hence, an increase in subchondral bone remodelling (Burr and Gallant, 2012). Simultaneously, cartilage microdamage occurs in the form of microcracks, which span across the osteochondral unit to subchondral bone. These microcracks facilitate later increased vascularization and the bidirectional passage of important cytokines and growth factors throughout the osteochondral junction, thus connecting the cartilage and subchondral bone biochemically as well as mechanically (Sharma et al., 2013; Li et al., 2013). However, the precise signalling molecules and cellular sources involved in the biochemical cross talk between articular cartilage and subchondral bone have not yet been fully elucidated.

As mentioned in Section 1.1.4, the current literature presents different routes of OA progression, driven primarily by the commonly observed cartilage damage or subchondral bone OA-associated changes. Some authors describe OA progression to start in the articular cartilage where extracellular matrix is remodelled by the resident under the influence of inflammation. Alterations of extracellular matrix lead to changes in the biomechanical environment of chondrocytes, which further drives the progression of the disease (Maldonado and Nam, 2013). Conversely, others place the initiation of the disease below the cartilage, driven by abnormal biomechanics which enhance subchondral remodelling activities, potentially as a response to repair bone damage, and that these bone alterations could primarily affect cartilage degeneration (Burr and Gallant, 2012). However, current evidence is unclear with respect to which of these routes contribute more to OA development. Irrespective of the site of initiation, the alterations on either side merge together in the osteochondral junction, leading to a common feature of hip OA represented by an osteochondral breach. In addition to the multiple osteochondral alterations described extensively by the literature (Suri and Walsh, 2012), patients with severe degenerative OA of the hip reportedly have impaired venous drainage from the juxta-chondral trabecular bone across the cortex and hypoxia of the subchondral bone (Findlay, 2007).

Some MRI studies indicated that hip OA accompanied with joint pain has bone alterations and radiographic OA can progress to more advanced stage OA over a short time period (Kamimura et al., 2014). This rapid progressive form of hip OA was first reported by Forestier in 1950s and subsequent case series and reports emphasized the clinical, radiographic and pathologic findings of this unusual condition, defined as joint space loss at a rate greater than 2 mm per year or if more than 50% of joint space is lost in 1 year (Batra et al., 2008; Flemming and Gustas-French, 2017). In the early stages, radiographic appearance showed either normal appearance or mild OA changes however within a few months of the onset of symptoms, the destruction of the femoral head and acetabulum with sclerosis, subchondral cysts, and minimal or no osteophytes were observed (Batra et al., 2008). While these authors noted that it can be easily mistaken for other conditions, all the pathologic findings, however, were consistent with OA (Batra et al., 2008) and may be associated with enhanced bone remodelling activities.

The pivotal importance of bone involvement in rapidly progressive hip OA is strongly suspected in humans. Some studies suggested that rapidly destructive hip OA may result from subchondral bone insufficiency fractures, documented as non-traumatic fractures immediately below the articular cartilage and commonly associated with the presence of BMLs and reduced bone mineral density (Yamamoto and Bullough, 2000). Furthermore, severe subchondral alterations were later documented in an MRI study on 12 patients diagnosed with rapidly progressive OA (Boutry et al., 2002). The alterations were mainly represented by subchondral bone sclerosis, abnormal trabeculae and cyst-like subchondral defects (Boutry et al., 2002).

1.1.9.1 Diagnosis and clinical features

It is often possible to diagnose hip OA on the basis of clinical presentation alone, but radiographic investigation is useful to confirm the diagnosis and to monitor disease progression (Murphy et al., 2016). However, it is important to note that patients with evident radiographic changes may not necessarily show correlating clinical symptoms and vice versa, some patients with severe radiographic hip OA may be asymptomatic (Pereira et al., 2011). Using pelvic radiographs data from the Framingham Osteoarthritis Study a community based study of OA, and Osteoarthritis Initiative, a multicentre longitudinal cohort study of OA, it was shown that 15.6% of patients with frequent hip pain had radiographic evidence of OA, while only 20.7% of patients with radiographic hip OA had frequent pain (Kim et al., 2015).

Therefore, diagnostic criteria of hip OA according to American College of Rheumatology uses a combination of clinical and radiographical assessment. This involves a combination of hip pain and either femoral and/or acetabular osteophytes on radiograph or erythrocyte sedimentation rate (ESR) ≤ 20mm/hour together with axial joint space narrowing on radiograph (Altman et al., 1991). Patients with hip OA typically develop pain over months to years rather than acutely, however as mentioned some patients can progress with rapidly-developing form of the disease. During clinical investigation, patients describe pain and stiffness that is worse in the morning or after sitting or resting, usually in the groin or thigh regions that radiates into the buttocks or knee (Woolhead et al., 2010). Stiffness in the hip joint makes it difficult to walk or bend and upon examination, muscle weakness can also be observed. "Locking" or "sticking" of the joint and a grinding noise (crepitus) during movement caused by loose cartilage fragments and other tissues interfering with smooth hip motion are also reported. Internal rotation is the most sensitive single indicator of hip OA, with decreased range of motion in the hip commonly affecting the ability to walk (Birrell et al., 2001).

The Kellgren-Lawrence (KL) scale is often used to classify the degree of deterioration of the joint using radiologic assessment of OA (Kellgren and Lawrence, 1957); The KL grading system uses a scale between 0-4, as follows: Grade 0: normal; Grade 1: doubtful joint space narrowing (JSN) and possible osteophytic lipping; Grade 2: definite osteophytes and possible JSN on anteroposterior weight-bearing radiograph; Grade 3: multiple osteophytes, definite JSN, sclerosis, possible bony deformity; Grade 4: large osteophytes, marked JSN, severe sclerosis and definite bony deformity. However, this scale is not specific for hip OA grading. Therefore in 1963, Kellgren used the knee classification to describe similarly four grades of hip OA, based on the degree of joint space narrowing, osteophyte formation, arthritic changes affecting the bone margins, and gross deformity. This grading has been recently updated by Altman *et al.* (Altman and Gold, 2007) and relies on the radiological evaluation of the typical radiographic features of hip OA, illustrated in Figure 1.6. These include joint space narrowing, marginal osteophytes and other alterations that can be observed radiologically, such as subchondral bone cysts in the acetabulum or femoral head, flattening of the femoral head or thickening of the medial femoral calcar (Aresti et al., 2016).

Radiological investigation can provide information on joint space narrowing, presence of cysts and in later stages of disease, sclerosis of the subchondral bone and osteophyte formation. Radiography is widely available, cost effective and interpretation is relatively

simple when compared to more sophisticated imaging modalities such as MRI, which in turn is more sensitive in detecting early structural changes (Guermazi et al., 2012).

MRI has many advantages over radiography and allows the assessment of more joint tissues and their morphological changes in three dimensions, with more types of available contrast. Abnormalities that can be observed using MRI include joint space narrowing, alterations in the subchondral bone including BMLs and presence of osteophytes. Unlike radiography, MRI can directly visualize articular cartilage and other joint tissues, such as meniscus (knee), tendon, muscle, or effusion. This led to OARSI to recommend MRI for the assessment of cartilage morphology (Conaghan et al., 2011). However, MRI assessment of the hip is more challenging than in the knee for several reasons. The hip joint is deep within the body and it is not in the isocentre of the magnet while the cartilage is very thin making very difficult to differentiate between the acetabular and femoral cartilage. Furthermore, the hip is a spherical joint and therefore partial volume effects are stronger than in the knee joint. Surface coils need to be used which allow high signal and high resolution imaging, but there are no dedicated hip coils (Gold et al., 2015).

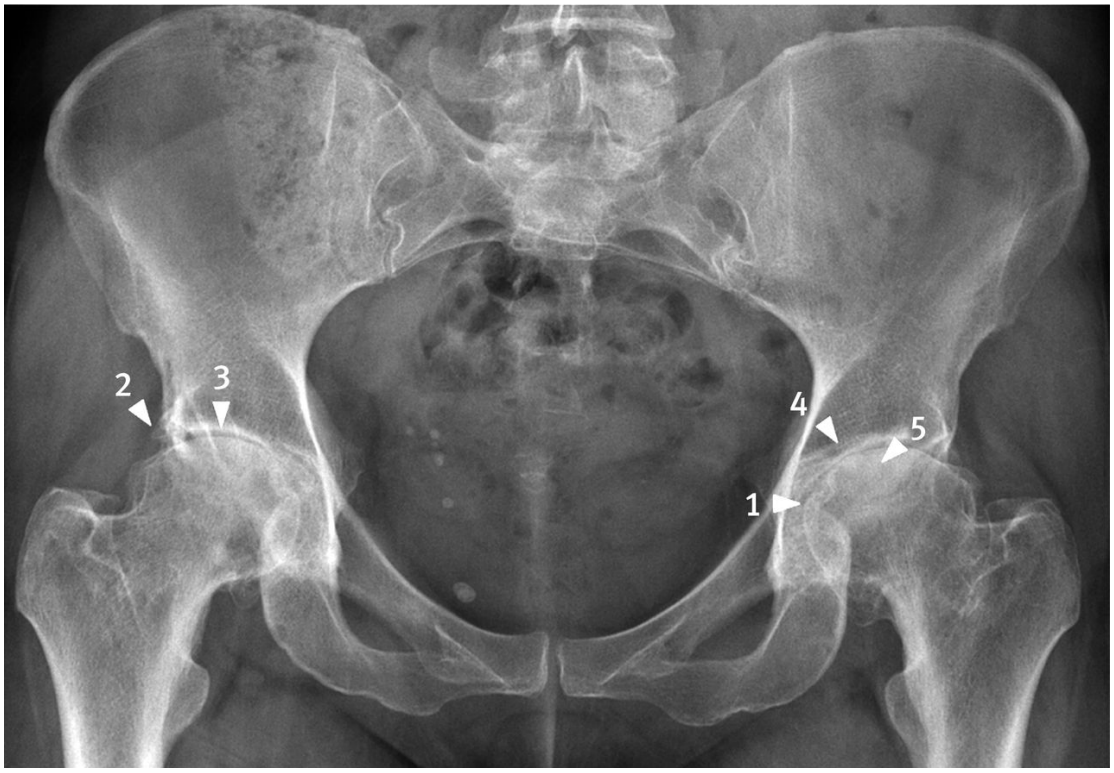

Figure 1.6. Typical plain radiograph of bilateral hip osteoarthritis. *Notice the loss of joint space (1), osteophytes (2), subchondral sclerosis (3), and subchondral cysts (4). In this advanced case, there is also evidence of deformity of the femoral head (5). Joint space narrowing is the best diagnostic criterion* (Croft et al., 1990)*. Figure adapted from* (Aresti et al., 2016)

1.2 Bone remodelling

Recognising that bone is a living organ rather than simply a hard carcass was a major advance in bone biology, thereby establishing the fundamental idea that bone is metabolically active and that cell dynamics facilitate the duality of bone construction and deconstruction by processes commonly referred to as bone modelling and remodelling. Both processes involve formation of bone by osteoblasts and its degradation by osteoclasts (Kenkre and Bassett, 2018). Osteoclasts are of haematopoietic origin and their main role is to resorb bone while osteoblasts are the main bone forming cells, with a mesenchymal origin. Both cell types are discussed in more detail in Section1.2.3.

In bone modelling bone resorption and formation occur at distinct skeletal sites to accomplish the major changes in bone shape and mass, such as during skeletal growth and development of long bones with large diameter. By contrast, in remodelling, these two processes are tightly coupled both spatially and temporally so that the overall bone volume and structure remain unchanged (Allen and Burr, 2014).

1.2.1 Bone remodelling process

Bone remodelling is a continuous and co-ordinated process that results in both formation and degradation of bone in order to maintain bone homeostasis. This active and dynamic process depends on the tightly regulated balance between bone formation and bone resorption as well as a complex interaction between different cell types which is regulated by a variety of biochemical and mechanical factors (Rucci, 2008). Particularly for trabecular bone which is mainly affected by OA, bone remodelling occurs as a cycle of cellular events at the bone surfaces and can be divided into five phases: activation, resorption, reversal, formation, and quiescence (Allen and Burr, 2014).

Anatomically, these processes in health take place within defined areas, described as basic multicellular units (BMU), which contain the main cellular players, osteoblasts and osteoclasts, as well as a capillary blood supply (Frost, 1990). As described in Figure 1.7, the bone remodelling process starts with the recruitment of osteoclasts precursors at the site of bone remodelling and their differentiation into mature, active osteoclasts. Once mature osteoclasts are present, bone lining cells retract from the surface of the bone by yet unknown mechanisms and form a raised canopy over the site to be resorbed (Hauge et al., 2001). Osteoclasts adhere to the exposed mineralised matrix and create a sealing zone allowing to dramatically increase cell surface and providing an ideal secretory environment to start dissolving the bone (Figure 1.7).

Soluble factors are released in the microenvironment during bone matrix degradation and the cells present at the bone surface are thought to be involved in the coupling of bone resorption and bone formation processes (Kenkre and Bassett, 2018). The exact transition signals that mediate the coupling mechanisms are still not elucidated, but evidence so far point to an important, but incompletely understood role for bone lining cells. These soluble factors, including bone morphogenetic proteins (BMPs), fibroblast growth factors (FGFs) and transforming growth factor β (TGF β), are likely responsible for the formation and accumulation of the osteoblasts in the reabsorbed area (Rucci, 2008). Bone formation is achieved by osteoblast and takes approximately 4 months in humans (Eriksen, 2010) The termination of the bone remodelling cascade is marked by the complete mineralisation of the newly formed osteoid. At this stage, osteoblasts end their life cycle by either apoptosis, become flattened as bone lining cells while some embed into their own matrix and differentiate into the terminal stage of maturation, becoming osteocytes (Figure 1.7). Osteocytes play a key role at this stage by releasing bone formation inhibitors, such as sclerostin (SOST) (Bonewald, 2011), and will be discussed in detail as part of Chapter 4.

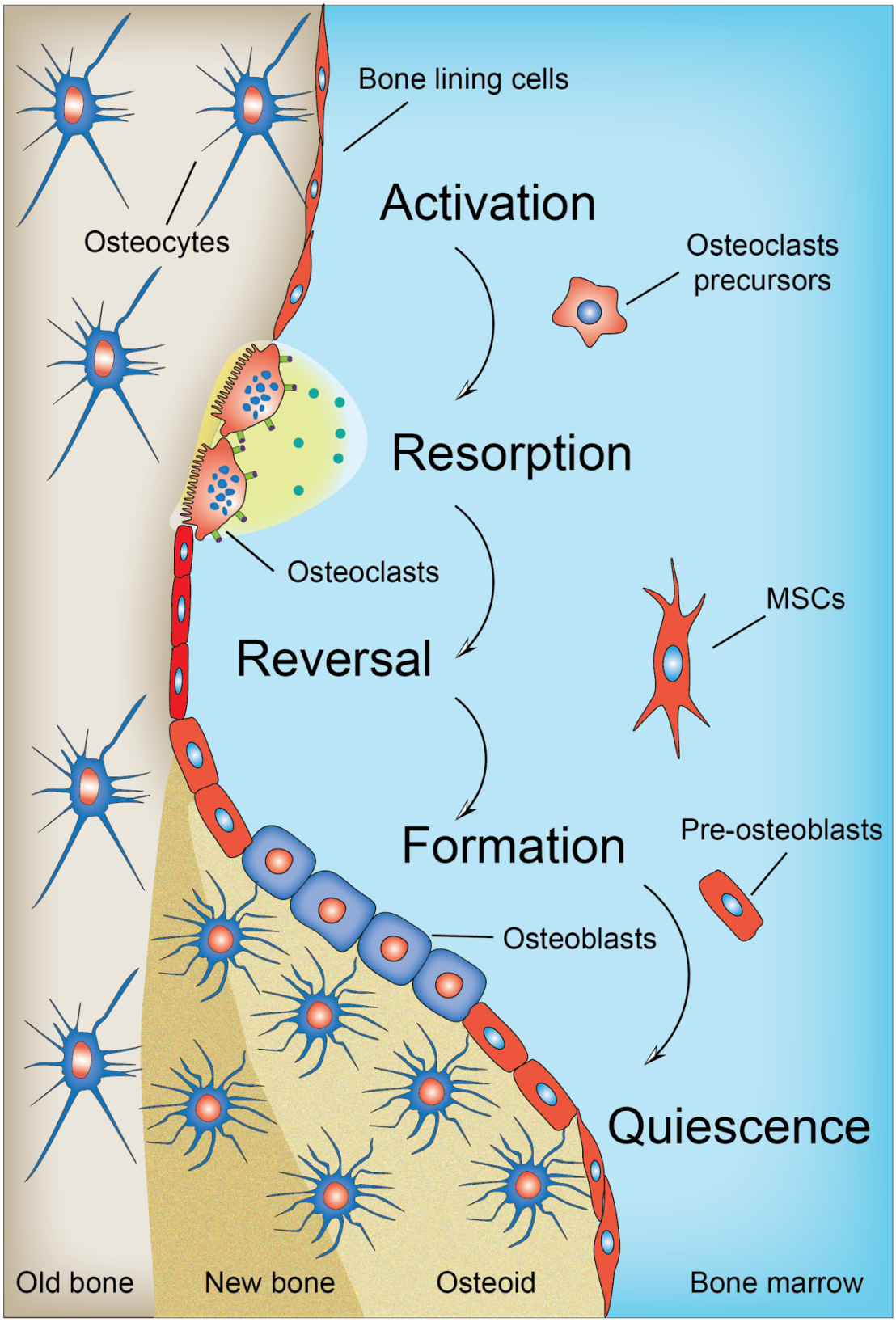

Figure 1.7. Bone remodelling cycle in health. *Bone turnover follows a sequence of events that includes activation, recruitment of osteoclasts to begin resorption, degradation and removal of bone, reversal stage and clearance of bone surface preparing it for formation of new bone by osteoblasts. After this phase a quiescent or resting period occurs.*

1.2.2 Cellular mechanisms of bone remodelling

Osteoarthritis is characterized by marked alterations in the composition, structure and functional properties of periarticular bone. These changes are mediated by the cells that remodel and model bone under physiological conditions and hence they may hold the key to understanding the pathophysiological processes associated with the skeletal changes in OA. This section provides a basic description of the cells involved.

1.2.2.1 Osteoclasts and bone resorption

Osteoclasts are large, multinucleated cells that form through fusion of mononuclear precursors of the hematopoietic lineage that also give rise to macrophages. Osteoclasts formation, activation and their unique functional property to resorb bone is regulated by the soluble molecules macrophage colony stimulating factor (M-CSF), receptor activator of NF-κB ligand (RANKL), osteoprotegerin (OPG), and signaling through the cell surface receptor activator of NF-κB (RANK) (Brendan F Boyce and Xing, 2007).

Resident cells at the site of bone remodelling initiation, including BM stromal cells and osteoblasts, are known to produce the main regulators of osteoclasts formation M-CSF and RANKL (Lacey et al., 1998). Mononuclear precursor cells undergo proliferation in response to stimulation by M-CSF and upon RANKL ligation to its receptor RANK, the osteoclasts form by cytoplasmic, but not nuclear, fusion of their mononuclear precursors (Wada et al., 2006) (Figure 1.8). In most circumstances, the number of nuclei correlates positively with the bone-resorbing activity of osteoclasts (Brendan F. Boyce and Xing, 2007). Inhibition of osteoclasts formation is achieved by OPG, which acts as a 'decoy' receptor by competing with RANKL for its receptor RANK, consequently preventing osteoclast differentiation and the survival of pre-existing osteoclasts (Figure 1.8) (Hsu et al., 1999).

The unique functional property of osteoclasts is the resorption of bone. As discussed in section 1.2.1, bone resorption is a process of bone matrix destruction accomplished by osteoclasts through a series of orchestrated molecular and physical changes.

In the early stages, osteoclasts bind to collagen, fibronectin, and laminin via β1 family of integrin receptors, especially the αvβ3 which binds to osteopontin and bone sialoprotein (Ross and Teitelbaum, 2005). Upon contact with bone matrix the osteoclast forms a ruffled border by transforming its fibrillar actin cytoskeleton into an actin ring, thereby allowing the formation of a sealing zone around the periphery of osteoclast attachment to the matrix, commonly referred to as Howship's lacuna (Väänänen et al., 2000) (Figure

1.8). The Howship's lacunae seal and isolate the acidified resorption compartment from the surrounding bone surface and facilitates the dissolution of the inorganic component. Osteoclasts pump protons through H+-ATPase, generated by Carbonic Anhydrase II into the sealing zone to dissolve the bone mineral, causing the ambient pH within the resorptive lacuna to fall to less than 4 (Silver et al., 1988; Tolar et al., 2004). This allows the release of acid-optimal lysosomal enzymes, such as cathepsin K (CTSK) activated by tartrate resistant-acid phosphatase (TRAP) and matrix metalloproteinases, which degrade the collagen-rich matrix by cleaving the helical and telopeptide regions of collagen (Delaissé et al., 2003). This results in the release of peptides that are endocytosed, transported through the cell and extruded through a functional secretory domain at the dorsolateral surface (Väänänen et al., 2000). These peptides can be used clinically to determine the rates of bone resorption (Greenblatt et al., 2017) while histochemical TRAP staining is widely used to identify osteoclasts *in vivo* and *in vitro*. The resorption process is terminated by osteoclasts apoptosis, ensuring no excess resorption occurs.

1.2.2.2 Osteoblasts and bone formation

Osteoblasts are responsible for the production of the organic constituents of the bone matrix. Osteoblasts do not function individually, but are found in clusters along the bone surface, lining on the layer of bone matrix that they are producing. However, how the osteoblasts emergence from their mesenchymal progenitors and the molecular mechanisms controlling their differentiation are still unclear.

Once the osteogenically-committed MSCs stop proliferating, they change shape from spindle-shape to large cuboidal differentiated osteoblasts. The morphological characteristics of osteoblasts indicate their main function as protein synthesizing cells, including the large cuboidal shape, abundant rough endoplasmic reticulum and prominent Golgi apparatus, as well as various secretory vesicles (Florencio-Silva et al., 2015). Following their short cycle as bone matrix synthesisers, the majority of osteoblasts have one of the three fates: most of the osteoblasts (90%) die through apoptosis and are replaced by new osteoblasts for as long as the formation process is necessary and undergoing; another fraction of osteoblasts are incorporated in the osteoid matrix as living cells and become osteocytes while others return to a quiescent state lining the bone surface as bone lining cells (Franz-Odendaal et al., 2006).

Bone formation takes approximately 4 to 6 months to complete (Eriksen, 2010) and occurs in two main steps: deposition of organic matrix and its subsequent mineralization.

Osteoblasts contribute to bone matrix formation by synthesis and directional secretion of type I collagen, which makes up over 90% of bone matrix protein (Morgan et al., 2008). Together with other types of collagen, proteoglycans, fibronectin and specific bone proteins, such as osteopontin, bone sialoprotein and osteocalcin, osteoblasts give shape to the unmineralised osteoid. This flexible hydrated protein matrix is further mineralised, providing the stiffness and rigidity specific to bone, as opposed to other collagenous matrices. Osteoblasts contribute to osteoid mineralization by releasing small, membrane-bound matrix vesicles that concentrate calcium and phosphate and enzymatically destroy mineralization inhibitors such as pyrophosphate or proteoglycans, these events resulting in nucleation and growth of crystals of hydroxyapatite [$Ca_{10}(PO_4)6(OH)_2$] among the collagen cross-links (Anderson, 2003).

Molecular communication between all the bone cells in the BM compartment is a fundamental mechanism that regulates bone formation and resorption with remarkable precision. However, the research focus has traditionally been on the cells directly involved in removing and depositing bone, the osteoclasts and osteoblasts. The other cells along the osteogenic axis, namely MSCs and osteocytes, indirectly involved in the remodelling process, have been largely disregarded in OA studies. Given their active involvement in these processes, this gap in knowledge must be addressed for a full understanding of cellular mechanisms underlying bone associated pathologies in OA.

There is a stark absence of knowledge on the roles of MSCs and osteocytes in OA. Therefore, work in this thesis aim to shed more light on the place occupied by both MSCs and osteocytes in the bone remodelling series of events, how they contribute to the regulation of cellular and molecular events behind bone abnormalities in OA.

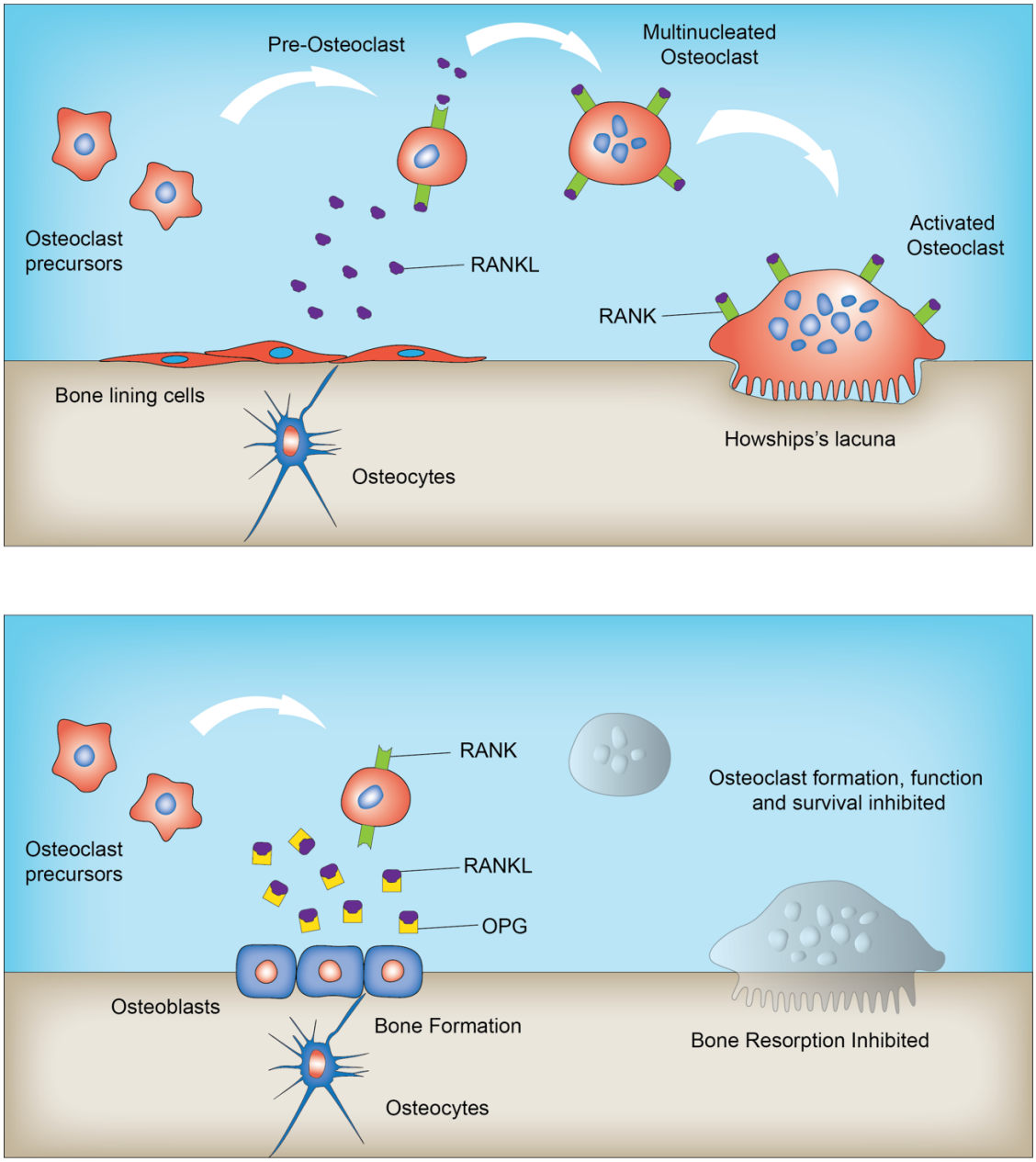

Figure 1.8. Osteoclasts differentiation and activation. *In the presence of RANKL released by stromal cells, RANK presenting monocytic precursors of osteoclasts differentiate and fuse together to form the osteoclasts which become active in contact with the bone matrix as they start resorbing the bone. Osteoclastogenesis is inhibited by the actions of OPG, which act as a 'decoy' receptor preventing the RANKL binding on the surface of osteoclasts precursors, preventing their differentiation and survival while allowing bone to form.*

1.2.3 Bone remodelling in OA

The imbalance between bone formation and bone resorption reflects an inappropriate bone remodelling activity (Rucci, 2008), which may lead to disturbances in bone mass, a characteristic often associated with various pathological conditions, such as OA (Li and Aspden, 1997).

Under homeostatic conditions, bone remodelling is tightly coupled playing an essential role in bone health and is a prerequisite for the maintenance of microdamaged bone that occurs as a result of normal terrestrial impact. As previously mentioned, coupling in this context refers to the temporal succession of events during the bone remodelling processes where the molecular signals that regulate the activities of osteoclasts and osteoblasts activity in a co-ordinated way. This equilibrium however is known to be altered in OA. Subchondral bone changes described in Section 1.1.7, as well as increased bone turnover in OA (Burr and Radin, 2003), are all results of alterations of bone remodelling processes and have been detected early in OA progression (Day et al., 2001; Hochberg et al., 2009).

The joint degeneration process in OA is therefore thought to be characterized by a spatial and temporal separation of the bone remodelling cycles (Burr and Gallant, 2012). Specifically, an increased remodelling was shown to dominate the early stages of the disease, marked by subchondral bone loss, and was considered as a determinant of OA progression (Bettica et al., 2002). As the disease progresses the remodelling rate reduces, shifting the balance towards an increase in bone formation (Burr and Gallant, 2012). This alteration results in increased bone volume, which can be associated with an apparent sclerosis, however the tissue is not well mineralised and may not be very stiff (L.G. Cox et al., 2012). While this may be partly attributed to an impaired mineralisation on behalf of osteoblasts (Sanchez et al., 2008), little is known about the roles of other osteogenic lineage cells in this process. On both sides of the osteoblasts stage of differentiation, the MSCs and the terminally differentiated osteocytes, may also be involved in the impaired bone remodelling activity, especially in the uncoupled mechanisms that seem to be skewed during the sequential phases of the bone remodelling cycle in OA (Burr and Gallant, 2012). However, there is very limited knowledge about how these various mesenchymal lineage cells achieve this in vivo.

1.3 Mesenchymal Stromal/Stem Cells

1.3.1 History and nomenclature of MSCs

In seminal studies during the 1960s and 1970s, pioneering work of Alexander Friedenstein, later working with Maureen Owen, provided evidence for an inherent osteogenic potential of a cell population in BM, distinguishable from the majority of hematopoietic cells (Friedenstein et al., 1968). They found that seeding BM cell suspensions at clonal density results in the establishment of a rapidly adherent fibroblastic cell originating from the BM stroma that can establish a colony in a density-independent manner, now known as colony forming unit fibroblasts (CFU-Fs) (Friedenstein et al., 1970). When the progeny (i.e. BM stromal cells) of these CFU-Fs were transplanted *in vivo* in a diffusion chamber (i.e. a closed system), cartilage formed in the relatively anaerobic interior and bone on the relatively aerobic exterior of the diffusion chamber. When transplanted *in vivo* using an appropriate scaffold (i.e. an open system), the colonies recreated a bone/marrow organ composed of bone, osteocytes, osteoblasts, haematopoiesis-supportive stroma and marrow adipocytes of donor origin, and haematopoiesis of recipient origin (Owen and Friedenstein, 1988). These observations were extended in 1980 and 1990 by other experiments demonstrating that these cells were multipotential and could give rise to osteoblasts, chondrocytes and adipocytes (Pittenger et al., 1999) and together with others that followed who demonstrated self-renewal (Sacchetti et al., 2007), clearly indicated that BM stroma contains a bona fide skeletal stem cell capable of reforming skeletal tissues (Bianco et al., 2008).

Adult stem cells, also known as somatic stem cells, possess the fundamental properties of stem cells, that is, self-renewal capacity and multipotency, although their differentiation capacity is restricted to the tissue where they reside (Kfoury and Scadden, 2015). The mechanisms controlling the fate of stem cells are not fully understood, but they are thought to depend on the interaction with other cells as well as with their microenvironment or niche (Ferraro et al., 2010). Niches are composed of other cells, extracellular matrix, and signalling factors, which, in combination with the inherent characteristics of stem cells, define their properties and potential (Fuchs et al., 2004). *In vivo*, adult stem cells are thought to divide asymmetrically to produce two kinds of daughter cells. Whereas one remains in the niche as a self-renewing stem cell, the other one becomes a precursor or progenitor cell, exits the niche, and enters a pathway of proliferation and differentiation, which leads to the formation of a mature cell type. Stemness refers to the biological pathways and mechanisms that preserve the cell in its

undifferentiated stem state, their ability to reconstruct the tissue of origin *in vivo* while also contributing to its maintenance and repair, thus demonstrating both multipotency and the ability to self-renew (Kolf et al., 2007).

Whether these cells should be considered true stem cells at all or as multipotent progenitors of mesenchymal lineages has been the focus of intense debate (Sipp et al., 2018). Since their initial description, these multipotent BM cells have been given different names. Friedenstein, who is generally credited for the discovery of MSCs, used the term osteogenic stem cells (Friedenstein et al., 1987), while Maureen Owen called them marrow stromal stem cells to underline that they generate stromal cells in long-term cultures (Owen et al., 1987). Based on their supposed capacity for self-renewal and differentiation capacities, Arnold Caplan was the first to introduce the term 'mesenchymal stem cells' (Caplan, 1991), which has become popular in the literature. Others have suggested an alternative term 'skeletal stem cell' to emphasise their potential to generate the cellular constituents of the skeleton (Bianco et al., 2008). In the absence of *in vivo* test for their self-renewal, the International Society for Cellular Therapy has therefore proposed the term 'multipotent mesenchymal stromal cell' (Horwitz et al., 2005).

1.3.2 Defining the MSCs

Decades of studies following their discovery have offered significant in-depth understanding of the biological features of MSCs, however much of the information has been obtained from *in vitro* studies on culture-expanded cells.

There are two main concepts by which the MSCs can be found in the current state of the art in MSC literature worldwide. Firstly, MSCs were defined as a heterogeneous population of cells that proliferate *in vitro* as plastic-adherent cells, have fibroblast-like morphology, form colonies *in vitro* and can differentiate into bone, cartilage and fat cells (Horwitz et al., 2005). However, some claim that stromal cells that apparently fulfil these criteria for an MSC have been isolated from almost every type of connective tissue (da Silva Meirelles et al., 2006) and therefore these features represent a common stromal cell adaptation to *in vitro* culture, and therefore do not reflect physiological functions of culture-initiating cells *in vivo*.

Secondly, others tried to not distort the initial concept of MSCs since its discovery by Friedenstein *et al*., recommending to define MSCs functionally, by experimentally demonstrate both self-renewal and multipotency *in vivo*, i.e. the MSCs would be able to

generate fully differentiated tissues *in vivo* and have the ability to reconstitute *in vivo* cells identical in phenotype and potency to those explanted (Bianco et al., 2013). Culture-expanded cells from the bone cavities (i.e. bone marrow) fulfil both these definitions, form adherent cultures and show self-renewal *in vivo*, which cannot be said for similar cells expanded from other tissues (Sacchetti et al., 2016).

There is currently no clear distinction between cultured and native cells when referred to MSCs and therefore this confusion is noteworthy. Knowledge of the natural identity of MSCs and how these cells are different from their culture-expanded counterparts represents a fundamental aspect, especially when handling MSCs experimentally to studying diseases, such as OA. Work in this thesis will tackle such issue in order to address important questions in the MSC field and more importantly, in their use to study OA pathogenesis.

1.3.2.1 Culture-expanded MSCs

The notion that all MSCs are equal is a common misconception (Phinney and Sensebé, 2013). Significant differences have been found between multipotentiality and function of MSCs derived from different tissues (Winter et al., 2003; Li et al., 2015), and even within the same type of tissues sourced from different anatomical sites (Lopa et al., 2014). It has been demonstrated that the cellular and functional properties can be affected in MSCs from different origins even when cultured under the same conditions. For example, Sakaguchi *et al*. showed that human MSCs isolated from the BM exhibited the strongest osteogenic potential whereas those isolated from synovium were predominant in chondrogenesis and adipogenesis (Sakaguchi et al., 2005).

As a consequence, the International Society for Cellular Therapy (ISCT) issued a position statement to establish a consensus over minimal criteria for designation of multipotent mesenchymal stromal cells, thereby also proposing the term "stromal" to be used instead of "stem" (Horwitz et al., 2005; Dominici et al., 2006). According to ISCT, the cells must adhere to plastic under standard culture conditions. Secondly, the cells should have a distinct and homogenous phenotype, with ≥95% of the population expressing the cell surface markers CD105 (endoglin), CD73 (ecto5'nucleotidase) and CD90 (Thy-19). Additionally, the cells should be negative or with ≤2% of the cells presenting CD45 (a pan-leukocyte marker), CD34 (the endothelial and haematopoietic marker), CD14 or CD11 (both monocyte/macrophage markers), CD79 or CD19 (both B-cell markers) or HLA-DR (a marker of professional antigen-presenting cells, only expressed on MSCs if stimulated by IFN-γ). Finally, the cells should have trilineage potentiality, with the ability

to differentiate into the osteogenic, the chondrogenic and the adipogenic lineages *in vitro* as assessed with standard staining methods (Dominici et al., 2006).

The defining function of *in vitro* MSCs for multipotentiality was described in the late 1990s by Pittenger *et al.* providing evidence of MSC commitment and differentiation towards osteogenic, adipogenic and chondrogenic lineages (Figure 1.9) (Pittenger et al., 1999). By using specific culture conditions, this differentiation capacity has been exploited *in vitro* to generate cells of the mesenchymal lineage, including bone, fat and cartilage which can be assessed by evaluating the formation of mineralized matrices, production of fat droplets and expression of type II collagen respectively (Pittenger et al., 1999).

The lineage commitment and differentiation of MSCs is driven by a tightly orchestrated cascade of transcription factors and signalling cascades. Osteogenic differentiation can be achieved by culturing the cells with ascorbic acid, β-glyceralphosphate and dexamethasone for 3 weeks in specialised osteogenic media (Pittenger et al., 1999). Osteogenic induction is marked by increased alkaline phosphatase activity at final week of differentiation, calcium deposition (positive for Alizarin Red) and mineral aggregation (positive for von Kossa staining). Gene expression analysis of differentiating cells normally confirms osteogenesis by elevation of osteogenesis-related master transcription factors runt-related transcription factor 2 (RUNX2) and osterix (SP7) expression at early time points and a later up-regulation of bone-matrix proteins, such as osteocalcin, encoded by BGLAP (Pittenger et al., 1999).

Adipogenesis, the process by which MSCs differentiate into adipocytes, is equally regulated by a complex and highly orchestrated gene expression program. The critical transcription factor documented to promote MSC adipogenesis while repressing osteogenesis is the peroxisome proliferator-activated receptor γ (PPARγ) while the fatty acid binding protein 4 (FABP4) and adiponectin are involved in the formation of mature adipocytes (Rosen and MacDougald, 2006). The expression of these molecules confirms adipogenic differentiation and can be used in combination with measuring the lipid droplets by Oil red and Nile red staining (Rosen and MacDougald, 2006).

The aim of the chondrogenic differentiation of MSCs *in vitro* is to mimic the natural process of cartilage development that occurs *in vivo*. Studies have documented benchmark genes associated with MSCs-derived chondrocytes, such as the transcription factor *SOX9*, responsible for driving the chondrogenic commitment (Bi et al., 1999) and

genes associated with cartilage extracellular matrix formation, including collagen type II, aggrecan or biglycan (Pittenger et al., 1999).

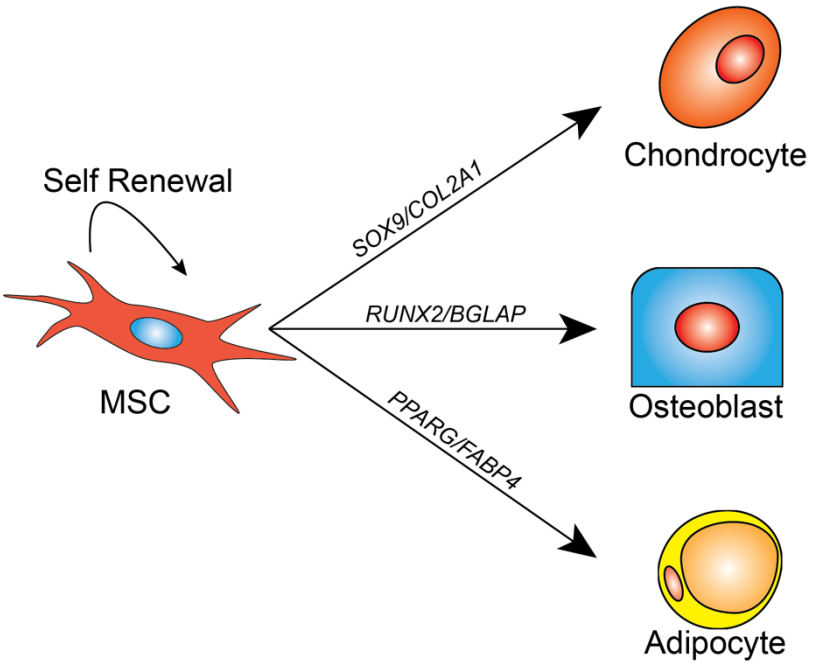

Figure 1.9. MSCs differentiation. *The MSCs have the potential to self-renew and differentiate towards the three mesodermal lineages (cartilage, bone and fat) driven by the actions of master transcription factors and microenvironmental cues.*

Noteworthy is that the ISCT criteria does not include the assessment of MSC's stemness, an important characteristic of adult stem cells. The common criteria established by the ISCT is used for identifying MSCs *in vitro* (Dominici et al., 2006), the surface markers having broad cell reactivity and are therefore not suitable alone for the detection of MSCs *in vivo* (Boxall et al., 2012). However, MSCs can be isolated and expanded with high efficiency (Pittenger et al., 1999). More recently it has been shown that placenta and umbilical cord blood/cord contain higher levels of MSCs than bone marrow, and these tissues are typically considered as biological waste and discarded after childbirth (Spitkovsky and Hescheler, 2008). Adipose tissue has also been shown to contain a much higher frequency of MSCs than bone marrow; with a study carried out finding 2% of nucleated cells in lipoaspirate after a low invasive subcutaneous lipoaspiration procedure were MSCs (Strem et al., 2005). It has been shown that MSCs from alternative areas other than the bone marrow may be more predisposed to differentiate into certain lineages, for example, MSCs isolated from the cartilaginous areas of the knee demonstrated increased levels of chondrogenesis when compared to bone marrow MSCs, but reduced levels of adipogenesis (English et al., 2007).

While culture-expanded MSCs are indeed capable of differentiating into bone, cartilage and fat cells and are readily available to be isolated from many adult tissue types, there are several limitations which hamper the understanding of their *in vivo* biology and particularly, their role in OA pathogenesis. These limitations mainly stem from the discrepancies between cultured and native MSCs, especially with regards to the changes induced by culture manipulations. More than one decade from the initial statement (Dominici et al., 2006), the ISCT criteria have not fully resolved the complexity of MSCs, moreover it can be misleading given the continuous waves of evidence marking the differences between native and culture expanded MSCs (Harichandan et al., 2012; Churchman et al., 2012), which will be further addressed in this thesis (Chapter 3).

1.3.2.2 Native MSCs

Since their first discovery in the BM, the MSCs were also demonstrated to be resident in both trabecular (Jones et al., 2010) and cortical bone (G. Cox et al., 2012). The BM represents a niche of intense activities with regards to haematopoiesis and bone remodelling. Bone marrow MSCs are critical to the bone microenvironment by virtue of their roles in providing a pool of progenitors for maintaining local tissue homeostasis and supporting haematopoiesis (Greenbaum et al., 2013). As mentioned, OA subchondral bone is marked by alterations in bone remodelling processes (Section 1.2.2), however the roles of local resident MSCs in these activities in OA have so far eluded scrutiny. One of the reasons for the scarcity of studies in native MSCs is the lack of specific surface markers, MSCs isolated by plastic adherence representing a heterogeneous mixture of cells with varying proliferation and differentiation potentials.

Currently, the purified human BM MSCs are characterized by a combination of markers, detailed in Table 1.2. These markers include and are not limited to, STRO-1, CD146, CD271 (LNGFR), MSCA-1, CD49a, CD73, CD105, CD106 (VCAM-1) and CD140b (Quirici et al., 2002; Jones et al., 2002; Gronthos et al., 2003; Aslan et al., 2006; Bühring et al., 2007; Sacchetti et al., 2007; Battula et al., 2009). However, some of the surface markers, such as CD49a, CD73, CD140b, and CD146 are widely expressed in other stromal cells (e.g., pericytes and reticular cells) and thus are not unique to MSCs. With this in mind, some negative markers are also used in combination with the aforementioned positive markers, including endothelial and haematopoietic cell markers, such as CD45 and CD31 (Pittenger et al., 1999; Jacobs et al., 2013).

Table 1.2. Positive markers used for native BM MSC identification

Marker	Name	Function	Reference
STRO-1	-	Unknown	(Simmons and Torok-Storb, 1991; Gronthos et al., 2003)
CD271	LNGFR, p75, p75NTR	Neurotrophin receptor	(Quirici et al., 2002; Jones et al., 2002; Jones et al., 2010)
CD105	Endoglin	Receptor for TGF-βI and III	(Barry et al., 1999)
CD106	VCAM-1	Mediates adhesion to leukocytes expressing alpha 4 integrins	(Gronthos et al., 2003; Mabuchi et al., 2013)
CD146	MCAM, MUC-18	Cell adhesion, highly expressed on endothelial cells, receptor for laminin alpha 4 and netrin-1.	(Shi and Gronthos, 2003; Sacchetti et al., 2007)
CD56	NCAM	Cell-cell or cell-matrix adhesion;	(Battula et al., 2009)
CD73	5'nucleotidase	Ectoenzyme, catalysis of purine 5' mononucleotides to nucleosides	(Barry et al., 2001)
CD90	Thy-1	Cell adhesion, highly expressed at sites of inflammation	(Jones et al., 2002; Mabuchi et al., 2013)
SSEA-4	-	Laminin binding; also hES marker	(Gang et al., 2007)
CD140b	PDGFR-β	MSC proliferation and migration	(Bühring et al., 2007)
MSCA-1	TNAP	Phosphate ectoenzyme	(Battula et al., 2009; Cuthbert et al., 2015; Busser et al., 2015)
CD49a	VLA-1	Receptor for collagen and laminin	(Deschaseaux et al., 2003)
CD140a	PDGFR-α	Mesoderm formation and connective tissue development during the embryogenesis	(Li et al., 2014)
GD2	-	Neural ganglioside	(Martinez et al., 2007)
CD10	Neprilysin	Metalloprotease	(Campioni et al., 2003)
SUSD2	-	Cell adhesion and migration	(Battula et al., 2009; Cuthbert et al., 2015; Busser et al., 2015)
CD166	ALCAM	Cell-cell adhesion	(Stewart et al., 2003)
D7-FIB	Fibroblast antigen	Unknown	(Jones et al., 2002)

Whereas for haematopoietic stem cells there is a gold standard to assess their self-renewal and multipotency as a single-cell level *in vivo* by reconstituting the haematopoietic niche in myeloablated recipients (Osawa et al., 1996), such an assay has not yet been universally established for MSCs to test their identity *in vivo*. As such, one group harnessed their capacity to form bone and heterotopic BM formation and identified a population of self-renewing MSCs covering the BM micro-vessels as recognized by the CD146 surface marker expression (Sacchetti et al., 2007) which was later found to also express CD271 (Tormin et al., 2011). The self-renewal capacity of these MSCs was demonstrated in an elegant mouse study by using the neural stem cell marker Nestin (Méndez-Ferrer et al., 2010). This was the first study to prove that MSCs in the BM represent the common pool for osteochondro-progenitors and that they can be serially transplanted following non-adherent culture conditions (Méndez-Ferrer et al., 2010).

The *in vivo* identity of BM MSCs is now firmly established as CD271+ cells (Boxall et al., 2012). CD271 (also named as low-affinity nerve growth factor receptor) is a receptor for neurotrophins, which stimulate neuronal cells to survive and differentiate (Tomellini et al., 2014). It was first suggested as an MSC marker for BM resident MSCs by Quirici *et al.* (Quirici et al., 2002) and further advanced by work in our laboratory and others (Jones et al., 2002; Bühring et al., 2007; Jones et al., 2010; Busser et al., 2015; H. Li et al., 2016).

The topography of CD271 positive MSCs in the BM placed them in the stromal reticular net, the perivascular region of the BM compartment as well as the endosteal region, lining the bone surface (Jones and McGonagle, 2008; Tormin et al., 2011; Sivasubramaniyan et al., 2018). It was further demonstrated that CD271 MSCs enriched more than 40-fold for CFU-Fs in the human BM alone or in combination with other cell surface markers, such as CD45 for negative selection of haematopoietic lineage cells (Quirici et al., 2002; Jones et al., 2002; Cuthbert et al., 2012). The removal of the haematopoietic lineage is commonly required as CD271 alone may not be sufficient to obtain a pure MSC population (Boxall et al., 2012) since CD271 was found to be expressed, although on low levels, on hematopoietic progenitor cells of the erythroid lineage (Cuthbert et al., 2012).

Cell population having the CD45-CD271+ phenotype has been extensively demonstrated by work in our laboratory and others to exhibit all the classical characteristics of MSCs, including the uniform expression of other MSC markers such as CD73, CD105 and CD90 (Jones et al., 2002; G. Cox et al., 2012; Churchman et al., 2013).

Using the CD146 marker, it was shown by work of Tormin *et al.* that the CD271+ MSC population exists within two different niches *in vivo*: endosteal and perivascular, MSCs being reported in both the CD271+CD146- and CD271+CD146+ fractions (Tormin et al., 2011). While these subsets have distinct cell-surface phenotypes based on CD146 expression, this was suggested to be related with their distinct BM topographies and consequently the access to different gradients of oxygen that exist between the endosteal surface and in the proximity of blood vessels where CD146+ cells reside. Both subsets demonstrated the lineage commonality of CD271+ cells and were evidenced to generate haematopoietic stroma *in vivo*, a key property which demonstrated the MSC nature of CD271+ cells (Tormin et al., 2011). This observation might be critical to understanding the link between MSCs and bone lining cells.

1.3.3 MSCs and bone formation

As previously discussed (Section 1.1.8), bone sclerosis in OA is characterised by an increase in the bone volume due to an increase in tissue density that is hypomineralised (Lajeunesse et al., 2003). This indicates an increase in the indices of bone formation in OA patients which may be explained by an aberrant MSC differentiation activity, which will be addressed by work in this thesis. However, the molecular mechanisms occurring in MSCs leading to bone formation must be defined first.

The differentiation process is believed to occur in two steps: the commitment of MSCs towards the specific lineage progenitor cells, and the subsequent maturation from progenitors to the specific cell type. The transcription factors involved in MSC commitment to osteogenesis that are commonly used for *in vitro* tests have been already outlines in Section 1.3.2. Whilst *in vitro* MSC differentiation is induced biochemically, osteogenic differentiation of MSCs *in vivo* relies on the concerted activation of a complex network of pathways controlled both locally and systemically during bone formation process. Wnt (a portmanteau of Wingless and integration 1) family and bone morphogenetic proteins (BMPs) are the main drivers of the early events in osteogenesis, while the helix-loop-helix Twist family of proteins maintain MSCs proliferation (Zaidi, 2007).

Wnt proteins are a family of 19 highly conserved Wnt secreted glycoproteins that play essential roles during development and tissue homeostasis and is a critical pathway for both skeletogenesis and skeletal remodelling (Baron and Kneissel, 2013). Some Wnt proteins, such as Wnt3a and Wnt10b, bind to Frizzled receptors, and recruit the LRP5/6 co-receptors to activate the canonical signalling pathway, leading to β-catenin

stabilization and translocation into the nucleus, enhancing the transcriptional activity of the downstream Wnt/β-catenin mediator, T-cell factor/lymphoid enhancer factor (TCF/LEF) (Cadigan and Waterman, 2012; Fakhry et al., 2013). Binding of Wnt proteins to LRP5/6 is inhibited by osteocyte-secreted factors, such as Dickkopf-related protein 1 (Dkk1) and SOST, both molecules produced by and therefore attributing critical roles to osteocytes in regulating bone remodelling (Tian et al., 2003; Li et al., 2005).

BMPs are considered to be a diverse group of phylogenetically conserved growth factors belonging to the TGF-β superfamily of signal molecules with 20 members identified so far. In the adult, BMP-2 acts as a potent stimulator of ectopic bone formation (Chen et al., 1997) and it is used clinically along with BMP-7 to enhance bone formation, for example, for the treatment of long bone open-fractures treated with intramedullary fixation, non-union fractures (Govender et al., 2002). BMP signalling through the recruitment and activation of heterodimeric Smad proteins controls the expression of Runt-related transcription factor 2 (*RUNX2*), also known as core binding factor alpha1 (*CBFA1*) (Ducy et al., 1997).

Indispensable for osteoblast differentiation, *RUNX2* transcription factor drives the early steps of MSC commitment towards the pre-osteoblast phenotype and no other lineages. This dominant effect was demonstrated by the fact that *RUNX2*-null mice are devoid of osteoblasts and lack bone formation (Komori et al., 1997; Ducy et al., 1997). Furthermore, *RUNX2* was also shown to upregulate osteoblast-related genes associated with bone formation, such as collagen type 1A1 (*COL1A1*), alkaline phosphatase (*ALP*), osteopontin (*SPP1*) and osteocalcin (*BGLAP*) (Fakhry et al., 2013). Osteopontin, encoded by *SPP1* gene (also known as bone sialopotein-1), is a polar linking protein in the extracellular matrix (Denhardt and Guo, 1993; Denhardt and Noda, 1998). Factors known to promote *RUNX2* activation include BMPs, TGF-β, parathyroid hormone (PTH) and FGFs, while the transcription factors *TWIST1* and *TWIST2* act as a negative regulator (Kaneki et al., 2006).

The transition from pre-osteoblasts to osteoblasts is facilitated by the second transcription factor unequivocally required for osteoblast differentiation, Osterix (also known as *SP7*). Osterix is a zinc finger-containing transcription factor belonging to the SP family of transcription factors, specifically expressed in osteoblasts, and required for bone formation (Komori, 2006). Similar to *RUNX2*, the activation of osterix in MSCs is achieved by anabolic signals, such as BMP-2 and insulin growth factor 1 (IGF-1) (Celil and Campbell, 2005). Its fundamental role in bone formation was demonstrated by studies

showing that osterix deficient mice lack bone formation, however they have normal levels of *RUNX2*, indicating osterix location downstream of *RUNX2* (Nakashima et al., 2002). At this stage, the osteoprogenitor cells stop proliferating, increase their expression of ALP, and begin to secrete type 1 collagen and other non-collagenous matrix proteins while anchoring to the newly formed osteoid by cadherin-11 (CDH11) and N-cadherin (Ferrari et al., 2010) exhibiting secretory functions resembling the osteoblasts (Section 1.2.3.2)

1.3.4 Native MSCs in OA

The transcriptional profile of healthy BM CD271+ MSCs has been previously characterised (Churchman et al., 2012; H. Li et al., 2016) and the expression of genes associated with bone, fat and cartilage were documented, indicating their multipotency. Furthermore, recent *in vitro* studies showed that some of the osteogenic molecules, including *SPARC* (osteonectin), *ALP* (alkaline phosphatase) and *TNFRSF11B* (osteoprotegerin) increased significantly following standard *in vitro* osteogenic differentiation (Churchman et al., 2017). Thus, the potential contribution of BM CD271+ MSCs to bone formation activities has been indicated by their gene expression profile in health. While aberrant bone remodelling activities and bone sclerosis are well-established features of OA (Burr and Gallant, 2012), the nature of MSCs in this disease has not been established yet. Furthermore, their roles in bone remodelling in humans are so far limited, but recent studies point to a potential involvement of native MSCs in OA pathophysiology.

While studies investigating the nature and the roles of native MSCs in OA are currently scarce, in one specific mouse model of OA, it was shown that the number of MSCs are increased in the subchondral BM of OA mice, attracted by an increase in TGF-β concentrations resulted following bone resorption (Zhen et al., 2013). This study suggested that the increase in MSCs is possibly due to changes in their topography, migrating from their perivascular location towards the surface of the bone where they participate in bone remodelling activities.

Some studies investigating the MSCs in human OA showed contrasting results to mouse work, with no differences observed in their numbers in comparison to healthy bone (Jones et al., 2010). However, emerging evidence documented aberrant MSCs activities in hip OA bone. The recent study of Campbell *et al*. showed an accumulation of MSCs in the damaged areas of hip OA marked by the presence of BMLs (Campbell et al., 2016) possibly as a repair attempt mechanism. While these MSCs exhibited functional and

transcriptional alterations *in vitro*, especially with regards to their mineralisation potential, their native state was not investigated. Furthermore, as mentioned (Section1.3.2) more recent evidence showed that MSCs isolated from OA bone exhibit phenotypical and transcriptional alterations *in vitro* (Barry and Murphy, 2013; Campbell et al., 2016), while their native profile in OA has not been explored yet. Together with their documented accumulation in altered areas of OA both in human (Campbell et al., 2016) and OA animal models (Zhen et al., 2013) is indicative that their native profile may also be affected.

1.4 Osteocytes

For a long period of time, osteocytes have been regarded as dormant cells 'entombed' within the mineralized bone matrix. While the other bone cells, such as osteoblasts and osteoclasts, were mainly defined by their functional role, the osteocytes were primarily defined by their morphology and location embedded in the bone. This was mainly due to their inaccessible location and the lack of tools to deepen the study of these cells. However, with the recent technological advances of high-resolution microscopic technologies and high-throughput molecular screening, as well as the development of cell- and tissue-specific transgenic animals, the research field involving osteocytes has experienced an increased growth over the last decades unravelling their biological properties and the important functions they have in the skeleton.

Osteocytes are the most abundant bone cells, making up more than 90% of all the cellular component of bone, with an estimated ~42 billion osteocytes in the adult human skeleton (Buenzli and Sims, 2015). As stated above, the osteocytes have been mainly defined by their morphology and represent the terminally differentiated stage of the osteogenic lineage cells, however the exact mechanisms that regulate how and why and osteoblast is destined to become embedded into the bone matrix and start a new life as an osteocyte are still not fully understood.

In humans, osteocytes were postulated to live long, with an estimated average half-life of a human osteocyte as long as 25 years (Frost, 1960). However, considering an overall bone-remodelling rate between 4 to 10% per year (Manolagas, 2000), the life of some osteocytes may be shorter and likely difficult to establish, especially given the differences between cortical and trabecular bone. Cortical bone has a higher density, organised in osteons (Harversian system) where the osteocytes are arranged in concentric layers around the central canal (Harversian canal) may have an increased life span due to large variations in the rate of cortical remodelling (Bach-Gansmo et al., 2015). In contrast, trabecular bone comprises a meshwork of thin trabeculae where the resident osteocytes are exposed to a higher remodelling activity, i.e. they are replaced at a higher rate. What is quite clear is that the lifespan of osteocytes greatly exceeds that of active osteoblasts, which is estimated to be only three months in human bones (Manolagas, 2000).

1.4.1 Osteocytogenesis and osteocyte morphology

Under normal conditions, the transition from osteoblast to osteocyte follows closely regulated steps that correlate intimately to the changes of the cell surroundings. The

incremental formation of osteoid and its subsequent mineralization would result in the temporal and spatial changes in matrix composition, oxygen tension, and mechanical stress, which consequently contribute to the physical transformation of these cells and changes in osteocyte morphology (Chen et al., 2018).

The research literature describes various stages of transition from osteoblasts to osteocytes, (Figure 1.10) as reviewed by Franz-Odendaal *et al*. (Franz-Odendaal et al., 2006). According to this scheme a subpopulation of osteoblasts on the bone surface slows down their matrix production as relative to neighboring cells and progressively immerse themselves in this newly formed osteoid. These cells gradually undergo radical morphological changes from large, cuboidal to a ramified, stellate shape. It was estimated that during the transition to nascent osteocytes, the cell shrinks its size by 30% and reaching a total reduction by 70% once the osteocyte is fully differentiated (Palumbo, 1986). Along their transition, the volume of the large cuboidal osteoblasts and the number of cytoplasmic organelles gradually decrease, including the rough endoplasmic reticulum, Golgi apparatus, and mitochondria (Florencio-Silva et al., 2015) while the nucleus-to-cytoplasm ratio increases (Schaffler et al., 2014) and cytoplasmic projections radiate away from the cell body towards the mineralizing front. Overall, this metamorphosis implies a change in their function, away from their role in extracellular matrix synthesis and more towards mediators in cellular communication and mechanosensory roles.

Accompanying all the physical transformations are changes in their molecular construct. During osteocyte development and maturation, a multitude of molecules are downregulated or switched off while others gradually start being expressed. These molecules include molecular markers specific to osteoblasts that decline in their expression, such as ALP, osteocalcin (BGLAP) and collagen type 1 (Paic et al., 2009) or osteocyte specific molecules, such as E11 (podoplanin) or SOST which start being expressed at different stages of maturation (Dallas et al., 2013). A more thorough discussion of the molecular mechanisms behind osteocyte development and maturation is presented in Chapter 4, Section 4.1.3.

In humans, mature osteocyte cell bodies measure ~9 μm in the short axis by 20 μm in the long axis (Mullender et al., 1996) with a gap present between the cell and the lacuna wall. Mature osteocytes are regularly dispersed throughout the bone matrix residing in ~15-20 μm lacunae (Bonewald, 2011). Originating from the lacunae, cytoplasmic extensions (dendritic processes) travel through the matrix via ~200-300 nm thick passageways called canaliculi, connecting the osteocytes between each other as well as with other bone cells

residing at the bone surface (You et al., 2004). The dendritic processes are approximately half the diameter of the canaliculi leaving a gap sufficient for two processes to lie side by side at points of gap junctional communication between two osteocytes. While the cell body orientation is aligned to the collagen fibres in the bone matrix, these dendritic processes are polarised towards the vasculature and the mineralised front and range in between 30-80 projections for each individual cell (Palumbo et al., 1990). Furthermore, the canalicular wall is wave-like with periodic conical protrusions in the form of collagen fibrils acting as anchoring points (hooks) for osteocyte attachment of the dendritic processes via integrins (McNamara et al., 2009).

Distinctive osteocyte morphologies were observed depending on the different types of bone as well as its stage of maturation. For example, in load-bearing long bones where the load is predominantly aligned with the longitudinal orientation of the bones, osteocytes were found to have mostly an elongated shape (Vatsa et al., 2008). On the other hand, round osteocytes were found in flat bones, such as calvariae, where the mechanical load has a lower amplitude and different directionality (Vatsa et al., 2008). Osteocyte morphology and orientation thus seem to also be affected by the mechanical loading direction.

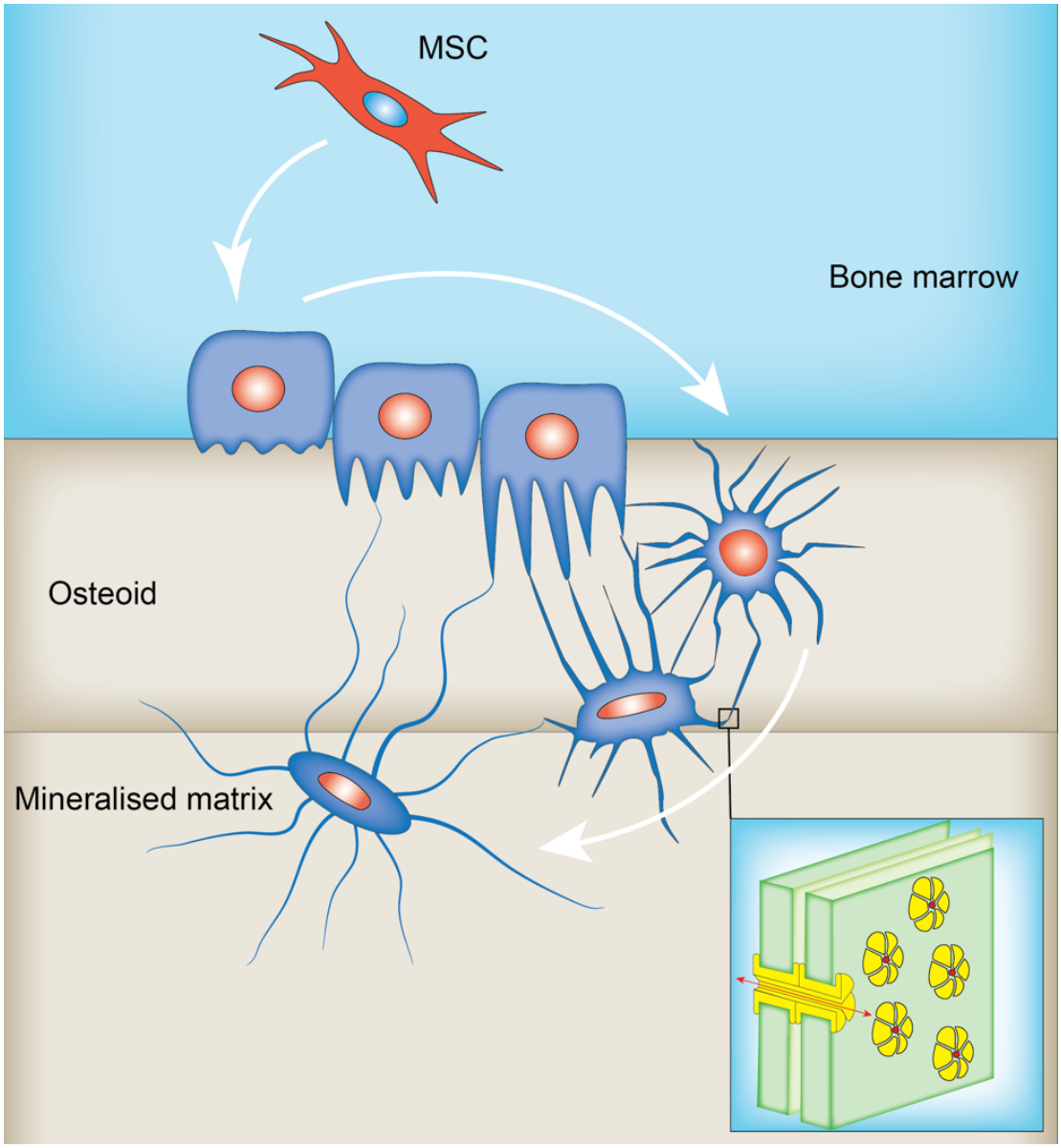

Figure 1.10. Osteocyte differentiation and maturation. *Active osteoblasts originating from MSC osteoprogenitors are gradually embedding into the collagenous matrix of the osteoid as young osteocytes which subsequently mature as the matrix mineralises. During this transformation process (white arrows), the embedding osteoblasts transform by extending dendritic processes and reducing cell body volume. Gap junctions are present between all cells for direct communication. The square panel shows gap junction between the cell processes, red arrow indicating the traffic of soluble molecules and nutrients. Diagram modified from (Franz-Odendaal et al., 2006).*

1.4.2 Lacuno-canalicular network

Due to their location buried in the mineral matrix, osteocytes have no space to proliferate and are also presented with challenges regarding intercellular communication and access to nutrients and oxygen. However, these cells have adapted exquisitely to these adverse

conditions by interconnecting into a complex network commonly referred to as the lacuno-canalicular network (LCN).

The LCN enable intercellular communication through gap junctions allowing the osteocytes to act as a functional syncytial network (Noble, 2008) and thus retaining connections with the surface layer of osteoblasts and bone lining cells. Furthermore, the LCN is also in the vicinity of vascular supply therefore allowing the cells to be supplied with oxygen and nutrients (Dallas et al., 2013).

The gap junctions connecting the dendritic processes between osteocytes as well as the hemichannels on the cell surface allow the exchange of nutrients and facilitate the transport of small signalling molecules among these cells. The osteocyte gap junctions at the tip of their dendritic projections is mainly composed by the most abundant member of the connexins family, Connexin 43, which plays an important role in the maintenance of intercellular communication and response (Civitelli, 2008). The LCN represents an ideal milieu for the transfer of exogenous and endogenous signals via mechanical and biochemical mechanisms (Knothe Tate, 2003).

1.4.3 Osteocyte functions

While osteocytes have been historically regarded as inactive placeholders in the bone matrix, recent data indicate that they are metabolically active and multifunctional cells (Noble, 2008).

Studies showed that osteocytes are necessary to maintain bone mass in response to normal load, but in the absence of load, they send signals that enhance bone resorption (Tatsumi et al., 2007). For example, during exercising or lifting heavy weights, the bone mass increases. Conversely, unloading, as occurs with space flight i.e. microgravity or immobilization, results in bone loss (Tatsumi et al., 2007). Bone tissue health depends on the ability of bone cells to recognize and respond to mechanical and biochemical stimuli, a process called mechanotransduction. The mechanotransduction biological process implies the transduction of a load-induced biophysical signal, such as fluid flow, substrate deformation, or electro-kinetic effects, to a cell and ultimately throughout a cellular network (Donahue, 2000).

Considering their unique location distributed throughout the bone matrix with extensive interconnectivity, osteocytes are the best candidates for detecting and coordinating responsiveness to mechanical signals (Klein-Nulend et al., 2013). Since osteocyte dendritic processes are in contact with osteoblasts on the bone surface and with adjacent

osteocytes, it is believed that osteocyte communicate mechanical signals to osteoblasts and perhaps other skeletal cells to affect their function (Klein-Nulend et al., 2013).

The exact mechanisms by which osteocytes sense and respond to mechanical signals are still unclear. It is believed that the mechanical signals are transmitted to the osteocyte cytoskeleton via cell surface receptors directly, through the compact bone matrix structure, or indirectly via fluid pressure and shear stress conveyed by fluid moving through the canaliculi due to load-induced fluid flow (Knothe Tate, 2003). The extracellular fluid in the lacunar-canalicular space is believed to be the coupling medium through which the osteocytes are stimulated and able to translate the mechanical loading-induced fluid flow shear-stress into biochemical effects at cellular level (Weinbaum et al., 1994). Deformation of the bone matrix surrounding osteocytes during mechanical strain imposes a shear stress by the movement of fluid along the canaliculi and is believed to produce perturbations in the osteocyte cell body or dendritic processes. *In vitro* studies using osteocytes cell lines demonstrated the importance of actin cytoskeleton along with the other filament networks and focal adhesion molecules in mechanotransduction by osteocytes (Alenghat and Ingber, 2002; Ponik et al., 2007; Santos et al., 2010). Furthermore, other studies suggested that crucial in sensing the changes in surroundings are a mechanosensory protein complex formed by a cilium and its associated proteins PolyCystins 1 and 2 (Xiao et al., 2006).

Several biologic effects in response to mechanical forces or lack of them have been described. Upon mechanical stimulation, osteocytes immediately respond by producing several secondary messengers, such as adenosine triphosphate (ATP), nitric oxide (NO), Ca^{2+}, and prostaglandins (PGE_2 and PGI_2,) which influence bone physiology (Klein-Nulend et al., 1995; Genetos et al., 2007). Conversely, targeted deletion of osteocytes leads to bone loss and unresponsiveness to loading (Tatsumi et al., 2007). This was attributed to the osteocyte specific protein sclerostin, the product of the SOST gene (van Bezooijen et al., 2004). Sclerostin was shown to inhibit bone formation, both *in vitro* and *in vivo,* by its effects on Wnt pathway in osteoblast lineage cells (Li et al., 2005). Furthermore, it was demonstrated that SOST is elevated during reduced loading and it is reduced during increased loading (Robling et al., 2008).

Osteocytes have been lately recognised to have critical regulatory roles in bone homeostasis, orchestrating the functions of osteoblasts and osteoclasts, thus acting as a master regulator of bone remodelling (Prideaux, Findlay, et al., 2016). Their control on bone formation is achieved through the aforementioned molecule SOST, which is

mechanically dependent and is a very potent bone formation inhibitor with demonstrated implications in OA pathology (Poole et al., 2005; Jia et al., 2018). Osteocytes have also regulatory roles in bone resorption by activating osteoclastogenesis. Recent evidence demonstrated that osteocytes are the main producer of RANKL and directly modulate bone resorption by promoting osteoclasts formation (Nakashima et al., 2011; Xiong et al., 2015). Furthermore, apoptosis or injury-induced necrosis of osteocytes defines the spatial domains in which bone remodelling occurs. It was observed that osteocyte apoptosis can occur at sites of microdamage, and it is proposed that dying osteocytes are targeted for removal by osteoclasts (Verborgt et al., 2002), possibly due to the release of RANKL along the canaliculi from the dying osteocytes.

Osteocytes also have endocrine functions, regulating mineral and phosphate metabolism at a local and systemic levels. Systemically, osteocytes play an important role in bone-kidney axis through the production of the phosphaturic factor, fibroblast growth factor 23 (FGF23) (Riminucci et al., 2003). Additionally, as cells embedded in the bone matrix, osteocytes also contribute to the maintenance of that matrix. As reviewed by Plotkin *et al.*, osteocytes produce phosphoproteins like dentin matrix protein 1 (DMP1), matrix extracellular phosphoglycoprotein (MEPE) and phosphate-regulating neutral endopeptidase, X-linked (PHEX) regulating mineral deposition, signalling with other bone cells in addition to regulating FGF23 production (Plotkin and Bellido, 2016).

The molecular mechanisms through which osteocytes exert their control on bone formation and bone resorption as well as their secretory profile that contributes to mineral and phosphate homeostasis are discussed further in Chapter 4.

Independently of the mechanisms involved, it is important to note that the regulatory and mechanosensory role of osteocytes are mainly possible due to their extensive LCN. The dendritic processes radiate in different directions and cover a vast bone area, allowing the communication with other bone cells as well as the transduction of cellular signals in response to biomechanics. Given their function as transducers of mechanical strains, it is likely that osteocytes might undergo enormous changes during biomechanical associated conditions, such as OA. Together with their regulatory roles in bone remodelling and mineral homeostasis, these changes may affect osteocytes not only morphologically but also at a transcriptional level, with noteworthy consequences in the overall bone microenvironment.

1.5 Hypothesis and aims

It was hypothesised that subchondral bone sclerosis as well as other bone abnormalities in hip OA result from alterations in the bone remodelling activities. The MSCs and osteocytes play a profound role in driving these alterations and therefore contributing to OA pathology.

The aims of this thesis are:

1. To investigate the transcriptional and topographical changes in native MSCs of hip OA bone using healthy iliac crest as control bone (Chapter 3).

2. To develop a method to study native osteocytes transcriptional profile in both OA and healthy bone and to study their transcriptional and topographical changes in hip OA compared to healthy bone (Chapter 4).

3. To determine the existence of an osteogenic committed subset of MSCs in OA bone (Chapter 5

Chapter 2 General methods

The basic methods described in this chapter have been used throughout the whole project, with more specific methods described in the Materials and Methods sections of individual chapters. The complete list of reagents, solutions and buffers used in this project is listed in Appendix 1 while plastics, consumables and equipment in Appendix 2. All illustrations were created in Adobe Illustrator by the author of this thesis unless otherwise stated.

2.1 Patient samples

In total, 63 donors were recruited following written informed consent. This research was undertaken after approval from the Leeds East and Leeds West Research Ethic Committees as well as local National Health Service Research and Development (Appendix 3).

All the samples in the OA group used across this project were harvested from 42 donors with end-stage OA (18 males and 24 females) undergoing total hip arthroplasty (median age 71 years old, range 40-89). Control bone was from iliac crest (IC) samples collected from 18 patients (9 males and 9 females) undergoing orthopaedic surgery for metal removal following previous fracture, who were otherwise healthy (median age 51 years old, range 24-87). The choice of healthy IC as control bone was due to the limited availability of healthy femoral heads. However, recent published data provided compelling evidence with regards to the validity of this type of bone is studying both osteocytes and MSCs (Ilas et al., 2019) and the cellular identity of MSCs has been previously documented to be similar between the two sites with regards to their surface markers phenotype and functional properties (Jones et al., 2010). Furthermore, in addition to IC, for histological analyses n=3 femoral heads were included from non-OA donors undergoing total hip arthroplasty for neck of femur fracture (all females, 54, 88 and 93 years old respectively). All samples were collected and processed on the day of the surgery and basic patient demographics were recorded and included in Appendix 4.

2.2 Tissue harvest, processing and overall study design

Whole femoral heads excised following total hip arthroplasty or iliac crest bone samples were collected in saline solution and transported in sealed sterile containers. Figure 2.1 illustrates the overall experimental design used in this thesis while the detailed description of each procedure is included in the Materials and Methods section of each chapter. The bone samples were used either for histological assessment (Chapter 4 and Chapter 5) or

enzymatically digested to obtain the MSCs (Chapter 3 and Chapter 5) and osteocytes (Chapter 4). To avoid culture manipulations, the bone treatment procedure was developed to simultaneously obtain pure osteocyte-enriched fragments and matched native MSCs. The MSCs were isolated by fluorescence activated cell sorting (FACS) from the enzymatically extracted cell suspension and used for gene expression analysis and functional assays, described in detail in Chapter 3 and Chapter 5. From the same cell suspension, MSCs were also isolated by plastic adherence and culture expanded to be used for CFU-F assays and gene expression analysis, detailed in Chapter 3. The remaining bone fragments following enzymatic treatment were further processed for complete tissue denudation in order to obtain pure native osteocytes which were also assessed for gene expression, described in detail in Chapter 4.

2.2.1 Bone mechanical processing and enzymatic treatment

Tissue processing was performed under strict aseptic conditions in the cell culture facility. From all bone samples, bone resident MSCs were extracted by enzymatic digestion as described previously (Jones et al., 2010) and followed by either cell sorting or culture expansion, using well established protocols by work in our laboratory (Jones et al., 2010; Churchman et al., 2012; Campbell et al., 2016). First, the cartilage was carefully removed from the femoral heads using a No. 24 blade scalpel (Swan-Morton) and 19 cm Stille-Liston bone cutting forceps (Sklar). Iliac crest bone fragments were processed intact due to their smaller size and weight (<1g). Bone samples from femoral heads were broken down into small fragments (<1 g) using a 22 cm Stille-Luer bone rongeur (Sklar) and washed repeatedly with phosphate buffered saline (PBS, Sigma) to remove fat, haematopoietic cells and clots. After weighing the bone fragments, they were subjected to 4 hours' incubation at 37º C with collagenase solution (Appendix 1) containing Collagenase I (Worthington Biochemical) in 20% Foetal Calf Serum (FCS, Biosera) and 80% Dulbecco's Modified Eagle Medium (DMEM, Thermo Fisher) (corresponding to 3000U/g of bone). The samples were kept in a water bath with regular shaking every 20 minutes to remove all adherent cells from the bone surfaces and disperse the bone pieces evenly in the collagenase solution.

Following digestion, the collagenase solution containing the released cells was separated from the bone chips by filtering it through a 70 μm cell strainer, while the bone fragments were further washed in large volumes of PBS to remove any residual cells, fat or clots. The PBS washes were filtered and pooled with the original collagenase solution,

centrifuged at 100x*g* for 10 minutes) and resuspended in DMEM (commonly 15-30 ml), containing 10% FCS and 1% penicillin/streptomycin (P/S, Thermo Fisher).

The remaining digested bone fragments were kept in PBS (no more than 1 hour) for further processing and RNA extraction from native osteocytes, described in detail in the 'Methods' section of Chapter 4.

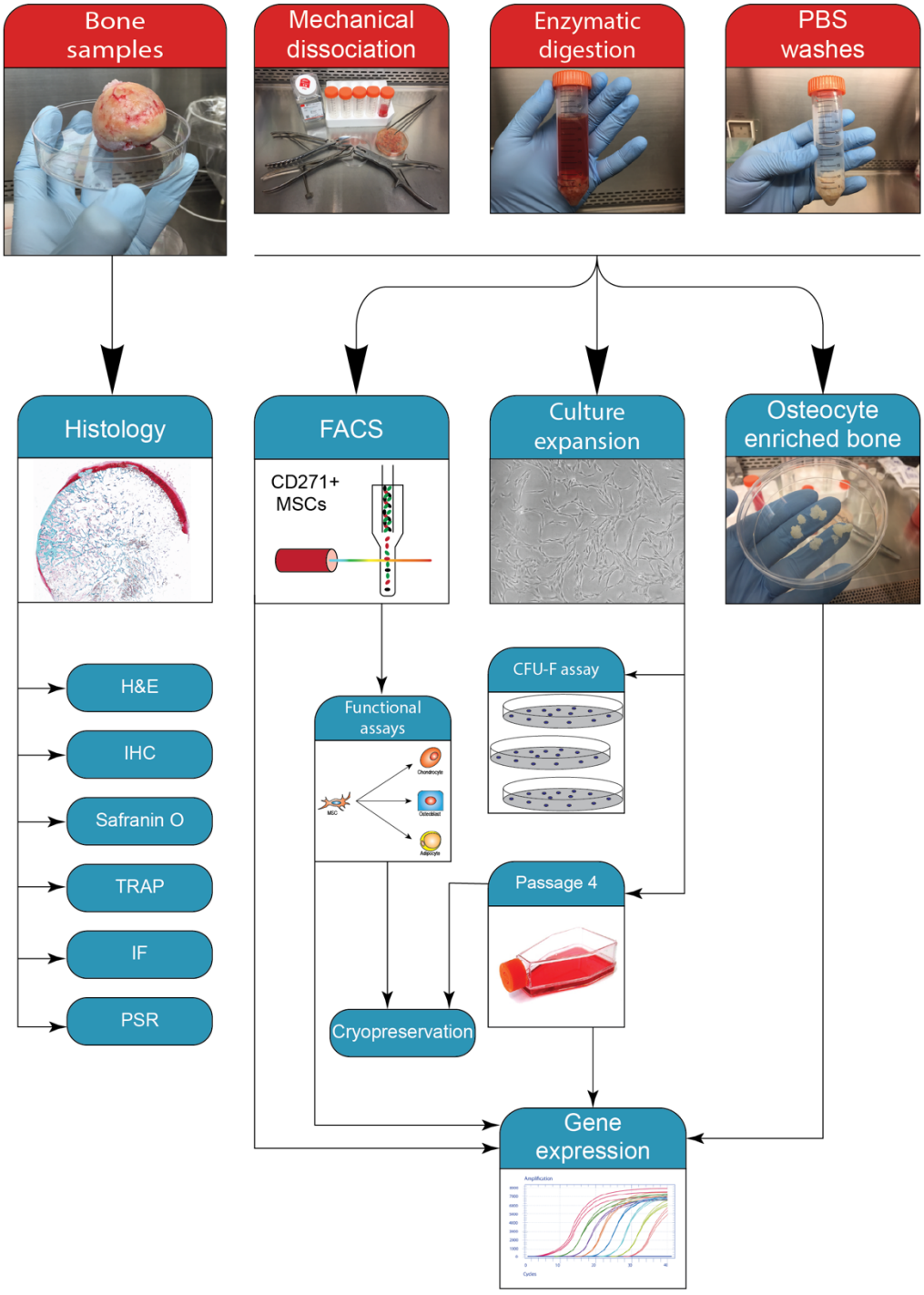

Figure 2.1. The overall design of experimental procedures. *Trabecular bone samples (OA and controls) were used for histological assessment or cell extraction. To obtain the stromal cell suspension and denuded osteocyte-enriched bone, the bone samples were mechanically broken down into small fragments and enzymatically digested. From the obtained cell suspension, the MSCs were isolated by FACS or by plastic adherence and used for subsequent gene expression analysis and functional in vitro assays. The remaining bone fragments were used for RNA isolation and gene expression analysis. For histological assessment bone samples were EDTA-decalcified and embedded in paraffin before the staining procedures.*

2.3 Cell culture

2.3.1 Determination of cell number and viability

The number of viable nucleated cells released by enzymatic digestion was determined using the trypan blue exclusion method using a haemocytometer with a Neubauer counting chamber and an inverted light microscope.

The cell suspension to be counted was prepared at the appropriate dilution in DMEM and subsequently diluted 1:1 in Trypan blue solution (Sigma) for counting. Approximately 10 µl of the mixture was transferred by capillary action to the haemocytometer and viewed under a bright field microscope at 10x magnification. The method is described in Figure 2.2 and is based on the observation that viable cells exclude the dye and non-viable cells stain blue due to a breakdown in cell membrane integrity. Viable cells were counted on four 1mm^2 squares which were then averaged. In order to maintain accuracy, a minimum number of 100 cells were counted. Where the cell number was difficult to count, the procedure was repeated following appropriate dilution of cell suspension.

The number of viable cells/ml in the cell suspension were determined using the formula below. In brief, the average cell count of the four large squares was multiplied by 10^4 and then multiplied again by the dilution factor (e.g. multiplied by two if cell : dye ratio is 1:1). The total number of viable cells represents the value of cells/ml in the original cell suspension multiplied by total volume.

$$No.of\ nucleatedcells/ml = No.of\ cells\ counted\ x\ 10^4 x\ Dilution\ factor$$

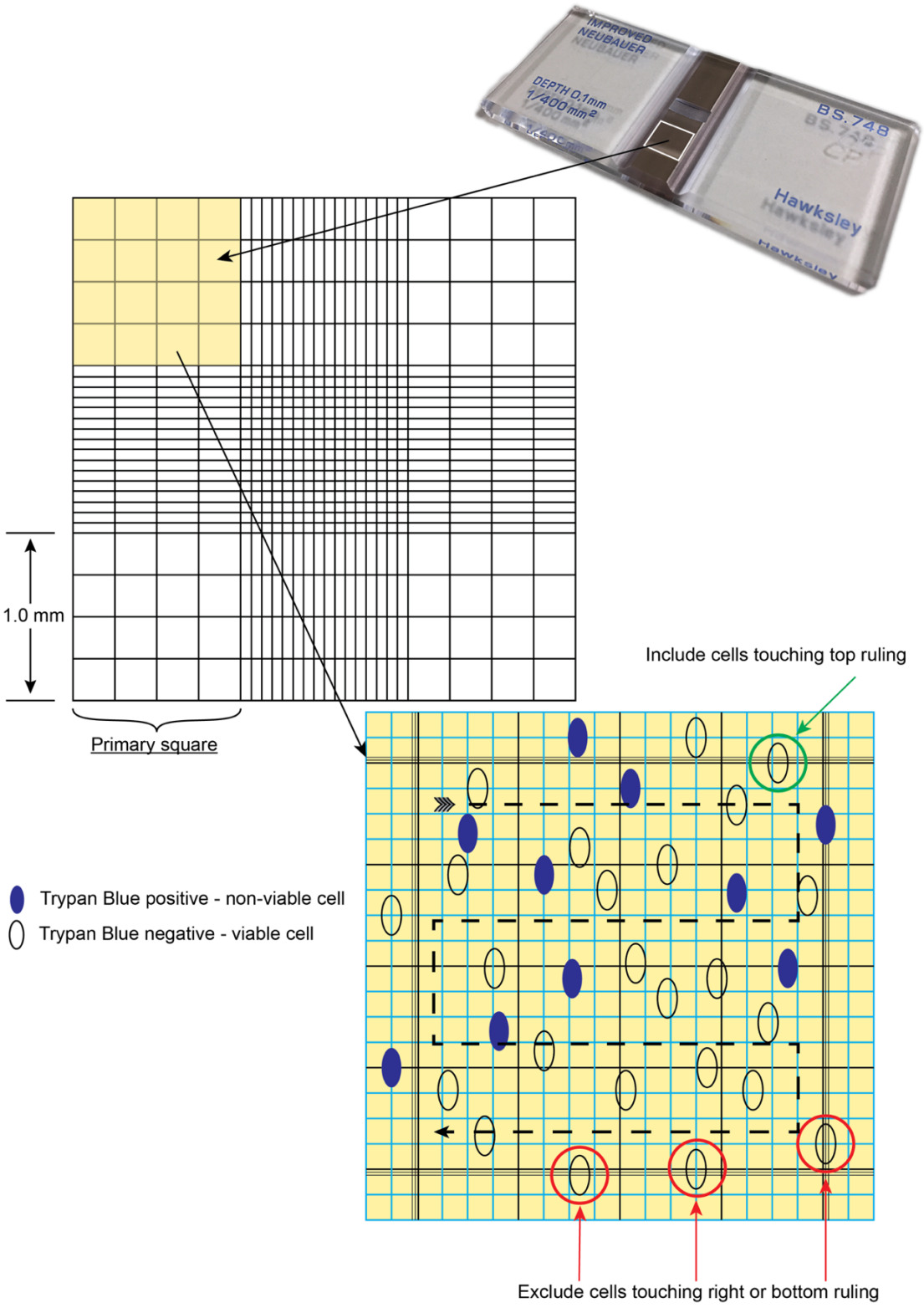

Figure 2.2. Manual cell counting using trypan blue exclusion method. *The cells were diluted 1:1 using trypan blue and placed in the counting chamber. Live cells with intact membrane exclude the dye (empty symbols) while dead cells stain blue (blue symbols). Viable cells that are on the border lines on two sides only are then counted in each large square.*

2.3.2 MSCs Isolation by plastic adherence and culture expansion

Cultures were initiated by plating a known number of nucleated cells from the enzymatically released cell suspension. Specifically, 10^6 cells as manually counted by Trypan Blue exclusion method were plated directly in 7 ml of Stem MACS MSC expansion media (Miltenyi Biotec) in T25 flasks and incubated at 37º C, 5% CO_2. Cells were allowed to attach for 48 hours and at this time-point non-adherent cells were removed by washing with 5 ml PBS and replacing the medium. These cells were expanded until sub-confluence, i.e. the cells just started to touch each other (~70% confluence), denoted as passage 0 (P0) and then passaged.

Passaging the MSCs was performed by removing the media and washing the cells with PBS before detaching them from the plastic surface using Trypsin solution (Appendix 1). Trypsin is a proteolytic enzyme of serine protease family with optimum activity at 37º C. The exact mechanism involves cutting away the focal adhesions, which anchor the cells onto the culture dish, at the C-termini side of Lysine or Arginine. Cell detachment was assessed under an inverted phase-contrast microscope following 2-3-minute incubation with 1 ml of Trypsin solution. The trypsin containing the detached cells along with any residual cells from the flask were collected with 8 ml of DMEM and centrifuged at room temperature for 5 minutes at 300xg. The supernatant was discarded and the cell pellet disrupted and resuspended in 1 ml of DMEM. The number of cells at each passage were determined by Trypan Blue exclusion method and an appropriate cell solution volume was transferred in T25 flasks corresponding to a cell density of 10^4 cells/cm^2 (i.e. $2.5x10^5$ cells/flask) for all subsequent passages up to passage 4 (P4). At this point they were lysed for RNA isolation from each flask while the remaining cells were frozen for future use as described in Section 2.3.3.

2.3.3 Cryopreservation and thawing cells

Cryopreservation of cells following tissue processing is a common technique used for long term storage. The solution of mixed, uncultured cells released following enzymatic treatment of bone was centrifuged at 300xg for 5 minutes and resuspended in an appropriate amount of freezing media containing 45% DMEM/1% P/S, 45% FCS and 10% Dimethyl sulfoxide (DMSO, Sigma) at 10^7 cells/ml. Cell suspension was then transferred in 1 ml aliquots into each 1.8ml labelled cryovials and then rapidly placed into an isopropanol based freezing container (Mr. Frosty, Nalgene) and kept at -80° C overnight for slow freezing (rate of approximately 1º C per minute). The vials were subsequently transferred to liquid nitrogen for long term storage.

The culture-expanded MSCs (cMSCs) remaining following passaging and at the end of culture-expansion experiments were also frozen and stored for further use. The cryopreservation of cMSCs was performed following the same method and freezing media using 10^6 cells/ml aliquots or less per cryovial.

Frozen and thawed enzymatically-released cells were used during the project in some experiments for cell sorting (Section 2.4), MSC culture expansion (Section 2.3) or CFU-F assays (Chapter 3, Section 3.3.3). Frozen cryovials were thawed at 37° C in a water bath until no ice-crystals were visible. The cells were then transferred using a sterile pastette to a 15 ml tube and resuspended in DMEM/10% FCS/1% P/S which was added to the cells drop-wise up to a total volume of 10 ml with gentle mixing every time. To reduce cell clumping, especially for the vials containing uncultured cells, the DMEM/10% FCS/1% P/S was prior supplemented with DNase I (20 U/ml, Sigma). In order to remove the DMSO used for cryopreservation, the cells were centrifuged at 300xg for 10 minutes at room temperature and resuspended in an appropriate amount of DMEM/10% FCS/1% P/S. After counting, the cells were seeded in T25 culture flasks, placed in a humidified incubator at 37º C and 5% CO_2 at cell densities specified in corresponding sections and grown in Stem MACS media until the cells reached confluence.

2.4 Native MSCs purification by FACS

Fluorescence activated cell sorting (FACS) was used in experiments presented in Chapter 3 to enumerate the native MSCs frequency in the enzymatically released cells from healthy and OA bone and to isolate pure MSC populations for gene expression analysis. For experiments described in Chapter 5 FACS was employed to enumerate and isolate pure native MSCs subpopulations for culture-expansion (Chapter 5, Section 5.3.5) and gene expression analysis (Chapter 5, Section 5.3.6). Specifically, in Chapter 3 the MSCs were selected based on the CD45-CD271+ phenotype (Jones et al., 2010) (Chapter 1, Section 1.3.2) while in Chapter 5 the CD45-CD271+ MSC population was segregated into distinct subsets based on the expression of CD146 (Tormin et al., 2011) and CD56 (Battula et al., 2009; Sivasubramaniyan et al., 2018) (Chapter 1.3.2). Details of each of these experiments are provided in the Materials and Methods section of each chapter.

By using FACS various cell properties are simultaneously analysed, such as cell size (forward scatter, FSC) and granularity (side scatter, SSC). This can be combined with the detection of surface markers labelled with different fluorescent dyes which emit at certain

wavelengths. When light from a laser interrogates a cell, that cell scatters light in all directions (Figure 2.3A). The light that is diffracted in the forward direction (i.e. along the same axis the laser is travelling) is detected in the Forward Scatter Chanel. The intensity of this signal has been attributed to cell size. Laser light that is scattered at 90º to the axis of the laser path is detected in the Side Scatter Channel when there is a change in the refractive index. The intensity of this signal is proportional to the amount of cytosolic structure in the cell, such as granularity. As the fluorescent molecule present in or on the antibody bound to the cell is interrogated by the laser light, it will absorb energy from the laser light and release the absorbed energy at a longer wave length. The emitted light passes through the optical filters and is detected by photodetectors, converted to electrical impulses which are then digitalised and quantified.

The BD Influx 6 flow cytometer (BD Bioscience) used in this project is equipped with four lasers at 355 nm (ultra-violet), 405 nm (violet), 488 nm (blue), 561 nm (green/yellow) and 633 nm (red) complemented by fluorescence detectors that can detect a total of 19 colour parameters from all lasers. Therefore, the fluorochromes chosen for the four antibodies in this project (CD271-APC, CD45-FITC, CD56-BV421 and CD146-PE) spanned across the spectrum and minimised the cross-over, as depicted in Figure 2.3B. Any spill-over (e.g. from FITC to PE) was corrected as detailed in Section 2.4.2.

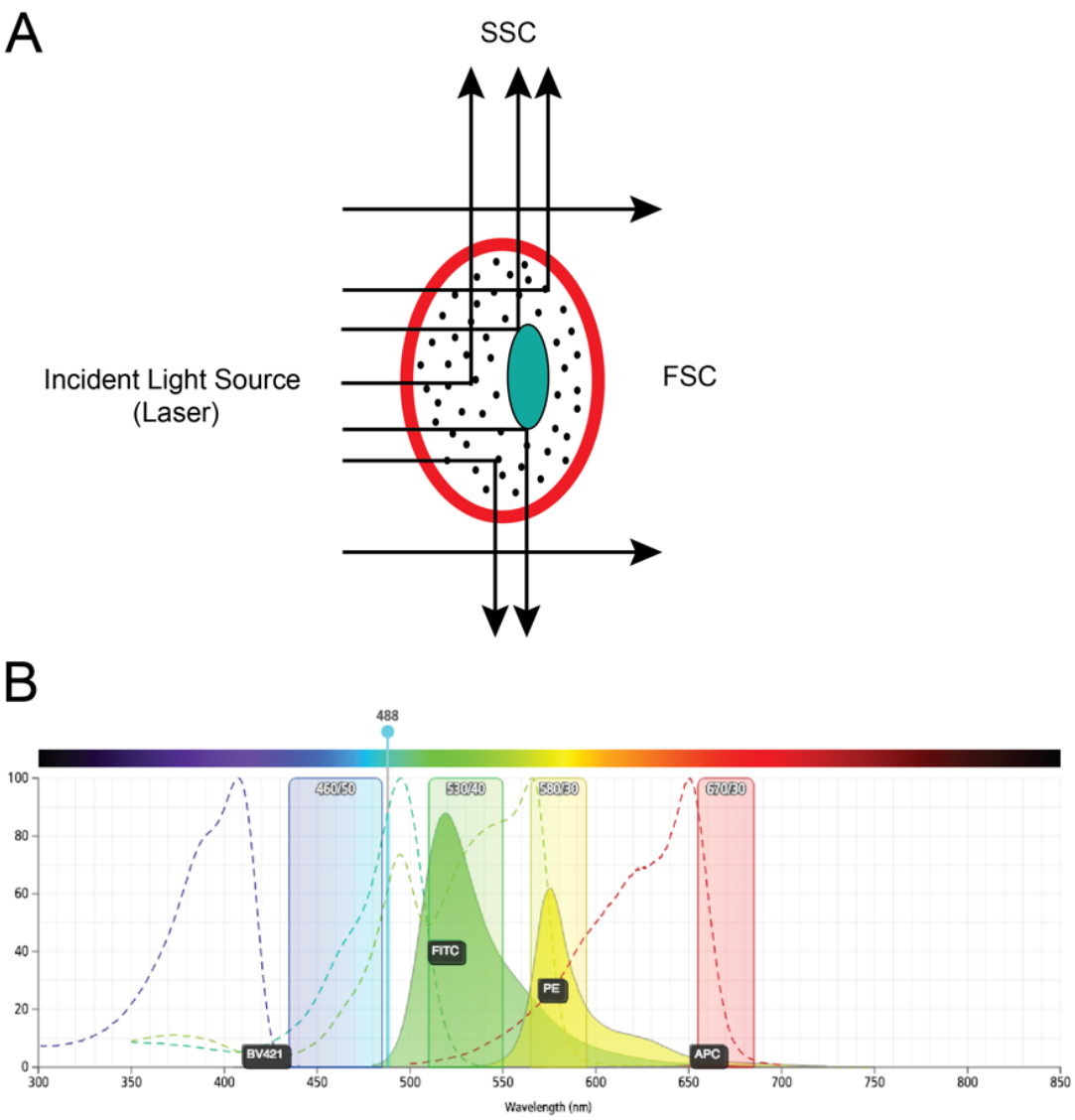

Figure 2.3. Light scattering and fluorochromes spectrum in flow cytometry. *(A) Determination of cell size and granularity by using the Forward Side Scatter (FCS) and Side Scatter (SSC). (B) Spectrum chart indicating the four fluorochrome for the antibodies used in sorting experiments as well as the filters (coloured rectangles) used for their detection in the corresponding channel. Dotted lines represent the excitation wave length while their emission is in full colour.*

2.4.1 Staining cells for cell sorting

Data in Chapter 3 include MSCs purification using the CD45-CD271+ phenotype (Jones et al., 2010) while in Chapter 5, this population was further divided by using antibodies for CD56 (Battula et al., 2009; Sivasubramaniyan et al., 2018) and CD146 (Tormin et al., 2011). As previously discussed in Chapter 1, Section 1.3 and detailed in Chapter 3, CD271 is the most common surface marker used for native MSCs isolation from the BM (Quirici et al., 2002; Bühring et al., 2009; Jones et al., 2010). Within this population of MSCs previous studies revealed the existence of distinct subsets based on the surface marker expression of CD146 (Tormin et al., 2011) and CD56 (Battula et al., 2009), as described in Chapter 1, Section 1.3 and Chapter 5, Section 5.1.3. In this thesis, the MSCs were isolated by using antibody for CD271 while the haematopoietic lineage cells (HLCs) were identified by using antibody for CD45, the most commonly used haematopoietic lineage marker (Shivtiel et al., 2008). A standard experimental arrangement and distribution of staining tubes for cell sorting calibration, the isotype controls as well as the antibody cocktails used in this thesis are detailed in Table 2.1.

Fluorescence compensation settings were optimised by using anti-mouse Ig κ/negative control CompBeads (BD Biosciences). The set contains both positive and negative microparticles which were mixed with the same conjugated antibodies used in the experiment providing an accurate compensation correction for spectral overlap for any combination of fluorochrome-labelled antibodies. The positive beads population binds to all isotypes conjugates of the specific immunoglobulin while the negative beads have no binding capacity. For example, as shown in Figure 2.3B, an antibody conjugated with FITC may emit light which crosses over with the light emitted by another antibody conjugated with PE, therefore light from FITC spills over into the channel for PE and vice-versa. This crossover can be compensated by using single colours compensation beads. Therefore, each conjugate needs to be tested in every channel and the spill-over subtracted from the channels other than its own. This was performed by flow cytometry staff members as part of instrument calibration prior to each sorting experiment.

Unstained cells and IgG1 isotype controls (Table 2.1) were used in each experiment to determine cells auto-fluorescence and non-specific background staining as described in each chapter and position the gate for each cell population investigated.

Table 2.1. List with complete set of antibodies and isotype controls used across all experiments

Surface molecule	Conjugate	Excitation/ Emission	Clone	Manufacturer
CD271	APC	595 nm/660 nm	ME20.4-1.H4	Miltenyi Biotec
CD45	FITC	488 nm/530 nm	T29/33	DAKO
CD56	BV-421	405 nm/421 nm	HCD56	Biolegend
CD146	PE	488 nm/580 nm	P1H12	Miltenyi Biotec
Isotype control	APC	595 nm/660 nm	X40	Miltenyi Biotec
Isotype control	FITC	488 nm/530 nm	MCA928F	BioRad
Isotype control	BV-421	405 nm/421 nm	MOPC-21	Biolegend
Isotype control	PE	488 nm/580 nm	MCA1210	BioRad

2.4.1.1 Sample staining

Depending on the cellularity of each sample, form the enzymatically released cell suspension, approximately 1.5-3x10^6 cells were resuspended in each staining tube in 100 µl of FACS buffer (Appendix 1) and incubated in a 10% Fc receptor blocking solution (Appendix 1) for 10 minutes at room temperature before the fluorophore-conjugated antibodies were added. Blocking step is required to inhibit non-specific binding and reduce background fluorescence. The cells were incubated with the conjugated antibodies for 20 minutes at room temperature, washed in FACS buffer and centrifuged for 5 minutes at 300xg. Cells were re-suspended in 500 µl FACS buffer, filtered through a 72 µm cell strainer cap (Corning Falcon) into a fresh tube to remove any remaining bone debris or cell clumps. To exclude the dead cells, 10 µl 7-amino-actinomycin (7-AAD) (Miltenyi Biotec) was added before the cell sorting procedure. Similar to trypan blue, 7-AAD only penetrates the disrupted membrane then binds to DNA and can be fluorescently detected in dead cells.

2.4.1.2 Controls and compensation beads staining

Compensation beads and isotype controls were stained simultaneously with the sample sorting tube. Approximately 200,000 cells were used in the isotype control tubes which were stained using 10 µl of each isotype control of the same species as the conjugated antibodies (all IgG1) and the corresponding fluorochrome. The unstained tubes contained the same number of cells as the isotype controls and were subjected to the same treatments, without the addition of antibodies. The compensation beads were first

vortexed and one drop of each was added to 100 µl FACS buffer in separate FACS tubes corresponding to each antibody. Then the conjugated antibodies (10 µl each) were added to the beads, one antibody in each tube, and incubated for 15 minutes at room temperature in the dark. The stained beads together with the sample and controls were then washed with 1 ml of FACS buffer, centrifuged at 300xg for 5 minutes and resuspended in 500 µl of FACS buffer before being analysed.

Table 2.2. Standard list of tubes used for FACS experiments

Tube	Antibody	Amount added	Approx. no of cells used	Role
1	Unstained Add 7AAD before sort	N/A 7AAD-10 µl	2-5x10^5	Setting the FSC/SSC gate
2	Sample sorting tube Add 7AAD before sort	CD45-15 µl CD56-7.5 µl* CD271-30 µl CD146-30 µl* 7AAD-10 µl	1.5-3x10^6	Sorting tube
3	Isotype Control Add 7AAD before sort	IgG1 FITC/APC/PE/BV 10 µl each	2-5x10^5	Setting gates, correct for non-specific background
4	CD45 Comp Beads	10 µl CD45	Comp Beads (no cells) 1 Drop each	Compensation
5	CD146 Comp Beads	10 µl CD146*	Comp Beads (no cells) 1 Drop each	
6	CD271 Comp Beads	10 µl CD271	Comp Beads (no cells) 1 Drop each	
7	CD56 Comp Beads	10 µl CD56*	Comp Beads (no cells) 1 Drop each	

* only used for FACS experiments in Chapter 5

2.4.2 Data acquisition and analysis of MSC frequencies

The acquisition of all tubes, compensation and instrument settings were performed by staff members of flow cytometry facility. The voltages for FSC and SSC were kept the same for every experiment, as changing the voltages would result in altered profiles making consistent gating more difficult. Data was acquired on the BD Influx flow cytometer and the raw data files were analysed using the FlowJo Software (Tree Star).

Several steps were taken in order to guarantee a pure MSC population and accurate selection of the positive cells. The stained beads were run first and compensation was altered for each channel prior to sorting of cells from the samples. Hence, spectral

compensation was first performed by using the CompBeads as described above, by recording 10,000 events form each positive controls of the conjugated antibody. Similarly, 10,000 events from the isotype controls were then acquired for each antibody using cells from the sample under investigation in order to set the correct gates for the desired populations. Next, the FSC and SSC voltages were set up by using unstained cells from the sample to be analysed. This would allow separation of contaminating small bone debris and other impurities, such as collagen or DNA, following the digestion procedure (Figure 2.1). To the unstained cells was then added 10 µl 7-AAD in order to separate the dead cells from viable cells on the red channel (Figure 2.4). In all experiments the cells were gated sequentially, first by using the FSC and SSC to eliminate debris and then the negative 7-AAD fraction was excluded to keep live cells only (Figure 2.4). As shown in Figure 2.4 physical gates were then created by selecting cells positive for CD271, comprising the MSC population, while the CD45 was used for HLCs selection, serving as control population for MSCs in subsequent gene expression experiments. In general, an average of $4x10^4$ MSC events (range $1x10^4$-$2.8x10^5$ events) and $4x10^5$ HLC events (range $1.6x10^4$-$2.3x10^6$ events) were collected after sorting. The cell sorting procedure, including calibration was usually performed within 2-4 hours, depending on the number of samples analysed for the experiment.

The analysis of MSC frequencies was performed by calculating the percentage of gated CD271 positive cells from the total of the gated live cells based on the total number of events acquired (Figure 2.4). Similarly, the subsequent MSC subsets were calculated as percentage of CD56, CD146- positive as well as the double negative cells of the gated CD271+ fraction, as depicted in Figure 2.4.

The purified sorted MSCs populations and control HLCs were collected directly into 100 µl of RNA lysis buffer (Norgen Biotek) and stored at -80º C for subsequent RNA isolation as detailed in Chapter 3 while the CD271+ MSC subsets where collected for both gene expression and culture-expansion, as detailed in Chapter 5, Section 5.3.5.

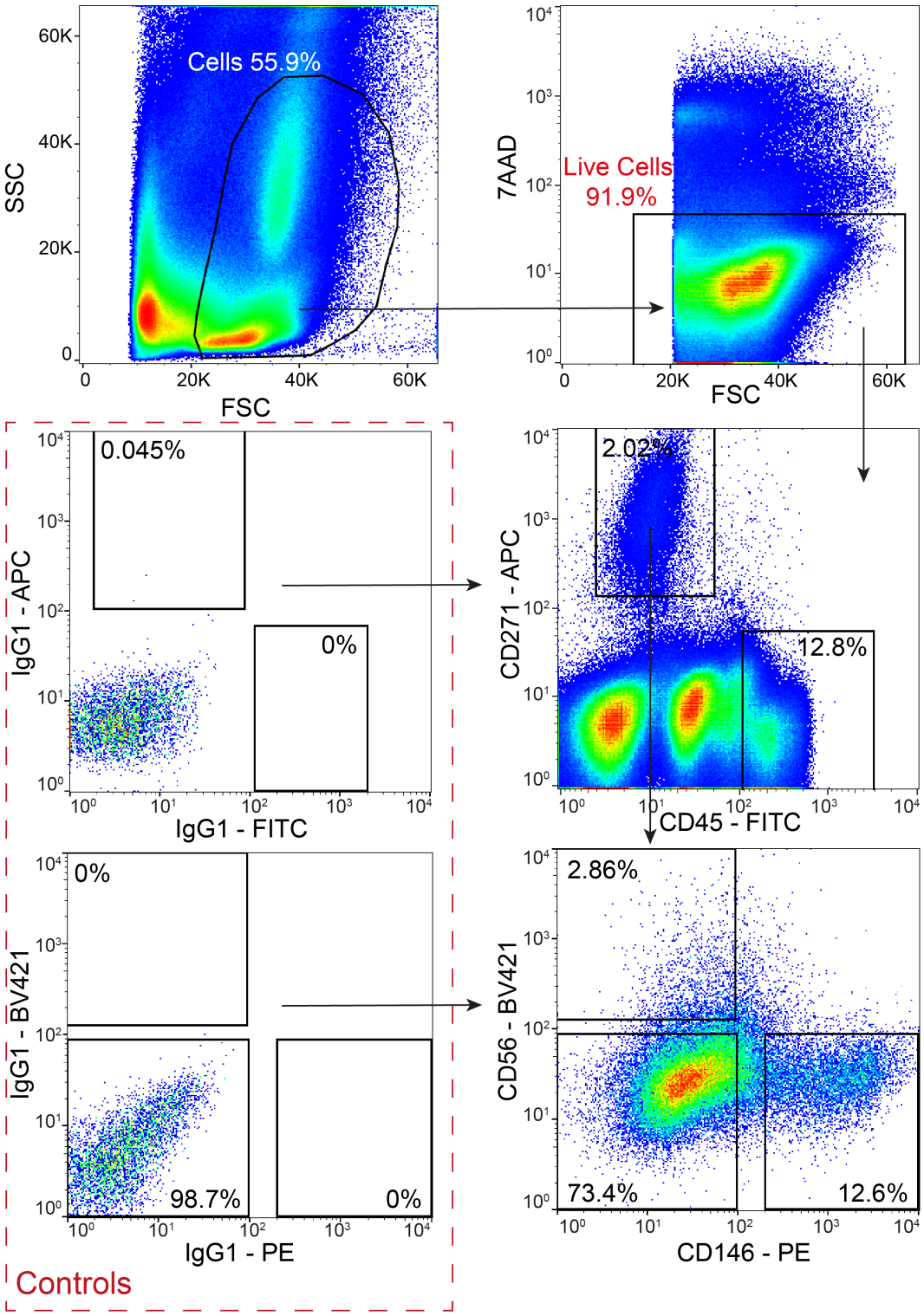

Figure 2.4. Gating strategy for MSCs enumeration and sorting. *Viable cells were identified using FSC and SSC then the live cells were selected using 7AAD. Isotype controls for each antibody conjugate were used to select positive populations while HLCs were defined using CD45. For further purification within the CD45-CD271+ gate, cells were selected for CD56+ and CD146+.*

2.5 Gene Expression

2.5.1 RNA isolation

Before RNA isolation the working surface and pipettes were wiped with RNase Away (Fisher Scientific) to remove any traces of RNase's. RNase free pipette tips and microcentrifuge tubes were used for all the steps during the isolation procedures in order to avoid RNA degradation or contamination.

The RNA isolation from osteocyte-enriched bone fragments is described in detail in Chapter 4, Section 4.3.3. In brief, the RNA was isolated using an adaptation of the methods of Chomczynski and Sacchi (Chomczynski and Sacchi, 1987) using chloroform extraction and isopropanol precipitation of RNA. For RNA isolation from culture-expanded cells or cell isolated by FACS, a column-based method was employed by using RNA isolation kits (all from Norgen Biotek) and following the manufacturer's protocol. The procedure is based on a column resin as the separation matrix for the RNA and a high-salt buffer system with guanidine salt which allows the RNA to be preferentially purified from other cellular components and contaminants based on its electrical charge within a spin column. Firstly, the cells were lysed with the lysis buffer provided by the kit supplemented fresh before each procedure with 1% β-mercaptoethanol (Sigma). This ensured the denaturation of RNases by reducing disulphide bonds and destroying the native conformation required for enzyme functionality. In combination with the strong, but temporary denaturing effects of guanidinium salts in lysis buffer any RNases present in the material to be extracted from will be completely inactivated, thus extending the life of the stored RNA.

As stated in Section 2.4, the cells isolated by FACS were sorted straight into 100 µl of RNA lysis buffer and vortexed for homogenisation before the RNA isolation procedure, while the cultured MSCs were lysed directly into the flask. For this, the culture media was removed and the cells were thoroughly washed with PBS (3 times), which was carefully removed using a pipette to prevent RNA lysis buffer dilution. Then 500 µl RNA lysis buffer was applied to the cell layer and collected by aspiration with a pipette following scraping the flask bottom using a sterile cell scraper (Corning). The collected lysate was stored at -80º C for subsequent RNA isolation.

The lysate was mixed with an equal volume of 95% ethanol (diluted in DEPC water) and then up to 600 µl of the mixture was applied to the column, in several steps if necessary. The samples were all treated with DNase-1 solution (Norgen Biotek) for 15 minutes at

room temperature, before the washing steps. Following 1-minute centrifugation at 13000xg, the RNA was retained onto the column while the remaining impurities were washed twice with 400 µl of the provided washing buffer. Purified RNA was then eluted in an appropriate volume of nuclease free water or elution solution provided by the kit.

The concentration and purity of RNA was assessed using the Nanodrop ND-1000 spectrophotometer and 2 µl of RNA per reading. Spectrophotometric analysis is based on the principles that nucleic acids absorb ultraviolet light in a specific pattern. In the case of DNA and RNA, a sample is exposed to ultraviolet light at a wavelength of 260 nm and a photo-detector measures the light that passes through the sample. Some of the ultraviolet light will pass through and some will be absorbed by the DNA/RNA. An optical density (OD) 260:280 ratio between 1.9 and 2.2 were used as a measure of pure RNA to be used for the gene expression experiments described in this project.

2.5.2 cDNA synthesis

The RNA was converted into cDNA by using a High-Capacity cDNA Reverse Transcription Kit (Applied Biosystems). To synthesize the cDNA, a reaction mix was made up as described in Table 3. The reaction mix comprising the appropriate amount of 10X Random primers, 100 mM dNTP mix, 10X RT buffer, MultiScribe reverse transcriptase and RNase inhibitor was then mixed with the appropriate amount of total RNA depending on the requirements for the downstream applications (e.g. qPCR). In order to have an equal starting material for qPCR reactions and therefore judge accurately the gene expression levels investigated, the RNA volume was normalised for every reaction depending on the amount of cDNA product required.

Table 2.3. Reaction components for cDNA synthesis

Component	Volume for 1 reaction
10X Random primers	2 µl
100 mM dNTP mix	0.8µl
10X RT buffer	2 µl
MultiScribe reverse transcriptase	1 µl
RNase inhibitor	1 µl
Total reaction master mix	10 µl
+	
Total RNA	10 µl

The volume was adjusted to 20 µl with nuclease-free water (Nalgene) in clean 0.2 ml tubes and PCR reaction performed by incubation of the samples in a Techne TC512 thermal cycler (Geneflow) using the following cycling conditions (Table 4): 25° C for 10 minutes to initiate the reaction then hold for 2 hours at 37°C; the reaction was terminated by incubation at 85° C for 5 minutes. Samples were kept frozen until use at -20° C.

Table 2.4. Thermal cycling conditions for cDNA synthesis

Settings	Step 1	Step 2	Step 3	Step 4
Temperature	25° C	37°C	85° C	4º C
Time	10 minutes	120 minutes	5 minutes	∞ (up to 5 hours)

2.5.3 qPCR reactions

Quantitative real-time polymerase chain reaction (qPCR) was performed using TaqMan reagents to evaluate the gene expression profiles of osteocytes and MSCs in this thesis. The TaqMan assays for the genes of interest are detailed in Appendix 5, all from Thermo Fisher and specified in the Methods section of each chapter.

This technique has a high degree of sensitivity and specificity, being commonly used for gene expression evaluation experiments. The detection system used by TaqMan involves dual labelled probe, with a fluorophore attached at the 5' of the oligonucleotide and a quencher at the 3' end (Figure 2.5). The juxtaposition of the fluorophore and quencher inhibits the fluorescence under the light excitation during cycling and therefore its detection. During the exponential stages of PCR, each target sequence is amplified by the Taq polymerase resulting in probe displacement and therefore the fluorescent signal can be detected and quantified in real time. The emitted fluorescence correlates with the cDNA template in the reaction and therefore can be quantified.

The qPCR was performed in 10 µl reactions on a 384 plate all in triplicate during each experiment. The reactions mix was prepared by adding 5µl of TaqMan gene expression master mix (Applied Biosystems), 0.5µl of TaqMan gene expression assay (Thermo Fisher) and a total of 4.5 µl mix of cDNA in nuclease free water resulted from the cDNA reaction. Additionally, a number of controls were also used, as follows: no template control was also used to assess the presence of any contamination or false positive results by omitting the cDNA in the reaction mix and no reverse transcription control was used to confirm the absence of genomic DNA contamination by simply omitting the reverse transcriptase during cDNA preparation.

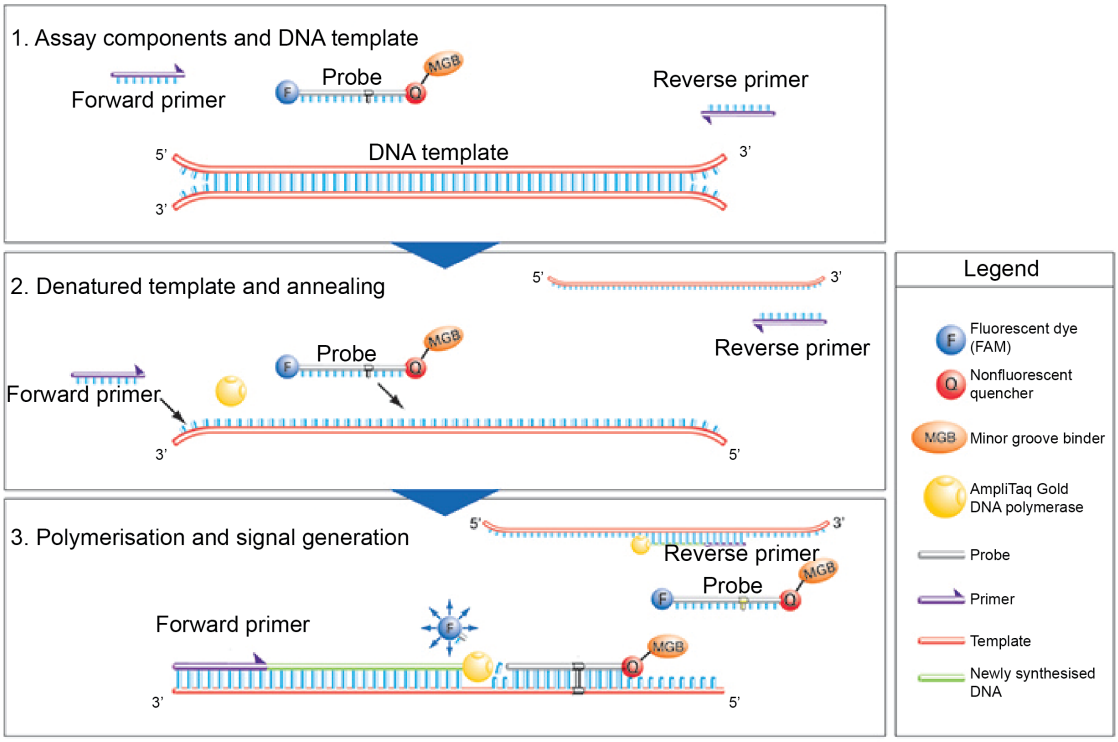

Figure 2.5. Schematic diagram of the TaqMan mechanisms in qPCR. *1. At the start of qPCR, the temperature is raised to denature the double-stranded cDNA. During this step, the signal from the fluorescent dye on the 5' end of the TaqMan probe is quenched on the 3' end. 2. The reaction temperature is lowered to allow the primers and probe to anneal to their specific target sequences. 3. Taq DNA polymerase synthesizes new strands using the unlabelled primers and the template. When the polymerase reaches a TaqMan probe, its endogenous 5' nuclease activity cleaves the probe, separating the dye from the quencher. Adapted from Thermo Fisher.*

Table 2.5. Reaction components for qPCR

Component	Volume for 1 reaction	Volume for 1 port
TaqMan Gene Expression Master Mix (2X)	5 µl	N/A
TaqMan Gene Expression Assay (20X)	0.5 µl	50 µl
cDNA template + H_2O	4.5 µl	50 µl
Total Volume	**10 µl**	**100 µl**

Some of the gene expression analysis in Chapter 3 and Chapter 5 was performed using a TaqMan Low Density Array (TLDA) card in a 96a format (Figure 2.6). The TaqMan probes for TLDA as well as for all the other experiments were designed to cover most of the isoforms commonly expressed and also using exon spanning wherever possible in order to avoid gDNA amplification, the full list of transcripts presented in Appendix 5. This micro fluidic technology utilizes eight sample-loading ports, each connected to 48 reaction chambers pre-loaded by the manufacturer with the specified probes. The reaction mix for each port contained 50 µl of cDNA and nuclease free water mix, containing a total amount of 200 ng of cDNA, and 50 µl of TaqMan Gene expression Master Mix, hence a 100 µl reaction mix per port. Following loading all the ports the card was centrifuged to dispense the cDNA samples to the reaction wells and then sealed and the ports trimmed using a scissors (Figure 2.6). The card was then loaded and data acquisition was similar to regular qPCR on the QuantStudio™ 7 Flex Real-Time PCR System (Applied Biosystems) using the same cycling conditions as used for all the experiments but with a block specifically designed for TLDA cards.

Data for normal qPCR and TLDA cards was acquired using ABI PRISM 7900HT SDS or QuantStudio™ 7 Flex Real-Time PCR System and SDS Software. Thermal cycling conditions (Table 8) used for qPCR comprised of initial steps of 2 minutes at 50º C and then 10 minutes at 95º C followed by 40 amplification cycles of 10 secs at 95º C and 1 min at 60º C. The fluorescence of the double stranded products was recorded in real time and the results obtained using the SDS Software (Applied Biosystems). A standard curve was previously constructed with serial dilutions of cDNA from a few samples.

Table 2.6. Thermal cycling conditions for qPCR experiments

Step	**Initial denaturation**	**Enzyme activation**	**PCR**	
	Hold	Hold	40 Cycles	
			Denature	Anneal/Extend
Temperature	50° C	95°C	95° C	60º C
Time	2 minutes	10 minutes	15 seconds	1 minute

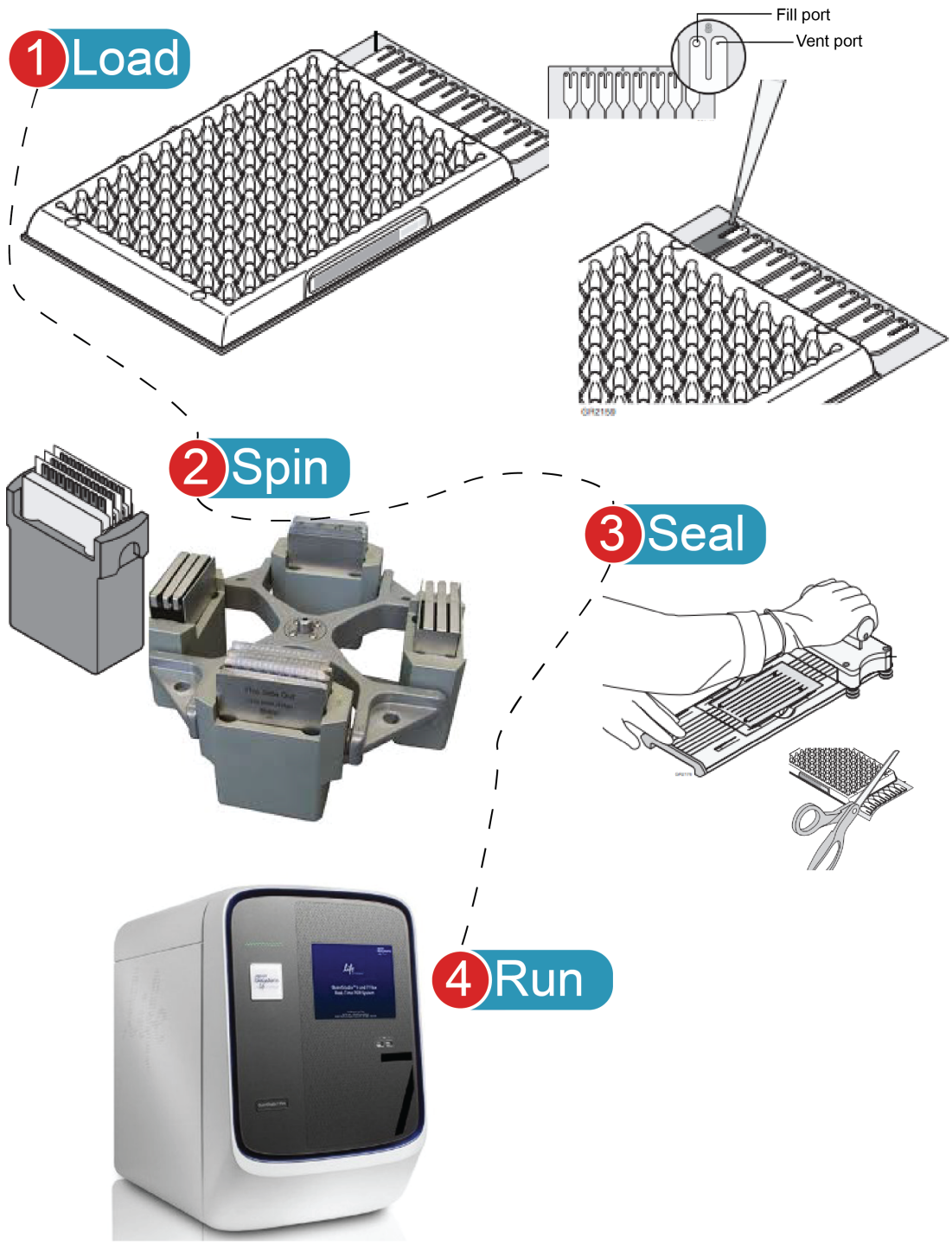

Figure 2.6. Experimental setup for gene expression analysis using TLDA. *The ports were first loaded with 100 µl of cDNA and TaqMan Master Mix then centrifuged to dispense the mix into each well. The wells were sealed using a sealer and the ports were trimmed off. qPCR was performed on a QuantStudio™ 7 Flex system.*

2.5.4 qPCR data analysis

The qPCR analysis relies on the Ct values (threshold cycle) values resulted following the qPCR run. These values were determined by the cycle number where the fluorescence produced by the amplified product accumulating exponentially over a defined threshold. The increase in the Ct value is inversely proportional to the amount of starting cDNA material, i.e. the lower the Ct value the higher the initial amount of cDNA.

In order to present the qPCR data as individual data points it was recommended to be presented as $2^{-\Delta Ct}$ rather than the raw Ct values (Livak and Schmittgen, 2001). When presenting the data from gene expression experiments, it is also recommended to normalize the values to an internal control to exclude variations arising from different inputs of total mRNA to the reaction (Schmittgen and Livak, 2008). Data in this project was therefore normalised to the reference gene hypoxanthine phosphoribosyltransferase 1 (*HPRT1*). The choice of reference gene had been previously determined and optimised by Dr. Sarah Churchman from previous published work (Churchman et al., 2012) following a screening of approximately 30 endogenous control genes, establishing therefore *HPRT1* as the most reliable transcript to use in MSCs related work. While *GAPDH* for example may be an excellent gene stably expressed at much higher levels across most of the cell types in comparison to *HPRT1*, the majority of the genes investigated in this project have a general low expression level (Ct values above 25), similar to *HPRT1* (Churchman et al., 2012). Together with the presumably low amount of starting genetic material obtained from sorted cells, *HPRT1* has been shown to be an appropriate endogenous control.

Therefore, to determine the relative expression of the genes of interest, following normalisation to *HPRT1*, data analysis was carried out and presented by the well-established $2^{-\Delta Ct}$ method (Schmittgen and Livak, 2008). Since all the reactions for all samples were performed in triplicate, the resulted values obtained from each reaction were averaged and used for subsequent calculations. Then normalisation (ΔCt) was calculated as: $\Delta \mathrm{Ct} = (\mathrm{Ct\ gene\ of\ interest} - \mathrm{Ct\ endogenous\ control})$

followed by the calculation of the $2^{-\Delta Ct}$.

2.6 Histology

2.6.1 Tissue preparation for histological analysis

2.6.1.1 Fixation

Prior de-calcification it is particularly important to thoroughly fix the specimens in order to stop autolysis and thereby preserving tissue integrity, poorly-fixed bone specimens become macerated during decalcification affecting the downstream histological analysis (Skinner et al., 1997; Callis and Sterchi, 1998). Bone fragments and whole femoral heads were processed for histologic analysis before and after collagenase digest. All bone samples were washed twice with PBS and immediately fixed in 10% neutral buffered formalin (Sigma). Some samples were cut in smaller pieces and agitated daily for better penetration of the fixative agent. Depending on sample size, the fixation was performed at room temperature between 24 hours for <1g iliac crest samples and up to 2 weeks for whole femoral heads in at least 20X volume of the tissue (Figure 2.8). Following fixation, the fixative was removed and disposed safely using the appropriate paraformaldehyde disposal bottles in the fume hood. All bone samples were washed three times with PBS before starting the decalcification procedure.

2.6.1.2 Decalcification

As mineralized bone is such a hard material, decalcification of the samples was performed to remove the mineral content so that good-quality paraffin sections can be prepared that will preserve all the microscopic elements, i.e. the highly cellular BM and complex trabecular structure. In order to protect the cellular and fibrous elements of bone from damage caused by the acids used in common decalcifying agents, such as formic acid, slow de-calcification with ethylenediaminetetracetic acid (EDTA) was used. The decalcification process is slow but gentle, causing little tissue damage (Callis and Sterchi, 1998) as compared to other methods for which stronger acids are required. Conventional stains are largely unaffected by EDTA calcification. Decalcification by using EDTA is pH dependent and is achieved by chelating calcium from the bone mineral i.e. dissolution of the bone hydroxyapatite complex, and can be represented by the following equation: $Ca_{10}(PO4)_6(OH)_2 + 8H \Leftrightarrow 10\ Ca^{++} + 6PO_4^{--} + 2H_2O$ (Skinner et al., 1997).

Following fixation, the samples were washed twice in PBS and then placed in 14% EDTA solution (pH 7.4, Appendix 1) for decalcification. Since EDTA progressively dissolves and moves calcium from the organic matrix into the surrounding liquid, the solution was

changed every week until decalcification was complete as confirmed by radiographic analysis.

Where whole femoral heads were used for histology, after 2-3 months when the decalcification process has penetrated more than half of the femoral head, the tissue was cut in half or quarters by using a general used histopathology knife in order to allow full penetration of EDTA (Figure 2.7).

It is important to determine the point at which all the calcium has been removed, because, from this point on, tissue damage seems to occur at an increasing rate. Over-decalcification may cause maceration of the softer tissue elements. On the other hand, specimens that are incompletely decalcified may be difficult or impossible to section. The method chosen for this study was to X-ray the specimens wherein transparency suggested complete decalcification. Bone specimens were scanned weekly to verify the stage of decalcification and decide whether further treatment was required (Figure 2.8). The x-ray machine used for this purpose was CS2200 (Carestream Health) with an exposure time of 0.113s at 70kV. The images were captured on standard dental films which were read on the automated unit with its corresponding installed software.

2.6.1.3 Paraffin embedding and Sectioning

Following decalcification, the samples were embedded in paraffin wax to offer support to the tissue for sectioning. Decalcified bone tissues were placed in plastic cassettes (Figure 2.9A) and processed for paraffin embedding using an overnight programme from neutral buffered formalin (10 % for 30 minutes) through graded ethanol (70% for 1 hour; 90% for 1 hour; 95%, for 1 hour; 100%, for 1 hour; 100%, for 2 hours; 100% for 2.5 hours) to xylene (3 buckets; 1 hour, 1 hour, 1.5 hour) to molten paraffin wax (2 buckets; 4 hours and 5 hours). Embedding in paraffin blocks took place in a Leica embedding centre using a hot paraffin dispenser and hot plate (Leica) (Figure 2.9B). Molten wax was poured into the plastic cassettes containing the tissue which were orientated to provide a transversal section of the whole femoral head. Wax then hardens within the plastic cassettes and makes up the finished block (Figure 2.9C), allowing blocks to be easily cut.

Tissue blocks were sectioned using a Leica RM2235 microtome (Leica Microsystems) fitted with a S+ type blade (CellPath). The blocks were initially trimmed by cutting serial 10 μm sections until tissue was fully exposed. Sections of 5 μm thickness were then cut, producing a string of serial slices joined together (Figure 2.9D). The strings, also called “ribbons”, were allowed to stretch and smooth out creases in a 45º C water bath and then

lifted out onto SuperFrost Plus glass slides. Residual water was dried from the slides in a 37º C incubator overnight.

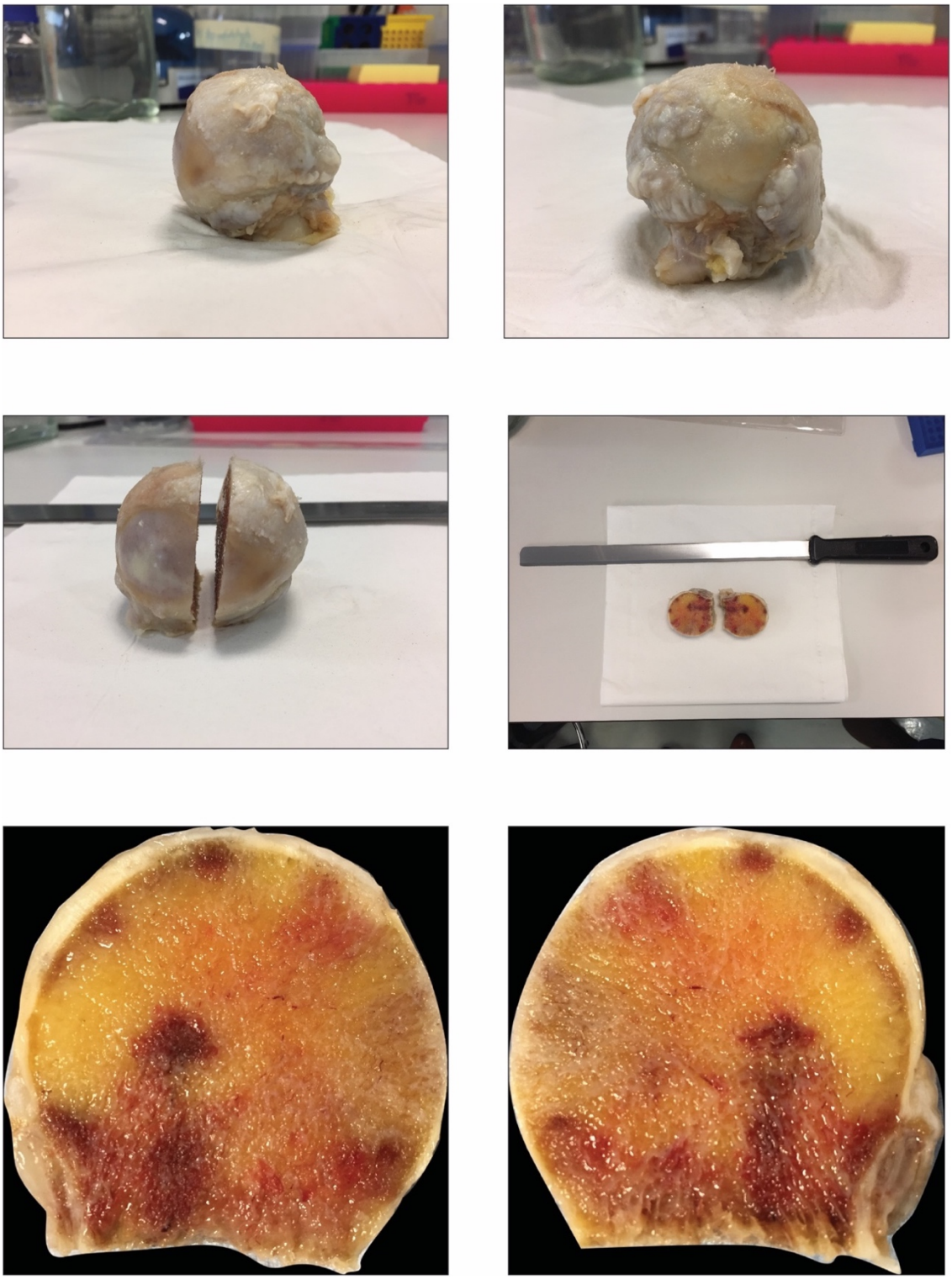

Figure 2.7. Sample preparation for fixation, decalcification and embedding. *Whole femoral head was fixed in PFA and partially decalcified. Then the femoral head was cut in half for complete EDTA penetration and decalcified completely.*

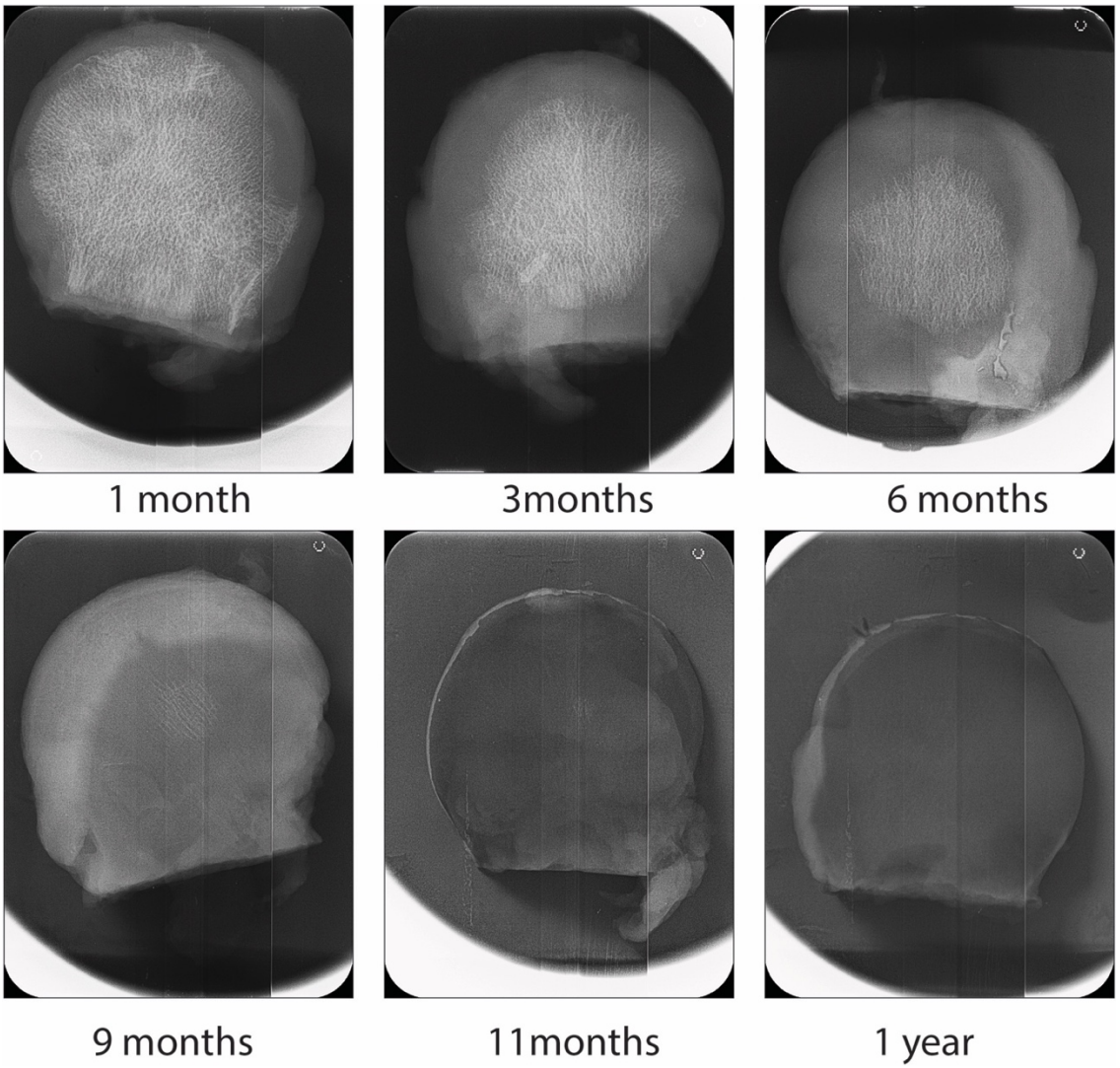

Figure 2.8. X-ray images showing gradual mineral removal by EDTA. *The images were captured monthly on standard dental films and read on the automated unit. Gradual loss in mineral content can be visualised as the increase in opacity on the x-ray images.*

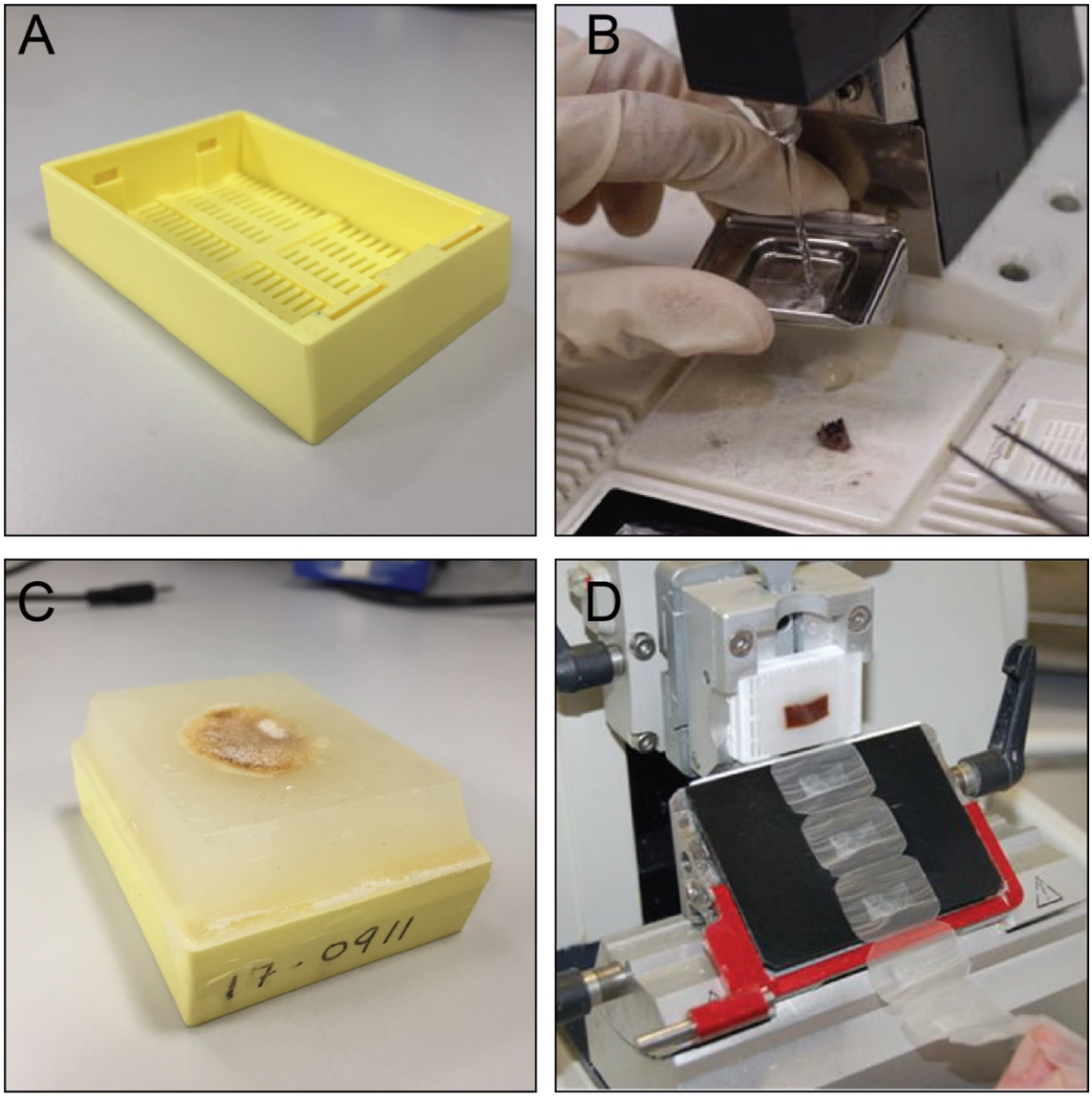

Figure 2.9. Paraffin embedding and sectioning of bone tissue for histology. *The bone tissue was placed in a cassette (A) and processed overnight for paraffin embedding. Using a Leica hot plate dispenser, liquid hot paraffin was poured onto the tissue (B) and placed on a cold plate until the block solidified (C). Tissue sections were cut using a Leica microtome for histological analysis (D).*

2.6.2 Haematoxylin and Eosin staining

Slides were deparaffinised by allowing to stand on a hot plate at 70º C for 20 minutes and then cleared in Xylene in a fume hood. The tissue was then rehydrated by placing the slides through graded ethanol, from high to low concentrations: absolute ethanol (3x3 minutes), 75% ethanol (1x3 minutes), 50% ethanol (1x3 minutes) and then into tap water for 2 minutes. Slides were then taken out of the fume hood and transferred to Harris Haematoxylin (Sigma) for 2 minutes after which they were cleared with tap water for 1 minute. To perform the 'blueing' of the nuclei the slides were placed in Scott's tap water (Appendix 1) for 2 minutes and washed in running tap water then immediately immersed in Eosin-Y (Appendix 1) solution for another 2 minutes. After washing in tap water for 1 minute the slides were dehydrated by immersing in absolute ethanol four times for 2 minutes each and then cleared in Xylene. The slides were then mounted with DPX medium (Sigma) and dried at room temperature before visualizing under light microscope.

2.6.3 Immunohistochemistry

For immunohistochemistry staining the Dako Envision Detection System (Peroxidase/DAB, Rabbit/Mouse) (Dako) kit was used according to the manufacturer instructions. The slides were first dewaxed and rehydrated similarly to H&E method. Next, hydrophobic round circles were drawn around the tissue using a PAP pen (Abcam) in order to designate the staining area and preventing reagents spill. The endogenous peroxidase activity was blocked by 5 minutes incubation with dual enzyme blocking solution (Dako kit) and the slides were then washed in tris buffered saline (TBS, Appendix 1) twice, for 1 minute and 5 minutes respectively. The non-specific binding was blocked using Antibody diluent (Dako) during 30 minutes incubation at room temperature in a humidified chamber. After washing the slides twice in TBS as before, the primary antibody was applied. The primary antibody had been previously diluted in Antibody diluent (Dako) at the appropriate dilution as described in each chapter and as previously determined by performing an antibody titre. Approximately 200 µl (enough to cover the tissue) was applied on the slide and incubated at room temperature for 1 hour. Slides were then washed twice in TBS to remove residual antibodies and incubated with the secondary reagent, Labelled polymer-HRP (Dako kit) for 30 minutes at room temperature. After washing in TBS, the slides were incubated with DAB reagent for 10 minutes at room temperature. Counterstaining was performed using Harris haematoxylin

(Sigma) with 2 minutes incubation followed by 1 minute in Scott's tap water until blue developed. Slides were washed in tap water and then dehydrated and cleared in Xylene.

2.6.4 Acquisition and initial image analysis

Slides were scanned on Leica Aperio AT2 up to an original magnification of ×20 and images were captured using Aperio Imagescope software (Leica). For OA femoral heads, antibody staining was also analysed using Nuance Multispectral Imaging System (Caliper Life Sciences) in selected regions differing in a degree of OA pathology based on the gross appearance of bone and cartilage as detailed in Chapter 4, Section 4.3.6 and Chapter 5, Section 5.3.2.

The digital images were acquired under a Nikon Eclipse bright-field microscope equipped with CRi multispectral camera. The regions of interests (ROIs) in the IHC images with characteristic sclerotic and non-sclerotic bone were selected using the ×20 magnification. Each ROI containing the trabecular space and positive DAB staining was captured at x20. To minimize selection bias, 10 images per slide were randomly selected from the ROI. For each IHC staining section, a total of six spectral cubes containing the complete spectral information at 20 nm wavelength intervals from 420 to 720 nm were randomly obtained from different areas of the section by CRi Nuance multispectral imaging systems. As a result, 20 bright-field IHC images were captured including identical 720p RGB images and 720p MS images, and all saved in Tagged Image File Format (TIFF) with consistent resolution of 1360 × 1024 pixels for analysis.

2.6.5 Quantitative image analysis

After imaging acquisition, the software package within CRi Nuance multispectral imaging system was used for quantification of IHC-positive areas using standard spectral unmixing and processing methods. CRi Nuance multispectral imaging system is comprising the Nikon Eclipse microscope, an attached CRi multispectral camera for image acquisition and the software Nuance 2.8 which was used to build the spectral libraries.

Spectral libraries contain spectral information which was extracted in both bright-field multispectral and red, green and blue (RGB), using images with a cube format (RGB images converted to Nuance specific cube format). Each chromogen has its unique spectral characteristics (curve), which is the basis for building the spectral library. The spectral characteristics (curve) for two chromogens (DAB and haematoxylin) in multispectral and RGB images were obtained by spectral unmixing. This spectral library

was built from the control slides, which was used to unmix the positive signals (DAB and haematoxylin) on each test slide by recognizing its unique spectral curves for quantification. Specific steps of CRi Nuance software have been previously described and briefed as the following: 1. Selection of targets for the specific antibodies used and background with different spectra; 2. Image un-mixing and elimination of background crosstalk: the target images with different spectra were automatically unmixed into DAB (molecular status) and haematoxylin component images by the software based on spectral library; and 3. Quantification of unmixed DAB component images.

Antibody expression levels stained on IHC slide were best quantitated as total optical density (OD) values per unit of positive area in one view field. The final quantitative results of each marker were the average values of the 10 cube images.

2.7 Statistics

The statistical analyses were performed using Mann-Whitney test for comparisons between two groups while Wilcoxon test was used for comparison between paired/matched samples. For the intergroup differences, Kruskal-Wallis analysis was used corrected with the Bonferroni-Dunn for multiple-group comparison and Friedman test for the donor matched samples. The normality test could not be used in all cases given the low sample numbers and the values were assumed to come from a non-Gaussian distribution. Specific details of the statistical tests carried out for each data set are provided in each chapter.

Results are presented as scatter dots plots with median lines or box and whisker plots, with boxes representing the upper and lower quartiles of the median, and whiskers representing the maximum and minimum values, calculated using GraphPad Prism version 7 software. Results were considered significantly different at $p < 0.05$ (with significance level denoted as $*p < 0.05$, $**p < 0.01$, $***p < 0.001$ and $****p < 0.001$).

Chapter 3 Native CD45-CD271+ MSCs in OA bone

3.1 Introduction

As a chronic, progressive and irreversible degenerative joint disease, OA affects millions of people in the UK and worldwide. Biomechanically abnormal joint loading resulting from obesity, joint instability, or trauma can affect the bone via progressive cartilage deterioration and subchondral bone remodelling (Martel-Pelletier et al., 2016). Although multiple risk factors including age, sex, obesity, genetics and joint trauma can likely contribute to the onset of OA, the cellular mechanism(s) underlying the disease are not clearly delineated. Given their high proliferative rates and ability for repair both bone and cartilage, mesenchymal stem cells have emerged as a theoretical therapy for OA in recent years. However, their roles in the pathology of human OA in vivo is still incompletely understood. Growing evidence indicate that MSCs may be implicated in OA, possibly by endogenous repair mechanisms or even in aberrant repair attempts such as the formation of osteophytes.

3.1.1 Joint resident MSCs

While knowledge of the BM resident MSCs has advanced significantly over the years in regards to their phenotypical characteristics and functional properties (Chapter 1, Section 1.3.2), the same cannot be said about the MSCs in other joint tissues. The up-to-date body of evidence indicate the presence of heterogeneous cell populations in joint tissues that display MSC-like characteristics, although their specific phenotype has yet to be established (McGonagle et al., 2017).

3.1.1.1 Synovium MSCs

The synovium consists of the synovial membrane which encapsulates the joint providing structural support and the synovial fluid for appropriate lubrication and nutrients essential for normal joint function (Smith, 2011).

Topographically, synovium MSCs were shown to be residing in the synovial membrane that lines the spaces of diarthrodial joints as well as in the synovial fluid (De Bari et al., 2001; Jones et al., 2004). Normal synovial fluid has been demonstrated to contain a resident MSC population (Jones et al., 2004) which was later demonstrated to increase during OA (Jones et al., 2008). Further investigation revealed that in comparison to normal joints, i.e. no obvious cartilage damage, the synovial membranes from OA patients also contained increased numbers of cells presenting an MSC phenotype, judged

by the expression of CD271, CD44 and CD90 (Hermida-Gómez et al., 2011). Evidence pertaining OA synovial MSCs documented the presence of different phenotypes of MSCs based on their topography, where CD55+ MSCs were found in the surface region, CD271-CD55- MSCs in the stromal region, and CD271+ MSCs in the perivascular region (Mizuno et al., 2018). However, these results need to be confirmed in healthy synovium but are in agreement with respect to the perivascular location of CD271+ MSCs in the BM (Tormin et al., 2011).

3.1.1.2 Cartilage MSCs

Studies reported the presence of a small population of MSC-like resident progenitors in the mature articular cartilage that are capable of differentiating into mature chondrocytes (Dowthwaite et al., 2004; Williams et al., 2010). Furthermore, it was shown that resident MSC-like progenitors had an increased frequency in OA cartilage (Fickert et al., 2004; Su et al., 2015) and diverged into two subpopulations, one of which exhibited an early senescent phenotype, which possibly reflects a replicative exhaustion following repeated but failed attempts at cartilage repair (Fellows et al., 2017). Recent evidence also implicate cartilage resident MSCs in cell clustering in OA cartilage, some of the clusters consisting entirely of cartilage resident MSC progenitors (Jayasuriya et al., 2018). This evidence confirms the presence of cartilage resident MSC progenitors and indicate their putative involvement in OA. Of note, since articular cartilage is an avascular tissue this evidence suggests that not all MSCs are perivascular.

Recently OA has been accepted as a disease of the whole joint, eventually affecting every tissue component. With plenty of evidence to indicate that MSCs resident in other joint tissues are also affected (McGonagle et al., 2017), this knowledge would facilitate a better understanding of how the bone-resident MSCs are affected by OA.

3.1.2 The current state-of-the art on native bone-resident MSCs in health and OA

As stated previously, MSCs have been documented in almost all vascular postnatal organs (Crisan et al., 2008), but there are tissues which contain a higher frequency of MSCs than others. Typically, MSCs are isolated from BM taken from the iliac crest or the hip, but MSCs represent only a very small fraction of nucleated cells in the BM, between 0.001-0.01% (Jones and McGonagle, 2008). However, previous work in our laboratory demonstrated that cells extracted by enzymatic digestion of the bone fragments contained 65-fold more CD271+ MSCs than BM aspirate, having the same cellular identity (Jones

et al., 2010). This indicated that not all bone resident MSCs can be released by BM aspirate and furthermore, it challenged the concept that MSCs were a rare population (McGonagle et al., 2017). In the enzymatically released fraction from OA femoral heads, the MSCs showed ageing-related loss of proliferation *in vitro*, but no gross osteogenic abnormalities (Jones et al., 2010). In a recent study, the MSC numbers were shown to be increased in areas of BML (Campbell et al., 2016) indicating a repair attempt of the bone resident MSC population, however the biology of native joint resident MSCs *in vivo* in OA is still incompletely understood.

Using different extraction methods have also recently revealed more information regarding the CD271+ MSC population. It was shown that in comparison to aspiration, MSCs isolated by rasping the femoral shaft of OA donors released more CD271+CD56+ MSCs, these cells having an increased chondrogenic potential *in vitro* in comparison to CD271+CD56- MSCs (Sivasubramaniyan et al., 2018). This recent study further supports the idea of multiple distinct MSC subsets within the CD271 fraction as well as the importance of isolation method with respect to their downstream use and site of extraction. It further indicated that some MSCs may be preferentially located onto the bone surface in OA, however this was not yet tested using functional assays.

As mentioned in Chapter 1, Section 1.3.2 the bone resident MSCs may play critical roles in mediating the coupling of bone resorption and formation. In an animal study it was shown that in response to osteoclastic bone resorption, MSCs migrate to the local site of repair, which is essential for coordinating bone remodelling (Zhang et al., 2009). However, in OA the bone remodelling process appears to be uncoupled. In a more recent OA animal study, in which anterior cruciate ligament transection was used to induce OA, nestin was employed as a surface marker to identify and track the MSCs. It was shown that MSCs accumulated and exhibited functional alterations in the joints affected by OA (Zhen et al., 2013). The high concentrations of TGF-β had been released from the subchondral bone during osteoclast-mediated bone resorption, facilitating MSCs recruitment and proliferation (Zhang et al., 2009).

As mentioned in Chapter 1, Section 1.3.4, numerical and topographic alterations have been recently reported in hip OA resident MSCs, specifically in the lesioned areas of OA femoral head bone (Campbell et al., 2016). In this study Campbell *et.al*. showed that the CD271+ MSCs resident in OA femoral heads accumulate in higher numbers in the areas of BML in comparison to non-lesioned areas. Furthermore, the MSCs isolated from the BML areas exhibited functional and transcriptional alterations *in vitro*. The BML MSCs

showed a decreased proliferation and mineralisation capacity as well as altered transcriptional expression of *RANKL* and C-X-C chemokine receptor type 4 (*CXCR4)*, encoding the receptor for C-X-C motif chemokine 12 (CXCL12) (Campbell et al., 2016). The CXCL12/CXCR4 signalling axis (Kitaori et al., 2009) has been regarded as a master regulator of stem cell migration and is essential in adult BM to maintain haematopoiesis (Sugiyama et al., 2006). It was shown to be expressed at high levels by CD271+ MSCs isolated from the BM (Churchman et al., 2012) and have important roles in stromal support of haematopoiesis (Greenbaum et al., 2013) and MSC migration to sites of injury (Kitaori et al., 2009).

Overall, these studies so far provided evidence which point to a global increase in the numbers of MSCs in all OA-affected joint tissues, possibly as a repair attempt on behalf of the tissue-resident MSCs population. Furthermore, these data indicate potential functional alterations of MSCs in OA in addition to their increased numbers.

3.1.3 Culture-expanded MSCs

Over the past two decades the research in the field of MSCs has grown exponentially, with a substantial focus on culture expanded MSCs (Schäfer et al., 2016). This is due not only to their ease of isolation, manipulation and maintenance but also because of their rapid proliferation in culture which can provide a known number of cells for delivery in musculoskeletal regenerative therapies. However, compelling evidence showed that this results in functional deficits as well as immuno-phenotypical and transcriptional changes (Harichandan et al., 2012; Churchman et al., 2012). Using the CD271 phenotype to identify native BM MSCs, recent studies showed that culture-expanded BM MSCs are not functionally and transcriptionally equivalent to their *in vivo* counterparts, notably with regard to bone related signalling pathways (Churchman et al., 2012), adhesion receptors and signalling molecules (Qian et al., 2012), and homing capacity (Morikawa et al., 2009). The "*in vitro* age" of MSC cultures was shown to detrimentally affect the proliferative and differentiation potential of the MSCs, eventually leading to culture senescence (Wagner et al., 2008).

Culture-expanded BM MSCs are also characterised by a poor haematopoietic-support (Qian et al., 2012; Churchman et al., 2012) and were shown to lose their ability to migrate to the BM having been in culture (Rombouts and Ploemacher, 2003). In addition, expanded MSCs have a decreased multilineage differentiation potential (Pevsner-Fischer et al., 2011) and lose their self-renewal capacity. Cultured primary cells do not grow infinitely, but undergo only a limited number of cell division leading to cellular

senescence (Hayflick, 1965) and as somatic stem cells, MSCs are no exceptions (Digirolamo et al., 1999). Moreover, MSCs isolated from trabecular bone samples from patients with OA showed an *in vitro* ageing-related loss of proliferation (Jones et al., 2010).

Since their identification, native MSCs have been classified as a heterogeneous population when considering morphology and surface marker expression. However, ISCT criteria suggested that culture expanded MSCs are homogeneous (Dominici et al., 2006) which emphasises the differences between native MSCs and culture-expanded cells defined by the ISCT. Adhesion molecules, extracellular matrix molecules, cytokines, growth factor receptors and antigens associated with numerous cell types are all associated with MSC cell interactions and functions (Bobis et al., 2006). For example, a variety of surface markers, such as CD44, are highly expressed on cultured cells, but not on native MSCs (Battula et al., 2009; Qian et al., 2012) and the expression of the native MSC marker CD271 is rapidly lost in culture (Tormin et al., 2011).

Altogether, these changes have been so far shown using BM MSCs, and no other types of MSCs including MSCs enzymatically extracted from bone. While *in vitro* MSCs have been extensively characterised, the current state of affairs with regards to their native counterparts is still growing and more work is need to advance the knowledge in order to fully understand the natural properties of these cells. The majority of OA related alterations were observed in MSCs under cultured conditions. Therefore, to understand their role in OA-associated pathology it is important to investigate their native state in both OA and under normal, healthy conditions.

Evidence pertaining the nature of bone-resident MSCs *in vivo* is currently scarce, however these studies provide some indication of changes that may occur in MSCs from OA affected bone. These may include loss of proliferation and changes in their mineralisation capacity (Campbell et al., 2016), but this has not been comprehensively investigated.

3.2 Chapter aims

1. To compare the number of native MSCs in OA femoral heads bone and control bone.

2. To compare the gene expression profile of native MSCs in OA and control bone.

3. To investigate whether any putative gene expression alterations are maintained in culture of MSCs.

3.3 Methods

3.3.1 Patient samples

For all the experiments in this chapter a total number of n=30 OA donors (12 males and 18 females) with age range between 40-90 years (median=72) and n=19 healthy donors (10 males and 9 females) with age ranging between 17-78 years (median=55) were recruited.

3.3.2 Experimental overview

Following the enzymatic digestion of the bone fragments (Chapter 2, Section 2.2) heterogeneous cell suspensions were obtained containing all the cellular component in the trabecular BM compartment from both healthy and OA donors. As shown in Figure 3.1, several experiments were performed at this stage. From this cell suspension the MSCs were enumerated and purified by FACS using the CD45-CD271^{+} phenotype in parallel with CFU-F assay. From the same cell suspension, the MSCs were also isolated by plastic adherence and culture-expanded for four passages. The freshly sorted cell populations along with donor-matched (in most cases) culture-expanded MSCs were subsequently used for gene expression analysis by qPCR.

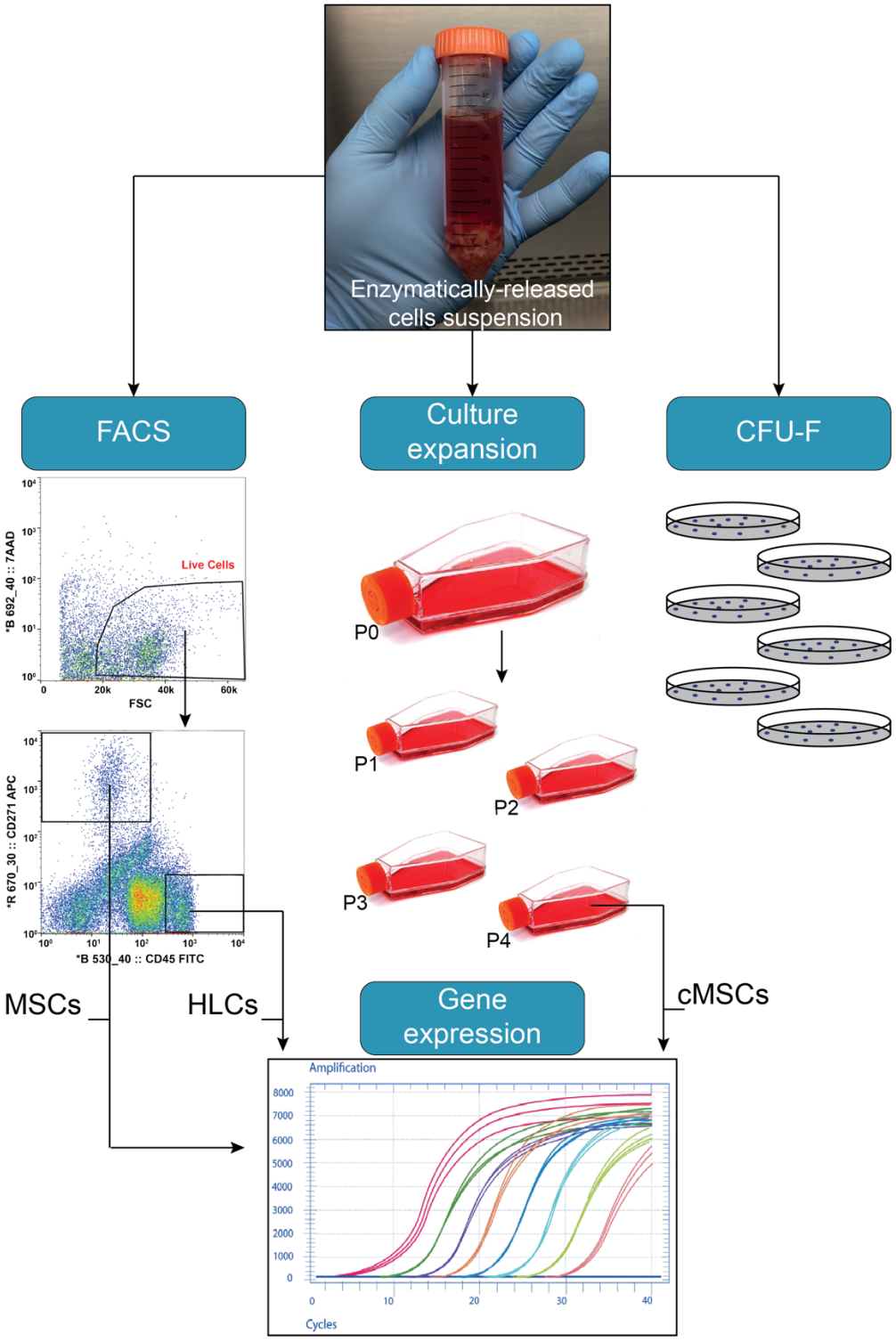

Figure 3.1. Experimental plan used to enumerate and analyse the native and cultured MSCs phenotype in healthy and OA bone. *From the pool of enzymatically extracted cell suspension MSCs were purified by FACS using the CD45-CD271+ phenotype or culture expanded up to four passages. MSCs obtained from both experiments along with control HLCs were used for gene expression analysis by qPCR. From the same pool of enzymatically released cells, CFU-F assays were set at three seeding densities in duplicate.*

3.3.3 MSC enumeration using CFU-F assay

The CFU-F assay is a well-established method for the quantification of native MSCs from the BM or other tissues (Chapter 1, Section 1.3.2). Due to previously-described high donor variation (Kuznetsov et al., 2009) the assay was performed using gradient seeding densities and set up with a defined cell concentration following optimisation.

The CFU-F assay was performed by plating the released cells at different densities, directly in standard MSC media (StemMACS, Miltenyi Biotec). Media was pre-warmed to 37º C in a water bath while the nucleated cells released from the bone fragments were re-suspended in DMEM/10%FCS/1%P/S and counted using the Trypan Blue exclusion method as described in Chapter 2 Section 2.3.1. The cells were then transferred to 60 mm culture dishes containing 3 ml of pre-warmed StemMACS at three different seeding densities of $1x10^4$, $2x10^4$ and $5x10^4$ cells/dish respectively, all in duplicate. After 48 hours, the non-adherent haematopoietic cells and debris were removed by one PBS wash and a full media change. The cells were cultured for 14 days at 37º C, 5% CO_2 with half media change twice per week.

Following 14 days in culture the media was removed and the dishes were washed twice with PBS. The colonies were fixed with 3.7% PFA (3 ml) at room temperature for 20 minutes. After removing the PFA, 3 ml of 1% methylene blue solution (in 10 mM borate buffer, pH 8.8, Appendix 1) was added and incubated for another 20 minutes to stain the colonies. After washing with tap water, the plates were left overnight to dry before counting the colonies. A colony was considered a group of 50 cells or more that were close to each other and distant from other groups of cells as visualised via low power microscopy (Gronthos et al., 2003). The colonies were manually counted and CFU-F frequency was established as percentage of cells seeded initially. The stained colonies were scanned at 360 dpi using a generic Epson scanner.

3.3.4 FACS

Since CD271 has been described as the most reliable marker for bone resident MSCs *in vivo* as discussed in Chapter 1, Section 1.3.2, the MSCs were purified using the CD45-CD271+ phenotype. Cell sorting was additionally employed to determine and compare the frequency of CD45-CD271+ bone resident MSCs between health and OA samples. In addition, the purified cell populations were used for gene expression analysis in order to investigate the differences in the transcriptional profile of native MSCs between health and OA while HLCs were also selected as negative control.

Staining and cell sorting were performed as described in Chapter 2, Section 2.4.1. The cells were sorted into MSCs (CD45-CD271+) and negative control HLCs (CD45+CD271-) fractions. For frequency analysis, a minimum of 100,000 events were acquired and analysed using a BD Influx system (BD Biosciences) as described in Chapter 2, Section 2.4.2. The MSCs fraction was gated as CD45-CD271+ and their proportion was then calculated as relative to total live cells. For gene expression analysis, the cells from the MSC ($CD45^{-}CD271^{+}$) and HLC ($CD45^{+}CD271^{-}$) fractions were sorted directly into 100 µl of RL RNA lysis buffer (Norgen Biotek) containing 1 µl of β-mercaptoethanol and immediately stored at -80º C for downstream RNA isolation and gene expression analysis (Section 3.3.6).

3.3.5 Cell culture

For culture expansion experiments, the nucleated cells from enzymatically-released cell suspensions were counted using Trypan blue and then seeded at a density of $1x10^6$ cells/flask in T25 tissue culture flasks (Corning) in 7 ml of StemMACS media and incubated at 37° C and 5% CO_2 as described in Chapter 2, Section 2.3. The majority of experiments were performed using fresh digest obtained on the day of processing, however in some instances, the cells were recovered following freezing in liquid nitrogen and culture-expanded after thawing as described in Chapter 2, Section 2.3.2.

After two days, the media was removed and the cells washed twice with 5 ml PBS to remove non-adherent cells. The media was replenished and expansion continued until cells achieved approximately 70-80% confluence which was assigned as passage 0 (P0); at this point cells were washed with 5 ml of PBS then the cells were detached using 1ml of trypsin solution (Invitrogen, Appendix 1) at 37° C for 2-5 minutes. The cells were then centrifuged at 600xg for 5 minutes, counted and re-seeded in StemMACS media at a density of $5x10^3$ cells/cm^2 in T25 tissue culture flasks and returned to incubation in the same conditions.

Cells were passaged when ~80% confluent, trypsinised and counted manually by trypan blue then reseeded at the same cell density. This was repeated from P0 onwards until P4 was achieved. Culture growth rates were then established by dividing the number of days between passages by the number of population doublings (PDs). The PDs before P0 were calculated using the CFU-F data and the following formula:

$$PD = Log2\left(\frac{Ni}{CFU-F}\right)$$

where Ni represents the cell numbers at the first trypsinisation and CFU-F represents the colony-forming number of seeded cells. For the following passages, the PDs were calculated as follows:

$$PD = Log2\left(\frac{Nt}{Ni}\right)$$

where Nt and Ni are the terminal and initial cell counts, respectively.

3.3.6 Gene expression analysis

Between $2x10^3$-$7x10^3$ cells from each fraction, CD45-CD271+ (MSCs) and CD45+CD271- (HLCs) respectively, were collected in 100 µl RNA lysis buffer. Total RNA was then extracted as described in Chapter 2, Section 2.5.1 using the Single Cell RNA isolation kit (Norgen Biotek) following the manufacturer instructions. Culture expanded MSCs were lysed at P4 and the RNA isolated using Total RNA extraction kit (Norgen Biotek) following the manufacturer instructions and as described in Chapter 2, Section 2.5.1. Briefly, the lysate was thawed on ice and an equal volume of 95% ethanol was added to precipitate the RNA. The mixture was loaded onto the spin column and centrifuged at 13000xg for 1 minute to bind the RNA. At this stage the flow-through was discarded and DNase digestion was performed. Following gDNA removal the RNA was washed twice using the kit washing buffer prior to be eluted using RNase free water in a small volume of 13 µl for sorted cells and 25 µl for cMSCs. The concentration and purity of RNA was assessed by Nanodrop and cDNA synthesised using the High Capacity Reverse Transcription kit (Applied Biosystems) as described in Chapter 2, Section 2.5.2 using a total amount of 200 ng RNA per sample.

The transcriptional profile of MSCs and HLCs purified by FACS from healthy (n=6) and OA (n=12) bone fragments was analysed using TaqMan probes and TLDA cards, while the cMSCs were analysed using TaqMan probes only (all from Thermo Fisher). The complete list of transcripts and assay IDs are detailed in Appendix 5. The genes of interest were selected based on previously published work by Dr. Sarah Churchman (Churchman et al., 2012). The genes selected for experiments in this chapter covered molecules specific to MSCs functional properties, especially associated with their multipotentiality, bone remodelling activities and stromal support. The reactions for qPCR were performed in triplicate as described in Chapter 2, Section 2.5. All gene expression levels were normalised to the house keeping gene *HPRT1* and analysed using the $2^{-\Delta Ct}$ method (Chapter 2, Section 2.5.4).

3.3.7 Statistics

The statistical analyses for gene expression experiments were performed using Mann-Whitney test for comparisons between two groups and Wilcoxon for matched paired data between two groups. The comparison between healthy and OA groups from FACS analysis and CFU-F assays included the Mann-Whitney test. Results were presented on a log scale as scattered dot plots with bars representing medians, connected dots plots for paired data or box and whisker plots, with boxes representing interquartile range, and whiskers representing the maximum and minimum values, calculated using GraphPad Prism version 7 software. Results were considered significantly different at $p < 0.05$ (with significance level denoted as $*p < 0.05$, $**p < 0.01$, $***p < 0.001$ and $****p < 0.001$).

3.4 Results

The first aim of this chapter was to investigate the number of native MSCs in OA femoral heads compared to control trabecular bone. In order to enumerate the MSCs and establish potential differences in their frequency in healthy and OA bone, two different techniques were used: the classic CFU-F assay (Jones et al., 2010) and the quantification of CD45-CD271+ cells using FACS (Jones et al., 2010). Without having access to healthy femoral heads, the cells extracted from healthy iliac crest bone were used as control instead. It was demonstrated previously in our laboratory that cells isolated using the CD45-CD271+ phenotype from BM aspirate from iliac crest and enzymatically digested iliac crest, and femoral head bone have the same MSC identity with regards to their phenotypical and functional characteristics (Jones et al., 2010).

3.4.1 Investigation of MSCs frequency in OA bone by CFU-F assay

To evaluate the frequency of MSCs in the enzymatically released cells from the bone fragments, the CFU-F assay was used and the resulted colonies following 14 days in culture were counted.

Following enzymatic digestion of bone fragments from healthy (n=10) and OA (n=13) donors, the total number of nucleated cells extracted was manually counted using trypan blue exclusion method. To account for the donor-to-donor variation the cells were seeded at three different densities and MSC frequency was calculated as a percentage of colonies in relation to total seeded cells based on the lowest seeding density which could be counted accurately. Representative CFU-F photographs are presented in Figure 3.2 showing the overall gradual increase of colonies in the dishes proportional to the increase in seeding density.

When counting colonies from dishes with a similar seeding density of $1x10^3$ cells, the number of colonies varied greatly between different donors of the same group (Figure 3.3A). The colonies resulted from CFU-Fs also showed a wide heterogeneity in size, which possibly reflects a different capacity to proliferate, a different stage of commitment of the initiating cells, or it may be due to different migration potentials (D'Ippolito et al., 1999; Gothard et al., 2013). Based on the median values of the CFU-Fs assay it was determined that the MSCs frequency as proportion of total nucleated cells was 2-fold higher ($p=0.0191$) in OA compared to the healthy bone-derived cells, with median values of 0.25% for healthy cells and 0.45% for OA (Figure 3.3B). This suggested that the

number of MSCs in OA bone is higher and will be further verified by cytometric quantification.

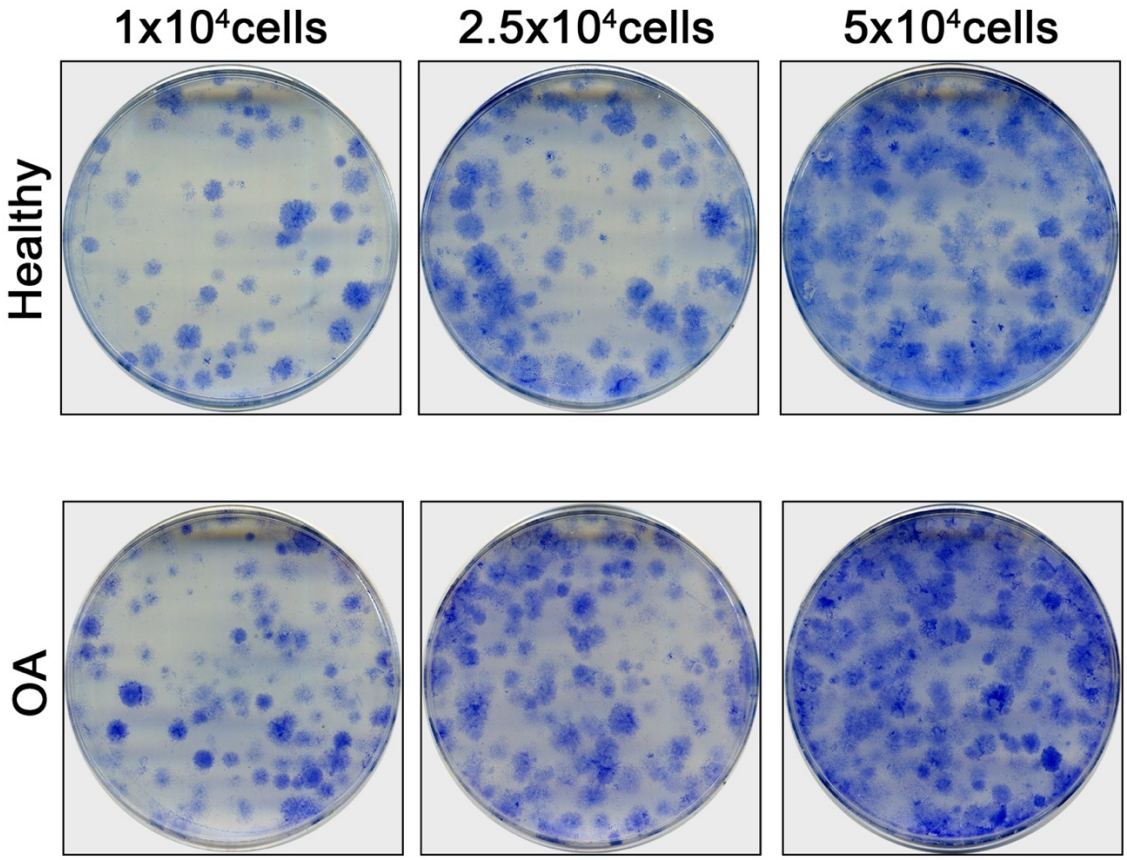

Figure 3.2. Cell seeding densities optimisation for CFU-F assays. *Representative CFU-F assays in 60mm culture dishes seeded with cells enzymatically released from bone of one healthy and one OA aged matched donors. Images show proportional increase of the colony formation when using gradient seeding densities of cells derived from both donor groups.*

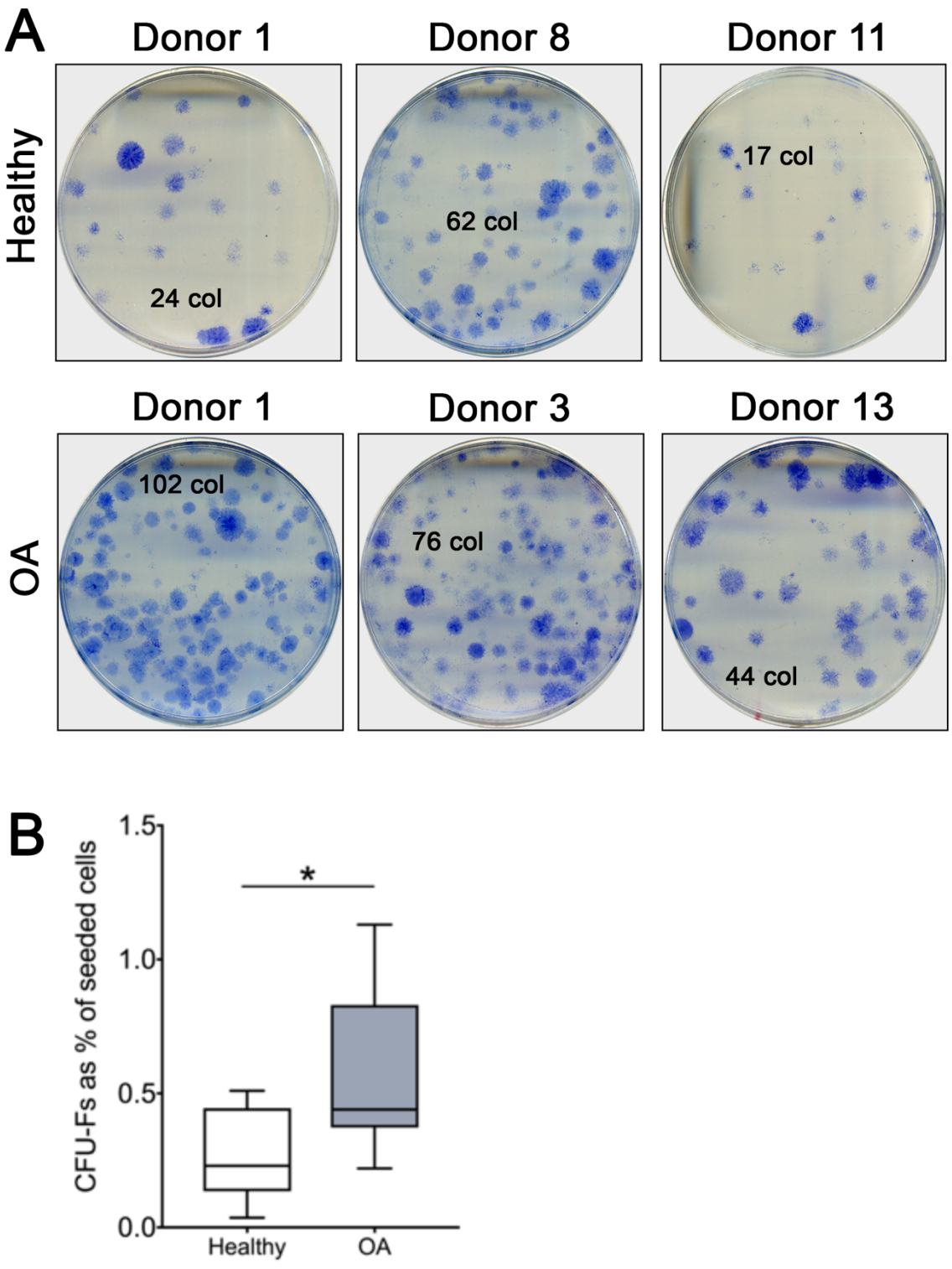

Figure 3.3. Examples of CFU-F dishes from healthy and OA donor cells and MSCs frequency. ***A.*** *CFU-Fs generated using equivalent seeding densities of cells enzymatically released from healthy and OA bone; col: colony. B. Graph showing the comparison between the CFU-F assays of the enzymatically released cells from healthy (n=10) and OA (n=13) bone calculated as percentage of the number of seeded cells; Mann-Whitney test.*

3.4.2 Enumeration and purification of MSCs from OA bone

To further validate the increased MSC frequency observed in OA as determined by the CFU-F assay, MSC enumeration was performed by FACS using the $CD45^{-}CD271^{+}$ phenotype on the cells released from bone immediately following the enzymatic digestion without any *in vitro* manipulation.

The analysis was performed using the acquisition and gating strategy described in Section 3.3.4 and Chapter 2, Section 2.4.2 on the enzymatically released cells from healthy (n=11) and OA (n=22) bone fragments. A minimum of $1x10^5$ events were acquired from all samples in order to obtain accurate statistical representations of the obtained cell populations. The resulting plots from the representative experiments are illustrated in Figure 3.4, noting an obvious variation between the donors.

The proportion of $CD45^{-}CD271^{+}$ MSCs as a percentage of total live cells was 3.4-fold higher in OA (p=0.0231) compared to cells from healthy iliac crest bone (medians 1.26% and 4.33%, Figure 3.5A). These results are contrasting previous studies where no difference was found when comparison was made between healthy and OA MSCs using the same cell phenotype (Jones et al., 2010). A close linear relationship (R=0.7416, p=0.0180) was found between the frequencies of MSCs as assessed by CFU-F and the proportion of $CD45^{-}CD271^{+}$ cells extracted from OA and healthy bone (Figure 3.5B), consistent with previous studies performed on BM aspirated MSCs (Cuthbert et al., 2012). Not all the CFU-F assays were matched with the FACS experiments therefore correlation was only calculated based on only donor matched samples from n=2 healthy and n=8 OA cells. It is important to note that while the fold difference in CFU-Fs between healthy and OA was only 2-fold, the differences in the proportion of $CD45^{-}CD271^{+}$ cells enumerated by FACS were higher (3.4-fold). However, this correlation indicated that the percentage of $CD45^{-}CD271^{+}$ cells was consistent with the CFU-F data, showing a higher proportion of MSCs in OA bone compared to healthy iliac crest.

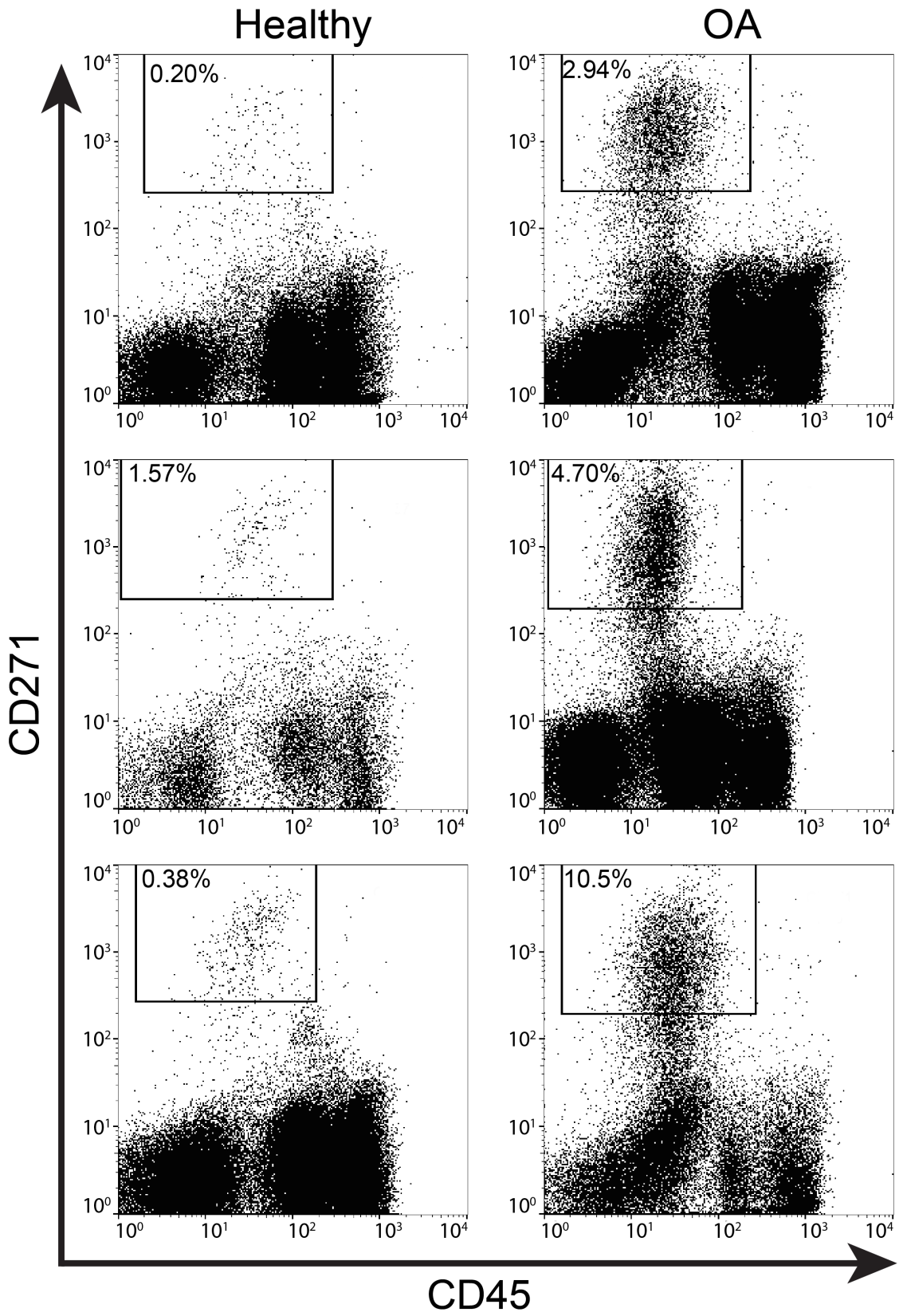

Figure 3.4. MSC enumeration by FACS. *Representative cell sorting plots illustrating FACS analysis of native, uncultured cells released from bone of three healthy and OA donors which were subsequently stained with CD45-FITC and CD271-APC following enzymatic treatment.*

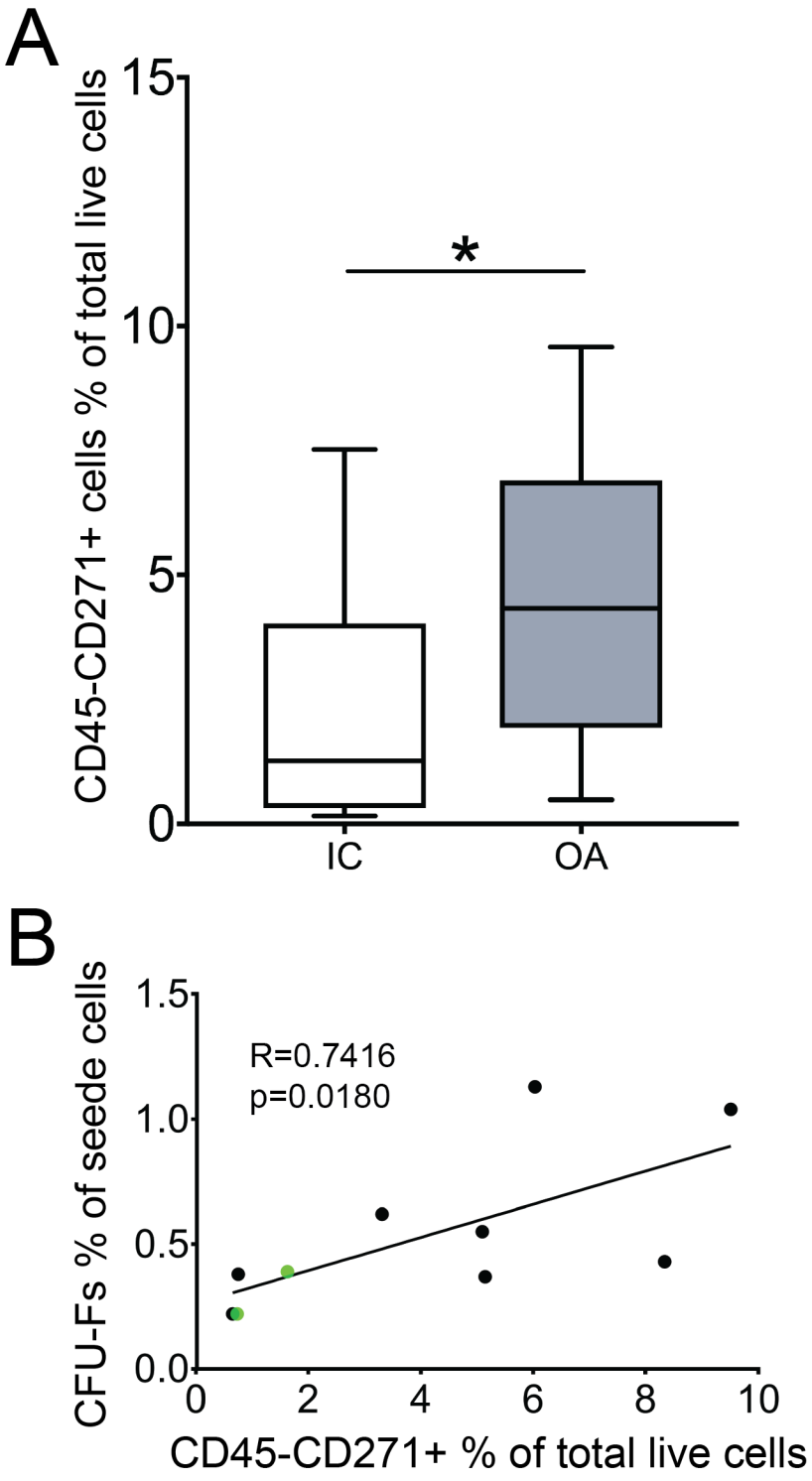

Figure 3.5. MSC frequency by FACS and correlation with CFU-F assay. *(A) Graph showing higher proportion of CD45-CD271+ cells as percentage of total live cells in OA (n=22, grey box) compared to healthy cells (n=11, white box); Mann-Whitney test. (B) Correlation of CFU-Fs and CD45-CD271+ cells from donor-matched samples of healthy (n=2, green dots) and OA (n=8, black dots); Spearman correlation.*

3.4.3 Molecular profile of native MSCs in OA femoral heads

Having determined a higher frequency of MSCs in OA femoral heads compared to IC bone, both by CFU-F assay and by cytometric analysis, the molecular profile of the CD45$^-$ CD271$^+$ cells from both healthy IC (n=6) and OA bone (n=11) was next investigated by qPCR.

In order to validate the MSC identity of the CD45-CD271+ cells, the gene expression levels of transcripts specific to MSCs (Churchman et al., 2012) were analysed in the sorted fractions from both healthy and OA samples. The donor-matched HLC sorted fractions, selected as CD45+CD271- by FACS, were used as a negative control cell population for confirmation of MSC molecular markers in the CD45-CD271+ cell population. A set of nine markers were selected to confirm MSC identity. These mesenchymal lineage genes, associated with stromal-support potential as well as multipotentiality, were previously shown to be specific to native BM MSCs released by aspiration (Tormin et al., 2011; Churchman et al., 2012).

Gene expression analysis showed that all the tested transcripts were significantly higher in the CD45-CD271$^+$ cells compared to donor matched HLCs isolated from healthy iliac crest (Figure 3.6). The highest level of expression in the CD45-CD271$^+$ cells was observed for *CXCL12* (1748-fold, $p<0.05$), a molecule associated with haematopoietic support (Greenbaum et al., 2013). Also, detected at higher levels were the transcripts associated with MSC osteogenic potential, such as *SPARC*, *SPP1* as well as *SP7* which was not expressed in any of the HLCs but was found in all tested CD45-CD271$^+$ cells. The MSC/early osteoblasts markers *CDH11* (2361-fold, $p<0.05$), *ALPL* (349-fold, $p<0.05$) and *COL1A1* (91-fold, $p<0.05$) (Kawaguchi et al., 2001; Ghazanfari et al., 2017) were found at higher levels in the CD45-CD271$^+$ cells compared to HLCs along with the MSC-specific adipogenic transcript *FABP4* (119-fold, $p<0.05$). MCAM, which is a surface marker for perivascular MSCs (Tormin et al., 2011) was also confirmed at higher levels in CD45-CD271$^+$ cells compared to HLCs (12-fold, $p<0.05$).

In the cells isolated from OA bone, all transcripts showed similar trends of expression (Figure 3.7). They all showed significantly higher level of expression in CD271$^+$ cells compared to HLCs, although the differential expression for some genes differed from their healthy counterparts which may indicate an alteration in their transcriptional profile in OA.

All the MSC-specific transcripts tested were therefore significantly higher in CD45-CD271$^+$ cells compared to HLCs and the fold change differences are detailed in Table

3.1. A similar study from our laboratory evaluated the same transcripts in healthy BM MSCs (Churchman et al., 2012) but this is the first study to investigate the gene expression profile of these cells enzymatically-released from bone. The results were consistent with the previous published study (Churchman et al., 2012) in regard to all the analysed transcripts, the gene expression profile of healthy BM MSCs being similar to the healthy enzymatically-released MSCs. Data in this chapter also introduced *CDH11* as a new molecule that showed higher expression levels in MSCs.

The bone remodelling associated genes encoding for RANKL and OPG (*TNFSF11* and *TNFRSF11B,* respectively) were also tested as they were previously shown to be expressed by MSCs (Churchman et al., 2012; Campbell et al., 2016) and are important modulators of bone remodelling processes. The mRNA levels of *TNFSF11* (encoding RANKL) were significantly higher in both healthy (15.6-fold, p=0.0312) and OA (10.8-fold, p=0.0156) CD45-CD271$^+$ cells compared to donor-matched HLCs (Figure 3.8). Similarly, *TNFRSF11B* (encoding OPG) was also shown to be specific to CD45-CD271$^+$ cells, being 76.6-fold higher in healthy CD45-CD271$^+$ cells compared to HLCs (p=0.0312) while in OA cells the mRNA levels for OPG were also higher in CD45-CD271$^+$ cells compared to HLCs (13.1-fold, p=0.0195) (Figure 3.8). So far, both molecules showed high specificity for MSCs in both healthy and OA samples indicating that CD45-CD271$^+$ cells may be the main source of these molecules, at least at a transcriptional level.

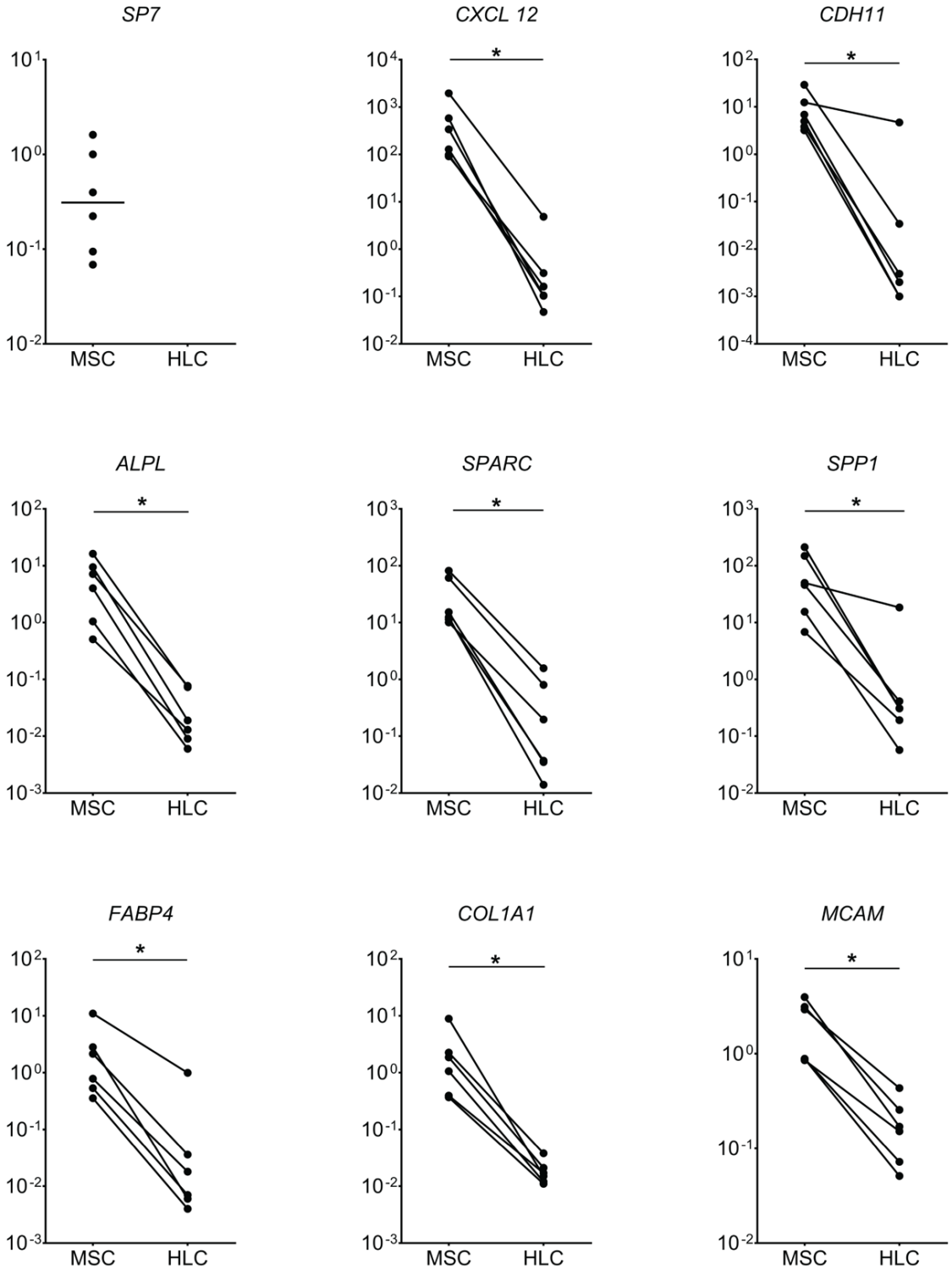

Figure 3.6. Comparative gene expression between healthy MSCs and HLCs. *Relative expression of genes associated with MSC multipotentiality and stromal support in donor matched MSCs and HLCs from healthy IC (n=6) bone fragments. Gene expression levels presented on a log scale and relative to HPRT1; Wilcoxon test for paired data. Missing dots represent values below detection in the respective data set.*

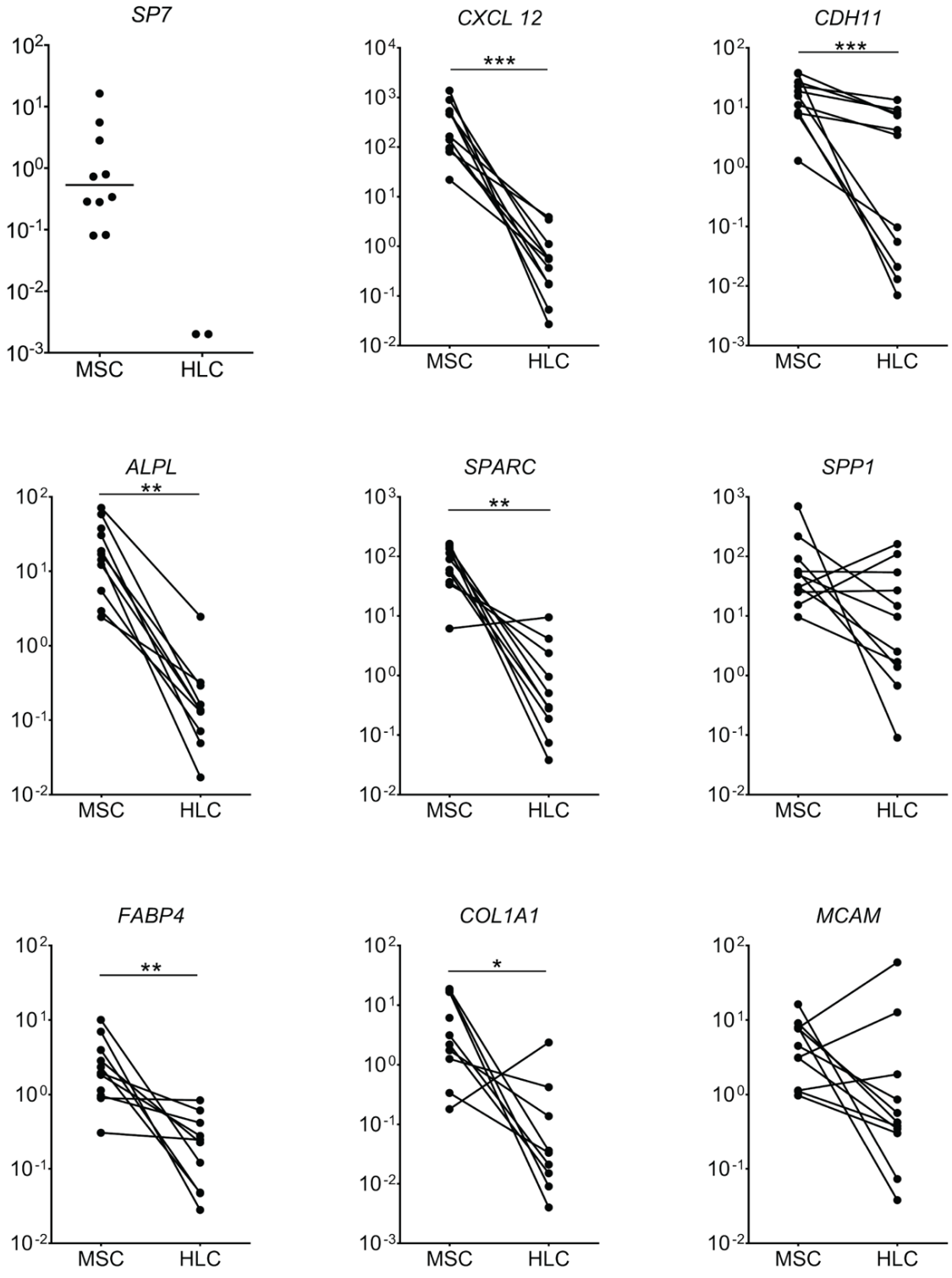

Figure 3.7. Comparative gene expression between OA MSCs and HLCs. *Relative expression of genes associated with MSC multipotentiality and stromal support in donor-matched MSCs and HLCs from OA (n=11) bone fragments. Gene expression levels are presented on a log scale and relative to HPRT1; Wilcoxon test for paired data. Missing dots represent values below detection in the respective data set.*

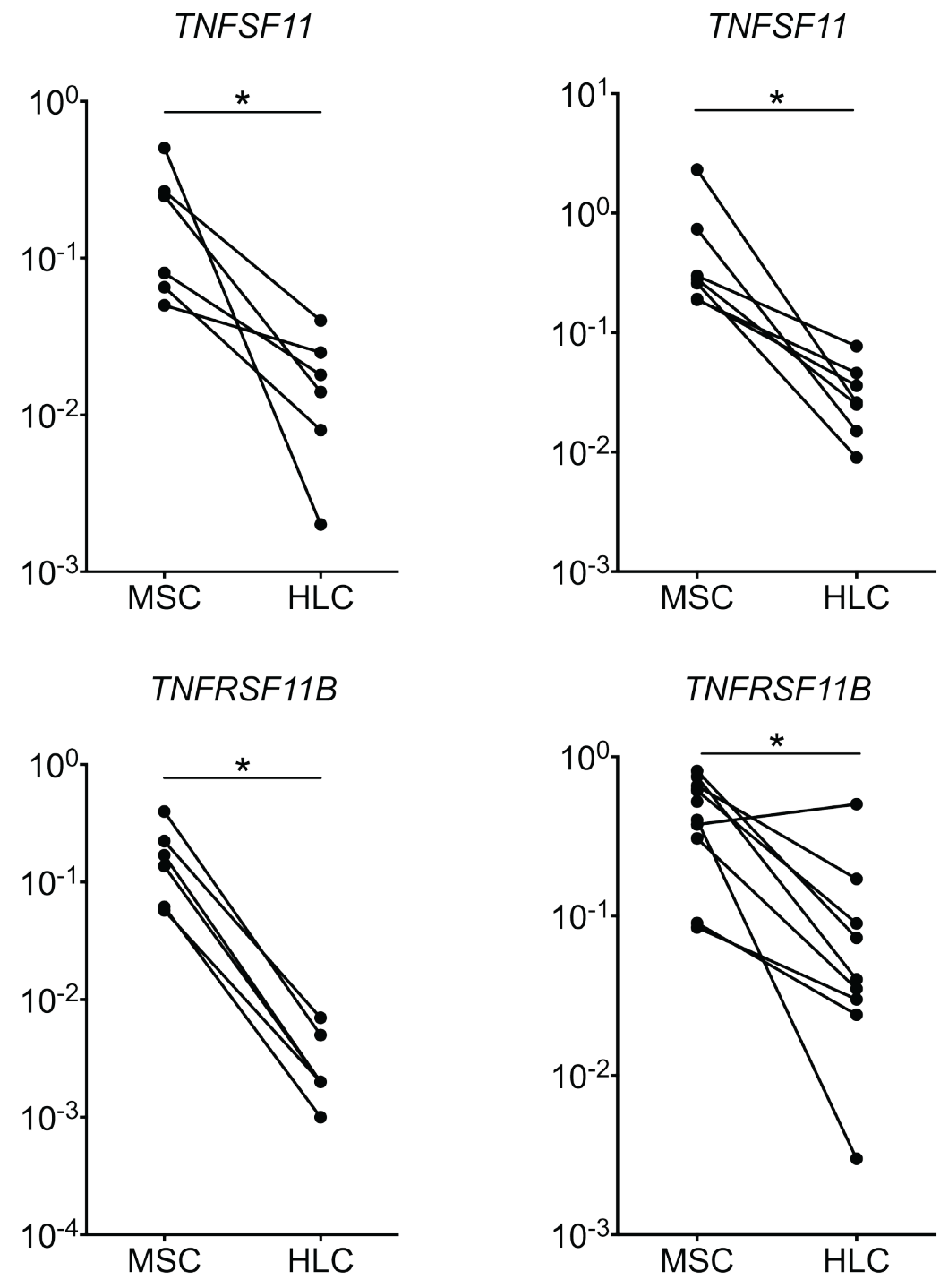

Figure 3.8. Bone remodelling genes in healthy and OA MSCs and HLCs. *Gene expression levels comparison of genes associated with bone remodelling in donor-matched MSC and HLC sorted from healthy (n=6) and OA (n=11) bone fragments. Gene expression levels are presented on a log scale and relative to HPRT1; Wilcoxon test for paired data.*

Table 3.1. Fold differences in gene expression based on median values of MSCs and HLCs sorted as CD45-CD271+ and CD45+CD271- respectively, from healthy and OA bone.

	Healthy		OA	
Gene	**Fold higher in MSC**	**p Value**	**Fold higher in MSC**	**p Value**
SP7	BD in HLC	NT	LD in HLC	NT
CDH11	2360.8	* 0.0313	390.8	*** 0.0010
CXCL12	1747.6	* 0.0313	298.7	*** 0.0010
ALPL	348.6	* 0.0313	126.5	** 0.0020
SPP1	155.2	* 0.0313	20.6	NS 0.2061
SPARC	118.5	* 0.0313	224.6	** 0.0039
FABP4	117.1	* 0.0313	18.9	** 0.0020
COL1A1	91.4	* 0.0313	94.6	* 0.0391
TNFRSF11B	76.6	* 0.0312	13.1	* 0.0195
TNFSF11	15.6	* 0.0312	10.8	* 0.0156
MCAM	11.9	* 0.0313	10.6	NS 0.4131

BD – below detection

LD – low detection

NS – not significant

NT – not tested

Altogether, this data confirmed the molecular identity of CD45-CD271+ cells as MSCs based on the significantly high expression of multiple MSC markers in comparison to matched HLCs. Next a 96-gene TaqMan Low Density Array was used to investigate, in greater depth, the transcriptional profile of native MSCs and how OA may alter their RNA expression levels. The panel of 96 gene transcripts are detailed in Appendix 5 and included molecules associated with the Wnt pathway, MSC stromal support, osteogenesis, chondrogenesis, migration and stimulation of angiogenesis. The qPCR raw data generated by this array was obtained from Dr. Sarah Churchman using the CD45-CD271+ sorted cells (n=6 healthy and n=7 OA) processed as part of the experiments described in this chapter. Expression levels were calculated based on the $2^{-\Delta\Delta Ct}$ method and normalised to *HPRT1*. These expression levels were pooled with the values from the MSCs molecular identity described in the above experiments and analysed together. The data generated by the 96-gene array as well as the panel used for MSC molecular identity used the same TaqMan assay and the same samples were used for both experiments.

Comparison was made between the CD45-CD271+ sorted cells from IC and OA bone. The fold differences for each group was calculated and the genes with expression levels higher than 2-fold were selected for further analysis. This revealed significant differences in MSCs' osteogenesis-related genes, most of these genes found to be higher in OA MSCs compared to healthy IC bone control (Figure 3.9). A significant increase in the levels of *RUNX2*, the master transcription factor involved in osteogenic differentiation (Nakashima et al., 2002) was detected in OA MSCs (7-fold, p=0.0177). Other osteogenic transcripts that were found to be elevated OA MSCs compared to healthy IC bone controls included *SPARC* (5-fold, p=0.0034), *ALPL* (3-fold, p=0.0477) and *CDH11* (3-fold, p=0.0249) (Figure 3.9). No significant difference was noted in the levels of other osteoblast-associated molecules (*SP7, SPP1, COL1A1* and *COL1A2*), although a trend for higher expression was noted for *SP7* and *COL1A2* (Figure 3.9). This data potentially indicated an early osteogenic commitment of the MSCs extracted from OA femoral heads.

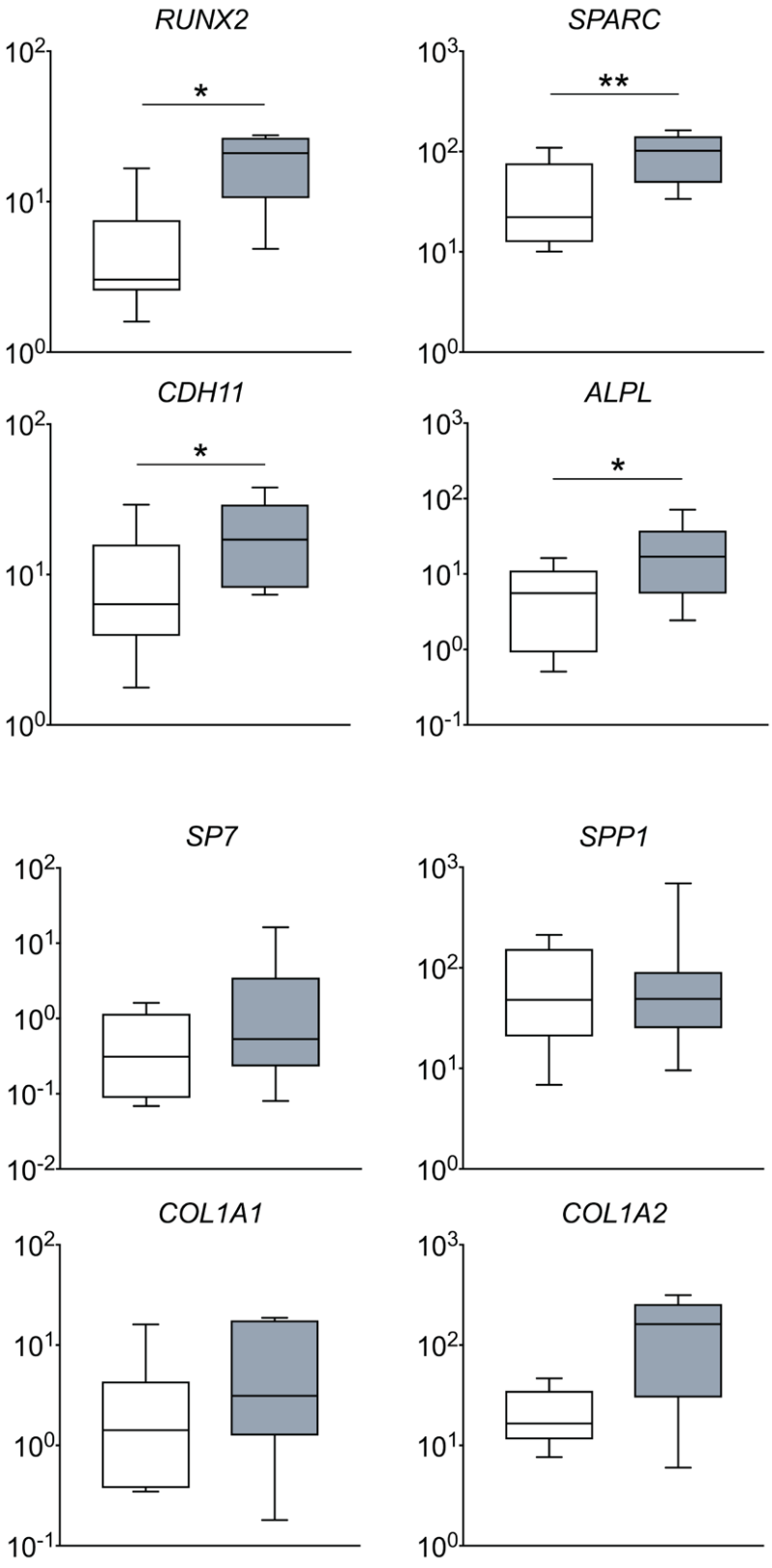

Figure 3.9. Comparative gene expression of osteogenesis molecules between healthy and OA MSCs. *The mRNA levels of genes associated with osteogenesis and bone formation in native MSCs sorted from healthy (n=6, empty boxes) and OA (n=11, grey boxes) bone fragments. Gene expression levels presented as relative to HPRT1 and Mann-Whitney test was used for statistical analysis.*

As major players in bone remodelling and expressed at considerably higher levels in MSCs compared to HLCs as shown in Figure 3.10, the mRNA levels for RANKL and OPG were also tested (Brendan F Boyce and Xing, 2007). Based on median values, the levels of *TNFRSF11B* were found at higher levels in OA MSCs (3.4-fold, p=0.0202) while *TNFSF11* expression was similar between both groups (Figure 3.10). In addition to the enhanced osteogenic commitment judged by the transcriptional analysis described here, the native MSCs in OA may also be more biased towards inhibition of bone resorption.

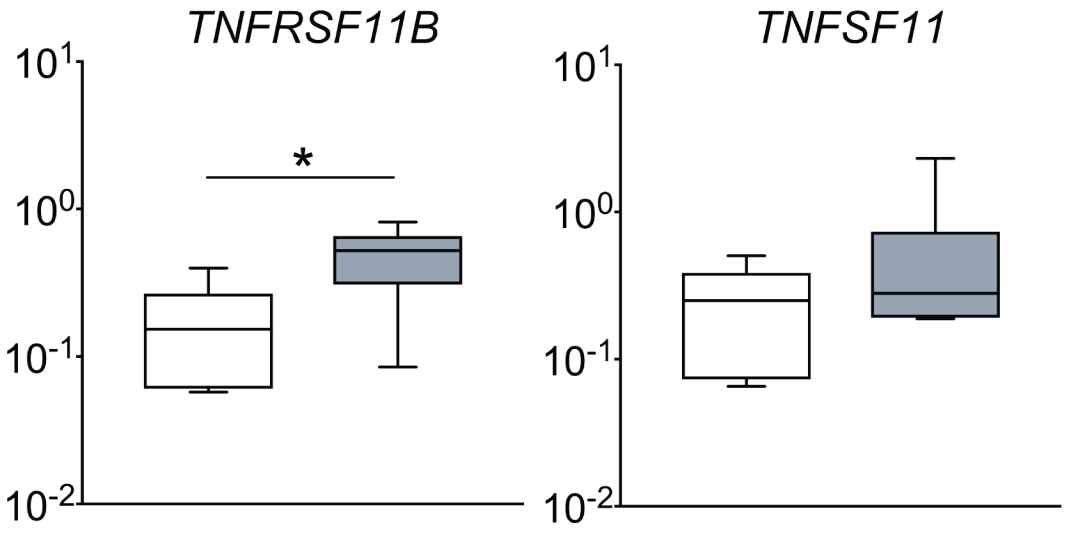

Figure 3.10. Comparative gene expression of bone remodelling molecules between healthy and OA MSCs. *The mRNA levels of bone remodelling associated genes encoding for OPG (TNFRSF11B) and RANKL (TNFSF11) in native MSCs sorted from healthy (n=6, empty boxes) and OA (n=11, grey boxes) bone fragments. Gene expression levels presented as relative to HPRT1 and Mann-Whitney test was used for statistical analysis.*

As shown in Figure 3.11, the expression level of genes associated with chondrogenesis and cartilage formation showed an overall decrease in OA. The major chondrogenic transcription factor *SOX9* (Bi et al., 1999) was significantly reduced in OA MSCs (5-fold, p=0.0082) as well as the levels of *CHAD* (chondroadherin), encoding a protein involved in chondrocytes adhesion (Camper et al., 1997), which was only expressed at lower levels in 2 out of 6 tested samples compared to healthy MSCs (Figure 3.11). Decreased gene expression levels were also observed for *UGDH* (14-fold, p=0.0140) and *PAPSS* (6-fold, p=0.0260), both encoding enzymes involved proteoglycan synthesis and cartilage formation (Haque et al., 1998; Wen et al., 2014). Although not statistically significant, a 6-fold increase in the levels of *ACAN* (p=0.0519) and 4-fold in *PRELP* (p=0.1797) was noted in OA MSCs. This is intriguing since both genes encode extracellular matrix proteins that play an important part in the structural integrity of the cartilaginous tissue and contrasts the significant decrease of other chondrogenesis-related genes in native OA MSCs.

No difference was observed in the genes associated with adipogenesis. The main adipogenic transcription factor *PPARG* as well as the mature adipogenic protein transcript; *FABP4,* showed similar levels in the MSCs isolated from both healthy and OA bone (Figure 3.12).

The α-smooth muscle actin gene, *ACTA2* was observed to be 9-fold increased (p=0.0411) in OA MSCs while the levels of *MCAM*, a gene encoding the CD146 antigen, were also higher in OA MSCs (2.4-fold, p=0.0365) compared to healthy MSCs. Noteworthy, both genes were shown to be expressed in BM CD271+ MSCs (Churchman et al., 2012), however since the CD146 marks an MSC subset associated with a perivascular location (Tormin et al., 2011), these differences between healthy and OA may be associated with an increased presence of perivascular MSCs subsets in OA. Furthermore, no differences were noted in the expression levels of the stromal support molecule, *CXCL12* between healthy and OA native MSCs (Figure 3.13), these results may indeed point to a potential implication of a perivascular subset of MSCs in OA bone. This would be further investigated by FACS to determine both the protein expression levels as well as the proportion of this MSC subset in OA bone.

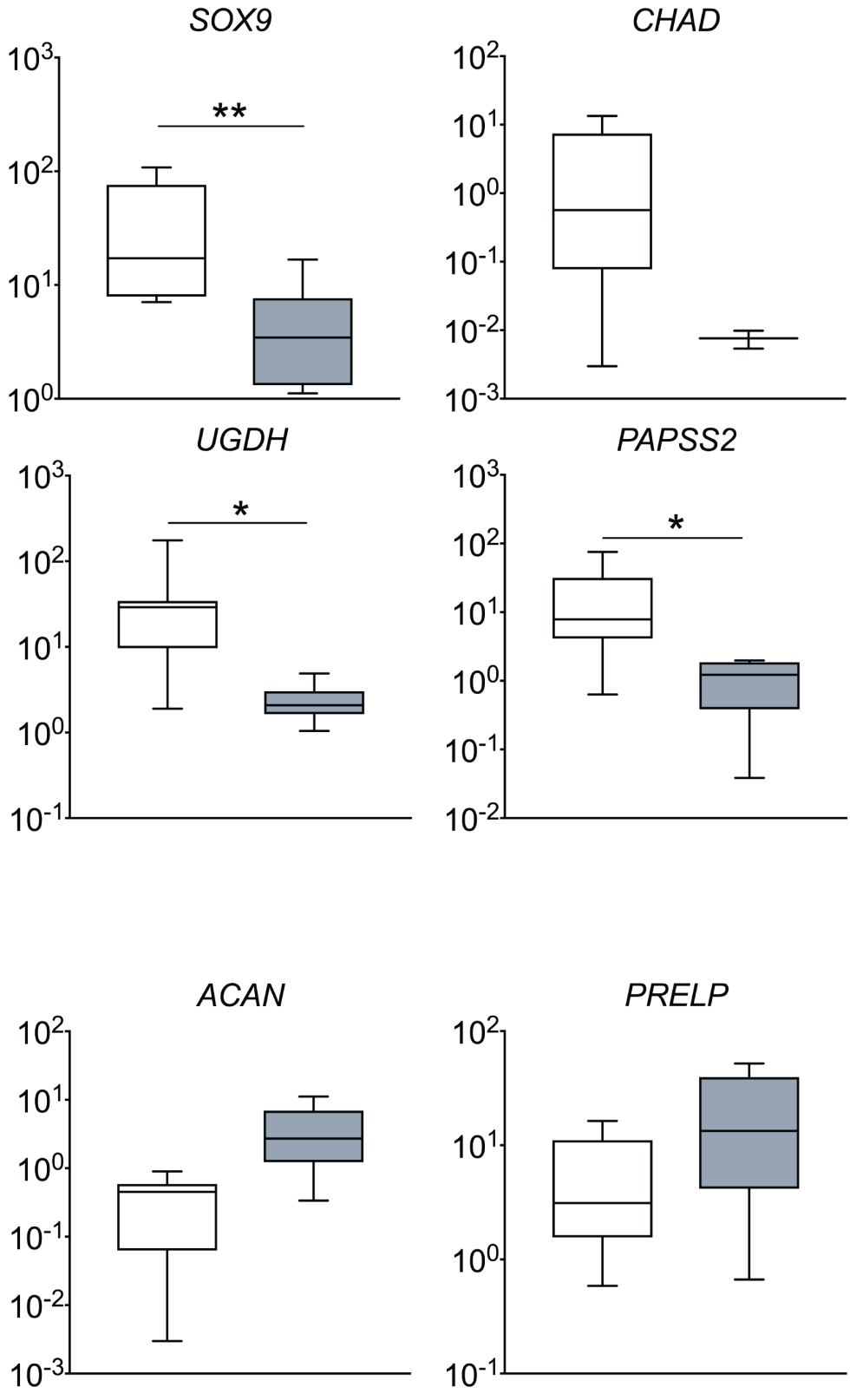

Figure 3.11. Comparative gene expression of chondrogenesis molecules between healthy and OA MSCs. *The mRNA levels of chondrogenic transcripts in native MSCs sorted from healthy (n=6, empty boxes) and OA (n=11, grey boxes) bone fragments. Gene expression levels presented as relative to HPRT1 and Mann-Whitney test was used for statistical analysis.*

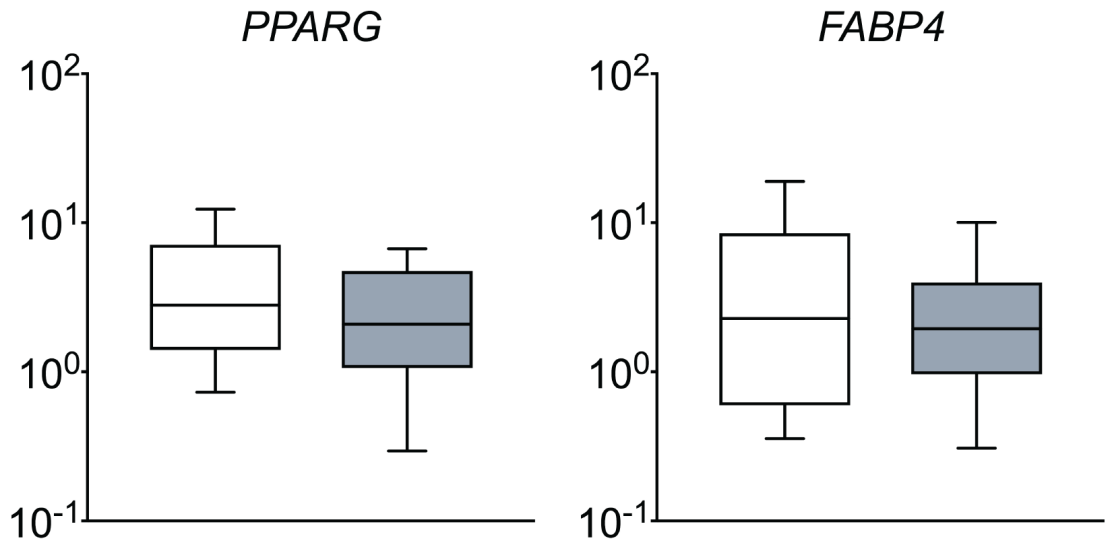

Figure 3.12. Comparative gene expression of adipogenesis molecules between healthy and OA MSCs. *The mRNA levels of adipogenic transcripts in native MSCs sorted from healthy (n=6, empty boxes) and OA (n=11, grey boxes) bone fragments. Gene expression levels presented as relative to HPRT1 and Mann-Whitney test used for statistical analysis with no significant difference found for either of the two genes between healthy and OA groups.*

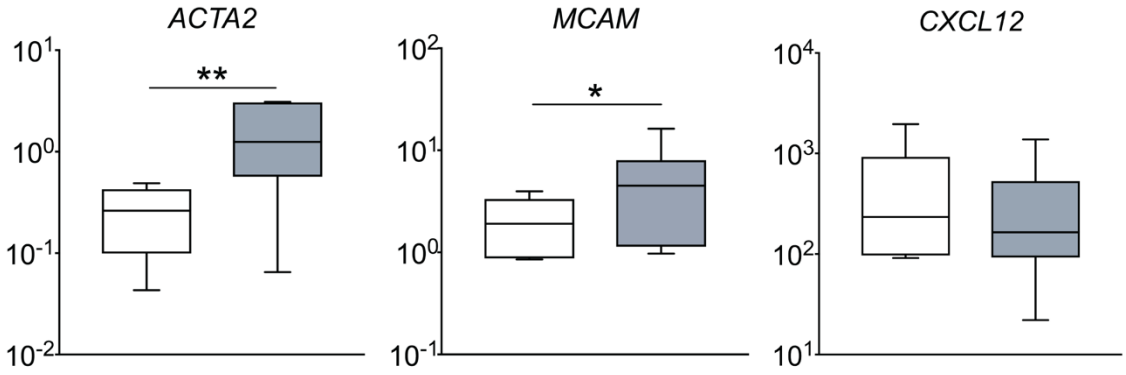

Figure 3.13. Comparative gene expression of vascular and stromal support molecules between healthy and OA MSCs. *The mRNA levels of angiogenic-related transcripts in native MSCs sorted from healthy (n=6, empty boxes) and OA (n=11, grey boxes) bone fragments. Gene expression levels presented as relative to HPRT1 and Mann-Whitney test was used for statistical analysis.*

Table 3.2. Fold changes based on median values in the expression levels between healthy and OA native MSCs

	Gene	Medians		Fold change	p Value
		Healthy	OA		
Osteogenesis	*RUNX2*	3.036	21.04	6.9	* 0.0177
	SPARC	22.14	101.9	4.6	** 0.0034
	CDH11	6.358	17.05	2.7	* 0.0249
	ALPL	5.577	17.01	3.1	* 0.0477
	SP7	0.3101	0.5323	1.8	NS 0.4923
	SPP1	47.96	49.15	1.0	NS 0.8836
	COL1A1	1.416	3.121	2.2	NS 0.2115
	COL1A2	16.54	161.7	9.8	NS 0.0734
Bone remodelling	*TNFRSF11B*	0.1531	0.5225	3.4	* 0.0202
	TNFSF11	0.2494	0.2801	1.1	NS 0.2677
Chondrogenesis	*SOX9*	17.15	3.456	5.0	**0.0082
	CHAD	0.5644	BD	NT	NT
	UGDH	29.00	2.080	13.9	* 0.0140
	PAPSS2	7.849	1.222	6.4	* 0.0260
	ACAN	0.4522	2.717	6.0	NS 0.0519
	PRELP	3.118	13.35	4.3	NS 0.1797
Adipogenesis	*FABP4*	1.464	1.945	1.3	NS 0.5908
	PPARG	2.801	2.088	1.3	NS 0.4452
Vascular and stromal support	*ACTA2*	0.2617	1.249	4.8	* 0.0411
	MCAM	1.908	4.501	2.4	* 0.0365
	CXCL12	233.2	164.6	0.7	NS 0.8075

BD – below detection

NT – not tested

NS – not significant

3.4.4 Cultured MSCs

To determine whether the observed differences in gene expression are maintained in culture, the MSCs isolated from bone of healthy and OA donors were culture-expanded in StemMACS media up to P4 and then gene expression analysed. First, the morphology and growth kinetics of the culture expanded cells were investigated.

Following the enzymatic digestion, approximately one million cells from the obtained cell suspension were seeded in a T25 flask. Morphological features of MSCs were examined by phase-contrast microscopy. Within hours after seeding, the cells attached to the culture surface and exhibited a typical fibroblastic-like spindle-shaped appearance (Figure 3.14A and B). When observed under the inverted microscope, the cells released from both healthy and OA bones contained a heterogeneous pool of cells, including a high number of plastic-adherent and proliferative stem-like adherent cells (Figure 3.14). During the first week in culture, the MSC showed increased proliferation, which gradually resulted in maintaining a homogeneous fibroblastic morphology (Figure 3.14C and D).

The majority of non-adherent cells were subsequently removed during the media exchanges throughout passages. Visual assessment of cultures from both healthy and OA groups showed indistinguishable morphology, with no differences in cell size and shape, which was maintained between passages. Of importance, the cells maintained their proliferative and plastic-adherent properties after freezing down and recovering from liquid nitrogen. When the cells reached confluence, they were trypsinised, counted and seeded back at a cell density of 10^4cells/cm^2 representing 2x10^5 cells per T25 flask. During the four passages the cells showed no differences in morphology, both healthy and OA cells maintaining their elongated MSC-like shape (Figure 3.15).

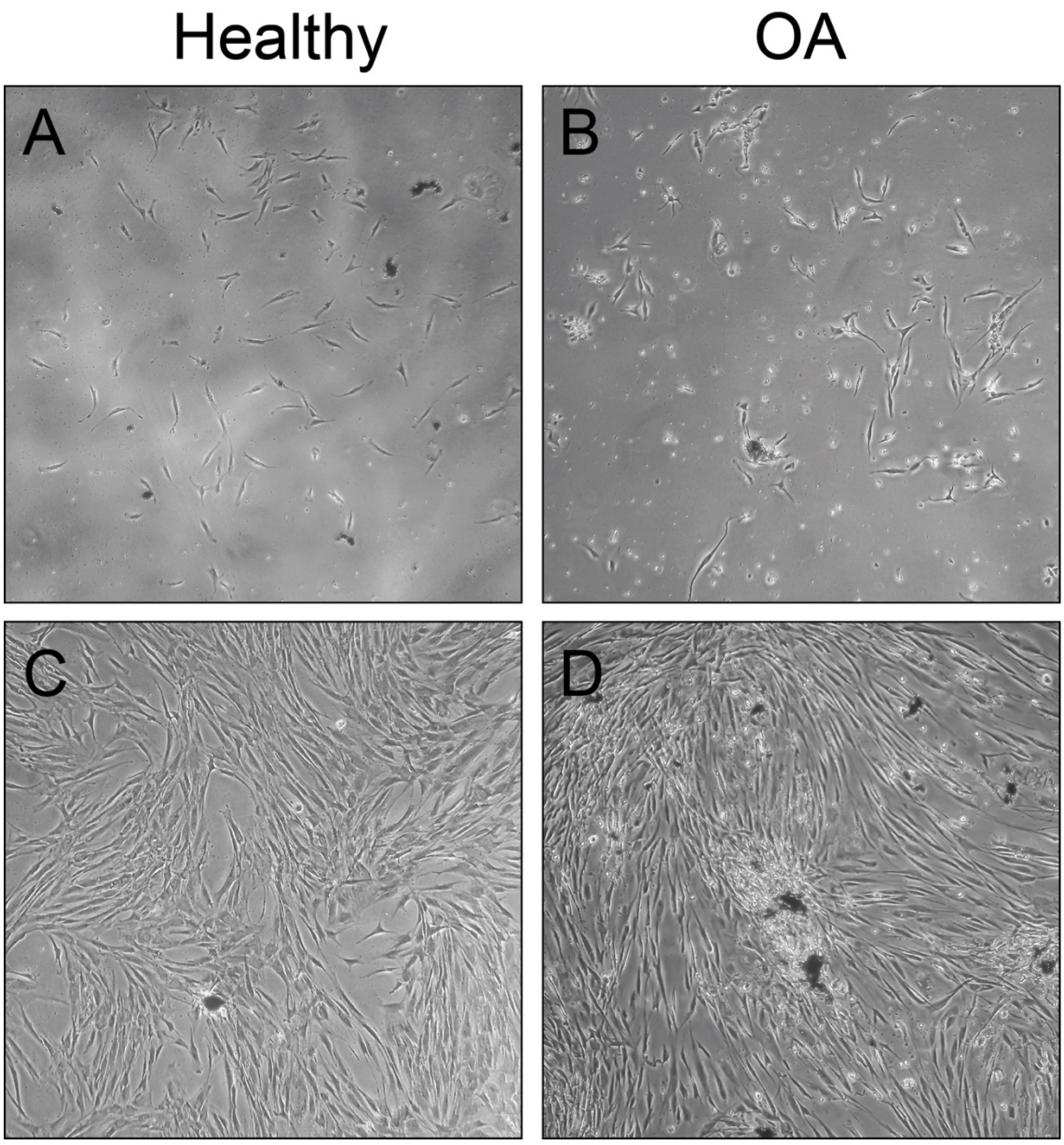

Figure 3.14. Culture expanded cells from healthy and OA bone prior to first passage. *MSCs early in culture isolated from healthy (A) and OA (B) bone have started to attach to the surface and proliferate as soon as 24 hours following extraction and seeding. After approximately 7 days the cells from both healthy (C) and OA (D) bone were confluent with no distinguishable differences in morphology. Some bone debris could be observed in cultures from both sources.*

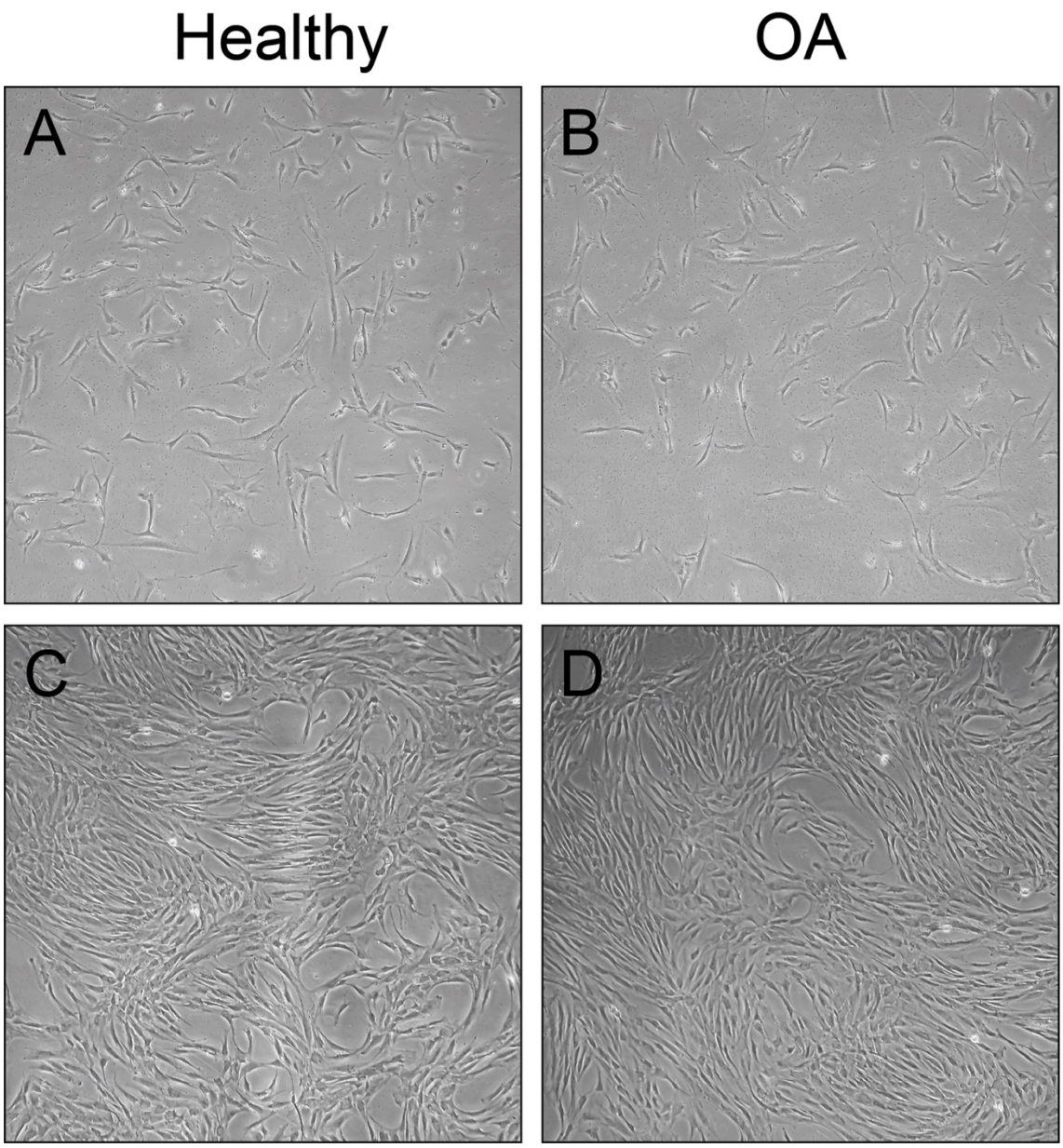

Figure 3.15. Late-passage culture expanded cells from healthy and OA bone. *Culture expanded cells from healthy (A) and OA (B) bone at the start of passage 4 (24 hours after seeding) showed signs of proliferation. Following 2-3 days in culture both healthy (C) and OA (D) bone MSCs have reached confluence, less debris present and a more homogenous cell population with cells that look similar in size and shape.*

For each passage the cell number was evaluated after trypsinization when 70–80% of cell confluence was achieved. The culture expansion experiment was performed with cells extracted from n=10 healthy and n=12 OA bone. The initiating cultures needed on average 6 days to reach sub-confluence and only 2-3 days were required between each passage. The cultures were stopped after four passages and the population doublings as well as cell counts between the passages were calculated based on seeded CFU-Fs as described in Materials and Methods (Section 3.3.3). While no statistically significant differences were found in the growth rates measured as days/PD, across the four passages between healthy and OA derived MSC cultures (median values of 2.03 and 2.59, respectively, Figure 3.16), a trend for higher PDs was observed for OA MSCs.

Interestingly this suggest that the higher CFU-Fs observed in the OA group compared to healthy IC may be associated with slower proliferation as the doubling times of MSCs released from OA bone were longer than healthy IC MSCs. However, another explanation may be the increased frequency of MSCs in the extracted cells from OA bone as assessed by FACS. Also noteworthy is the OA donor variability in comparison to healthy cMSCs. While the age spread on healthy donors was higher than in OA (Appendix 3), the results were opposite, which may indicate that the higher variability in OA may be associated with the disease.

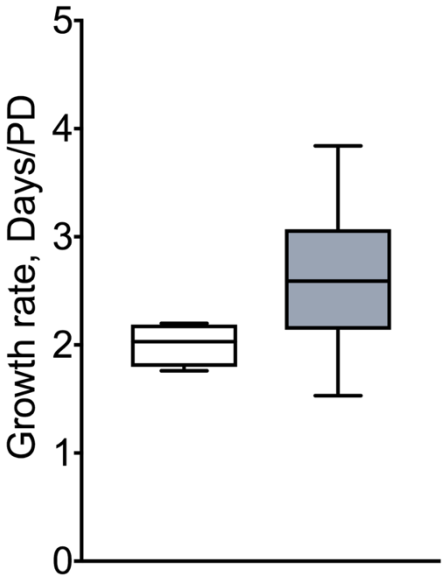

Figure 3.16. Comparative growth rate between healthy and OA bone cMSCs. *Graphs showing the growth rate of cultured MSCs derived from healthy (n=10, white box) and OA (n=12, grey box) bone measured as days/PD. A trend for higher growth rate and increased variability was observed in OA MSC cultures. However, the PD rates showed no significant differences between healthy and OA donors calculated as days/PD based on Mann-Whitney test.*

3.4.5 Gene expression comparison between native and cultured MSCs from OA bone

As mentioned in the introduction of this chapter (Section 3.1.3), healthy IC BM MSCs lose their native gene expression following passaging in culture. However, the molecular profile of culture-expanded MSCs from other sources, i.e. healthy iliac crest and OA femoral heads have not been investigated yet. Therefore, analysis in this chapter aimed at establishing the differences of cMSCs in comparison to their *in vivo* counterparts in both healthy and OA bone-derived MSCs. Furthermore, comparison between healthy and OA cMSCs were also performed to establish whether the differences observed in native MSCs were maintained in culture.

Once the cells have reached four passages, the culture was stopped and gene expression was analysed in OA cMSCs while healthy IC cMSCs were used as control. These comparisons were made between native $CD45^{-}CD271^{+}$ MSCs isolated by FACS from healthy (n=6) and OA (n=11) bone previously described above in Section 3.4.3 and culture-expanded MSCs seeded from the pool of cells extracted from healthy (n=9) and OA (n=11) bone, out of which n=4 were donor matched.

As expected, a drastic difference in the gene expression cMSCs from healthy bone occurred when the cells were culture expanded. The levels of many of the tested molecules were lower in cMSCs compared to native $CD45^{-}CD271^{+}$ MSCs. The MSCs markers associated with their osteogenic and adipogenic potentials showed the highest differences, the level of osteogenic transcription factor *SP7* were found to be 470-fold (p=0.0043) lower in cMSCs as well as the adipogenic protein *FABP4*, which was 236-fold (0.0004) lower in cMSCs (Figure 3.17). Furthermore, the other osteogenic related genes were also significantly lower in cMSCs compared to native cells, including *SPP1* (85-fold, p=0.0004) and *ALPL* (17-fold, p=0.0360) (Figure 3.17) along with the stromal support molecule, *CXCL12* which was 11-fold (p=0.0004) lower in healthy cMSCs compared to native cells. Two other molecules associated with osteogenesis, *SPARC* and *COL1A1* were both significantly higher in cMSCs compared to native MSCs (Figure 3.17). The only genes that did not show any changes while in culture were adhesion molecules *CDH11* and *MCAM* (Figure 3.17). Taken together this data indicated that the trends for lower expression in cMSCs compared to native CD271+ MSCs were consistent with those found for MSC from IC aspirates (Churchman et al., 2012; Ghazanfari et al., 2017). Furthermore, these results indicate that osteogenic pathway genes may be affected by the culture conditions.

Next, the same panel of genes was investigated in native and cultured MSCs extracted from OA femoral heads as OA MSCs were also susceptible to these changes. Results showed that the same trends observed in healthy MSCs were present in OA MSCs. All the transcripts that were found to be lower in healthy cMSCs, *SP7*, *CXCL12*, *ALPL, SPP1* and *FABP4* (Figure 3.18) were as well significantly decreased in the cultured MSCs isolated from OA bone. All the fold changes are listed in Table 3.3 and it was notable that some fold changes were different in the OA group as compared to the healthy MSCs. For example, while the MCAM levels were unchanged when comparing the healthy MSCs, there was a significant decrease observed in the cells expanded from the OA bone (5-fold, p=0.0006). This may be due to the perturbations observed in native MSCs and documented in Section 3.4.3 above, or it may indicate that these differences caution against using cMSCs to understand OA since they fail to reflect their native phenotype.

When comparing the levels of the molecules responsible for bone remodelling regulation in healthy and OA derived MSCs, alterations were also found in both mRNA levels for RANKL (*TNFSF11*) and OPG (*TNFRSF11B*) (Figure 3.19).

In both healthy and OA cMSCs a significant decrease was observed in RANKL mRNA levels, being 121-fold (p=0.0016) and 35-fold (p=0.0001) decreased in healthy and OA cMSCs respectively compared to native MSCs. Opposite trends were observed in the levels of OPG, which was shown to be significantly up-regulated in both healthy (5-fold, p=0.0048) and OA group (3-fold, p=0.0032).

The changes observed in the levels of OPG however were not as distinct as the ones observed for RANKL. This may be explained by the increased levels of OPG in native OA MSCs compared to healthy MSCs (Figure 3.10). However, regardless of the expression levels in native MSCs, the similar pattern was observed for both molecules, in both healthy and OA, although at different extents.

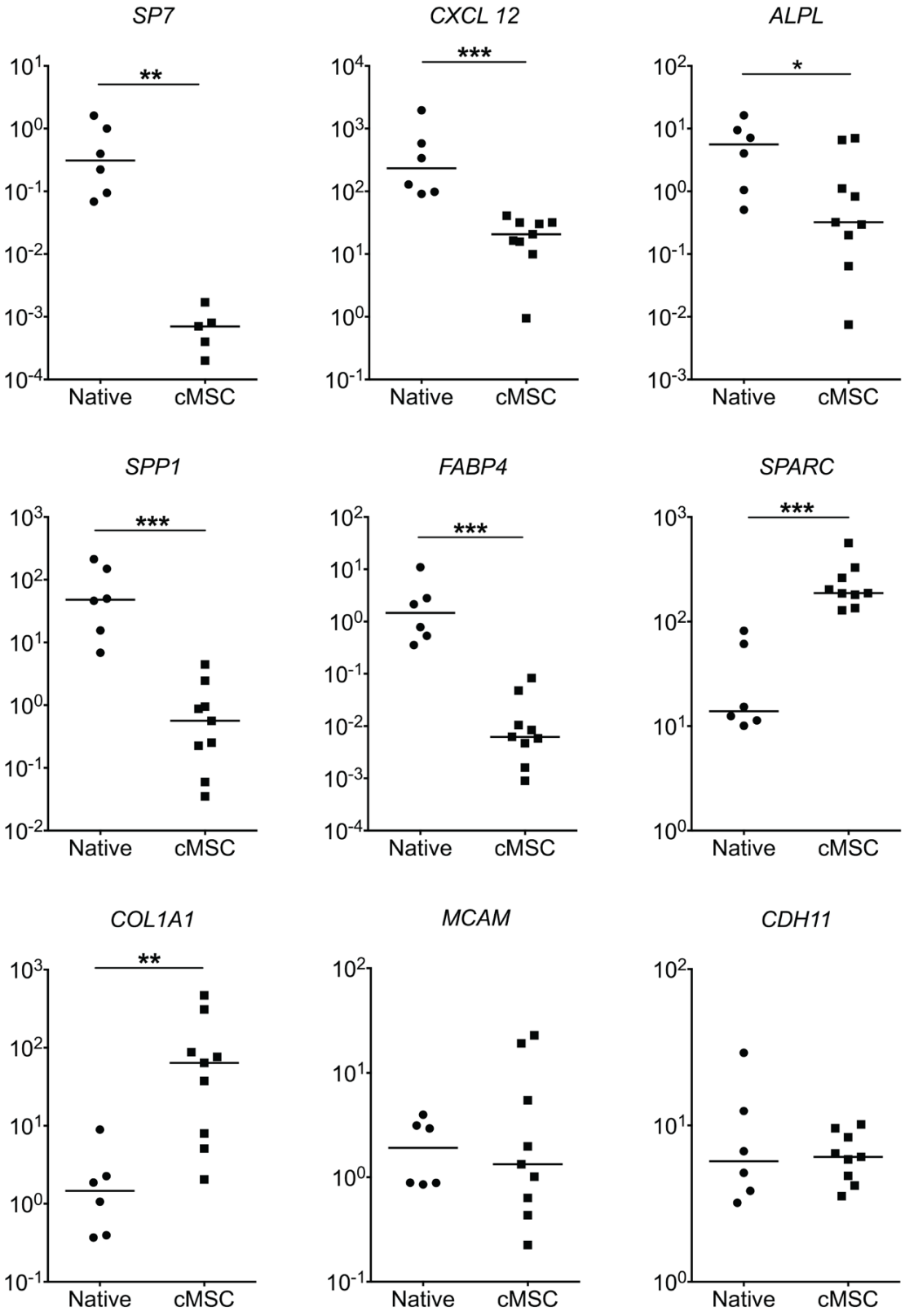

Figure 3.17. Comparative gene expression between native and cMSCs derived from healthy bone. *Graphs showing the comparison in mRNA levels between native (CD45-CD271+, n=6) MSCs and culture-expanded MSCs (cMSCs, n=9) isolated from healthy iliac crest bone. Gene expression levels presented as relative to HPRT1 and Mann-Whitney test was used for statistical analysis.*

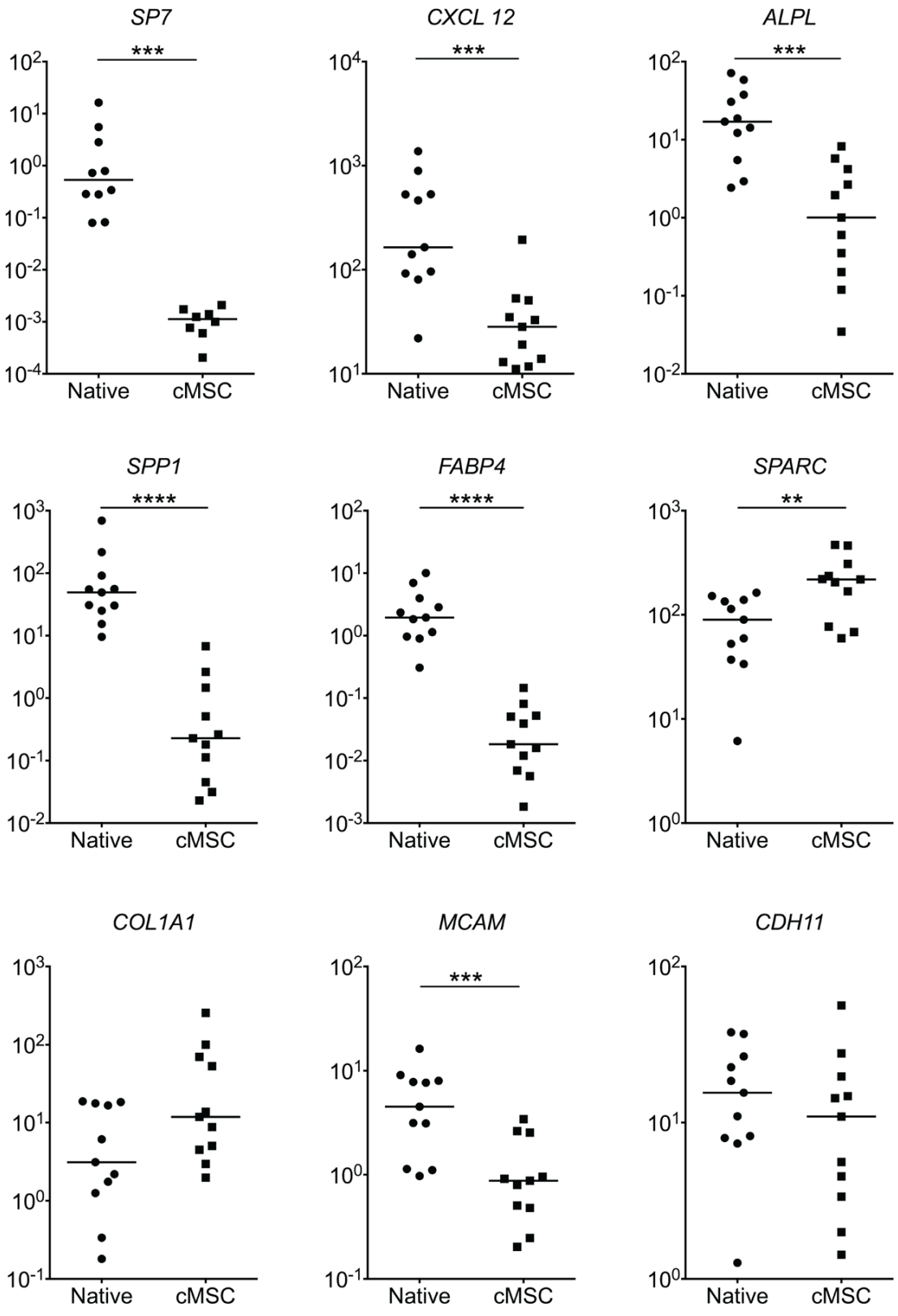

Figure 3.18. Comparative gene expression between native and cMSCs derived from OA bone. *Graphs showing the comparison in gene expression levels between native (CD45-CD271+, n=11) MSCs and culture-expanded MSCs (cMSCs, n=11) isolated from OA femoral head bone. Gene expression levels presented as relative to HPRT1 and Mann-Whitney test was used for statistical analysis.*

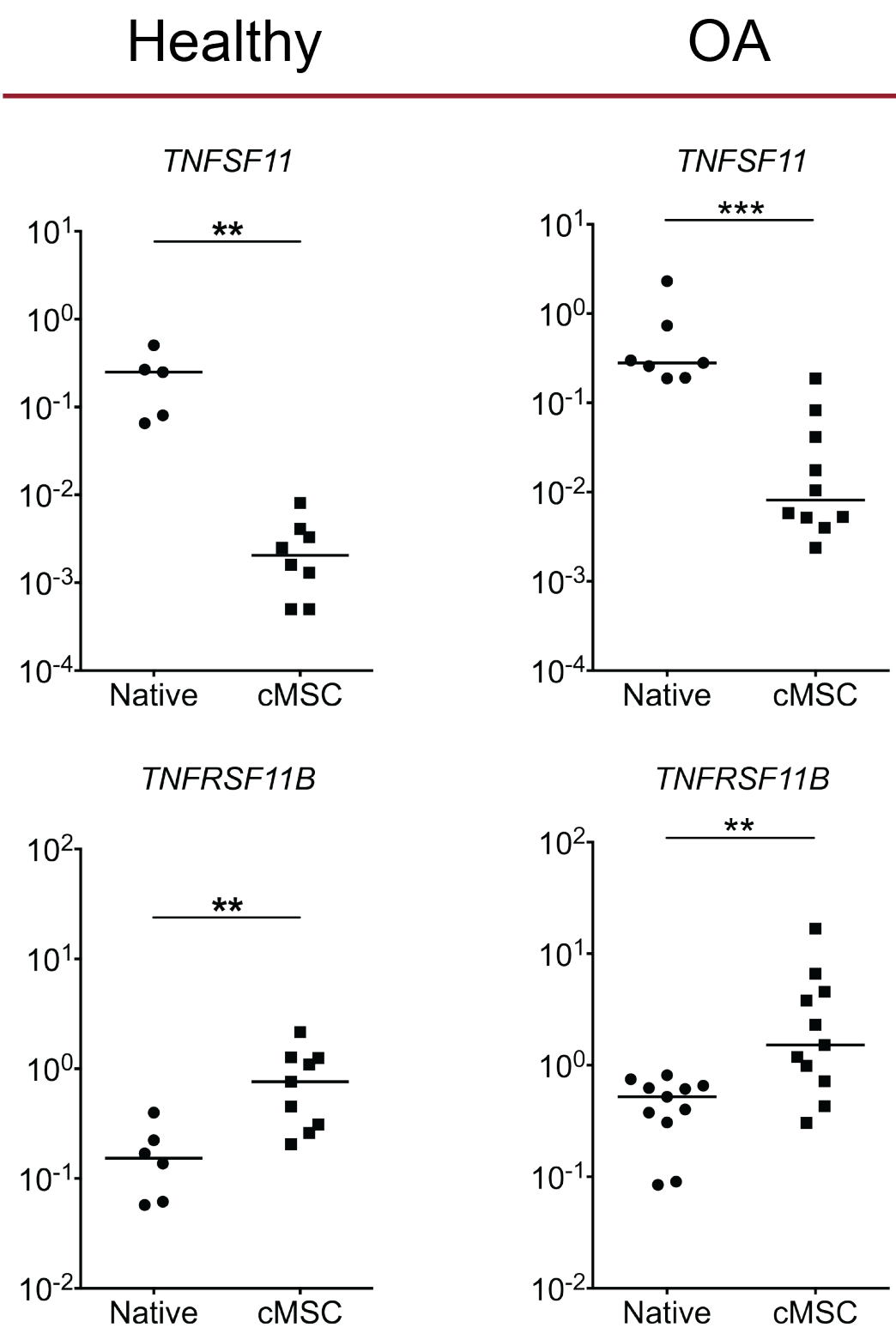

Figure 3.19. Comparative gene expression of bone remodelling molecules between native and cMSCs derived from healthy and OA bone. *The mRNA levels of bone remodelling associated genes in native and culture-expanded MSCs extracted from healthy and OA bone. Gene expression levels presented as relative to HPRT1 and Mann-Whitney test was used for statistical analysis.*

Table 3.3. Table summarising the median fold differences in gene expression levels between native and culture-expanded MSCs extracted from healthy and OA bone.

		Healthy		OA	
	Gene	**Fold difference**	**p Value**	**Fold difference**	**p Value**
Higher in CD45-CD271+ MSCs	*SP7*	443	0.0043	470	<0.0001
	CXCL12	11.25	0.0004	5.81	0.0006
	ALPL	17.36	0.0360	16.90	0.0003
	CDH11	1.07	NS	1.42	NS
	SPP1	85.03	0.0004	215.78	<0.0001
	FABP4	236.07	0.0004	106.61	<0.0001
	MCAM	1.44	NS	5.11	0.0006
	TNFSF11	121.66	0.0016	35.01	0.0001
Higher in cMSCs	*COL1A1*	43.71	0.0048	3.79	NS
	SPARC	13.50	0.0004	2.43	0.0041
	TNFRSF11B	4.97	0.0048	2.91	0.0032

BD – below detection

NS – not significant

NT – not tested

In summary, the gene expression differences observed between healthy and OA native MSCs were not found to be maintained following culture-expansion. The only difference observed between healthy and OA cMSCs was in the bone remodelling associated molecules, particularly the mRNA levels of RANKL. In comparison to healthy cMSCs the levels of RANKL mRNA were 4-fold higher (p=0.0043) in the OA cMSCs (Figure 3.20). The mRNA levels for the resorption inhibitor OPG (*TNFRSF11B*) also indicated a trend for higher expression in the OA cMSCs, however it failed to reach statistical significance (Figure 3.20). Noteworthy are the opposite trends observed for RANKL and OPG when the cells were exposed to culture, particularly the increased expression of RANKL in OA cMSCs.

None of the other transcripts tested in relation to MSC identity or their multipotential nature showed any differences between the healthy and OA-derived cultures (Figure 3.21). Although the fold differences observed in native cells were not notably high, a similar trend would still be expected to be observed in the cultures.

Considering these overall changes in gene expression observed between native and cMSCs, especially with regards to the two main mediators of bone resorption, it strengthens the message that cMSCs should be used with more caution in understanding OA pathophysiology.

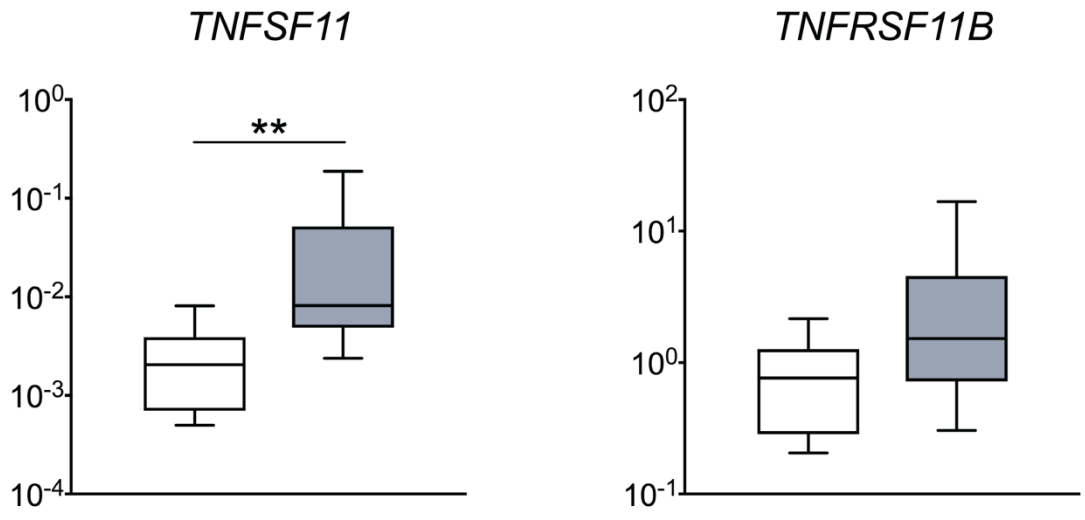

Figure 3.20. Comparison of bone remodelling associated gene ex between healthy and OA cMSCs. *The mRNA levels of bone remodelling associated genes in culture-expanded MSCs extracted from healthy (n=9, white boxes) and OA (n=11, grey boxes) bone. Gene expression levels presented as relative to HPRT1 and Mann-Whitney test was used for statistical analysis.*

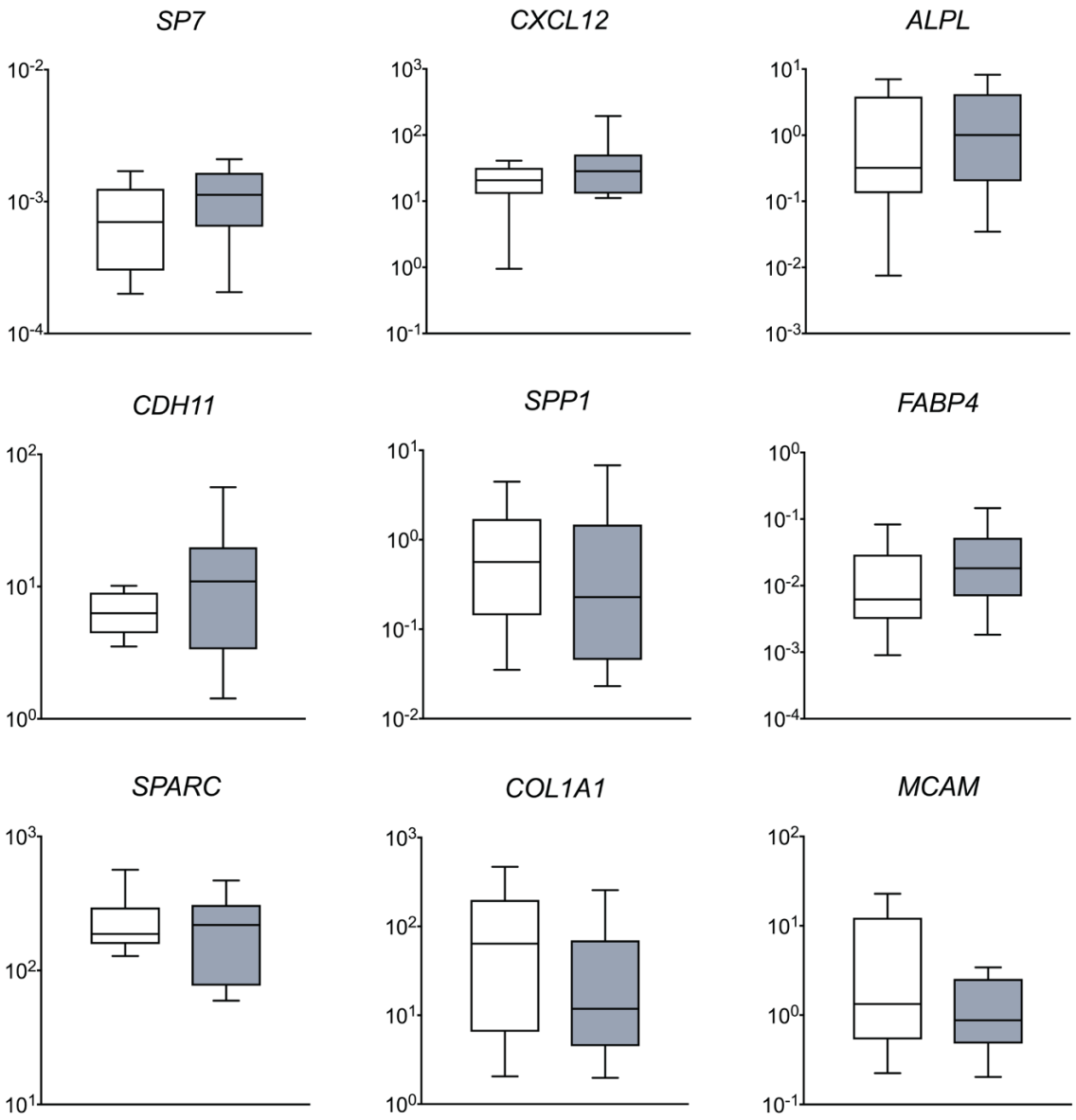

Figure 3.21. Comparative gene expression between healthy and OA cMSCs. *Comparison of mRNA levels of genes associated with MSC phenotype in culture-expanded MSCs from healthy (n=9, white boxes) and OA (n=11, grey boxes) bone. All the transcripts showed no significant differences between healthy and OA extracted cells. Gene expression levels presented as relative to HPRT1 and Mann-Whitney test was used for statistical analysis.*

3.5 Discussion

The main aim of this chapter was to test whether MSC numbers and their gene expression profile are altered in OA affected bone. The current understanding of the contribution of MSCs to the mechanisms underlying OA pathology and endogenous repair mechanisms is limited, however, their importance may be reasonably assumed given their wide distribution in all of the joint tissues (Barry and Murphy, 2013; McGonagle et al., 2017). Furthermore, recent OA studies in both animal models (Zhen et al., 2013) and humans (Campbell et al., 2016) point to an involvement of bone resident MSCs in OA pathology. Therefore, this chapter focused on investigating the MSC numbers in OA femoral heads by means of enumeration and purification to establish their presence in OA affected bone. In order to ascertain how the OA pathological environment may affect their gene expression, the transcriptional profile was also analysed in their native state and was further verified if it is faithfully preserved following culture expansion.

3.5.1 Investigation of MSCs numbers in OA

In order to obtain an accurate quantification of the MSCs numbers in OA bone, their enumeration was performed using two different assays, CFU-F and cell sorting using surface marker selection. Data in this chapter obtained from the CFU-F assays showed that the frequency of MSC among the cells extracted from OA bone was significantly higher compared to the cells from healthy iliac crest. This result is in contrast to a previous study in our laboratory, where no alterations in the CFU-Fs were found in cells from OA in comparison to healthy bone (Jones et al., 2010). The 2-fold increase described in the current chapter may be attributable to the technical improvement in the MSC extraction protocol. The bone fragments were subjected to more stringent washing following the enzymatic treatment (Chapter 2, Section 2.2.1) as well as an additional low speed centrifugation step, which all contributed to the release and capture of more cells, possibly some that were tightly attached to the bone surface. This may point to bone lining cells as a strong candidate responsible for the observed differences and moreover, a potentially increased presence of these cells in OA.

Variations were observed in the CFU-Fs among donors from the same group and were further found similarly variable among the $CD45^{-}CD271^{+}$ population of cells enumerated from healthy and OA samples by FACS. This may be indeed attributed to patient variability, but given the limited supply of human tissue, especially healthy iliac crest bone, an analysis between age- and sex-matched donors of healthy and OA bone was not always possible. However, efforts have been made to narrow the age gap by selecting

older IC and younger OA donors. Additionally, to account for the inter-donor variability and optimise for a feasible colony count, the CFU-F assays were performed by plating the cells at different seeding densities. To obtain an accurate quantification of the native MSC frequencies, optimal density was chosen based on the number of cells that were seeded initially in order to generate the most reliable number of colonies that could be counted accurately.

The CFU-F assay is a very common, robust and straight forward technique for enumeration of native MSCs (Kuznetsov et al., 2009). However, it is also time consuming and retrospective, being reflective of many variables that may affect the end-point result, such as initial cell seeding density, subjectivity in scoring the colonies or merged colonies, all leading to a high degree of variability. Meanwhile, flow cytometry, which is rapid, reliable, and reproducible, could provide a useful alternative to CFU-F assay, but the prerequisite to using this method is a clear understanding of the phenotype of native MSCs.

Thus far the low-affinity nerve growth factor receptor; CD271, has been considered one of the most specific and reliable markers for native MSCs (Quirici et al., 2002; Jones et al., 2002; Bühring et al., 2007; Bühring et al., 2009; H. Li et al., 2016) while CD45 is commonly employed as a negative selection marker to identify the haematopoietic lineage cells. This phenotype has been used in previous studies to purify MSCs from cells isolated from many joint tissues, including trabecular (Jones et al., 2010) and cortical (G. Cox et al., 2012) bone and BM (Quirici et al., 2002; Jones et al., 2002; Bühring et al., 2007) and described as functionally and phenotypically similar.

The enumeration of MSCs extracted from both healthy and OA bone was therefore performed utilising the $CD45^{-}CD271^{+}$ phenotype in parallel to CFU-F assays. Enzymatic digestion of trabecular bone fragments from OA femoral heads released an abundance of $CD45^{-}CD271^{+}$ cells. This is in accordance with previous studies in our laboratory that showed a high number of $CD45^{-}CD271^{+}$ MSCs in the trabecular bone from OA femoral heads expressing the common MSC surface markers CD105, CD73 and CD90 (Jones et al., 2010). Data in this chapter showed that the proportion of $CD45^{-}CD271^{+}$ MSCs extracted from the OA femoral heads was 3.4-fold higher than in healthy iliac crest bone. This finding corroborates the CFU-F data and may be similar attributed to technical improvement of MSC extraction. However, there was only a 2-fold difference observed in the MSC frequency based on the CFU-F assay, which may be explained by the fact that not all CD271+MSCs form CFU-F, as previously reported (Cuthbert et al., 2012).

The differences between health and OA as well as inter-donor variability could be attributable to variations in the extent of damage of OA femoral heads. The heterogeneity of OA and the variable extent of associated bone damage has been well documented (Suri and Walsh, 2012; Burr and Gallant, 2012). Previous studies assessing the presence of MSCs in OA bone indicated no differences in comparison to healthy bone (Jones et al., 2010) although their numbers were later shown to increase with pathology (Campbell et al., 2016). However, the lack of repair observed in OA joints is not due to a decrease in MSCs population, which may explain the common addition of exogenous MSCs in cell-based therapies. Hence this evidence led to the assumption that MSCs presence in OA femoral heads were not altered. Data presented here showed that MSCs are present in higher in numbers in OA bone, which may be due to a pathological repair attempt. Previous work in our laboratory showed that MSCs were increased in areas of OA damage, specifically more MSCs were shown to inhabit areas affected by BM lesions in comparison to non-lesioned areas (Campbell et al., 2016).

3.5.2 Transcriptional profiling of native bone resident $CD45^{-}CD271^{+}$ MSCs in OA bone

While showing that OA trabecular bone harbours a higher concentration of MSCs relative to healthy bone, the questions still remain on how these MSCs participate in the attempted repair or contribute to the disease process and whether they inhibit or trigger the abnormalities associated with OA. To address this, the $CD45^{-}CD271^{+}$ MSCs purified by FACS were investigated at a transcriptional level for a more comprehensive characterisation of their native phenotype in both health and OA.

In addition to their surface phenotype that has been previously evidenced in several studies (Quirici et al., 2002; Jones et al., 2002; Bühring et al., 2007; Jones et al., 2010; Churchman et al., 2012), the transcriptional profile of the $CD45^{-}CD271^{+}$ cells and their MSC identity has also been previously described (Qian et al., 2012; Churchman et al., 2012; Ghazanfari et al., 2017), but in cells aspirated from healthy BM. In contrast, in this chapter the identity of MSCs extracted from the bone of healthy and OA donors was established by means of gene expression. In comparison to donor-matched HLCs, the MSCs extracted from healthy and OA bone and purified using the $CD45^{-}CD271^{+}$ phenotype showed a distinct gene expression signature specific to mesenchymal lineage and similar to BM MSCs (Churchman et al., 2012). Among the most specific MSC marker observed in this chapter, was SP7, also known as osterix. As a bone-specific transcription factor, SP7 is required for osteoblast differentiation and is therefore critical

for bone formation (Nakashima et al., 2002; Kaback et al., 2008). In both healthy and OA samples *SP7* was found to be expressed in $CD45^{-}CD271^{+}$ MSCs while in HLCs was completely absent in the healthy samples and at very low levels on only two out of 11 OA tested samples. Another robust marker was identified as *CXCL12*. Consistent with previous findings using BM MSCs (Churchman et al., 2012), the expression of *CXCL12*, a highly-expressed molecule characteristic of MSC stromal support activity (Greenbaum et al., 2013), was also significantly higher in MSCs compared to HLCs. All the other MSC markers were expressed in a distinct manner at significantly higher levels in MSCs compared to matched haematopoietic cells, confirming simultaneous osteogenic, adipogenic and haematopoiesis supporting transcriptional activity in bone resident $CD45^{-}$ $CD271^{+}$ cells, thus confirming, at the molecular level, their multipotential stromal nature.

A plethora of studies have been carried out on culture expanded MSCs isolated from various sources, although their native profile is still unexplored. Gene expression of native MSCs analysed in this chapter revealed an increased osteogenic commitment of MSCs from OA bone. This can be evidenced by the increased expression of several genes associated with osteogenesis and bone formation, including *RUNX2*, *ALPL*, *SPARC* and *CDH11*. This finding may provide a mechanistic explanation to the global increase in bone formation and sclerosis observed at the late stages of this disease (Burr and Gallant, 2012) considering the samples used here were from later-stage OA.

The first step in MSC lineage commitment and formation of osteoprogenitors is regulated by key transcription factors, such as *RUNX2* and *SP7* (osterix) (Nakashima et al., 2002) (Chapter 1, Section 1.3.2). This step involves expression of lineage inducing factors as well as inhibition of factors that maintain lineage plasticity. The initial progenitor are still bi-potential and can commit to either osteo- or chondro-lineage depending upon the threshold of *SOX9* and *RUNX2*/*SP7* (Nishimura et al., 2008). Compared to healthy MSCs, OA MSCs had significantly lower levels of *SOX9* (5-fold) while the levels of *RUNX2* and *SP7* were both elevated (8-fold and 2-fold, respectively). This indicated that the osteogenic commitment of OA MSCs was also supported by the higher levels of bone matrix markers and early osteoblasts, such as *CDH11* and *ALPL* (Anh et al., 1998; Ferrari et al., 2010) as well as *COL1A1*, *SPP1*, *SPARC* (osteonectin), which were also at higher levels to different degrees in OA MSCs compared to healthy IC bone controls. Therefore, a relatively higher expression of these genes in OA MSCS suggest a fairly appreciable bone anabolic activity supported by their osteogenic commitment. Histological studies would be needed to confirm at a protein level the association of abnormal bone formation

with the $CD45^{-}CD271^{+}$ MSCs investigated in this chapter. Further, immunohistological studies are needed to investigate the presence of MSCs in relation to new bone formation in OA femoral heads.

Age-related decreases in proliferation and osteoblast differentiation in human MSCs have been described (Zhou et al., 2008) therefore the increased osteogenic potential observed in MSCs in OA are unlikely to be influenced solely by the age of the patients, but more likely by the active and strenuous environment they reside in. Dominant aberrations within the MSC microenvironment may alter their gene expression and consequently the way MSCs modulate bone homeostasis and repair. MSCs reside in a highly interconnected niche (Isern and Méndez-Ferrer, 2011), interacting with all the other cells around them which are all subjected to the same physical stress exerted by a biomechanical disease like OA. In a mouse model of OA, Cao *et al*. described an increase in MSC numbers following OA induction which were recruited by the increase in TGF-β activated by bone resorption (Zhen et al., 2013) and led to aberrant bone formation. Data presented here revealed a similar increase in MSC numbers in OA bone and taken together with their osteogenic bias may suggest a similar mechanism in human OA, thus confirming the findings observed in the mouse models, although more work is needed in order to determine the triggers of these changes and how can the balance be re-established.

During skeletal development and throughout life, the cells in the bone compartment synthesize and secrete molecules that in turn initiate and control osteoclast differentiation (Teitelbaum, 2007). As described in Chapter 1, Section 1.2.3, OPG acts as a decoy receptor that binds to RANKL and prevents it from interacting with its receptor RANK, inhibiting osteoclastogenesis (Brendan F Boyce and Xing, 2007). Higher levels of OPG observed in OA MSCs in comparisons to their healthy counterparts described in this chapter suggest an MSC involvement in bone resorption inhibition in addition to their enhanced osteogenic commitment and anabolic activity. Although this finding comes as a supportive evidence of an exacerbated bone phenotype in OA, a more thorough investigation is needed, including an assessment of bone resorption activity in OA bone to assess the osteoclasts presence as well as more confirmatory experimental procedures that may directly implicate MSCs in bone resorption inhibition. Studies investigating the RANKL/OPG pathway in OA also suggested an altered expression of these molecules in OA subchondral osteoblasts (Kwan Tat et al., 2008), indicating an osteoblast lineage specific aberration in the expression of these molecules. It would be interesting to

investigate the levels of these molecules on the remaining line of MSC differentiation, the bone embedded osteocytes, as they have been described to be the main producers of RANKL (Xiong et al., 2015).

Another interesting finding in native OA MSCs was the low expression levels of *SOX9*, the major transcription factor inducible of chondrogenesis (Bi et al., 1999). Similarly, other molecules involved in cartilage formation were also lower, such as *UGDH* and *PAPSS*. Interestingly, an early study carried out by Murphy *et al.* reported that OA MSCs, even in locations remote from sites of damage, had reduced chondrogenic and adipogenic potential *in vitro* (Murphy et al., 2002).

These findings together with the reduced levels of many chondrogenesis molecules presented in this chapter point to an alteration in the commitment of MSCs in OA, with the switch locked into forming bone, rather than replacing the damaged cartilage. But very intriguing was the high level of aggrecan transcript (*ACAN*) observed in the OA MSCs, which encodes the proteoglycan, an integral part of cartilage tissue. This contrasts previous studies showing lower expression of *ACAN* in OA MSCs (Campbell et al., 2016), however this study was performed using cultured MSCs. In another *in vitro* study it was shown that *ACAN* expression can be induced by elevated TGF-β levels (Tuli et al., 2003). It is possible therefore to assume that this increase in *ACAN* observed in native OA MSCs may be due to an increase in the levels of TGF-β previously described by Cao *et al*. in the subchondral bone in OA mouse models (Zhen et al., 2013). As shown here and in other studies (Churchman et al., 2012; Ghazanfari et al., 2017) there are considerable differences in the gene expression levels between native and *in vitro* expanded MSCs, discussed in more detail in the next section.

Differences in the transcriptional profile between healthy and OA native MSCs described here may be due to the existence of a subpopulation within the $CD45^{-}CD271^{+}$ fraction which is increased in OA. It is already known that native $CD45^{-}CD271^{+}$ MSCs in the BM stroma reside in both endosteal and perivascular niches (Chapter 1, Section 1.3.2), the latter around the blood vessels, marked by the $CD271^{+}CD146^{+}$ MSC phenotype (Tormin et al., 2011). The increased levels of *MCAM,* which encodes the surface MSC marker CD146 (Tormin et al., 2011), observed in the OA native MSCs may indicate an increase in this particular MSC subset. This could be verified by FACS or flow cytometry by selecting for this population from the CD45-CD271+ MSC pool. Additionally, the expression levels of *ACTA2* was shown to be elevated in OA MSCs, a gene encoding the α-smooth muscle actin, known to be expressed by pericytes (Schmitt-Gräff et al., 1989;

da Silva Meirelles et al., 2008) as well as BM MSCs (Churchman et al., 2012) and the marrow sinusoidal pericytes that also express CD271 *in situ* (Cattoretti et al., 1993; Tormin et al., 2011). Given the increased angiogenesis and vascular invasion that has been described in OA bone (Findlay, 2007), an increase of a perivascular population of MSCs would not be surprising. More intriguing is their osteogenic commitment described here which still remain to be deciphered with regards to the causative mechanism behind it.

3.5.3 Culture-expanded MSCs

Using FACS directly after the enzymatic extraction of cells from the bone tissue allowed a pure population of MSCs to be obtained in comparison to the plastic adhesion method, where the waiting time to obtain comparable homogeneity was considerably high. Culture expanded MSCs provide heterogeneous progeny which do not faithfully reflect the properties of their native counterparts, alterations in the transcriptional and functional profile having been previously documented on BM MSCs (Churchman et al., 2012; Ghazanfari et al., 2017). These changes that occur between native and cultured cells may be due to the biochemical changes in the MSCs consequently to their adaption to *in vitro* culture conditions. While the cMSCs investigated in this chapter were not subjected to immunophenotyping using standard ISCT criteria (Dominici et al., 2006), the experimental methods were used in accordance with previous published literature. Multiple studies using culture-expanded cells showed that by using this isolation method (Chapter 2, Section 2.3.2) the cMSCs maintain their phenotype and multipotency as stated by the ISCT for more than four passages (Churchman et al., 2012; H. Li et al., 2016; Ghazanfari et al., 2017).

Previous published data documented transcriptional and phenotypic alterations following culture expansion in MSCs derived from healthy BM aspirate (Qian et al., 2012; Churchman et al., 2012; Ghazanfari et al., 2017). Results presented here are consistent and showed for the first time similar alterations in bone-resident MSCs, providing more evidence concerning the differences between native cells and their *in vitro* counterparts. The markers tested in relation to their osteogenic and adipogenic potential as well as stromal support, were all altered in culture in the same pattern, in MSCs from both healthy and OA bone. Comparison of culture-expanded cells between healthy and OA showed no differences with regards to the transcripts associated with MSC multipotential and stromal support activity, contrasting the distinct alterations observed in native cells. These alterations documented similarly in cultured MSCs isolated from healthy BM

(Churchman et al., 2012) showed the same transcripts changed under cultured conditions. Furthermore, the transcripts associated with bone remodelling encoding for RANKL and OPG have also been previously documented. Elevated levels of RANKL mRNA (Wagner et al., 2008) as well as decreased OPG (Churchman et al., 2017) showed similar changes following culture expansion of MSCs from healthy BM MSCs as documented in this chapter using bone-resident MSCs.

Irrespective of the site of extraction (bone or BM) or pathological state of the bone (healthy or OA), these MSCs suffer changes *in vitro* that should be taken into consideration in future studies and are not a good tool to study disease pathophysiology. Conversely, these changes may also be reversible as cMSCs can differentiate and upregulate these molecules following differentiation induction.

Chapter 4 Osteocytes in OA bone

4.1 Introduction

In the previous chapter, investigations were performed to uncover any potential abnormalities in MSCs resident in OA bone. The presented data showed that OA MSCs were proportionally increased, and that they had gene expression bias towards bone formation and inhibition of bone resorption. Furthermore, upon culture-expansion, important gene expression patterns were lost, emphasizing the drawbacks of culture-expansion methodologies in the study of mesenchymal-lineage cells. This chapter will investigate if MSC abnormalities have an impact on their most differentiated osteogenic – lineage progeny – osteocytes, and whether osteocyte pathology can also contribute to pathogenesis of OA.

4.1.1 Subchondral bone changes in OA and the role of osteocytes

As mentioned in Chapter 1, OA has a multifactorial anatomical (McGonagle et al., 2010) and pathogenetic basis (Martel-Pelletier et al., 2016). It is recognised as a disease of the whole joint and is characterised by pathological changes to cartilage, subchondral bone and the synovium (Lories and Luyten, 2011; Goldring and Goldring, 2016a). Irrespective of the site of initiation, subchondral bone sclerosis is an important feature in OA pathophysiology (Henrotin et al., 2012). Other changes in OA bone include alterations in overall shape, mineral density and bone remodelling rates, osteophyte formation, development of subchondral bone cysts and advancement of the tidemark with vascular invasion into the calcified cartilage (Goldring, 2008; Goldring, 2009; Burr and Gallant, 2012). Altered bone architecture and other signs of ongoing, or recent, bone remodelling activity were proposed as an early and very important events in OA (Lajeunesse and Reboul, 2003) particularly evident in BMLs (Zanetti et al., 2000), which are predictive of OA progression (Bowes et al., 2016). .

It is still not clear whether the bone abnormalities observed in OA are a consequence of the disease or a trigger. However, the interface between subchondral bone and the outer surface of the joint- including cartilage- is disrupted, which may allow the exchange of molecular signals that could influence the progression of the disease in both directions. It is also possible that abnormal mechanical loading on the joint is a critical factor affecting both subchondral bone and cartilage tissues simultaneously. This may lead to a combined effort of the bone derived cells to engage an endogenous repair mechanism which in OA seems to be unsuccessful.

The alterations in the subchondral bone that characterise the osteoarthritic process represent adaptations to local biomechanical and biological signals. These changes are mediated by bone cells that modify the architecture and properties of the bone through active cellular processes of modelling and remodelling (Goldring, 2009). Remodelling of microdamaged bone in both health and OA is essential for the maintenance of bone strength. The majority of studies into bone remodelling in OA have focused on osteoblasts (Couchourel et al., 2009), their parent: MSCs (Zhen et al., 2013; Campbell et al., 2016), and osteoclasts (Durand et al., 2013). However, there is a paucity of data on osteocytes in OA, which is surprising given that osteocytes are the most abundant and longest living bone cells (Boskey and Coleman, 2010).

Osteocytes play a cardinal role in bone mechano-transduction (Klein-Nulend et al., 2013) and are increasingly viewed as master regulators of the bone remodelling cascade (Prideaux, Findlay, et al., 2016). In an elegant study by Zhen *et al.* in a murine model of OA it was shown an increase of MSCs in the osteochondral areas in response to abnormal mechanical loading due to OA and furthermore, the inhibition of TGF-β in these MSCs attenuated the disease (Zhen et al., 2013). In this study it was hypothesised that the altered microenvironment induced by abnormal mechanical loading in OA may lead to "*in situ*" commitment of osteoprogenitors in the BM cavities (Zhen et al., 2013). Given the osteocytes function as mechano-sensors and master regulators of bone formation and resorption (Prideaux, Findlay, et al., 2016), these findings indicated that osteocytes may be acting as triggers of OA bone pathology and rises the awareness of the importance of the whole mesenchymal lineage in OA bone. Another study reported increased osteocytes death in OA (Jaiprakash et al., 2012) suggesting an altered OA osteocyte phenotype which may be a consequence of the disease progression and relates to an altered MSC phenotype described in Chapter 3 of this project and by others (Zhen et al., 2013; Campbell et al., 2016) which may influence their downstream progenies and vice-versa. However, the role of osteocytes in OA pathophysiology is still unexplored and more work is needed to understand the cellular mechanisms behind OA bone pathology.

4.1.2 Current methodologies for studying osteocyte biology in health and disease

While bone MSCs are easily accessible for direct study following enzymatic extraction and cell sorting as shown in the previous chapter, the study of osteocytes *in vivo* has proved challenging due to their location, embedded in the mineralized matrix. This makes them difficult to isolate and therefore other experimental approaches for their study have

been undertaken. Prior to the discovery of genetic markers specific to osteocytes, these cells were identified by their morphology and spatial relationships within bone. Osteocytes were defined by their location, which may translate into a lack of knowledge regarding their function.

Further on, the 'gold-standard' for the study of osteocytes nowadays is the use of *in vitro* cell lines, such as MLO-Y4 (Kato et al., 1997) or generation of *in vitro* surrogate cells (Thompson et al., 2015) and more recently, 3D cultures using differentiating osteoblastic cells into gel matrices (Sun et al., 2015) or the co-culture of osteoblasts on top of MLO-Y4 osteocyte cell line cultured in three dimensional collagen gels (Vazquez et al., 2014). Although these cultures likely give a better approximation of the natural environment of the osteocyte, they still require the use of cell lines or isolated cells, with all their limitations. In addition, gels do not exactly mimic the biochemical make-up of the matrix. These methods may be effective in generating a morphologically similar cell type, but it is unlikely that they resemble the *in vivo* phenotype of osteocytes, as the conditions where they exert their functions are largely different. As opposed to culture conditions, *in vivo* osteocytes reside encased in a mineralised matrix forming an interconnected osteocyte-canalicular cell network with a central and multi-functional role in regulating skeletal homeostasis (Bonewald, 2011). Mechanosensing is widely accepted as one of the principal function of osteocytes. This functionality places these cells as transducers of mechanical strains that are translated into biochemical signals with influence over the communication among osteocytes and between osteocytes and other bone cells, including the MSCs. Their location is a determinant of their three-dimensional shape, and thereby likely affecting their ability to sense mechanical signals and the communication within the lacuno-canalicular network as well.

Attempts to isolate osteocytes from mouse (Stern et al., 2012) and human bone (Prideaux, Schutz, et al., 2016) have been performed previously but the cell population remained impure. Without a specific cell marker, the population would contain other cell types from the surrounding microenvironment. Also, as native osteocytes are no longer able to divide, osteocytes cultures may quickly be overgrown by other cell types, limiting the useful life span of the culture. It remains to be shown to what extent osteocytes cultured in two dimensions on tissue culture plastic retain their complete osteocyte-like phenotype.

4.1.3 Osteocyte molecular markers

To assess the osteocyte purity and stage of maturation, a panel of genes has been proposed comprising classical osteocyte markers (Dallas et al., 2013) summarised in Figure 4.1.

The molecular signature of osteocytes comprises genes and proteins that control dendritic morphology and canaliculi formation, phosphate metabolism and matrix mineralization, bone formation and bone resorption (Plotkin and Bellido, 2016). Knowledge of this signature of osteocytes in their native state would allow a more direct and thorough examination of the molecular and cellular biology of these cells in the context of OA pathology.

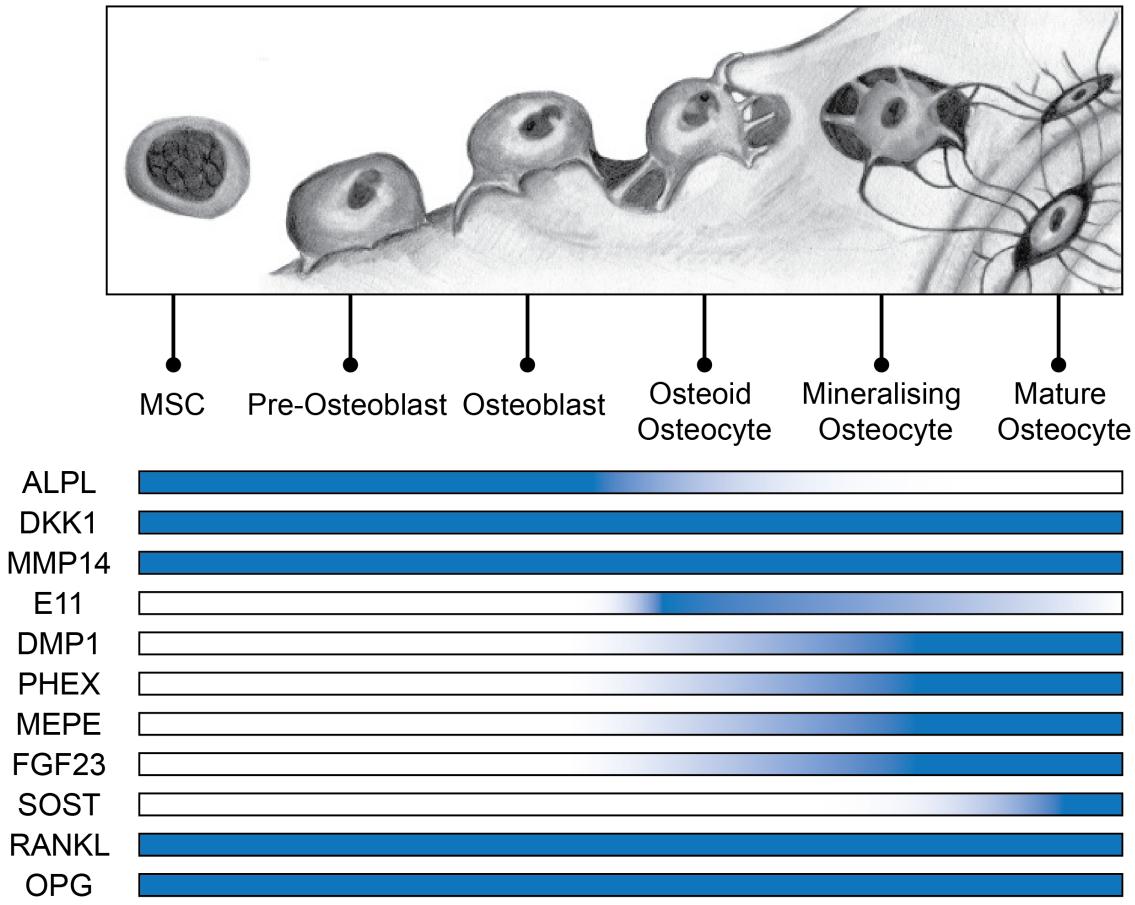

Figure 4.1. Osteocyte molecular signature during differentiation process. *As the osteoblast differentiate into embedding osteocytes a decrease expression of ALP concomitant with an increase expression of proteins associated with canalicular formation (E11, MMP14) is maintained in early osteocytes and decreases as they terminally differentiate. During the maturation process osteocytes secrete Wnt pathway inhibition (DKK1, SOST) and paracrine phosphate regulation (FGF23). Cytokines responsible for bone resorption activation (RANKL) or inhibition (OPG) are also secreted at all stages of differentiation. MEPE, PHEX and DMP1 are proteins responsible for mineralisation process and are expressed at more mature stages. SOST is exclusively expressed by mature osteocytes. Adapted from (Compton and Lee, 2014).*

Osteocyte's osteoblastic origins are well recognised (Aubin and Turksen, 1996), however while in their mature stage of differentiation the nature of the relationship between osteocytes and their mesenchymal ancestry, the MSCs is still unclear. Osteocyte-specific molecules start being expressed once the osteoblasts stop actively producing bone matrix and they become entrapped within the formed osteoid where they differentiate into osteocytes (Dallas et al., 2013). As discussed in Chapter 1, Section 1.4.1, approximately 10-20% of the osteoblasts continue their differentiation process to osteocytes, while some are cleared by apoptosis or become quiescent bone lining cells (Miller et al., 1989; Aubin and Turksen, 1996), however the determinant behind osteoblasts' fate it is still unknown.

Osteocytogenesis is not a passive process, on the contrary, is invasive and requiring the cleavage of collagen and potentially other matrix molecules (Karsdal et al., 2004). Holmbeck *et al*. showed that the dramatic morphological changes during the initial embedding are facilitated by MMP14, also known as MT1-MMP. This membrane bound matrix metalloproteinase is required for the development of the dendritic processes as they protrude in the newly forming osteoid (Holmbeck et al., 2005). One of the earliest molecules also demonstrated to be responsible for the cytoskeletal changes during osteocytic differentiation is E11, also known as podoplanin. This transmembrane glycoprotein was shown to be responsible for dendrite elongation in response to mechanical strain (Zhang et al., 2006). E11 has been proven by various studies to play an essential important role in osteocyte formation. E11 is highly expressed during the transition from osteoblast to the nascent osteocyte concomitant with matrix mineralisation and the formation of dendritic processes (Staines et al., 2016). E11 expression was demonstrated by an *in vitro* study using the MLO-Y4 osteocytic cell line to be intimately modulated by the extent of mineralisation of the extra cellular matrix, revealing the importance of the interaction between the cells and the matrix they reside in (Prideaux et al., 2012). The mineralization of the extracellular matrix proved therefore essential for terminal osteoblast differentiation to the osteocyte phenotype. Studies in mice also showed that conditional deletion of this protein in bone leads to a disrupted osteocyte network and shorter dendritic processes (Staines et al., 2017).

Osteocytes express molecules with important roles in mineralisation and phosphate metabolism, such as dentin matrix protein 1 (DMP1), phosphate-regulating neutral endopeptidase on chromosome X (PHEX) and matrix extracellular phosphoglycoprotein (MEPE). DMP1 is required for osteocytes maturation and bone mineralisation (Rios et al., 2005; Feng et al., 2006). DMP1-null mice displayed a defective bone mineralisation

accompanied by an altered osteocyte phenotype, with increased expression of osteoblastic and early osteocyte genes in mature osteocytes as well as lack of sclerostin expression (Rios et al., 2005). Although the exact function of PHEX has not yet been elucidate, mutations in either DMP1 or PHEX were associated hypophosphatemic rickets and elevated levels of fibroblast growth factor 23 (FGF23) (Feng et al., 2006). Osteocytes have also been described as exerting endocrine functions through the actions of FGF23 (Dallas et al., 2013), mainly expressed by osteocytes (Yoshiko et al., 2007). Factors secreted by osteocytes act in concert not only to regulate skeletal mineral homeostasis locally, but also to control serum phosphate levels systemically by actions on the kidney. The most direct link between osteocytes and the kidney is provided by FGF23, a phosphaturic hormone produced by osteocytes that acts on kidney tubule cells to suppress tubular phosphate reabsorption (Riminucci et al., 2003).

4.1.4 Osteocytes roles in bone resorption and formation

Osteocytes play a central role in bone remodelling (Prideaux, Findlay, et al., 2016). Their contribution to bone resorption has been documented by numerous studies. One of the means by which osteocytes modulate bone resorption is through their death. Osteocyte apoptosis can occur at sites of microdamage and it was proposed that dying osteocytes are targeted for removal by osteoclasts (Verborgt et al., 2002). Apoptotic osteocytes release signals to stimulate the remodelling of the bone at specific sites and time points (Manolagas, 2006). Such signals include the osteoclastogenesis activator, RANKL that binds to precursor and mature osteoclasts, which stimulates their differentiation, function and survival (Nakashima et al., 2011), as discussed in Chapter 1, Section 1.2.3. Osteocytes also produce the main inhibitor of RANKL; OPG, and the ratio of RANKL to OPG at a particular location determines the magnitude of bone resorption at that site (O'Brien et al., 2013).

Emerging evidence also supports the idea that osteocytes actively participate in bone resorption by remodelling the lacunae in which they reside (Wysolmerski, 2012), a process known as osteocytic osteolysis. Osteocytes lacunae of lactating mice were shown to be larger during lactation and it comes back to normal after lactation in both cortical bone and trabecular bone (Qing et al., 2012). It was also shown that osteocytes express genes that osteoclasts use for resorption, including Acid Phosphatase 5, Tartrate Resistant (ACP5, commonly known as TRAP) and cathepsin K (CTSK) and these genes are significantly increased during lactation and decrease after (Qing et al., 2012). Enlarged perilacunar matrix was also found increased and shown to be remodelled by osteocytes

during stress, such as glucocorticoid treatment (Fowler et al., 2017). By perilacunar remodelling osteocytes dynamically resorb and replace the surrounding perilacunar bone matrix to maintain mineral homeostasis (Fowler et al., 2017) although this process in OA have not been investigated yet. Osteocyte-mediated bone resorption may represent an attractive therapeutic target to delay or prevent the development of OA as well as other associated bone conditions.

At the same time, osteocytes have also been recognised for their role in controlling bone formation by their production of *SOST* (van Bezooijen et al., 2004) and *DKK1*, another Wnt inhibitor, which was also reported to contribute to osteophyte formation in OA (Diarra et al., 2007; Weng et al., 2010). When sclerostin binds to the LRP5/6 and Frizzled co-receptors on the cell surface of osteoblasts, Wnt/β-catenin signalling is inhibited (Li et al., 2005), thereby inhibiting osteoblast differentiation, proliferation, and activity, resulting in reduced osteoblastic bone formation (Li et al., 2008). Both *SOST* and *DKK1* have been recently shown to be implicated in OA subchondral bone changes (Weng et al., 2010; Zarei et al., 2017; Jia et al., 2018) and limited data also suggests their important role in osteocyte survival or apoptosis in human OA bone pathology (Jaiprakash et al., 2012). A recent study showed that the low levels of sclerostin induced by mechanical loading in severe late-stage OA in mice as well as the elevation of bone formation in the subchondral plate are the major mechanisms characterizing subchondral bone phenotypes observed in this murine model of OA (Jia et al., 2018).

Emerging evidence from animal models and *in vitro* studies revealed critical functions of osteocytes in bone homeostasis and consequently there are indications of their potential involvement in bone associated pathologies. However, the biology of human osteocytes and especially their implication in OA is currently unexplored. More work is needed for a better understanding of their *in vivo* biology and the crosstalk with their progenitors, the MSCs.

4.2 Chapter aims

1. To establish robust gene markers for human native osteocytes and to test their specificity by comparing their expression with donor-matched MSCs.
2. To investigate the gene expression signature of osteocytes in OA bone in comparison to healthy IC control bone
3. To document the topographic relationships between MSCs and osteocytes in OA femoral head bone, and in relation to disease associated pathology.

4.3 Methods

To avoid culture manipulations, the bone treatment procedure was developed to simultaneously obtain pure osteocyte-enriched fragments and matched native $CD45^-$ $CD271^+$ MSCs (Chapter 2, Section 2.2). The enzymatic extraction of MSCs was described in Chapter 2, Section 2.2.1. The remaining bone fragments following this procedure were further used for RNA isolation from native osteocytes and to confirm their purity by gene expression and histology.

4.3.1 Patient samples

The bone samples obtained following the MSC extraction procedure described in Chapter 3 were used in parallel for osteocyte-enrichment during this study. For all the experiments in this chapter a total number of n=30 OA donors (12 males and 18 females) with age range between 40-90 years (median=72) and n=19 healthy donors (10 males and 9 females) with age range between 17-78 years (median=55) were recruited. The osteocytes-enriched bone fragments were obtained from control IC bone biopsies of n=11 healthy donors and from n=9 OA femoral heads and used for gene expression analysis. In addition, healthy (n=6) and OA (n=11) sorted MSCs and HLCs which were obtained following MSC isolation described in Chapter 3 were used here as controls for gene expression analysis along with the osteocytes-enriched bone fragments. Amongst these samples, total number of 5 samples were donor matched for MSCs, HLCs and osteocytes (n=2 IC and n=3 OA). While IC bone was used as healthy control for experiments in this chapter, recent published literature (Ilas et al., 2019) provided supportive evidence of its suitability and comparable gene expression for both osteocytes and MSCs.

For histological studies a total of n=4 OA femoral head samples were used while n=3 healthy IC were used as control bone. The samples used for histology in some cases were different from the ones used for MSC extraction and osteocyte-enrichment. The healthy IC bone specimens obtained from surgery were not sufficient to perform both experiments while some femoral heads were used as whole only to have a global (macroscopic) view of hip OA pathology.

4.3.2 Sample processing to produce osteocyte-enriched bone fragments

As described in Chapter 2, Section 2.2, the enzymatic treatment during MSC extraction procedure was first optimised to remove most of the cellular material from the bone surfaces while the osteocytes remained embedded in the bone. For this, the denuded bone fragments were washed repeatedly with sterile PBS to remove any contaminant tissue.

The bone fragments were distributed equally in conical tubes (approximately 5g in each tube) with 15ml of sterile PBS and shaken rigorously to dislodge any remaining soft tissue in the trabecular cavities. After every wash, organic residue consisting of fat, blood clots and other stromal tissue was cleared away leaving the PBS of clear appearance. At this stage the bone fragments were visibly clean of any residual tissue and they were clear white in appearance (Figure 4.2). Some of the bone fragments were used for RNA isolation (approximately 1g for each RNA isolation procedure) while the rest were placed in 3.7% PFA for overnight fixation and used for histological validation of this method.

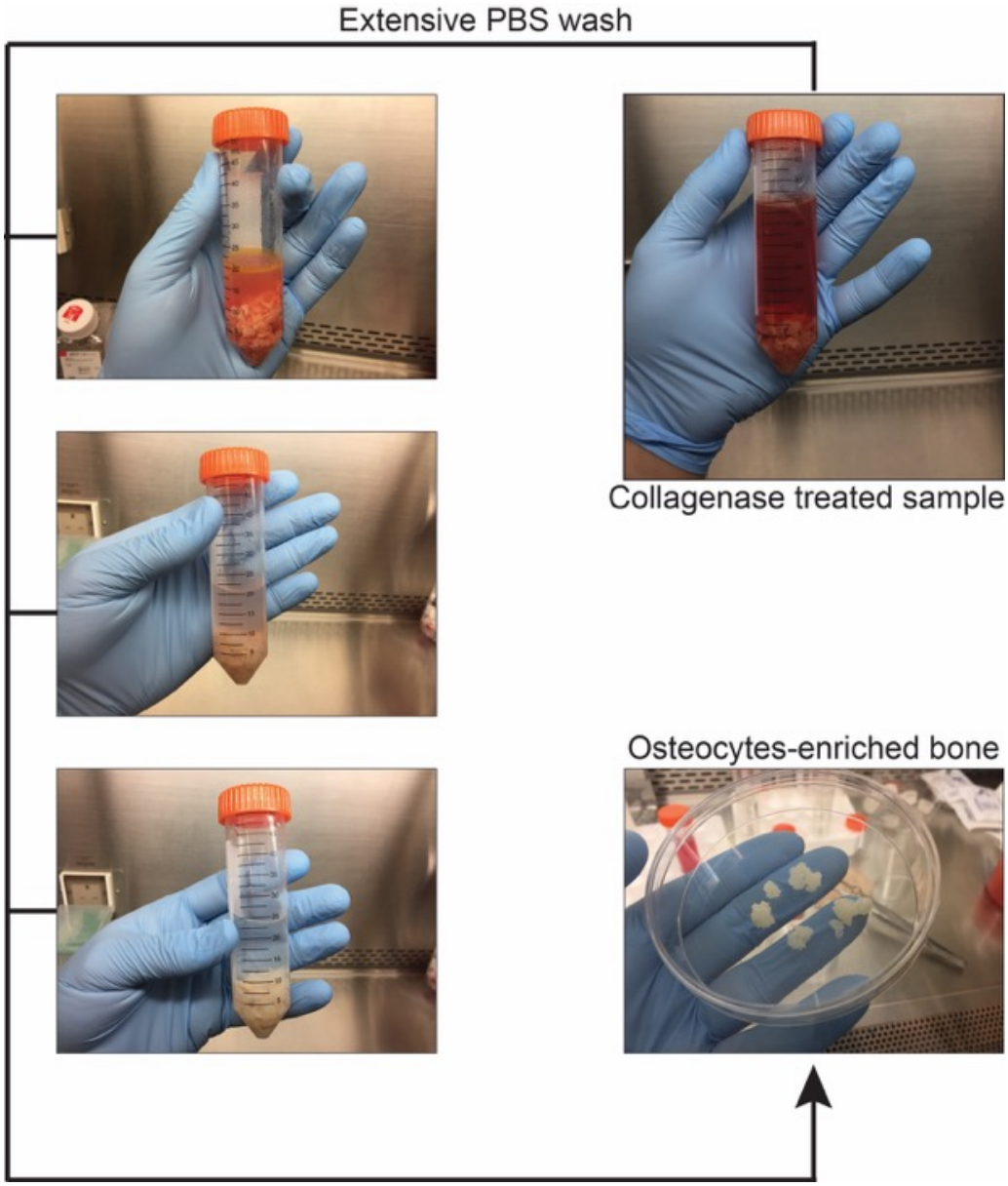

Figure 4.2. Bone processing for osteocytes enrichment. *The remaining bone fragments following enzymatic treatment were further depleted of all soft tissue by extensive PBS washes. After each wash the residual tissue cleared away until the bone was white in appearance. The bone fragments were lysed in situ for RNA extraction from osteocytes.*

4.3.3 Osteocytes-enriched bone RNA isolation and gene expression

As described in Chapter 2, Section 2.2 and 2.5, osteocyte-enriched bone obtained following collagenase digestion and osteocyte enrichment procedure from healthy IC and OA femoral heads were used for RNA isolation and subsequent gene expression analysis. To extract pure native osteocyte RNA, the tissue-denuded bone fragments were homogenised in Guanidine isothiocyanate (GITC) lysis buffer (GITC solution containing 0.4% sodium citrate, 1% N-lauryl sarcosine and 0.5% β-mercaptoethanol, Appendix 1). The bone fragments were homogenised by using a pipette tip or scalpel with a number 10 blade to break the fragments into the smallest sizes and allow the lysis buffer to penetrate the bone chips and lyse the osteocytes *in situ*. The lysate was immediately transferred to 1.5ml centrifuge tubes and kept at -80 ºC until RNA isolation was performed.

Total RNA was extracted as outlined in Chapter 2, Section 2.5.1 using an adaptation of the previously described method by Chomczynski and Sacchi (Chomczynski and Sacchi, 1987) and summarised in Figure 4.3. After homogenisation, the samples were mixed with an equal volume of acid phenol (pH 5, Sigma), 0.1 volume of 2M sodium acetate (Sigma) and 0.2 volume of chloroform : isoamyl alcohol (24:1, Sigma) and let to settle on ice for 10 minutes. The tubes were then centrifuged at 4 ºC and 15000 g for 30 minutes. The aqueous phase formed (Figure 4.3) was carefully retained without disrupting the interphase and transferred into a new tube. The RNA was precipitated by adding an equal volume of isopropanol and incubated at -80 ºC for 2 hours or at -20 ºC overnight, followed by DNase (Invitrogen) treatment as described in Section 2.2.1. Total RNA was pelleted down with 5 minutes centrifugation at 15000 g at 4 ºC and resuspended in 50 µl of RNase free water. After quantification with Nanodrop the RNA was stored at -80 ºC.

The isolated RNA was used to synthesize first-strand cDNA using the High-Capacity cDNA Reverse Transcription Kit (Applied Biosystems) described in Chapter 2, Section 2.5.2. qPCR was performed on a QuantStudio™ 7 Flex Real-Time PCR System (Applied Biosystems) as described in Chapter 2, Section 2.5.3 using the same cycling conditions. The gene expression levels were normalised relative to housekeeping gene *HPRT1* and calculated using the $2^{-\Delta Ct}$ method similarly to all experiments in this study. The TaqMan probes for the genes of interest used for these experiments are detailed in Appendix 4, all from Thermo Fisher.

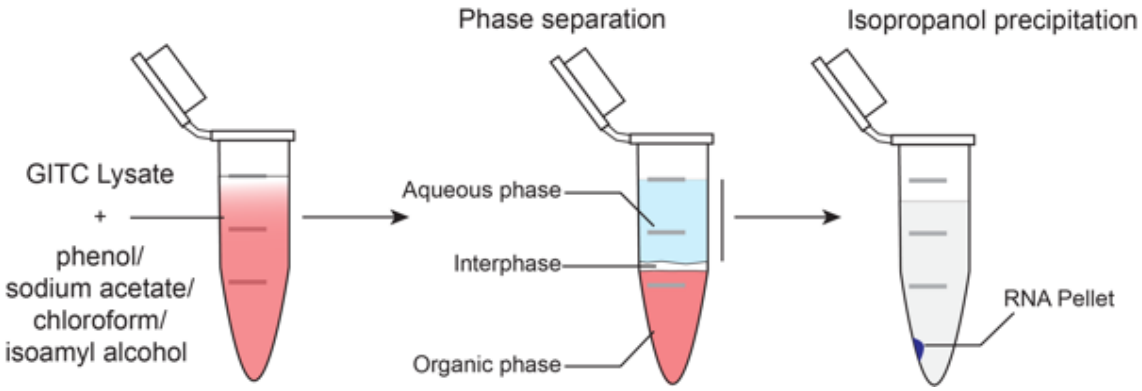

Figure 4.3. Schematic representation of the RNA isolation from osteocytes-enriched bone. *The tissue lysate was mixed with phenol:chloroform:isoamyl alcohol (25:24:1 ratio) and allowed to settle. After 30 minutes' centrifugation, the mixture separated into different layers (phases) based on density gradient. The upper aqueous phase containing the RNA was carefully removed and mixed with an equal volume of isopropanol for RNA precipitation.*

4.3.4 *In vitro* method validation

Since the principal function of osteocytes is to sense and respond to mechanical forces it was hypothesised that the mechanical processing of the bone prior to collagenase treatment may affect the gene expression of these cells. To assess whether the mechanical stimulation of the bone fragments affected the gene expression levels of the embedded osteocytes, an *in vitro* assay was developed (Figure 4.4). The principle of this experiment was to allow the bone fragments to rest in culture and then mechanical stimulation would be applied by means of breaking down the bone in a similar manner as per the processing protocol described above. Bone fragments from different time points and with or no mechanical stimulation were homogenised for RNA extraction and gene expression analysis.

Following enzymatic digestion and osteocytes-enrichment as described above, bone fragments from three donors were placed in 60 mm culture dishes with 3 ml of DMEM supplemented with 10% FCS and 1% P/S. After one day in culture, bone fragments were considered at rest. Approximately 100 mg of bone fragments were washed thoroughly with PBS and lysed for RNA isolation with no manipulation, straight from culture. Same weight of bone was then mechanically broken down to smaller fragments and then homogenised and lysed for RNA extraction. Similarly, RNA was isolated at Day 7 before and after mechanical stimulation and samples were all further analysed for gene expression using the osteocyte-specific gene markers.

Bone fragments from each time point were also tested for cell viability using a live/dead staining kit (Thermo Fisher) and viewed with a confocal microscope (Nikon A1R). Intracellular esterase activity and an intact plasma membrane are distinguishing characteristics of live cells. This kit was used to discriminate live from dead cells by simultaneously staining with green-fluorescent calcein to indicate intracellular esterase activity and red-fluorescent ethidium homodimer-1 to indicate loss of plasma membrane integrity. The bone fragments (100 mg or less) were washed with PBS and incubated for 1 hour with 4 μM calcein (Thermo Fisher) and 8 μM ethidium homodimer-1 (Thermo Fisher) in 1ml of sterile PBS in the dark at room temperature. After a brief wash in PBS the bone fragments were examined with a confocal microscope Nikon A1R by using the 488 nm laser line to detect calcein (green) and the 647 nm laser line for ethidium homodimer-1 (red). The background levels were negligible or completely absent because both stains fluoresce only in contact with the cells. The images were captured and generated using the integrated software, Nikon Elements (Nikon).

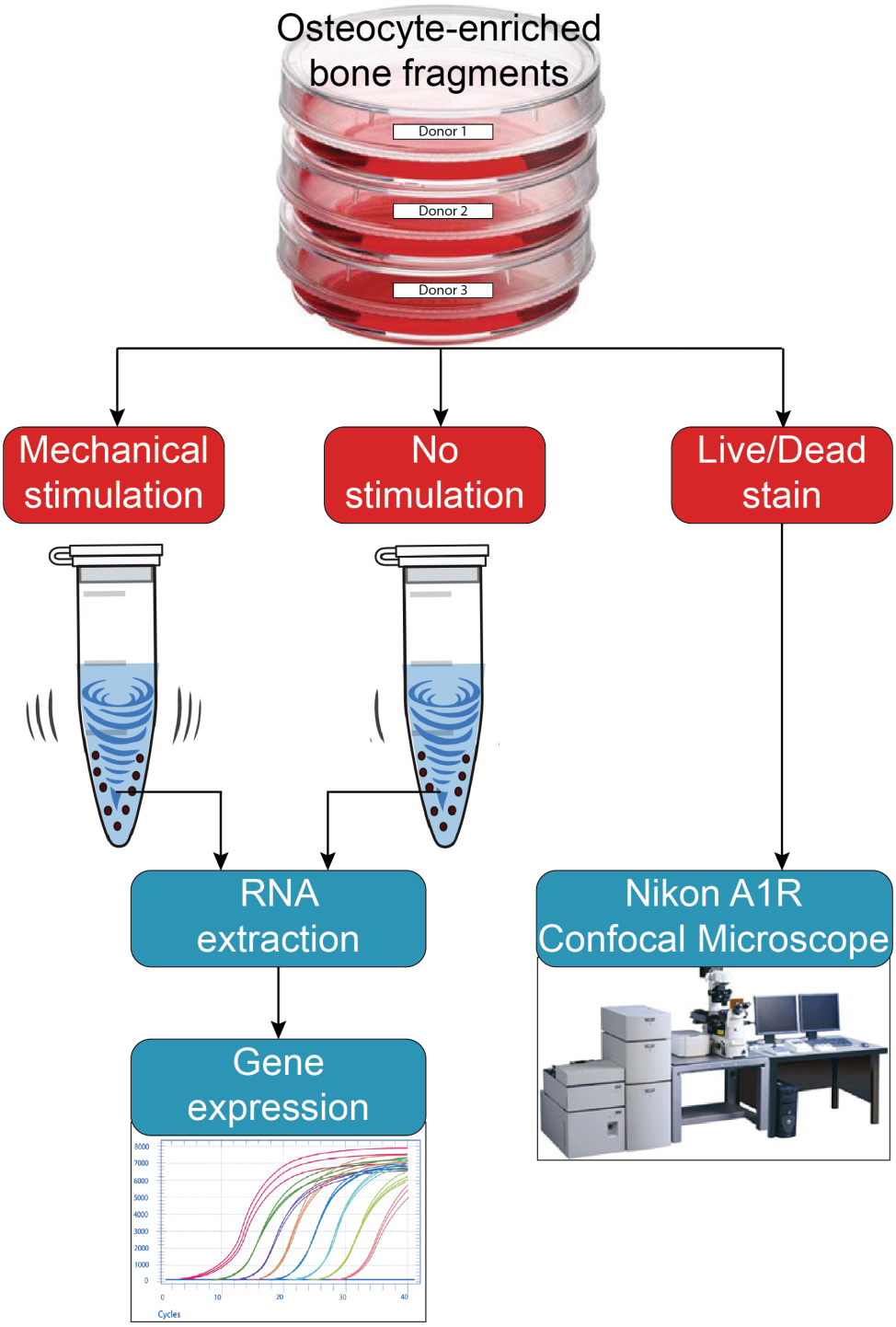

Figure 4.4. Schematic illustration of experimental setup for in vitro culture of osteocyte-enriched bone fragments. *Bone fragments from n=3 OA donors were split into fractions at two different time-points following culture, at Day 1 and Day 7 respectively. At each time point bone fragments from one fraction were homogenised in RNA lysis, second fraction was broken down (mechanically stimulated) and then homogenised in RNA lysis and the third fraction was stained with live/dead stain which was further visualised using a confocal microscope. Both first and second fractions were processed for gene expression analysis by qPCR.*

4.3.5 Histology

Osteoarthritic femoral heads (n=4) and IC bone fragments (n=3) were fixed in PFA and decalcified in EDTA as described in Chapter 2 Section 2.6.1. Decalcified bone sections (5 μm thick) were used for immunohistochemistry or stained with HE, Safranin O and fast green, and TRAP.

4.3.5.1 Haematoxylin and Eosin

Tissue samples from bone fragments used in MSC extraction and osteocyte-enrichment were used for HE staining to assess the complete soft tissue removal from the bone fragments. Bone samples were collected before any enzymatic treatment and after the osteocyte-enrichment procedure. All the collected bone fragments were fixed and decalcified as described in Chapter 2, Section 2.6.1. Additionally, whole femoral heads were decalcified and embedded in large cassettes in order to provide a global view of hip OA, as described in Chapter 2, Figure 2.8. Slides with 5 μm tissue sections were deparaffinised and rehydrated as described in Chapter 2, Section 2.6.2. The slides were then transferred to Harris Haematoxylin (Sigma) for 2 minutes after which they were cleared with tap water for 1 minute. To perform the ‘blueing’ of the nuclei the slides were placed in Scott’s tap water for 2 minutes and washed in running tap water then immediately immersed in Eosin-Y solution for another 2min. After washing in tap water for 1 minute the slides were dehydrated and cleared in Xylene. The samples were then mounted with DPX medium (Sigma) and dried at room temperature before visualizing under light microscope.

4.3.5.2 Safranin O

Safranin 'O' was used for the detection of articular cartilage and its distinct separation from the bone tissue, as well as to evaluate any pathological changes in relation to disease. The intensity of safranin 'O' staining is directly proportional to the proteoglycan content in the cartilage while Fast green provides a clear contrast to the Safranin O staining. For this method Safranin O solution was prepared at 1% in distilled water by dissolving 2.5g of Safranin O powder (Sigma) in 250ml dH2O. Following deparaffinisation and rehydration, the slides were incubated in Weigert’s Iron Hematoxylin solution (Sigma) for 5 minutes followed by immersion for 2 seconds in 1% Acid Alcohol (1% HCl in 80% ethanol) to remove excess stain and define the nuclei. Slides were then counterstained in 0.02% Fast Green for 1 minute and cleared in 1% Acetic acid for 30 seconds. The slides were then incubated for 10 minutes at room temperature in Safranin O solution and rinsed

briefly in absolute ethanol. Slides were dehydrated and cleared in xylene then mounted with DPX.

4.3.5.3 Tartrate resistant acid phosphatase staining

To detect osteoclast activity, TRAP staining was performed histochemically. The enzyme TRAP is expressed by osteoclasts during the process of bone resorption. The stain utilises Fast Red (Sigma) as a chromogenic substrate and tartrate with an acidic pH (pH 4.7-5) which relies on the chemical interaction between the cells expressing the enzyme and tartrate combined with a chromogenic substrate. The TRAP staining solution mix was prepared fresh, before every staining procedure, by dissolving 0.06% Fast Red Violet LB salt (Sigma) and 0.01% Naphthol AS-MX Phosphate in 200ml of already made TRAP basic incubation media (0.2 M sodium acetate and 50 mM L (+) tartaric acid in dH2O, pH 5.0). Paraffin sections of 5 μm thickness were deparaffinised in three changes of xylene (3 min each) and rehydrated (3 changes 95% ethanol, 3 min each; 1 change 75% and 50% ethanol each 3 min, dH2O for 2 min). After rehydration, samples were placed in pre-warmed TRAP staining solution mix for 30 min at 37ºC or until osteoclasts appeared bright red. Subsequently sections were rinsed with dH2O and counterstained with 0.02% Fast Green. Fast Red salt is soluble in ethanol therefore common graded ethanol dehydration was avoided and the slides were air dried overnight instead and mounted with aqueous Leica CV Ultra mounting media (Leica) the next day. Slides were scanned as described in Chapter 2 Section 2.6.4 and staining analysed in regions of bone sclerosis compared to non-sclerotic regions.

4.3.6 Immunohistochemistry

Immunohistochemistry staining was performed using the EnVision+ Dual Link System-HRP (DAB+) (DAKO) as described in Chapter 2, Section 2.6.3. The antibodies used for this study were against CD271 (1:100, clone NGFR5, Abcam), E11 (1:200, clone NZ1, Merck Millipore), OPG (1:500, polyclonal, Abcam), RANKL (1:500, polyclonal, Abcam) and CTSK (1:300, Proteintech). Endogenous peroxidase activity was blocked for 10 minutes by enzyme blocking solution (DAKO kit) and non-specific binding was blocked for 30 minutes using antibody diluent (DAKO). Tissue slides were then incubated with primary antibodies for 1 hour and secondary antibody for 30 minutes. The secondary antibody consisted of a labelled-polymer horse radish peroxidase (HRP) which was applied first for 30 minutes followed by 10 minutes incubation with 3,3'-diaminobenzidine tetra hydrochloride (DAB) (both included in the DAKO kit). DAB reacts with HRP forming an insoluble brown-coloured precipitate at locations where

labelled-polymer HRP is bound to primary antibodies. The slides were then counterstained with haematoxylin for 2 minutes and mounted using DPX media. The optimal concentration of primary antibody was determined in dilution series on test tissue sections. No primary antibody was used as negative control; these slides were incubated with antibody diluent alone.

Slides were scanned on Leica Aperio AT2 up to an original magnification of ×20 and images were captured using Aperio Imagescope (Leica) as described in Chapter 2 Section 2.6.4. Semi-automatic counting of E11-positive osteocytes was performed within a defined bone area and region of interest from OA femoral head sections from n=3 donors, using a minimum of 10 regions per patient. Percentage of positive osteocytes from total number of osteocytes per region analysed was calculated to determine the number of early/immature osteocytes in sclerotic and non-sclerotic areas of hip OA. The abundance of CD271-positive MSCs was assessed as percentage of positively stained area within a defined trabecular bone cavity area and region of interest, using a minimum of 10 regions per patient as described in Chapter 2, Section 2.6.5. This quantification was performed to ascertain the abundance of CD271-positive MSCs in sclerotic and non-sclerotic regions of hip OA, similarly to E11. No quantification was performed for OPG, RANKL and CTSK, the expression of these proteins was analysed qualitatively in regions of bone sclerosis and compared to non-sclerotic regions and healthy IC.

4.3.7 Statistics

The statistical analyses for gene expression experiments were performed using Mann-Whitney test for comparisons between two groups and Wilcoxon for matched paired data between two groups. Kruskal-Wallis analysis was employed for intergroup differences, corrected with the Bonferroni-Dunn multiple-group comparison. For the immunohistochemistry experiments, the statistical analysis for area quantifications included Mann-Whitney test for comparisons between the sclerotic and non-sclerotic areas for each patient.

Results are presented as scatter dots plots with medians or box and whisker plots; with boxes representing interquartile range, and whiskers representing the maximum and minimum values, calculated using GraphPad Prism version 7 software. Results were considered significantly different at $p < 0.05$ (with significance level denoted as $*p < 0.05$, $**p < 0.01$, $***p < 0.001$ and $****p < 0.001$).

4.4 Results

4.4.1 Preparation of osteocyte-enriched bone fragments

In order to investigate the gene expression profiles of native human osteocytes a protocol was first optimised to extract RNA from pure native osteocytes, depleted of any contaminating cells present on the bone surfaces and BM cavities. To test its purity, the gene expression was analysed and compared to their MSC progenitors. Therefore, a protocol for the simultaneous preparation of osteocyte-enriched bone and donor-matched, pure uncultured MSCs from that same bone was first optimised derived from the already established method used for MSC extraction described in Chapter 3, Section 3.3.2.

Histological examination of the bone fragments following osteocyte enrichment was employed to visually assess the complete removal of cellular material from the bone surface. The aim was to keep the osteocytes embedded in the bone as the only cellular material in the denuded bone fragments.

Haematoxylin-eosin stained trabecular bone before enzymatic treatment showed a delicate meshwork of bony trabeculae covered by bone-lining cells in which the highly cellular BM tissue resided (Figure 4.5A). Following collagenase treatment and extensive PBS washes, the stromal tissue and bone lining cells were completely removed from the trabecular cavities, with only occasional cells remaining attached to the bone surface in small deep pores (Figure 4.5B). These bone fragments were further washed with PBS to ensure complete removal of bone lining cells leaving only embedded osteocytes as the remaining cellular material (Figure 4.5C, D). This osteocyte-enriched bone was subsequently used for gene expression analysis.

To obtain a better view over the osteocyte's phenotype, their gene expression was compared to the MSCs and HLCs extracted from the stromal compartment following the collagenase digestion and purified by FACS, as described in Chapter 2, Section 2.4. The analysis was therefore performed using the osteocytes-enriched bone in comparison with the donor matched MSCs (CD45-CD271+ cells), while HLCs (CD45+CD271- cells) were used as a control non-mesenchymal lineage population.

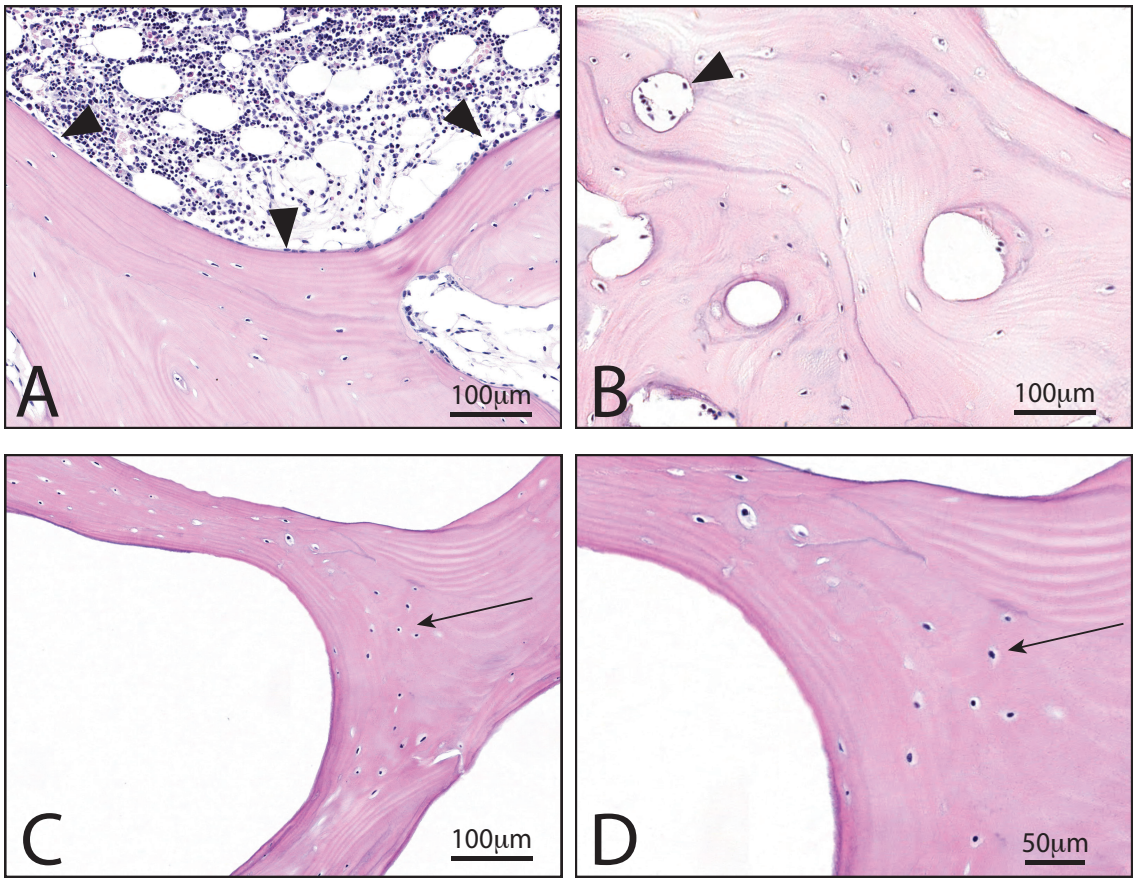

Figure 4.5. Haematoxylin and Eosin staining of trabecular bone illustrating the generation of osteocyte-enriched bone fragments. *(A) Histological appearance of the bone trabeculae and BM tissue before processing. (B) After collagenase digestion, most of the marrow tissue, containing the MSCs, was removed by the enzymatic digestion, with minimal cells remaining in the deep pores of the bone. (C) Bone trabeculae showing the complete removal of residual bone lining cells by the extensive washes. (D) Higher magnification photomicrograph showing osteocytes embedded in the bone matrix as the only visible cellular material left following enzymatic digestion and extensive wash. Arrow heads: stromal cells, arrows: osteocytes. Sample ID: DIFHOA010*

4.4.2 Expression of osteocyte-specific genes in osteocyte-enriched bone and MSCs

To assess osteocyte enrichment following the above procedure, gene expression analysis was first conducted on healthy IC bone followed by OA femoral head bone. The first aim of the gene expression analysis performed in osteocytes and MSCs was to verify osteocytes identity based on specific osteocyte markers as described in Section 4.1.3 and secondly to assess the potential alterations that occur in OA bone. The HLCs fraction was used as negative control population for the mesenchymal lineage cells.

In addition to the selected osteocytes markers, three MSCs markers used previously in Chapter 3, *CXCL12, ALPL* and *SP7*, were also selected as specific for MSCs and to serve therefore as negative markers for osteocytes.

In the RNA from IC bone, as expected, the expression of classical late osteocytes markers *SOST*, *DMP1, MEPE* and *PHEX* was higher in osteocyte-enriched bone compared to purified MSCs (Figure 4.6A). *SOST* and *PHEX* were particularly low in MSCs (detectable only in 1 out of 6 tested samples) and could therefore be considered the most differentially-expressed molecules between osteocytes and MSCs. *DMP1* and *MEPE* were also confirmed to be osteocyte specific, being 60-fold ($p=0.002$) and 18-fold ($p=0.013$) higher, respectively, in osteocytes compared to MSCs. Apart from *PHEX,* all other tested osteocyte-specific transcripts were expressed at considerably lower levels in HLCs, confirming their mesenchymal lineage specificity (Figure 4.6A). The expression of *FGF23*, *E11* and *DKK1* in osteocytes compared to MSCs failed to reach statistical significance, although a trend for lower expression in MSCs was observed (Figure 4.6A).

In respect to the selected native MSC specific molecules, these were tested here for the first time in native osteocytes. Compared to MSCs, osteocytes expressed lower levels of all three MSCs specific transcripts *CXCL12, ALPL* and *SP7*, in line with their more mature differentiation stage (Figure 4.6B). However, these differences were not as large as those between MSCs and HLCs, consistent with anticipated differences between cells of different lineages (MSCs and HLCs) and cells representing different maturation stages within the same lineage (MSCs and osteocytes).

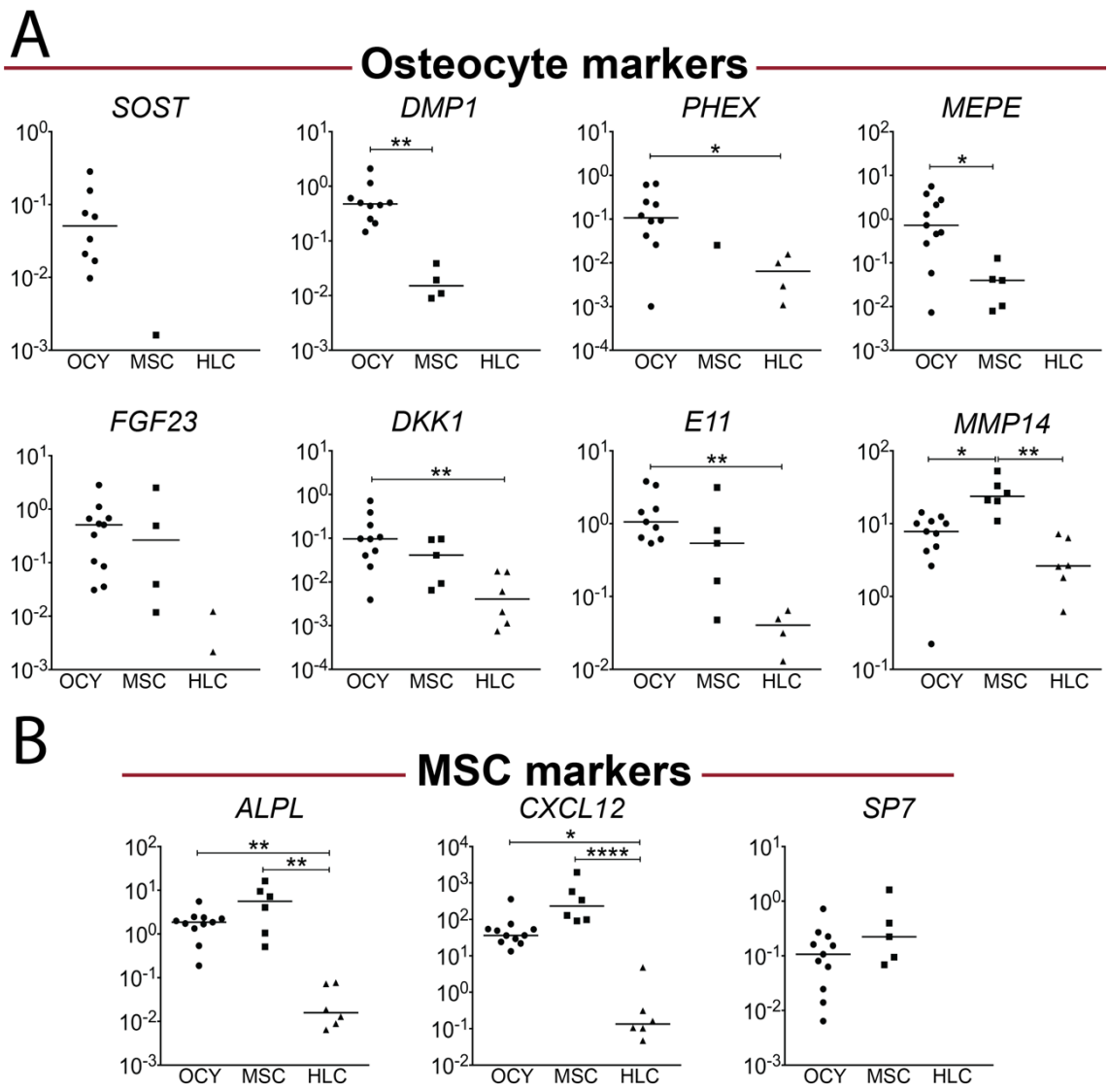

Figure 4.6. Comparative gene expression of osteocytes and MSC markers in healthy bone. *Comparison of (A) osteocyte-, (B) MSC -specific gene expression in osteocyte-enriched fragments (OCY) (n=11), CD45-CD271+ mesenchymal stem cells (MSC) (n=6) and CD45+CD271- haematopoietic lineage cells (HLC) (n=6) from healthy bone. Results are expressed relative to HPRT1. Absence of dots indicate that values were below detection thus precluding full statistical analysis of the respective data set.*

Similar trends were observed between MSCs and osteocytes following analysis of femoral head bone samples from OA patients (Figure 4.7A). The greatest differences between osteocytes and MSCs were found for late osteocyte markers *SOST, DMP1, PHEX*, *MEPE* and *FGF23.* The genes for *SOST*, *DMP1* and *PHEX* were expressed in all osteocytes group while these transcripts were detected in only some of the either MSCs or HLCs fractions, similarly to the healthy group described above. In the cases where transcripts could be detected on more than half of the tested samples statistical analysis confirmed the increased levels in osteocytes compared to MSCs and HLCs. The levels of *E11* and *DKK1* showed a trend for lower expression in MSCs compared to osteocytes (Figure 4.7A), similar to the ones observed in the cells derived from healthy bone (Figure 4.6A) although they failed to reach statistical significance. All the three MSC markers were consistently higher in MSCs as compared to osteocytes and HLCs (Figure 4.7B), consistent with the levels observed in the healthy group.

Gene expression analysis described here confirmed the specificity of the selected molecules to verify osteocyte identity. Furthermore, this data taken together with the histological assessment of the enrichment-procedure serve as evidence that the protocol optimised to study the gene expression profiles of native osteocytes was successful. Although all the tested molecules showed specificity to the cells that were selected to be tested for, several differences were noted. Some molecules analysed in both MSCs and osteocytes were expressed at different levels between healthy and OA groups and were further investigated in the following sections.

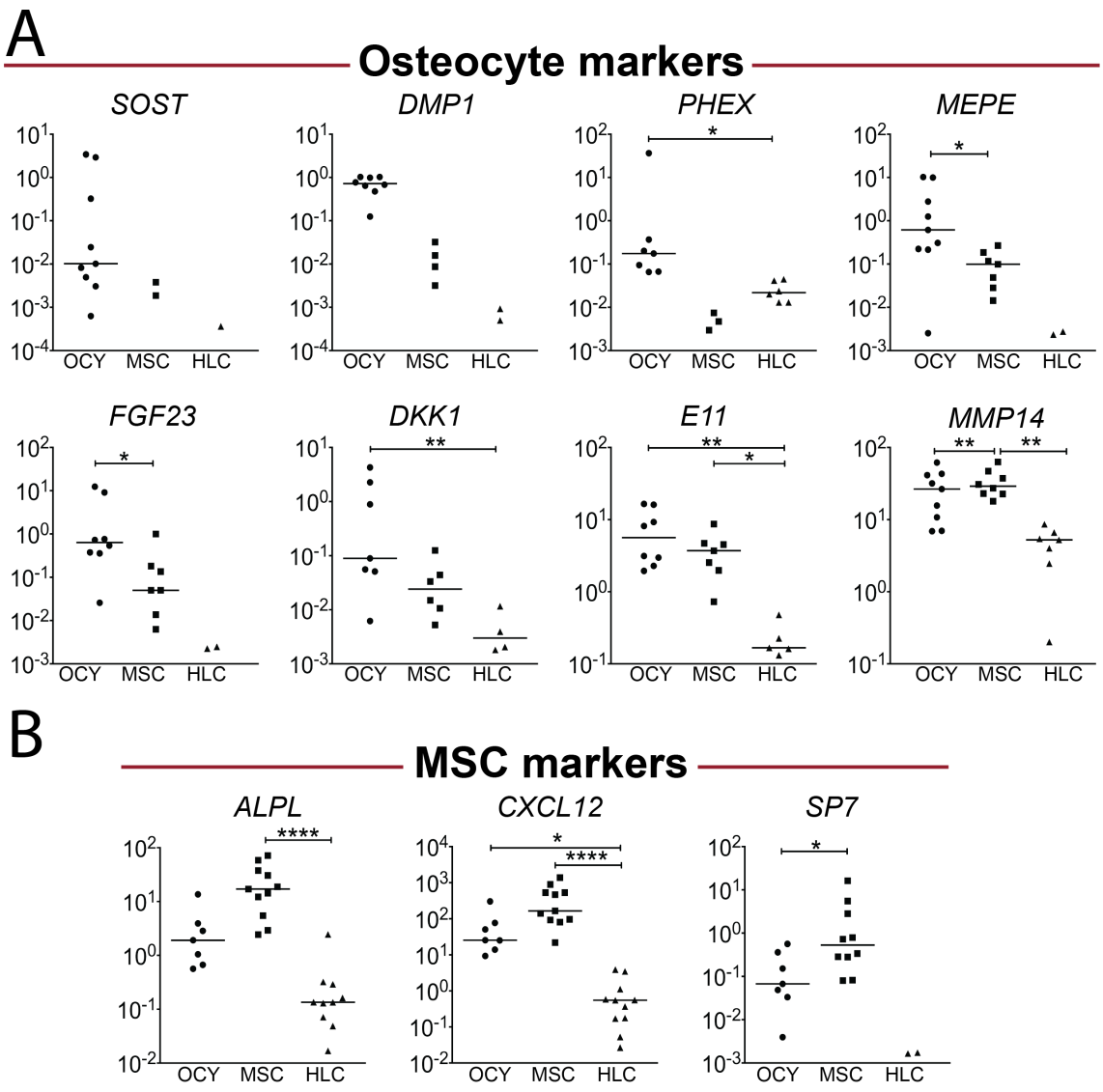

Figure 4.7. Comparative gene expression of osteocytes and MSC markers in OA bone. *Comparison of osteocyte- (A), MSC and early osteoblast-specific (B) gene expression in osteocyte-enriched fragments (OCY) (n=9), CD45-CD271+ mesenchymal stem cells (MSC) (n=11) and CD45+CD271- haematopoietic lineage cells (HLC) (n=11) from OA bone. Results are expressed relative to the values of HPRT1. Missing dots indicate that values were below detection thus precluding full statistical analysis of the respective data set.*

4.4.3 *In vitro* assessment of osteocyte-enriched bone fragments

Since osteocytes are mechano-sensory cells it was hypothesised that the mechanical processing of the bone fragments may affect gene expression levels in osteocytes. To investigate this the fragments were mechanically broken down at several intervals while being in culture at rest. The RNA was isolated from osteocytes before and after mechanical processing, at day 1 and day 7.

To confirm the viability of osteocytes under culture conditions, the bone fragments were incubated with a live/dead stain comprising of calcein and ethidium homodimer-1. Before incubation however, the bone fragments were observed under an inverted microscope to identify any potential cell outgrowths from the denuded bone fragments. As shown in Figure 4.8A there were no visible cells in the culture dish or surrounding the bone chips after a week under tissue culture conditions, suggesting successful depletion of any remaining stroma or bone lining cells. Using confocal microscopy, the samples after one week in culture medium had a considerable number of live cells present (Figure 4.8B). It is difficult to discriminate osteocytes from any other cells that may have grown on the bone surface, however these cells may originate from a rather low number of contaminating cells at the start of the experiment.

The gene expression levels of the main osteocyte markers assessed in samples from the three donors showed no specific pattern either before or after mechanical processing (Figure 4.9). However, the results confirmed the expression of all osteocyte-specific molecules. Without any specific expression pattern, this data may also indicate that the gene expression levels are more likely affected by the culture conditions rather than mechanical stimulation. Considering data obtained from fresh osteocytes (Figure 4.7), an overall reduction in gene expression was observed in Day 7 as compared to Day 1. Especially noticeable is the reduced expression of *FGF23* under culture conditions, both at Day 1 and Day 7.

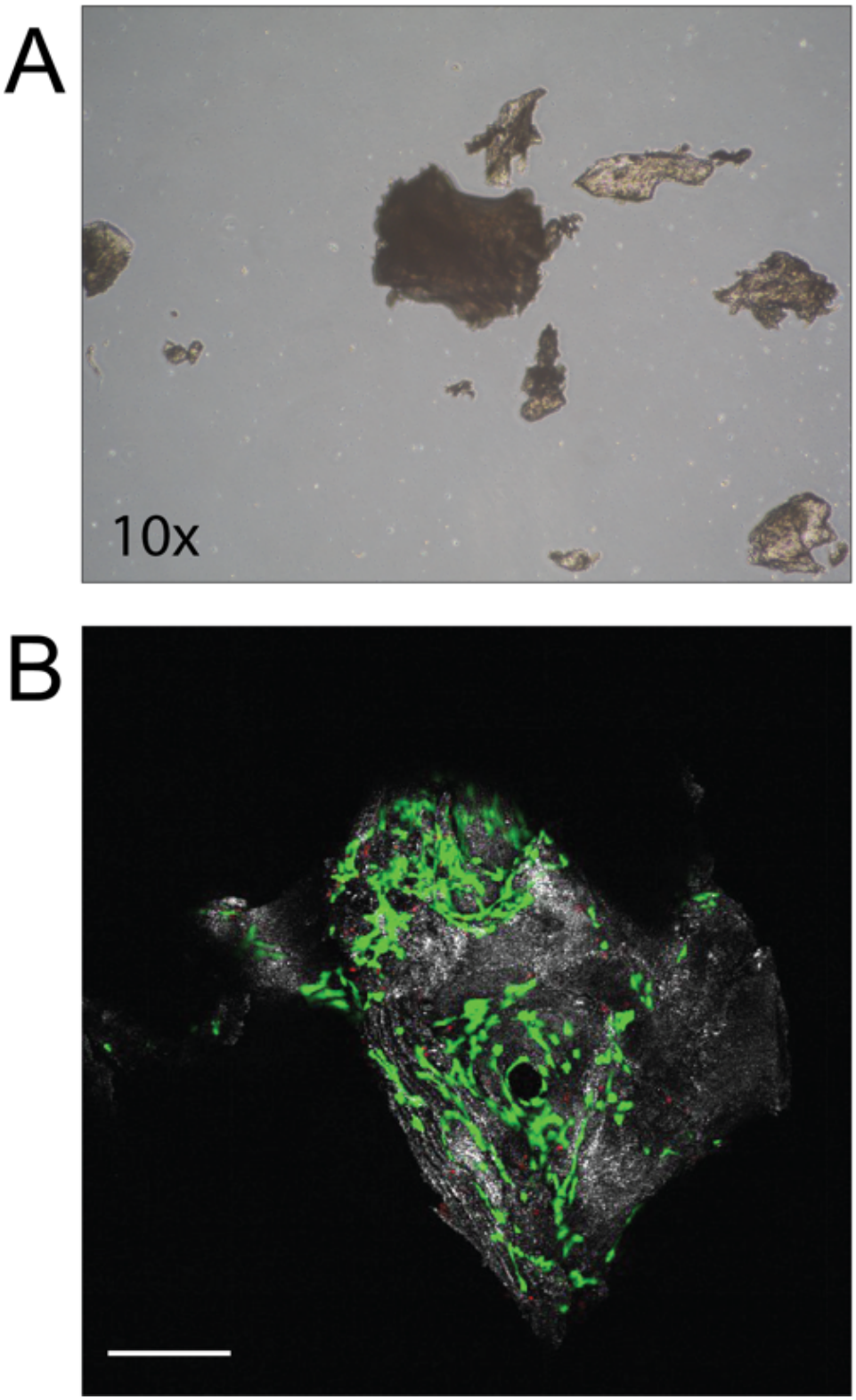

Figure 4.8. Viability of osteocyte-enriched bone fragments culture. *(A) shows the absence of cells in the culture dishes and around the bone fragments following one week in culture. (B) shows the live (green) and dead (red) staining of osteocyte-enriched bone fragments in culture conditions after 1 week. Scale bar, 200 μm*

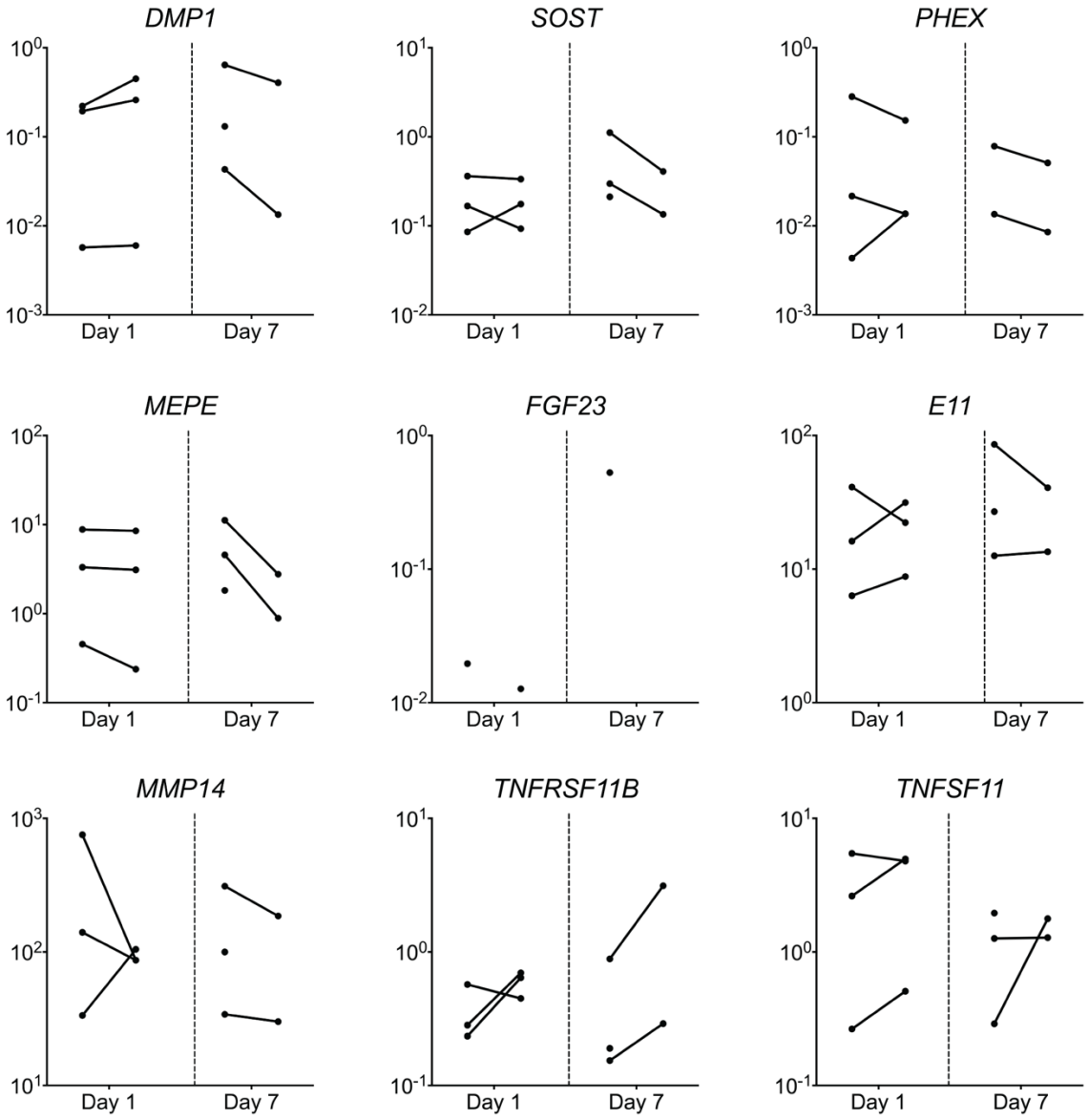

Figure 4.9. Gene expression of osteocyte transcripts and molecules associated with bone remodelling in cultured enriched-bone fragments. *Graphs show relative gene expression levels of osteocyte specific molecules under culture conditions and mechanical stimulation after one day and one week. Dots with connecting lines represent expression levels on a log scale between rest and mechanical stimulation while unconnected dots denote levels below detection of the corresponding data points. Expression levels were normalised to the reference gene HPRT1.*

4.4.4 Gene expression in osteocytes from OA bone

Having established a reliable method to study gene expression in native osteocytes and MSCs from the same bone, the next aim was to analyse potential differences between healthy and OA osteocytes in their native state. The gene expression analysis was performed on fresh samples using native osteocytes RNA obtained from n=9 OA and n=11 healthy donors.

4.4.4.1 Osteocyte-specific markers

No significant differences in the expression of classical osteocyte transcripts (*SOST*, *DMP1, MEPE*, *PHEX, FGF23* and *DKK1)* were noted between healthy and OA bone osteocytes, apart from the early osteocyte markers *E11* and *MMP14* (Figure 4.10).

Both molecules are specifically expressed by osteocytes at their early stage of differentiation facilitating their embedding in the newly formed osteoid (Holmbeck et al., 2005; Zhang et al., 2006). *E11* was 9-fold higher in OA femoral head osteocytes compared to IC osteocytes (p=0.0028, Figure 4.10) whereas the level of *MMP14,* involved in the maintenance of osteocytic dendritic processes (Holmbeck et al., 2005), was 4-fold higher in OA compared to IC osteocytes (p=0.0097, Figure 4.10).

These elevated levels observed in the early osteocyte marker *E11* and the osteocyte specific *MMP14* indicate an immature osteocyte phenotype with an active embedding activity. In support to this idea, all the other markers tested are mainly expressed by more mature osteocytes (Dallas et al., 2013) and no significant differences between healthy and OA groups was noted (Figure 4.10). .

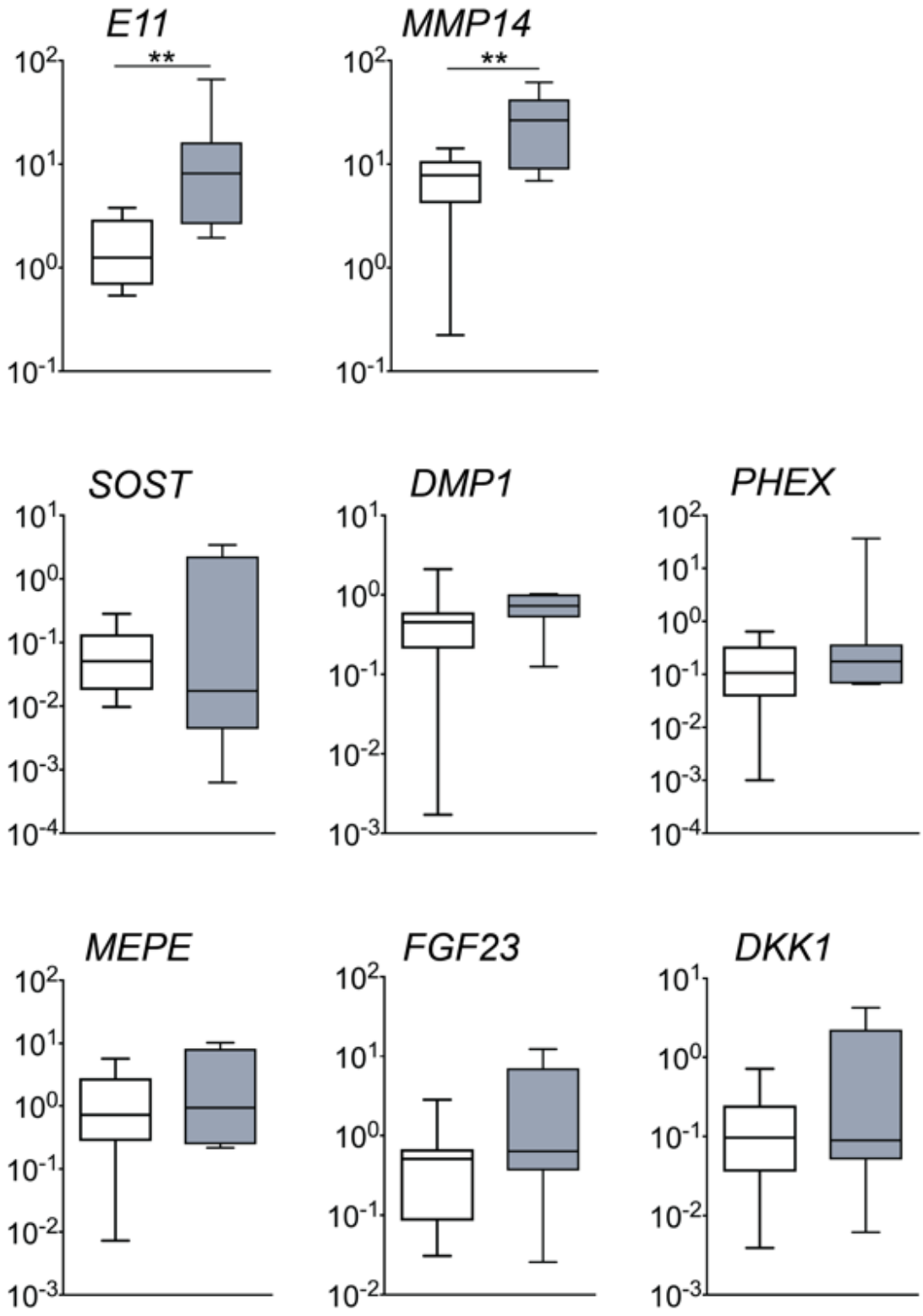

Figure 4.10. Comparative gene expression of osteocyte-specific molecules between healthy and OA osteocytes. *Gene expression levels in osteocytes from healthy (empty boxes, n=11) and OA bone (grey boxes, n=9) revealed that only the molecules that are expressed on early osteocytes showed significant differences (E11 and MMP14). No significant differences were observed in the levels of the late osteocyte markers; Results are expressed relative to the values of HPRT1.*

4.4.4.2 Bone resorption molecules

To investigate whether the OA environment modulated molecules involved in bone remodelling, the expression of RANKL (encoded by *TNFSF11*), OPG (encoded by *TNFRSF11B*), and resorption molecules cathepsin K (encoded by *CTSK*) and TRAP (encoded by *ACP5*) also implicated in osteocyte osteolysis pathways (Qing et al., 2012; Wysolmerski, 2013; Dole et al., 2017) were analysed in parallel to the classical osteocyte transcripts described above.

Interesting differences were observed in expression of the selected genes associated with bone or bone matrix remodelling (Figure 4.11). While the mRNA levels for RANKL showed no significant difference between healthy and OA osteocytes, mRNA expression levels for OPG were 5-fold higher in osteocytes from OA bone ($p=0.0185$). The molecular balance between the osteoclastogenesis activator RANKL and its antagonists, OPG, dictates the rate of osteoclastogenesis (Brendan F Boyce and Xing, 2007) and hence, bone resorption. The ratio between these two molecules was calculated and it was determined that the OPG/RANKL mRNA ratio in OA osteocytes was 7-fold increased ($p=0.0083$, Figure 4.11) compared to healthy osteocytes, suggesting a bias towards bone resorption inhibition modulated by the osteocytes. Interestingly, similar trends were found on OA MSCs (Chapter 3, Section 3.4.3).

The other molecules involved in the activity of bone resorption process, *CTSK* and *TRAP*, were also analysed alongside RANKL and OPG but with no significant differences between the healthy and OA osteocytes was observed, although a trend to increase expression in OA was noted in both genes (Figure 4.11). To validate this data, the expression of all resorption associated molecules will be further investigated at a protein level by immunohistochemistry.

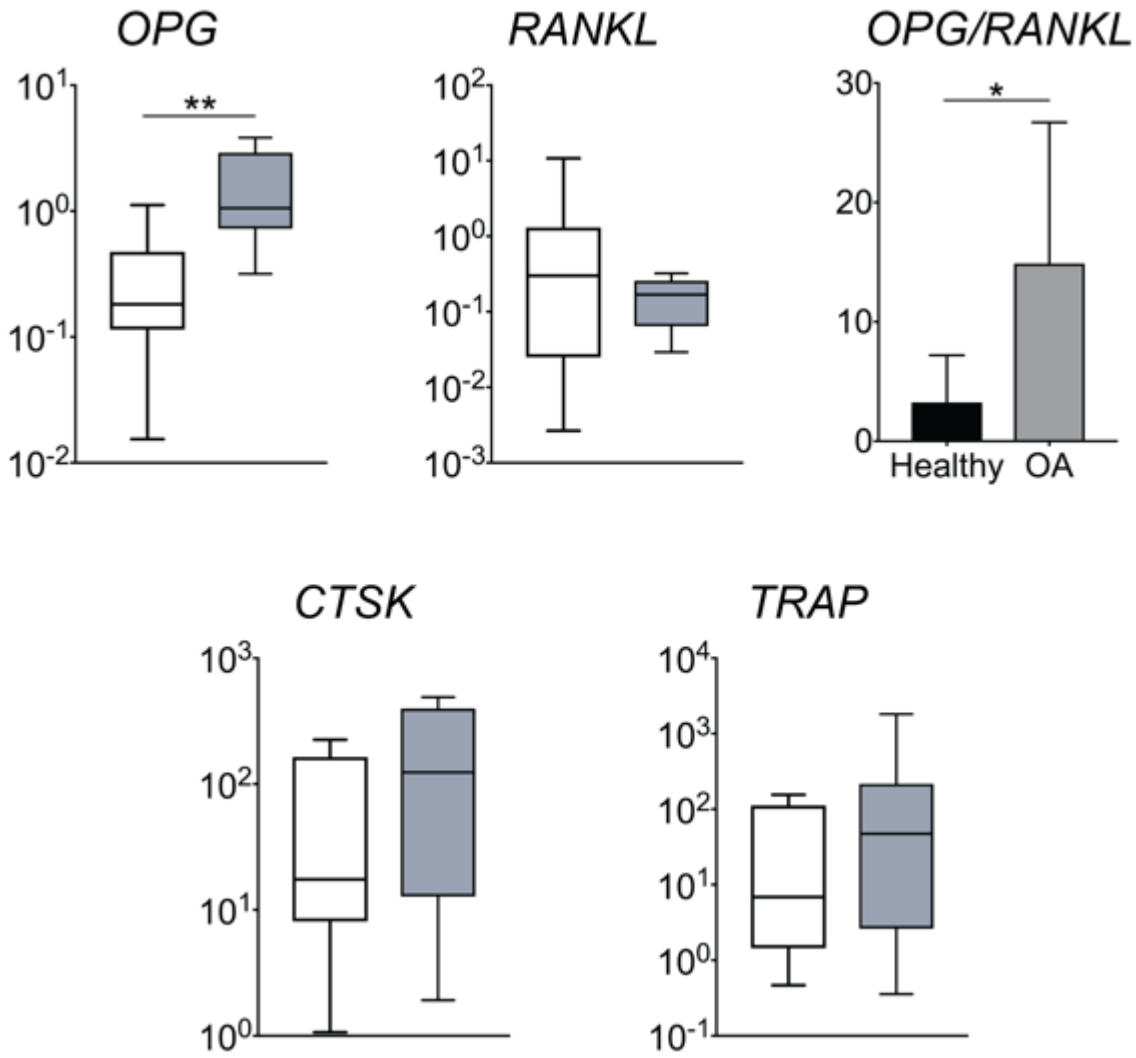

Figure 4.11. Comparative gene expression of bone remodelling molecules between healthy and OA osteocytes. *Comparison of gene expression levels between osteocytes from healthy bone (empty boxes, n=11) and OA bone (grey boxes, n=9) of the main molecules associated with bone resorption: osteoprotegerin (OPG), receptor activator of nuclear factor kappa-B ligand (RANKL), cathepsin k (CTSK) and tartrate resistant acid phosphatase (TRAP). Results are expressed relative to the values of HPRT1. Mean ratio for OPG/RANKL is expressed as columns with error bars representing standard deviation.*

Taken together, these patterns of gene expression suggested higher early osteocyte activity and a potential bias for inhibition of bone resorption by osteocytes in OA femoral head bone. This data points to an underestimated role of osteocytes in OA bone pathology with implications to their early progenitors, the MSCs, which were shown to have a similar profile as described in Chapter 3.

No age-dependent trends were observed for differentially expressed genes (*E11, MMP14, OPG* and *RANKL*) neither in IC nor OA osteocytes (Figure 4.12) indicating that the observed differences in the genes between healthy and OA osteocytes were likely to be characteristic of OA bone pathology rather than a result of systemic changes in bone homeostasis related to donor age.

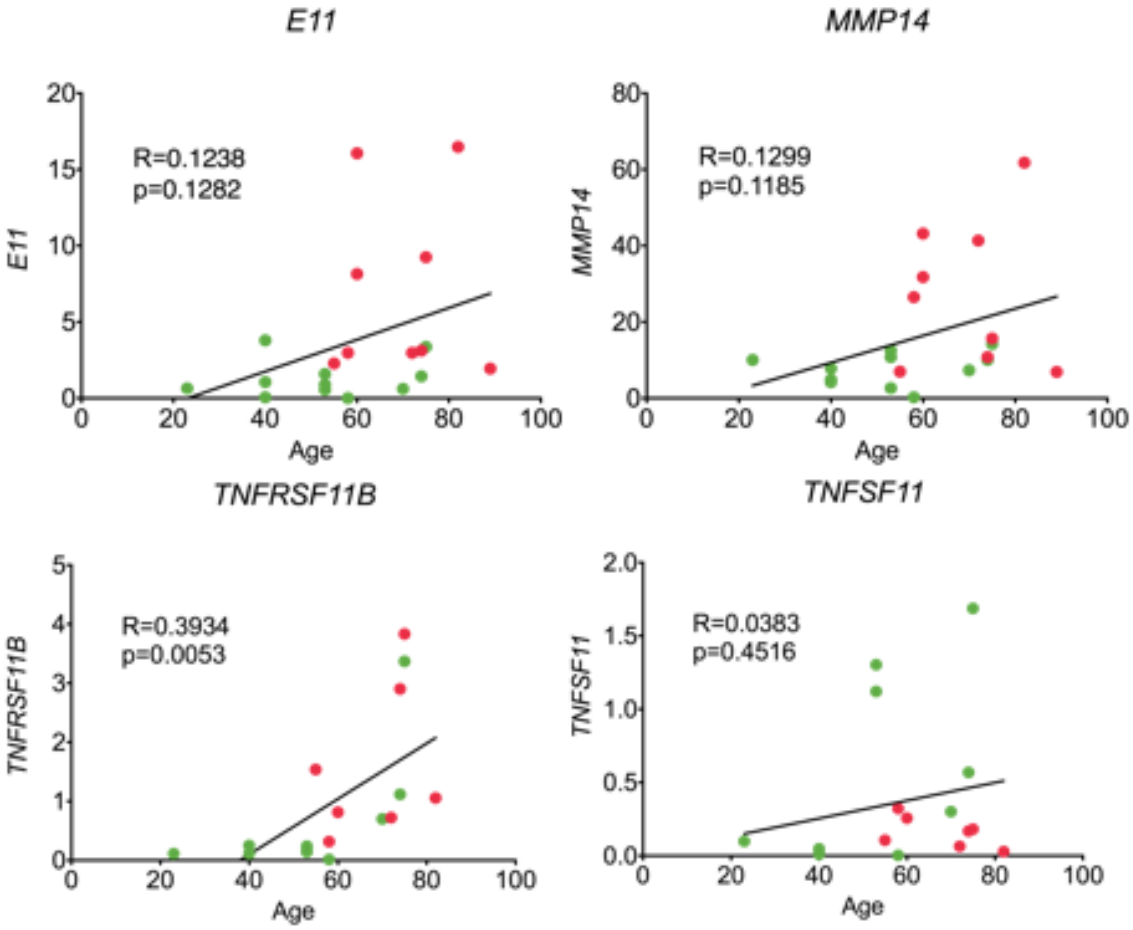

Figure 4.12. Donor age correlations of differentially expressed genes in healthy and OA osteocytes. *Correlation between the gene expression levels of differentially expressed molecules from healthy (green dots) and OA (red dots) osteocytes and the donor age (years). Trend lines are shown in each graph with correlation coefficients and p values calculated using non-parametric Spearman correlation test.*

4.4.5 Histological assessment of molecules of interest

Gene expression analysis in osteocytes as well as MSCs (Chapter 3) showed an altered expression of genes involved in bone formation and remodelling. The differentially expressed genes were further assessed at protein level by using immunohistochemistry and in addition, their tissue distribution in relation to OA pathology was investigated. Of specific interest, this whole tissue distribution would also indicate potential topographical relationships between osteocytes and MSCs, the main cells under investigation as specified in the aims of this thesis.

Based on the visual appearance of the articular cartilage and the underlining subchondral bone, it was observed that within the same femoral head, the degree of tissue damage was heterogeneous. To identify areas of bone and cartilage pathology, Safranin O staining was first performed on whole OA femoral heads (Figure 4.13A). Safranin O is a basic stain which binds with proteoglycans (acids) in cartilage with a strong affinity forming a red complex. The intensity of the staining depends on proteoglycan's quantity contained in cartilage. This stain allowed for a distinctive separation of bone and cartilage making it possible to measure the bone areas in regions of visible damage and compare it to areas with a normal appearance. The areas of bone sclerosis commonly associated with increased bone volume (L.G. Cox et al., 2012) were identified below the regions of severe osteochondral damage, cartilage loss as well as fibrovascular tissue invasion beyond the tidemark (Figure 4.13B). Non-sclerotic regions (NS) (Figure 4.13B) representing minimally affected trabecular bone areas were localised distal from the diseased osteochondral regions or to the areas with the least osteochondral damage.

Bone area measurements associated with these regions were performed to assess the validity of S and NS regions selection and showed a significant increase in the areas occupied by bone in S regions. Using ImageScope software (Leica) the cartilage was excluded from the selected regions for analysis, and bone area calculated as percentage of total tissue area, comprised thereof bone and stromal cavity. In S regions, the area covered by bone was between 54.08%-90.38% (median of 61.72%) while in the NS regions the bone was significantly reduced ($p<0.0001$) being in the range of 8.72% - 32.26% with a median of 16.88% (Figure 4.14).

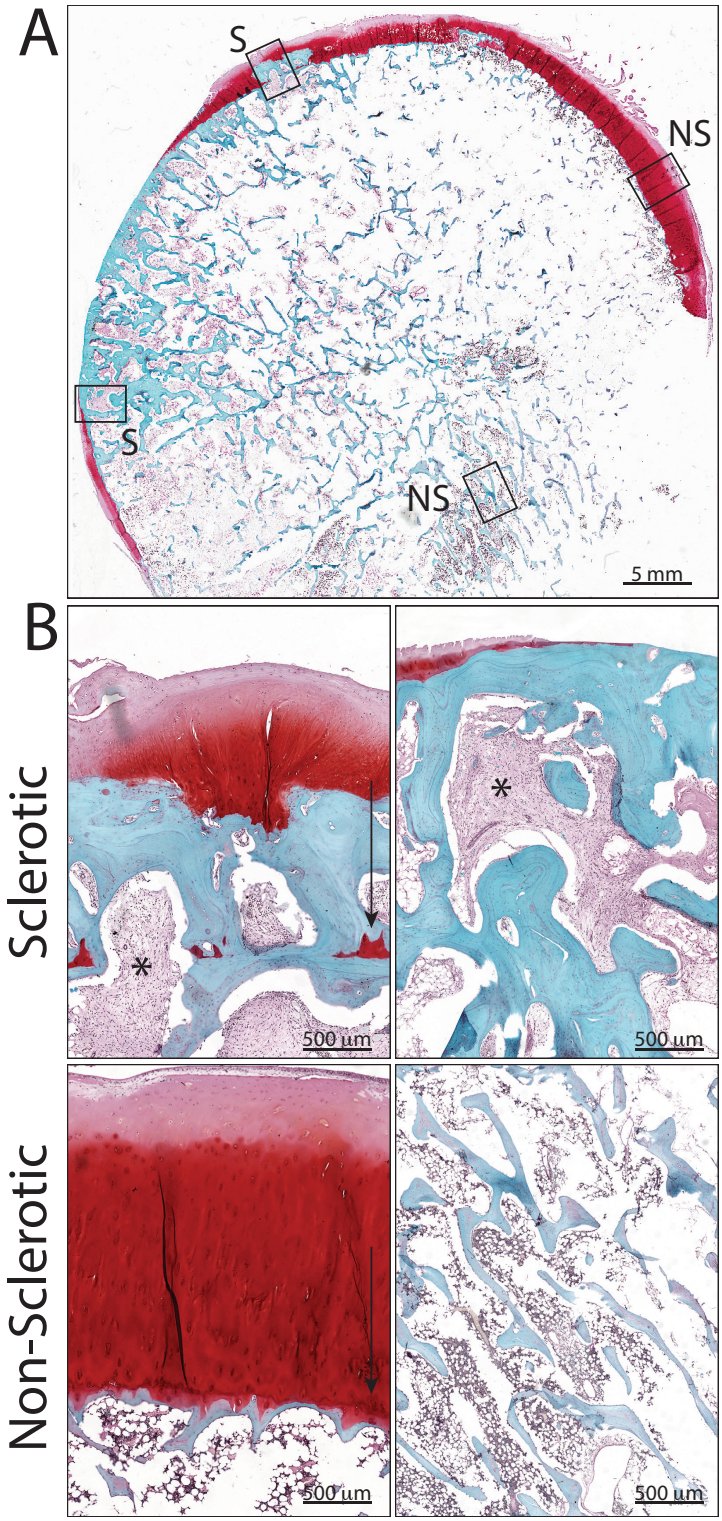

Figure 4.13. Representative histology images of the whole femoral head stained with Safranin O. *(A) Global picture of OA associated pathologies in a whole OA femoral head, noting the association between cartilage denudation and increased bone area. (B) Distinct bone and cartilage abnormalities characteristic to hip OA with the squares indicating the sclerotic (S) and non-sclerotic (NS) regions which were used for subsequent analysis and shown at higher magnification; arrow: tidemark, *: fibrovascular tissue. Sample ID: DIFHOA018*

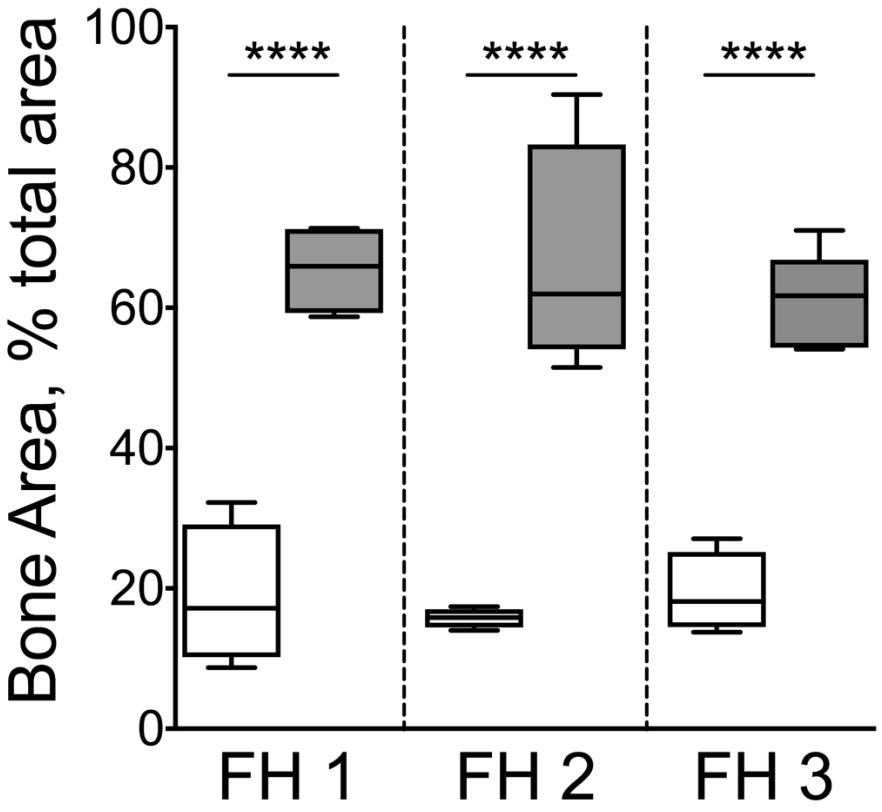

Figure 4.14. Comparison of bone area measurements between non-sclerotic (empty boxes) and sclerotic (grey boxes) areas of hip OA from three different donors. *A minimum of 10 regions each in three femoral heads (FH) from all donors were used for area measurements and represented as percentage of bone out of total tissue area from the region of interest selected for analysis.*

4.4.6 Bone resorption associated molecules

To investigate the expression of the bone remodelling molecules as well as their tissue distribution in relation to the areas of OA bone pathology, IHC was employed using antibodies against OPG, RANKL and CTSK. The expression of TRAP was assessed histochemically by staining for the acid phosphatase enzymatic activity using a TRAP assay. This would facilitate the investigation of active osteoclasts but would also help to determine whether the TRAP enzymatic activity is present in osteocytes, having had shown its expression at a gene level. The immunohistological staining for RANKL and OPG was analysed in S and NS regions of n=2 OA femoral heads, selected based on the measurements described above as well as in n=1 healthy iliac crest.

In the severe sclerotic regions of OA femoral head, strong OPG staining was observed, most obvious being in the fibrovascular tissue that had replaced the BM and breached the tidemark into the cartilage (Figure 4.15, upper panels); osteoblasts and some osteocytes were also strongly OPG-positive (Figure 4.15, bottom panels). In contrast, RANKL was absent or very low expressed (Figure 4.15, bottom panels). No obvious OPG or RANKL staining was found in the articular cartilage of this particular sample with a severe degree of osteochondral damage (Figure 4.15, upper panels).

In the subchondral areas of the same femoral head, but distant from the osteochondral damage, the cartilage in this area was thicker and of normal appearance but with no positivity for either of the proteins (Figure 4.16). This area was characterised by no visible alteration in bone or stromal tissue and no expression of RANKL and OPG was observed in either stromal cells or osteocytes (Figure 4.16, bottom panels).

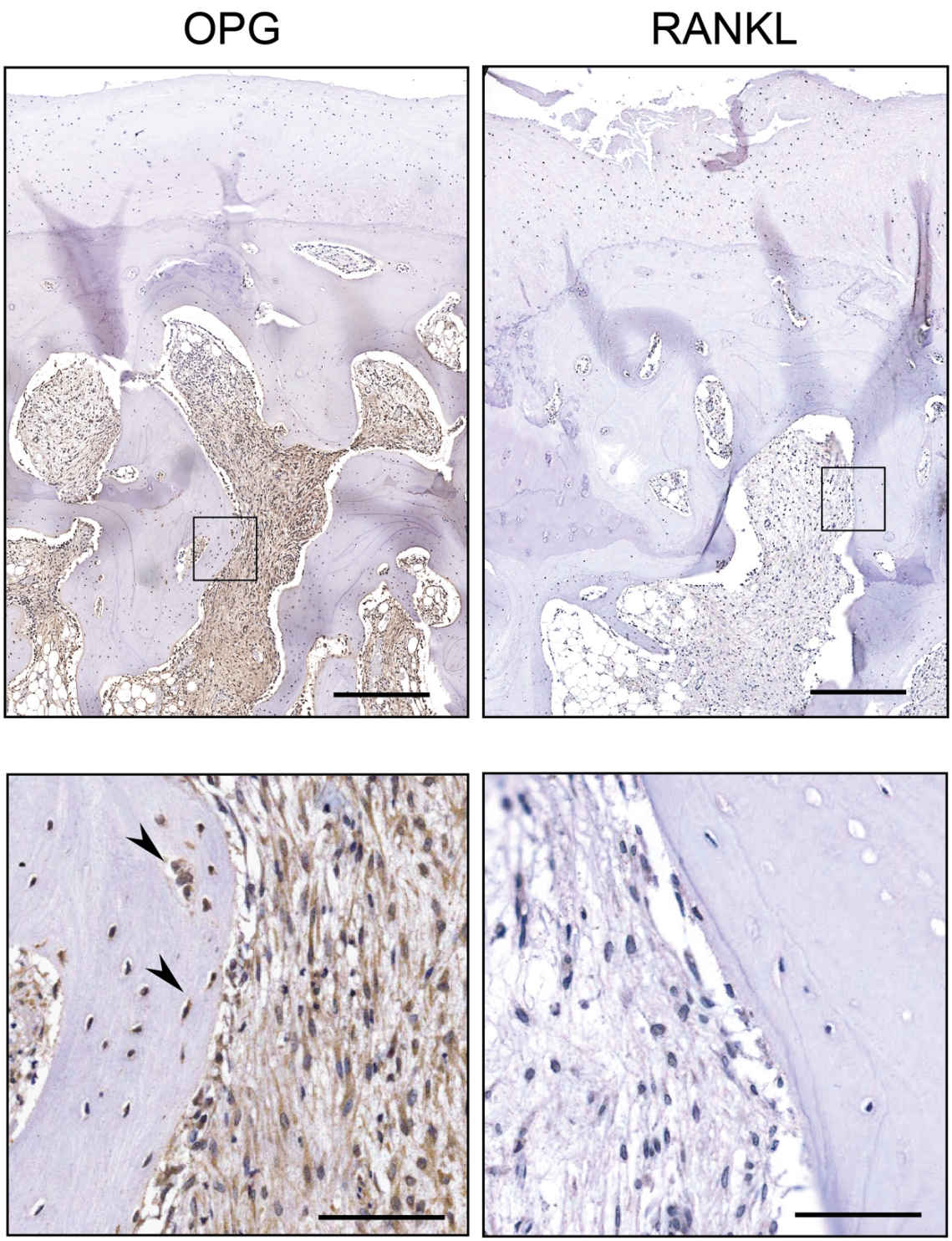

Figure 4.15. Immunohistochemical staining of OA femoral head showing the topography of OPG and RANKL positive cells in subchondral S regions. *Square areas magnified from upper panels showing the proximity of OPG positive osteocytes (arrow heads) to bone lining osteoblasts and the abundance of OPG in the dense fibrovascular tissue. In contrast RANKL is not expressed in any of the osteocytes from the same area while its expression in the fibrovascular tissue is notably lower. Scale bars: 300 μm upper panels, 100 μm bottom panels. Sample ID: DIFHOA018*

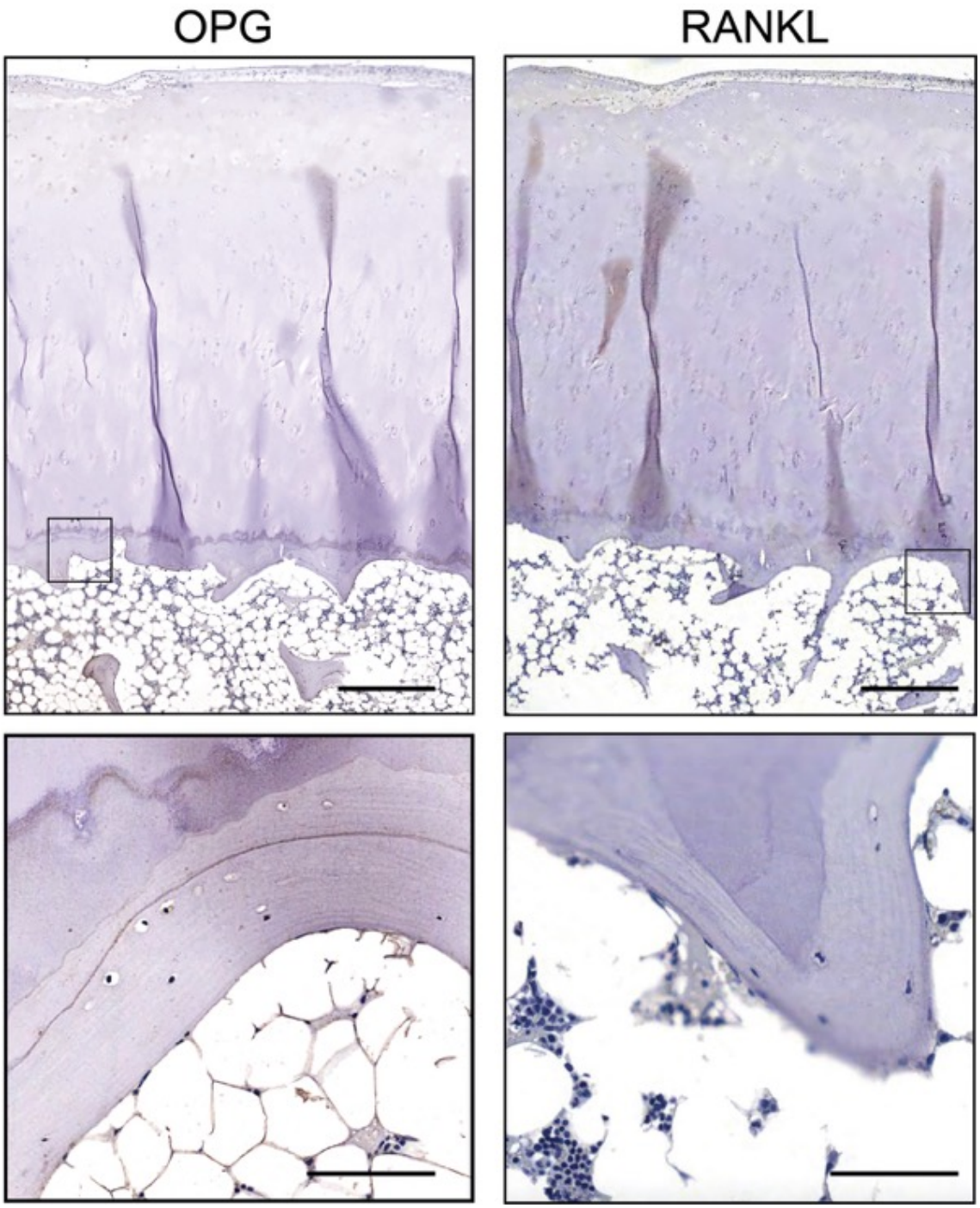

Figure 4.16. Immunohistochemical staining of OA femoral head bone showing the topography of OPG and RANKL positive cells in subchondral NS regions. *Square areas magnified from upper panels confirming the absence of OPG and RANKL positivity in those regions of hip OA. Scale bars: 300 μm upper panels, 100 μm bottom panels. Sample ID: DIFHOA018*

Due to the heterogonous nature of OA bone alterations (Burr and Gallant, 2012), a second femoral head was analysed. It was noted that in this sample with less cartilage damage, the extent of bone sclerosis and fibrovascular tissue invasion was not as evident, suggesting a different stage of progression of the disease. In those samples, the expression of OPG was located similarly to previous sample, in the subchondral regions (Figure 4.17 upper panels). However, in contrast to the regions with more severe bone sclerosis and general OA associated pathology documented in previous sample (Figure 4.15), RANKL was also found to be expressed here at similar levels and locations to OPG (Figure 4.17, bottom panels). Furthermore, in this sample the osteocytes and chondrocytes also showed positivity for both RANKL and OPG, suggesting a general remodelling modulation in this patient at a tissue level (Figure 4.17, magnified areas, left panels). In this sample, a notable number of bone remodelling sites was observed in the subchondral area, defined as an increased presence of osteo/chondroclasts and osteoblasts. This may be a consequence of the general RANKL expression which facilitated osteoclastogenesis while the presence of osteoblasts may indicate a high number of MSCs in that area in response to the high remodelling activity.

In both samples analysed, osteocytes from the trabecular bone, that was non-sclerotic and distant from the subchondral area, were weakly positive for both RANKL and OPG, while expression in stromal tissue was not as evident as in the subchondral sclerotic areas (Figure 4.18).

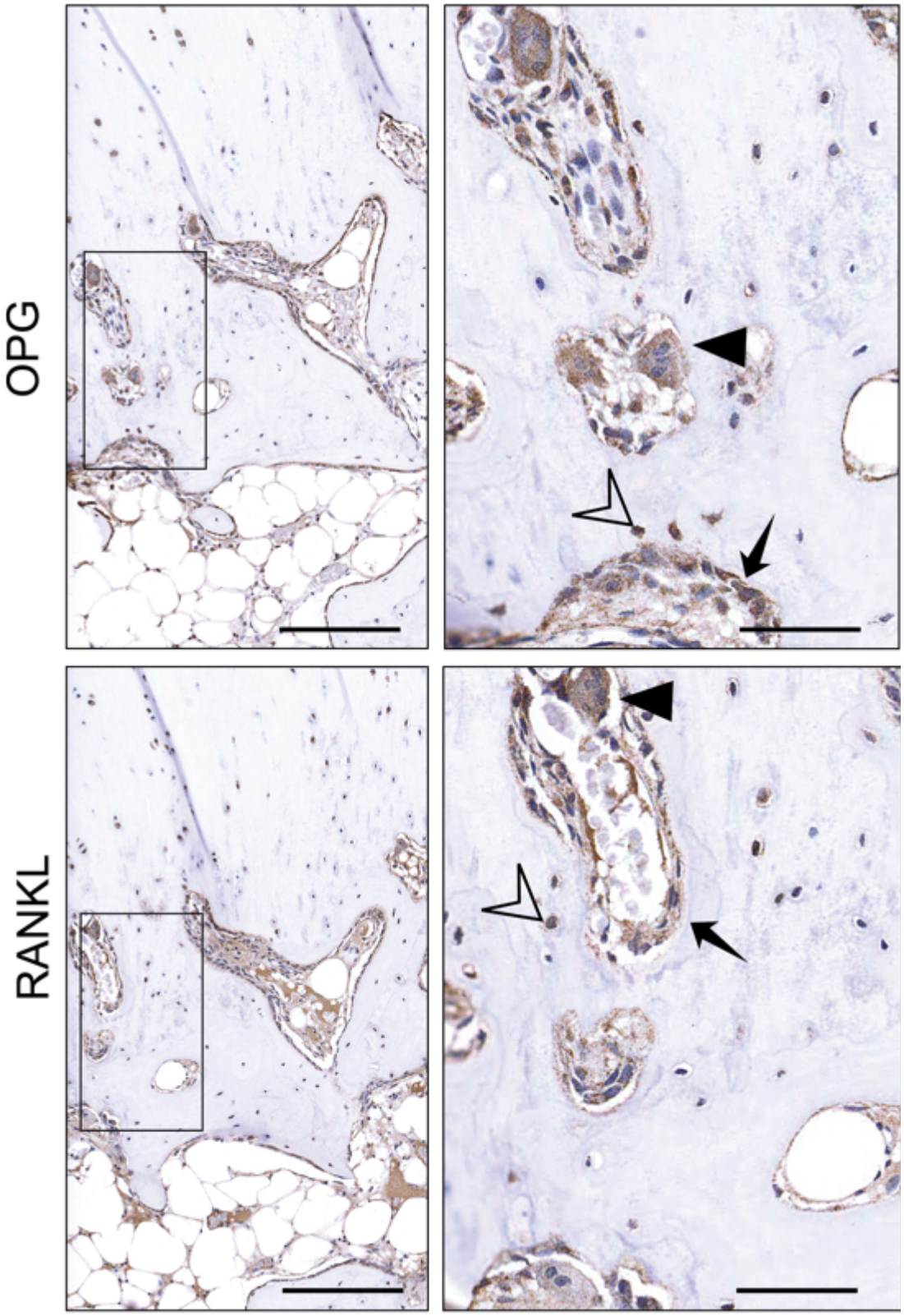

Figure 4.17. Staining of OPG and RANKL in S regions of hip OA from second patient marked by severe osteochondral damage. *Magnified rectangular areas show that there is evident staining of both molecules in the cells from areas of bone remodelling. Arrows: osteoblasts; arrow heads: osteo/chondroclasts; empty arrow heads: osteocytes. Scale bars: 200 μm left panels, 50 μm right panels. Sample ID: DIFHOA012*

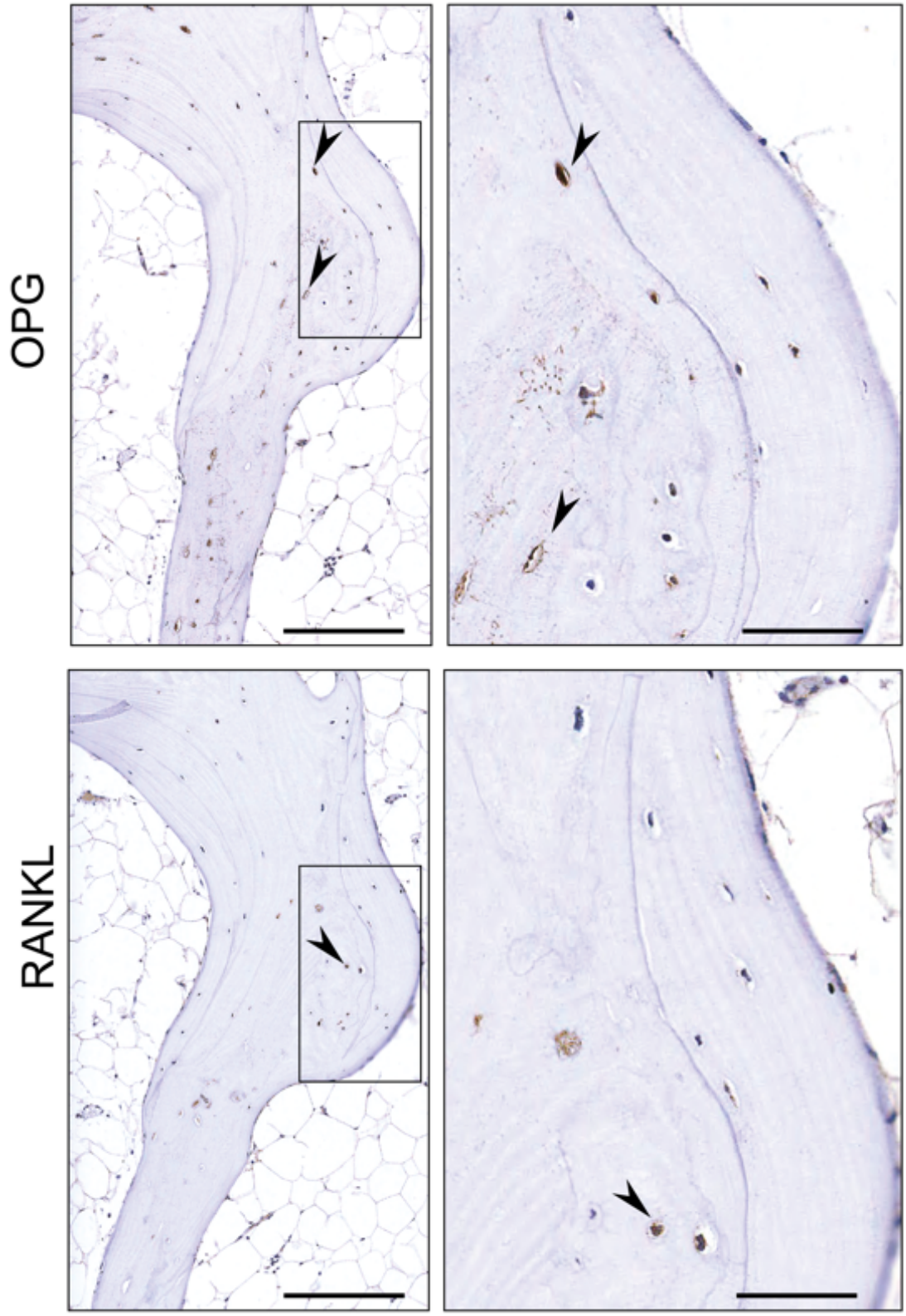

Figure 4.18. Staining of OPG and RANKL in non-sclerotic areas of hip OA from the second patient, located distant from subchondral area. *Magnified rectangular areas show that expression in the stromal tissue is not as evident, although some osteocytes are positive, for both RANKL and OPG (arrow heads). Scale bars: 200 μm left panels, 50 μm right panels. Sample ID: DIFHOA012*

Following the analysis of OPG and RANKL in these two samples of apparent different stages of degree progression, the expression of the two resorption modulation molecules was found to be heterogeneous between these patients. However, in both patients the expression of OPG and RANKL was predominantly found in the osteochondral regions while the distal regions were similar in appearance in both patients. In the second patient, the expression of RANKL was found strongly positive in bone remodelling areas. The positivity was detected on osteo/chondroclasts, as expected probably due to its membrane binding during their differentiation, as well as on the other cells, including the osteoblasts, bone lining cells and osteocytes. Further assessment using TRAP staining will be used to determine osteo/chondroclasts clasts activity in those regions of interest. In contrast, in the first patient there were no osteoclasts visible and the RANKL expression was absent.

The expression of both molecules was found on osteocytes and corroborates the gene expression data. Both OPG and RANKL were found in osteocytes from regions of bone sclerosis as well as regions with no sclerosis or distal from the osteochondral area. Although no visible difference of expression was observed in the osteocytes between the different regions, their expression would be further investigated in the healthy IC in order to confirm the gene expression findings while the expression in MSCs will be investigated subsequently.

While RANKL and OPG are molecules regulating the osteoclastogenesis and have mainly a regulatory role over the osteoclast differentiation, CTSK and TRAP are both enzymes with joined roles in the resorption activity itself. To investigate these molecules, antibody staining was performed using antibodies against CTSK while TRAP was assessed cytochemically using an acid phosphatase chromogenic based assay. Both stainings were performed on whole femoral head tissue sections from n=3 OA donors. Safranin O was also employed to allow the visual separation between bone and cartilage, making it possible to identify the nature of the tissue where the resorption takes place and hence differentiate between chondroclasts and osteoclasts, based on their tissue location.

Numerous resorption pits could be observed in the subchondral areas of hip OA. Osteoclasts with ≥3 nuclei were frequently seen in those areas and were usually localized in resorbing bays, often in apposition to bone tissue as confirmed by Safranin O (Figure 4.19). CTSK staining revealed the enzyme expression in the subchondral areas with high specificity only to osteoclasts. The osteoclasts activity was confirmed by the presence of TRAP as revealed in Figure 4.19, bottom panels. TRAP-positive cells adjacent to bone

surface in the same location with the CTSK positive cells indicate the presence of active osteoclasts in those areas and inherently, bone remodelling activity.

Osteocytes in those areas were found to be negative for CTSK as well as TRAP, both molecules showing specificity to osteoclasts only.

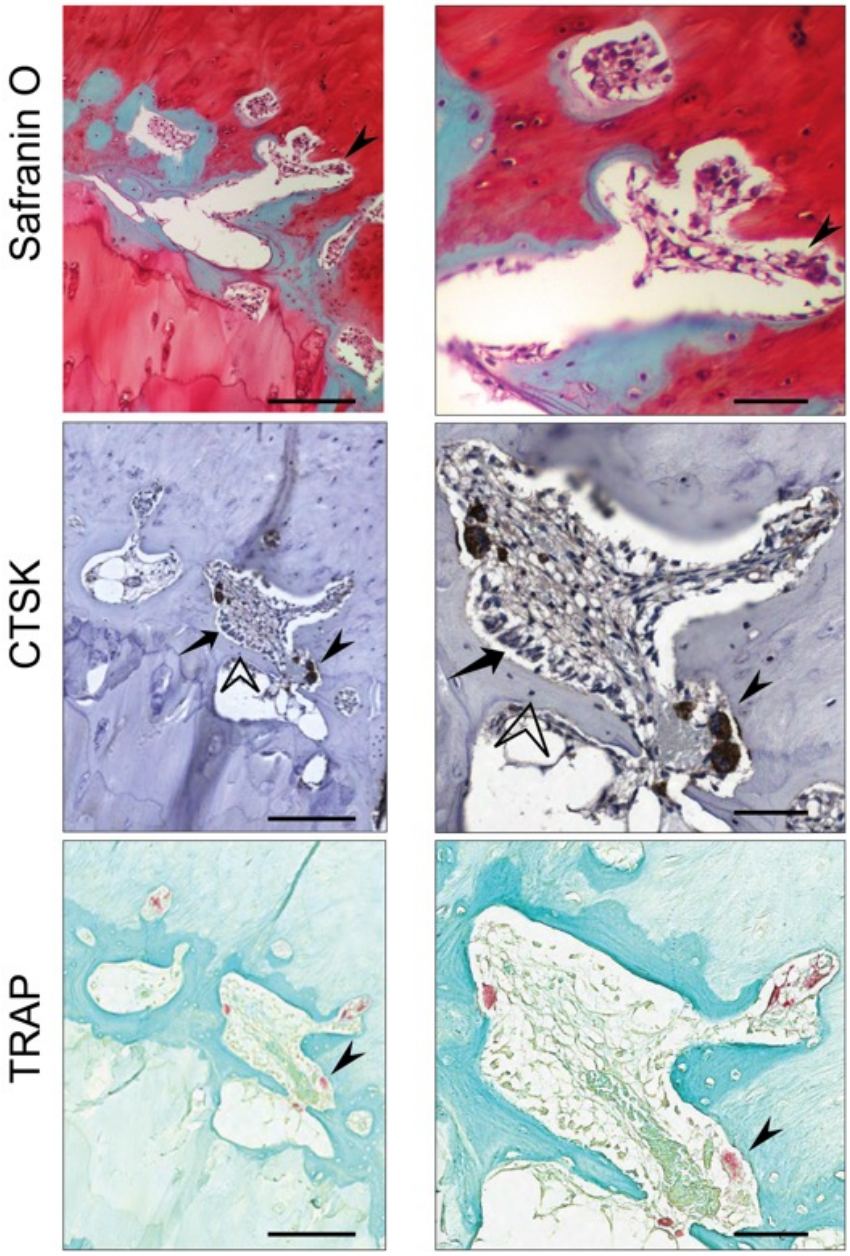

Figure 4.19. Cartilage replacement by bone in subchondral regions of hip OA. *OA femoral heads stained with Safranin O (upper panels), anti-Cathepsin K (CTSK, middle panels) and tartrate resistant acid phosphatase (TRAP, bottom panels). Safranin O indicates new bone formation breaching the cartilage. Increased bone remodelling activity is marked by CTSK- and TRAP-positive osteoclasts (arrow heads) within the same site with osteoblasts (arrows) and osteocytes (empty arrow heads) which are both negative. Scale bars: 200 μm, left panels; 50 μm, right panels. Sample ID: DIFHOA018*

Assessing the expression of these resorption molecules in relation to osteocytes as well as MSCs was important to be evidenced here and served as part of the aims of this chapter. To correlate with the data obtained by gene expression, bone resorption associated molecules were investigated by immunohistochemistry in healthy IC.

In healthy control IC bone, OPG staining was confined to stromal cells (Figure 4.20), with no expression observed in osteocytes. Similarly, RANKL was not expressed in healthy IC osteocytes or stromal tissue. CTSK was found on very low levels in IC, being restricted to osteoclasts only, which were limited to occasional bone remodelling sites (Figure 4.20, upper panels). This is expected because in IC the bone remodelling has minimal activity (Clarke, 2008).

Since osteoclasts presence is minimal in healthy IC, but elevated in OA subchondral areas concomitant with tissue remodelling sites (Figure 4.20), the gene expression levels observed in the resorption molecules in OA osteocytes (CTSK and TRAP, Figure 4.11) could be in theory, attributed to osteoclasts contamination. However, histological evidence in Section 4.4.1 clearly shows complete soft tissue denudation. Moreover, as shown so far in the histological images, osteoclasts are rare cells with a short life-span, only present in the tissue remodelling areas and of orders of magnitude lower numbers compared to osteocytes. This suggests that the detected signal can only come from osteocytes. The absence of TRAP and CTSK expression at protein level may be due to an inability of these molecules to be translated from mRNA in osteocytes. Moreover, TRAP enzymatic activity is detected under a low pH (4.7-5), which may not be the case in the lacunar environment where osteocytes reside in.

In summary, the expression of OPG was found elevated in all mesenchymal lineage cells, with an overall increased expression in the S areas of OA femoral heads. Meanwhile, the levels of RANKL were only noted in areas of active tissue remodelling, in both osteocytes and MSCs. These active areas were also associated with the presence of osteoclasts, which absence was corroborated with the increase expression of OPG, hence inhibiting their differentiation and survival. All together, these results confirm the involvement of both MSCs and osteocytes in the active process of tissue remodelling in OA.

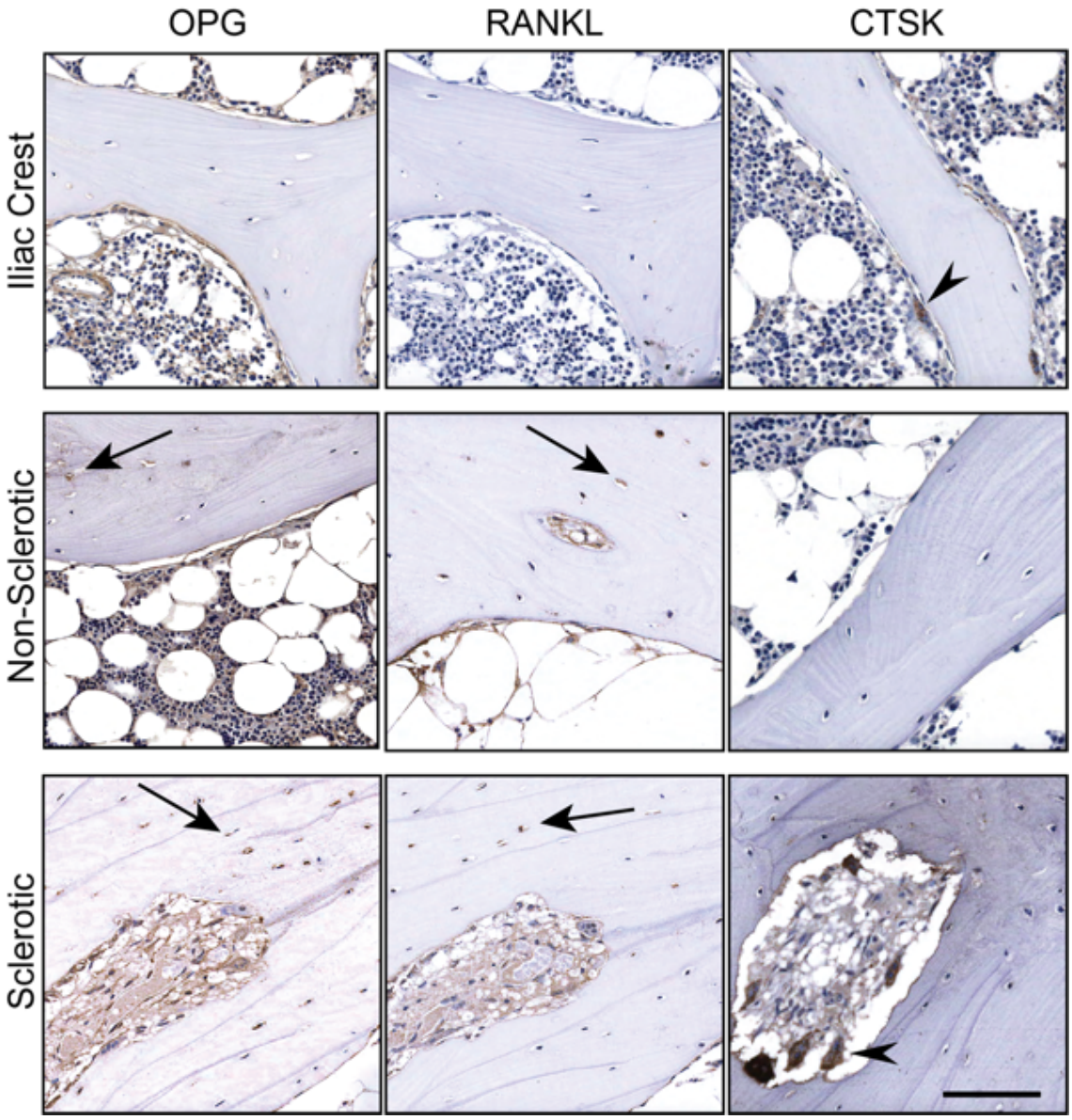

Figure 4.20. Representative images from healthy IC in comparison to OA femoral head bone. *OPG and RANKL are not expressed in healthy IC although OPG is present in the stromal compartment. Cathepsin K (CTSK) specificity for osteoclasts (arrow heads) was evident and no osteocytes were found positive. No osteoclasts were found in healthy IC where sites of remodelling were scarce. Scale bar: 100 μm. Sample IDs: IC: DIHIC03; OA: DIFHOA012*

4.4.7 Osteocyte and MSC distribution in relation to bone pathology in OA

Osteocytes gene expression analysed previously showed elevated levels of the early osteocyte marker *E11* (Figure 4.7 and 4.10). To confirm this at a protein level and to investigate the topography of MSCs in relation to osteocytes, the distribution of E11-positive osteocytes and CD271-positive MSCs were next analysed on large sections of OA femoral heads from three patients in relation to OA bone pathology and in one control IC bone.

Similar to analysis of OPG and RANKL, some variation in the degree of pathology was evident between femoral heads. The antibody staining was compared between evidently sclerotic regions and the regions with no evidence of bone sclerosis as described in Figure 4.13.

In sclerotic regions, intense E11-positive staining was found in all the osteocytes which were mostly concentrated near the outer edges of thick trabeculae of OA femoral head, with the highest density proximal to cuboidal osteoblasts (Figure 4.21). Their presence in the proximity of osteoblasts is consistent with them being newly embedded in bone, also suggested by their morphology. In contrast, the osteocytes in non-sclerotic regions of the osteochondral area (Figure 4.21) showed noticeable differences, both in their distribution and morphology. The frequency of E11-positive osteocytes is visibly reduced compared to the sclerotic regions while the cells appeared smaller in size and with less dendritic processes. To confirm these differences, their distribution will be further assessed in this chapter.

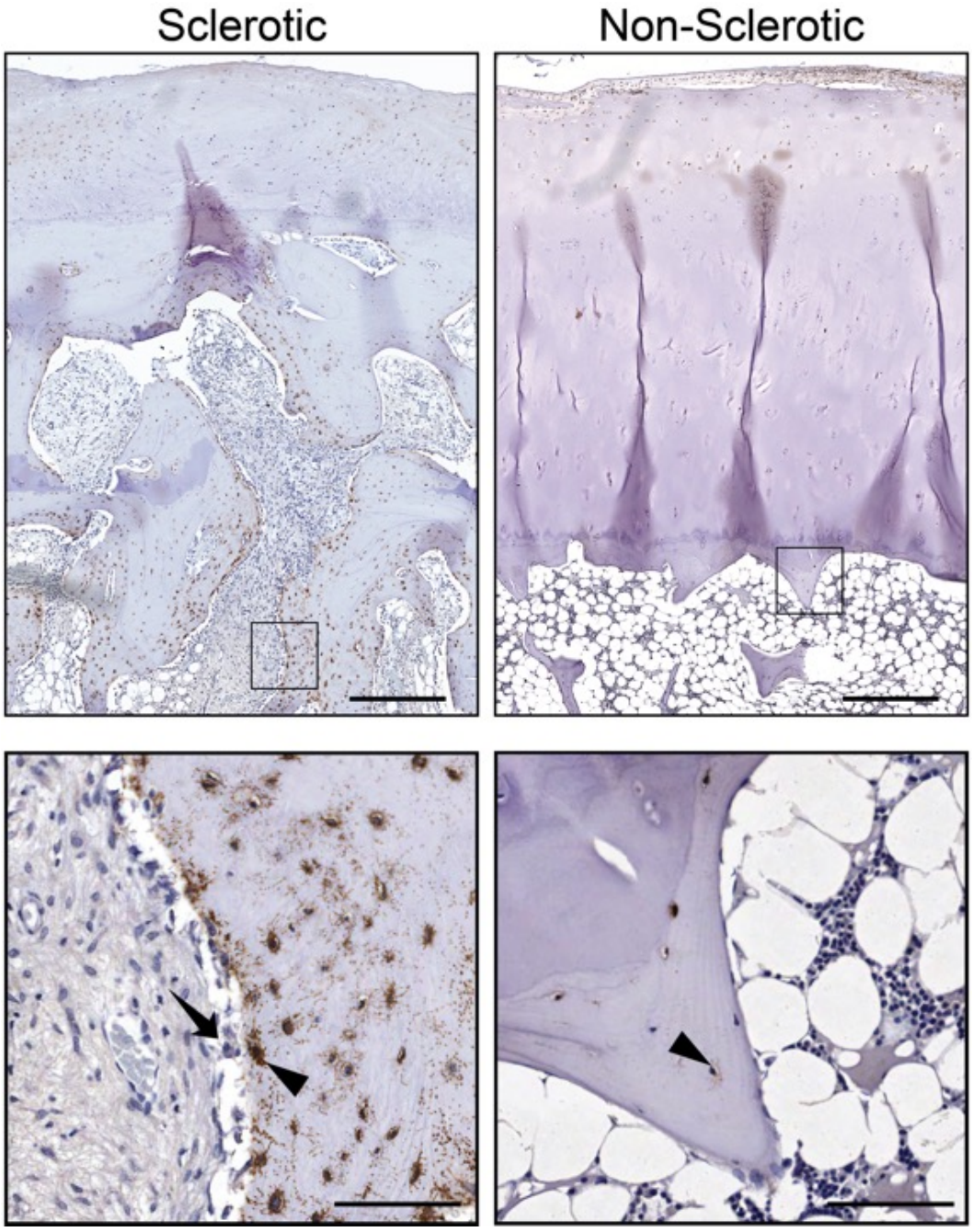

Figure 4.21. Immunohistochemical staining of OA femoral head showing the topography of E11 positive cells. *Global view of E11 positive osteocytes in sclerotic regions (left panels) and non-sclerotic regions (right panels) of the osteochondral region. Square areas magnified from upper panels showing the abundance of E11 positive osteocytes in the sclerotic areas (left panel) with increased presence in proximity to the bone lining osteoblasts (arrows). In non-sclerotic areas (right panels) E11 positivity was not as evident, with only some positive osteocytes and of distinctive morphology, with smaller, more elongated cell body and less dendritic processes compared to the ones from sclerotic areas. Arrow heads: E11 positive osteocytes; arrows: osteoblast. Scale bar: 200 μm (upper panels) and 50 μm (bottom panels). Sample ID: DIFHOA018*

Having observed the noticeable difference in morphology of the osteocytes between the two distinct areas of OA pathology, the E11-positive osteocytes were examined at a higher magnification in both sclerotic and non-sclerotic regions, but also in healthy IC bone (Figure 4.22).

The E11-positive osteocytes from healthy IC resemble a morphology consistent with previous published work (Zhang et al., 2006; Prideaux et al., 2012; Staines et al., 2017). They were characterised by an elongated morphology with a small cell body and organised dendritic processes aligned towards the surface of the bone. The E11-positive osteocytes from the non-sclerotic regions of femoral heads had an indistinguishable morphology to IC ones, with the osteocytes having a similar elongated body and aligned dendritic processes. Also, their size seems to decrease proportionally with their embedding distantly from the bone surface (non-sclerotic, Figure 4.22). In contrast, the osteocytes from the sclerotic areas had numerous and disorganised dendritic processes radiating chaotically from their body, with no specific orientation. Their cell body was visibly larger and more circular compared to osteocytes from non-sclerotic areas and healthy IC and they seem to be present at a higher density in the vicinity of the bone lining cells (Figure 4.22).

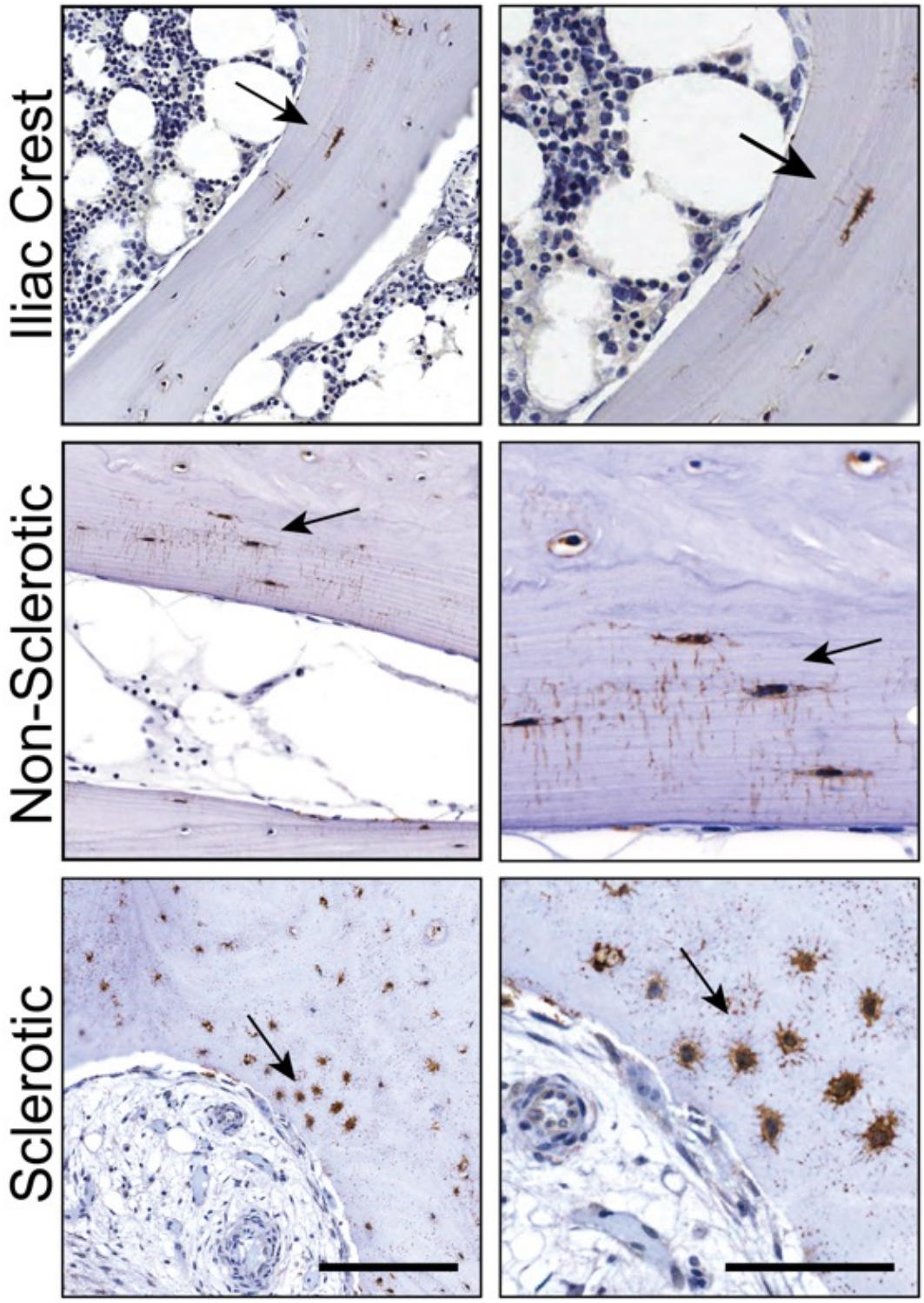

Figure 4.22. Morphology of E11 positive osteocytes in IC and OA bone. *Representative images showing immunostaining for E11 in healthy iliac crest bone (upper panel) and non-sclerotic (middle panel) and sclerotic (bottom panel) regions of OA femoral heads. High magnification images show the similar morphologies of E11 positive osteocytes between iliac crest and non-sclerotic regions of OA femoral head as opposed to the distinct morphologies of osteocytes from the sclerotic regions. Scale bar: 100 μm (left panels) and 50 μm (right panels). Sample IDs: IC: DIHIC03; OA: DIFHOA018*

E11 positivity was next analysed semi-quantitatively and compared between sclerotic (Figure 4.23A) and non-sclerotic (Figure 4.23B) regions of the femoral heads from three different donors. To avoid any bias in counting the positive osteocytes, the signal for E11-positivity was measured by using the computer software Nuance with the threshold set on negative control DAB-only positive slide. All the osteocytes were then counted in a minimum of 10 regions for each patient and the percentage of positive osteocytes out of total osteocytes in the bone area of a selected region of interest was calculated and presented as average for each S and NS region.

As shown in Figure 4.23C, the E11-positive osteocytes in the non-sclerotic areas were significantly less numerous (average 5-fold, $p<0.0001$) than in sclerotic areas. In all three donors, the percentage of E11-positive osteocytes in the non-sclerotic areas ranged between 6% and 49% with a median of 15% across all patients while in the sclerotic areas the majority were E11 positive. In the sclerotic areas, the percentages of E11-positive osteocytes ranged between 40% and 96% with a median of 76% across all three donors. Statistically significant distinction in the presence of E11-positive osteocytes was observed in the samples from all three patients.

The significant increase of the E11-positive osteocytes in the sclerotic regions of the OA femoral heads allows an explanation for the differences observed in the gene expression analysis. The osteocytes from OA bone had a higher level of E11 gene expression, however this comparison was performed between global osteocytes from OA and healthy bone, irrespective of the site of damage. Here, the elevated numbers of E11-positive osteocytes indicate that the difference observed in gene expression may be due to their accumulation in the sclerotic areas of hip OA.

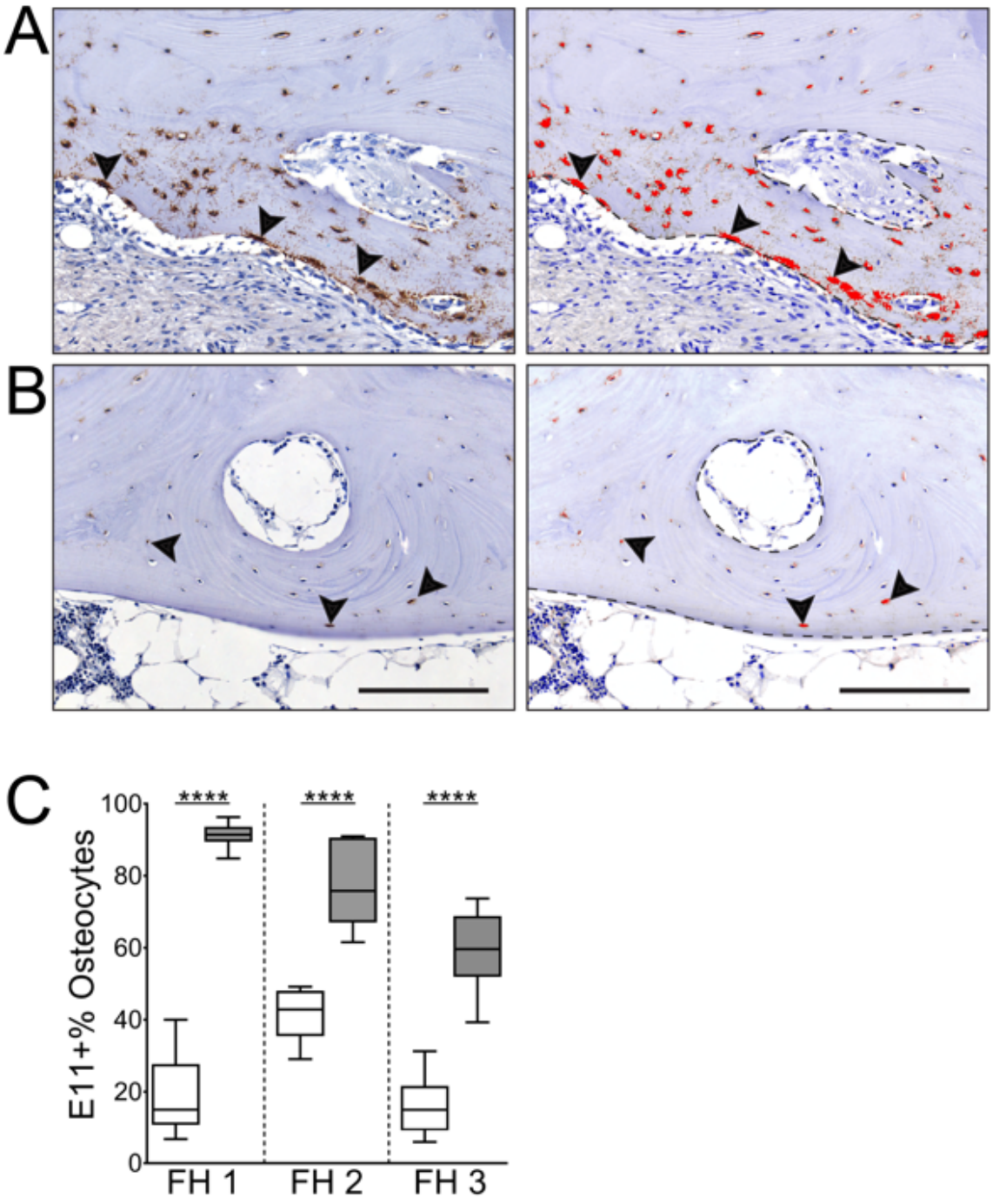

Figure 4.23. Quantification of E11 positive osteocytes in S and NS regions of OA bone. *Representative images showing immunostaining for E11 in sclerotic (A) and non-sclerotic (B) regions of OA femoral heads. Right panels A and B show the selection of regions of interest (within the dashed lines) in the bone area for semi-automatic counting of E11 positive osteocytes. Red colour indicates positive staining based on the negative control threshold set on DAB-only slide. (C) The proportions of E11-positive osteocytes in these regions was quantified in a minimum of 10 regions each in three femoral heads (FH) from three donors (empty boxes – non-sclerotic regions, grey boxes – sclerotic regions). Scale bars: 100 μm. Sample ID: DIFHOA018*

In Chapter 3, several alterations in the gene expression of native MSCs were observed between healthy and OA bone-derived cells. These included an increased expression of osteogenic molecules, such as *RUNX2*, *SPARC*, *ALPL*, *CDH11* and *OPG*. In the present chapter, so far it has been demonstrated that the OA osteocytes were also affected by the disease process, confirmed at both the gene expression level and protein level. Specifically, E11-positive osteocytes were shown to be accumulated in the sclerotic areas of the femoral heads of hip OA characterised by an increased bone area. Since the MSCs have been previously shown to be accumulated at sites of OA associated bone alterations (Campbell et al., 2016), this emphasises the value in investigating MSCs topography in relation to the E11-positive osteocytes in the sclerotic areas of hip OA.

In the sclerotic regions of OA femoral heads, CD271-positive MSCs were highly abundant in the fibrovascular tissue, that had replaced the BM, with the highest density of positive cells present around blood vessels and near bone surfaces lined with cuboidal osteoblasts (Figure 4.24, left panels). In non-sclerotic regions, especially in the subchondral area, CD271-positive cells were less numerous and had predominantly bone-lining topography (Figure 4.24, right panels). A dense fibrovascular tissue of yet unknown cellular origin, inhabits the sclerotic bone cavity which breached into the cartilage layer. Although other cells were present, such as osteoblasts and the dense fibrovascular tissue, the majority of them were CD271-positive cells with a high abundance around the blood vessels and in proximity to the bone surface. In the subchondral area of minimal osteochondral damage, the fibrovascular tissue was absent and the CD271-positive cells were restricted to a bone lining location (Figure 4.24, right panels).

The non-sclerotic trabecular bone that was distant from the subchondral areas was also lined with CD271-positive cells which were similar in localisation to healthy IC bone (Figure 4.25). Within non-sclerotic regions CD271 positivity was also detected in the stromal tissue cells with no visible distinction between the healthy IC and the non-sclerotic trabecular bone from OA femoral heads (Figure 4.25). The trabecular bone along with the lining CD271-positive cells from the IC bone and the femoral head are visibly indistinguishable.

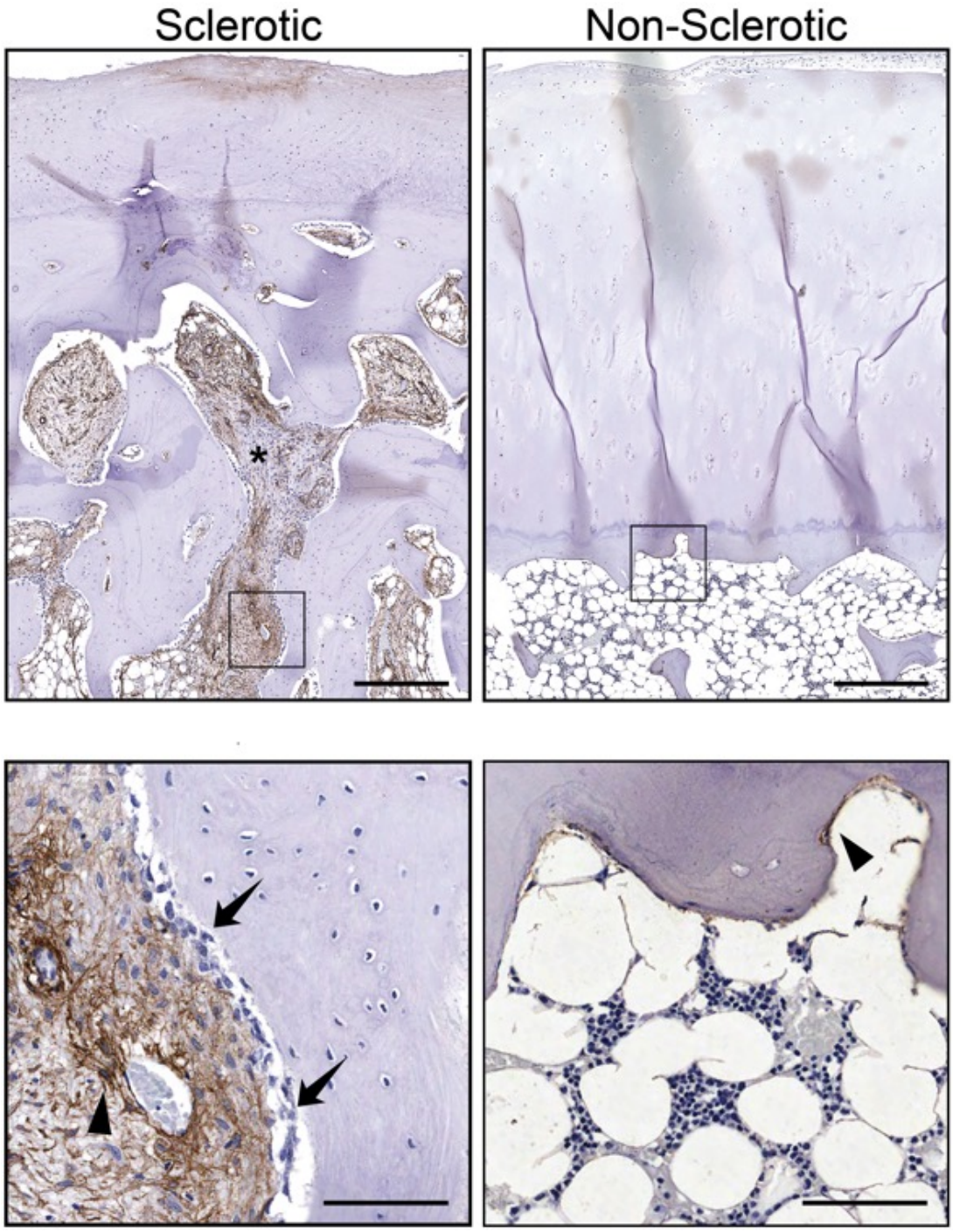

Figure 4.24. Immunohistochemical staining of OA femoral head showing the topography of CD271 positive cells in S regions (left panels) and NS regions (right panels) of the subchondral bone. *Square areas magnified from upper panels showing the abundance of CD271 positive cells in the dense fibrovascular tissue of sclerotic areas (left panel) with increased presence around blood vessels and adjacent to bone lining osteoblasts shown by long arrows. In non-sclerotic areas (right panels) CD271 positivity was less prominent, with only some bone lining cells positive. Arrow heads: CD271+ cells; arrows: osteoblasts. Scale bar: 200 μm (upper panels) and 50 μm (bottom panels). Sample ID: DIFHOA018*

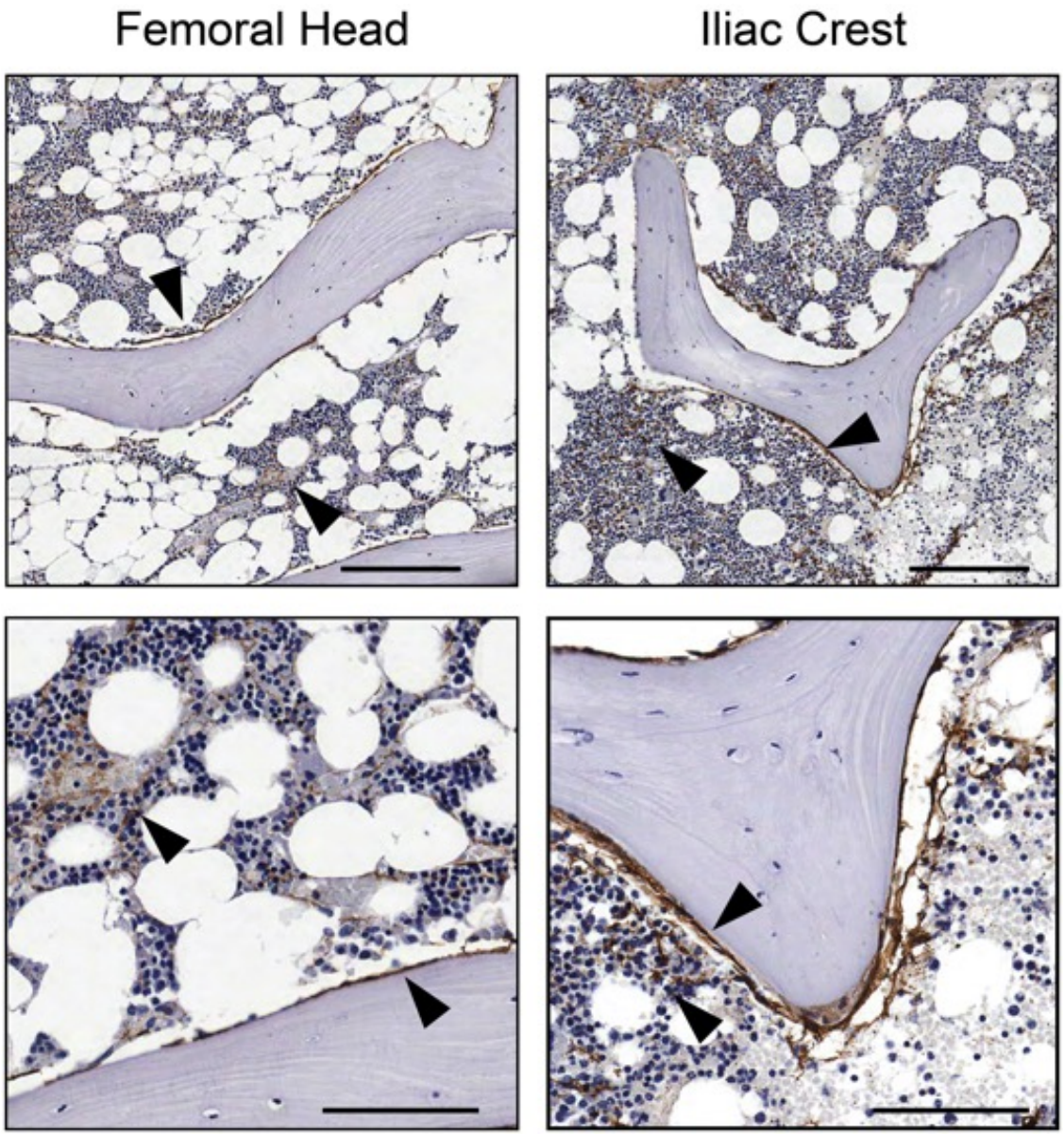

Figure 4.25. Topographical comparison of CD271 positive cells between healthy iliac crest and NS regions of OA bone. *Similarity in the topography of CD271+ cells from the trabecular bone distant from subchondral bone, in the non-sclerotic areas of OA femoral heads (left panels) and healthy iliac crest bone (right panels). Arrow heads point to CD271+ cells lining the bone in both regions as well as the scattered presence in the stromal tissue. Scale bar: 200μm (upper panels) and 50μm (bottom panels). Sample IDs: IC: DIHIC03; OA: DIFHOA018*

To quantify the presence of MSCs in regions of bone sclerosis (S) and compare it to regions of less damage (non-sclerotic, NS), the CD271 positivity was then measured within the trabecular space of S (Figure 4.26A) and NS (Figure 4.26B) regions of OA femoral heads (n=3). The quantification was done by using a computer software (Nuance) with the threshold set on a control DAB-only positive slide and calculation was performed as percentage of positive area in relation to total bone cavity area.

The density of CD271-positive cells in the S regions populated by the aforementioned dense fibrovascular tissue in all three patients was significantly higher than the donor-matched non-sclerotic areas. In the S regions, the area of CD271 positivity was 9-fold higher ($p<0.0001$) than in the non-sclerotic regions from the same femoral head (Figure 4.26C) based on the medians between the three donors analysed in this experiment. The differences between the two regions were statistically significant, consistently across all three donors (Figure 4.26 C).

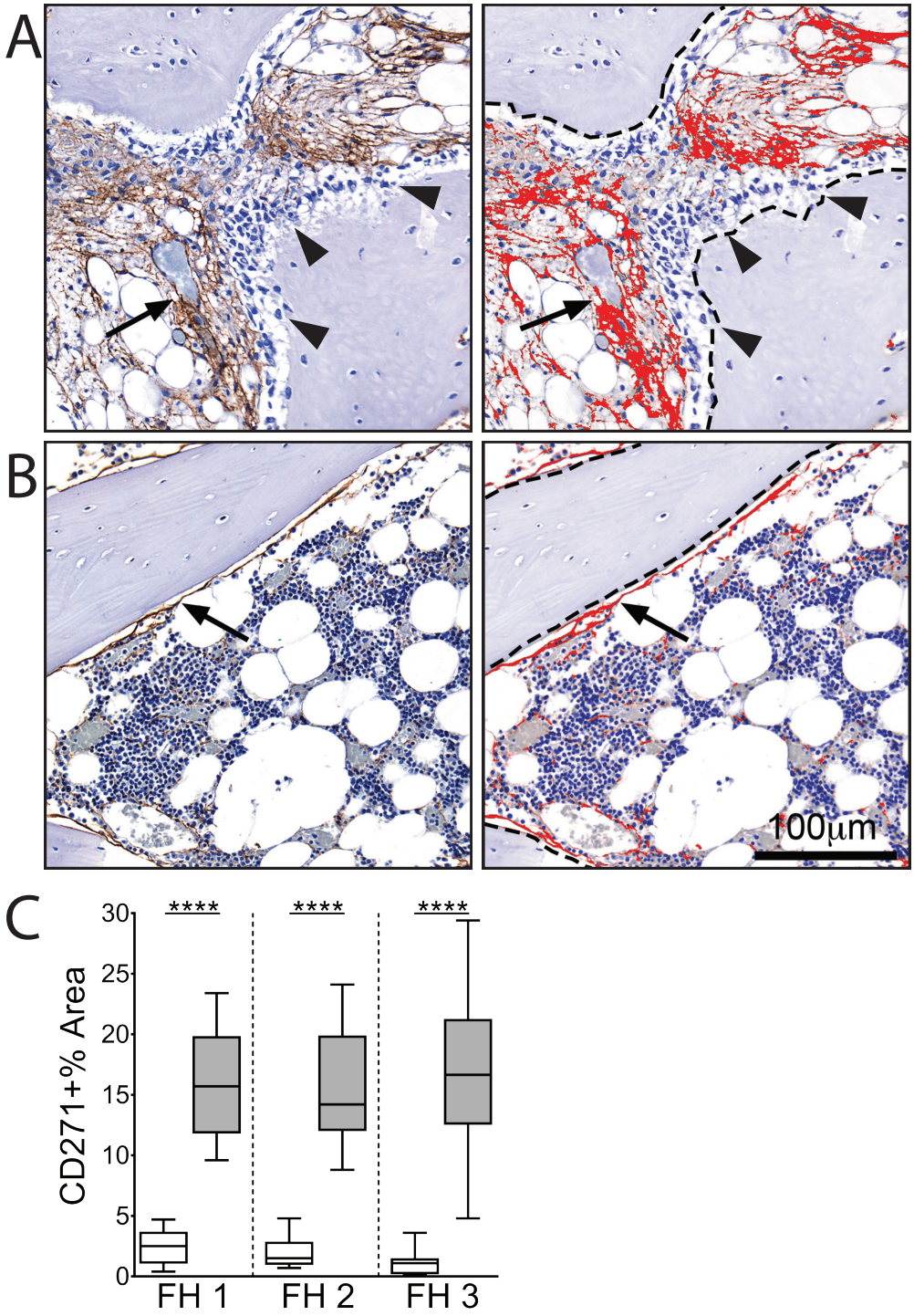

Figure 4.26. Quantification of CD271 staining in OA femoral head from sclerotic (A) and non-sclerotic (B) bone areas. *Left panels in A and B show representative DAB+ cells (brown) in the regions selected for analysis. Right panels show the selection of regions of interest (within the dashed lines) in the bone cavity area for CD271 quantification. Red colour indicates positive staining based on the negative control threshold set on DAB-only slide. (C) Quantification of CD271+ area of non-sclerotic (empty boxes) and sclerotic (grey boxes) regions from n=3 femoral heads (FH); Arrow heads: osteoblasts, arrows: CD271+ MSCs. Sample ID: DIFHOA018*

Altogether, this staining pattern revealed that, similar to E11-positive osteocytes, in sclerotic regions the CD271-positive MSCs also accumulated in sclerotic areas and that they were located near the bone surface as well as within the fibrovascular tissue, particularly around blood vessels as shown in Figures 4.24 and 4.26.

Next, the co-localisation of CD271+ MSCs and the early E11-positive osteocytes within the same area was analysed using adjacent sections from the same tissue samples (Figure 4.27). Many CD271+ MSCs can be seen concentrated in the vicinity of osteoblasts (Figure 4.27, right panel), in proximity to the bone. This suggests the possibility that MSCs located near the bone surface rather than perivascular MSCs may be specifically responsible for osteoblasts and subsequently, for osteocyte deposition. The left panel in Figure 4.27 shows the distinct morphologies of osteocytes strongly positive for E11 and situated near the bone surface, some in direct contact with these bone lining cells, which in the absence of osteoblasts are CD271+ as shown previously (Figures 4.25 and 4.26). Since E11 expression marks a new stage along the osteogenic progression, it would be interesting to investigate bone-lining MSC subset is more detail, particularly in relation to bone pathology in OA.

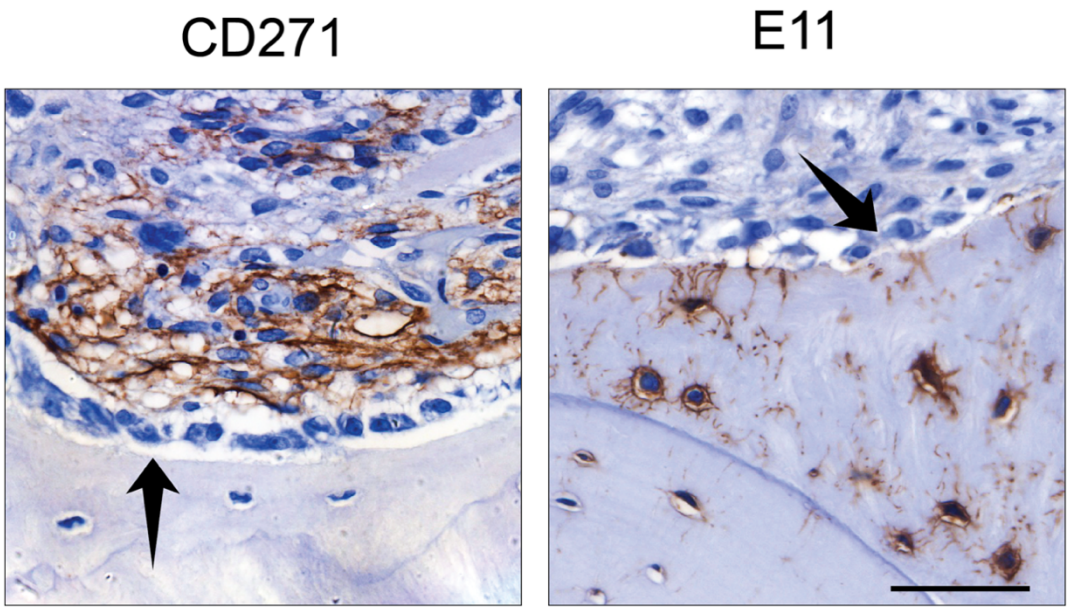

Figure 4.27. MSC and early-osteocyte co-localisation in S areas of hip OA. *Left panel: increased MSC presence is marked by abundance of CD271+ cells (brown) near bone surface and in the fibrovascular tissue, adjacent to bone lining cells and osteoblasts (arrows). Right panel: E11-positive osteocytes (brown) embedded in newly formed osteoid. A demarcation line separates the bone rich in E11-positive osteocytes from the more mineralised bone, inhabited by more mature and less E11-positive osteocytes with different morphology. Scale bar: 50 µm. Sample ID: DIFHOA018*

4.5 Discussion

The unexplored functional characteristics of osteocytes and MSCs during OA pathogenesis and progression, and the possibility of detecting novel molecular candidates responsible for their interaction under normal and pathological conditions holds great interest. Although the communication between osteocytes and other bone cells such as osteoblasts has been well documented (Kamioka et al., 2004; Paic et al., 2009; Dallas and Bonewald, 2010) their interactions with the MSCs are still unexplored. In the present work, it was hypothesised that abnormally committed MSCs would directly impact on their terminally differentiated osteocyte descendants with numerical and functional perturbations in OA bone.

4.5.1 The simultaneous analysis of osteocytes and MSC from human bone

Firstly, to address this, methodologies were optimised to investigate the gene expression signature of native osteocytes in osteocyte-enriched bone fragments and compare it to native uncultured MSCs from the same bone. The MSCs were isolated by enzymatic extraction as previously described (Jones et al., 2010), followed by cell sorting using the $CD45^{-}CD271^{+}$ cell surface phenotype and gene expression analysis as described in Chapter 3 Section x. The enzymatic removal of all the soft tissue from the bone surface was possible during the MSC extraction stage, leaving the bone-embedded osteocytes to be the only remaining cellular material. The approach was then to lyse the osteocytes *in situ* and extract the RNA from native osteocytes without any *in vitro* manipulation.

The first aim of this chapter was to establish robust gene markers for native human osteocytes and test their specificity by comparing them to native MSCs. The selected panel of genes have been previously documented and established as osteocytes markers based on extensive animal work and on cell lines as reviewed by Dallas et al. (Dallas et al., 2013), but their specificity to native human osteocytes has not yet been investigated.

The study of osteocytes in their native environment is complicated by their entrapment in a mineralised bone matrix (Prideaux, Findlay, et al., 2016) hence the biochemical data characterizing their precise role in bone associated pathologies have thus far been limited. Several *in vivo* models have been developed to study their function, however the studies on human osteocytes is scarce. Native gene expression of osteocytes has been documented in a mouse model for load induced adaptation of the vertebras (Wasserman et al., 2013) and similarly on osteocytes isolated by gene fractionation and FACS, also from mouse bones. Pertaining human studies, some focused on the analysis of their

viability and molecular responses following short-term culture of the osteocyte-enriched bone chips (Shah et al., 2016; Pathak et al., 2016). However, in these two studies, osteocytes were studied *in vitro*, their purity was not confirmed histologically and no comparisons were made with other bone-lineage cells such as MSCs.

Data in this chapter showed that markers of mature osteocytes, such as the bone formation inhibitor *SOST* and the mineral and phosphate regulating molecules, *DMP1, MEPE* and *PHEX* (Martin et al., 2011) were the most specific markers for human osteocytes when compared to MSCs. Although *SOST* is commonly known as a classical osteocyte molecule (van Bezooijen et al., 2004), and its specificity was confirmed in this chapter, the variable expression levels found here suggest more caution in the use of this molecule as a positive marker on its own for osteocytes studies.

On the other hand, the expression of *DMP1*, *PHEX* and *MEPE* were reliably expressed in all osteocytes samples at higher levels than the MSCs from the same bone. *MEPE*, originally identified as a substrate for *PHEX*, is primarily expressed by osteocytes (Nampei et al., 2004). Evidence for a direct role of *MEPE* in bone mineralisation came from the increased mRNA expression levels of *MEPE* seen during osteoblast matrix mineralisation (Petersen et al., 2000). *DMP1* and *PHEX* are both expressed by osteocytes and were also shown to regulate the expression of *FGF23* (Martin et al., 2011). The key regulator of phosphate homeostasis, *FGF23*, is expressed predominantly by osteocytes (Yoshiko et al., 2007; Ubaidus et al., 2009) and data presented here showed higher levels of expression in osteocytes compared to MSCs in both health and disease. As expected, the early osteocyte marker *E11* was the least differentially expressed between osteocytes and MSCs.

The expression of these markers in osteocytes *in vitro* however, requires further investigation. While most of the markers showed stability in culture (for 7 days), the expression of *FGF23* was clearly affected (Figure 4.9). Moreover, the expression of RANKL and OPG also showed dysregulated expression while subjected to mechanical stimulation and while in culture conditions. Current studies using osteocytes culture methods should take into consideration the effect of culture conditions on the phenotype of these cells. An *in vitro* study by Pathak *et al*. investigated the effect of RA-serum or inflammatory cytokines on expression of human osteocyte-specific proteins and cytokines (Pathak et al., 2016). While osteocytes are viable after one week in culture as shown in this chapter and by this study as well (Pathak et al., 2016), and still express their specific markers as described in Section 4.4.3, the osteocyte phenotype is likely to be

different than its native counterpart. Data obtained from these cultures should consider potential differences induced by culture conditions to the factors secreted by osteocytes and more work is needed to determine the extent of these changes. This may include analysis of gene expression and measurement of osteocytes-secreted soluble factors during a lengthier time course with multiple and closer time points. Furthermore, osteocyte-specific mechanical stimulation methods could also be employed, such as fluid flow, hydrostatic pressure, mechanical stretching or low-magnitude, high-frequency vibration (Lau et al., 2010).

Altogether, this differential gene expression pattern observed in native osteocytes by the methodology described in this chapter confirmed that the optimised bone processing protocol produced osteocyte-enriched bone and could be used to compare osteocyte gene expression between healthy and OA bone.

4.5.2 Osteocytes in hip OA

The second aim was therefore to investigate the gene expression profiles of native osteocytes in OA as compared to their healthy counterparts. It was shown that native osteocytes in OA resemble an early phenotype marked by increased expression of *E11* and *MMP14* and may be involved in bone resorption inhibition indicated by elevated levels of *OPG*.

Osteocytes sense biomechanical signals through a highly interconnected network of dendritic processes (Bonewald, 2011). The formation of these dendritic processes occurs at the early stages of osteocytes development during their entrapment in the bone matrix. While the elongation of dendritic processes is facilitated by E11, also known as podoplanin (Zhang et al., 2006) the embedding of osteocytes in the collagenous osteoid has been described to involve the expression of *MMP14* (Holmbeck et al., 2005). Data in this chapter showed high levels of *E11* transcripts in native OA osteocytes which indicated a young and immature profile of these cells in OA. The increased expression of *MMP14* observed here is therefore more owing to these elevated early-osteocytes, actively embedding into the osteoid. In response to changes in bone biomechanics, osteocytes adapt by modulating the local and global environment (Rubin et al., 2002), by recruiting osteoclasts to resorb bone and osteoblast to form bone, maintaining normal tissue homeostasis. However, this adaptation may be also possible by means of their own ability to resorb bone and modulate its matrix attachment. The elevated levels of *MMP14* found in OA osteocytes may also indicate an active osteocytic osteolysis during the early stages of osteocytes maturation. Indeed, two animal model studies have shown that peri-

canalicular osteopenia is a feature of osteocyte remodelling (Fowler et al., 2017; Dole et al., 2017).

The RANKL/OPG system is a pathway of important clinical implications with potential therapeutic role in skeletal diseases such as osteoporosis (Cummings et al., 2009), rheumatoid arthritis (Haynes et al., 2008), juvenile Paget's disease (Whyte et al., 2002) and a range of bone tumours (Mundy, 2002). When the mRNA expression levels of *RANKL* and *OPG* were compared between OA osteocytes, it was observed that a trend exists for increased *OPG* expression in OA bone however, *RANKL* levels were unaltered. As mentioned before, several lines of evidence have now established a key role for osteocytes in the regulation of bone resorption by its expression of RANKL, showing that deletion of RANKL in osteocytes leads to increased bone mass (Nakashima et al., 2011; Xiong et al., 2015). However, equally important is its main inhibitor, OPG, and little is known about the role of OPG in osteocytes. Data presented in this chapter with regards to OPG suggest that osteocytes may act together with MSCs for a global enhancement of bone formation and inhibition of bone resorption. MSCs were documented in Chapter 3 as having a committed osteogenic profile while here data suggest that osteocytes may play a role in supporting that osteogenic activity by inhibition of bone resorption. However, confirmation of these mechanisms requires further work.

In addition, the mRNA levels for the other two molecules with active roles in bone resorption, cathepsin K and TRAP, showed trends for increased expression at a gene level in OA osteocytes, but not statistically significant. However, using histology and IHC osteocytes in OA showed no positivity for either TRAP or CTSK, indicating they are not involved directly in resorption activities. This comes in contradiction with other studies reporting TRAP positive osteocytes and a potential contribution to OA subchondral bone pathogenesis (Jaiprakash et al., 2012), however that study was performed in knee OA. Hip and knee OA have distinct clinical presentations (Le Marshall et al., 2013) which may indicate different progression rates and, biochemical and cellular responses due to the different anatomical sites with distinct biomechanical properties of the joints.

Sclerostin is a known potent inhibitor of bone formation which was confirmed to be secreted mostly by mature, late osteocytes (Poole et al., 2005). The variable low levels of *SOST* observed in OA osteocytes in this study as well as by others (Jaiprakash et al., 2012) may represent their response to the magnitude of altered biomechanics of the OA joint (Jia et al., 2018). Furthermore, a more viable explanation may be the variable rates

of early-osteocyte formation from MSCs, these immature cells being unlikely to produce *SOST* as suggested by data in this chapter.

4.5.3 Topographic relationships between osteocytes and MSCs in OA femoral head bone

The final aim of this chapter was to map the topographical relationships between osteocytes and MSCs in relation to OA associated bone alterations. With the use of antibodies against E11 for early osteocytes and CD271 for MSCs, active osteocytogenesis was documented in osteoarthritic femoral heads in the vicinity of MSCs, in sclerotic areas associated with severe osteochondral damage. This provided an indication of the cellular mechanism for pathological subchondral bone changes including subchondral bone sclerosis in hip OA.

High densities of E11-positive osteocytes were found in the outer edges of thick bone trabeculae in areas of bone sclerosis and cartilage loss and in proximity to CD271-positive MSCs and osteoblasts confirming an ongoing osteocyte formation process in OA femoral heads at the protein level. These early osteocytes were also characterised by disorganised dendritic processes which may translate into poor mechanosensing capabilities (Burra et al., 2010). In healthy bone, osteocytes are well connected, and the dendritic processes are oriented in the direction of the blood supply and along the pressure lines induced by mechanical forces (Palumbo, 1986; Petrtýl et al., 1996; You et al., 2004). In osteoarthritic bone, there is a notable distortion of the dendritic processes, which may indicate a decreased connectivity. All the molecules secreted by osteocytes reach their target through the interconnected canalicular network (Schaffler et al., 2014). Changes in osteocyte connectivity could have a dramatic effect not only on osteocyte function and viability, but also on the mechanical properties of bone. Although IHC and histological assessment in this chapter provided an indication of a disrupted osteocyte network, this could be further investigated by means of 3D visualisation of the whole lacuno-canalicular network in the sclerotic areas associated with OA.

Immunohistochemical staining showed strong OPG protein positivity in the whole of the fibrovascular tissue which invaded into the articular cartilage in non-weight bearing areas where it could be a forerunner to a central osteophyte. Previous studies proposed fibrovascular tissue, which also carries nerves, as a contributor to OA joint pain (Suri and Walsh, 2012). The present data indicated its potential contribution to central osteophytosis in hip OA.

It would be interesting to establish whether the reported subchondral bone softening in OA bone (L.G. Cox et al., 2012; Burr and Gallant, 2012) is attributable to an inability of the newly formed osteocytes to mineralise their surrounding tissue or it is the hypomineralisation that prevents the maturation of these cells. Studies on animal models suggest the latter. It was shown that the maturation of osteocytes was halted by inhibiting matrix mineralisation, suggesting that mineralization of the matrix surrounding the osteocyte is the trigger for their differentiation from an immature osteoblastic-like form to a mature osteocyte (Irie et al., 2008). This was later confirmed by Prideaux *et al*. in a *in vitro* study using MLO-Y4 cell line demonstrating that the mineralisation of the extracellular matrix drives the osteocytes maturation and moreover, it induces the expression of E11 (Prideaux et al., 2012). Data presented in this chapter provides evidence of increased human early osteocytes presence in areas of bone sclerosis in hip OA, in the vicinity of MSCs however further work is needed to establish the degree of tissue mineralisation in these areas of interest. This can be done by micro-CT in the first instance followed by tissue decalcification and Mason Trichrome staining to observe the newly formed bone (osteoid) and immunohistochemistry using antibodies against E11 to confirm the presence of early osteocytes in these regions.

The present findings demonstrated for the first time, the high specificity of the selected genes for discriminating between native human osteocytes and MSCs, and a pattern of differences reflective of osteocyte maturation stage from the earliest markers such as *E11* to the late markers, *DMP1* and *SOST*. The results in this chapter have implicated subchondral bone MSCs as a key population driving subchondral bone abnormalities in hip OA with direct consequences in their descendants, the osteocytes. No previous study has documented early osteocytes in OA, in regions of active bone formation where their immature progenitors, the MSCs, accumulate in high numbers. Highly heterogeneous MSC topographies prevented accurate quantification of individual MSCs *in situ*, however surface area measurements indicated their significant accumulation in sclerotic areas. The cellular origin of the fibrovascular tissue formation is intriguing, but its fibroblast and bone lineage cellular elements are likely to be derived from MSCs. Furthermore, given the heterogeneous nature of MSCs and the increased expression of MCAM in the OA-resident CD271+ MSCs it is possible that a certain perivascular subset may be the driver of this osteogenic bias and if true, may be harnessed for therapy interventions.

The present findings documenting an exaggerated MSC-early osteocyte maturation axis in hip OA (Figure 4.28) provide a cellular mechanism for pathological subchondral bone

sclerosis in this condition and implicate aberrant differentiation of local bone-resident MSCs in human OA pathogenesis. The dynamics of osteocytes in respect to morphology, gene expression and implicitly, their function, depend upon the cell's prior differentiation history as well as its living environment within the tissue. Exploiting this method to extract biochemical information from osteocytes will greatly facilitate a more complete understanding of their biology *in vivo* both in health and disease.

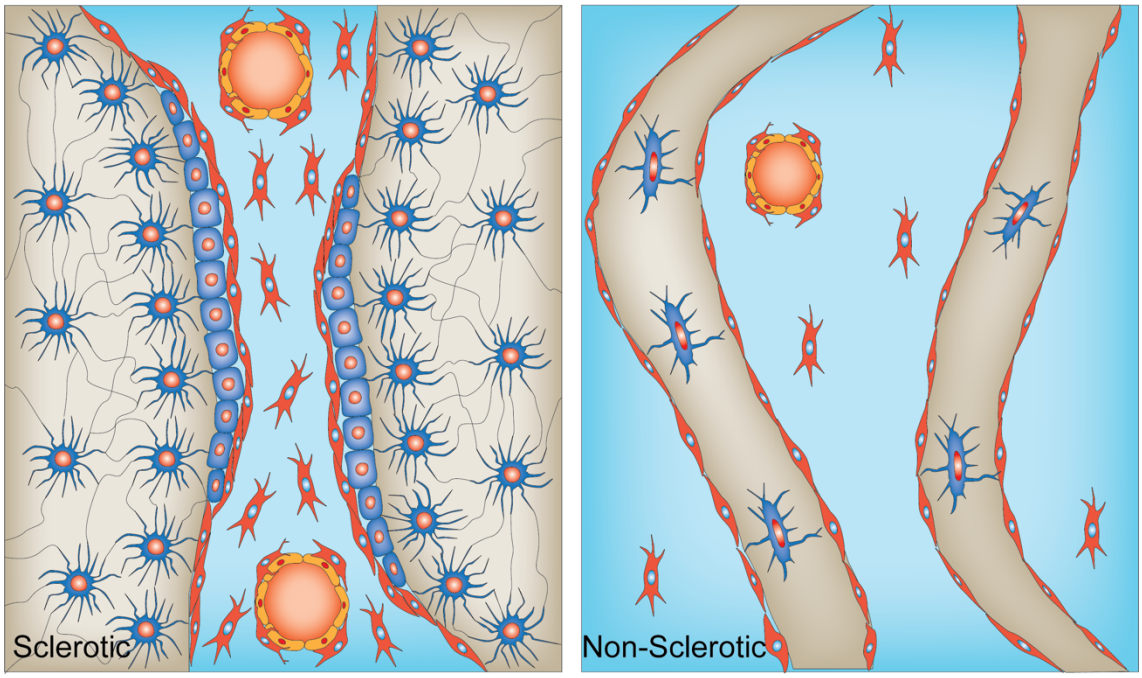

Figure 4.28. Cellular mechanisms of bone sclerosis in OA: The schematic illustrating the spatial cellular relationships along the "MSC – Osteocyte axis". *Sclerotic regions in the OA subchondral bone are characterised by thickened trabeculae. Resident osteocytes are morphologically distinct, with a rounded cell body and high number of dendritic projections. They are E11-positive and densely distributed in the vicinity of bone lining osteoblasts and adjacent MSCs. The fibrovascular tissue replacing the BM in the sclerotic regions is populated by a high number of bone lining and perivascular MSCs. In non-sclerotic regions, the trabeculae are much thinner with a significantly lower density of E11-positive osteocytes and MSCs. Osteoblasts are absent from the surface of the bone due to lower bone remodelling activity while MSCs are lining the bone instead, forming an interconnected meshwork with the other stromal and perivascular MSCs.*

Chapter 5 The roles of a novel $CD45^{-}CD271^{+}CD56^{+}$ MSC subset in OA bone

5.1 Introduction

Skeletal tissue undergoes constant remodelling throughout adult life in order to maintain bone strength and tissue homeostasis. As described in previous chapters, bone remodelling is an active and dynamic process involving the participation of multiple cell types as well as the secretion and uptake of numerous growth factors and cytokines by these cells during different stages of this process (Rucci, 2008). Osteoprogenitor lineage differentiation is one of the key processes involved in bone formation and remodelling. During this process, a subpopulation of mesenchymal progenitors undergoes osteoblast lineage commitment and matures through a series of differentiation steps. In response to appropriate signals the progenitor cells first proliferate, then secrete extracellular matrix that will then mineralize, embedding the cells within the matrix (Aubin, 1998). The osteocytes, engulfed in this mineralized matrix, represent the terminal differentiation stage of osteoblast lineage. While the osteocytes and MSCs were discussed in previous chapters, little is known about the intermediate stage of differentiation which is commonly represented by a still poorly defined subpopulation of osteoprogenitors. Furthermore, data presented in Chapter 3 and Chapter 4 indicate that it is this osteogenically-committed MSC subsets that may be increased in OA. This chapter follows with the aims to identify the surface phenotype of these osteoprogenitor cells in health and disease and investigate their gene expression profile, with reference to their effectors, the osteoblasts and terminally differentiated osteocytes as well as their progenitors, the MSCs. Progress in this area may provide new insights into how these cells may be harnessed to prevent damage and re-establish bone homeostasis in OA.

5.1.1 Osteogenic commitment of MSCs

So far data presented in this project indicated an increased osteogenic activity in OA bone, with evidence implicating both MSCs and osteocytes in the abnormal bone phenotype observed in OA. The MSCs present in OA femoral heads were shown to accumulate in areas of bone sclerosis while gene expression analysis suggested an altered phenotype with a predilection for bone formation. Furthermore, an increased density of young and immature osteocytes inhabiting the sclerotic bone areas where MSCs and osteoblasts were found to accumulate (Figure 4.28) may indicate a result of a skewed differentiation balance in the resident MSCs population. Along the osteogenic differentiation axis

however, there are other cellular stages that are still not clearly defined yet, such as the committed osteoprogenitor MSCs which subsequently give rise to the bone forming osteoblasts.

The specific differentiation pathways of MSC are guided by a complex multigenic process under the control of key regulatory and transcriptional factors, such as *RUNX2* and osterix (*SP7*) (Komori, 2006), as described in detail in Chapter 1, Section 1.3.3. *RUNX2* is well known as an early osteogenic marker (Komori et al., 1997) regulating, amongst other genes, the expression of *BGLAP* (osteocalcin) (Sierra et al., 2003), a protein involved in matrix mineralization and calcium ion homeostasis (Wei and Karsenty, 2015) also widely used as a marker for new bone formation (Chapurlat and Confavreux, 2016). Other molecules known to be commonly attributed to the osteogenic MSC lineage are *SPP1* (osteopontin), type I collagen and *ALP*. Bone specific ALP, encoded in MSCs by *ALPL* gene, is necessary to supply phosphate for bone mineral and is a good indicator of bone synthesis (Garnero and Delmas, 1998) while type I collagen represents the major protein component of bone (Tamma et al., 2014). Both molecules were shown to be expressed by native MSCs (Churchman et al., 2012). Along the osteogenic differentiation process, the cells also express osteomodulin (OMD), also known as osteoadherin (Rehn et al., 2008). OMD is an extracellular matrix keratan sulphate proteoglycan member of the small leucine-rich repeat protein family (Sommarin et al., 1998) secreted into the matrix at the time of mineralization (Lucchini et al., 2004; Rehn et al., 2008) and is proposed to be a reliable marker for mature osteoblasts. Its overexpression was shown to enhance the differentiation and maturation of osteoblasts *in vitro* (Rehn et al., 2008) and may be implicated in mineralization processes, regulating osteoblast metabolism by binding alpha (V) beta (3)-integrin (Lucchini et al., 2004; Rehn et al., 2008). The expression of many genes associated with osteoblasts on undifferentiated MSCs is intriguing. The simultaneous expression of mature fat molecules may indicate they are present in a poised state ready for differentiation (Nombela-Arrieta et al., 2011). It was therefore hypothesised that the osteogenic committed MSCs subset is likely to have upregulated bone associated genes while the fat transcripts would be downregulated.

5.1.2 Bone lining cells: the candidate subset and novel players in bone remodelling

The topographical localisation of native $CD45^{-}CD271^{+}$ MSCs in the BM stroma places these cells in both endosteal and perivascular niches (Chapter 1, Section 1.3.2), the latter

marked by the $CD271^{+}CD146^{+}$ MSC phenotype (Tormin et al., 2011). The results in Chapter 3 revealed that OA native MSCs were characterised by an increased transcriptional level of the surface perivascular MSC marker CD146 (Tormin et al., 2011) together with high expression of multiple osteogenesis-related transcripts. Considering the increased vascular presence in the OA affected bone (Walsh et al., 2010), this prompted the idea that in OA there was an increase in this particular MSC subset and may represent a good candidate for the osteogenic aberrations observed in OA bone. However, the cells lining the bone surface, including the already documented bone-lining CD271+CD146- MSCs (Tormin et al., 2011), may represent a runner-up candidate.

As stated in Chapter 1, the proportion of osteoblasts and osteoclasts in the skeleton represents a relatively small fraction in the pool of all bone cells. With regards to bone surface cells in particular, nearly 75% of cancellous bone surfaces and about 95% of intracortical surfaces is covered by a lining layer of flat cells (Miller et al., 1989). Bone lining cells (BLCs) much as their name suggests, are found lining the endosteal surfaces considered "inactive" or “resting” in terms of remodelling or modelling activities (neither resorption nor formation takes place), hence the commonly attributed name of quiescent bone lining cells (Matic et al., 2016).

These cells have long been observed histologically, primarily characterised based on their flat, elongated bone lining morphology and so far, their physiological functions in normal bone homeostasis has remained elusive. One of their roles proposed due to their location is that of a functional cellular barrier between bone and BM, separating the bone interstitial fluid from the general extracellular fluid (Wein, 2017). In addition, their location may also favour a direct contact with bone matrix embedded osteocytes, acting as a cellular link in calcium exchange and other substrates released by osteocytes (Wein, 2017). As such, these cells are best positioned to be the cells mediating MSC-osteocyte axis in OA.

To date, no markers have been described specific to BLCs or effective techniques to selectively isolate these cells, although they are thought to constitute part of the osteoblast lineage due to the expression of various bone related molecules (Miller et al., 1989; Andersen et al., 2009; Matic et al., 2016). Recent evidence in mouse models showed that BLCs represent a major source of osteoblasts during adulthood using cell tracing of osterix expressing bone lining cells. It was demonstrated that following osteoblasts ablation, the BLCs were proliferative and contributed significantly to new bone

formation, with little input from the nearby mesenchymal progenitors, identified by Gremlin marker (Matic et al., 2016).

More compelling evidence has recently emerged to support the idea that BLCs represent an osteoblastic progenitor pool. As discussed in both Chapter 1, Section 1.4 and Chapter 4, Section 4.1, SOST is a potent bone formation inhibitor secreted exclusively by osteocytes (van Bezooijen et al., 2004). Studies demonstrated the activation of bone formation following administration of antibodies against SOST in animal models (Li et al., 2009) and humans (McClung et al., 2014). Of importance is that the antibodies blocking SOST induced conversion of BLCs into active osteoblasts by their direct reactivation, contributing to increased osteoblast numbers following treatment in mice (Kim et al., 2017). Therefore, SOST neutralization caused BLCs to reacquire an osteoblastic phenotype. This followed a previous study in which it was demonstrated that BLCs reactivation was induced by intermittent parathyroid hormone treatment which additionally lowered SOST levels in bone (Keller and Kneissel, 2005). Altogether this indicated that BLCs reactivation could occur via reducing SOST production by osteocytes.

In addition to providing a source of osteoblasts (Matic et al., 2016), BLCs were shown to be critical in more bone remodelling processes. As discussed in Chapter 1, Section 1.2, the first phase of the bone remodelling process is activation of the endosteal surface. This implied that resorption was initiated at inactive sites, still coated by BLCs. The activation phase involves the recruitment of osteoclasts precursors at these sites moving on to the next stage of bone resorption by osteoclasts following their attachment to the bone surface (Allen and Burr, 2014). More evidence implicating BLCs in bone remodelling processes, indicate their role in coupling these phases of bone formation and bone resorption. As discussed in Chapter 1, Section 1.2, coupling requires the input of the cells present in the BMU following bone resorption, also known as reversal cells. These cells have been described to be present at the convergence of osteoclasts and osteoblasts and identified as BLCs (Andersen et al., 2013). Furthermore, some authors studying these events suggested their contribution to the progenitor pool of cells present in the BMU canopy (Kristensen et al., 2014). Furthermore, BLCs are thought to clean the surface of Howship's lacunae following osteoclastic bone resorption (Everts et al., 2002). Specifically, BLCs were shown to digest the remnant of collagen fibrils following bone resorption by osteoclasts. More interestingly, it was revealed that following the clean-up of the resorption pit, the BLCs deposited a thin layer of a collagenous matrix along the Howship's lacuna, in close

association with an osteopontin-rich cement line, thus preparing the grounds for the bone forming osteoblasts. Their catabolic functions were also demonstrated by their increased expression of matrix metalloproteinases (Dierkes et al., 2009). Given that CD271 was found expressed on BLCs (Figure 4.25), particularly in areas of bone remodelling and on canopies (Figure 4.26) in OA bone, it represents a good candidate for the osteogenic committed subset of MSCs.

At the endosteal level of the trabecular bone, a flat spindle-shaped cell layer was previously documented to express CD56, also known as neural adhesion molecule (Andersen et al., 2009). This molecule was also shown to be strongly expressed in most osteoblasts along bone trabeculae that coincide with the presence of collagen I and alkaline phosphatase activity (Lee and Chuong, 2009). Further histological studies showed that the CD56 expressing cells lining the surface of the bone (Andersen et al., 2009) were also expressing osterix (SP7) (Kristensen et al., 2013), indicating cells of osteoblastic lineage. On the bone surfaces, canopies have also been described as structures separating remodelling sites from the BM, consisting of CD56-positive osteoblasts at an early differentiation stage (Kristensen et al., 2013; Kristensen et al., 2014). Altogether this evidence indicates that CD56 represents a good candidate marker for the osteogenic committed MSCs subset.

5.1.3 Current state of the art in CD271 MSCs subsets

As mentioned in Chapter 1, Section 1.3.2, the topography of MSCs resident in the BM places them in a perivascular and bone lining location as well as in the stromal reticular niche, known as adventitial reticular cells where they are anchoring the other cells providing structural support of the stromal tissue (McGonagle et al., 2017). While the perivascular localisation would give MSCs easy access to most tissues for repair if needed (François et al., 2006), MSCs are also thought to be lining the bone surface (Tormin et al., 2011), as confirmed in this study (Figure 4.25 and 4.26). This endosteal localisation may provide them an ideal advantage to be involved in the bone remodelling activities.

As discussed in previous chapters, CD271 is accepted as the most specific marker for native BM MSCs (Quirici et al., 2002; Bühring et al., 2007; Jones et al., 2010). However, this population is heterogenous with studies indicating multiple subsets that form part of the same CD271+ phenotype (Battula et al., 2009; Tormin et al., 2011). The availability of appropriate molecular and cell surface markers that can be used to isolate and characterize these cell populations may lead to isolation of homogeneous cell samples.

Cluster of differentiation 146 (CD146), also known as melanoma cell adhesion molecule (MCAM) or cell surface glycoprotein Muc18, was originally identified as an endothelial cell marker with a role in cell-matrix interaction and angiogenesis (Lehmann et al., 1989; Bardin et al., 2001). CD146 defines the self-renewing MSC population located in the perivascular space of the BM (Sacchetti et al., 2007) which was also later introduced as an MSC surface marker in combination with CD271 (Tormin et al., 2011). Both the CD271+CD146- and CD271+CD146+ cells were later shown to have self-renewal properties as well as enriched CFU-Fs. Although they display a similar phenotype, the CD271+CD146+ population was associated with a perivascular location in the BM cavity where they have access to elevated oxygen levels close to the blood vessels as opposed to the more hypoxic conditions in the proximity of the bone surface (Tormin et al., 2011). Both CD271 and CD146 have been described to identify uncultured multipotent MSCs (Sacchetti et al., 2007; Tormin et al., 2011; Mabuchi et al., 2013) and are altered when the cells are expanded in culture. CD271 expression is lost during culture expansion (Quirici et al., 2002; Churchman et al., 2012) while CD146 surface marker expression is upregulated once the cells are cultured but is downregulated when cultured under hypoxic conditions (Tormin et al., 2011). Furthermore, data in Chapter 3 suggested an increased presence of a perivascular MSCs subset in OA based on overall higher proportion of CD271+ MSCs in OA bone determined by FACS as well as the increased mRNA expression of MCAM (encoding CD146) in OA CD271+ MSCs.

Another surface marker used in conjunction with CD271 is CD56, also known as neural cell adhesion molecule. As a known marker for natural killer, neural, and more recently for muscle cells (Van Acker et al., 2017) it was additionally shown to be expressed on a small subset of BM CD271+ cells (Bühring et al., 2007) and having a particular chondrogenic bias (Battula et al., 2009). In a more recent study, Sivasubramaniyan *et al*. isolated MSCs based on this phenotype from sites distant from the affected bone of OA patients and confirmed the enhanced chondrogenic potential of the CD271+CD56+ cells but moreover, demonstrated the distinct topographical location of this subset in the endosteal region (Sivasubramaniyan et al., 2018).

All the evidence presented above indicates the existence of at least two topographical subsets within the CD271+ MSC fraction, and that either of them may contain osteoprogenitors increased in number in OA. However, CD56+ BLCs may represent a stronger candidate for such cells based on their proximity to osteoblasts and osteoclasts as shown in the previous chapter (Figure 4.28). Based on this, the focus of this chapter

was the isolation of osteoprogenitor MSCs and their enumeration and characterisation from healthy and OA bone using CD56 and CD146 surface markers, used for the first time in combination with CD271.

5.2 Chapter aims

1. To document the topography of CD56+ cells in OA and control bone and establish the existence of CD271+CD56+ bone lining MSC subset.
2. To enumerate the CD271+CD56+ and CD271+CD146+ MSC subsets in OA and healthy bone.
3. To explore the native CD271+CD56+ and CD271+CD146+ MSC subsets in OA by investigating their osteogenic commitment using gene expression analysis and *in vitro* functional assays.

5.3 Methods

5.3.1 Patient samples

For all the experiments in this chapter a total number of n=18 OA donors (8 males and 10 females) with age range between 40-90 years (median=72) and n=11 healthy donors (5 males and 6 females) with age range between 17-78 years (median=55) were recruited. The MSC subsets were enumerated and isolated using FACS from the cell suspensions obtained following bone digestion procedures described in Chapter 2, Section 2.2.1.

For histological studies a total of n=4 OA femoral head samples were used while n=3 healthy IC and n=3 non-OA neck of femur fractures femoral heads were used as control bone. As described in Chapter 4, the samples used for histology in some cases were different from the ones used for MSC extraction.

5.3.2 Immunohistochemistry

Sequential sections (5 μm) of decalcified trabecular bone (Chapter 2, Section 2.6.1) were deparaffinized in xylene and rehydrated through graded ethanol series to water. EnVision + Dual Link System-HRP (DAB+) (DAKO, UK) was used for the staining procedure as described in Chapter 2, Section 2.6.3. The primary antibody used for CD271 has been described in Chapter 4, Section 4.3.6 while for CD56 a rabbit monoclonal antibody (clone EPR2566, Abcam, UK) was used at a 1:300 dilution. The staining procedure was similar as described in Chapter 4, Section 4.3.6. The optimal concentration of primary antibody had been determined in dilution series on test tissue sections similar to CD271 in Chapter 4.

5.3.3 Immunofluorescence

Immunofluorescence was chosen to investigate the co-localisation of the two markers, CD271 and CD56 in OA femoral heads. Tissue sections were dewaxed and rehydrated as described in Chapter 2, Section 2.6.2. The tissue was then permeabilised to allow intracellular staining with 0.25% Triton-X-100 (Sigma) for 15 minutes at room temperature and washed several times in TBS. Antigen sites were blocked using 5% Casein solution (Appenix 3) for 30 minutes at room temperature before subsequent addition of the same primary antibodies used for IHC (Section 5.3.2). After 1-hour incubation at room temperature, the primary antibody was washed in TBS for 5 minutes and the appropriate conjugated secondary antibody was added to the tissue sections for 1 hour at room temperature. The CD271 antibody was raised in mouse and therefore a goat

anti-mouse antibody was used conjugated with Alexa Fluor 488 (1:200, Thermo Fisher). The CD56 antibody was raised in rabbit and therefore a donkey anti-rabbit was used conjugated with Alexa Fluor 647 (1:200, Abcam). After washing, the slides were mounted with a coverslip using VectaShield with DAPI (Vector Laboratories). Fluorescence was analysed using a Nikon A1 confocal laser microscope (Nikon) and multiple fluorescent images were acquired and presented using NIS Elements software (Nikon). The maximum excitation wavelength for Alexa Fluor 488 is 495 nm and emission peaks at 519 nm, therefore the blue 488 nm laser line was used to detect cells positive for CD271. To detect the CD56 cells, the excitation wavelength for Alexa Fluor 647 is 650 nm and emission peaks at 665 nm, therefore the red 647 nm laser line was used. No primary antibody slide was used as control with both secondary antibodies in order to set the threshold and normalise for background signal.

5.3.4 Picrosirius Red staining

Picrosirius red (PSR) was employed to stain and visualise the collagen fibres in OA femoral heads (n=4) in order to determine areas of new bone formation. The staining procedure was performed following dewaxing and rehydration as described in Chapter 2, Section 2.6.2. The slides were then incubated for 1 hour at room temperature in 0.1% PSR solution (Appendix 1). Next, the slides were briefly washed for 1-2 seconds in 0.5% acetic acid before being mounted with DPX (Leica).

The slides were visualised using brightfield (Nikon) as well as polarized light (Nikon) microscopes in order to evaluate the size and organization of collagen fibrils of subchondral bone in parallel with adjacent slides stained for CD56 by IHC.

5.3.5 Cell sorting

Based on topography, the CD271+ MSCs were shown to reside in a perivascular location, marked by the expression of CD146 (Tormin et al., 2011) as well as lining the bone, marked by the expression of CD56 (Battula et al., 2009). Therefore, FACS was employed to enumerate and isolate these distinct subsets within the CD271+ MSCs fraction in order to investigate their presence in healthy and OA bone in addition to gene expression comparison between these subsets.

Staining and cell sorting experiments were performed similar to MSCs enumeration and sorting described in Chapter 3, Section 3.3.4, with the addition of the two antibodies (CD56 and CD146) for further segregation of the CD271 fraction. All antibodies used in this study as well as the gating strategy used for the identification and sorting of CD45-

CD271+ population and its sub-fractioning in the CD271+CD56+CD146- (designated as CD56+), CD271+CD56-CD146+ (CD146+) and CD271+CD56-CD146- (double negative, DN) subsets was described in Chapter 2, Section 2.4.

5.3.5.1 FACS analysis and sorting for gene expression analysis

Bone fragments from healthy IC and OA femoral heads were mechanically processed as described in Chapter 2, Section 2.2 and enzymatically treated. Following enzymatic extraction of all cellular material from the bone fragments, the cells were filtered and manually counting using Trypan blue exclusion method as described in Chapter 2, Section 2.3.1. Depending on cellularity, approximately $3x10^6$ cells were centrifuged at 300xg for 5 minutes and resuspended in 100 µl of FACS buffer. Following 10 minutes incubation with Fc block, the four antibodies (CD271, CD45, CD56 and CD146) were added at the dilution described in Chapter 2, Section x and incubated for 15 minutes in the dark, at room temperature. After staining, cells were washed and processed for cell sorting and FACS analysis using the gating strategy described in Chapter 2, Section 2.4.1.

The percentages of the MSC subsets was calculated as percentage of number of events in the gated live CD271+ MSCs population, as described in Chapter 2, Section 2.4.2. Additionally, together with the CD271+CD146+ and CD271+CD56+ fractions, the double negative subset (designated as DN) was also selected for analysis as described in Chapter 2, Section 2.4.2. On average, $6x10^4$ events were acquired to gate the CD271+ fraction across all OA experiments, ranging between $0.8x10^4$ -$2.8x10^5$ while from healthy bone an average of $2.5x10^4$ events, ranging between $2.3x10^4$ -$9.9x10^4$ events. The MSC subsets were sorted from this CD271+ population for downstream processing for *in vitro* functional assays (Section 5.3.5.2 and 5.3.7) or gene expression analysis by qPCR (Section 5.3.5.3).

5.3.5.2 Cell sorting for functional assays

Following FACS analysis the MSC subsets from n=3 OA donors were collected for *in vitro* functional assays in 500 µl of StemMACS media. Immediately following cell sorting, cells from each MSC subset were seeded in 6-well culture plates at similar cell densities, while the CD45+ subset was seeded at a higher cell density due to less likely chance to have adherent cells (Tormin et al., 2011) and served as control population. The number of cells required for differentiation assay of MSC subset was not sufficient following cell sorting, therefore all sorted fractions were minimally expanded up to P1 as

described in Chapter 2, Section 2.3.2 and used for each assay as described in Section 5.3.7.

5.3.6 Gene expression of the sorted MSC subsets

Following the cell sorting experiments, the selected subsets (CD56+, CD146+ and DN) were collected for gene expression analysis in 100 µl or RNA lyses buffer (Norgen Biotek). Due to the different cell proportions within the selected subsets, an average number of $5x10^3$ cells were collected for the CD146+ (range $0.5x10^2$- $1.3x10^4$ cells) and 7.6 $x10^4$ for DN subsets (range $1.2x10^4$-$1.5x10^5$), however due to low and variable numbers of the CD56+ subset, only an average of $3x10^3$ cells (range $0.5x10^3$-1.5 $x10^4$ cells) were collected. Additionally, $1x10^5$ cells from the CD45+ fraction were collected as control. The RNA was then isolated from all collected cells using a Single Cell RNA extraction kit (Norgen Biotek) and cDNA synthesised from all volume of extracted RNA using High Capacity Reverse Transcription kit (Applied Biosystems) as described in Chapter 2 and based on manufacturer instructions.

For gene expression analysis a custom pre-designed TLDA card (format 96a; Applied Biosystems) was used as described in Chapter 2, Section 2.5.3 and manufacturer instructions. Exon-spanning TaqMan assays were selected for the array when possible, generally comprising genes associated with MSCs multipotentiality and stromal support, similar to the panel used in Chapter 3. The complete list of transcripts is detailed in Appendix 5. The cDNA (50 µl for each sample in nuclease free water) and TaqMan master mix (50 µl) (Applied Biosystems) were prepared as a single mix and 100 µl was used per port, allocating 2 ports/sample corresponding to a total of 96 assays (48 genes/port), as described in Chapter 2, Section 2.5.3. Data analysis was carried out using $2^{-\Delta Ct}$ method, with results normalized to the values for the reference gene *HPRT1*. The hierarchical cluster analysis was performed using the Cluster 3.0 open source software as described previously (Churchman et al., 2012). Using this software, the gene expression values were first transformed to a logarithmic scale and then hierarchical clustering was performed for genes and samples arrays using Spearman rank correlation and complete linkage. This method clusters the genes with similar levels of expression between the subsets, the results being visualised as a dendrogram using the Tree View software.

5.3.7 Differentiation assay

Trilineage differentiation of MSCs is a defining property of MSCs and was used to compare the potential of the sorted MSCs subtypes to undergo osteogenic, adipogenic

and chondrogenic differentiation *in vitro* using standard techniques. In particular, these functional assays were aimed at confirming the gene expression results and therefore to verify the reflection of the osteogenic commitment of subsets under investigation.

All differentiation assays were performed for the three MSC subsets isolated by FACS from n=3 OA donors and culture expanded up to P1. Exemplified in Figure 5.1 are the details of cells distribution for functional assays together with the number of cells seeded and replicates for each MSC subset from each donor, hence a total number of n=9 samples (n=3 donors and n=3 MSC subsets).

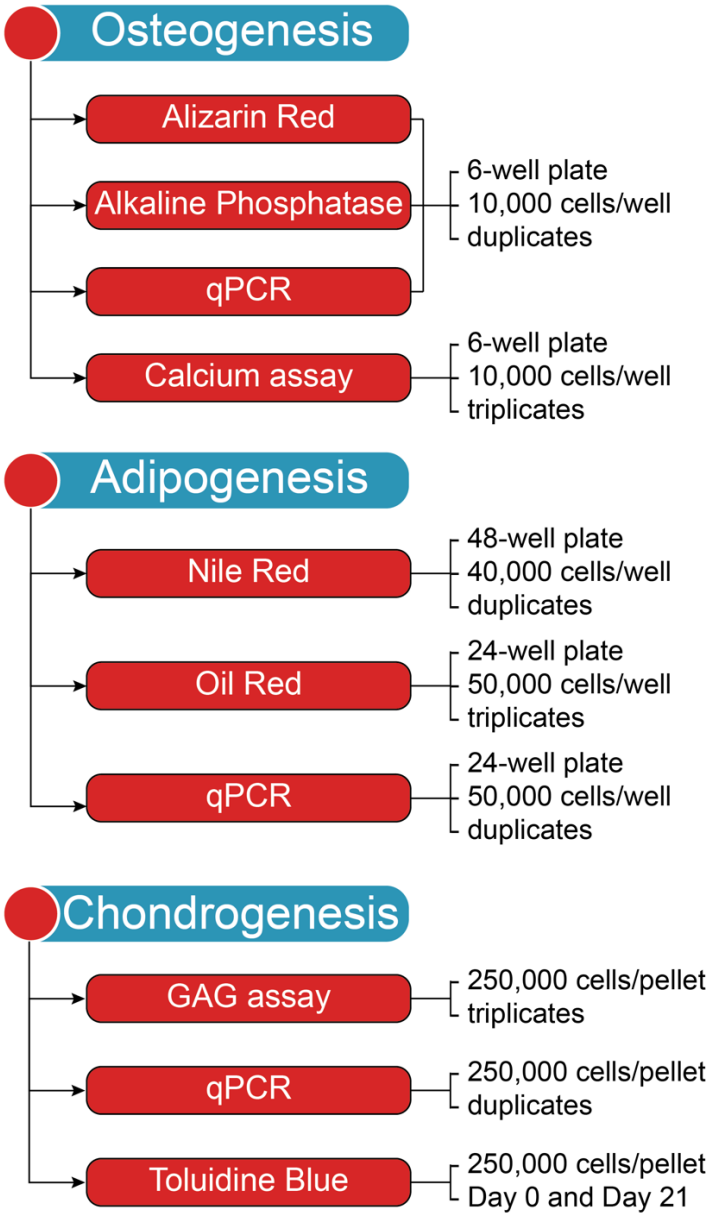

Figure 5.1. The flowchart of differentiation assays experimental plan. *The MSC subsets were induced towards osteogenic, adipogenic and chondrogenic lineages. The functional assays were performed for each of the three MSC subsets (CD56+, CD146+ and DN) isolated by FACS from n=3 OA donors.*

5.3.7.1 Osteogenic differentiation

Following isolation by FACS and subsequent culture expansion of all three cell types from OA patients (n=3) (Section 5.3.5.2), the MSCs were seeded in duplicate into 6-well tissue culture plates (Corning) at a seeding density of $1x10^4$ cells/well and incubated at 37° C, 5% CO_2 (Figure 5.1). Osteogenesis was induced with ready-made osteogenic differentiation media OsteoDiff from Miltenyi Biotec. Half of the media was changed twice weekly and cultures were maintained for 14 or 21 days when they were stopped depending on the assay performed: the level of osteogenic differentiation was determined by assessing the alkaline phosphatase (ALP) activity, measuring the accumulated calcium using a calcium liquid colorimetric assay and staining the deposited calcium with Alizarin Red. For ALP and Alizarin Red assays, cells were seeded in a 6-well plate in duplicate at a cell density of $3x10^4$ cells/well. For calcium detection, the cells were seeded similarly in 6-well plate at the same cellular density, in triplicate. Additionally, qPCR was also performed to analyse the expression of osteogenic specific molecules, *RUNX2* and *BGLAP* using TaqMan assays (Thermo Fisher), detailed in Appendix 5.

5.3.7.2 Detection of alkaline phosphatase activity

For determination of ALP activity, osteogenic cultures were terminated on day 14 post-induction (Pittenger et al., 1999). The media was removed from the adherent cells, which were washed gently with 1 ml PBS and subsequently fixed with the addition of 2 ml of citrate fixative solution (Appendix 1) for 30 seconds at room temperature. The fixative was then removed, and wells were washed twice with dH_2O. The assessment of ALP activity was performed by adding 1 ml fast blue salt solution (Appendix 1) to each well and incubated in the dark at room temperature for 30 minutes to allow colour development. Following incubation, the wells were washed gently with 1 ml dH_2O until clear and allowed to air dry. Dishes were subsequently scanned using an Epson digital scanner and high magnification images acquired using an inverted microscope with an Olympus camera attached.

5.3.7.3 Alizarin Red staining

This assay was performed to assess the *in vitro* osteogenesis by determination of the accumulated calcium in the extracellular matrix of the cultured cells. Alizarin Red staining solution was prepared fresh prior to performing the assay (Appendix 1). The cells were first fixed by incubation on ice for 1 hour with cooled (at -20º C) absolute ethanol. After fixation, the cells were gently washed several times with dH_2O and incubated with

Alizarin Red staining solution for 10 minutes at room temperature. Following staining the cells were washed twice with dH_2O and air-dried over-night. Dishes were subsequently scanned using an Epson digital scanner and high magnification images acquired using an inverted microscope with an Olympus camera attached.

5.3.7.4 Determination of total calcium accumulation

Colorimetric assay was used for quantification of calcium content produced by and accumulated in the osteogenically differentiated MSCs. At the culture end-point (21 days post induction) the cells were washed gently with sterile calcium-free PBS (Invitrogen) and subsequently incubated at room temperature for 5 minutes with 0.5 M hydrochloric acid (HCl) to extract calcium from the mineralized extracellular matrix. Using a disposable cell scraper (Fisher Scientific) cells were mobilised from each well and along with the HCl were transferred using a sterile pastette into 1.5 ml microcentrifuge tubes. Calcium was extracted by 4 hours' agitation at 4° C in a rotator and subsequently stored at -20º C. Prior to calcium production assay, samples were equilibrated to room temperature and centrifuged at 5000xg for 5 minutes to remove any remaining cellular debris (Jaiswal et al., 1997).

For determination of calcium content, the Sentinel Calcium kit (Sentinel Diagnostics) was used following the producer instructions. First, standards were prepared ranging from 0 to 800 ng calcium/well using the calcium standard solution provided. Flat bottomed 96-well plates were loaded with 6 µl of standards and 6 µl of samples' supernatant in triplicate to which 200 µl of the 'working dye' solution (0.3 mM o-cresolphthalein-complexone, provided in the kit) was added for each corresponding MSC sample (n=3 donors, n=3 MSC subtype each, i.e. 9 samples). The mixture was incubated in the dark for 10 minutes at room temperature and the calcium content was measured using a microplate reader with a 570 nm wave length filter. Cresolphtalein-complexone reacts with calcium ions at pH>10 to form a purple coloured complex and the colour intensity is directly proportional to the concentration of calcium; this was quantified by measuring the absorbance at 570 nm. When samples did not fall within the standard curve, a 1:1 dilution was performed for those samples only and the plate was read again. Once measured, the absorbance can be converted to concentration of calcium by comparing the absorbance of the known calcium standards to the sample absorbance (Jaiswal et al., 1997).

5.3.7.5 Adipogenic differentiation

Following culture expansion to obtain the required cell number for differentiation, cells were induced towards the adipogenic lineage using the commercially available adipogenic media (AdipoDiff, Miltenyi Biotec). Quantitative measurement of adipogenesis was performed by Oil red and Nile red staining in parallel with gene expression analysis using established adipogenic markers, *PPARγ* and *FABP4* (both from Thermo Fisher) (Aldridge et al., 2013) detailed in Appendix 5.

For Oil red staining $5x10^4$ MSCs/well were seeded in triplicate into 24-well tissue culture plates (Corning) containing 1ml adipogenic media and incubated at 37° C, 5% CO_2. For Nile red staining the cells were seeded in triplicate in a 48-well plate at a seeding density of $4x10^4$ MSCs per well in 500 µl of adipogenic media. For both assays, half of the culture media was replaced twice every week and cultures were terminated on day 21 (Aldridge et al., 2013).

5.3.7.6 Detection of lipid vacuoles by uptake of Oil Red

On day 21, seeded cells were washed twice with PBS and fixed with 500 µl of 3.7% PFA at room temperature for 15 minutes. Oil Red solution was prepared fresh before the staining procedure.

After fixation, the Oil red staining solution was applied at 1 ml/well and incubated for 20 minutes at room temperature before washing twice with 1 ml PBS. For qualitative assessment of oil red uptake, a brightfield microscope was used and images captured using a digital camera (Olympus).

5.3.7.7 Quantification of adipogenesis by Nile Red fluorescence measurement

Nile red assay was performed similar to the Oil red staining up to the post-fixation stage. After the fixative was removed and the cells washed gently, the PBS was fully aspirated from the wells and replaced with an exact volume of 200 µl in each well. This was used as a background reading to be used for an accurate quantification of the fluorescent dyes, Nile red (excitation at 450-500 nm and emission at >528 nm) and DAPI (excitation at 358 nm and emission at 461 nm) (both from Sigma). The wells containing PBS were used therefore to measure emission at 460 nm and 535 nm following excitation at 355 nm and 485 nm respectively. The PBS was then replaced with 200 µl of a solution mix containing 0.2% saponin (Sigma), 1µg/ml DAPI and 1µg/ml Nile red in PBS (Aldridge et al., 2013). Additionally, DMSO only wells were also used as baseline controls. Saponin was used to facilitate the penetration of Nile red into the cells which becomes fluorescent in contact

with lipids, while DAPI was used to stain for nuclei. The plate was incubated in the dark, wrapped in foil, for 15 minutes at room temperature. After staining the cells were washed twice, then 200 µl PBS was added to each well and the plate was read again as before.

To quantify adipogenic induction, the Nile red to DAPI ratio was calculated. But first, the background from the first readings was subtracted from the second readings. Then the mean emission value for each triplicate for both Nile red and DAPI were calculated and this value divided by the mean value from control readings containing DMSO only to obtain the fold changes in adipogenic differentiation.

5.3.7.8 Chondrogenic differentiation

For chondrogenic differentiation the cells were cultured in the form of a 3D pellet (Jones et al., 2002). To form each pellet, $2.5x10^5$ MSCs were suspended in 0.5 ml of chondrogenic media (ChondroDiff, Miltenyi Biotec) and centrifuged for 5 minutes in screw top 1.5 ml microcentrifuge tubes at 400xg. Screw caps were fastened loosely in order to allow gas exchange and incubated at 37º C, 5% CO_2; half the media was replaced every 3 days for a total culture period of 21 days. From each sample, a total of n=6 pellets were generated and investigated, as follows: n=2 pellets were snap-frozen in optimal cutting temperature (OCT) compound (Fisher Scientific) using the vapour phase of liquid nitrogen prior to cryo-sectioning and staining with toluidine blue; n=3 pellets were prepared for papain digestion followed by glycosaminoglycan (GAG) assay while n=1 pellet was lysed for RNA extraction using standard RNA lysis buffer from a kit (Norgen Biotek) and qPCR using chondrogenic transcripts for *SOX9* and *COL2A1* detailed in Appendix 5.

5.3.7.9 Papain digestion

The chondrogenic pellets (n=3 for each subset) were degraded using a papain-based digestion in order to be able to quantify the content of GAGs in the samples. The activated papain enzyme digestion solution was prepared as described in Appendix 1. The chondrogenic pellets were incubated overnight with 200 µl of this solution in a 60º C water-bath. Following incubation, the digested pellets were mixed thoroughly and centrifuged at 15,000xg for 10 minutes at room temperature and immediately stored at -20º C until GAG quantitation.

5.3.7.10 Glycosaminoglycan assay

This assay was performed using the commercially available kit Blyscan (Biocolor) by using the papain digest from n=3 pellets for each MSC subset from the n=3 donors. This kit relies on the interaction between the sulphated polymers and 1.9 dimethylmethylene blue (DMMB) dye. Similar to the calcium assay, a standard curve for GAG content was prepared using the standard reagents provided in the kit, ranging between 0-5 μg/well. Samples assessment was performed by mixing 1 ml of DMMB with 200 μl of the papain digest sample, vortexed and mixed by constant agitation in a circular rotator for 30 minutes at room temperature. The mixture was then centrifuged at 15,000xg for 10 minutes so that the dye bounded to the GAG content in the samples was pelleted on the bottom of the tubes. The excess dye was gently removed without disrupting the coloured pellet, then 1 ml of dye dissociation agent was added to the sample and mixed similarly in a circular rotator for 30 minutes at room temperature. In a clear round-bottom 96-well plate 200 μl of each standard and samples were plated in triplicate and absorbance was read on a Berthold plate reader (Appendix 1) using a 656 nm wave length filter. The quantification was performed based on the GAG standard curve and the absorbance which was converted to concentration of GAGs/pellet by comparing the absorbance of the known GAG standards to the sample absorbance.

5.3.7.11 Toluidine blue staining

For toluidine blue staining, 7 μm thick sections were prepared from snap-frozen pellets (n=2 for each subset) using a CM3050S cryostat (Leica) and adhered to SuperFrost histology slides (Fisher Scientific). Slides were allowed to air-dry overnight then incubated with cooled methanol (Sigma) for 20 minutes at -20° C. Subsequently, slides were removed from methanol and allowed to air dry for 30 minutes. Once dry, slides were incubated in pre-warmed toluidine blue solution (Appendix 1) at 37° C for 30 minutes then briefly washed in isopropanol (Sigma Aldrich) to remove excess toluidine blue. Slides were incubated in xylene (Sigma Aldrich) for 5 minutes at room temperature and mounted using coverslips and DPX mounting media (Sigma Aldrich). Slides were examined using an Eclipse 1000 (Nikon) microscope and images captured using a digital camera (Olympus).

5.3.8 Statistics

The statistical analyses for gene expression experiments were performed using Kruskal-Wallis for intergroup differences, corrected with the Bonferroni-Dunn for multiple-group comparison. Mann-Whitney analysis was employed for comparisons between two groups and Wilcoxon for matched paired data between two groups. Results were presented on a log scale as scattered dot plots with bars representing medians, connected dots plots for paired data or box and whisker plots, with boxes representing interquartile range, and whiskers representing the maximum and minimum values, calculated using GraphPad Prism version 7 software. Results were considered significantly different at $p < 0.05$ (with significance level denoted as $*p < 0.05$, $**p < 0.01$, $***p < 0.001$ and $****p < 0.001$).

5.4 Results

In previous chapter an increased presence of young immature osteocytes was detected in areas of bone sclerosis in OA femoral heads using staining for the expression of the early-osteocyte marker E11. Within the stromal compartment of the same areas an increased presence of MSCs marked by the CD271 expression was also observed by IHC. The BLCs that were located interposed between these young osteocytes and the stromal compartment showed positivity for CD271 (i.e. flat cells on the endosteal surface) (Figure 4.25 and 4.26), while osteoblasts were CD271 negative (Figure 4.27). Previous studies described cells lining the bone surface to be positive for the adhesion molecule CD56 (Kristensen et al., 2013) and since they localised within the same location with the endosteal CD271 cells, it was hypothesised that some of the BLCs may represent an osteogenic subset of CD271+ MSCs. Another subset - CD146+ - was also analysed as CD271+ OA MSCs showed an increased expression of *MCAM*, encoding CD146 (Chapter 3, Section 3.4.3) pointing to an involvement of this perivascular subset in OA bone.

5.4.1 Identification of CD56+ cells in OA bone by IHC

Given the altered MSCs phenotype in late stages of OA, CD56 was first employed as a candidate marker to investigate the osteogenic lineage cells in OA femoral heads. Based on the literature, the CD56 positivity would be present on cells in both sclerotic and non-sclerotic areas (Kristensen et al., 2013; Kristensen et al., 2014). Therefore, to confirm the presence and determine the topographical location of these cells in relation to sclerotic areas, the investigation was performed first by using CD56 and CD271 alone, followed by the study of double-positive cells.

Upon examination, it was observed that CD56 was indeed expressed on all cells present on the bone surface, in both S and NS areas (Figure 5.2). The expression of CD56 in S areas was not limited to BLCs (Figure 5.2A black arrow), but was also expressed by the mature bone forming osteoblasts (Figure 5.2A black arrow head) and bone resorbing osteoclasts (Figure 5.2A white arrow), although their presence was scarce, only present at bone remodelling sites. In contrast to the CD271 expression documented in Chapter 4, the expression of CD56 was negative in the stromal tissue. Active osteoblasts could be detected visually based on their morphology as large cuboid cells, while BLCs are much flatter in relation to the bone surface and osteoclasts have the defining multinucleated characteristic as described in Chapter 4, Section 4.4.5.

In NS areas the expression of CD56 was also found to be expressed in the cells covering the bone surface. However, the NS areas, as mentioned in Chapter 4, Section 4.4.7, were characterised by decreased trabecular bone area which was covered by bone lining cells only. No bone remodelling compartments were observed in these regions and therefore the osteoblasts and osteoclasts were absent.

The expression of CD56 in both S and NS areas was consistent with the initial hypothesis and with the published research (Kristensen et al., 2014), indicating that only the cells on the bone surface showed positivity for this marker.

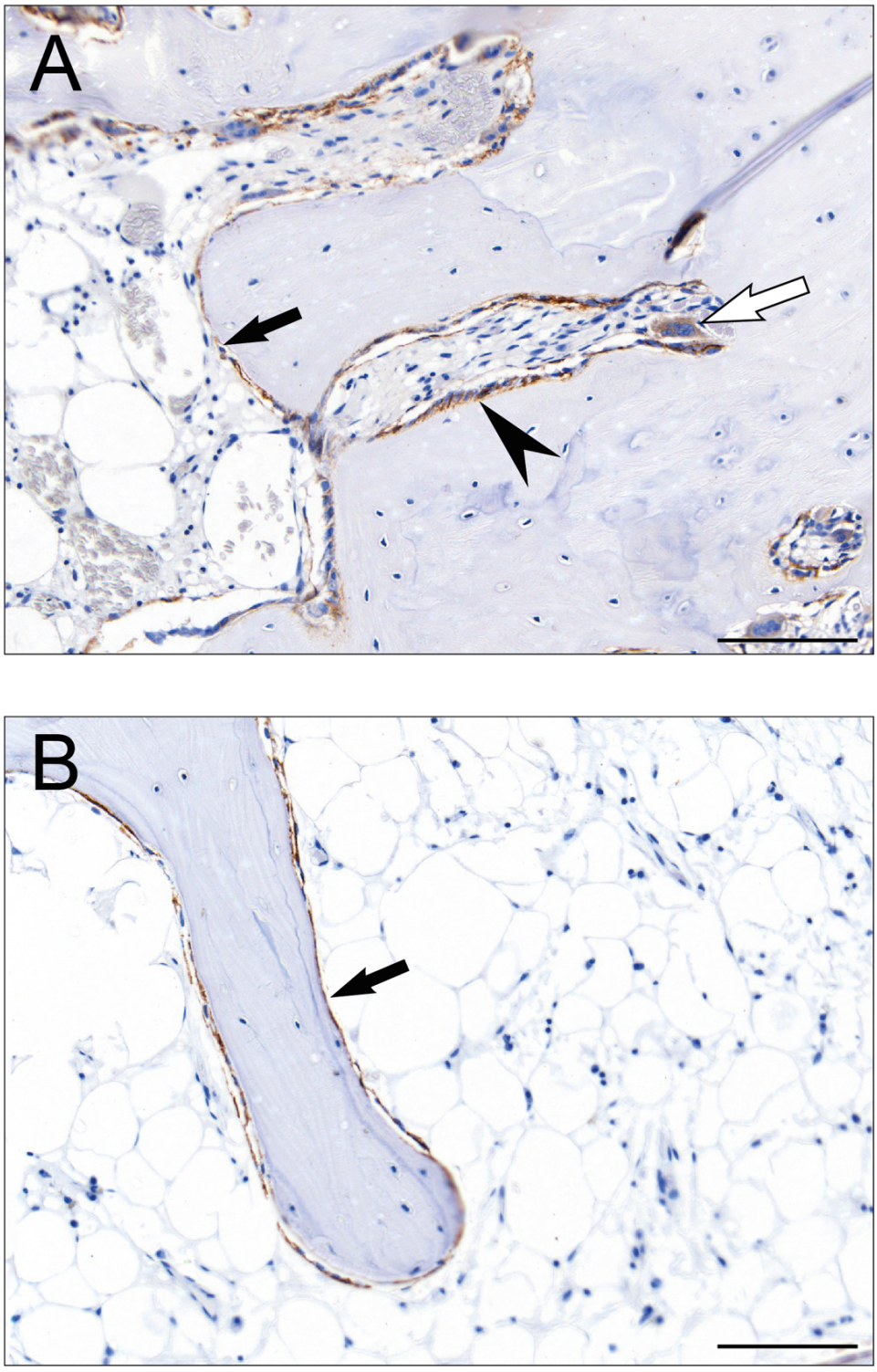

Figure 5.2. Representative IHC images showing CD56 positive cells in OA femoral heads from S areas (A) and NS areas (B). *S areas are characterised by fibrovascular cones invading the articular cartilage dominated by bone remodelling units where all bone surface cells showed positivity for CD56, including the single thick layer of BLCs (black arrow), osteoblasts (black arrow head) and osteoclasts (white arrow). In NS areas a continuous single layer of bone lining cells was present and shown positivity for CD56 (black arrow). Scale bar: 100μm. Sample ID: DIFHOA010*

The positivity of CD56 staining was next assessed in large sections of bone from four OA femoral heads in order to quantify the distribution of CD56+ cells in relation to OA bone pathology. The analysis was performed in sclerotic (S) (Figure 5.3A) and non-sclerotic (NS) (Figure 5.3B) areas of OA bone, using the same samples and similar approach described in Chapter 2, Section 4.4.7 while assessing the topography of CD271+ MSCs. The areas of interest were traced selecting out the bone tissue while the percentage of positive area in relation to total stromal compartment area was calculated based on the signal detected (Figure 5.3C and D) by Nuance software as described in Chapter 2, Sections 2.6.4. and 2.6.5.

The area of CD56 positivity was expected to be higher in S areas due to increased presence of osteoblasts and osteoclasts in S areas (Chapter 4, Section 4.4.6), as well as higher concentrations of CD56+ cells near the areas of new bone formation.

Area analysis revealed that indeed the CD56 positive areas were significantly increased in the S areas from all four femoral heads of OA donors in comparison to donor matched NS areas (Figure 5.3E). This trend was found to be consistent across all four femoral heads and indicated a similar pattern to the increased presence of CD271+ MSCs in the same areas of the same femoral heads, described previously in Chapter 4, Section 4.4.7. Based on median values it was determined that the CD56 presence was 5.8-fold higher in S areas ($p<0.0001$, Figure 5.3F) compared to the NS areas of the same femoral head.

The area analysis indicated that CD56+ cells are more abundant in areas of bone sclerosis in OA femoral heads, which point to their involvement in enhanced osteogenesis leading to bone sclerosis. However, the calculation included osteoblasts and scattered osteoclasts which also shown positivity for CD56 (Figure 5.2) but were negative for CD271 and therefore cannot be considered as MSCs. A new approach was adopted in order to obtain a more accurate quantification of the bone lining CD56+ cells in these areas. Specifically, since the osteoblasts and osteoclasts that showed positivity for CD56 were clearly not MSCs, confirmed by the negative expression of CD271, they were manually excluded leaving the possibility that the remaining cells positive for CD56 may contain an MSC subset.

Since the presence of osteoblasts and osteoclasts was only observed in areas of bone sclerosis, only these areas were re-analysed. To this end, the positive areas that comprised osteoblasts and osteoclasts (Figure 5.4A) were excluded from the analysis as shown in Figure 5.4B and it was determined that the same trend for higher CD56 positivity in S regions was maintained (Figure 5.4C). New positivity area measurements comprising all

the cells without osteoblasts and osteoclasts in the S areas revealed that the CD56 positivity was found to be 3.5-fold higher ($p<0.0001$) in the cells from S areas compared to the non-sclerotic areas (Figure 5.4D). Although osteoblasts and osteoclasts role is well established in bone turnover (Burr and Gallant, 2012) and their number were expected to be elevated in S regions, results presented here indicated that CD56+ BLCs may also be involved in the bone sclerosis given their elevated number in sclerotic areas.

The increased expression of CD56 in the S areas was corroborated with a visible increase in the cell numbers that were lining the bone (Figure 5.5). This observation indicated that in the S regions of OA femoral heads, the bone surface was often lined by a multiple layer of cells and in some places, the cells were organised into a canopy, a structure known to be present in areas of active bone formation (Kristensen et al., 2014).

This data suggests that the abundance of bone lining and canopy cells may account for the higher CD56 positivity observed in the S regions compared to NS, as determined by analysis of CD56 positivity in the whole FH of OA donors. This indicated that CD56+ cells may indeed represent a reservoir of osteoprogenitors that actively contribute to the enhanced bone formation activity associated with OA. Further in this chapter, their co-localisation with CD271+ cells will be investigated, in order to ascertain if these cell topographies can indeed represent the osteogenically committed MSCs.

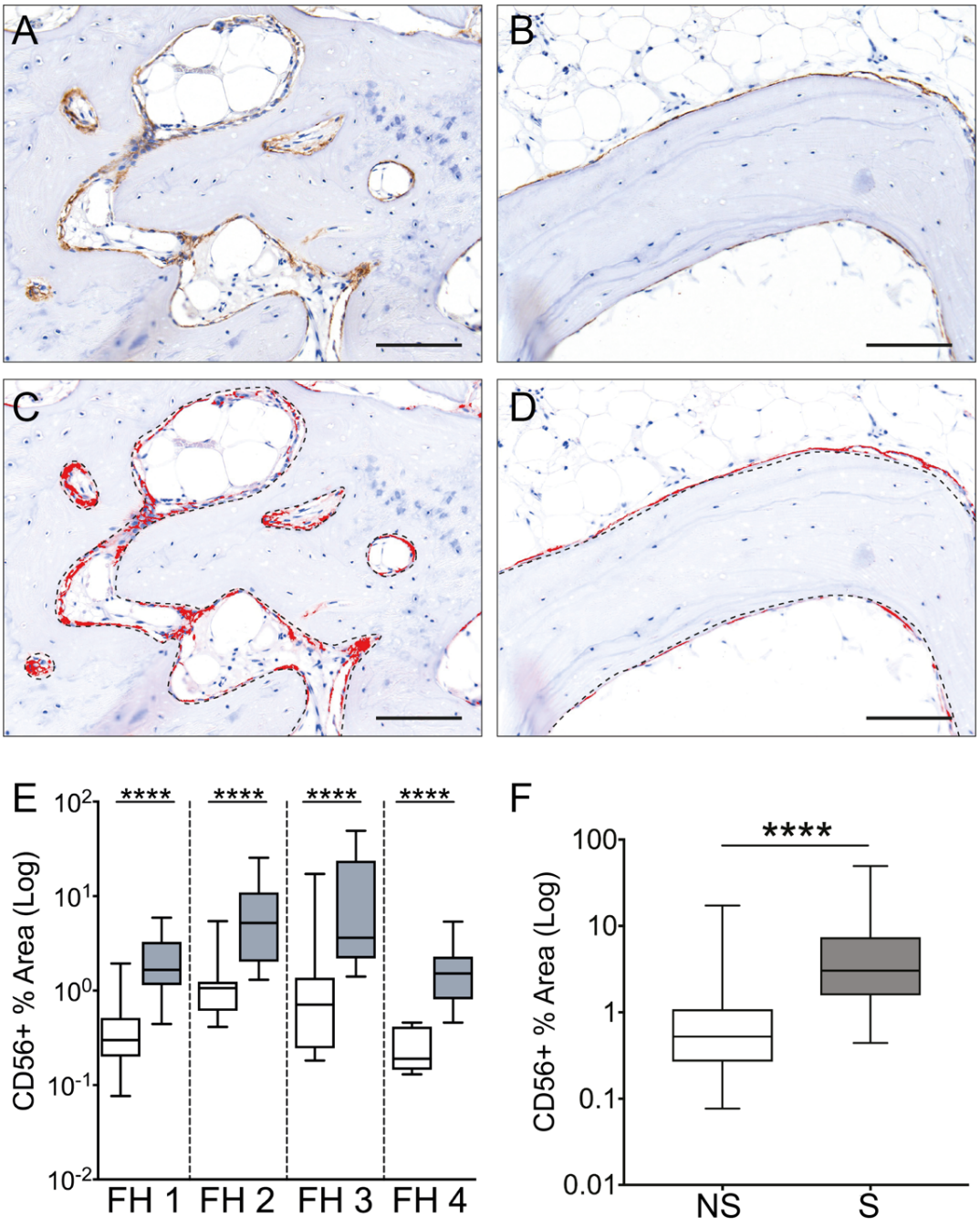

Figure 5.3. Quantification of CD56 positive cells in OA femoral head bone. *Representative images showing IHC of CD56 positive cells in OA femoral heads from S areas (A) and NS areas (B). The areas were selected for quantification using Nuance software by tracing a dotted line around the stromal compartment in S areas (C) and NS areas (D). The threshold was set according to control DAB+ only slides. The area measurements of CD56 positivity was graphed as percentage of total stromal area in all four femoral heads (FH) (D). Box plots show interquartile range, median and extreme values (empty boxes as NS areas, grey boxes S areas). All values from all four patients were pooled, the graph showing the percentage of CD56+ cells from NS (white box) and S (grey box) areas (F); Scale bar: 100 μm. Sample ID: DIFHOA016.*

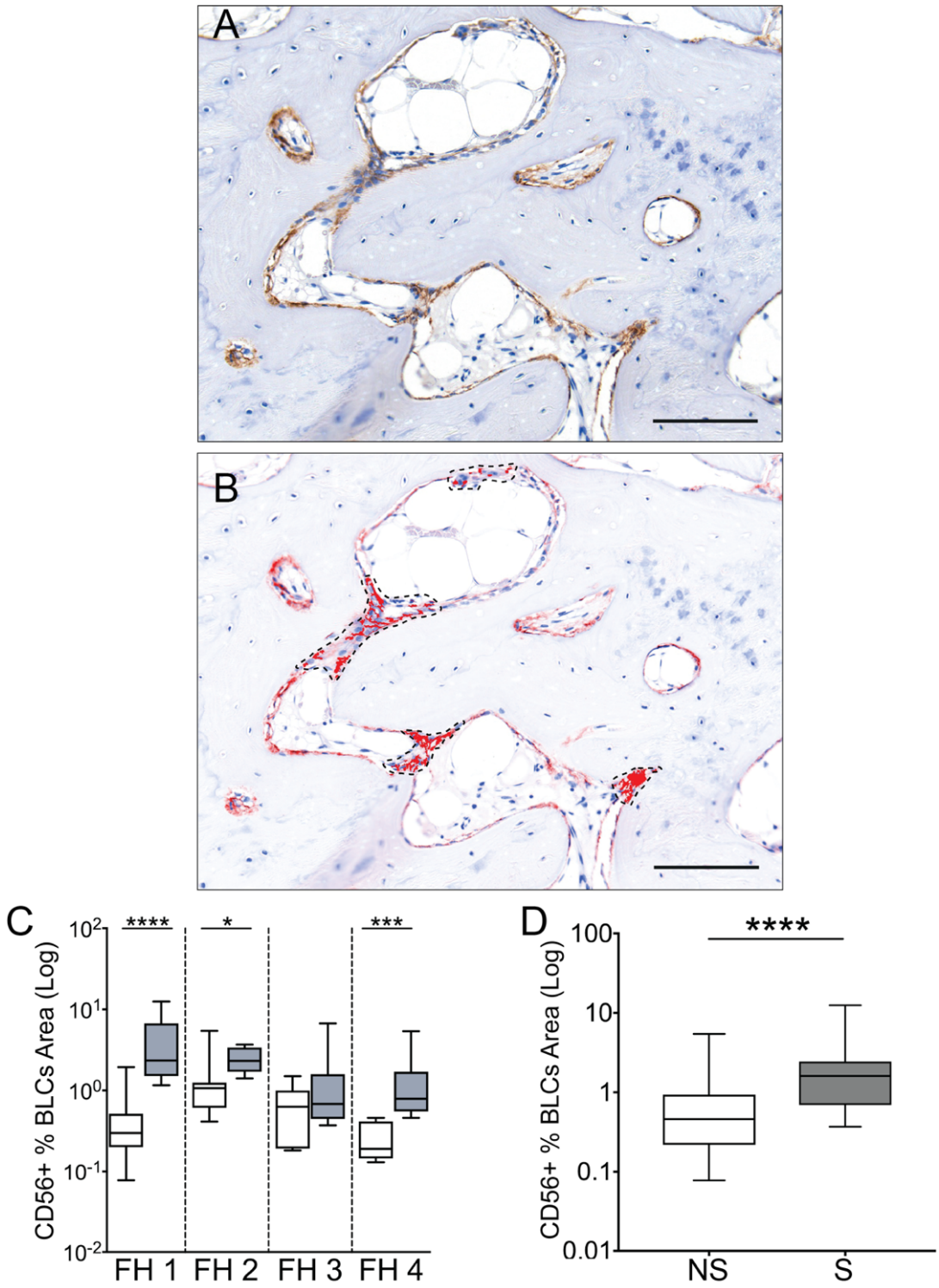

Figure 5.4. Quantification of CD56 positive cells in OA femoral head bone following osteoblasts and osteoclasts exclusion. *In the S areas of OA bone, CD56 was expressed on all cells on the bone surface (A). Selection and measurement of area occupied by osteoblasts and osteoclasts positive for CD56 (B). Graph showing the areas occupied by other cells, after excluding osteoblasts and osteoclasts (C). All values from all four patients were pooled, the graph showing the percentage of CD56+ bone lining cells from NS (white box) and S (grey box) areas (F); Scale bar: 100 μm. Sample ID: DIFHOA016.*

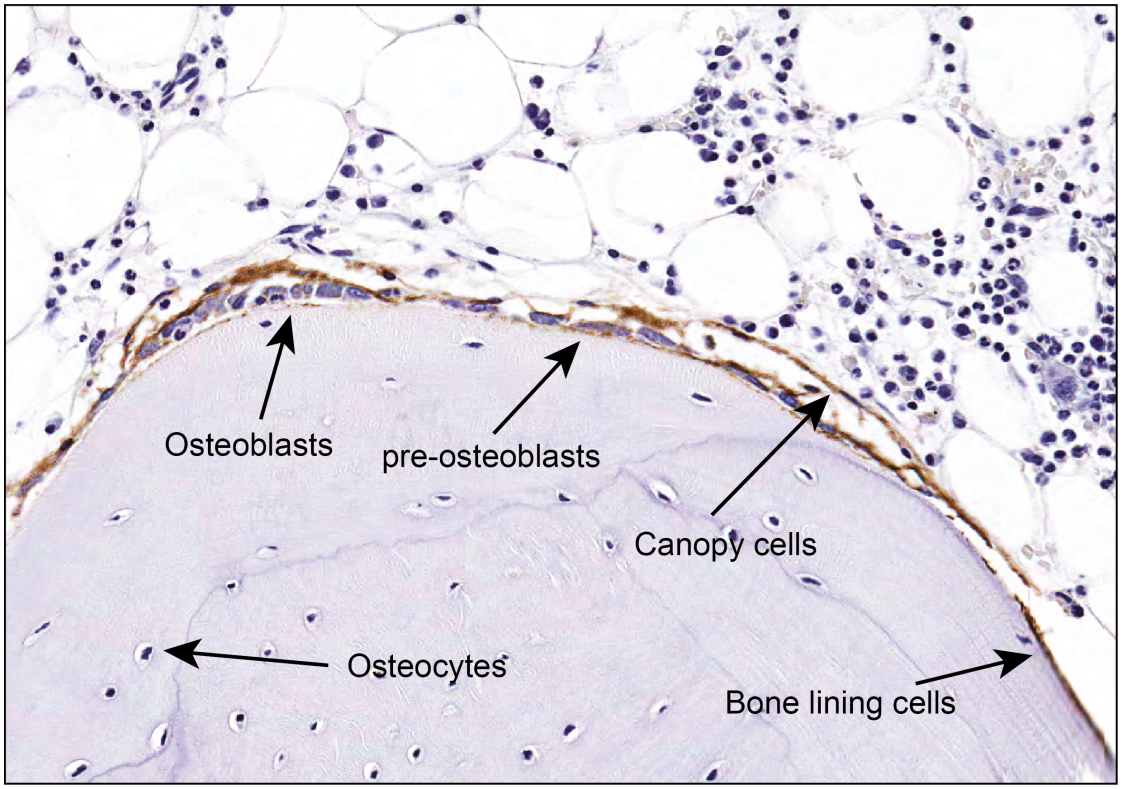

Figure 5.5. Representative IHC showing a sclerotic area of OA bone comprising the cells positive for CD56 on the bone surface. *The CD56+ cells are only present at the bone surface, with no positive cells in the stromal compartment. The S areas of OA bone were characterised by the presence of CD56 positive bone lining cells as a single layer. These cells were observed to be more numerous in the presence of osteoblasts and pre-osteoblasts, also CD56 positive, forming a canopy as a sealing zone for bone formation and osteogenic differentiation activities. Sample ID: DIFHOA010.*

5.4.2 CD56+ cells in areas of new bone formation

In order to obtain information with regards to new bone formation in the sclerotic areas of OA femoral heads as well as to corroborate this information with the spatial localisation of the CD56+ cells, PSR staining was employed together with CD56+ IHC. If CD56+ BLCs and canopy cells were directly involved in osteogenesis in S areas, their abundance would be co-localised to new bone formation areas. Since the tissue had been decalcified, assessment of new bone formation was assessed based on the colour profile and intensity of birefringence of the PSR-stained collagen fibres, bone formation and mineralisation undergoing changes in collagen fibrils thickness, orientation and their molecular packing (Viguet-Carrin et al., 2006).

Adjacent slides from n=4 OA femoral heads were used for PSR staining and CD56 IHC. The expression of CD56 detected in areas of bone sclerosis were commonly associated with active bone remodelling activity based on the presence of osteoblasts and osteoclasts (Figure 5.6A). Within these same areas, the PSR slides were visualised under bright field microscopy revealing differences in the collagen content of the bone based on the intensity of red colouring. It was observed that the areas where the CD56+ bone lining cells and osteoblasts were present had a brighter red colour while the areas more distant from the bone surface where lighter.

Under polarised light, the differences between the collagen fibres adjacent to the bone surface and the collagen content of the inside areas of the bone tissue were better revealed in the pattern of birefringence. With PSR staining under cross-polarized light, polarization colours of thin collagen fibres are green to greenish-yellow, and thick fibres range from yellowish-orange to orange to red. A predominance of green polarization in the OA sclerotic areas may indicate that the collagen molecules are loosely packed and could be composed of procollagens or intermediate collagens. The red areas proximal to the bone surface represent thicker collagen fibrils which may indicate newer laid collagen in the form of osteoid, due to an active bone formation process which corresponds to areas of CD56+ osteoblasts presence. The bone surface areas where CD56+ bone lining cells were present appeared yellow while the majority of the tissue appeared green.

All together this data places the CD56+ cells in areas of bone with an increased immature collagen content, i.e. thicker collagen fibres, based on the yellow and red birefringence in the endosteal regions. Of importance, the gradual difference in collagen thickness could also be related to bone mineral deposition. Newly laid bone, also known as osteoid, represents sections of unmineralized matrix containing bundles of collagen fibrils which

would consequently be mineralised as the bone tissue mature (Reddi et al., 1977). These results confirmed that the CD56+ BLCs were localised in area of new bone formation.

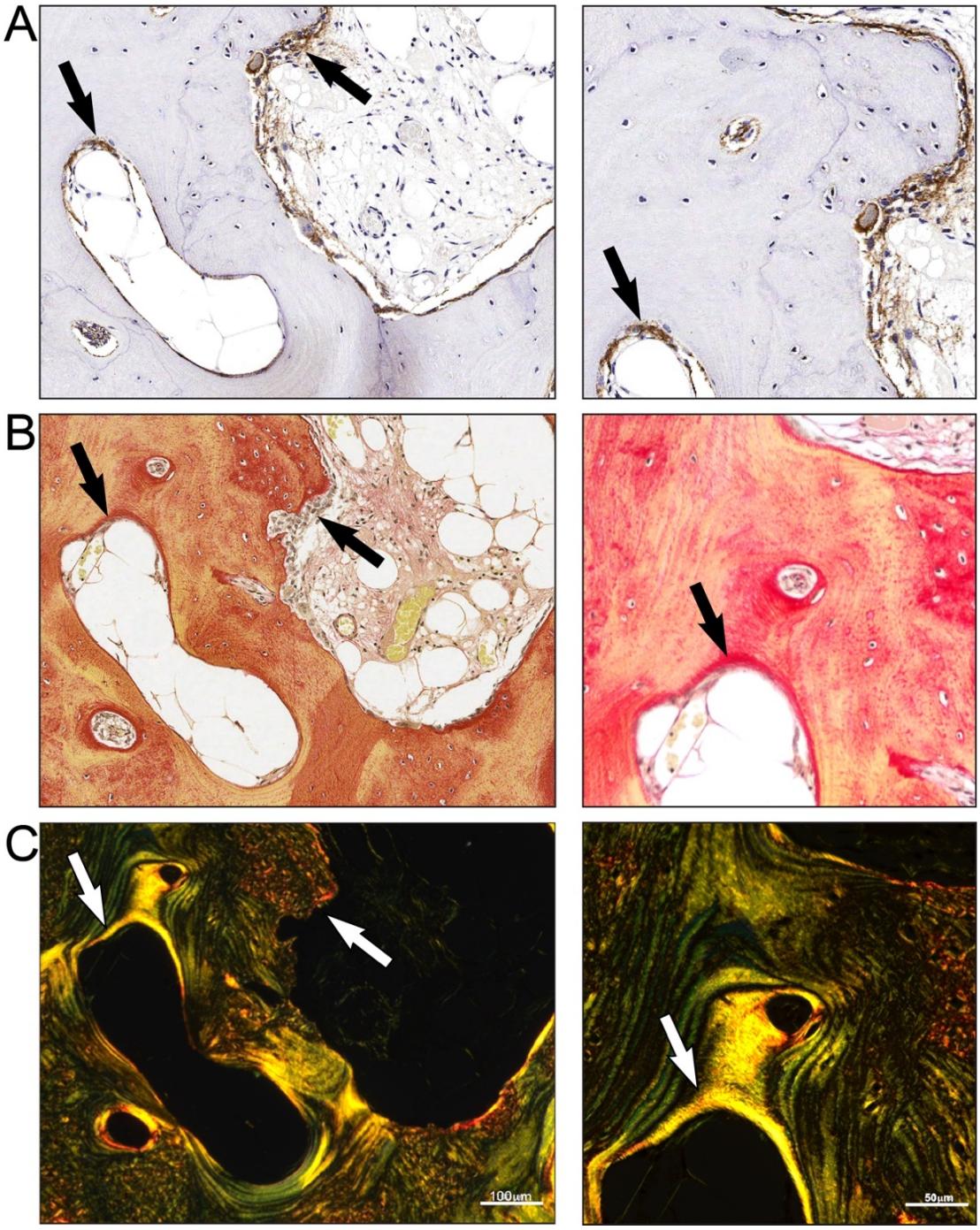

Figure 5.6. Representative photomicrographs of CD56 IHC and PSR staining in sclerotic area of OA bone. *(A) CD56 is expressed by osteoblasts and bone lining cells (black arrows). (B) Picrosirius red staining of OA sclerotic bone visualised under bright field microscopy showing the different red colour intensities within the same area. (C) Polarised light microscopy showing red birefringence in areas of osteoblasts presence, yellow corresponding to areas occupied by bone lining cells and green for majority of bone tissue (magnified panels). Sample ID: DIFHOA016*

5.4.3 Co-localisation of CD271 and CD56 using adjacent slides

Current literature documented the existence of a CD271+CD56+ subset within the BM CD271+MSC population (Bühring et al., 2009). Together with data in Chapter 3 that revealed an osteogenic bias of the CD271+ MSCs in OA, it was hypothesised that the CD271+CD56+ MSCs would be the responsible subset driving the observed osteogenic commitment of CD271+ MSCs. Therefore, in order to demonstrate this, it was necessary to firstly prove the presence of double-positive cells in both healthy and OA bone.

Next, IHC was further used to determine whether the CD56+ cells are unique to OA or they are present on other bone surfaces. So far it was shown that CD56+ cells were residing on the endosteal surface of the OA trabecular bone in both S and NS regions, although in higher numbers in the S regions. Similarly, in previous chapter it was shown that CD271+ MSCs were occupying the same locations, however they were also shown to be residing in the stromal and perivascular location as well, consistent with published literature (Tormin et al., 2011) and highlighted in Figure 5.7, right panels. Therefore, the topographic relationship of CD56+ cells with respect to CD271+ endosteal MSCs was assessed by using adjacent tissue slides in bone tissues from multiple sources and degree of pathology.

To determine the co-localisation of CD271+ and CD56+ cells, IHC staining was performed using the antibodies against CD271 (as used in previous chapter) and against CD56. As shown in Figure 5.7, it was determined that both CD56 and CD271 were found expressed in bone from all tissue sources and their endosteal location was consistent across all samples, however a difference in the number of cells positive for the two markers was noted.

As expected, the CD56 positive cells were found abundant in the S areas of OA bone, comprising osteoblasts and osteoclasts present in areas of bone remodelling, its expression being restricted to all the cells lining the bone (Figure 5.2A and 5.7, top panel). Meanwhile, consistent with data obtained in previous chapter, the CD271 expression was also found in the vast majority of cells within the same areas, including some stromal cells (Figure 5.7, top panel). Furthermore, noteworthy was the absence of CD271 staining in osteoclasts and osteoblasts, consistent with previously shown data in Chapter 4, Section 4.4.7.

In NS areas of OA bone, the expression of both markers was observed under the same pattern, with the CD56+ cells lining the bone while CD271+ was expressed by cells present both on the bone surfaces, as well as in the stromal compartment. When

comparing the sclerotic and non-sclerotic area of OA, there was notable difference in the number of cells in these areas. This confirmed the increased presence of CD271+ cells in S areas, presented and discussed in Chapter 4, Section 4.4.7 as well as the CD56+ accumulation in S areas presented in Section 5.4.1.

Interestingly, the expression of both CD56 and CD271 in healthy iliac crest was similar to the NS areas from OA bone as expected. A single layer of cells appears to be lining the bone, showing positivity for both CD56 and CD271. The expression of CD271 in the stromal compartment of IC was also consistent with the NS area as previously documented in Chapter 4, Figure 4.25.

When the expression of CD56 and CD271 was investigated in femoral head bone from non-OA donors, represented by femoral heads of neck of femur fracture patients, the positive cells showed the same topographical pattern although their number was notably lower. This may be due to decreased BM cellularity and its replacement with the apparent fatty stromal cells, which is commonly observed with increasing age of these patients. Of note, areas selected for comparison for the non-OA samples corresponded to the S areas from OA samples, both located in the subchondral zone.

It was concluded therefore that CD56+ cells were present on bone surfaces irrespective of site or tissue status and it was noted that CD271+ cells in the endosteal regions were potentially co-localised with CD56+ cells. However, since the analysis was performed on adjacent slides it was still insufficient evidence to determine whether the CD56+ and CD271+ BLCs were the same cells. To verify this, double staining IF was used.

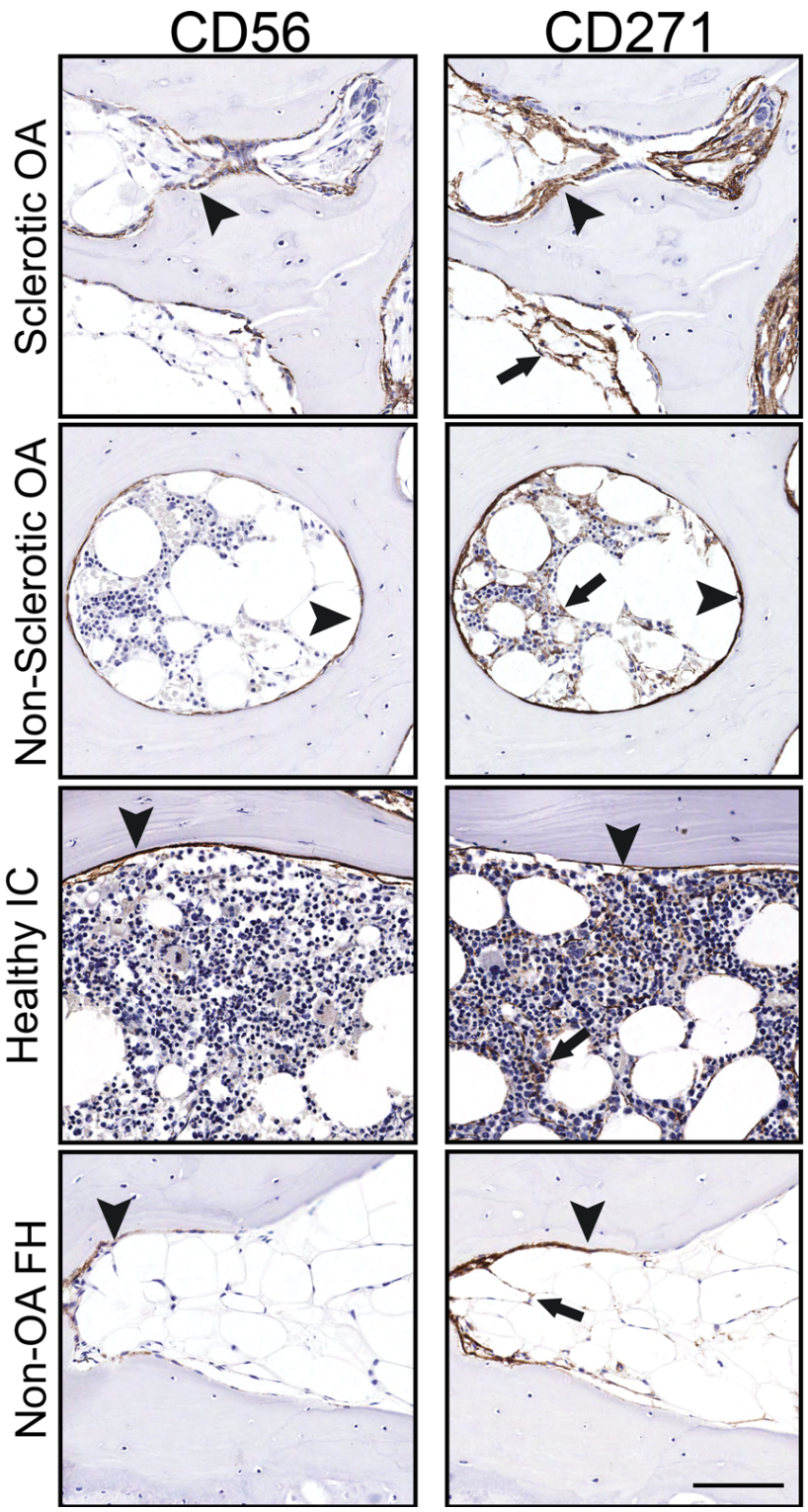

Figure 5.7. The comparison of CD56 and CD271 positive cells in bone from multiple sources. *Staining was performed in S and NS regions of OA bone, healthy IC and femoral head bone from femoral neck fractures (non-OA FH). The CD56+ cells were located lining the bone surfaces of all samples while CD271+ cells were in the same bone lining locations where CD56+ cells were present as well as in the stromal compartment. Arrows: CD271+ cells; arrow heads: CD56+ cells. Scale bar:100 μm. Sample IDs: OA: DIFHOA010; IC: DIHIC03; Non-OA: DIFHOP03.*

5.4.4 Co-localisation of CD271 and CD56 using immunofluorescence

Following IHC staining it was determined that a subset of CD271+ cells and CD56+ cells was located in the endosteal region, lining the bone surface. However, this was not sufficient to determine whether the cells lining the bone were co-expressing both markers and therefore have one cellular identity characterised by CD271+CD56+ phenotype, or there are two distinct cell populations condensed within the same area. To validate the co-expression of CD56 and CD271 on the same cell as well as the endosteal topography, IF double staining was employed using the same antibodies from IHC experiments and visualised by confocal microscopy in OA bone sections. The antibody against CD56 was tagged with Alexa Fluor 647, emitting a red colour when excited by confocal microscopy lasers, while the antibody against CD271 were tagged with Alexa Fluor 488 which can be visualised in the green spectrum, as described in Section 5.3.3. Negative control using secondary antibodies only was used to detect any background fluorescence in order to set the threshold of fluorescence as well as to validate the antibody binding, described in Section 5.3.3.

Initial examination confirmed the location of both markers as previously assessed by IHC. While CD56+ cells were located lining the bone surface, the CD271 positivity was detected in both endosteal and the stromal cells, consistent with the IHC findings (Figure 5.8). The CD56+ cells coloured red could be observed in the bone lining region only (Figure 5.8A), consistent with the IHC data. Similarly, CD271+ cells stained green were found localised both on the endosteal surface as well as throughout the stromal tissue (Figure 5.8B). When the images were merged by using the Elements software (Nikon), co-localisation of these molecules can be observed in yellow colour, marking the double positive cells as shown by the arrows in Figure 5.8D. By using immunofluorescence merged sections it is possible to also visualise the single positive cells, which based on the IHC data may belong to osteoblasts, osteoclasts or CD271+ MSCs which do not express CD56.

This data confirmed the existence of CD271+CD56+ cells on the bone surface. While the presence of an individual marker (CD56) had been described by the literature on BLCs (Kristensen et al., 2013; Andersen et al., 2013; Kristensen et al., 2014), this was the first time when they were both shown on the same cells. Therefore, by using FACS, from the CD271+ MSCs population a novel endosteal CD271+CD56+ subset could be sorted, in addition to the already discovered perivascular CD271+CD146+ subset (Tormin et al., 2011).

When visualised at a higher magnification (Figure 5.9) the presence of double positive cells can be observed more easily on the bone surface, while the positivity for CD271 alone was found only in the stromal compartment (Figure 5.9). Some positive CD56 cells were also detected indicated by the red arrows in Figure 5.9 and based on their size and location they were potentially differentiated osteoblasts.

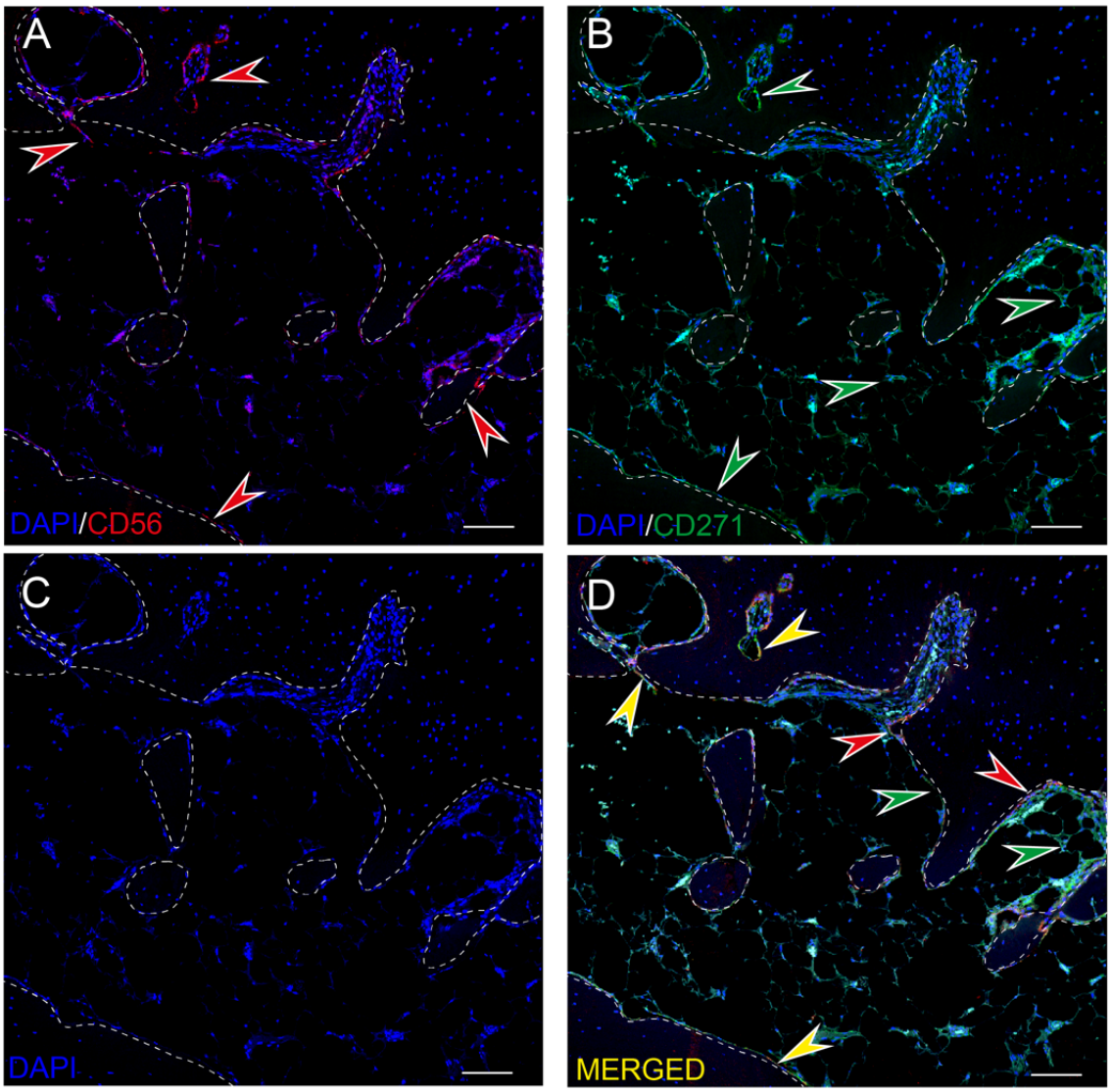

Figure 5.8. Immunofluorescence staining of OA femoral head bone tissue from sclerotic area. *(A) CD56+ cells found exclusively on the bone surfaces. (B) CD271 was expressed by cells within the stromal area as well as by the cells lining the bone. (C) DAPI nuclear staining showing the presence of all cells in the tissue slide. (D) Merged images of all planes of view showing the cells that only express CD56 (red arrows) and CD271 (green arrows) while the co-expression can be observed in yellow colour, but not in all areas (yellow arrows). Scale bar: 100 μm. Sample ID: DIFHOA010*

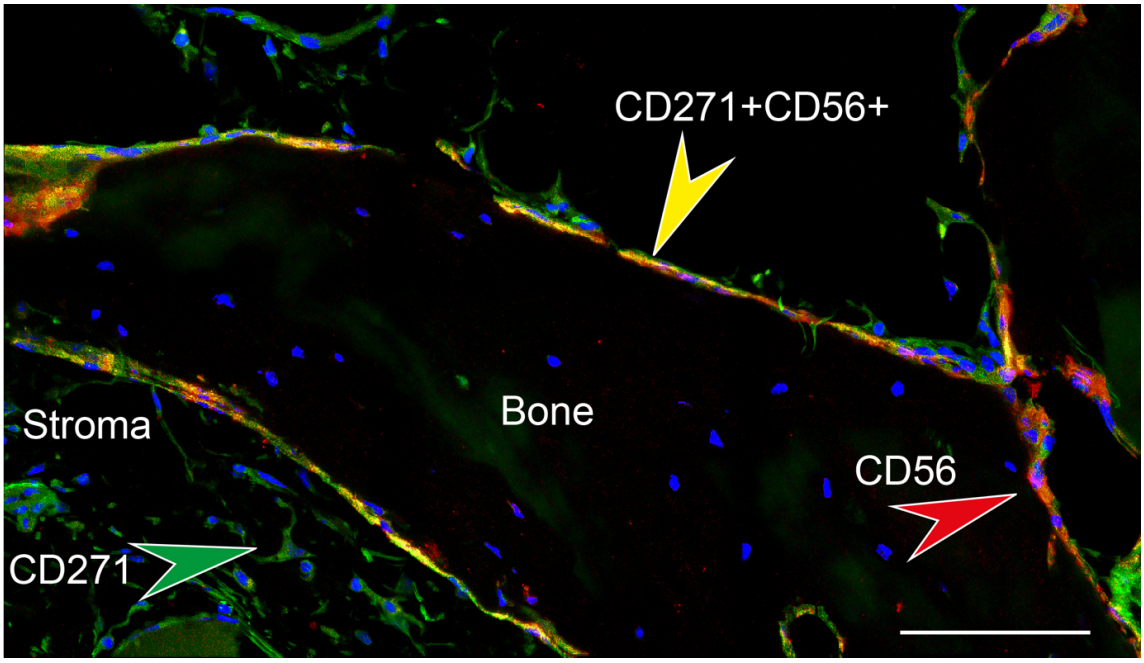

Figure 5.9. High magnification IF image showing the co-localisation of CD56 and CD271 on cells in OA bone. *The CD271+ cells (green arrows) can be seen in the stromal compartment while CD56+ cells (red arrows) are observed on the bone surface. When the two markers were detected by the software to be co-localised, it appeared yellow (yellow arrows). Scale bar: 50 μm. Sample ID: DIFHOA010*

5.4.5 MSCs subsets enumeration and cell sorting by FACS

The CD271 antigen represents a marker of native MSCs in the BM which can be further sub fractionated using additional cell surface markers. Following IHC and IF, the existence and topography of CD271+CD56+ phenotype was confirmed by FACS and compared to CD271+CD146+ phenotype, which was used as a comparator. Gating was set on the CD45-CD271+ phenotype as described in Chapter 2, Section 2.4 and was performed on enzymatically released cells form healthy (n=8) and OA (n=15) bone. Based on IHC data in Section 5.4.1 and the increased osteogenic commitment observed in CD271+ MSCs from Chapter 3, the presence of CD271+CD56+ subset was expected to be increased in the OA samples.

The MSC subsets were then enumerated as percentage of CD271+ MSCs and phenotypically distinct MSC subsets could be distinguished based on the expression of CD56 and CD146 within the CD271 gated fraction (Figure 5.10). Unexpectedly, the double negative (DN) fraction of CD271+ MSCs was found to be the most numerous in comparison to the CD56+ and CD146+ fractions (Figure 5.10 and 5.11).

A minimum number of $1x10^3$ events were collected and cytometric analysis revealed that the percentage of CD56+ subset within the CD271+ MSC population, gated as CD45-CD271+CD56+CD146- was 8-fold ($p<0.0001$) higher in OA samples in comparison to healthy IC controls. Based on median values, the CD56+ subset accounted for 0.52% of the CD271+ MSCs isolated from the healthy bone samples while in OA they represented 4.21% (Figure 5.11A).

The DN population gated as CD45-CD271+CD56-CD146- represented the majority of CD271+ population. Based on median values, the DN subset represented 70.7% of healthy CD271+ cells while in OA their frequency was found to be at 58.51%. Although notably different, their percentages were not significantly different between healthy and OA cells. No difference was also observed in the percentages of CD146+ subset, gated as CD45-CD271+CD56-CD146+ between healthy and OA, with medians of 14.26% in healthy samples and 17.31% in OA samples (Figure 5.11B). While a trend for higher expression in OA was observed, these data validated the increased transcriptional levels of *MCAM* (Chapter 3, Figure 3.14) at the protein level without reaching statistical significance.

These results confirm the increased presence of the CD271+CD56+ subset in OA bone. However, in comparison to other subsets, the CD271+CD56+ subset represented only a small proportion of the entire CD271+ population, the majority of cells being actually

DN. These are stromal reticular cells (non-BLCs, non-pericytes) which in OA can represent the stromal cells in the fibrovascular tissue previously documented in Chapter 4, Figure 4.24.

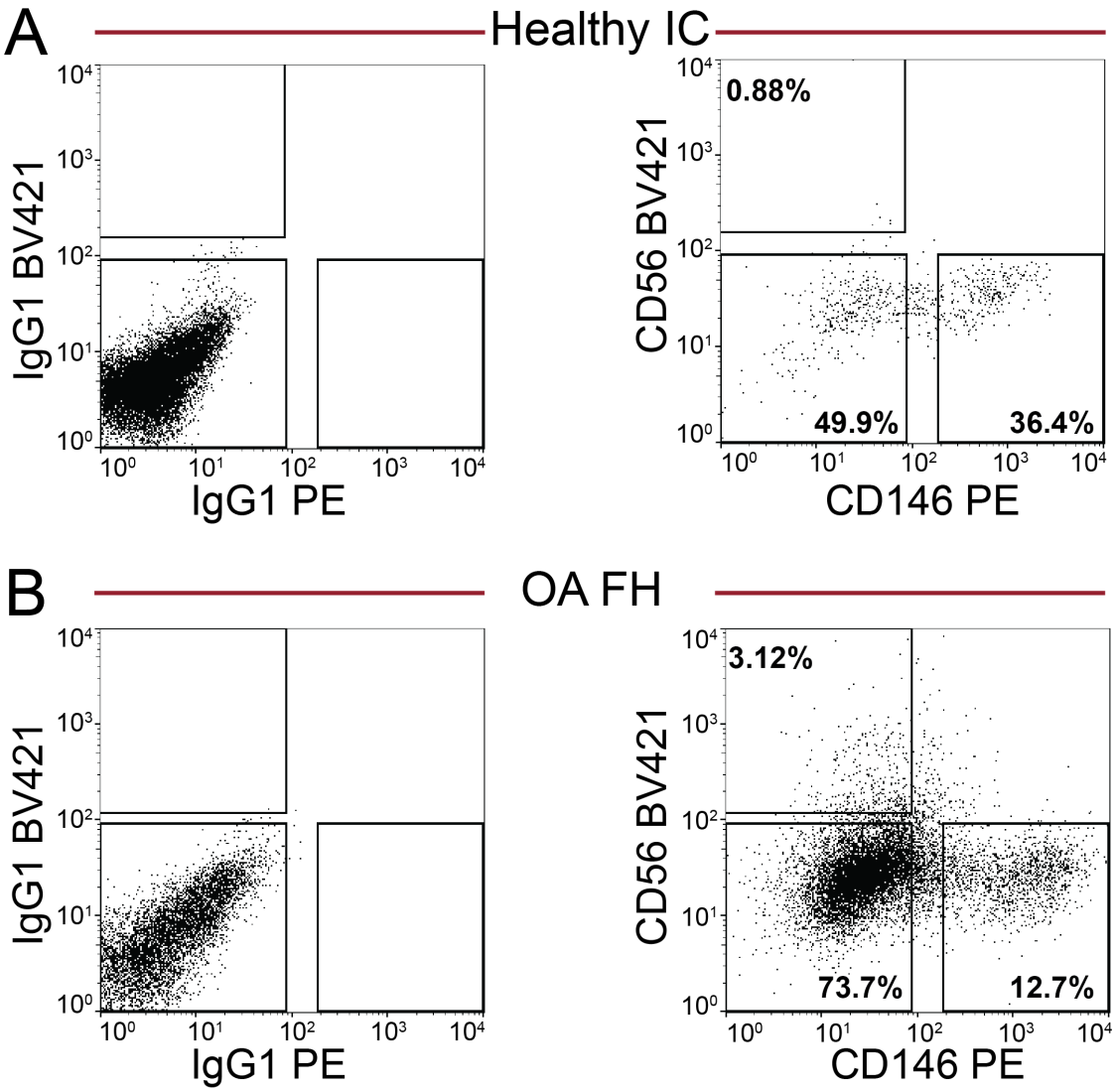

Figure 5.10. Enumeration by FACS of CD271+ MSCs subsets from healthy and OA bone. *Dot plots showing FACS analysis of fresh, uncultured cells enzymatically extracted from healthy IC and OA FH bone, stained with BV421-CD56 and PE-CD146 following gating on the APC-CD271+ cell population and HLCs removal by negative gating with FITC-CD45. (A) Gates set using the isotype control IgG1 BV421 corresponding to CD56 antibody conjugate and IgG1 PE for CD146 antibody on cells isolated from iliac crest. (B) Gates were set using isotype controls for each antibody used to stain the cells extracted from OA bone.*

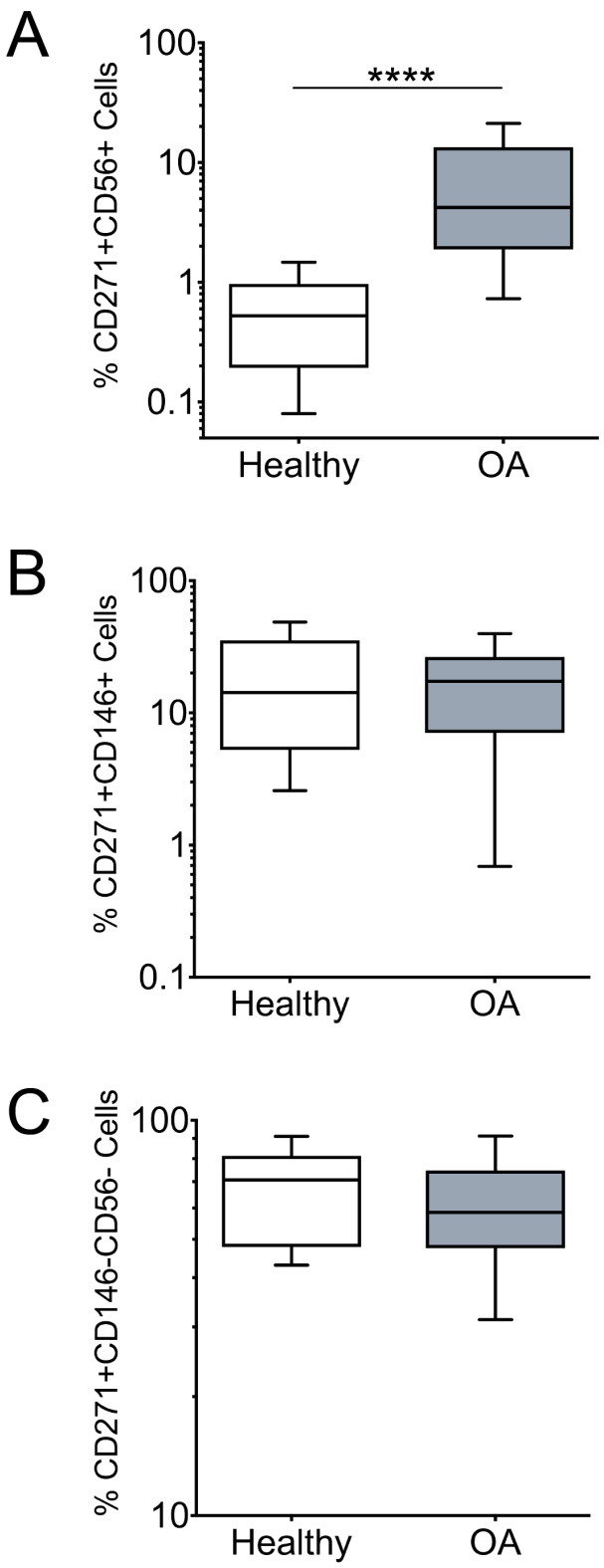

Figure 5.11. Comparison of CD271+ MSC subsets percentages between healthy and OA bone. *Graphs showing the enumeration of CD271+ MSC subsets extracted and purified by FACS from healthy and OA bone. (A) Graphs representing the percentage of CD56+ cells out of CD45-CD271+ cells. (B) Graphs representing the percentage of CD146+ cells out of CD45-CD271+ cells (C) Graphs representing the percentage of DN population gated as CD56-CD146- cells out of CD45-CD271+ cells.*

5.4.6 Gene expression analysis of native CD271$^+$ MSC subsets

In addition to enumeration, the CD271+ MSC subsets were also sorted for downstream analysis. This included investigation of gene expression levels of CD271+CD56+ subset in comparison to CD271+CD146+ and DN subsets as well as functional assessments. Based on the data cumulated so far, this further analysis aimed at testing the hypothesis that the increased osteogenic commitment observed in the CD271+ MSCs from Chapter 3 was attributed to a specific osteogenic committed CD271+CD56+ subset.

Donor matched FACS purified MSCs subpopulations from OA donors (n=6) were collected for gene expression analysis using TaqMan low density array (TLDA). Due to difficulties in obtaining large cell numbers from healthy iliac crest, cells of all three MSC subsets were only collected from OA bone. Analysis was performed using cells isolated from donor-matched subsets of n=6 OA samples comprising the CD45-CD271+CD146-CD56+ (CD56+ subset), CD45-CD271+CD146+CD56- (CD146+ subset), CD45-CD271+CD146-CD56- (DN subset) while CD45+CD271- (HLCs) were used as a control for all three subsets. All gene expression values were normalised to the housekeeping gene levels of HPRT1 and presented as $2^{-\Delta Ct}$, as described in Chapter 2, Section 2.5.4.

The TLDA panel comprised a total number of 96 genes known to be specific to MSCs and influence their functional properties, summarised in Appendix 5. These included transcription factors and mature proteins as markers for osteogenic, adipogenic and chondrogenic differentiation, proliferation and migration as well as stimulation of angiogenesis. These results were subjected to hierarchical clustering for visualization as described previously (Churchman et al., 2012), allowing fold differences to be observed more easily. Hierarchical clustering was performed based on Spearman rank correlation of the log transformed values, the software grouping the genes with similar differential expression between the MSC subsets. As expected, this analysis clustered the data from the four sorted fractions into two separate branches of the dendrogram, HLCs and MSCs respectively based on their level of expression and differences between the groups (Figure 5.12). It can be observed a segregation between the genes expressed higher in the HLC lineage (Figure 5.12, white rectangle) than MSC subsets and similarly, the genes higher expressed in CD271+ MSCs subsets as compared to HLCs (Figure 5.12, blue rectangle). Furthermore, another group of genes clustered under the CD56+ subset (Figure 5.12, yellow rectangle), however some of the DN samples were observed to overlap within the same cluster.

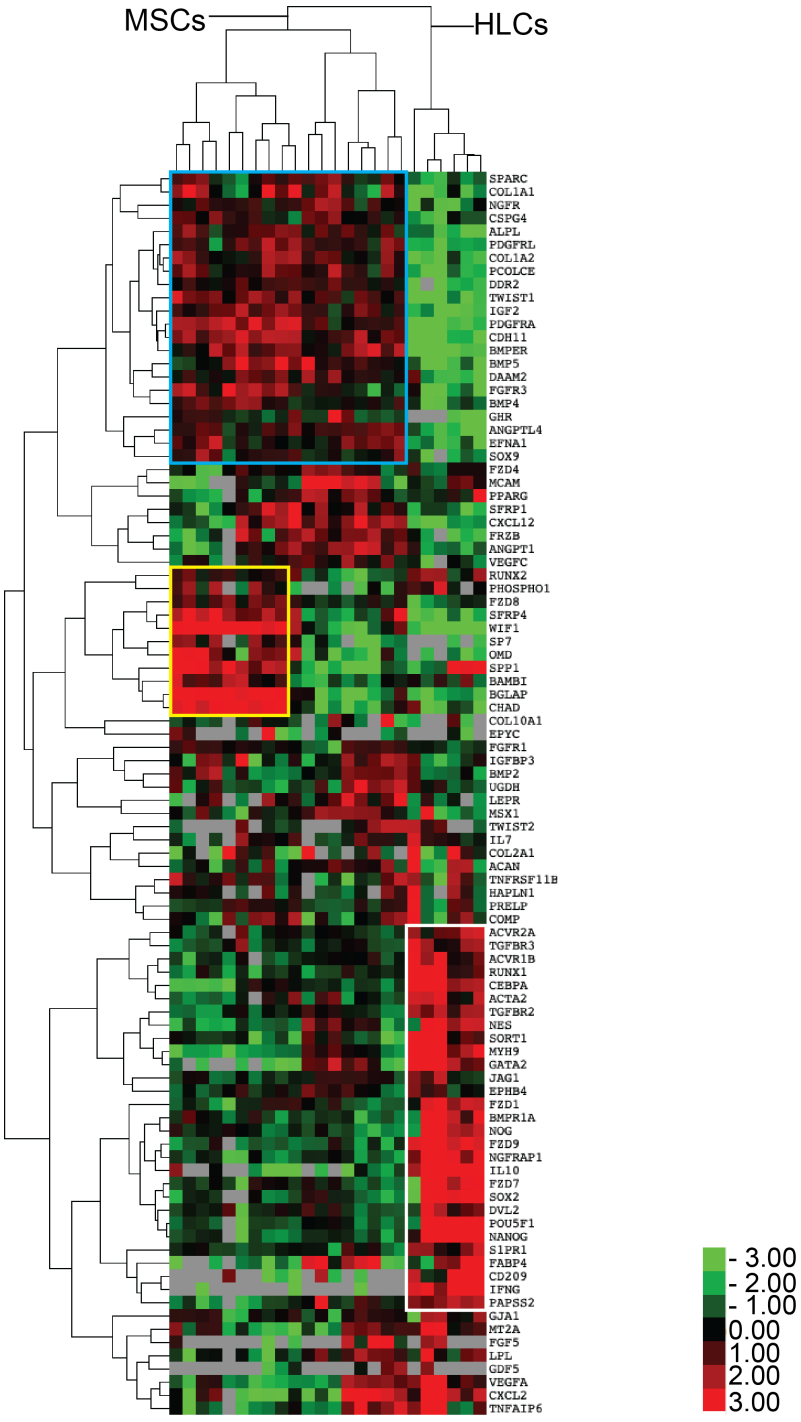

Figure 5.12. Hierarchical cluster analysis of FACS sorted fractions isolated from OA bone. *Dendrogram showing hierarchical cluster analysis of log2 transformed relative gene expression of FACS-purified native MSCs subsets and HLCs from OA bone (n=6). Values were calculated by the* $2^{-\Delta Ct}$ *normalised to HPRT1. Green < HPRT1, Red>HPRT1, Black=HPRT1, Grey-missing values. White rectangle: HLCs specific cluster; blue rectangle: CD271+ common genes; yellow rectangle: CD271+CD56+ specific cluster, overlapping with DN.*

It is known that data pre-processing steps, such as gene normalisation and how missing values are dealt with can affect the clustering outcome (D'haeseleer, 2005). Following hierarchical clustering it was decided that a more exhaustive comparison was needed for the genes that showed notable changes between the CD56+, CD146+ and DN subsets belonging to the CD271+ MSC population. The clusters obtained were not compact and well separated with regards to the genes within the CD271+ MSC population, which was comprised of three subsets as selected by FACS. Therefore, the genes were scrutinised individually to investigate their expression levels by direct comparison between the sorted fractions.

But first, quality control was assessed at a transcriptional level to verify the sorting procedure and to test whether the isolated fractions under investigation actually belong to the corresponding populations. The cluster analysis segregation confirmed distinct molecular identities reflecting different cell lineages, the two clusters highlighted on the dendrogram including genes associated with the cellular identities of MSCs and HLCs. The HLCs group included genes associated with the haematopoietic lineage, such as GATA binding protein 2 (*GATA2*), *RUNX1*, interleukin 10 (*IL10*) and interferon gamma (*IFNG*) which were all differentially expressed in comparison to the MSC group. As shown in Figure 5.13, the expression levels of *IFNG* was only detected in HLCs with no detectable signals in any of the three subsets. Similarly, *IL10* was only detected in some of the MSCs subsets and at lower levels in comparisons to HLCs.

In addition, the levels of *NGFR,* the gene encoding the CD271 antigen was expressed at similar levels across the three MSC subsets, all significantly higher than HLCs. This confirmed at a transcriptional level the positive selection of the three MSCs subsets under the CD271 marker. Furthermore, the gene encoding CD146 marker (*MCAM*) also confirmed the FACS sorting procedure, the levels of expression being significantly higher in the CD146+ MSC subsets in comparison to the other two MSC fractions and HLCs.

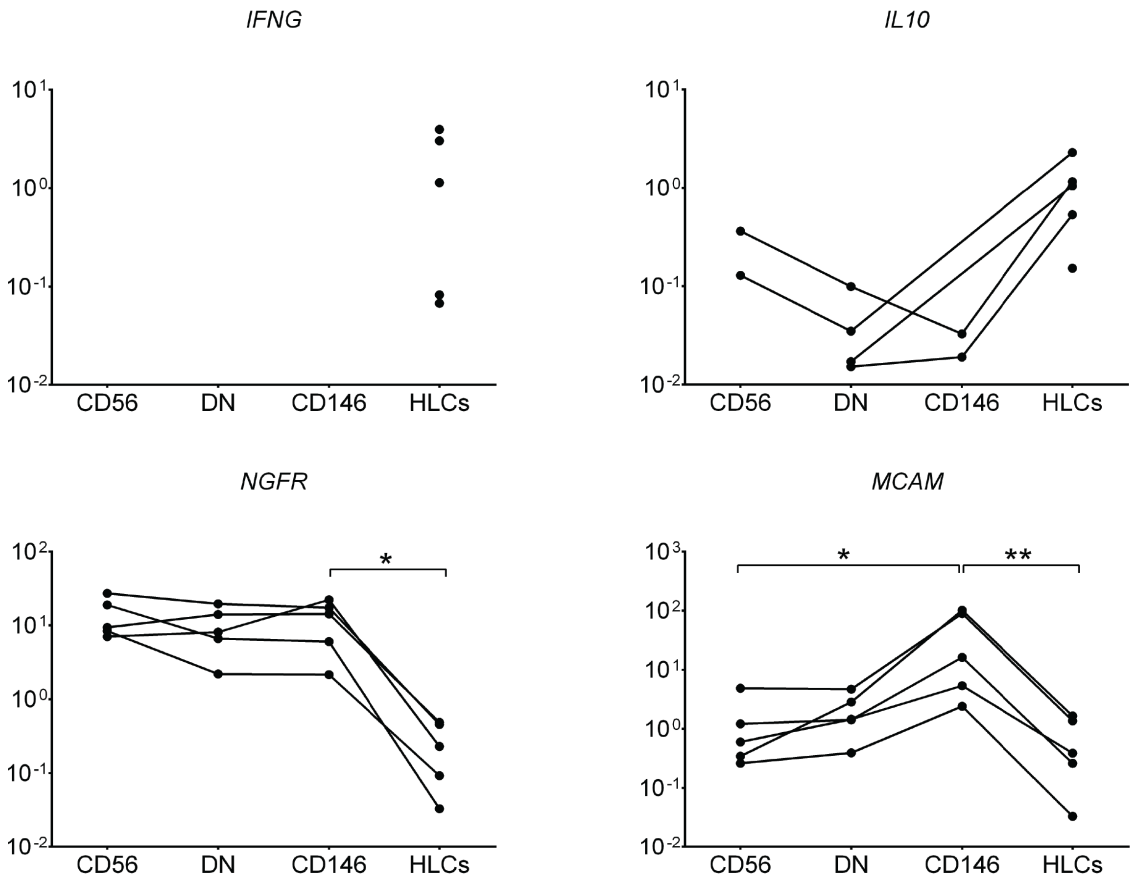

Figure 5.13. Assessment of positive control gene expression in the FACS sorted fractions. *Gene expression levels of CD45+ HLCs (IFNG and IL10) and CD271+ MSCs subsets (NGFR and MCAM) associated molecules were compared across all fractions. The expression levels confirmed the sorting procedure in sorted fractions from OA bone. Data represented as connecting dots for donor-matched samples and gene expression values as relative to HPRT1 on a log scale.*

5.4.7 Osteo-chondrogenic gene expression profile of OA CD45^{-}CD271^{+} CD56^{+} MSCs

As previously stated, within the CD271+ MSCs there may be a subset of enhanced osteogenic commitment responsible for the altered MSC phenotype observed in OA. Based on histological assessment and in consensus with the published literature (Bühring et al., 2009), it was determined that the CD271+CD56+ exists and is located on the bone lining surface. In order to determine whether CD56+ MSC subset are the culprit fraction responsible for the osteogenic bias observed in OA MSCs, a detailed analysis of the gene expression differences between the three MSC subsets selected from the TLDA was next performed. This indicated a strong osteogenic commitment of the CD56+ MSC subset as well as an increase in some chondrogenic related molecules. Although the experiment was performed by using MSC subsets from n=6 OA donors, for a better interpretation of results, the analysis was performed only on the complete set of donor-matched gene expression values (Figures 5.14 and 5.15).

The CD56+ subset gene expression profile was first determined to be significantly different in comparison to the CD146+ subset. Furthermore, it was noted that a trend for higher expression corresponds to the CD56+ subset in comparison to DN, however it failed to reach statistical significance between these two data sets (Figures 5.14). The gene expression levels of *SPP1* were 508-fold higher in the CD56+ subset (p=0.0016) compared to CD146+ subset while *BGLAP*, a robust marker for bone formation and active osteoblasts (Wei and Karsenty, 2015) was 163-fold higher in the CD56+ subset (p=0.0045) compared to CD146+. The levels of *OMD*, encoding an extracellular matrix protein with important roles in osteoblasts formation and the mineralisation process (Rehn et al., 2008), were 86-fold higher (p=0.0047) in the CD56+ subset in comparison to the CD146+ subset. Furthermore, the levels of the key osteogenic transcription factors *SP7* and *RUNX2* were both significantly higher expressed in the CD56+ subset in comparison to CD146+ subset. The levels of *SP7* were found to be 26-fold elevated (p=0.0140) in the CD56+ subsets while *RUNX2* levels were 14-fold higher (p=0.0117) in comparison to CD146+ subset. Another molecule associated with the MSC's osteogenic lineage commitment, *ALPL,* was 3-fold higher (p=0.0342) in the CD56+ subset compared to CD146+ cells. The analysis was performed based on median values, representing the medians calculated based on the donor matched expression levels for each gene and detailed in Table 5.1.

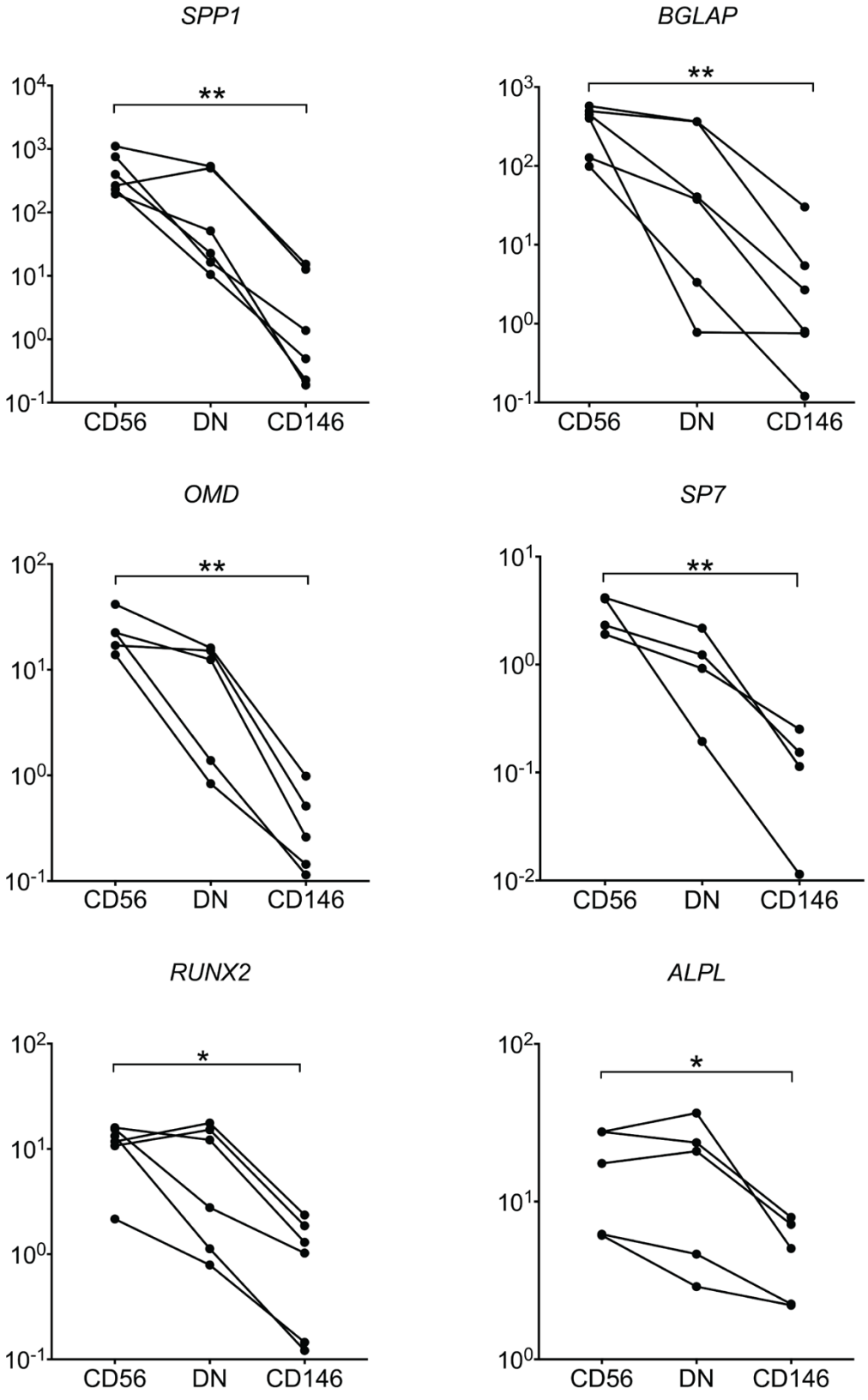

Figure 5.14. Gene expression levels of osteogenesis-related molecules in sorted CD271+ fractions from OA bone. *Data represented as connecting dots for donor-matched samples and gene expression values as relative to HPRT1 on a log scale.*

Following analysis of genes associated with osteogenesis, the CD56+ and DN subsets also expressed higher levels of molecules associated with the chondrogenic lineage compared to CD146+. The transcription factor *SOX9*, the main controller of the chondrogenic lineage commitment (Bi et al., 1999) was expressed at higher levels in the CD56+ subset compared to CD146+ cells (5-fold, p=0.0400). The expression levels of *CHAD*, another gene implicated in cartilage formation and MSC chondrogenic differentiation (Camper et al., 1997), were 221-fold higher in the CD56+ subset (p=0.0133) compared to CD146+ subset.

Similar to the trend observed in the expression levels of osteogenic molecules, the DN subset also showed similar expression levels to the CD56+ subset with regards to the chondrogenic transcription factor *SOX9,* but was significantly higher than in CD146+ subset. The levels of *CHAD* were also higher in DN compared to CD146+, however it was not statistically significant.

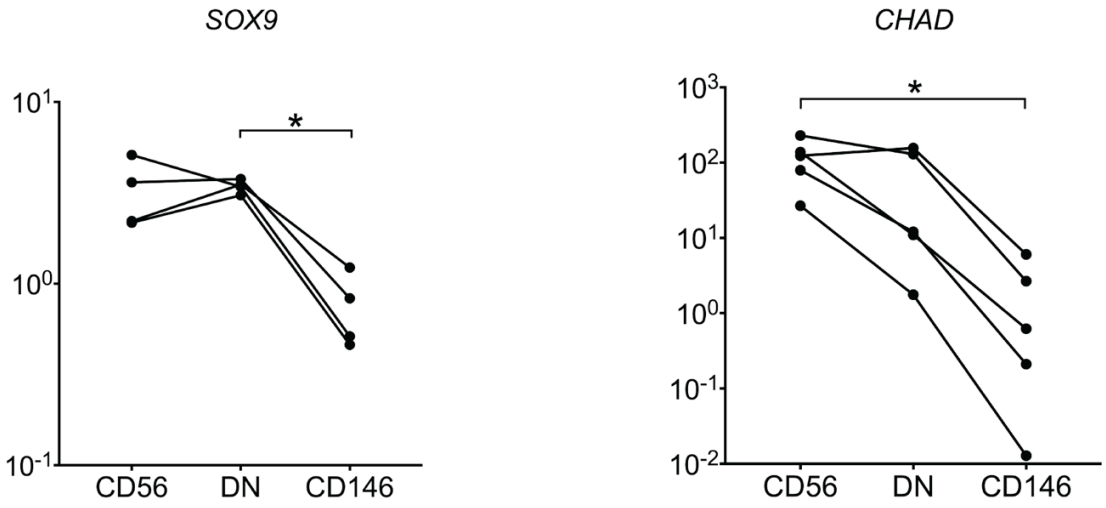

Figure 5.15. Gene expression of chondrogenic molecules SOX9 and CHAD in sorted cell fractions from OA bone. *Data represented as connecting dots for donor-matched samples and gene expression values as relative to HPRT1 on a log scale.*

Table 5.1. Fold differences in gene expression based on median values of CD56+ and CD146+ subsets sorted from OA bone

Gene	Fold difference to CD146+	P value	Fold difference to DN	P value
SPP1	508.62	** 0.0016	10.68	NS
BGLAP	163.11	** 0.0045	7.23	NS
OMD	86.02	** 0.0047	2.58	NS
SP7	25.78	** 0.0140	1.99	NS
RUNX2	13.57	* 0.0117	2.02	NS
ALPL	2.78	* 0.0342	1.17	NS
CHAD	221.22	* 0.0133	6.57	NS
SOX9	4.53	* 0.0400	1.23	NS

Taken together, this pattern of expression points to an osteo-chondro profile of both CD56+ and DN subsets of MSCs but although not statistically significant, the CD56+ subsets expressed higher levels of these genes compared to DN. Therefore, this is the first time when the gene expression profile of CD271+ subsets were analysed in native cells. While a chondrogenic bias of the CD271+CD56+ subset was previously documented in healthy BM MSCs (Battula et al., 2009), this analysis was done following culture expansion of the respective subset and knowledge about their native biology was lacking. The enhanced osteogenic profile documented in this chapter suggest a more complex molecular profile of the different subpopulations of native bone resident MSCs and may provide important insights with respect to MSCs implications in OA pathophysiology.

5.4.8 Genes higher expressed in CD146+ and DN subsets

Further analysis revealed the distinction between the CD56+ and DN subsets. It was found that *CXCL12*, a well-known stromal support chemokine (Greenbaum et al., 2013), showed significantly higher expression levels in DN compared to both CD56+ and CD146+ subsets (Figure 5.15A). Based on median values CXCL12 was 7-fold elevated in DN compared to CD56+ subset (p=0.0133) and 4-fold higher in comparison to the CD146+ subset, although the latter was not statistically significant. This was consistent with the stromal topography of this subset (Chapter 4, Figure 4.24) as CXCL12 encodes SDF-1, a critical chemokine with roles in MSC migration and stromal support (Kitaori et al., 2009; Greenbaum et al., 2013).

While CXCL12 seemed to be higher expressed in DN subset and therefore indicating a separation of the three subsets, it was interesting to verify the identity of the CD146+ subset, which was only characterised based on functional assays and localisation in previous studies, with no indication of their molecular signature (Tormin et al., 2011). The gene that showed higher specificity to CD146+ compared to both CD56+ and DN was *FABP4,* encoding a mature adipogenic protein. In comparison to DN and CD56+ median values, the expression levels of *FABP4* were 17-fold higher (p=0.0140) in CD146+ subset. Furthermore, the adipogenic transcription factor PPARγ was also shown to be higher expressed in CD146+ subset compared to DN and CD56+, although it was not statistically significant.

In addition, another gene that showed specificity for CD146+ perivascular subset was a transcript expressed by cells associated with a haematopoietic origin (Figure 5.15B). *GATA2* is a transcription factor required for expansion and differentiation of haematopoietic stem cells (Tsai et al., 1994) but several roles have also been documented in MSCs, including roles in maintenance of stemness (X. Li et al., 2016). The *GATA2* expression levels were found to be 6-fold higher (p=0.0159) in CD146+ subset in comparison to DN and no expression was detected in the CD56+ subset.

Transcriptional profile of the three subsets indicated so far distinct gene expression signatures in OA. It was shown that CD56+ cells had an enhanced osteochondro profile while DN is characterised by increased CXCL12, consistent with its location within the stromal compartment. Perivascular topography of CD146+ has been previously documented (Tormin et al., 2011) and here it was shown that this subset expressed low osteogenic related genes, but higher levels of *GATA2* in addition to the fat associated molecules, *FABP4* and *PPARγ.*

Based on the results following both topographical assessment and gene expression analysis, there has been an indication of a gradient gene expression pattern in MSCs from bone lining location towards the perivascular MSCs. The osteogenesis related genes were at low levels in the perivascular CD146+ subset which were observed at an intermediate level in DN and reaching significantly higher levels in the CD56+ subset, which was topographically shown to be located on the bone surface. Most importantly, this enhanced osteogenic profile was exhibited by the CD271+CD56+ cells lining the bone surface, excluding the bone forming osteoblasts, previously shown to be negative for CD271 (Chapter 4, Figure 4.27).

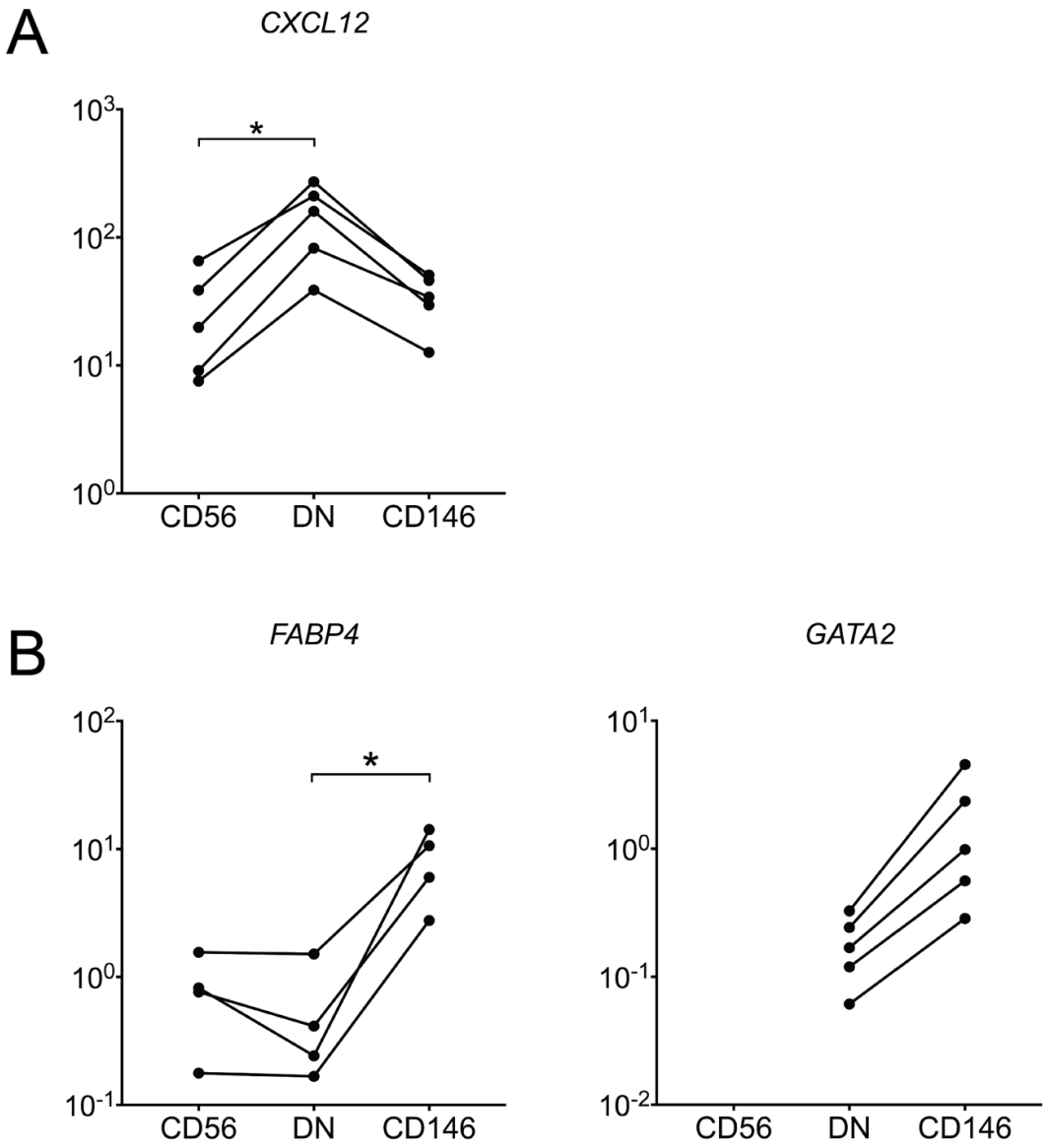

Figure 5.16. Gene expression levels of molecules expressed higher in DN and CD146+ in comparison to CD56+ subset. *Higher gene expression levels of CXCL12 in the DN subset compared to CD56+ and CD146+ subsets (A) and the levels of higher expressed molecules in the CD146+ subset compared to DN and CD56+ subsets (B). Data represented as connecting dots for donor-matched samples and gene expression values as relative to HPRT1 on a log scale.*

5.4.9 Differentiation assay

One of the key biological properties of MSCs is their potential to differentiate into mesodermal lineages. Therefore, the phenotypical characteristics of the purified subsets were further tested for their multipotentiality *in vitro*. Based on gene expression data, it was expected that the *in vitro* osteogenic potential of CD56+ was higher in comparison to the other two fractions. Similarly, the adipogenic potential of CD146+ subset would also confirm the higher levels of adipogenic transcripts observed by gene expression analysis of this subset in comparison to DN and CD56+ subsets.

By using enzymatically released cells from three OA donors, cultures were initiated from all three FACS-purified CD271+MSC subsets (CD56+, CD146+ and DN) and subjected to standard osteogenic, adipogenic and chondrogenic differentiation to determine which of these fractions represent a population of BM MSCs with enhanced osteogenic potential. The *in vitro* differentiation was evaluated by functional assays, histochemical and qPCR analysis.

5.4.9.1 Cell culture

The collected numbers of cells following cell sorting procedure ranged between $0.3x10^4$ – $2.2x10^4$ cells for the lowest fraction (CD56) and were insufficient for the differentiation assays, therefore minimal culture expansion was performed to allow the cells to proliferate. Thus, between $0.5x10^4$ - $1x10^4$ cells from the three subsets were seeded in 6-well culture dishes and allow to proliferate over the same period for 6 days post isolation by FACS. Following trypsinisation, the cells were seeded at a density of 5,000 cells/cm^2 and cultured for further 48 hours thereafter when they were trypsinised and seeded in the corresponding media for either osteogenic, adipogenic or chondrogenic assay. Altogether, the cells were in culture for 8 days and were used at passage 1 for these assays.

The three MSCs cultured subsets were found to be heterogeneous regarding cell size and morphology immediately after they were placed in culture (Figure 5.16). The CD56+ subset took on a circular in shape, while the DN and CD146+ cells displayed an MSC-like spindle shape (Figure 5.17). However, following 3 to 7 days respectively, all the cells adopted a similar fibroblastic morphology characteristic to cultured MSCs (Figure 5.17). No obvious differences were noted, all three subtypes displaying a morphology varying from elongate to broad as well as small flat cells. The HLCs (CD45+) isolated following FACS analysis were also cultured and displayed a morphology characteristic to haematopoietic cells, with spindle shaped monocytes progenitors attached while other CD45+ cells suspended in media were sequentially removed during media changes.

Following the 7 days in culture some of the attached CD45+ cells adopted a flat morphology, indicating differentiating monocytes (Figure 5.17).

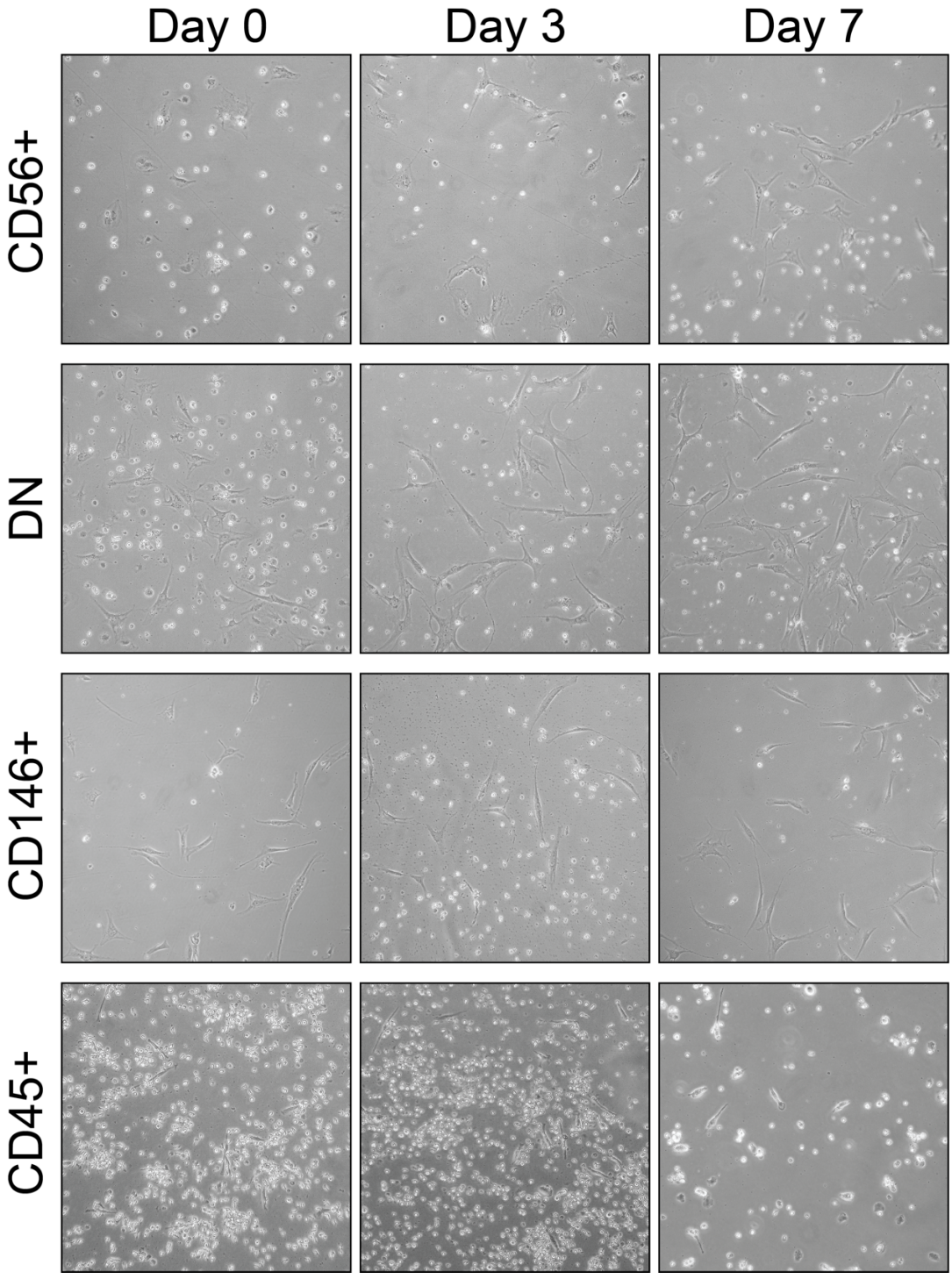

Figure 5.17. Cell cultures generated from the isolated cells following sorting by FACS from the four fractions. *Photos were taken at Day 0, Day 3 and Day 7. While the cells showed different morphologies at Day 0, representing first day after sorting, they were all distinct from CD45+ cells and adopted a fibroblastic morphology after Day 3. Images were taken using an inverted microscope with a 20x objective and an Olympus camera.*

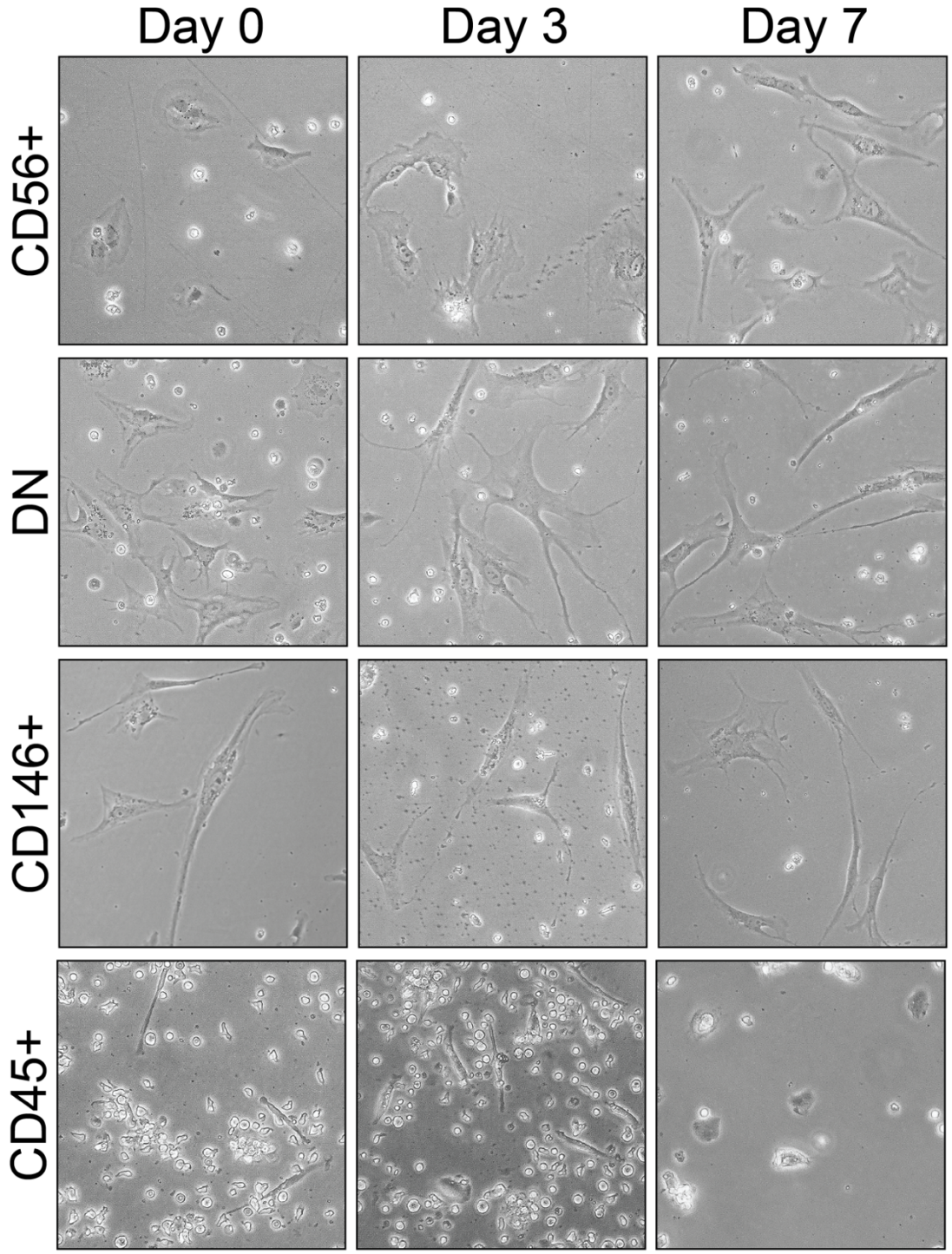

Figure 5.18. Higher magnification of the FACS isolated cells from the four fractions at Day 0, Day 3 and Day 7. *While the cells showed different morphologies at Day 0, representing first day after sorting, they were all distinct from CD45+ cells and adopted a fibroblastic morphology after Day 3. Note that morphology of some attached CD45+ cells changed from a spindle shape to flat shape through the 7 days in culture. Images were taken using an inverted microscope with a 40x objective and an Olympus camera.*

5.4.9.2 Osteogenesis

In order to determine whether any of the three CD271+ MSC subsets have an enhanced osteogenic potential, osteogenic assays were next used. By using this assay, it was expected to obtain a confirmation of the gene expression data of enhanced osteogenic bias observed in native CD56+ subset.

Osteogenesis was assessed following induction in standard commercially available osteogenic media of the three MSCs subsets expanded for 1 passage from the three donors. Following 14 days in culture under osteogenic conditions, the cells were stained to detect the ALP activity (Figure 5.19) showing positive results in all samples judged by the blue colour developed in the culture plate following incubation with ALP staining solution. The MSCs subsets displayed no visible differences between the subsets or the donors with regards to the intensity of blue colour, while a degree of variability was noted.

Alizarin red staining was performed to assess the calcium production in the three MSCs subsets following 21 days' post-induction. Similarly, no differences were observed in the calcium deposition marked by the red staining between the MSCs subsets from all three donors (Figure 5.20) while similar variability between donors and subsets was observed.

Both staining methods provided a qualitative assessment of the osteogenic differentiation potential of the three subsets from three different donors. It was observed that all subsets responded well to osteogenic induction. This indicated a potential for *in vitro* osteoblastic lineage commitment of all the three MSC subsets, based on the positive alkaline phosphatase activity as well as their increased calcium production. In order to determine any potential differences between these subsets in their osteogenic potential, the three subsets were subjected to quantitative assessments, including measurements of calcium production and transcriptional analysis following osteogenic induction.

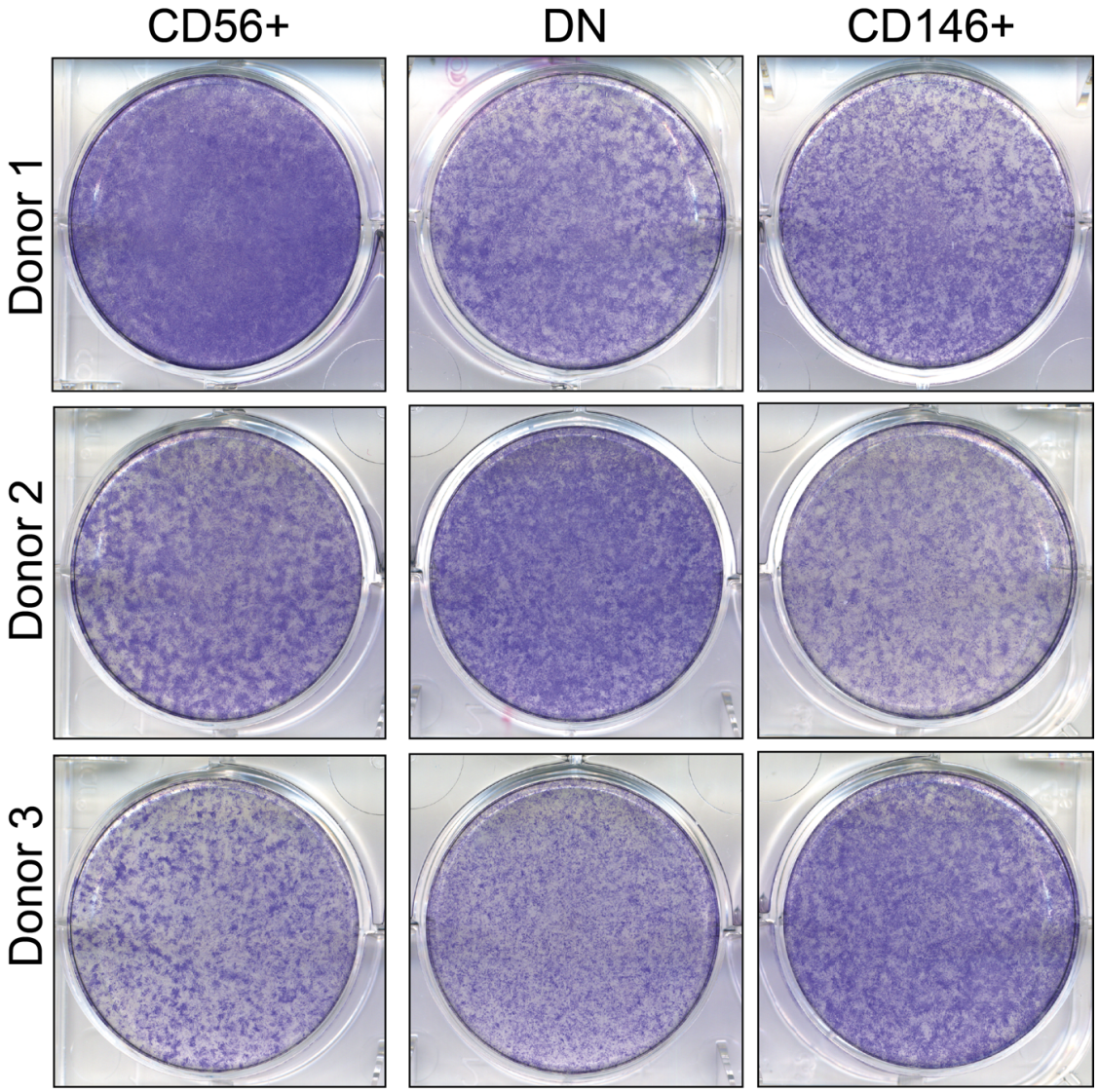

Figure 5.19. Assessment of alkaline phosphatase activity in the culture-expanded CD271+ MSCs subsets. *Representative osteogenesis assay dishes showing ALP staining at 14 days post-induction using Fast Blue RR salt for all CD271+ MSC subsets following culture (n=3 donors, each subset in duplicate). No visible difference was observed between the MSC subsets.*

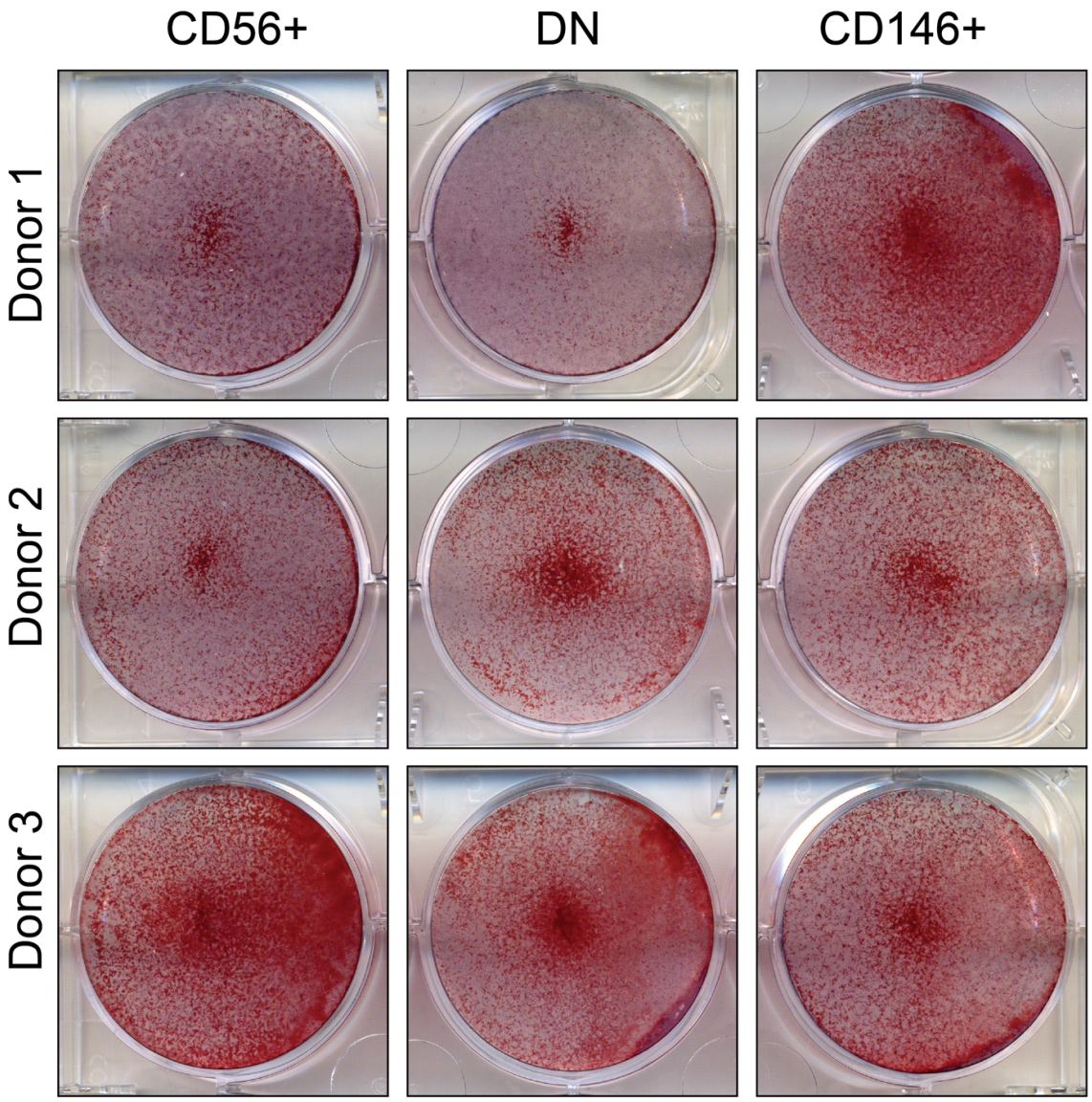

Figure 5.20. Assessment of calcium production by Alizarin red in the culture-expanded CD271+ MSCs subsets. *Osteogenesis assay dishes showing Alizarin red staining at 21 days post-induction to assess calcium deposition of sorted MSC subsets (n=3 donors, each subset in duplicate) indicating inter-donor variability and no visible differences across the subsets.*

Total calcium production per well was measured in triplicate in all MSC subsets from the three donors following 21 days under osteogenic conditions. Calcium was detected in all samples, and no statistically significant difference was observed between the MSCs subsets (Figure 5.21). Inter-donor variability was observed across all subsets and may be attributed to cell characteristics and their ability to adapt to *in vitro* conditions.

Correspondence between total calcium measured and alizarin red staining was observed but not in ALP staining. For example, the CD146+ MSCs subset from Donor 1 showed stronger alizarin red staining in comparison to DN and CD56+ subset. The same trend was observed by calcium measurements where CD146+ MSCs produced on average 8 µg Calcium/well while DN and CD56+ only 19 µg/well and 24 µg/well respectively.

Osteogenic differentiation was also quantified at a transcriptional level using gene expression by qPCR and analysing the mRNA levels of genes encoding lineage-specific markers, such as the key transcription factor *RUNX2* and the mature bone protein *BGLAP* (osteocalcin).

Interestingly, gene expression results were variable with regards to the MSC subsets' response to osteogenesis induction. The levels of both transcripts varied among the three MSC subtypes without a clear trend that would be expected to reflect the results observed following functional assays. Moreover, it was observed that the levels of *RUNX2* tend to decrease following induction in all three MSC subtypes which may be explained by previous studies suggesting that *RUNX2* activity is more regulated at post-transcriptional level and was also shown to be elevated early during differentiation and decreased on day 21 (Jaiswal et al., 1997). However, the functional assays quantifying alkaline phosphatase activity and calcium deposition indicated a positive and active osteogenesis.

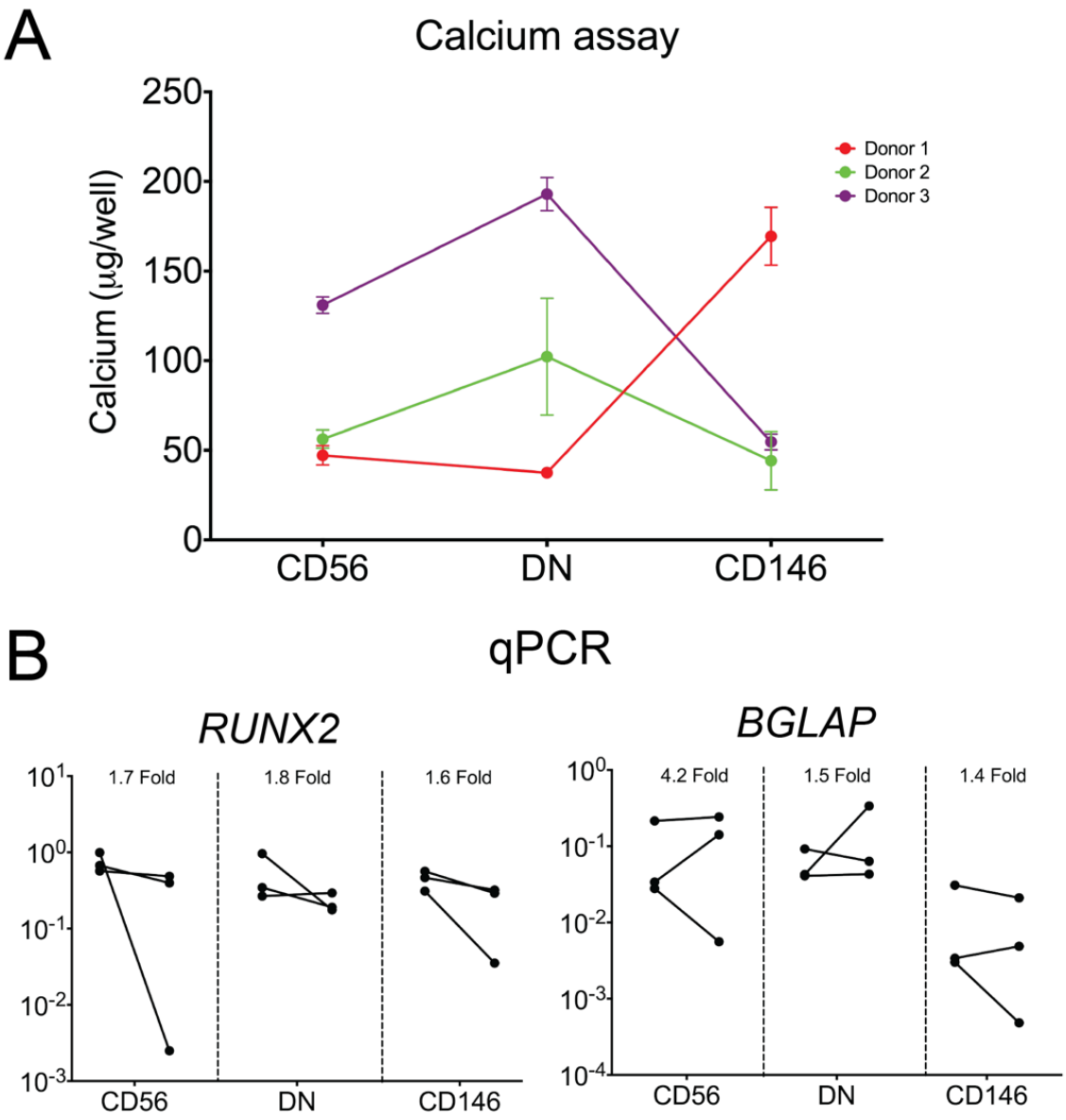

Figure 5.21. Osteogenic differentiation assessment by Calcium assay and qPCR. *(A) Calcium production of sorted cells following culture expansion represented as µg of calcium/well. Data presented as donor-matched connected dot plots with average values and bars as standard deviation of triplicate wells for each of the three MSC subsets in the three donors. (B) Transcriptional analysis at day 0 (left data set) and day 21 (right data set) post-osteogenic induction showing the fold changes in relative expression of RUNX2 and BGLAP in the three MSC subsets. Data represented as connected dot plots for donor-matched samples and fold changes calculated based on average values of duplicates for each subset.*

5.4.9.3 Chondrogenesis

In order to determine which of the three CD271+ MSC subsets have a more pronounced chondrogenic potential, functional assays were used on all three MSC subsets from the same three OA donors. These chondrogenic assays were expected to confirm the enhanced chondrogenic potential observed by gene expression and indicated by the published literature (Bühring et al., 2009; Sivasubramaniyan et al., 2018). Chondrogenesis was hereby investigated using pellet-cultured MSCs in chondrogenic media for 21 days. Pellets of the three MSC subsets from the same n=3 OA donors were used for toluidine blue staining, GAG assay and qPCR.

After 21 days of differentiation, all MSC subsets undergone chondrogenesis and all samples formed large pellets with prominent matrix metachromasia (Figure 5.22A and B). Pellets were removed from media, photographed and diameter measured in duplicate (Figure 5.22B and C) then embedded in OCT for cryo-sectioning and toluidine blue staining in duplicate. All pellets had a similar shape and size with no obvious differences between subsets or donors. The diameter measurements of the pellets were averaged for each subset and then across all donors with no significant differences observed between the MSC subsets (Figure 5.22C).

Toluidine blue is a standard procedure for the histological assessment of chondrogenic differentiated cells and cartilaginous tissue maturity and quality (Bergholt et al., 2018). This dye permits the visualisation of the proteoglycans presence in a tissue because of its high affinity for the sulphate groups of proteoglycans (Schmitz et al., 2010). As shown in Figure 5.22A, all pellets exhibited an intense blue/purple colour suggesting a high proteoglycan content present in the pellets formed by the differentiated cells. However, no visible differences were observed between the three subsets with regards to matrix composition. Toluidine blue was used to stain the chondrogenic pellets formed by the differentiating cells as a qualitative assessment of the chondrogenic induction. Therefore, the potential to differentiate towards a chondrogenic lineage was positive for all MSCs subset, however this assay was insufficient for a quantitative assessment.

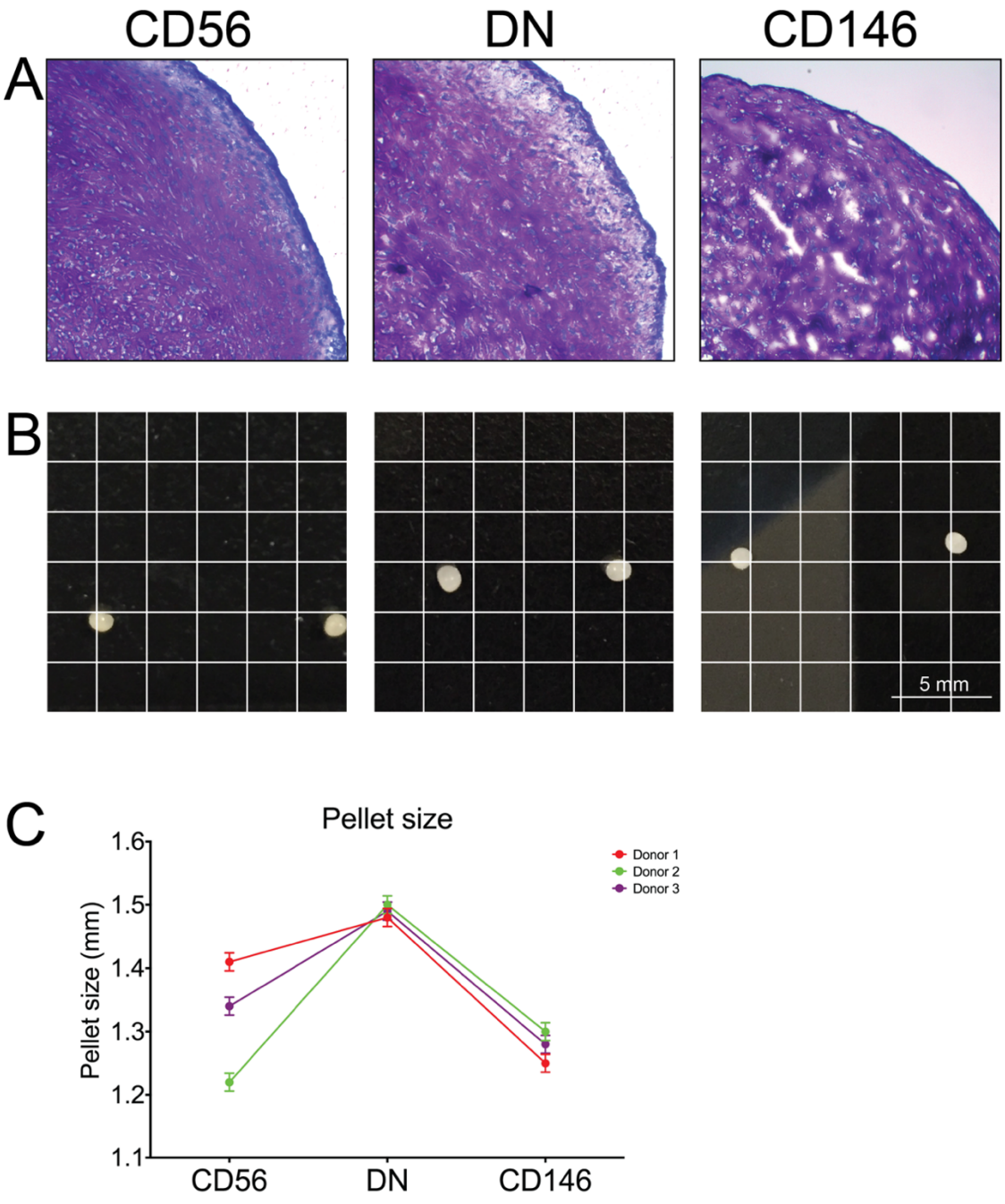

Figure 5.22. Assessment of chondrogenic pellets formation in the culture-expanded CD271+ MSCs subsets. *(A) Representative sections of chondrogenic pellets stained with Toluidine blue from the three FACS sorted fractions following culture expansion and chondrogenic induction. (B) Photograph of the chondrogenic pellets before embedding in OCT and snap freezing in liquid nitrogen. (C) Graph showing the diameter in mm of the two pellets represented as averages and standard deviation as connecting dots for donor matched samples.*

Following histological evaluation, GAGs were measured in pellets from all MSC subsets as processed after the overnight papain digestion from the three donors. The accumulation of GAGs in chondrogenic pellets was assessed in triplicate pellets for each MSCs subset.

Mean values for the 6 measurements for each subset (i.e. 3 pellets/subset in triplicate) were pooled and shown in Figure 5.21 indicating that although a degree of inter-donor variability was observed in the chondrogenic capacity, there were no differences between the MSCs subsets in their GAG production (Figure 5.23).

Chondrogenesis was also assessed at a transcriptional level. Gene expression of the cells contained in the chondrogenic pellets was evaluated by qPCR using the lineage-specific transcripts, *SOX9* and *COL2A1*. Analysis revealed that the CD56+ MSC subset responded better to chondrogenesis induction in comparison to the other subsets. The increase in gene expression levels of both transcripts following chondrogenic induction was higher in the CD56+ subset in comparison to CD146+ and DN subsets. Based on median values, the increase in *SOX9* following 21 days of chondrogenic induction in CD56+ derived cells increased 8.4-fold compared to Day 0, while the increase was in CD146+ and DN was 2.3- and 3.4-fold respectively. Similarly, the expression of the mature chondrogenic molecule *COL2A1* was almost below detection before chondrogenic induction but elevated significantly (more than 20,000-fold) in the CD56+ cells. In comparison, the levels of *COL2A1* following chondrogenic induction were lower in the other two subsets, similar to the trend observed in *SOX9* expression. The expression levels in some samples were below the detection level and therefore the fold changes were calculated based on the median values for the paired data sets.

Although all three subsets were able to form cartilage *in vitro*, these results indicate that at least at a transcriptional level CD56+ and DN cells, may have an increased chondrogenic potential in comparison to CD146+ subset, although not statistically significant.

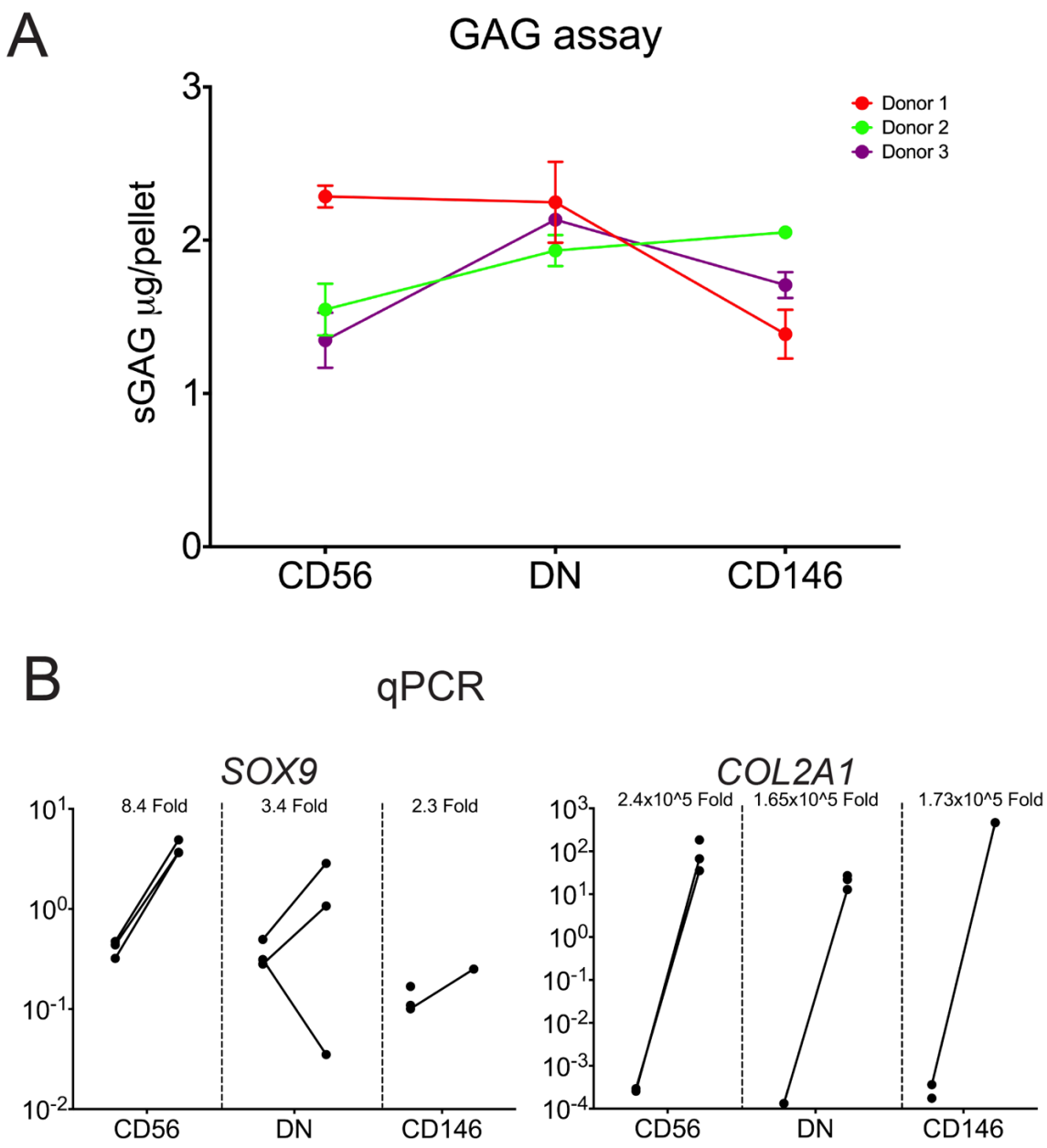

Figure 5.23. Chondrogenic differentiation assessment by GAG assay and qPCR. *(A) Quantification of GAG in µg per chondrogenic pellet obtained from FACS sorted fractions following culture expansion and chondrogenic induction represented as connected dot plots of the average value of donor-matched MSC subsets with bars as standard deviation. (B) Transcriptional analysis before and after chondrogenic induction showing the fold change differences in relative expression of SOX9 and COL2A1 in the three MSC subsets. Data represented as connected dot plots for donor-matched samples and fold changes calculated based on average values of each sample. Missing dots represent values below detection, fold change calculate based only on the average values of paired data sets.*

5.4.9.4 Adipogenesis

Adipogenic potential of the different MSCs subsets was investigated using the sorted cells from the three donors expanded to passage 1 and cultured thereafter in adipogenic media for 21 days.

The accumulation of lipid vacuoles was assessed in the MSC subsets using bright-field microscopy following Oil red staining. This assay confirmed the presence of adipogenic droplets in all three MSC subsets, but no obvious differences were observed across the three fractions as highlighted by the uptake of oil red (Figure 5.22). Inter-donor variability was noted, more oil red positive lipid vacuoles being detected in the third donor in comparison to the other two donors. The representative photomicrographs were taken using bright-field inverted microscope with a x20 objective directed in the middle of each well of the assay following Oil red staining.

Oil red staining provided a qualitative assessment of the adipogenic differentiation but in order to quantify the extent of adipogenesis in the three subsets, a more exhaustive method was then chosen. Quantitative analysis was employed using Nile red staining in order to investigate further any potential differences between the MSC subsets. Fluorescence emission following Nile red staining was measured in all samples and no significant differences were observed between the MSCs subsets from the three donors based on the median measured fluorescence. To ensure this was not due to a result of cell proliferation and hence, increased adipogenic induction, the ratio of Nile red to DAPI fluorescence was compared between the two sets (Figure 5.23A). Although not statistically significant, a trend for higher NR/DAPI ratio in the CD146+ MSC subset compared to DN and CD56+ MSCs was noted. This may be caused by the lower fluorescence levels of nuclear stain DAPI, suggesting a smaller number of cells in that subset due to different rates of proliferation.

Indication of higher adipogenic potential of the CD146+ MSCs compared to CD56+ and DN was further observed by qPCR using genes specific to adipogenic lineage cells. Although all subsets responded to adipogenic induction by increasing the expression of *FABP4* and *PPARG*, the fold change between Day 0 and Day 21 post-induction of these two adipogenic lineage markers were notably higher in the CD146+ MSC subset as compared to DN and CD56+ MSCs (Figure 5.23B). This suggested that the CD146+ subsets responded better to adipogenic induction since the transcription factor *PPARG* was increased 8-fold in this subset, while in CD56+ and DN cells the detected levels were only elevated 4-fold and 3-fold, respectively. Similarly, the expression levels of the

adipogenic protein *FABP4* increased almost 2000-fold in the CD146+ subset following adipogenic induction, while in the CD56+ and DN subsets this gene increased 100-fold and 70-fold, respectively.

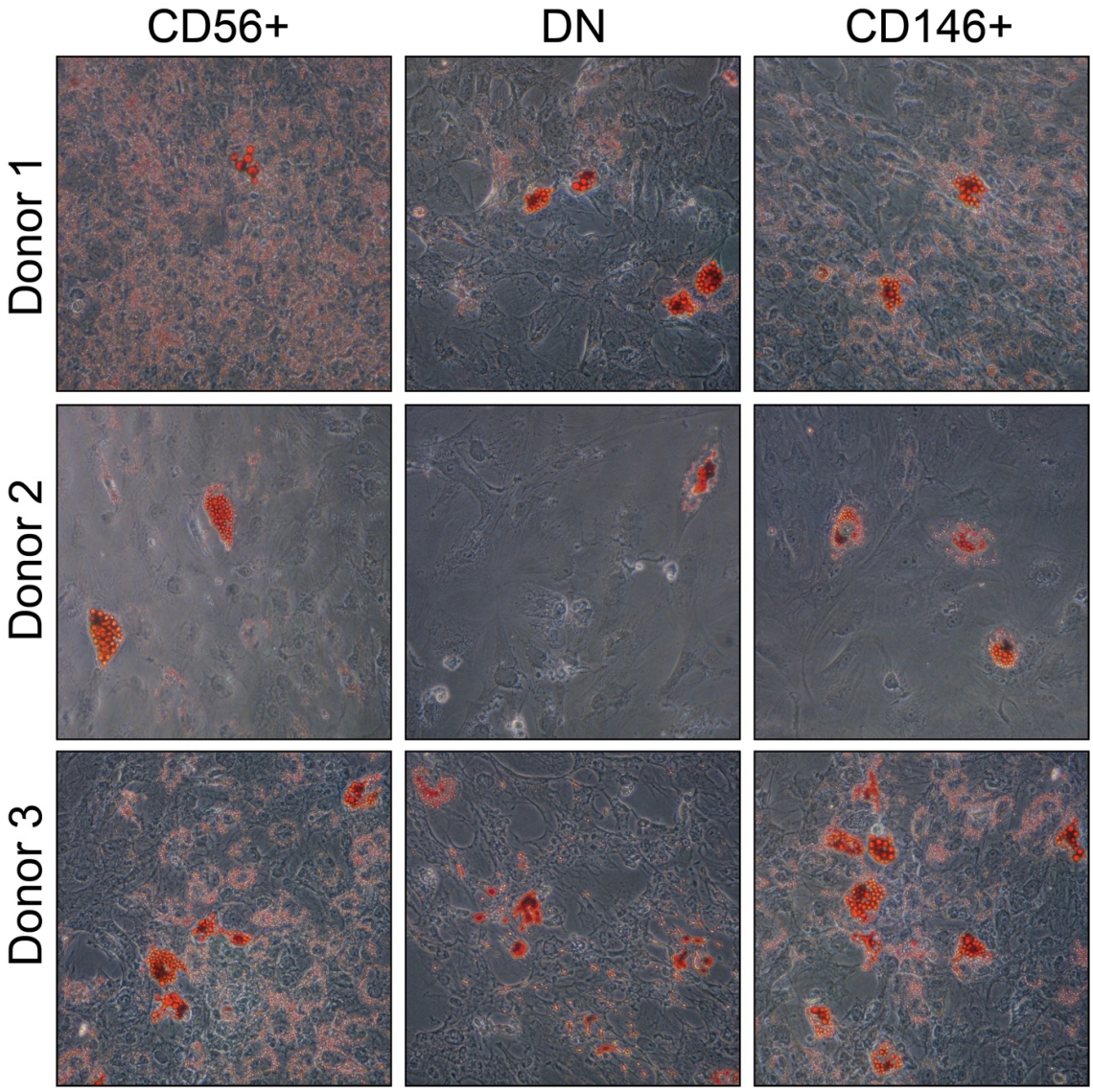

Figure 5.24. Assessment of lipid accumulation by Oil red following adipogenic induction in the culture-expanded CD271+ MSCs subsets. *Oil red staining of lipid droplets accumulation in the FACS sorted fractions following culture expansion and adipogenic induction from OA bone at 21-days post-induction. Images were taken at the centre of the wells of 24-well flask at 20X using inverted light microscope and an attached Olympus camera.*

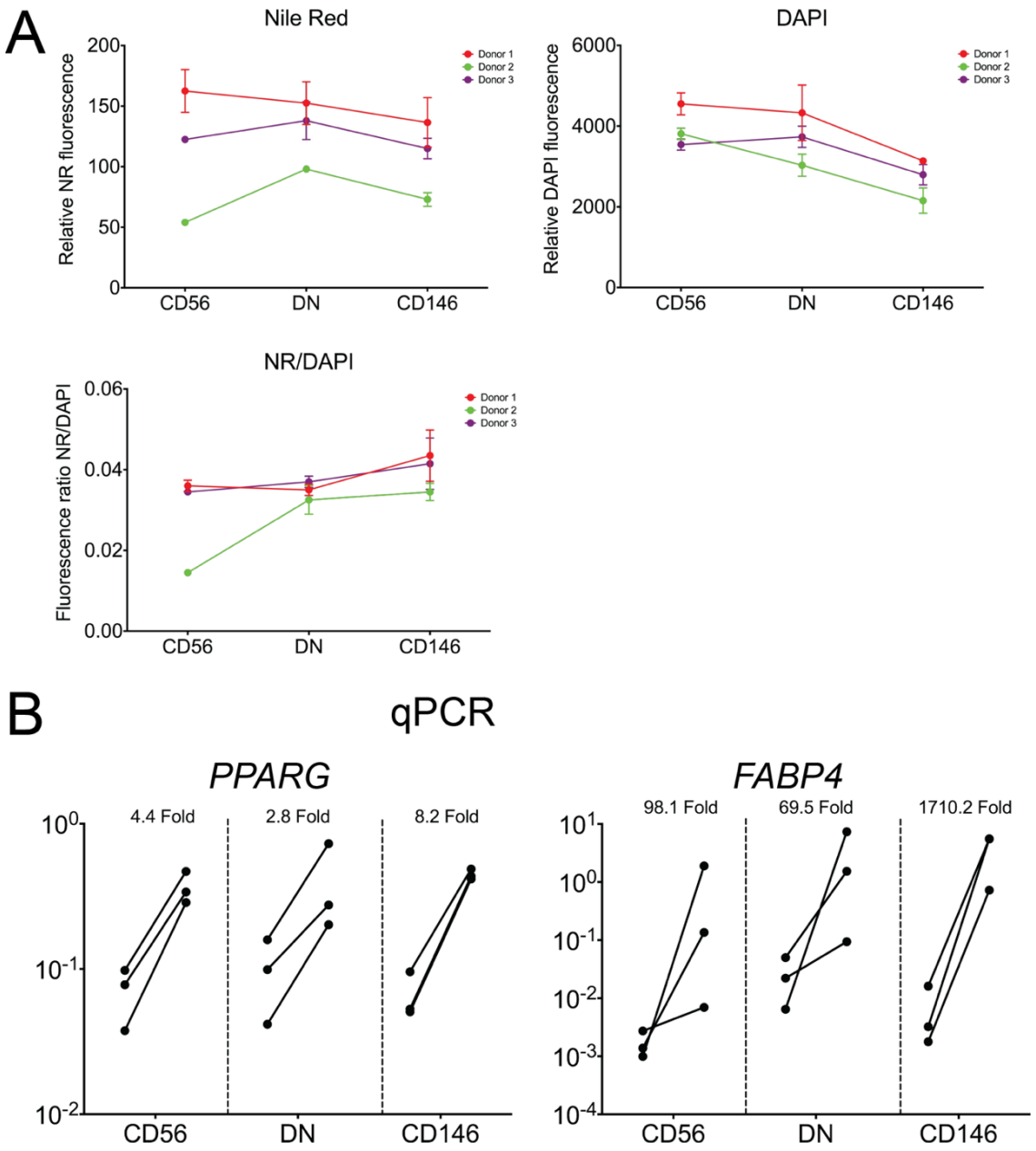

Figure 5.25. Assessment of adipogenesis in the culture-expanded CD271+ MSCs subsets by Nile red assay and qPCR. *(A) Adipogenic quantification by uptake of Nile red following 21 days post-adipogenic induction. Average fluorescence absorbance of Nile red and DAPI was measured and the ratio calculated, data represented as donor-matched connected dot plots of triplicate wells average with bars as standard deviation for the three MSC subsets in all donors. (B) Transcriptional analysis before and after adipogenic induction showing the fold change differences in relative expression of PPARG and FABP4 in the three MSC subsets. Data represented as connected dot plots for donor-matched samples and fold changes calculated based on median values of each set of paired data.*

Overall data presented in this section provides evidence of multipotentiality for all the OA CD271+ MSCs subsets investigated. It was shown that the perivascular, stromal and bone lining MSCs, as selected based on surface marker expression by FACS, possessed and maintained their capacity to adhere, grow and differentiate under culture conditions. While no major differences were observed between the three MSC subsets with regards to their multipotential *in vitro,* it was observed that CD56+ MSC subset responded better to chondrogenesis compared to CD146+ and DN MSC subsets. While the functional assays demonstrated an enhanced chondrogenic potential of the CD56+ subset, the strong osteogenic commitment observed by gene expression in the native cells was not reflected during the *in vitro* assays. Furthermore, it was also noted a trend of higher adipogenic potential of the CD146+ MSC subset, based on gene expression analysis following adipogenic induction.

Taken together, these results indicate that the native CD45-CD271+ phenotype represents a heterogeneous population of MSCs comprising of multiple subsets differing in their lineage commitment bias. It was demonstrated that *in vivo* the CD271+CD56+ had an increased osteogenic gene expression and was found in higher proportions in OA compared to healthy bone. The differences in gene expression observed in the native state of these subsets in OA bone had a greater amplitude which were not faithfully maintained under *in vitro* conditions.

5.5 Discussion

The cellular mechanisms behind bone sclerosis observed in OA is still poorly understood, however previous chapters revealed new evidence indicating involvement of both MSCs and osteocytes in the pathological mechanisms behind bone sclerosis. An aberrant CD271+ MSCs accumulation was observed in the sclerotic areas of OA femoral heads bone, putatively participating in an active bone formation process evident by the abundance of new and immature osteocytes inhabiting those areas (Chapter 4). As shown in Chapter 3, these MSCs also had an enhanced osteogenic commitment evidenced by their increased gene expression of molecules associated with osteogenesis and bias for bone formation. Additionally, as described in Chapter 1 and thoroughly documented by decades of research, it is clear that an abnormal bone phenotype dominate the late stage of disease (Lajeunesse et al., 2003; Suri and Walsh, 2012; Burr and Gallant, 2012). By dissecting the CD271+ MSC population into phenotypically different subsets, work in this chapter tested the hypothesis of the existence of an osteogenically committed MSC subpopulation that may be increased and OA and have possible implications in the bone sclerosis of late stage hip OA.

5.5.1 Bone lining resident CD271+CD56+ MSC subset

Data presented here showed that the CD271+CD56+ MSCs are restricted to the bone lining region of the stromal compartment in bone tissue from multiple sites and donors with the remaining CD271+ population located within the stromal architecture and around the blood vessels. Among the stromal CD271+ population, the perivascular fraction had been demonstrated previously to be represented by the CD146 expression (Tormin et al., 2011) while the remaining subset, represented by the CD271+CD56-CD146- (DN), comprises the population of MSCs in the stromal reticular net.

The presence of CD56 in cells at the bone surface has been previously documented as a transient molecule during osteoblast differentiation (Lee and Chuong, 2009). The CD56 expression was described as transient because was not found expressed in MSCs before osteogenic initiation and was lost in osteocytes in later stages (Lee and Chuong, 2009). This indicated that CD56 may be a marker for osteogenically committed cells and represented a viable molecule of choice for work in this chapter. It was shown however that the expression of CD56 was present in all bone surface cells, including the osteoblasts and osteoclasts present at the bone remodelling sites on the bone surface as well as BLCs (Andersen et al., 2009). Although these same locations have also been shown in Chapter 4 and by others (Tormin et al., 2011; Campbell et al., 2016) to be inhabited by CD271+

MSCs, data in Chapter 4 also indicated that both osteoblasts and osteoclasts were negative for the CD271 MSC marker. With this in mind, the CD271 and CD56 markers were chosen to identify a putative osteogenic committed MSC subset, suspected to drive abnormal bone formation in OA.

Data presented in this chapter confirmed the expression of CD56 in all bone surface bound cells, including osteoblasts and osteoclasts, consistent with previous studies (Andersen et al., 2009). Performing area expression quantification, it was determined that the expression of CD56 was increased in areas of bone sclerosis. This was not surprising considering the increased remodelling activities characteristic to subchondral areas (Burr and Gallant, 2012). Therefore, by excluding the osteoblasts and osteoclasts from area measurements, it was determined that the remaining CD56+ cells were increased in areas of bone sclerosis and bone formation, confirmed by PSR staining. Immunohistochemical analysis in this chapter placed these CD56+ cells in the vicinity of bone forming osteoblasts which were also shown to be increased particularly in areas of bone sclerosis, indicating a potential involvement in this pathological event. The PSR staining confirmed areas of bone formation by facilitating the visualisation of collagen content in proximity of CD56+ cells. The new bone formation was judged by the presence of immature collagen fibrils (Paschalis et al., 2003) in the vicinity of CD56+ cells. This was consistent with previous studies showing that CD56 was strongly expressed in cells along bone trabeculae that coincided with the presence of markers of new bone formation, such as collagen I and ALP (Lee and Chuong, 2009).

The presence of CD56+ cells was also documented in this chapter in the canopy cells covering areas of bone remodelling. This may confirm a theory suggested by Kristensen *et al*. that canopy cells represent a route of recruitment for osteoblasts (Kristensen et al., 2014). The CD56+ cells identified in this chapter in areas of bone sclerosis were found occasionally to resemble previous descriptions by the literature. Canopies have been described as specialised structures comprising cells expressing osteoblastic markers overarching the BMUs and separating this area from the BM (Hauge et al., 2001). The location of CD56+ as BLCs make them ideal candidates as osteoprogenitors. By demonstrating the co-localisation of the MSC marker CD271 it further extended the characterization of this cell type which so far has been limited. While evidence so far has indicated BLCs as being an osteoblast precursor (Kristensen et al., 2014; Matic et al., 2016), data in this chapter showing the enhanced osteogenic profile and proximity to bone formation areas of the CD271+CD56+ cells indicate that this MSC subset may be an

excellent candidate. In a previous mouse study it was already demonstrated that osterix expressing BLCs have the ability to proliferate, activate and become osteoblasts (Matic et al., 2016), which in this chapter was shown to be highly expressed by the CD271+CD56+ MSCs.

It has been established that bone restoration during remodelling demands recruitment of osteoprogenitors onto reversal surfaces, possibly from the canopy cells or nearby BLCs (Jensen et al., 2015). Data here has established the co-expression of CD271+ and CD56+ as new markers for the BLCs and demonstrated their presence both on the bone lining surface and in the adjacent bone remodelling canopies which point to their roles in bone formation process.

5.5.2 Overview of the CD271+ MSCs subsets

The inherent heterogeneity of MSC populations can present problems that obscure gene expression in a particular subset of cells. To circumvent these obstacles and obtain cell-type-specific native expression profiles, the approach adopted in this study was cell surface marker-based cell purification in order to isolate more homogeneous subsets of MSCs. This procedure utilized FACS sorting of cells that have been enzymatically released from healthy and diseased bone tissue. Utilizing this approach and by avoiding *in vitro* cell manipulation, facilitated gene expression analysis of the different MSCs subtypes reflecting their native phenotypes.

Previous studies have reported on the co-existence of distinct MSC subsets within the same MSC pool, both CD146 and CD56 have been used for investigating the different subsets of the CD271+ MSC population (Bühring et al., 2007; Battula et al., 2009; Tormin et al., 2011), but this is the first time when these markers were used together. This facilitated the segregation of CD271+ MSCs based on their topography, thus identifying the bone lining fraction by using antibodies for CD56 and the perivascular fraction by using CD146. Furthermore, this resulted in a third double negative fraction (DN), represented by the CD271+ MSCs resident in the stromal reticular net. The results determined that the CD271+CD146-CD56+ MSCs have distinct phenotypic and functional properties resembling an osteogenic committed cell population, differentiating them from the DN and CD146+ subsets.

Their most remarkable osteogenic commitment was evidenced not only by their *in vitro* potential to generate bone but also by the increased expression of a vast array of bone formation associated genes in their native state. In comparison to the other two subsets,

the CD56+ subset in OA was characterised by significantly higher levels of *SPP1* and *BGLAP*, two major components of extracellular matrix and bone formation markers (Denhardt and Noda, 1998; Wei and Karsenty, 2015). Additionally, both transcriptional regulators of osteogenesis, *RUNX2* and *SP7* (Komori, 2006), were also highly expressed by this subset. It has been shown previously that proliferating cells may contain more *RUNX2* (Schroeder et al., 2005), thus proliferating *RUNX2*-rich MSCs would enter osteogenic differentiation more efficiently. *OMD* encodes osteomodulin, a minor proteoglycan found in the mineralized matrix of bone, where it binds to hydroxyapatite (Wendel et al., 1998). It was previously shown to be expressed in healthy BM CD271+ MSCs (Churchman et al., 2012) as well as in mature osteoblasts located superficially on trabecular bone and has been proposed as an organiser of mineral formation (Sommarin et al., 1998). Thus, the high expression levels of *OMD* found in OA CD271+CD56+ MSCs may account for mineralization changes in OA (L.G. Cox et al., 2012). Furthermore, *OMD* is known to regulate the extracellular matrix during bone formation, by controlling the diameter of type I collagen fibrils (Tashima et al., 2015), which may explain the differences in birefringence and sizes of collagen fibrils observed following PSR staining, with thicker collagen fibres present in the proximity of CD56+ cells.

By gauging their native differentiation potential with a variety of stringent differentiation assays, it was demonstrated that CD271+CD56+ cells are inherently geared to generate bone, cartilage and fat. However, it was expected that their native documented prominent osteogenic bias would be reflected *in vitro* but this was not the case. This may be due to the thoroughly documented effects of culture conditions which may have interfered with these results fading the differences observed in their native counterparts.

The surface marker CD56 was first described by work of Buhring *et al*. research group in 2007 and 2009 (Bühring et al., 2007; Battula et al., 2009; Bühring et al., 2009). Using antibodies against CD271+ and CD56+ they identified distinct CD271+ MSCs subpopulations from healthy BM (Battula et al., 2009). The resulted CD271+CD56+ subset displayed distinct phenotypic and functional properties from its negative counterpart, with an increased chondrogenic potential of these cells based on standard *in vitro* functional assay.

Data in this chapter on the native gene expression of the CD56+ subset showed higher levels of *SOX9*, a major transcription factor that controls chondrogenesis (Bi et al., 1999) as well as high levels of *CHAD*, a major component of cartilage (Camper et al., 1997) in comparison to the other CD271+ subsets. This may indicate a ready-state of this subset

for chondrogenic differentiation considering the *SOX9* and *COL2A1* upregulation following chondrogenesis induction *in vitro*. However, this was only evident based on a limited number of samples. While transcriptional evaluation of the differentiated cells in this chapter pointed to a chondrogenic bias of CD56+ subset in comparison to the other two CD271+ MSC subsets, judging by the pellet sizes and GAG concentration following culture, there was no difference between all three MSC subsets. Importantly, the samples analysed in this chapter were obtained from OA donors, which may also be an influencing factor, data in Chapter 1 showing a significantly lower level of these molecules in OA bone derived CD271+ MSCs compared to healthy bone (Figure 3.12). Previous studies had assessed the chondrogenic potency of the CD271+CD56+ MSC subset isolated from healthy BM and shown a higher capacity of these cells to form chondrocytes in comparison to CD271+CD56- counterpart (Battula et al., 2009). Unfortunately, the analysis of healthy CD271+MSC subsets was not possible in this project due to the low cell numbers obtained following FACS purification procedure. This is needed to establish whether the phenotype of these subsets is associated with the disease.

Recently, a study showed that MSCs isolated after rasping of the femoral canal resulted in a higher percentage of CD271+CD56+ cells compared to donor-matched aspirate and these cells were significantly more chondrogenic than the CD271+CD56- cells (Sivasubramaniyan et al., 2018). Histological assessment presented in this chapter clearly indicated the bone lining location of the CD271+CD56+ MSCs both by IF and IHC (Sections 5.4.3 and 5.4.4). Thus, the findings in Sivasubramaniyan *et al.* study (Sivasubramaniyan et al., 2018) that bone rasping contained higher numbers of CD271+CD56+ cells in comparison to aspiration was in agreement with data found in this chapter. The histological appearance of the chondrogenic pellets indeed showed a correlation with the number of CD271+CD56+ cells (Sivasubramaniyan et al., 2018), however this may not reflect the nature of the specific CD271+CD56+ population. This is because in contrast to work presented here, that study (Sivasubramaniyan et al., 2018) investigated the difference in chondrogenic potential of MSCs isolated by different methods (rasping and aspiration) followed by plastic adherence, thus the cells were not selectively purified by surface marker expression, but belonged to a heterogeneous population of MSCs. Hence, the cells with an increased chondrogenic potential shown by Sivasubramaniyan *et al* isolated by rasping of the femoral canal of OA donors may indeed be attributed to CD271+CD56+ MSCs, but it may as well be influenced by any of the other CD271+ fractions. Although, this may also be explained by the distant MSC extraction sites. Data presented here was obtained from cells isolated from OA femoral

heads, while that study used MSCs isolated from the femoral shaft of OA donors, which are relatively distant from each other.

Cytometric analysis presented in Section 5.4.5 showed an increases proportion of CD271+CD56+ MSCs within the CD271+ MSC population in OA femoral heads compared to healthy bone. Corroborated with data in Chapter 3, this suggested that the osteogenic profile of CD271+ MSCs may be linked to one candidate subpopulation, hereby determined to be the CD56+ subset. However, this subset only accounted for a small percentage of the whole CD271+ MSCs. Meanwhile the DN subset accounted for the majority of the CD271+ cell population (about 70%) therefore, it may be possible that this may be increased in OA as well. Although no statistical significance was found, a trend for an increased DN subset in OA was indeed observed by FACS and it may become statistically significant if more samples would be analysed. In support to this idea, the DN subset resides in the stromal reticular net which in Chapter 4, Section 4.4.7 was shown to accommodate the fibrovascular tissue in areas of bone sclerosis. Based on the increased expression of *CXCL12* (SDF-1) in DN, it may be possible for this subset to diverge from the perivascular location, occupied by the CD271+CD146+ subset, which may represent a more primitive MSC subpopulation. Thus, what differentiate DN from the two subsets is the distinct localisation in the stromal reticular net and the high transcriptional levels of *CXCL12*. Given the well explored roles played by the MSC-derived *CXCL12* in stromal support, haematopoiesis and migration (Sugiyama et al., 2006; Kitaori et al., 2009; Greenbaum et al., 2013), this suggests that the DN subset may be involved in facilitating the migration, proliferation and re-location to the bone surface of more osteogenic committed progenitors in the OA CD271+ MSC population (Figure 5.26).

While the osteogenic commitment of DN subset was similar to CD56+ and CD146+, the endosteal CD56+ subset had the most osteogenic gene expression signature of all three subsets. However, transcriptional analysis identified progressive changes between the subsets which may correlate with their topography in OA. While the CD146+ subset is located perivascular (Tormin et al., 2011) and CD56+ lining the bone surface, the remaining CD271+ subset resides as an intermediate MSC population with a progressive osteogenic commitment. This was shown to be lowered to an intermediate level in the stromal-resident DN and a significant reduction in all osteogenesis related genes was observed in the perivascular CD146+ subset, which revealed higher expression of transcripts associated with fat, indication of an early MSC phenotype. Given the high osteogenic profile similar across both CD56 and the most numerous DN subset, from a

therapeutic perspective, targeting the CD271+ MSC population in OA as a whole seems favourable while the exact nature of these subtypes is still under investigation.

As previously discussed in Chapter 1, Tormin *et al.* (Tormin et al., 2011) also showed that the CD271+ MSC population from healthy BM has distinct topography based on the CD146 surface marker expression. Thus, it was shown that CD271+CD146+ MSCs were located in a perivascular location while the CD271+CD146- were mostly lining the bone surface. However, transcriptional differences of these subsets were not described in that study and all experiments were performed using cells isolated from the BM of healthy donors. Their MSC identity was however demonstrated, showing that both subsets can form bone and haematopoietic stroma *in vivo* (Tormin et al., 2011). Data presented in this chapter further characterised this perivascular fraction by similarly using the CD271+CD146+ phenotype, obtaining more knowledge about their nature in both healthy and OA bone, expressing more fat and early-MSCs transcripts. This was also demonstrated *in vitro*, transcriptional analysis of the differentiated cells having showed an overall lower osteogenesis in the CD146+ compared to both DN and CD56+.

In this chapter, the CD271+CD146- fraction described by Tormin *et al*. has been further separated by using the novel marker CD56, while the CD271+CD146+ fraction served as comparator. In the study by Tormin *et al.*, no gene expression analysis was performed in the native subsets represented by the aforementioned phenotype. Another study suggested that the two MSC subsets may not necessarily be distinct cell types, but a reflection of the distinct microenvironments due to access to different oxygen levels (Maijenburg et al., 2011). Data in this chapter however documented some transcriptional differences between the CD271+CD146+ subset and the other CD271+ MSCs subsets. Gene expression analysis showed significantly higher levels of *GATA2* in the CD146+ subset, while this molecule was significantly lower in the DN subset and below detection levels in the CD56+. The roles of *GATA2* in the mesenchymal lineages based on *in vitro* studies suggests that *GATA2* maintains MSCs in an undifferentiated state and loss of this gene in osteogenically differentiating MSCs has detrimental effects on bone formation (X. Li et al., 2016; Tolkachov et al., 2018). In addition, *GATA2* was shown to positively modulate adipocyte differentiation (Kamata et al., 2014). Gene expression indicated that CD146+ subset may represent early adipogenic progenitors. This was backed up by the significantly higher levels of adipogenic molecule *FABP4* expressed in the CD146+ subset in comparison to both DN and CD56+ subsets. An increased capacity of CD146+ subset to differentiate towards the adipocytic lineage was evidenced by the *in vitro*

adipogenic differentiation potential, showing consolidating evidence of its adipogenic bias.

While previous studies have already documented the MSCs characteristics of CD271+ MSCs (Jones et al., 2010; Tormin et al., 2011; Li et al., 2014), this is the first study were the CD271+ native MSCs were dissected into multiple subsets and compared between each other, revealing the distinct phenotypes of its subpopulations in their native state. Furthermore, this was the first time to compare the differentiation capacity across topographically different CD271+ MSC subsets *in vitro*, all three MSC subsets showing multipotentiality with some expected variation between donors.

5.5.3 Final considerations

A major limitation of this study is represented by the low number of cells obtained from the healthy control IC bone. While FACS and IHC provided evidence pertaining the different presence of the CD56+ MSCs subset in bone from healthy and OA, gene expression analysis was not successful using the cells from IC and was only assessed in the OA group. A more sensitive approach is therefore needed to obtain a gene expression profile of these cells from their healthy environment and thus allowing a direct comparison to their diseased counterpart. This would provide more information about how OA environment modulate the changes in gene expression and confirm whether the CD56+ subset of MSCs are indeed responsible for the abnormal bone formation at the end-stage OA. As shown in this chapter and by others (Bühring et al., 2007; Sivasubramaniyan et al., 2018), the CD56+ MSC subset is not unique to OA and is present on other bone surfaces. More work is needed to establish whether the osteochondrogenic profile of the CD56+ MSC subset is mediated by the OA environment or it is due to their progressive commitment as they migrate towards the bone surface. This information may have great consequences with regards to novel cellular targets and open new avenues for treatment strategies in many bone-associated pathologies, including OA.

In a recent study involving nearly 100 OA patients, gene expression alterations were documented in BMLs of knee OA. Genes associated with neuronal, osteogenic and chondrogenic pathways, such as stathmin 2, thrombospondin 4, matrix metalloproteinase 13 and Wnt/Notch/catenin/chemokine signalling molecules were shown to be the most up-regulated in bone from BMLs of knee OA in comparison to non-affected areas (Kuttapitiya et al., 2017). While this study showed strong indication of gene expression changes in bone affected by OA, more work is needed to establish the exact cellular source of these aberrant signals. Of great interest would represent an investigation of these

genes in the MSCs subsets presented here. More intriguing is the potential role that CD271+ MSC population may play in modulating the pain pathways in OA.

This study brought forward the importance of BLCs in OA and offers new insights in the identity of the bone lining CD271+ MSCs previously documented. Work in this chapter uncovered a new phenotype of bone lining osteoprogenitors and while the native osteogenic profile of CD271+CD56+ cells was demonstrated, their roles in the BM environment are still being unravelled (Figure 5.26).

Identifying and characterising these osteoprogenitor cells may provide novel therapeutic targets not only for diseases associated with an abnormal bone forming phenotype, such as osteoarthritis or spondyloarthropathies but can also be extended to other conditions where bone formation is lacking, such as osteoporosis

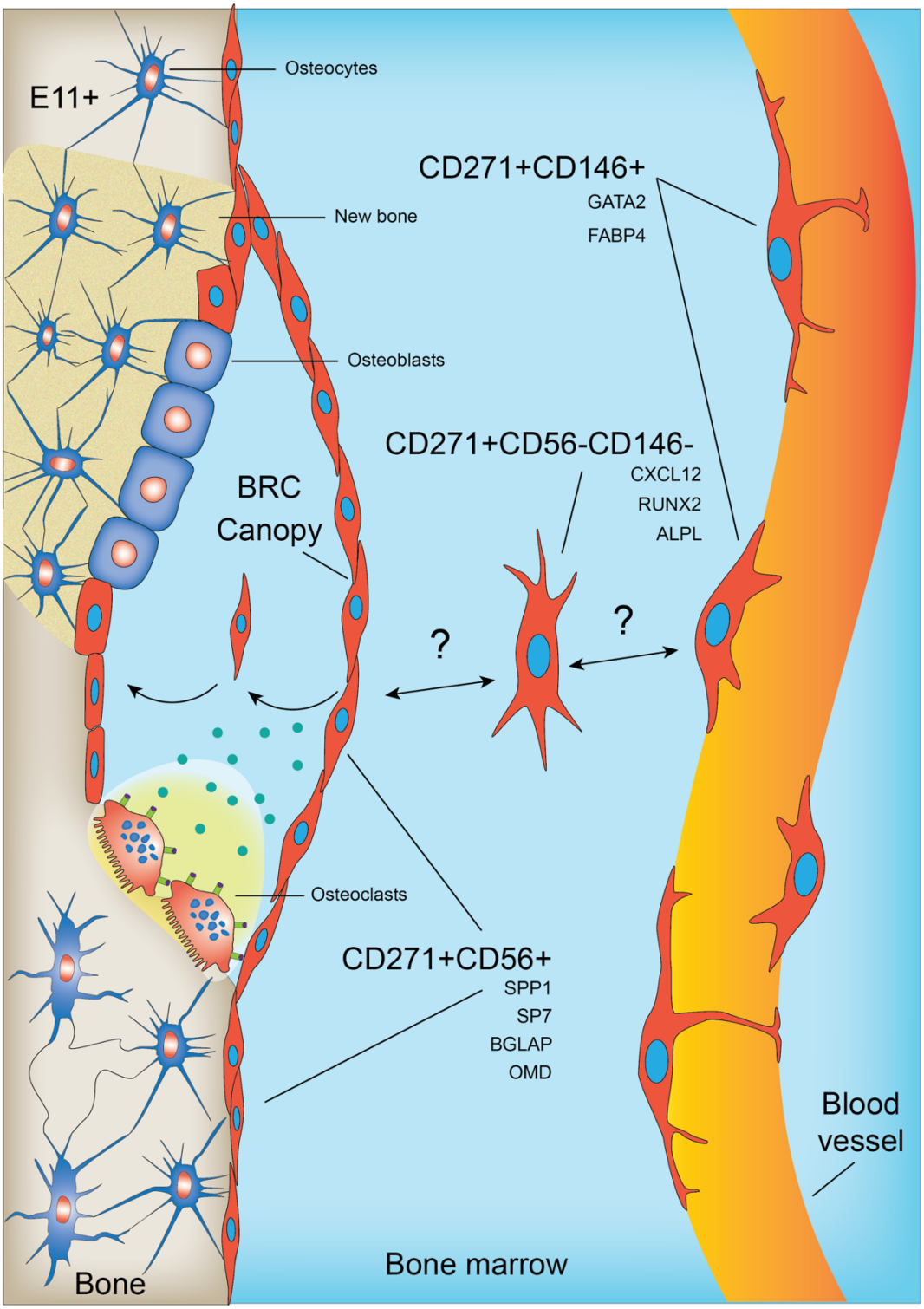

Figure 5.26. Illustration of CD271+CD56+ subset in OA bone. *Bone lining MSCs identified by CD271+CD56+ phenotype represent a reservoir of osteoprogenitors for the bone remodelling compartment (BRC) marked by the presence of osteoblasts and osteoclasts. The MSC subset marked by the CD271+CD146+ phenotype reside in perivascular location possibly supplying the pool of stromal reticular population of CD271+ MSCs, which are negative for both CD56 and CD146 and acts as an intermediate osteoprogenitor subset.*

Chapter 6 General discussion

6.1 Main findings

Osteoarthritis is an undisputedly complex disease and is a growing worldwide problem. As a reflection of the anabolic bone in the late stages of the disease, this project confirmed the hypothesis that there is an accumulation of MSCs in hip OA femoral heads and they exhibit an osteogenic phenotype. This aberration was further found to be partially attributed to a novel MSC subset marked by the CD271+CD56+ phenotype and reflected in the increased presence of young immature osteocytes in OA bone. An improvement of the MSC extraction procedure may have contributed to the release of these previously inaccessible bone resident MSCs and their proportion was shown to be higher in OA compared to healthy bone by both IH and flow cytometry. Furthermore, this method allowed the study of osteocytes in their native state for the first time, revealing for the first time their transcriptional and topographical differences between healthy and OA bone.

This study represents a novel aspect in the MSC field by investigating distinct subsets of MSCs within the native CD271+ population from OA and healthy bone. Although various surface markers were reported for association with MSC populations while echoing their heterogeneity, the current study isolated and investigated at a transcriptional level the MSC subpopulations based on their natural topography in the BM. By using the CD271+CD56+ phenotype, work in this thesis established a novel marker to the bone lining MSCs in addition to their perivascular location marked by expression of CD146 (Tormin et al., 2011). Furthermore, transcriptional analysis provided evidence of an osteogenic profile of this MSC subset in OA, although this remains to be tested in healthy bone to ascertain whether this was modulated by the disease or it reflects the actual cell identity as an osteoprogenitor MSC subset.

Although osteocytes are by far the most numerous cells in the bone, making up more than 90% of all bone cells (Prideaux, Findlay, et al., 2016), due to their inaccessibility there is a paucity of data on human osteocytes, this being the first study to investigate their native gene expression in healthy and OA bone. Of importance, this study revealed an immature phenotype of bone resident osteocytes in OA both by gene expression and IHC. While the different maturation stages during osteoblasts to osteocyte transition can be recognized morphologically using *in vitro* studies while documenting the molecular changes during these transformations, some questions still remained unanswered. For

example, the decision for an osteoblast to become an osteocyte is still ambiguous. It is unknown whether all osteoblasts are equally capable of embedding as osteocytes or their fate is predefined by osteoprogenitors cells, possibly by the CD271+CD56+ MSCs. It is still unclear whether the osteoblast's fate is dictated by a specific gene expression pattern in this subset of osteogenic precursors and also whether this is a cell-autonomous response or one that is controlled via the bone surface cells receiving signals from the already embedded osteocytes (Dallas and Bonewald, 2010). Answering these questions may provide a mechanistic explanation of the enhanced bone formation and remodelling activities dominating the late stages of OA bone which may be further explored in other bone associated conditions.

6.2 Study limitations

Most of the recruited patients in these studies were diagnosed with OA and the samples used for this study were at the late stage of the disease, collected following joint replacement. OA is known to be a progressive degenerative disease (Lajeunesse and Reboul, 2003; Martel-Pelletier et al., 2016) exhibiting various bone-related pathological manifestations and bone remodelling imbalances at different stages, such as an enhanced bone resorption activity at the early stages progressing to prominent bone formation and sclerosis in the late stages (Burr and Gallant, 2012). An investigation of osteoprogenitors in relation to other cellular components in this strenuous environment at different stages of disease progression is preferable. This would provide a more detailed picture of the putative cellular events that trigger and allow the progression of OA with respect to the subchondral bone.

Another limitation of this study was the number of samples, which were not representative of all disease phenotypes. As a multifactorial disease, the late stage pathological manifestations may be different considering the patient variability with regards to age, sex, body mass index, genetics or level of activity, all of which may be highly influential in a biomechanical condition like OA. Furthermore, as discussed in Chapter 1, Section 1.1, initiation of disease may take place at different sites in the joint. It is possible that progression of the disease from subchondral bone towards the cartilage may resemble different pathologies in comparison to secondary OA where the initiation factor may be ligamentous or cartilage damage. Data in Chapter 4, Section 4.4.6 presented highly heterogeneous expression of RANKL and OPG in two OA patients. This may reflect different stages of disease progression previously suggested by Burr *et al*. (Burr

and Gallant, 2012), but it could also represent different tissue responses to the site of initiation.

The control bone used for this study was IC. Femoral head and iliac crest are distant sites and may present major differences with regards to the cellular activities and biomechanics. The iliac crest is not generally a weight bearing zone as opposed to the femoral head. Since osteocytes are established mechanosensory cells (Klein-Nulend et al., 2013), their gene expression profile may be different between femoral head and iliac crest even under normal conditions. Furthermore, their response to altered biomechanics can also be different since the osteocytes resident in the femoral head are being exposed and possibly adapted to different strains in comparison to iliac crest bone. However, recent published data showed that gene expression and morphology of osteocytes are comparable between the two sites with regards to both gene expression and IHC evaluation of molecules of interest (Ilas et al., 2019). Similarly, when compared to similar weight-bearing sites, such as the femoral heads of NFF donors, the changes in gene expression were similar to healthy IC bone (Ilas et al., 2019) while the MSC topography seemed notably similar to healthy IC and NS areas from OA bone, however no quantification was performed to confirm. This indicates that their accumulation in sclerotic areas is modulated by OA and not by tissue distribution or mechanical load.

The changes observed in both osteocytes and MSCs in this study would be ideally analysed by comparing them to non-OA femoral heads, but the availability of these samples is very low. While it may be possible to obtain normal femoral heads from recently deceased donors, studies have shown that RNA degradation in femoral head bone occurs at fast rates and is recommended to be extracted within a 48 hours window post-mortem (Kuliwaba et al., 2005). Another option would imply the isolation of MSCs and osteocytes from segregated regions of damaged and unaffected areas within the same femoral head. This may involve high technical difficulty and subjectivity, especially with regards to visual assessment of damaged areas. To overcome this, MRI can be used immediately after sample collection, as described in previous studies (Campbell et al., 2016; Kuttapitiya et al., 2017).

Knowing the biology of MSCs in their native state is crucial when aiming to characterise the fundamental differences between health and disease. It only emphasises that however convenient, *in vitro* studies are not sufficient neither for a correct assessment of the disease process nor for the deduction of the MSC biology *in vivo*. A better understanding of native MSCs phenotype would contribute considerably to development of better

treatment strategies for OA that are efficient, correctly targeted, more financially viable and less invasive.

6.3 Future directions and clinical implications

As stated in Chapter 1, Section 1.1.5, due to the lack of effective treatment strategies, the cell-based therapies have surfaced as alternative methods for treatment of OA (Zhang, Ouyang, Crispin R Dass, et al., 2016), however only limited data proved their efficacy. Furthermore, as shown in Chapter 3, with an increased number present in the joints already, the addition of exogenous MSC may prove redundant, especially without properly characterising the MSCs used for therapy. Evidence discussed so far indicate a defective phenotype in OA and drastic changes following culture expansion. Thus, more efforts should be made to target the existent endogenous pool of MSCs with the aim to restore the homeostasis and trigger a natural healing mechanism. Such approaches have recently emerged involving mobilisation of synovial MSCs in order to populate and repair the cartilage defects in OA (Baboolal et al., 2018).

Some cell-based therapies may aim to stimulate the biological restoration of the damaged tissues in OA, such as the subchondral bone. The MSCs might be capable of facilitating tissue repair through paracrine signalling, immunomodulation and extracellular vesicles (EVs), with direct MSC differentiation likely playing a minor role in some instances (Barry and Murphy, 2013; Cosenza et al., 2017). The 'secretome' of MSCs, although not fully understood, generally has functions associated with chemoattraction and modulation of immune cells, angiogenesis, and support of cellular growth and proliferation (da Silva Meirelles et al., 2009). Extracellular vesicles are predominantly endosomal in origin, comprising mainly of exosomes and microvesicles containing a cargo of miRNA, mRNA, and proteins usually delivered to the target cells (Keshtkar et al., 2018). Hence, this may facilitate the use of intra-articular healthy EV delivery with the aim to enhance the inherent repair mechanisms of resident MSCs at the sites of damage. In fact, EVs derived from MSCs could potentially be easier to manage and be safer due to the lower extra-cellular proteins, such as the major histocompatibility complex (MHC) molecules and their ability to form tumours (Yu et al., 2014). This may provide MSCs-derived EVs with a great therapeutic advantage and be superior to whole cells treatments.

It is still unknown whether the osteogenic commitment and increased numbers described in this thesis have any deleterious impact on the joint and whether inhibiting the osteocytic maturation program in MSC-lineage cells could be beneficial to the joint. Increased accumulation of MSCs in areas of bone formation may represent a reparative

response mechanism. The immature osteocytes inhabiting the sclerotic bone indicated the bone was newly formed and therefore may provide support for the joint in compensation to cartilage damage. In any case, the high bone remodelling activity observed in this study and documented extensively by others (Burr and Gallant, 2012) point to increased repair capacity, which seems the key for the spontaneously reversible course of this disease. Evidence pertaining E11 is of great importance as it may be harnessed therapeutically. Inhibition of osteocytic maturation program in MSC-lineage cells may re-establish the bone homeostasis in late stage OA by preventing early osteocyte differentiation concomitantly with bone formation. Its protective role against OA has been recently evidenced in a mouse model of OA showing that bone-specific conditional deletion of E11 protects against load-induced OA (Staines et al., 2018).

Progression of OA has been described as a bi-phasic process, with increased remodelling during early disease and its reduced rate as the disease progresses (Burr and Gallant, 2012). Given the emerging insights into the osteocytes' role in regulating bone homeostasis (Prideaux, Findlay, et al., 2016), and therapies for targeting them pharmacologically (Plotkin and Bellido, 2016), data in this thesis provided a conceptual basis for targeting their precursors MSCs in OA. Specifically, the high levels of OPG in OA-osteogenic lineage cells caution against a subchondral bone manipulation strategy aimed at osteoclast inhibition in advanced stages of OA. The use of anti-resorptive therapeutic agents in OA, such as bisphosphonates and cathepsin K inhibitors, requires a better understanding of the 'window of opportunity' in which these therapies could lead to restoration of normal bone homeostasis.

Subchondral bone has been considered as one of the most promising targets for OA drug development (Hayami et al., 2004). Identification and prospective isolation of tissue-residents MSCs with known and different functionalities may provide novel approaches for targeted tissue repair in regenerative medicine. These findings could provide the basis for the use of osteochondroprogenitors purified from different sources in clinical protocols of cell-based therapies for the repair of osteochondral defects. These cells may as well be targeted by bisphosphonates. Bisphosphonates can attach to hydroxyapatite binding sites in bone lining locations, particularly those which are undergoing active bone resorption (Walsh and Chapman, 2011). The location of CD271+CD56+ MSCs lining the bone surface may also facilitate the development of novel biologics allowing to target these cells similarly to bisphosphonates in order to re-establish the normal bone turnover.

6.4 Concluding remarks

With the increasing life span of the human population, the need to maintain bone quality and strength is more relevant as ever, and significant effort is being put into studying bone remodelling and additional factors influencing bone quality. Due to ageing everyone has some degree of wear and tear damage in the joints, however not everyone develops OA. Therefore, while the initiation of the disease may be imminent, therapeutic strategies aimed at stopping or slowing the progression of the disease may prove more efficient. Early correction of the MSCs abnormal migration and osteogenesis bias could prevent an excessive bone formation and the corresponding cartilage destruction in this disease.

This project has revealed important roles played by the MSCs and their osteogenic lineage progenies in OA pathophysiology. Little is known about the native biology of MSCs while their roles in bone remodelling activities have not been investigated so far. Using native and minimally manipulated cells provided more relevant information regarding cellular aberrations, the results not being biased by culture induced transcriptional and functional changes. Furthermore, this study revealed the existence of a novel osteogenic MSC subset residing on the bone surface with potential implications in driving the OA bone sclerosis. So far neglected, discovering the increased accumulation of young and immature osteocytes in the vicinity of MSCs of OA sclerotic bone revealed the buried proof that clearly implicates the MSCs and its entire osteogenic lineage in the subchondral bone alterations in OA.

Appendix 1. Reagents

Manufactured reagents

Product	Manufacturer
Absolute Ethanol	Sigma
Acetone	Sigma
Alizarin Red	Sigma
β–Mercaptoethanol	Sigma
Bovine Serum Albumin	Sigma
Citrate Concentrated Solution	Sigma
Collagenase I Type A, AOF	Worthington
Dimethyl Sulfoxide (DMSO)	Sigma
Disodium Tetraborate	Sigma
Disodium Tetraborate	Fisher Scientific
DNase (cell culture)	Sigma
DNase I (RNA)	Norgen Biotek
DPX Mounting Media	Sigma
Dulbecco's Modified Eagle Medium	Gibco
Dulbecco's Phosphate Buffered Saline	Gibco
Eosin Y	Sigma
Ethylene Glycol Monoethyl Ether	Sigma
Ethylenedinitrilotetraacetic Acid (EDTA)	Fisher Scientific
Fast blue RR Salt (tablets)	Sigma
Fast Green FCF	Alfa Aesar
Foetal Bovine Serum	Biosera
Formalin (10% neutral buffered)	Sigma
Guanidine Isothiocyanate Solution	Invitrogen
Haematoxylin (Harris)	Fisher Scientific
Haematoxylin (Weigert's)	Sigma
Human Serum	Sigma
Hydrochloric Acid	Fisher Scientific
Isopropanol	Sigma
L-Cysteine	Sigma
Live/dead staining kit (contains calcein AM and ethidium homodimer-1)	Invitrogen
Magnesium Sulphate	Sigma
Methanol	Sigma
Methylene Blue	Sigma

Naphtol AX-MX Phosphate	Sigma
Nile Red	Thermo Fisher
Nuclear Fast Red	Sigma
Nuclease-free Water	Ambion
Oil Red O	Sigma
Optimal Cutting Temperature (OCT) compound	VWR
PBS Tablets	Sigma
Penicillin/streptomycin (Pen/Strep)	Gibco
Phenol : Chloroform : Isoamyl Alcohol (25:24:1)	Sigma
Phosphate buffered saline (without calcium and magnesium)	Gibco
Picric Acid (Saturated, Aqueous)	Fisher Scientific
Potassium Chloride	Sigma
Saponin	Sigma
Sirius Red F3B	Sigma
Sodium Acetate Anhydrous	Sigma
Sodium Bicarbonate	Sigma
Sodium Hydroxide	Sigma
StemMACS AdipoDiff Media	Miltenyi Biotec
StemMACS ChondroDiff Media	Miltenyi Biotec
StemMACS MSC Expansion Media	Miltenyi Biotec
StemMACS OsteoDiff Media	Miltenyi Biotec
TaqMan Gene Expression Master Mix	Applied Biosystems
Toluidine Blue	Sigma
Tris Base	Fisher Scientific
Trypan Blue Solution	Sigma
Xylene	Fisher Scientific

Standard solutions

Activated papain enzyme digestion solution (GAG assay)

For 100 mM sodium phosphate buffer/5 mM EDTA/10 mM L-cysteine (0.125 mg/ml papain): Just before use, add 63 mg of L-cysteine hydrochloride hydrate in 40 ml papain buffer and sterile filter using syringe and 20 μm filter. Transfer 1 ml of papain solution to a microcentrifuge tube using a syringe and 20-gauge needle then add 125 μg/ml papain enzyme.

Alizarin red staining solution (Osteogenesis)

Prepared by dissolving 342 mg Alizarin Red (Sigma) in 25 ml of dH_2O and pH adjusted to 4.1

Borate buffer (CFU-F assay)

10mM borate buffer: 1.91g disodium tetraborate dehydrate (Sigma) dissolved in 500 ml dH_2O and pH adjusted to 8.8 with 1M boric acid (made up by dissolving 6.183g boric acid (Sigma) in 100 ml dH_2O = 1M)

Cell freezing media

90% FCS (Biosera) + 10% DMSO (Sigma).

Citrate fixative (ALP assay)

6 ml acetone (Sigma) and 4 ml of 1:50 dilution of citrate concentrate solution (Sigma)

EDTA decalcification solution

0.5 M EDTA solution (pH 7.4): 186.1 g EDTA disodium dehydrate (Fisher Scientific) dissolved in 800 ml dH_2O. The disodium salt of EDTA will not go into solution until the pH of the solution is adjusted to ~8.0 by the addition of NaOH. The pH was therefore first adjusted to 8.0 with approximately 20 g of Sodium Hydroxide pellets (NaOH) (Fisher Scientific) and following complete dissolution adjusted to 7.4 with neat HCl (Sigma).

Fast Blue solution (ALP assay)

One Fast blue salt tablet (Sigma) dissolved in 48 ml of dH_2O with the addition of 2 ml of 0.25% Naphtol AX-MX phosphate solution (Sigma)

Fast Green staining solution (Safranin O staining)

0.02% solution by dissolving 0.05 g Fast Green FCF (Sigma) in 250 ml dH_2O

FACS Buffer

500 ml PBS + 1% w/v bovine serum albumin (5 g) (Sigma) + 200 µl EDTA 0.5M (Fisher Scientific)

Fc blocking buffer

1 ml aliquots containing 10% mouse serum (Sigma), 1% human IgG (Sigma) in FACS Buffer

GITC lysis buffer

GITC solution (Invitrogen) containing 0.4% sodium citrate (Sigma), 1% N-lauryl sarcosine (Fisher Scientific) and 0.5% β-mercaptoethanol (Sigma).

HCL solution (Calcium assay)

0.5N HCl; 26.5 ml of 37% HCl (Fisher Scientific) in 473.5 ml dH_2O.

Methylene blue solution (CFU-F assay)

1% w/v methylene blue solution: 1 g methylene blue (Sigma) dissolved in 100 ml of 10mM borate buffer (pH 8.0).

Naphthol AS-MX Phosphate Substrate

20 mg of Naphtol AX-MX phosphate (Sigma) dissolved in 1 ml Ethylene Glycol Monoethyl Ether (Sigma)

Nile red

Make up Nile red stock solution at 0.1 mg/ml in methanol. Before use, add 4 µl Nile red stock in 80 µl PBS to obtain 1:2000 working dilution.

Oil red (Adipogenesis)

Prepared at 0.5% by dissolving 50 mg Oil red (Sigma) in 10 ml of isopropanol (Sigma), incubated for 30 minutes at 37° C and then diluted 3:2 w/v with dH_2O, filtered twice using a 45 µm filter (Millex) for first filtration followed by a 22 µm filter (Millex) to remove any undissolved material.

Papain buffer extract (PBE) (GAG assay)

For 100 ml of 100 mM sodium phosphate buffer/5 mM EDTA (pH 6.5): To 90 ml of dH_2O add 0.653 g sodium phosphate dibasic (Na_2HPO_4, MW 142.0), 0.648 g of sodium dihydrogen phosphate (NaH_2PO_4, MW 120.0) and 1 ml of 500 mM EDTA (Sigma). Adjust pH to 6.5 using HCl and make up volume to 100 ml using dH_2O then filter sterile.

Phosphate buffer saline

1 PBS tablet (Sigma) dissolved in 200 ml dH_2O

Picrosirius red

0.1% Picrosirius red solution: dissolve 0.25g Sirius red F3B (Sigma) in 250 ml saturated aqueous picric acid (Fisher scientific)

Scott's tap-water substitute

3.5 g of 42 mM Sodium bicarbonate ($NaHCO_3$) (Sigma), 20 g of 8 mM magnesium sulphate ($MgSO_4$) (Sigma) dissolved in 1L of dH_2O.

Toluidine blue solution (Chondrogenesis)

1% Toluidine Blue (Sigma) in 50% v/v isopropanol (Sigma) 50% v/v dH_2O: Dissolve 2 g of Toluidine Blue in a mix of 100 ml isopropanol and 100 ml dH_2O.

TRAP basic incubation media

1 L of 50 mM tartrate solution: 9.2 g Sodium Acetate Anhydrous (Sigma) + 11.4 g L-(+) Tartaric Acid (Sigma) + 950 ml dH_2O; pH adjusted to 4.7-5 with 5M Sodium Hydroxide (Fisher Scientific) to increase or more HCl (Sigma) to decrease.

TRAP staining solution mix

200 ml of 0.06% Fast Red: dissolving 120 mg Fast Red/Violet LB (Sigma) in 200 ml TRAP basic incubation media with the addition of 1 ml Naphthol AS-MX Phosphate Substrate mix

Tris-buffered saline

16 g Sodium chloride (NaCl), 0.4 g Potassium chloride (KCl) and 6 g Tris base (all from Sigma) dissolved in 800 ml dH2O adjust pH to 7.4 with HCl and make up volume to 1L with dH2O

Appendix 2. Plasticware, consumables and equipment

Plasticware and Consumables

Item	Manufacturer
12-well Culture Plate	Corning
24-well Culture Plate	Corning
384-well PCR Plate	Thermo Fisher
48-well Culture Plate	Corning
6-well Culture Plate	Corning
60 mm Culture Dish	Corning
Bijous (5 ml)	Star Lab
Cell strainer (72 μm)	Corning
Cryo Boxes	Sarstedt
Cryovials (2 ml)	Sarstedt
Falcon Tubes (15 ml and 50 ml)	Corning
Falcon Tubes (5 ml polypropylene FACS)	Corning
Filter (0.22 μm)	Millex
Histology Cassettes	Scientific Laboratory Supplies
Microtome Blades (CellEdge R+)	Cell Path
PCR Tubes and Caps	Star Lab
Pipette Tips (10 μl, 200 μl and 1000 μl)	Gilson
Safe-lock Tubes (0.5 ml and 1.5 ml)	Eppendorf
Scalpel (blade sizes 10 and 22)	Swann-Morton
Sterile Pot (150 ml)	Medfor
Stripette (5 ml, 10 ml and 25 ml)	Corning
SuperFrost Plus Microscope Slides	Thermo Fisher
T25, T75, T150 Culture Flask	Corning
Tubes and Tethered Cap with 0-Ring	Star Lab

Equipment

Equipment	Manufacturer
Bone Cutting Forceps (Stille-Liston)	Sklar
Bone Rongeur (Stille-Luer)	Sklar
Bone saw	Exakt
Cell Culture Cabinet (Class II)	Nuaire
Centrifuge (5424 R - for molecular biology)	Eppendorf
Centrifuge (5810 R - for cell culture)	Eppendorf
Centrifuge (Heraeus™ Multifuge™ - TLDA)	Thermo Fisher
Digital Camera (for microscope)	Olympus
Freezer (-20° C)	Liebherr
Freezer (-80° C)	Panasonic
Freezing Container (Mr.Frosty)	Nalgene
Fridge (2°-4° C)	Zanussi
Fume Hood	
Haemocytometer	Hawksley
Hot plate – SH3 (histology)	Stuart Scientific
Hot plate stirrer (PC-351)	Corning
Incubator (37° C)	Sanyo
Metal Mesh Glove	Niroflex
Microcentrifuge	Star Lab
Microscope (Brightfield)	Leica Microsystems
Microscope (Confocal)	Nikon A1R
Microscope (Fluorescent)	Nikon Eclipse
Microscope (Inverted)	Olympus
Microtome – RM2235	Leica
Nanodrop Spectrophotometer	Thermo Fisher
pH Meter	Jenway
Plate reader (Mithras LB 940)	Berthold
QuantStudio™ 7 Flex Real-Time PCR System	Applied Biosystems
Rotator/hybridisation Oven (HB-500)	Ultra-Violet Products
Vortex	Star Lab
Water Bath	Grant
Weighing Scale	Mettler Toledo
X-Ray Machine (CS2200)	Carestream Health

Appendix 3. Ethics

NHS
Health Research Authority

NRES Committee Yorkshire & The Humber - Leeds East
Yorkshire and Humber REC Office
First Floor, Millside
Mill Pond Lane
Meanwood
Leeds
LS6 4RA

Tel: 0113 3050108
Fax:

12 April 2012

Prof Peter Giannoudis
Consultant
Department of Trauma and Orthopaedics
St James's University Hospital
LS9 7TF

Dear Prof Giannoudis

Study title:	**Biological properties of Mesenchymal Stem Cells in Fracture Healing**
REC reference:	**06/Q1206/127**
Amendment number:	**3/1**
Amendment date:	**11 April 2012**

Thank you for submitting the above amendment, which was received on 12 April 2012. It is noted that this is a modification of an amendment previously rejected by the Committee (our letter of 22nd February 2012 refers).

The modified amendment has been considered on behalf of the Committee by the Vice-Chair.

Ethical opinion

I am pleased to confirm that the Committee has given a favourable ethical opinion of the modified amendment on the basis described in the notice of amendment form and supporting documentation.

Approved documents

The documents reviewed and approved are:

Document	Version	Date
Parental Agreement - Consent Form	1.1	23 March 2012
Participant Consent Form: Patient Consent Form 16 - 17 years old	1.0	23 March 2012
Participant Consent Form: Children Assent Form	1.0	01 February 2012
Participant Information Sheet: Patient Information Sheet 16 - 17 years old	1.0	23 March 2012
Participant Information Sheet: Parental Information Sheet	1.1	23 March 2012
Participant Information Sheet: Children Information Sheet	1.1	23 March 2012
Protocol	6.0	19 December 2011
Modified Amendment		11 April 2012

The Leeds Teaching Hospitals NHS
NHS Trust

Ref: Amy Dickinson

17/07/2014

Research & Development
Leeds Teaching Hospitals NHS Trust
34 Hyde Terrace
Leeds
LS2 9LN

Tel: 0113 392 2878
Fax: 0113 392 6397

r&d@leedsth.nhs.uk
www.leedsth.nhs.uk

Professor Dennis McGonagle
Rheumatology Department
Chapel Allerton Hospital
Chapeltown Road
Leeds
LS7 4SA

Dear Professor Dennis McGonagle

Re: NHS Permission at LTHT for: Collection of joint Mesenchymal Stem Cells by aspiration, biopsy, joint retrieval at arthroplasty or by synovium agitation during arthroscopy
LTHT R&D Number: RR14/11102 (100077/WY)
REC: 14/YH/0087

I confirm that *NHS Permission for research* has been granted for this project at The Leeds Teaching Hospitals NHS Trust (LTHT). NHS Permission is granted based on the information provided in the documents listed below. All amendments (including changes to the research team) must be submitted in accordance with guidance in IRAS. Any change to the status of the project must be notified to the R&D Department.

Permission is granted on the understanding that the study is conducted in accordance with the *Research Governance Framework for Health and Social Care*, ICH GCP (if applicable) and NHS Trust policies and procedures available at http...

This permission is granted only on the understanding that you comply with the requirements of the *Framework* as listed in the attached sheet "Conditions of Approval".

If you have any queries about this approval please do not hesitate to contact the R&D Department on telephone 0113 392 2878.

Indemnity Arrangements

The Leeds Teaching Hospitals NHS Trust participates in the NHS risk pooling scheme administered by the NHS Litigation Authority 'Clinical Negligence Scheme for NHS Trusts' for: (i) medical professional and/or medical malpractice liability; and (ii) general liability. NHS Indemnity for negligent harm is extended to researchers with an employment contract (substantive or honorary) with the Trust. The Trust

Appendix 4. Patient details

OA						
Sample ID	***Age***	***Sex***		***Sample ID***	***Age***	***Sex***
OA01	89	Female		OA022	53	Male
OA02	82	Male		OA023	71	Male
OA03	75	Male		OA024	68	Male
OA04	79	Female		OA025	67	Male
OA05	77	Female		OA026	69	Male
OA06	84	Female		OA027	67	Male
OA07	82	Female		OA028	69	Male
OA08	77	Male		OA029	82	Male
OA09	57	Female		OA030	40	Male
OA010	75	Female		OA031	57	Female
OA011	60	Female		OA032	74	Male
OA012	55	Female		OA033	74	Female
OA013	56	Female		OA034	67	Male
OA014	71	Female		HO13	72	Female
OA015	57	Female		HO19	73	Female
OA016	68	Male		HO44	70	Female
OA017	82	Female		HO41	43	Male
OA018	74	Female		HO55	78	Female
OA019	81	Female		HO27	59	Male
OA020	72	Female		HO40	63	Male
OA021	61	Female		HO13	72	Female
Controls						
Sample ID	***Age***	***Sex***		***Sample ID***	***Age***	***Sex***
IC01	58	Male		APB22	31	Male
IC02	58	Male		APB23	87	Female
IC03	55	Female		APB24	24	Male
IC04	49	Male		APB1	54	Male
IC05	46	Male		APB2	70	Female
IC06	53	Female		APB3	24	Female
IC07	38	Female		APB13	39	Female
IC08	78	Male		NFF01	88	Female
IC09	42	Male		NFF02	54	Female
IC10	40	Female		NFF03	93	Female
IC11	74	Female				

Appendix 5. TaqMan assays

TaqMan probes used for MSC gene expression analysis in Chapter 3 and 5

Assay ID	Gene Symbol	Synonyms	Group
Hs00244715_m1	*ACVR1B*	activin A receptor, type IB	Bone
Hs00155658_m1	*ACVR2A*	activin A receptor, type IIA	Bone
Hs00758162_m1	*ALPL*	alkaline phosphatase, liver/bone/kidney	Bone
Hs01101127_m1	*ANGPTL4*	angiopoietin-like 4	Bone
Hs03044164_m1	*BAMBI*	BMP and activin membrane-bound inhibitor homolog	Bone
Hs00609452_g1	*BGLAP*	bone gamma-carboxyglutamate protein (osteocalcin)	Bone
Hs00154192_m1	*BMP2*	bone morphogenetic protein 2	Bone
Hs00370078_m1	*BMP4*	bone morphogenetic protein 4	Bone
Hs00234930_m1	*BMP5*	bone morphogenetic protein 5	Bone
Hs00403062_m1	*BMPER*	BMP binding endothelial regulator	Bone
Hs00831730_s1	*BMPR1A*	bone morphogenetic protein receptor, type IA	Bone
Hs00253550_m1	*CD209* *CLEC4M*	CD209 molecule,C-type lectin domain family 4, member M	Bone
Hs01076777_m1	*COL1A1*	collagen, type I, alpha 1	Bone
Hs01028971_m1	*COL1A2*	collagen, type I, alpha 2	Bone
Hs00322497_m1	*DAAM2*	dishevelled associated activator of morphogenesis 2	Bone
Hs00182901_m1	*DVL2*	dishevelled, dsh homolog 2	Bone
Hs00241111_m1	*FGFR1*	fibroblast growth factor receptor 1	Bone
Hs00179829_m1	*FGFR3*	fibroblast growth factor receptor 3	Bone
Hs00173503_m1	*FRZB*	frizzled-related protein	Bone
Hs00268943_s1	*FZD1*	frizzled homolog 1	Bone
Hs00201853_m1	*FZD4*	frizzled homolog 4	Bone
Hs00275833_s1	*FZD7*	frizzled homolog 7	Bone
Hs00259040_s1	*FZD8*	frizzled homolog 8	Bone
Hs00268954_s1	*FZD9*	frizzled homolog 9	Bone
Hs01075601_m1	*GHR*	growth hormone receptor	Bone

Hs00181211_m1	*IGFBP3*	insulin-like growth factor binding protein 3	Bone
Hs02379661_g1	*MT2A*	metallothionein 2A	Bone
Hs00182120_m1	*NGFR*	nerve growth factor receptor (TNFR superfamily, member 16)	Bone
Hs00271352_s1	*NOG*	noggin	Bone
Hs00192325_m1	*OMD*	osteomodulin	Bone
Hs00170179_m1	*PCOLCE*	procollagen C-endopeptidase enhancer	Bone
Hs00998018_m1	*PDGFRA*	platelet-derived growth factor receptor, alpha polypeptide	Bone
Hs00185122_m1	*PDGFRL*	platelet-derived growth factor receptor-like	Bone
Hs01370291_g1	*PHOSPHO1*	phosphatase, orphan 1	Bone
Hs00231079_m1	*RUNX1*	runt-related transcription factor 1	Bone
Hs00231692_m1	*RUNX2*	runt-related transcription factor 2	Bone
Hs00173499_m1	*S1PR1*	Sphingosine-1-Phosphate Receptor 1	Bone
Hs00610060_m1	*SFRP1*	secreted frizzled-related protein 1	Bone
Hs00180066_m1	*SFRP4*	secreted frizzled-related protein 4	Bone
Hs00361747_m1	*SORT1*	sortilin 1	Bone
Hs00541729_m1	*SP7*	Sp7 transcription factor	Bone
Hs00277762_m1	*SPARC*	secreted protein, acidic, cysteine-rich (osteonectin)	Bone
Hs00959010_m1	*SPP1*	secreted phosphoprotein 1 (osteopontin, bone sialoprotein I)	Bone
Hs00559661_m1	*TGFBR2*	transforming growth factor, beta receptor II (70/80kDa)	Bone
Hs00234257_m1	*TGFBR3*	transforming growth factor, beta receptor III	Bone
Hs00900360_m1	*TNFRSF11B*	tumor necrosis factor receptor superfamily, member 11b (osteoprotegerin)	Bone
Hs00361186_m1	*TWIST1*	twist homolog 1	Bone
Hs00382379_m1	*TWIST2*	twist homolog 2	Bone
Hs00183662_m1	*WIF1*	WNT inhibitory factor 1	Bone
Hs00153936_m1	*ACAN*	Aggrecan	Cartilage
Hs00154382_m1	*CHAD*	Chondroadherin	Cartilage
Hs00166657_m1	*COL10A1*	collagen, type X, alpha 1	Cartilage

Hs00264051_m1	*COL2A1*	collagen, type II, alpha 1	Cartilage
Hs00164359_m1	COMP	Cartilage Oligomeric Matrix Protein	Cartilage
Hs00191912_m1	*EPYC*	epiphycan	Cartilage
Hs00167060_m1	*GDF5*	Growth Differentiation Factor 5	Cartilage
Hs00157103_m1	*HAPLN1*	Hyaluronan And Proteoglycan Link Protein 1	Cartilage
Hs00190682_m1	PAPSS2	3'-Phosphoadenosine 5'-Phosphosulfate Synthase 2	Cartilage
Hs00160431_m1	*PRELP*	Proline and Arginine Rich End Leucine Rich Repeat Protein	Cartilage
Hs00165814_m1	*SOX9*	SRY (sex determining region Y)-box 9	Cartilage
Hs01113602_m1	*TNFAIP6*	TNF Alpha Induced Protein 6	Cartilage
Hs01097550_m1	*UGDH*	UDP-Glucose Dehydrogenase	Cartilage
Hs00170454_m1	*FGF5*	fibroblast growth factor 5	Early/ES/neural
Hs02387400_g1	*NANOG*	Nanog homeobox	Early/ES/neural
Hs00707120_s1	*NES*	nestin	Early/ES/neural
Hs00999632_g1	*POU5F1*	POU class 5 homeobox 1	Early/ES/neural
Hs01053049_s1	*SOX2*	SRY (sex determining region Y)-box 2	Early/ES/neural
Hs00181613_m1	*ANGPT1*	angiopoietin 1	Endo/ mural
Hs00156438_m1	*CDH11*	cadherin 11, type 2, OB-cadherin	Endo/ mural
Hs00901463_m1	*CDH5*	cadherin 5, type 2, VE-cadherin	Endo/ mural
Hs00426981_m1	*CSPG4*	chondroitin sulfate proteoglycan 4	Endo/ mural
Hs00358886_m1	*EFNA1*	ephrin-A1	Endo/ mural
Hs00174752_m1	*EPHB4*	EPH receptor B4	Endo/ mural
Hs00748445_s1	*GJA1*	gap junction protein, alpha 1, 43kDa	Endo/ mural
Hs00174838_m1	*MCAM*	melanoma cell adhesion molecule	Endo/ mural
Hs00269972_s1	*CEBPA*	CCAAT/enhancer binding protein (C/EBP), alpha	Fat
Hs00609791_m1	*FABP4*	fatty acid binding protein 4, adipocyte	Fat
Hs00174492_m1	*LEPR*	leptin receptor	Fat
Hs01012571_m1	*LPL*	lipoprotein lipase	Fat
Hs01115513_m1	*PPARG*	peroxisome proliferator-activated receptor gamma	Fat

Hs00231119_m1	*GATA2*	GATA binding protein 2	Haematopoietic
Hs99999041_m1	*IFNG*	interferon, gamma,	Haematopoietic
Hs00961622_m1	*IL10*	interleukin 10	Haematopoietic
Hs99999905_m1	*GAPDH*	glyceraldehyde-3-phosphate dehydrogenase	Housekeeping
Hs99999909_m1	*HPRT1*	hypoxanthine phosphoribosyltransferase 1	Housekeeping
Hs00909449_m1	*ACTA2*	actin, alpha 2, smooth muscle, aorta	Muscle
Hs00178815_m1	*DDR2*	discoidin domain receptor tyrosine kinase 2	Muscle
Hs00427183_m1	*MSX1*	msh homeobox 1	Muscle
Hs00159522_m1	*MYH9*	myosin, heavy chain 9, non-muscle	Muscle
Hs00171022_m1	*CXCL12*	chemokine (C-X-C motif) ligand 12 (stromal cell-derived factor 1)	Stromal
Hs00601975_m1	*CXCL2*	C-X-C Motif Chemokine Ligand 2	Stromal
Hs00174202_m1	*IL7*	interleukin 7	Stromal
Hs01070036_m1	*JAG1*	jagged 1	Stromal
Hs00900058_m1	*VEGFA*	vascular endothelial growth factor A	Stromal
Hs01099206_m1	*VEGFC*	vascular endothelial growth factor C	Stromal

TaqMan probes used for osteocytes and MSC gene expression analysis in Chapter 4

Assay ID	*Gene*	Gene name	Role
Hs00366766_m1	*PDPN*	Podoplanin/E11/gp38	Early osteocyte development
Hs00237119_m1	*MMP14*	Membrane-Type-1 Matrix Metalloproteinase	
Hs01011692_m1	*PHEX*	Phosphate-regulating neutral endopeptidase, X-linked	Mineralisation and phosphate metabolism
Hs00189368_m1	*DMP1*	Dentin matrix acidic phosphoprotein 1	
Hs00220237_m1	*MEPE*	Matrix Extracellular Phosphoglycoprotein	
Hs00221003_m1	*FGF23*	Fibroblast growth factor 23	
Hs00228830_m1	*SOST*	Sclerostin	Bone remodelling
Hs00183740_m1	*DKK1*	Dickkopf WNT Signaling Pathway Inhibitor 1	
Hs00900360_m1	*TNFRSF11B*	Tumor necrosis factor receptor superfamily, member 11b (OPG)	
Hs01092186_m1	*TNFSF11*	Tumor necrosis factor (ligand) superfamily, member 11 (RANKL)	
Hs00166156_m1	*CTSK*	Cathepsin K	
Hs00356261_m1	*ACP5*	Acid Phosphatase 5, Tartrate Resistant (TRAP)	
Hs00758162_m1	*ALPL*	Alkaline phosphatase	Native MSC markers
Hs00541729_m1	*SP7*	Sp7 Transcription Factor	
Hs00171022_m1	*CXCL12*	Chemokine (C-X-C motif) ligand 12	
*Hs99999909_m1	*HPRT1*	Hypoxanthine phosphoribosyltransferase 1	Housekeeping

Bibliography

Van Acker, H.H., Capsomidis, A., Smits, E.L. and Van Tendeloo, V.F. 2017. CD56 in the Immune System: More Than a Marker for Cytotoxicity? *Frontiers in immunology*. **8**, p.892.

Aldridge, A., Kouroupis, D., Churchman, S., et al. 2013. Assay validation for the assessment of adipogenesis of multipotential stromal cells—a direct comparison of four different methods. *Cytotherapy*. **15**(1), pp.89–101.

Alenghat, F.J. and Ingber, D.E. 2002. Mechanotransduction: All Signals Point to Cytoskeleton, Matrix, and Integrins. *Science Signaling*. **2002**(119), pp.pe6-pe6.

Allen, M.R. and Burr, D.B. 2014. Bone Modeling and Remodeling. *Basic and Applied Bone Biology*., pp.75–90.

Altman, R., Alarcón, G., Appelrouth, D., et al. 1991. The American College of Rheumatology criteria for the classification and reporting of osteoarthritis of the hip. *Arthritis and rheumatism*. **34**(5), pp.505–14.

Altman, R., Asch, E., Bloch, D., et al. 1986. Development of criteria for the classification and reporting of osteoarthritis. Classification of osteoarthritis of the knee. Diagnostic and Therapeutic Criteria Committee of the American Rheumatism Association. *Arthritis and rheumatism*. **29**(8), pp.1039–49.

Altman, R.D. 1991. Classification of disease: Osteoarthritis. *Seminars in Arthritis and Rheumatism*. **20**(6), pp.40–47.

Altman, R.D. and Gold, G.E. 2007. Atlas of individual radiographic features in osteoarthritis, revised. *Osteoarthritis and Cartilage*. **15**, pp.A1–A56.

Andersen, T.L., Abdelgawad, M.E., Kristensen, H.B., et al. 2013. Understanding Coupling between Bone Resorption and Formation. *The American Journal of Pathology*. **183**(1), pp.235–246.

Andersen, T.L., Sondergaard, T.E., Skorzynska, K.E., et al. 2009. A Physical Mechanism for Coupling Bone Resorption and Formation in Adult Human Bone. *The American Journal of Pathology*. **174**(1), pp.239–247.

Anderson, D.D., Chubinskaya, S., Guilak, F., et al. 2011. Post-traumatic osteoarthritis: Improved understanding and opportunities for early intervention. *Journal of Orthopaedic Research*. **29**(6), pp.802–809.

Anderson, H.C. 2003. Matrix vesicles and calcification. *Current rheumatology reports*. **5**(3), pp.222–6.

De Angelis, G. and Chen, Y. 2013. Obesity among women may increase the risk of arthritis: observations from the Canadian Community Health Survey, 2007–2008.

Rheumatology International. **33**(9), pp.2249–2253.

Anh, D.J., Dimai, H.P., Hall, S.L. and Farley, J.R. 1998. Skeletal alkaline phosphatase activity is primarily released from human osteoblasts in an insoluble form, and the net release is inhibited by calcium and skeletal growth factors. *Calcified tissue international*. **62**(4), pp.332–40.

arcOGEN Consortium, arcOGEN Collaborators, Zeggini, E., et al. 2012. Identification of new susceptibility loci for osteoarthritis (arcOGEN): a genome-wide association study. *The Lancet*. **380**(9844), pp.815–823.

Aresti, N., Kassam, J., Nicholas, N. and Achan, P. 2016. Hip osteoarthritis. *BMJ (Clinical research ed.)*. **354**, p.i3405.

Arthritis Research UK 2013. *Osteoarthritis in general practice* [Online]. [Accessed 1 November 2018]. Available from: https://healthinnovationnetwork.com/wp-content/uploads/2017/01/Osteoarthritis_in_general_practice__July_2013__Arthritis_Research_UK_PDF_421_MB.pdf.

Aslan, H., Zilberman, Y., Kandel, L., et al. 2006. Osteogenic Differentiation of Noncultured Immunoisolated Bone Marrow-Derived CD105 $^{+}$ Cells. *Stem Cells*. **24**(7), pp.1728–1737.

Aubin, J.E. 1998. Bone stem cells. *Journal of cellular biochemistry. Supplement*. **30**–**31**, pp.73–82.

Aubin, J.E. and Turksen, K. 1996. Monoclonal antibodies as tools for studying the osteoblast lineage. *Microscopy Research and Technique*. **33**(2), pp.128–140.

Baboolal, T.G., Khalil-Khan, A., Theodorides, A.A., et al. 2018. A Novel Arthroscopic Technique for Intraoperative Mobilization of Synovial Mesenchymal Stem Cells. *The American journal of sports medicine*. **46**(14), pp.3532–3540.

Bach-Gansmo, F.L., Weaver, J.C., Jensen, M.H., et al. 2015. Osteocyte lacunar properties in rat cortical bone: Differences between lamellar and central bone. *Journal of Structural Biology*. **191**(1), pp.59–67.

Bardin, N., Anfosso, F., Massé, J.M., et al. 2001. Identification of CD146 as a component of the endothelial junction involved in the control of cell-cell cohesion. *Blood*. **98**(13), pp.3677–84.

De Bari, C., Dell'Accio, F., Tylzanowski, P. and Luyten, F.P. 2001. Multipotent mesenchymal stem cells from adult human synovial membrane. *Arthritis and rheumatism*. **44**(8), pp.1928–42.

Baron, R. and Kneissel, M. 2013. WNT signaling in bone homeostasis and disease: from human mutations to treatments. *Nature Medicine*. **19**(2), pp.179–192.

Barry, F., Boynton, R., Murphy, M., Zaia, J. and Zaia, J. 2001. The SH-3 and SH-4 Antibodies Recognize Distinct Epitopes on CD73 from Human Mesenchymal Stem Cells. *Biochemical and Biophysical Research Communications*. **289**(2), pp.519–524.

Barry, F. and Murphy, M. 2013. Mesenchymal stem cells in joint disease and repair. *Nature Reviews Rheumatology*. **9**(10), pp.584–594.

Barry, F.P., Boynton, R.E., Haynesworth, S., Murphy, J.M. and Zaia, J. 1999. The Monoclonal Antibody SH-2, Raised against Human Mesenchymal Stem Cells, Recognizes an Epitope on Endoglin (CD105). *Biochemical and Biophysical Research Communications*. **265**(1), pp.134–139.

Batra, S., Batra, M., McMurtrie, A. and Sinha, A.K. 2008. Rapidly destructive osteoarthritis of the hip joint: a case series. *Journal of orthopaedic surgery and research*. **3**, p.3.

Battula, V.L., Treml, S., Bareiss, P.M., et al. 2009. Isolation of functionally distinct mesenchymal stem cell subsets using antibodies against CD56, CD271, and mesenchymal stem cell antigen-1. *Haematologica*. **94**(2), pp.173–184.

Bergholt, N.L., Lysdahl, H., Lind, M. and Foldager, C.B. 2018. A Standardized Method of Applying Toluidine Blue Metachromatic Staining for Assessment of Chondrogenesis. *Cartilage*., p.194760351876426.

Bettica, P., Cline, G., Hart, D.J., Meyer, J. and Spector, T.D. 2002. Evidence for increased bone resorption in patients with progressive knee osteoarthritis: longitudinal results from the Chingford study. *Arthritis and rheumatism*. **46**(12), pp.3178–84.

van Bezooijen, R.L., Roelen, B.A.J., Visser, A., et al. 2004. Sclerostin is an osteocyte-expressed negative regulator of bone formation, but not a classical BMP antagonist. *The Journal of experimental medicine*. **199**(6), pp.805–14.

Bi, W., Deng, J.M., Zhang, Z., Behringer, R.R. and de Crombrugghe, B. 1999. Sox9 is required for cartilage formation. *Nature Genetics*. **22**(1), pp.85–89.

Bianco, P., Cao, X., Frenette, P.S., et al. 2013. The meaning, the sense and the significance: translating the science of mesenchymal stem cells into medicine. *Nature Medicine*. **19**(1), pp.35–42.

Bianco, P., Robey, P.G. and Simmons, P.J. 2008. Mesenchymal Stem Cells: Revisiting History, Concepts, and Assays. *Cell Stem Cell*. **2**(4), pp.313–319.

Birrell, F., Croft, P., Cooper, C., et al. 2001. Predicting radiographic hip osteoarthritis from range of movement. *Rheumatology (Oxford, England)*. **40**(5), pp.506–12.

Bobis, S., Jarocha, D. and Majka, M. 2006. Mesenchymal stem cells: characteristics and clinical applications. *Folia histochemica et cytobiologica*. **44**(4), pp.215–30.

Bonewald, L.F. 2011. The amazing osteocyte. *Journal of bone and mineral research : the official journal of the American Society for Bone and Mineral Research*. **26**(2), pp.229–38.

Boskey, A.L. and Coleman, R. 2010. Aging and Bone. *Journal of Dental Research*. **89**(12), pp.1333–1348.

Boutry, N., Paul, C., Leroy, X., et al. 2002. Rapidly Destructive Osteoarthritis of the Hip: MR Imaging Findings. *American Journal of Roentgenology*. **179**(3), pp.657–663.

Bowes, M.A., McLure, S.W., Wolstenholme, C.B., et al. 2016. Osteoarthritic bone marrow lesions almost exclusively colocate with denuded cartilage: a 3D study using data from the Osteoarthritis Initiative. *Annals of the Rheumatic Diseases*. **75**(10), pp.1852–1857.

Boxall, S.A., Jones, E., Boxall, S.A. and Jones, E. 2012. Markers for Characterization of Bone Marrow Multipotential Stromal Cells. *Stem Cells International*. **2012**, pp.1–12.

Boyan, B.D., Hart, D.A., Enoka, R.M., et al. 2013. Hormonal modulation of connective tissue homeostasis and sex differences in risk for osteoarthritis of the knee. *Biology of Sex Differences*. **4**(1).

Boyce, B.F. and Xing, L. 2007. Biology of RANK, RANKL, and osteoprotegerin. *Arthritis research & therapy*. **9 Suppl 1**, p.S1.

Boyce, B.F. and Xing, L. 2007. The RANKL/RANK/OPG pathway. *Current Osteoporosis Reports*. **5**(3), pp.98–104.

Brittberg, M. 2008. Autologous chondrocyte implantation—Technique and long-term follow-up. *Injury*. **39**(1), pp.40–49.

Buchanan, W.W., Kean, W.F. and Kean, R. 2003. History and current status of osteoarthritis in the population. *Inflammopharmacology*. **11**(4), pp.301–16.

Buenzli, P.R. and Sims, N.A. 2015. Quantifying the osteocyte network in the human skeleton. *Bone*. **75**, pp.144–150.

Bühring, H.-J., Battula, V.L., Treml, S., et al. 2007. Novel markers for the prospective isolation of human MSC. *Annals of the New York Academy of Sciences*. **1106**, pp.262–71.

Bühring, H.-J., Treml, S., Cerabona, F., et al. 2009. Phenotypic characterization of distinct human bone marrow-derived MSC subsets. *Annals of the New York Academy of Sciences*. **1176**, pp.124–34.

Burr, D.B. 2004. Anatomy and physiology of the mineralized tissues: Role in the pathogenesis of osteoarthrosis. *Osteoarthritis and Cartilage*. **12**, pp.20–30.

Burr, D.B. and Gallant, M.A. 2012. Bone remodelling in osteoarthritis. *Nature reviews. Rheumatology*. **8**(11), pp.665–73.

Burr, D.B. and Radin, E.L. 2003. Microfractures and microcracks in subchondral bone: are they relevant to osteoarthrosis? *Rheumatic diseases clinics of North America*. **29**(4), pp.675–85.

Burra, S., Nicolella, D.P., Francis, W.L., et al. 2010. Dendritic processes of osteocytes are mechanotransducers that induce the opening of hemichannels. *Proceedings of the National Academy of Sciences*. **107**(31), pp.13648–13653.

Busser, H., Najar, M., Raicevic, G., et al. 2015. Isolation and Characterization of Human Mesenchymal Stromal Cell Subpopulations: Comparison of Bone Marrow and Adipose Tissue. *Stem Cells and Development*. **24**(18), pp.2142–2157.

Cadigan, K.M. and Waterman, M.L. 2012. TCF/LEFs and Wnt signaling in the nucleus. *Cold Spring Harbor perspectives in biology*. **4**(11).

Callis, G. and Sterchi, D. 1998. Decalcification of Bone: Literature Review and Practical Study of Various Decalcifying Agents. Methods, and Their Effects on Bone Histology. *Journal of Histotechnology*. **21**(1), pp.49–58.

Campbell, T.M., Churchman, S.M., Gomez, A., et al. 2016. Mesenchymal stem cell alterations in bone marrow lesions in hip osteoarthritis. *Arthritis & rheumatology (Hoboken, N.J.)*.

Camper, L., Heinegârd, D. and Lundgren-Akerlund, E. 1997. Integrin alpha2beta1 is a receptor for the cartilage matrix protein chondroadherin. *The Journal of cell biology*. **138**(5), pp.1159–67.

Campioni, D., Lanza, F., Moretti, S., et al. 2003. Functional and immunophenotypic characteristics of isolated CD105+ and fibroblast+ stromal cells from AML: implications for their plasticity along endothelial lineage. *Cytotherapy*. **5**(1), pp.66–79.

Caplan, A.I. 1991. Mesenchymal stem cells. *Journal of Orthopaedic Research*. **9**(5), pp.641–650.

Carrino, J.A., Blum, J., Parellada, J.A., Schweitzer, M.E. and Morrison, W.B. 2006. MRI of bone marrow edema-like signal in the pathogenesis of subchondral cysts. *Osteoarthritis and Cartilage*. **14**(10), pp.1081–1085.

Cattoretti, G., Schiró, R., Orazi, A., Soligo, D. and Colombo, M.P. 1993. Bone marrow stroma in humans: anti-nerve growth factor receptor antibodies selectively stain reticular cells in vivo and in vitro. *Blood*. **81**(7), pp.1726–38.

Celil, A.B. and Campbell, P.G. 2005. BMP-2 and Insulin-like Growth Factor-I Mediate Osterix (Osx) Expression in Human Mesenchymal Stem Cells via the MAPK and Protein Kinase D Signaling Pathways. *Journal of Biological Chemistry*. **280**(36),

pp.31353–31359.

Chapman, K., Takahashi, A., Meulenbelt, I., et al. 2008. A meta-analysis of European and Asian cohorts reveals a global role of a functional SNP in the 5' UTR of GDF5 with osteoarthritis susceptibility. *Human Molecular Genetics*. **17**(10), pp.1497–1504.

Chapurlat, R.D. and Confavreux, C.B. 2016. Novel biological markers of bone: from bone metabolism to bone physiology. *Rheumatology*. **55**(10), pp.1714–1725.

Chen, D., Harris, M.A., Rossini, G., et al. 1997. Bone morphogenetic protein 2 (BMP-2) enhances BMP-3, BMP-4, and bone cell differentiation marker gene expression during the induction of mineralized bone matrix formation in cultures of fetal rat calvarial osteoblasts. *Calcified tissue international*. **60**(3), pp.283–90.

Chen, X., Wang, L., Zhao, K. and Wang, H. 2018. Osteocytogenesis: Roles of Physicochemical Factors, Collagen Cleavage, and Exogenous Molecules. *Tissue Engineering Part B: Reviews*. **24**(3), pp.215–225.

Choi, K., Kuhn, J.L., Ciarelli, M.J. and Goldstein, S.A. 1990. The elastic moduli of human subchondral, trabecular, and cortical bone tissue and the size-dependency of cortical bone modulus. *Journal of Biomechanics*. **23**(11), pp.1103–1113.

Chomczynski, P. and Sacchi, N. 1987. Single-step method of RNA isolation by acid guanidinium thiocyanate-phenol-chloroform extraction. *Analytical biochemistry*. **162**(1), pp.156–9.

Christensen, R., Bartels, E.M., Astrup, A. and Bliddal, H. 2006. Effect of weight reduction in obese patients diagnosed with knee osteoarthritis: a systematic review and meta-analysis. *Annals of the Rheumatic Diseases*. **66**(4), pp.433–439.

Churchman, S.M., Boxall, S.A., McGonagle, D. and Jones, E.A. 2017. Predicting the Remaining Lifespan and Cultivation-Related Loss of Osteogenic Capacity of Bone Marrow Multipotential Stromal Cells Applicable across a Broad Donor Age Range. *Stem Cells International*. **2017**, pp.1–10.

Churchman, S.M., Kouroupis, D., Boxall, S.A., et al. 2013. Yield optimisation and molecular characterisation of uncultured CD271+ mesenchymal stem cells in the Reamer Irrigator Aspirator waste bag. *European cells & materials*. **26**, pp.252–62.

Churchman, S.M., Ponchel, F., Boxall, S.A., et al. 2012. Transcriptional profile of native CD271+ multipotential stromal cells: evidence for multiple fates, with prominent osteogenic and Wnt pathway signaling activity. *Arthritis and rheumatism*. **64**(8), pp.2632–43.

Civitelli, R. 2008. Cell-cell communication in the osteoblast/osteocyte lineage. *Archives of biochemistry and biophysics*. **473**(2), pp.188–92.

Clarke, B. 2008. Normal Bone Anatomy and Physiology. *Clinical Journal of the*

American Society of Nephrology. **3**(Supplement 3), pp.S131–S139.

Compton, J.T. and Lee, F.Y. 2014. A review of osteocyte function and the emerging importance of sclerostin. *The Journal of bone and joint surgery. American volume*. **96**(19), pp.1659–68.

Conaghan, P.G., Hunter, D.J., Maillefert, J.F., Reichmann, W.M. and Losina, E. 2011. Summary and recommendations of the OARSI FDA osteoarthritis Assessment of Structural Change Working Group. *Osteoarthritis and Cartilage*. **19**(5), pp.606–610.

Cosenza, S., Ruiz, M., Toupet, K., Jorgensen, C. and Noël, D. 2017. Mesenchymal stem cells derived exosomes and microparticles protect cartilage and bone from degradation in osteoarthritis. *Scientific Reports*. **7**(1), p.16214.

Couchourel, D., Aubry, I., Delalandre, A., et al. 2009. Altered mineralization of human osteoarthritic osteoblasts is attributable to abnormal type I collagen production. *Arthritis and rheumatism*. **60**(5), pp.1438–50.

Cox, G., Boxall, S.A., Giannoudis, P. V, et al. 2012. High abundance of CD271(+) multipotential stromal cells (MSCs) in intramedullary cavities of long bones. *Bone*. **50**(2), pp.510–7.

Cox, L.G., van Donkelaar, C.C., van Rietbergen, B., Emans, P.J. and Ito, K. 2012. Decreased bone tissue mineralization can partly explain subchondral sclerosis observed in osteoarthritis. *Bone*. **50**(5), pp.1152–1161.

Crema, M.D., Roemer, F.W., Zhu, Y., et al. 2010. Subchondral Cystlike Lesions Develop Longitudinally in Areas of Bone Marrow Edema–like Lesions in Patients with or at Risk for Knee Osteoarthritis: Detection with MR Imaging—The MOST Study. *Radiology*. **256**(3), pp.855–862.

Crisan, M., Yap, S., Casteilla, L., et al. 2008. A Perivascular Origin for Mesenchymal Stem Cells in Multiple Human Organs. *Cell Stem Cell*. **3**(3), pp.301–313.

Croft, P., Cooper, C., Wickham, C. and Coggon, D. 1990. Defining osteoarthritis of the hip for epidemiologic studies. *American journal of epidemiology*. **132**(3), pp.514–22.

Cummings, S.R., Martin, J.S., McClung, M.R., et al. 2009. Denosumab for Prevention of Fractures in Postmenopausal Women with Osteoporosis. *New England Journal of Medicine*. **361**(8), pp.756–765.

Cuthbert, R., Boxall, S.A., Tan, H.B., et al. 2012. Single-platform quality control assay to quantify multipotential stromal cells in bone marrow aspirates prior to bulk manufacture or direct therapeutic use. *Cytotherapy*. **14**(4), pp.431–440.

Cuthbert, R.J., Giannoudis, P. V., Wang, X.N., et al. 2015. Examining the Feasibility of Clinical Grade CD271+ Enrichment of Mesenchymal Stromal Cells for Bone

Regeneration P. Menendez, ed. *PLOS ONE*. **10**(3), p.e0117855.

D'haeseleer, P. 2005. *How does gene expression clustering work?* [Online]. [Accessed 23 December 2018]. Available from: http://www.nature.com/naturebiotechnology.

D'Ippolito, G., Schiller, P.C., Ricordi, C., Roos, B.A. and Howard, G.A. 1999. Age-Related Osteogenic Potential of Mesenchymal Stromal Stem Cells from Human Vertebral Bone Marrow. *Journal of Bone and Mineral Research*. **14**(7), pp.1115–1122.

Dallas, S.L. and Bonewald, L.F. 2010. Dynamics of the transition from osteoblast to osteocyte. *Annals of the New York Academy of Sciences*. **1192**, pp.437–43.

Dallas, S.L., Prideaux, M. and Bonewald, L.F. 2013. The osteocyte: an endocrine cell ... and more. *Endocrine reviews*. **34**(5), pp.658–90.

Day, J.S., Ding, M., van der Linden, J.C., et al. 2001. A decreased subchondral trabecular bone tissue elastic modulus is associated with pre-arthritic cartilage damage. *Journal of Orthopaedic Research*. **19**(5), pp.914–918.

Delaissé, J.-M., Andersen, T.L., Engsig, M.T., et al. 2003. Matrix metalloproteinases (MMP) and cathepsin K contribute differently to osteoclastic activities. *Microscopy Research and Technique*. **61**(6), pp.504–513.

Denhardt, D.T. and Guo, X. 1993. Osteopontin: a protein with diverse functions. *FASEB journal : official publication of the Federation of American Societies for Experimental Biology*. **7**(15), pp.1475–82.

Denhardt, D.T. and Noda, M. 1998. Osteopontin expression and function: role in bone remodeling. *Journal of cellular biochemistry. Supplement*. **30**–**31**, pp.92–102.

Deschaseaux, F., Gindraux, F., Saadi, R., et al. 2003. Direct selection of human bone marrow mesenchymal stem cells using an anti-CD49a antibody reveals their CD45med,low phenotype. *British journal of haematology*. **122**(3), pp.506–17.

Diarra, D., Stolina, M., Polzer, K., et al. 2007. Dickkopf-1 is a master regulator of joint remodeling. *Nature medicine*. **13**(2), pp.156–63.

Dieppe, P., Cushnaghan, J., Young, P. and Kirwan, J. 1993. Prediction of the progression of joint space narrowing in osteoarthritis of the knee by bone scintigraphy. *Annals of the rheumatic diseases*. **52**(8), pp.557–63.

Dieppe, P.A. and Lohmander, L.S. 2005. Pathogenesis and management of pain in osteoarthritis. *The Lancet*. **365**(9463), pp.965–973.

Dierkes, C., Kreisel, M., Schulz, A., et al. 2009. Catabolic Properties of Microdissected Human Endosteal Bone Lining Cells. *Calcified Tissue International*. **84**(2), pp.146–155.

Digirolamo, C.M., Stokes, D., Colter, D., et al. 1999. Propagation and senescence of human marrow stromal cells in culture: a simple colony-forming assay identifies samples with the greatest potential to propagate and differentiate. *British journal of haematology*. **107**(2), pp.275–81.

Dole, N.S., Mazur, C.M., Acevedo, C., et al. 2017. Osteocyte-Intrinsic TGF-β Signaling Regulates Bone Quality through Perilacunar/Canalicular Remodeling. *Cell Reports*. **21**(9), pp.2585–2596.

Dominici, M., Le Blanc, K., Mueller, I., et al. 2006. Minimal criteria for defining multipotent mesenchymal stromal cells. The International Society for Cellular Therapy position statement. *Cytotherapy*. **8**(4), pp.315–7.

Donahue, H.. 2000. Gap junctions and biophysical regulation of bone cell differentiation. *Bone*. **26**(5), pp.417–422.

Dowthwaite, G.P., Bishop, J.C., Redman, S.N., et al. 2004. The surface of articular cartilage contains a progenitor cell population. *Journal of Cell Science*. **117**(6), pp.889–897.

Ducy, P., Zhang, R., Geoffroy, V., Ridall, A.L. and Karsenty, G. 1997. Osf2/Cbfa1: a transcriptional activator of osteoblast differentiation. *Cell*. **89**(5), pp.747–54.

Durand, M., Komarova, S. V., Bhargava, A., et al. 2013. Monocytes from patients with osteoarthritis display increased osteoclastogenesis and bone resorption: The In Vitro Osteoclast Differentiation in Arthritis study. *Arthritis & Rheumatism*. **65**(1), pp.148–158.

Engesæter, L.B., Dale, H., Schrama, J.C., Hallan, G. and Lie, S.A. 2011. Surgical procedures in the treatment of 784 infected THAs reported to the Norwegian Arthroplasty Register. *Acta orthopaedica*. **82**(5), pp.530–7.

English, A., Jones, E.A., Corscadden, D., et al. 2007. A comparative assessment of cartilage and joint fat pad as a potential source of cells for autologous therapy development in knee osteoarthritis. *Rheumatology (Oxford, England)*. **46**(11), pp.1676–83.

Eriksen, E.F. 2010. Cellular mechanisms of bone remodeling. *Reviews in endocrine & metabolic disorders*. **11**(4), pp.219–27.

Evangelou, E., Chapman, K., Meulenbelt, I., et al. 2009. Large-scale analysis of association between GDF5 and FRZB variants and osteoarthritis of the hip, knee, and hand. *Arthritis & Rheumatism*. **60**(6), pp.1710–1721.

Evans, J.T., Evans, J.P., Walker, R.W., et al. 2019. How long does a hip replacement last? A systematic review and meta-analysis of case series and national registry reports with more than 15 years of follow-up. *Lancet (London, England)*. **393**(10172), pp.647–654.

Everts, V., Delaissé, J.M., Korper, W., et al. 2002. The Bone Lining Cell: Its Role in Cleaning Howship's Lacunae and Initiating Bone Formation. *Journal of Bone and Mineral Research*. **17**(1), pp.77–90.

Fakhry, M., Hamade, E., Badran, B., Buchet, R. and Magne, D. 2013. Molecular mechanisms of mesenchymal stem cell differentiation towards osteoblasts. *World Journal of Stem Cells*. **5**(4), p.136.

Fazzalari, N.L. and Parkinson, I.H. 1997. Fractal Properties of Subchondral Cancellous Bone in Severe Osteoarthritis of the Hip. *Journal of Bone and Mineral Research*. **12**(4), pp.632–640.

Fellows, C.R., Williams, R., Davies, I.R., et al. 2017. Characterisation of a divergent progenitor cell sub-populations in human osteoarthritic cartilage: the role of telomere erosion and replicative senescence. *Scientific reports*. **7**, p.41421.

Felson, D.T. 2013. Osteoarthritis as a disease of mechanics. *Osteoarthritis and Cartilage*. **21**(1), pp.10–15.

Felson, D.T., Gale, D.R., Elon Gale, M., et al. 2005. Osteophytes and progression of knee osteoarthritis. *Rheumatology*. **44**(1), pp.100–104.

Felson, D.T., McLaughlin, S., Goggins, J., et al. 2003. Bone marrow edema and its relation to progression of knee osteoarthritis. *Annals of internal medicine*. **139**(5 Pt 1), pp.330–6.

Felson, D.T., Niu, J., Gross, K.D., et al. 2013. Valgus malalignment is a risk factor for lateral knee osteoarthritis incidence and progression: Findings from the multicenter osteoarthritis study and the osteoarthritis initiative. *Arthritis & Rheumatism*. **65**(2), pp.355–362.

Felson, D.T. and Zhang, Y. 2015. Smoking and osteoarthritis: A review of the evidence and its implications. *Osteoarthritis and Cartilage*. **23**(3), pp.331–333.

Felson, D.T., Zhang, Y., Anthony, J.M., Naimark, A. and Anderson, J.J. 1992. Weight loss reduces the risk for symptomatic knee osteoarthritis in women. The Framingham Study. *Annals of internal medicine*. **116**(7), pp.535–9.

Felson, D.T., Zhang, Y., Hannan, M.T., et al. 1997. Risk factors for incident radiographic knee osteoarthritis in the elderly: the Framingham Study. *Arthritis and rheumatism*. **40**(4), pp.728–33.

Feng, J.Q., Ward, L.M., Liu, S., et al. 2006. Loss of DMP1 causes rickets and osteomalacia and identifies a role for osteocytes in mineral metabolism. *Nature genetics*. **38**(11), pp.1310–5.

Ferrari, S.L., Traianedes, K., Thorne, M., et al. 2010. A Role for N-Cadherin in the Development of the Differentiated Osteoblastic Phenotype. *Journal of Bone and Mineral Research*. **15**(2), pp.198–208.

Ferraro, F., Celso, C. Lo and Scadden, D. 2010. Adult stem cells and their niches. *Adv Exp Med Biol*. **695**, pp.155–168.

Fickert, S., Fiedler, J. and Brenner, R.E. 2004. Identification of subpopulations with characteristics of mesenchymal progenitor cells from human osteoarthritic cartilage using triple staining for cell surface markers. *Arthritis Research & Therapy*. **6**(5), p.R422.

Findlay, D.M. 2007. Vascular pathology and osteoarthritis. *Rheumatology*. **46**(12), pp.1763–1768.

Flemming, D.J. and Gustas-French, C.N. 2017. Rapidly Progressive Osteoarthritis: a Review of the Clinical and Radiologic Presentation. *Current Rheumatology Reports*. **19**(7), p.42.

Florencio-Silva, R., Sasso, G.R. da S., Sasso-Cerri, E., Simões, M.J. and Cerri, P.S. 2015. Biology of Bone Tissue: Structure, Function, and Factors That Influence Bone Cells. *BioMed research international*. **2015**, p.421746.

Fowler, T.W., Acevedo, C., Mazur, C.M., et al. 2017. Glucocorticoid suppression of osteocyte perilacunar remodeling is associated with subchondral bone degeneration in osteonecrosis. *Scientific Reports*. **7**, p.44618.

François, S., Bensidhoum, M., Mouiseddine, M., et al. 2006. Local Irradiation Not Only Induces Homing of Human Mesenchymal Stem Cells at Exposed Sites but Promotes Their Widespread Engraftment to Multiple Organs: A Study of Their Quantitative Distribution After Irradiation Damage. *STEM CELLS*. **24**(4), pp.1020–1029.

Franz-Odendaal, T.A., Hall, B.K. and Witten, P.E. 2006. Buried alive: How osteoblasts become osteocytes. *Developmental Dynamics*. **235**(1), pp.176–190.

Friedenstein, A.J., Chailakhjan, R.K. and Lalykina, K.S. 1970. The development of fibroblast colonies in monolayer cultures of guinea-pig bone marrow and spleen cells. *Cell Proliferation*. **3**(4), pp.393–403.

Friedenstein, A.J., Chailakhyan, R.K. and Gerasimov, U. V 1987. Bone marrow osteogenic stem cells: in vitro cultivation and transplantation in diffusion chambers. *Cell and tissue kinetics*. **20**(3), pp.263–72.

Friedenstein, A.J., Petrakova, K. V, Kurolesova, A.I. and Frolova, G.P. 1968. Heterotopic of bone marrow. Analysis of precursor cells for osteogenic and hematopoietic tissues. *Transplantation*. **6**(2), pp.230–47.

Frost, H.M. 1960. In vivo osteocyte death. *The Journal of bone and joint surgery. American volume*. **42**–**A**, pp.138–43.

Frost, H.M. 1990. Skeletal structural adaptations to mechanical usage (SATMU): 2. Redefining Wolff's Law: The remodeling problem. *The Anatomical Record*. **226**(4), pp.414–422.

Fuchs, E., Tumbar, T. and Guasch, G. 2004. Socializing with the neighbors: stem cells and their niche. *Cell*. **116**(6), pp.769–78.

Gang, E.J., Bosnakovski, D., Figueiredo, C.A., Visser, J.W. and Perlingeiro, R.C.R. 2007. SSEA-4 identifies mesenchymal stem cells from bone marrow. *Blood*. **109**(4), pp.1743–1751.

Garnero, P. and Delmas, P.D. 1998. Biochemical markers of bone turnover. Applications for osteoporosis. *Endocrinology and metabolism clinics of North America*. **27**(2), pp.303–23.

Genetos, D.C., Kephart, C.J., Zhang, Y., Yellowley, C.E. and Donahue, H.J. 2007. Oscillating fluid flow activation of gap junction hemichannels induces ATP release from MLO-Y4 osteocytes. *Journal of cellular physiology*. **212**(1), pp.207–14.

Ghazanfari, R., Zacharaki, D., Li, H., et al. 2017. Human Primary Bone Marrow Mesenchymal Stromal Cells and Their in vitro Progenies Display Distinct Transcriptional Profile Signatures. *Scientific Reports*. **7**(1), p.10338.

Glyn-Jones, S., Palmer, A.J.R., Agricola, R., et al. 2015. Osteoarthritis. *The Lancet*. **386**(9991), pp.376–387.

Gold, G.E., Cicuttini, F., Crema, M.D., et al. 2015. OARSI Clinical Trials Recommendations: Hip imaging in clinical trials in osteoarthritis. *Osteoarthritis and cartilage*. **23**(5), pp.716–31.

Goldring, M.B. and Goldring, S.R. 2010. Articular cartilage and subchondral bone in the pathogenesis of osteoarthritis. *Annals of the New York Academy of Sciences*. **1192**(1), pp.230–237.

Goldring, M.B. and Goldring, S.R. 2007. Osteoarthritis. *Journal of Cellular Physiology*. **213**(3), pp.626–634.

Goldring, S.R. 2012. Alterations in periarticular bone and cross talk between subchondral bone and articular cartilage in osteoarthritis. *Therapeutic advances in musculoskeletal disease*. **4**(4), pp.249–58.

Goldring, S.R. 2009. Role of Bone in Osteoarthritis Pathogenesis. *Medical Clinics of North America*. **93**(1), pp.25–35.

Goldring, S.R. 2008. The Role of Bone in Osteoarthritis Pathogenesis. *Rheumatic Disease Clinics of North America*. **34**(3), pp.561–571.

Goldring, S.R. and Goldring, M.B. 2016a. Changes in the osteochondral unit during osteoarthritis: structure, function and cartilage-bone crosstalk. *Nat Rev Rheumatol*. **12**(11), pp.632–644.

Goldring, S.R. and Goldring, M.B. 2016b. Changes in the osteochondral unit during

osteoarthritis: structure, function and cartilage–bone crosstalk. *Nature Reviews Rheumatology*. **12**(11), pp.632–644.

Gothard, D., Dawson, J.I. and Oreffo, R.O.C. 2013. Assessing the potential of colony morphology for dissecting the CFU-F population from human bone marrow stromal cells. *Cell and Tissue Research*. **352**(2), pp.237–247.

Govender, S., Csimma, C., Genant, H.K., et al. 2002. Recombinant human bone morphogenetic protein-2 for treatment of open tibial fractures: a prospective, controlled, randomized study of four hundred and fifty patients. *The Journal of bone and joint surgery. American volume*. **84**–**A**(12), pp.2123–34.

Greenbaum, A., Hsu, Y.-M.S., Day, R.B., et al. 2013. CXCL12 in early mesenchymal progenitors is required for haematopoietic stem-cell maintenance. *Nature*. **495**(7440), pp.227–230.

Greenblatt, M.B., Tsai, J.N. and Wein, M.N. 2017. Bone Turnover Markers in the Diagnosis and Monitoring of Metabolic Bone Disease. *Clinical chemistry*. **63**(2), pp.464–474.

Gronthos, S., Zannettino, A.C.W., Hay, S.J., et al. 2003. Molecular and cellular characterisation of highly purified stromal stem cells derived from human bone marrow. *Journal of cell science*. **116**(Pt 9), pp.1827–35.

Guermazi, A., Niu, J., Hayashi, D., et al. 2012. Prevalence of abnormalities in knees detected by MRI in adults without knee osteoarthritis: population based observational study (Framingham Osteoarthritis Study). *BMJ (Clinical research ed.)*. **345**, p.e5339.

Haque, M.F. ul, King, L.M., Krakow, D., et al. 1998. Mutations in orthologous genes in human spondyloepimetaphyseal dysplasia and the brachymorphic mouse. *Nature Genetics*. **20**(2), pp.157–162.

Harichandan, A., Sivasubramaniyan, K. and Bühring, H.-J. 2012. Prospective Isolation and Characterization of Human Bone Marrow-Derived MSCs *In*: *Advances in biochemical engineering/biotechnology* [Online]., pp.1–17. [Accessed 11 June 2018]. Available from: http://www.ncbi.nlm.nih.gov/pubmed/22825720.

Hauge, E.M., Qvesel, D., Eriksen, E.F., Mosekilde, L. and Melsen, F. 2001. Cancellous Bone Remodeling Occurs in Specialized Compartments Lined by Cells Expressing Osteoblastic Markers. *Journal of Bone and Mineral Research*. **16**(9), pp.1575–1582.

Havdrup, T., Hulth, A. and Telhag, H. 1976. The subchondral bone in osteoarthritis and rheumatoid arthritis of the knee. A histological and microradiographical study. *Acta orthopaedica Scandinavica*. **47**(3), pp.345–50.

Hayami, T., Pickarski, M., Wesolowski, G.A., et al. 2004. The role of subchondral bone remodeling in osteoarthritis: Reduction of cartilage degeneration and prevention of osteophyte formation by alendronate in the rat anterior cruciate ligament transection

model. *Arthritis & Rheumatism*. **50**(4), pp.1193–1206.

Hayflick, L. 1965. The limited in vitro lifetime of human diploid cell strains. *Experimental cell research*. **37**, pp.614–36.

Haynes, D., Crotti, T., Weedon, H., et al. 2008. Modulation of RANKL and osteoprotegerin expression in synovial tissue from patients with rheumatoid arthritis in response to disease-modifying antirheumatic drug treatment and correlation with radiologic outcome. *Arthritis & Rheumatism*. **59**(7), pp.911–920.

Henrotin, Y., Pesesse, L. and Sanchez, C. 2012. Subchondral bone and osteoarthritis: biological and cellular aspects. *Osteoporosis international : a journal established as result of cooperation between the European Foundation for Osteoporosis and the National Osteoporosis Foundation of the USA*. **23 Suppl 8**, pp.S847-51.

Hermida-Gómez, T., Fuentes-Boquete, I., Gimeno-Longas, M.J., et al. 2011. Quantification of cells expressing mesenchymal stem cell markers in healthy and osteoarthritic synovial membranes. *The Journal of rheumatology*. **38**(2), pp.339–49.

Hochberg, M.C., Lethbridge-Cejku, M., Scott, W.W., et al. 2009. Upper extremity bone mass and osteoarthritis of the knees: Data from the baltimore longitudinal study of aging. *Journal of Bone and Mineral Research*. **10**(3), pp.432–438.

Holmbeck, K., Bianco, P., Pidoux, I., et al. 2005. The metalloproteinase MT1-MMP is required for normal development and maintenance of osteocyte processes in bone. *Journal of cell science*. **118**(Pt 1), pp.147–56.

Horwitz, E.M., Le Blanc, K., Dominici, M., et al. 2005. Clarification of the nomenclature for MSC: The International Society for Cellular Therapy position statement. *Cytotherapy*. **7**(5), pp.393–5.

Hsu, H., Lacey, D.L., Dunstan, C.R., et al. 1999. Tumor necrosis factor receptor family member RANK mediates osteoclast differentiation and activation induced by osteoprotegerin ligand. *Proceedings of the National Academy of Sciences of the United States of America*. **96**(7), pp.3540–5.

Hui, M., Doherty, M. and Zhang, W. 2011. Does smoking protect against osteoarthritis? Meta-analysis of observational studies. *Annals of the Rheumatic Diseases*. **70**(7), pp.1231–1237.

Ilas, D.C., Churchman, S.M., Baboolal, T., et al. 2019. The simultaneous analysis of mesenchymal stem cells and early osteocytes accumulation in osteoarthritic femoral head sclerotic bone. *Rheumatology (Oxford, England)*.

Irie, K., Ejiri, S., Sakakura, Y., Shibui, T. and Yajima, T. 2008. Matrix mineralization as a trigger for osteocyte maturation. *The journal of histochemistry and cytochemistry : official journal of the Histochemistry Society*. **56**(6), pp.561–7.

Isern, J. and Méndez-Ferrer, S. 2011. Stem Cell Interactions in a Bone Marrow Niche.

Current Osteoporosis Reports. **9**(4), pp.210–218.

Jacobs, S.A., Roobrouck, V.D., Verfaillie, C.M. and Van Gool, S.W. 2013. Immunological characteristics of human mesenchymal stem cells and multipotent adult progenitor cells. *Immunology and Cell Biology*. **91**(1), pp.32–39.

Jaiprakash, A., Prasadam, I., Feng, J.Q., et al. 2012. Phenotypic Characterization of Osteoarthritic Osteocytes from the Sclerotic Zones: A Possible Pathological Role in Subchondral Bone Sclerosis. *International Journal of Biological Sciences*. **8**(3), pp.406–417.

Jaiswal, N., Haynesworth, S.E., Caplan, A.I. and Bruder, S.P. 1997. Osteogenic differentiation of purified, culture-expanded human mesenchymal stem cells in vitro. *Journal of Cellular Biochemistry*. **64**(2), pp.295–312.

Jakobsen, R.B., Engebretsen, L. and Slauterbeck, J.R. 2005. An Analysis of the Quality of Cartilage Repair Studies. *The Journal of Bone and Joint Surgery (American)*. **87**(10), p.2232.

Jayasuriya, C.T., Hu, N., Li, J., et al. 2018. Molecular characterization of mesenchymal stem cells in human osteoarthritis cartilage reveals contribution to the OA phenotype. *Scientific Reports*. **8**(1), p.7044.

Jensen, P.R., Andersen, T.L., Hauge, E.-M., Bollerslev, J. and Delaissé, J.-M. 2015. A joined role of canopy and reversal cells in bone remodeling — Lessons from glucocorticoid-induced osteoporosis. *Bone*. **73**, pp.16–23.

Jia, H., Ma, X., Wei, Y., et al. 2018. Loading-Induced Reduction in Sclerostin as a Mechanism of Subchondral Bone Plate Sclerosis in Mouse Knee Joints During Late-Stage Osteoarthritis. *Arthritis and Rheumatology*. **70**(2), pp.230–241.

Jones, E., English, A., Churchman, S.M., et al. 2010. Large-scale extraction and characterization of CD271+ multipotential stromal cells from trabecular bone in health and osteoarthritis: implications for bone regeneration strategies based on uncultured or minimally cultured multipotential stromal cells. *Arthritis and rheumatism*. **62**(7), pp.1944–54.

Jones, E. and McGonagle, D. 2008. Human bone marrow mesenchymal stem cells in vivo. *Rheumatology (Oxford, England)*. **47**(2), pp.126–31.

Jones, E.A., Crawford, A., English, A., et al. 2008. Synovial fluid mesenchymal stem cells in health and early osteoarthritis: detection and functional evaluation at the single-cell level. *Arthritis and rheumatism*. **58**(6), pp.1731–40.

Jones, E.A., English, A., Henshaw, K., et al. 2004. Enumeration and phenotypic characterization of synovial fluid multipotential mesenchymal progenitor cells in inflammatory and degenerative arthritis. *Arthritis and rheumatism*. **50**(3), pp.817–27.

Jones, E.A., Kinsey, S.E., English, A., et al. 2002. Isolation and characterization of bone marrow multipotential mesenchymal progenitor cells. *Arthritis and rheumatism*. **46**(12), pp.3349–60.

Juhakoski, R., Heliovaara, M., Impivaara, O., et al. 2008. Risk factors for the development of hip osteoarthritis: a population-based prospective study. *Rheumatology*. **48**(1), pp.83–87.

Kaback, L.A., Soung, D.Y., Naik, A., et al. 2008. Osterix/Sp7 regulates mesenchymal stem cell mediated endochondral ossification. *Journal of Cellular Physiology*. **214**(1), pp.173–182.

Kamata, M., Okitsu, Y., Fujiwara, T., et al. 2014. GATA2 regulates differentiation of bone marrow-derived mesenchymal stem cells. *Haematologica*. **99**(11), pp.1686–1696.

Kamimura, M., Nakamura, Y., Uchiyama, S., et al. 2014. The Pathophysiology and Progression of Hip Osteoarthritis Accompanied with Joint Pain are Potentially Due to Bone Alterations - Follow-up Study of Hip OA Patients. *The open rheumatology journal*. **8**, pp.46–53.

Kamioka, H., Sugawara, Y., Honjo, T., Yamashiro, T. and Takano-Yamamoto, T. 2004. Terminal differentiation of osteoblasts to osteocytes is accompanied by dramatic changes in the distribution of actin-binding proteins. *Journal of bone and mineral research : the official journal of the American Society for Bone and Mineral Research*. **19**(3), pp.471–8.

Kaneki, H., Guo, R., Chen, D., et al. 2006. Tumor Necrosis Factor Promotes Runx2 Degradation through Up-regulation of Smurf1 and Smurf2 in Osteoblasts. *Journal of Biological Chemistry*. **281**(7), pp.4326–4333.

Karsdal, M.A.A., Andersen, T.A.A., Bonewald, L. and Christiansen, C. 2004. Matrix metalloproteinases (MMPs) safeguard osteoblasts from apoptosis during transdifferentiation into osteocytes: MT1-MMP maintains osteocyte viability. . **23**(3).

Kato, Y., Windle, J.J., Koop, B.A., Mundy, G.R. and Bonewald, L.F. 1997. Establishment of an osteocyte-like cell line, MLO-Y4. *Journal of bone and mineral research : the official journal of the American Society for Bone and Mineral Research*. **12**(12), pp.2014–23.

Katz, J.N. 2006. Total joint replacement in osteoarthritis. *Best Practice & Research Clinical Rheumatology*. **20**(1), pp.145–153.

Kawaguchi, J., Kii, I., Sugiyama, Y., Takeshita, S. and Kudo, A. 2001. The Transition of Cadherin Expression in Osteoblast Differentiation from Mesenchymal Cells: Consistent Expression of Cadherin-11 in Osteoblast Lineage. *Journal of Bone and Mineral Research*. **16**(2), pp.260–269.

Kazakia, G.J., Kuo, D., Schooler, J., et al. 2013. Bone and cartilage demonstrate changes localized to bone marrow edema-like lesions within osteoarthritic knees. *Osteoarthritis and Cartilage*. **21**(1), pp.94–101.

Keller, H. and Kneissel, M. 2005. SOST is a target gene for PTH in bone. *Bone*. **37**(2), pp.148–158.

Kellgren, J.H. and Lawrence, J.S. 1957. Radiological assessment of osteo-arthrosis. *Annals of the rheumatic diseases*. **16**(4), pp.494–502.

Kenkre, J. and Bassett, J. 2018. The bone remodelling cycle. *Annals of Clinical Biochemistry: International Journal of Laboratory Medicine*. **55**(3), pp.308–327.

Keshtkar, S., Azarpira, N. and Ghahremani, M.H. 2018. Mesenchymal stem cell-derived extracellular vesicles: Novel frontiers in regenerative medicine. *Stem Cell Research and Therapy*. **9**(1).

Kfoury, Y. and Scadden, D.T. 2015. Mesenchymal cell contributions to the stem cell niche. *Cell stem cell*. **16**(3), pp.239–53.

Kim, C., Nevitt, M.C., Niu, J., et al. 2015. Association of hip pain with radiographic evidence of hip osteoarthritis: diagnostic test study. *BMJ*. **351**, p.h5983.

Kim, S.W., Lu, Y., Williams, E.A., et al. 2017. Sclerostin Antibody Administration Converts Bone Lining Cells Into Active Osteoblasts. *Journal of bone and mineral research : the official journal of the American Society for Bone and Mineral Research*. **32**(5), pp.892–901.

Kitaori, T., Ito, H., Schwarz, E.M., et al. 2009. Stromal cell-derived factor 1/CXCR4 signaling is critical for the recruitment of mesenchymal stem cells to the fracture site during skeletal repair in a mouse model. *Arthritis & Rheumatism*. **60**(3), pp.813–823.

Klein-Nulend, J., Bakker, A.D., Bacabac, R.G., Vatsa, A. and Weinbaum, S. 2013. Mechanosensation and transduction in osteocytes. *Bone*. **54**(2), pp.182–190.

Klein-Nulend, J., Semeins, C.M., Ajubi, N.E., Nijweide, P.J. and Burger, E.H. 1995. Pulsating fluid flow increases nitric oxide (NO) synthesis by osteocytes but not periosteal fibroblasts--correlation with prostaglandin upregulation. *Biochemical and biophysical research communications*. **217**(2), pp.640–8.

Knothe Tate, M.L. 2003. "Whither flows the fluid in bone?" An osteocyte's perspective. *Journal of Biomechanics*. **36**(10), pp.1409–1424.

Kolf, C.M., Cho, E. and Tuan, R.S. 2007. Mesenchymal stromal cells: Biology of adult mesenchymal stem cells: regulation of niche, self-renewal and differentiation. *Arthritis Research & Therapy*. **9**(1), p.204.

Komori, T. 2006. Regulation of osteoblast differentiation by transcription factors. *Journal of Cellular Biochemistry*. **99**(5), pp.1233–1239.

Komori, T., Yagi, H., Nomura, S., et al. 1997. Targeted disruption of Cbfa1 results in a complete lack of bone formation owing to maturational arrest of osteoblasts. *Cell*. **89**(5), pp.755–64.

Koshino, T., Wada, S., Ara, Y. and Saito, T. 2003. Regeneration of degenerated articular cartilage after high tibial valgus osteotomy for medial compartmental osteoarthritis of the knee. *The Knee*. **10**(3), pp.229–36.

van der Kraan, P.M. and van den Berg, W.B. 2007. Osteophytes: relevance and biology. *Osteoarthritis and Cartilage*. **15**(3), pp.237–244.

Kraus, V.B., Blanco, F.J., Englund, M., Karsdal, M.A. and Lohmander, L.S. 2015. Call for standardized definitions of osteoarthritis and risk stratification for clinical trials and clinical use. *Osteoarthritis and cartilage*. **23**(8), pp.1233–41.

Kristensen, H.B., Andersen, T.L., Marcussen, N., Rolighed, L. and Delaisse, J.-M. 2013. Increased presence of capillaries next to remodeling sites in adult human cancellous bone. *Journal of Bone and Mineral Research*. **28**(3), pp.574–585.

Kristensen, H.B., Andersen, T.L., Marcussen, N., Rolighed, L. and Delaisse, J.-M. 2014. Osteoblast Recruitment Routes in Human Cancellous Bone Remodeling. *The American Journal of Pathology*. **184**(3), pp.778–789.

Kuliwaba, J.S., Fazzalari, N.L. and Findlay, D.M. 2005. Stability of RNA isolated from human trabecular bone at post-mortem and surgery. *Biochimica et Biophysica Acta (BBA) - Molecular Basis of Disease*. **1740**(1), pp.1–11.

Kuttapitiya, A., Assi, L., Laing, K., et al. 2017. Microarray analysis of bone marrow lesions in osteoarthritis demonstrates upregulation of genes implicated in osteochondral turnover, neurogenesis and inflammation. *Annals of the rheumatic diseases*. **76**(10), pp.1764–1773.

Kuznetsov, S.A., Mankani, M.H., Bianco, P. and Robey, P.G. 2009. Enumeration of the colony-forming units-fibroblast from mouse and human bone marrow in normal and pathological conditions. *Stem cell research*. **2**(1), pp.83–94.

Kwan Tat, S., Pelletier, J.-P., Lajeunesse, D., et al. 2008. The differential expression of osteoprotegerin (OPG) and receptor activator of nuclear factor kappaB ligand (RANKL) in human osteoarthritic subchondral bone osteoblasts is an indicator of the metabolic state of these disease cells. *Clinical and experimental rheumatology*. **26**(2), pp.295–304.

Lacey, D.L., Timms, E., Tan, H.L., et al. 1998. Osteoprotegerin ligand is a cytokine that regulates osteoclast differentiation and activation. *Cell*. **93**(2), pp.165–76.

Lajeunesse, D., Hilal, G., Pelletier, J.-P. and Martel-Pelletier, J. 1999. Subchondral bone

morphological and biochemical alterations in osteoarthritis. *Osteoarthritis and Cartilage*. **7**(3), pp.321–322.

Lajeunesse, D., Massicotte, F., Pelletier, J.-P. and Martel-Pelletier, J. 2003. Subchondral bone sclerosis in osteoarthritis: not just an innocent bystander. *Modern Rheumatology*. **13**(1), pp.0007-0014.

Lajeunesse, D. and Reboul, P. 2003. Subchondral bone in osteoarthritis: a biologic link with articular cartilage leading to abnormal remodeling. *Current opinion in rheumatology*. **15**(5), pp.628–33.

Lau, E., Al-Dujaili, S., Guenther, A., et al. 2010. Effect of low-magnitude, high-frequency vibration on osteocytes in the regulation of osteoclasts. *Bone*. **46**(6), pp.1508–15.

Lee, Y.-S. and Chuong, C.-M. 2009. Adhesion molecules in skeletogenesis: I. transient expression of neural cell adhesion molecules (NCAM) in osteoblasts during endochondral and intramembranous ossification. *Journal of Bone and Mineral Research*. **7**(12), pp.1435–1446.

Lehmann, J.M., Riethmüller, G. and Johnson, J.P. 1989. MUC18, a marker of tumor progression in human melanoma, shows sequence similarity to the neural cell adhesion molecules of the immunoglobulin superfamily. *Proceedings of the National Academy of Sciences of the United States of America*. **86**(24), pp.9891–5.

Lementowski, P.W. and Zelicof, S.B. 2008. Obesity and osteoarthritis. *American journal of orthopedics (Belle Mead, N.J.)*. **37**(3), pp.148–51.

Leydet-Quilici, H., Le Corroller, T., Bouvier, C., et al. 2010. Advanced hip osteoarthritis: magnetic resonance imaging aspects and histopathology correlations. *Osteoarthritis and Cartilage*. **18**(11), pp.1429–1435.

Li, B. and Aspden, R.M. 1997. Composition and Mechanical Properties of Cancellous Bone from the Femoral Head of Patients with Osteoporosis or Osteoarthritis. *Journal of Bone and Mineral Research*. **12**(4), pp.641–651.

Li, C., Wu, X., Tong, J., et al. 2015. Comparative analysis of human mesenchymal stem cells from bone marrow and adipose tissue under xeno-free conditions for cell therapy. *Stem Cell Research & Therapy*. **6**(1), p.55.

Li, G., Yin, J., Gao, J., et al. 2013. Subchondral bone in osteoarthritis: insight into risk factors and microstructural changes. *Arthritis Research & Therapy*. **15**(6), p.223.

Li, H., Ghazanfari, R., Zacharaki, D., et al. 2014. Low/Negative Expression of PDGFR-α Identifies the Candidate Primary Mesenchymal Stromal Cells in Adult Human Bone Marrow. *Stem Cell Reports*. **3**(6), pp.965–974.

Li, H., Ghazanfari, R., Zacharaki, D., Lim, H.C. and Scheding, S. 2016. Isolation and characterization of primary bone marrow mesenchymal stromal cells. *Annals of the New York Academy of Sciences*. **1370**(1), pp.109–118.

Li, X., Huynh, H., Zuo, H., Salminen, M. and Wan, Y. 2016. Gata2 Is a Rheostat for Mesenchymal Stem Cell Fate in Male Mice. *Endocrinology*. **157**(3), pp.1021–1028.

Li, X., Ominsky, M.S., Niu, Q.-T., et al. 2008. Targeted Deletion of the Sclerostin Gene in Mice Results in Increased Bone Formation and Bone Strength. *Journal of Bone and Mineral Research*. **23**(6), pp.860–869.

Li, X., Ominsky, M.S., Warmington, K.S., et al. 2009. Sclerostin Antibody Treatment Increases Bone Formation, Bone Mass, and Bone Strength in a Rat Model of Postmenopausal Osteoporosis. *Journal of Bone and Mineral Research*. **24**(4), pp.578–588.

Li, X., Zhang, Y., Kang, H., et al. 2005. Sclerostin Binds to LRP5/6 and Antagonizes Canonical Wnt Signaling. *Journal of Biological Chemistry*. **280**(20), pp.19883–19887.

Lievense, A.M., Bierma-Zeinstra, S.M.A., Verhagen, A.P., et al. 2002. Influence of obesity on the development of osteoarthritis of the hip: a systematic review. *Rheumatology (Oxford, England)*. **41**(10), pp.1155–62.

Livak, K.J. and Schmittgen, T.D. 2001. Analysis of Relative Gene Expression Data Using Real-Time Quantitative PCR and the 2−ΔΔCT Method. *Methods*. **25**(4), pp.402–408.

Loeser, R.F. 2009. Aging and osteoarthritis: the role of chondrocyte senescence and aging changes in the cartilage matrix. *Osteoarthritis and cartilage*. **17**(8), pp.971–9.

Loeser, R.F., Goldring, S.R., Scanzello, C.R. and Goldring, M.B. 2012. Osteoarthritis: a disease of the joint as an organ. *Arthritis and rheumatism*. **64**(6), pp.1697–707.

Lopa, S., Colombini, A., Stanco, D., et al. 2014. Donor-matched mesenchymal stem cells from knee infrapatellar and subcutaneous adipose tissue of osteoarthritic donors display differential chondrogenic and osteogenic commitment. *European cells & materials*. **27**, pp.298–311.

Lories, R.J. and Luyten, F.P. 2011. The bone–cartilage unit in osteoarthritis. *Nature Reviews Rheumatology*. **7**(1), pp.43–49.

Lucchini, M., Couble, M.-L., Romeas, A., et al. 2004. αvβ3 Integrin Expression in Human Odontoblasts and Co-localization with Osteoadherin. *Journal of Dental Research*. **83**(7), pp.552–556.

Mabuchi, Y., Morikawa, S., Harada, S., et al. 2013. LNGFR+THY-1+VCAM-1hi+ Cells Reveal Functionally Distinct Subpopulations in Mesenchymal Stem Cells. *Stem Cell Reports*. **1**(2), pp.152–165.

Madry, H., van Dijk, C.N. and Mueller-Gerbl, M. 2010. The basic science of the subchondral bone. *Knee surgery, sports traumatology, arthroscopy : official journal of the ESSKA*. **18**(4), pp.419–33.

Maijenburg, M.W., Kleijer, M., Vermeul, K., et al. 2011. Primary Bone Marrow-Derived MSC Subsets Have Distinct Wnt-Signatures Compared to Conventionally Cultured MSC and Differ in Their Capacity to Support Hematopoiesis in Vitro. *Blood*. **118**(21).

Maldonado, M. and Nam, J. 2013. The Role of Changes in Extracellular Matrix of Cartilage in the Presence of Inflammation on the Pathology of Osteoarthritis. *BioMed Research International*. **2013**, pp.1–10.

Maleki-Fischbach, M. and Jordan, J.M. 2010. New developments in osteoarthritis. Sex differences in magnetic resonance imaging-based biomarkers and in those of joint metabolism. *Arthritis Research and Therapy*. **12**(4).

Manolagas, S.C. 2000. Birth and Death of Bone Cells: Basic Regulatory Mechanisms and Implications for the Pathogenesis and Treatment of Osteoporosis. *Endocrine Reviews*. **21**(2), pp.115–137.

Manolagas, S.C. 2006. Choreography from the tomb: An emerging role of dying osteocytes in the purposeful, and perhaps not so purposeful, targeting of bone remodeling. *BoneKEy-Osteovision*. **3**(1), pp.5–14.

Le Marshall, K.F., Yee, B., Dieppe, P.A., et al. 2013. Differences between patients with hip and knee osteoarthritis. *Osteoarthritis and Cartilage*. **21**, p.S139.

Martel-Pelletier, J., Barr, A.J., Cicuttini, F.M., et al. 2016. Osteoarthritis. *Nature Reviews Disease Primers*. **2**, p.16072.

Martin, A., Liu, S., David, V., et al. 2011. Bone proteins PHEX and DMP1 regulate fibroblastic growth factor Fgf23 expression in osteocytes through a common pathway involving FGF receptor (FGFR) signaling. *The FASEB Journal*. **25**(8), pp.2551–2562.

Martinez, C., Hofmann, T.J., Marino, R., Dominici, M. and Horwitz, E.M. 2007. Human bone marrow mesenchymal stromal cells express the neural ganglioside GD2: a novel surface marker for the identification of MSCs. *Blood*. **109**(10), pp.4245–4248.

Matic, I., Matthews, B.G., Wang, X., et al. 2016. Quiescent Bone Lining Cells Are a Major Source of Osteoblasts During Adulthood. *Stem cells (Dayton, Ohio)*. **34**(12), pp.2930–2942.

McCauley, T.R., Kornaat, P.R. and Jee, W.-H. 2001. Central Osteophytes in the Knee. *American Journal of Roentgenology*. **176**(2), pp.359–364.

McClung, M.R., Grauer, A., Boonen, S., et al. 2014. Romosozumab in Postmenopausal Women with Low Bone Mineral Density. *New England Journal of Medicine*. **370**(5), pp.412–420.

McCrae, F., Shouls, J., Dieppe, P. and Watt, I. 1992. Scintigraphic assessment of osteoarthritis of the knee joint. *Annals of the rheumatic diseases*. **51**(8), pp.938–42.

McGonagle, D., Baboolal, T.G. and Jones, E. 2017. Native joint-resident mesenchymal stem cells for cartilage repair in osteoarthritis. *Nature Reviews Rheumatology*. **13**(12), pp.719–730.

McGonagle, D., Tan, A.L., Carey, J. and Benjamin, M. 2010. The anatomical basis for a novel classification of osteoarthritis and allied disorders. *Journal of anatomy*. **216**(3), pp.279–91.

McNamara, L.M., Majeska, R.J., Weinbaum, S., et al. 2009. Attachment of osteocyte cell processes to the bone matrix. *Anatomical record (Hoboken, N.J. : 2007)*. **292**(3), pp.355–63.

Méndez-Ferrer, S., Michurina, T. V., Ferraro, F., et al. 2010. Mesenchymal and haematopoietic stem cells form a unique bone marrow niche. *Nature*. **466**(7308), pp.829–834.

Miller, S.C., de Saint-Georges, L., Bowman, B.M. and Jee, W.S. 1989. Bone lining cells: structure and function. *Scanning microscopy*. **3**(3), pp.953-60; discussion 960–1.

Milz, S. and Putz, R. 1994. Quantitative morphology of the subchondral plate of the tibial plateau. *Journal of anatomy*. **185 (Pt 1)**(Pt 1), pp.103–10.

Minina, E., Kreschel, C., Naski, M.C., Ornitz, D.M. and Vortkamp, A. 2002. Interaction of FGF, Ihh/Pthlh, and BMP Signaling Integrates Chondrocyte Proliferation and Hypertrophic Differentiation. *Developmental Cell*. **3**(3), pp.439–449.

Mithoefer, K., McAdams, T., Williams, R.J., Kreuz, P.C. and Mandelbaum, B.R. 2009. Clinical Efficacy of the Microfracture Technique for Articular Cartilage Repair in the Knee. *The American Journal of Sports Medicine*. **37**(10), pp.2053–2063.

Mizuno, M., Katano, H., Mabuchi, Y., et al. 2018. Specific markers and properties of synovial mesenchymal stem cells in the surface, stromal, and perivascular regions. *Stem Cell Research & Therapy*. **9**(1), p.123.

Mollon, B., Kandel, R., Chahal, J. and Theodoropoulos, J. 2013. The clinical status of cartilage tissue regeneration in humans. *Osteoarthritis and Cartilage*. **21**(12), pp.1824–1833.

Morgan, E., Barnes, G. and Einhorn, T. 2008. Osteoporosis *In*: M. R, F. D, N. DA and R. CJ, eds. *Osteoporosis*. San Diego: Academic Press, pp.3–26.

Morikawa, S., Mabuchi, Y., Kubota, Y., et al. 2009. Prospective identification, isolation, and systemic transplantation of multipotent mesenchymal stem cells in murine bone marrow. *The Journal of experimental medicine*. **206**(11), pp.2483–96.

Mullender, M.G., van der Meer, D.D., Huiskes, R. and Lips, P. 1996. Osteocyte density changes in aging and osteoporosis. *Bone*. **18**(2), pp.109–13.

Mundy, G.R. 2002. Metastasis to bone: causes, consequences and therapeutic opportunities. *Nature Reviews Cancer*. **2**(8), pp.584–593.

Murphy, J.M., Dixon, K., Beck, S., et al. 2002. Reduced chondrogenic and adipogenic activity of mesenchymal stem cells from patients with advanced osteoarthritis. *Arthritis & Rheumatism*. **46**(3), pp.704–713.

Murphy, L.B., Helmick, C.G., Schwartz, T.A., et al. 2010. One in four people may develop symptomatic hip osteoarthritis in his or her lifetime. *Osteoarthritis and Cartilage*. **18**(11), pp.1372–1379.

Murphy, N.J., Eyles, J.P. and Hunter, D.J. 2016. Hip Osteoarthritis: Etiopathogenesis and Implications for Management. *Advances in Therapy*. **33**(11), pp.1921–1946.

Nakashima, K., Zhou, X., Kunkel, G., et al. 2002. The novel zinc finger-containing transcription factor osterix is required for osteoblast differentiation and bone formation. *Cell*. **108**(1), pp.17–29.

Nakashima, T., Hayashi, M., Fukunaga, T., et al. 2011. Evidence for osteocyte regulation of bone homeostasis through RANKL expression. *Nature Medicine*. **17**(10), pp.1231–1234.

Nampei, A., Hashimoto, J., Hayashida, K., et al. 2004. Matrix extracellular phosphoglycoprotein (MEPE) is highly expressed in osteocytes in human bone. *Journal of bone and mineral metabolism*. **22**(3), pp.176–84.

Neogi, T. and Zhang, Y. 2013. Epidemiology of Osteoarthritis. *Rheumatic Disease Clinics of North America*. **39**(1), pp.1–19.

Netter, F.H., Hansen, J.T. and Lambert, D.R. 2005. *Netter's clinical anatomy*. Icon Learning Systems.

Nevitt, M.C. and Felson, D.T. 1996. Sex hormones and the risk of osteoarthritis in women: Epidemiological evidence *In*: *Annals of the Rheumatic Diseases*. BMJ Publishing Group, pp.673–676.

NICE 2014. *Total hip replacement and resurfacing arthroplasty for end-stage arthritis of the hip* [Online]. NICE. [Accessed 11 March 2019]. Available from: https://www.nice.org.uk/guidance/ta304.

Nishimura, R., Hata, K., Ikeda, F., et al. 2008. Signal transduction and transcriptional regulation during mesenchymal cell differentiation. *Journal of Bone and Mineral Metabolism*. **26**(3), pp.203–212.

Noble, B.S. 2008. The osteocyte lineage. *Archives of Biochemistry and Biophysics*. **473**(2), pp.106–111.

Nombela-Arrieta, C., Ritz, J. and Silberstein, L.E. 2011. The elusive nature and function

of mesenchymal stem cells. *Nature reviews. Molecular cell biology*. **12**(2), pp.126–31.

O'Brien, C.A., Nakashima, T. and Takayanagi, H. 2013. Osteocyte control of osteoclastogenesis. *Bone*. **54**(2), pp.258–263.

Oliveria, S.A., Felson, D.T., Cirillo, P.A., Reed, J.I. and Walker, A.M. 1999. Body weight, body mass index, and incident symptomatic osteoarthritis of the hand, hip, and knee. *Epidemiology (Cambridge, Mass.)*. **10**(2), pp.161–6.

Osawa, M., Hanada, K., Hamada, H. and Nakauchi, H. 1996. Long-term lymphohematopoietic reconstitution by a single CD34-low/negative hematopoietic stem cell. *Science (New York, N.Y.)*. **273**(5272), pp.242–5.

Owen, M. and Friedenstein, A.J. 1988. Stromal stem cells: marrow-derived osteogenic precursors. *Ciba Foundation symposium*. **136**, pp.42–60.

Owen, M.E., Cavé, J. and Joyner, C.J. 1987. Clonal analysis in vitro of osteogenic differentiation of marrow CFU-F. *Journal of cell science*. **87 (Pt 5)**, pp.731–8.

Paic, F., Igwe, J.C., Nori, R., et al. 2009. Identification of differentially expressed genes between osteoblasts and osteocytes. *Bone*. **45**(4), pp.682–92.

Palazzo, C., Nguyen, C., Lefevre-Colau, M.-M. and Poiraudeau, S. 2016. Risk factors and burden of osteoarthritis. *Annals of Physical and Rehabilitation Medicine*. **59**(3), pp.134–138.

Palotie, A., Väisänen, P., Ott, J., et al. 1989. Predisposition to familial osteoarthrosis linked to type II collagen gene. *Lancet (London, England)*. **1**(8644), pp.924–7.

Palumbo, C. 1986. A three-dimensional ultrastructural study of osteoid-osteocytes in the tibia of chick embryos. *Cell and tissue research*. **246**(1), pp.125–31.

Palumbo, C., Palazzini, S. and Marotti, G. 1990. Morphological study of intercellular junctions during osteocyte differentiation. *Bone*. **11**(6), pp.401–6.

Pan, J., Zhou, X., Li, W., et al. 2009. In situ measurement of transport between subchondral bone and articular cartilage. *Journal of Orthopaedic Research*. **27**(10), pp.1347–1352.

Paschalis, E., Recker, R., Dicarlo, E., et al. 2003. Distribution of Collagen Cross-Links in Normal Human Trabecular Bone. *Journal of Bone and Mineral Research*. **18**(11), pp.1942–1946.

Pathak, J.L., Bakker, A.D., Luyten, F.P., et al. 2016. Systemic Inflammation Affects Human Osteocyte-Specific Protein and Cytokine Expression. *Calcified Tissue International*. **98**(6), pp.596–608.

Pereira, D., Peleteiro, B., Araújo, J., et al. 2011. The effect of osteoarthritis definition on prevalence and incidence estimates: a systematic review. *Osteoarthritis and cartilage*. **19**(11), pp.1270–85.

Petersen, D.N., Tkalcevic, G.T., Mansolf, A.L., Rivera-Gonzalez, R. and Brown, T.A. 2000. Identification of osteoblast/osteocyte factor 45 (OF45), a bone-specific cDNA encoding an RGD-containing protein that is highly expressed in osteoblasts and osteocytes. *The Journal of biological chemistry*. **275**(46), pp.36172–80.

Petrtýl, M., Hert, J. and Fiala, P. 1996. Spatial organization of the haversian bone in man. *Journal of biomechanics*. **29**(2), pp.161–9.

Pevsner-Fischer, M., Levin, S. and Zipori, D. 2011. The Origins of Mesenchymal Stromal Cell Heterogeneity. *Stem Cell Reviews and Reports*. **7**(3), pp.560–568.

Phinney, D.G. and Sensebé, L. 2013. Mesenchymal stromal cells: misconceptions and evolving concepts. *Cytotherapy*. **15**(2), pp.140–145.

Pittenger, M.F., Mackay, A.M., Beck, S.C., et al. 1999. Multilineage potential of adult human mesenchymal stem cells. *Science (New York, N.Y.)*. **284**(5411), pp.143–7.

Plotkin, L.I. and Bellido, T. 2016. Osteocytic signalling pathways as therapeutic targets for bone fragility. *Nature Reviews Endocrinology*. **12**(10), pp.593–605.

Ponik, S.M., Triplett, J.W. and Pavalko, F.M. 2007. Osteoblasts and Osteocytes Respond Differently to Oscillatory and Unidirectional Fluid Flow Profiles. *Journal of Cellular Biochemistry*. **100**, pp.794–807.

Poole, K.E.S., van Bezooijen, R.L., Loveridge, N., et al. 2005. Sclerostin is a delayed secreted product of osteocytes that inhibits bone formation. *The FASEB journal : official publication of the Federation of American Societies for Experimental Biology*. **19**(13), pp.1842–1844.

Pottenger, L.A., Phillips, F.M. and Draganich, L.F. 1990. The effect of marginal osteophytes on reduction of varus-valgus instability in osteoarthritic knees. *Arthritis and rheumatism*. **33**(6), pp.853–8.

Prideaux, M., Findlay, D.M. and Atkins, G.J. 2016. Osteocytes: The master cells in bone remodelling. *Current Opinion in Pharmacology*. **28**, pp.24–30.

Prideaux, M., Loveridge, N., Pitsillides, A.A. and Farquharson, C. 2012. Extracellular matrix mineralization promotes E11/gp38 glycoprotein expression and drives osteocytic differentiation. *PloS one*. **7**(5), p.e36786.

Prideaux, M., Schutz, C., Wijenayaka, A.R., et al. 2016. Isolation of osteocytes from human trabecular bone. *Bone*. **88**, pp.64–72.

Pritzker, K.P.H., Gay, S., Jimenez, S.A., et al. 2006. Osteoarthritis cartilage

histopathology: grading and staging. *Osteoarthritis and Cartilage*. **14**(1), pp.13–29.

Qian, H., Le Blanc, K. and Sigvardsson, M. 2012. Primary mesenchymal stem and progenitor cells from bone marrow lack expression of CD44 protein. *The Journal of biological chemistry*. **287**(31), pp.25795–807.

Qing, H., Ardeshirpour, L., Divieti Pajevic, P., et al. 2012. Demonstration of osteocytic perilacunar/canalicular remodeling in mice during lactation. *Journal of Bone and Mineral Research*. **27**(5), pp.1018–1029.

Quirici, N., Soligo, D., Bossolasco, P., et al. 2002. Isolation of bone marrow mesenchymal stem cells by anti-nerve growth factor receptor antibodies. *Experimental hematology*. **30**(7), pp.783–91.

Radin, E.L., Paul, I.L. and Tolkoff, M.J. 1970. Subchondral bone changes in patients with early degenerative joint disease. *Arthritis & Rheumatism*. **13**(4), pp.400–405.

Reddi, A.H., Gay, R., Gay, S. and Miller, E.J. 1977. Transitions in collagen types during matrix-induced cartilage, bone, and bone marrow formation. *Proceedings of the National Academy of Sciences of the United States of America*. **74**(12), pp.5589–92.

Rehn, A.P., Cerny, R., Sugars, R. V., Kaukua, N. and Wendel, M. 2008. Osteoadherin is Upregulated by Mature Osteoblasts and Enhances Their In Vitro Differentiation and Mineralization. *Calcified Tissue International*. **82**(6), pp.454–464.

Reynard, L.N. and Loughlin, J. 2013. Insights from human genetic studies into the pathways involved in osteoarthritis. *Nature Reviews Rheumatology*. **9**(10), pp.573–583.

Riminucci, M., Collins, M.T., Fedarko, N.S., et al. 2003. FGF-23 in fibrous dysplasia of bone and its relationship to renal phosphate wasting. *The Journal of clinical investigation*. **112**(5), pp.683–92.

Rios, H.F., Ye, L., Dusevich, V., et al. 2005. DMP1 is essential for osteocyte formation and function. *Journal of musculoskeletal & neuronal interactions*. **5**(4), pp.325–7.

Robling, A.G., Niziolek, P.J., Baldridge, L.A., et al. 2008. Mechanical Stimulation of Bone in vivo Reduces Osteocyte Expression of Sost/Sclerostin. *Journal of Biological Chemistry*. **283**(9), pp.5866–5875.

Rodriguez-Fontenla, C., Calaza, M., Evangelou, E., et al. 2014. Assessment of Osteoarthritis Candidate Genes in a Meta-Analysis of Nine Genome-Wide Association Studies. *Arthritis & Rheumatology*. **66**(4), pp.940–949.

Rombouts, W.J.C. and Ploemacher, R.E. 2003. Primary murine MSC show highly efficient homing to the bone marrow but lose homing ability following culture. *Leukemia*. **17**(1), pp.160–170.

Roos, E.M. and Juhl, C.B. 2012. Osteoarthritis 2012 year in review: rehabilitation and outcomes. *Osteoarthritis and cartilage*. **20**(12), pp.1477–83.

Rosen, E.D. and MacDougald, O.A. 2006. Adipocyte differentiation from the inside out. *Nature Reviews Molecular Cell Biology*. **7**(12), pp.885–896.

Ross, F.P. and Teitelbaum, S.L. 2005. Alphavbeta3 and macrophage colony-stimulating factor: partners in osteoclast biology. *Immunological Reviews*. **208**(1), pp.88–105.

Rubin, C., Judex, S. and Hadjiargyrou, M. 2002. Skeletal adaptation to mechanical stimuli in the absence of formation or resorption of bone. *Journal of musculoskeletal & neuronal interactions*. **2**(3), pp.264–7.

Rucci, N. 2008. Molecular biology of bone remodelling. *Clinical cases in mineral and bone metabolism : the official journal of the Italian Society of Osteoporosis, Mineral Metabolism, and Skeletal Diseases*. **5**(1), pp.49–56.

Sabokbar, A., Crawford, R., Murray, D.W. and Athanasou, N.A. 2000. Macrophage-osteoclast differentiation and bone resorption in osteoarthrotic subchondral acetabular cysts. *Acta Orthopaedica Scandinavica*. **71**(3), pp.255–261.

Sacchetti, B., Funari, A., Michienzi, S., et al. 2007. Self-renewing osteoprogenitors in bone marrow sinusoids can organize a hematopoietic microenvironment. *Cell*. **131**(2), pp.324–36.

Sacchetti, B., Funari, A., Remoli, C., et al. 2016. No Identical "Mesenchymal Stem Cells" at Different Times and Sites: Human Committed Progenitors of Distinct Origin and Differentiation Potential Are Incorporated as Adventitial Cells in Microvessels. *Stem Cell Reports*. **6**(6), pp.897–913.

Sakaguchi, Y., Sekiya, I., Yagishita, K. and Muneta, T. 2005. Comparison of human stem cells derived from various mesenchymal tissues: Superiority of synovium as a cell source. *Arthritis & Rheumatism*. **52**(8), pp.2521–2529.

Sanchez, C., Deberg, M.A., Bellahcène, A., et al. 2008. Phenotypic characterization of osteoblasts from the sclerotic zones of osteoarthritic subchondral bone. *Arthritis & Rheumatism*. **58**(2), pp.442–455.

Santos, A., Bakker, A.D., Zandieh-Doulabi, B., de Blieck-Hogervorst, J.M.A. and Klein-Nulend, J. 2010. Early activation of the β-catenin pathway in osteocytes is mediated by nitric oxide, phosphatidyl inositol-3 kinase/Akt, and focal adhesion kinase. *Biochemical and Biophysical Research Communications*. **391**(1), pp.364–369.

Schäfer, R., Spohn, G. and Baer, P.C. 2016. Mesenchymal Stem/Stromal Cells in Regenerative Medicine: Can Preconditioning Strategies Improve Therapeutic Efficacy? *Transfusion medicine and hemotherapy : offizielles Organ der Deutschen Gesellschaft fur Transfusionsmedizin und Immunhamatologie*. **43**(4), pp.256–267.

Schaffler, M.B., Cheung, W.-Y., Majeska, R. and Kennedy, O. 2014. Osteocytes: master

orchestrators of bone. *Calcified tissue international*. **94**(1), pp.5–24.

Schmitt-Gräff, A., Skalli, O. and Gabbiani, G. 1989. α-Smooth muscle actin is expressed in a subset of bone marrow stromal cells in normal and pathological conditions. *Virchows Archiv B Cell Pathology Including Molecular Pathology*. **57**(1), pp.291–302.

Schmittgen, T.D. and Livak, K.J. 2008. Analyzing real-time PCR data by the comparative CT method. *Nature Protocols*. **3**(6), pp.1101–1108.

Schmitz, N., Laverty, S., Kraus, V.B. and Aigner, T. 2010. Basic methods in histopathology of joint tissues. *Osteoarthritis and Cartilage*. **18**, pp.S113–S116.

Schroeder, T.M., Jensen, E.D. and Westendorf, J.J. 2005. Runx2: A master organizer of gene transcription in developing and maturing osteoblasts. *Birth Defects Research Part C: Embryo Today: Reviews*. **75**(3), pp.213–225.

Shah, K.M., Stern, M.M., Stern, A.R., et al. 2016. Osteocyte isolation and culture methods. *BoneKEy reports*. **5**, p.838.

Sharma, A., Jagga, S., Lee, S.-S. and Nam, J.-S. 2013. Interplay between Cartilage and Subchondral Bone Contributing to Pathogenesis of Osteoarthritis. *International Journal of Molecular Sciences*. **14**(10), pp.19805–19830.

Shi, S. and Gronthos, S. 2003. Perivascular Niche of Postnatal Mesenchymal Stem Cells in Human Bone Marrow and Dental Pulp. *Journal of Bone and Mineral Research*. **18**(4), pp.696–704.

Shivtiel, S., Kollet, O., Lapid, K., et al. 2008. CD45 regulates retention, motility, and numbers of hematopoietic progenitors, and affects osteoclast remodeling of metaphyseal trabecules. *The Journal of experimental medicine*. **205**(10), pp.2381–95.

Sierra, J., Villagra, A., Paredes, R., et al. 2003. Regulation of the bone-specific osteocalcin gene by p300 requires Runx2/Cbfa1 and the vitamin D3 receptor but not p300 intrinsic histone acetyltransferase activity. *Molecular and cellular biology*. **23**(9), pp.3339–51.

da Silva Meirelles, L., Caplan, A.I. and Nardi, N.B. 2008. In Search of the In Vivo Identity of Mesenchymal Stem Cells. *Stem Cells*. **26**(9), pp.2287–2299.

da Silva Meirelles, L., Chagastelles, P.C. and Nardi, N.B. 2006. Mesenchymal stem cells reside in virtually all post-natal organs and tissues. *Journal of Cell Science*. **119**(11), pp.2204–2213.

da Silva Meirelles, L., Fontes, A.M., Covas, D.T. and Caplan, A.I. 2009. Mechanisms involved in the therapeutic properties of mesenchymal stem cells. *Cytokine & Growth Factor Reviews*. **20**(5–6), pp.419–427.

Silver, I.A., Murrills, R.J. and Etherington, D.J. 1988. Microelectrode studies on the acid microenvironment beneath adherent macrophages and osteoclasts. *Experimental cell research*. **175**(2), pp.266–76.

Simmons, P.J. and Torok-Storb, B. 1991. Identification of stromal cell precursors in human bone marrow by a novel monoclonal antibody, STRO-1. *Blood*. **78**(1), pp.55–62.

Sipp, D., Robey, P.G. and Turner, L. 2018. Clear up this stem-cell mess. *Nature*. **561**(7724), pp.455–457.

Sivasubramaniyan, K., Ilas, D.C., Harichandan, A., et al. 2018. Bone marrow harvesting technique influences functional heterogeneity of mesenchymal stem/stromal cells and cartilage regeneration. *American Journal of Sports Medicine*.

Skinner, R.A., Hickmon, S.G., Lumpkin, C.K., et al. 1997. Decalcified Bone: Twenty Years of Successful Specimen Management. *Journal of Histotechnology*. **20**(3), pp.267–277.

Smith, M.D. 2011. The normal synovium. *The open rheumatology journal*. **5**, pp.100–6.

Sommarin, Y., Wendel, M., Shen, Z., Hellman, U. and Heinegârd, D. 1998. Osteoadherin, a cell-binding keratan sulfate proteoglycan in bone, belongs to the family of leucine-rich repeat proteins of the extracellular matrix. *The Journal of biological chemistry*. **273**(27), pp.16723–9.

Spitkovsky, D. and Hescheler, J. 2008. Adult mesenchymal stromal stem cells for therapeutic applications. *Minimally Invasive Therapy and Allied Technologies*. **17**(2), pp.79–90.

Srikanth, V.K., Fryer, J.L., Zhai, G., et al. 2005. A meta-analysis of sex differences prevalence, incidence and severity of osteoarthritis. *Osteoarthritis and Cartilage*. **13**(9), pp.769–781.

Staines, K.A., Ikpegbu, E., Javaheri, B., et al. 2018. Hypomorphic conditional deletion of E11/podoplanin in the subchondral bone protects against load-induced osteoarthritis. *Osteoarthritis and Cartilage*. **26**, p.S61.

Staines, K.A., Javaheri, B., Hohenstein, P., et al. 2017. Hypomorphic conditional deletion of E11/Podoplanin reveals a role in osteocyte dendrite elongation. *Journal of Cellular Physiology*. **232**(11), pp.3006–3019.

Staines, K.A., Prideaux, M., Allen, S., et al. 2016. E11/Podoplanin Protein Stabilization Through Inhibition of the Proteasome Promotes Osteocyte Differentiation in Murine in Vitro Models. *Journal of Cellular Physiology*. **231**(6), pp.1392–1404.

Steadman, J.R., Rodkey, W.G., Briggs, K.K. and Rodrigo, J.J. 1999. The microfracture technic in the management of complete cartilage defects in the knee joint. *Der Orthopade*. **28**(1), pp.26–32.

Stern, A.R., Stern, M.M., Van Dyke, M.E., et al. 2012. Isolation and culture of primary osteocytes from the long bones of skeletally mature and aged mice. *BioTechniques*. **52**(6), pp.361–73.

Stewart, K., Monk, P., Walsh, S., et al. 2003. STRO-1, HOP-26 (CD63), CD49a and SB-10 (CD166) as markers of primitive human marrow stromal cells and their more differentiated progeny: a comparative investigation in vitro. *Cell and Tissue Research*. **313**(3), pp.281–290.

Strem, B.M., Hicok, K.C., Zhu, M., et al. 2005. Multipotential differentiation of adipose tissue-derived stem cells. *Keio Journal of Medicine*. **54**(3), pp.132–141.

Su, X., Zuo, W., Wu, Z., et al. 2015. CD146 as a new marker for an increased chondroprogenitor cell sub-population in the later stages of osteoarthritis. *Journal of Orthopaedic Research*. **33**(1), pp.84–91.

Sugiyama, T., Kohara, H., Noda, M. and Nagasawa, T. 2006. Maintenance of the hematopoietic stem cell pool by CXCL12-CXCR4 chemokine signaling in bone marrow stromal cell niches. *Immunity*. **25**(6), pp.977–88.

Sun, Q., Gu, Y., Zhang, W., et al. 2015. Ex vivo 3D osteocyte network construction with primary murine bone cells. *Bone Research*. **3**, p.15026.

Suri, S. and Walsh, D.A. 2012. Osteochondral alterations in osteoarthritis. *Bone*. **51**(2), pp.204–211.

Taljanovic, M.S., Graham, A.R., Benjamin, J.B., et al. 2008. Bone marrow edema pattern in advanced hip osteoarthritis: quantitative assessment with magnetic resonance imaging and correlation with clinical examination, radiographic findings, and histopathology. *Skeletal Radiology*. **37**(5), pp.423–431.

Tamma, R., Carbone, C. and Colucci, S. 2014. Bone Matrix Proteins and Mineralization Process *In*: *Imaging of Prosthetic Joints* [Online]. Milano: Springer Milan, pp.15–25. [Accessed 24 December 2018]. Available from: http://link.springer.com/10.1007/978-88-470-5483-7_2.

Tanamas, S.K., Wluka, A.E., Pelletier, J.-P., et al. 2010. The association between subchondral bone cysts and tibial cartilage volume and risk of joint replacement in people with knee osteoarthritis: a longitudinal study. *Arthritis Research & Therapy*. **12**(2), p.R58.

Tande, A.J. and Patel, R. 2014. Prosthetic Joint Infection. *Clinical Microbiology Reviews*. **27**(2), pp.302–345.

Tashima, T., Nagatoishi, S., Sagara, H., Ohnuma, S. and Tsumoto, K. 2015. Osteomodulin regulates diameter and alters shape of collagen fibrils. *Biochemical and Biophysical Research Communications*. **463**(3), pp.292–296.

Tatsumi, S., Ishii, K., Amizuka, N., et al. 2007. Targeted ablation of osteocytes induces

osteoporosis with defective mechanotransduction. *Cell metabolism*. **5**(6), pp.464–75.

Teitelbaum, S.L. 2007. Osteoclasts: what do they do and how do they do it? *The American journal of pathology*. **170**(2), pp.427–35.

Thompson, W.R., Uzer, G., Brobst, K.E., et al. 2015. Osteocyte specific responses to soluble and mechanical stimuli in a stem cell derived culture model. *Scientific reports*. **5**, p.11049.

Tian, E., Zhan, F., Walker, R., et al. 2003. The role of the Wnt-signaling antagonist DKK1 in the development of osteolytic lesions in multiple myeloma. *The New England journal of medicine*. **349**(26), pp.2483–94.

Tolar, J., Teitelbaum, S.L. and Orchard, P.J. 2004. Osteopetrosis. *New England Journal of Medicine*. **351**(27), pp.2839–2849.

Tolkachov, A., Fischer, C., Ambrosi, T.H., et al. 2018. Loss of the Hematopoietic Stem Cell Factor GATA2 in the Osteogenic Lineage Impairs Trabecularization and Mechanical Strength of Bone. *Molecular and Cellular Biology*. **38**(12).

Tomellini, E., Lagadec, C., Polakowska, R. and Le Bourhis, X. 2014. Role of p75 neurotrophin receptor in stem cell biology: more than just a marker. *Cellular and Molecular Life Sciences*. **71**(13), pp.2467–2481.

Tormin, A., Li, O., Brune, J.C., et al. 2011. CD146 expression on primary nonhematopoietic bone marrow stem cells is correlated with in situ localization. *Blood*. **117**(19), pp.5067–77.

Troeberg, L. and Nagase, H. 2012. Proteases involved in cartilage matrix degradation in osteoarthritis. *Biochimica et Biophysica Acta - Proteins and Proteomics*. **1824**(1), pp.133–145.

Tsai, F.-Y., Keller, G., Kuo, F.C., et al. 1994. An early haematopoietic defect in mice lacking the transcription factor GATA-2. *Nature*. **371**(6494), pp.221–226.

Tuli, R., Tuli, S., Nandi, S., et al. 2003. Transforming Growth Factor-β-mediated Chondrogenesis of Human Mesenchymal Progenitor Cells Involves N-cadherin and Mitogen-activated Protein Kinase and Wnt Signaling Cross-talk. *Journal of Biological Chemistry*. **278**(42), pp.41227–41236.

Van Tunen, J.A.C., Peat, G., Bricca, A., et al. 2018. Association of osteoarthritis risk factors with knee and hip pain in a population-based sample of 29-59 year olds in Denmark: A cross-sectional analysis. *BMC Musculoskeletal Disorders*. **19**(1).

Ubaidus, S., Li, M., Sultana, S., et al. 2009. FGF23 is mainly synthesized by osteocytes in the regularly distributed osteocytic lacunar canalicular system established after physiological bone remodeling. *Journal of electron microscopy*. **58**(6), pp.381–92.

Väänänen, H.K., Zhao, H., Mulari, M. and Halleen, J.M. 2000. The cell biology of osteoclast function. *Journal of cell science*. **113 (Pt 3)**, pp.377–81.

Van Valburg, A.., Van Roermund, P.., Marijnissen, A.C.., et al. 2000. Joint distraction in treatment of osteoarthritis (II): effects on cartilage in a canine model. *Osteoarthritis and Cartilage*. **8**(1), pp.1–8.

Valdes, A.M. and Spector, T.D. 2011. Genetic epidemiology of hip and knee osteoarthritis. *Nature Reviews Rheumatology*. **7**(1), pp.23–32.

Valdes, A.M. and Spector, T.D. 2010. The clinical relevance of genetic susceptibility to osteoarthritis. *Best Practice & Research Clinical Rheumatology*. **24**(1), pp.3–14.

Varich, L., Pathria, M., Resnick, D., et al. 1993. Patterns of central acetabular osteophytosis in osteoarthritis of the hip. *Investigative radiology*. **28**(12), pp.1120–7.

Vatsa, A., Breuls, R.G., Semeins, C.M., et al. 2008. Osteocyte morphology in fibula and calvaria — Is there a role for mechanosensing? *Bone*. **43**(3), pp.452–458.

Vazquez, M., Evans, B.A.J., Riccardi, D., et al. 2014. A New Method to Investigate How Mechanical Loading of Osteocytes Controls Osteoblasts. *Frontiers in Endocrinology*. **5**, p.208.

Verborgt, O., Tatton, N.A., Majeska, R.J. and Schaffler, M.B. 2002. Spatial Distribution of Bax and Bcl-2 in Osteocytes After Bone Fatigue: Complementary Roles in Bone Remodeling Regulation? *Journal of Bone and Mineral Research*. **17**(5), pp.907–914.

Viguet-Carrin, S., Garnero, P. and Delmas, P.D. 2006. The role of collagen in bone strength. *Osteoporosis International*. **17**(3), pp.319–336.

Vingård, E., Alfredsson, L., Goldie, I. and Hogstedt, C. 1993. Sports and osteoarthrosis of the hip. *The American Journal of Sports Medicine*. **21**(2), pp.195–200.

Wada, T., Nakashima, T., Hiroshi, N. and Penninger, J.M. 2006. RANKL–RANK signaling in osteoclastogenesis and bone disease. *Trends in Molecular Medicine*. **12**(1), pp.17–25.

Wagner, W., Horn, P., Castoldi, M., et al. 2008. Replicative Senescence of Mesenchymal Stem Cells: A Continuous and Organized Process T. Zwaka, ed. *PLoS ONE*. **3**(5), p.e2213.

Walsh, D.A. and Chapman, V. 2011. Bisphosphonates for osteoarthritis. *Arthritis Research & Therapy*. **13**(5), p.128.

Walsh, D.A., McWilliams, D.F., Turley, M.J., et al. 2010. Angiogenesis and nerve growth factor at the osteochondral junction in rheumatoid arthritis and osteoarthritis.

Rheumatology (Oxford, England). **49**(10), pp.1852–61.

Warner, S.C., Valdes, A.M., Warner, S.C. and Valdes, A.M. 2016. The Genetics of Osteoarthritis: A Review. *Journal of Functional Morphology and Kinesiology*. **1**(1), pp.140–153.

Wasserman, E., Webster, D., Kuhn, G., et al. 2013. Differential load-regulated global gene expression in mouse trabecular osteocytes. *Bone*. **53**(1), pp.14–23.

Wei, J. and Karsenty, G. 2015. An overview of the metabolic functions of osteocalcin. *Reviews in Endocrine and Metabolic Disorders*. **16**(2), pp.93–98.

Wein, M.N. 2017. Bone Lining Cells: Normal Physiology and Role in Response to Anabolic Osteoporosis Treatments. *Current Molecular Biology Reports*. **3**(2), pp.79–84.

Weinans, H., Siebelt, M., Agricola, R., et al. 2012. Pathophysiology of peri-articular bone changes in osteoarthritis. *Bone*. **51**(2), pp.190–196.

Weinbaum, S., Cowin, S.C. and Zeng, Y. 1994. A model for the excitation of osteocytes by mechanical loading-induced bone fluid shear stresses. *Journal of biomechanics*. **27**(3), pp.339–60.

Wells, C. 1973. The palaeopathology of bone disease. *The Practitioner*. **210**(257), pp.384–91.

Wen, Y., Li, J., Wang, L., et al. 2014. UDP-glucose dehydrogenase modulates proteoglycan synthesis in articular chondrocytes: its possible involvement and regulation in osteoarthritis. *Arthritis research & therapy*. **16**(6), p.484.

Wendel, M., Sommarin, Y. and Heinegård, D. 1998. Bone matrix proteins: isolation and characterization of a novel cell-binding keratan sulfate proteoglycan (osteoadherin) from bovine bone. *The Journal of cell biology*. **141**(3), pp.839–47.

Weng, L.-H., Wang, C.-J., Ko, J.-Y., Sun, Y.-C. and Wang, F.-S. 2010. Control of Dkk-1 ameliorates chondrocyte apoptosis, cartilage destruction, and subchondral bone deterioration in osteoarthritic knees. *Arthritis & Rheumatism*. **62**(5), pp.1393–1402.

WHO Scientific Group 2003. The burden of musculoskeletal conditions at the start of the new millennium. *World Health Organization technical report series*. **919**, i–x, 1-218, back cover.

Whyte, M.P., Obrecht, S.E., Finnegan, P.M., et al. 2002. Osteoprotegerin Deficiency and Juvenile Paget's Disease. *New England Journal of Medicine*. **347**(3), pp.175–184.

Williams, R., Khan, I.M., Richardson, K., et al. 2010. Identification and Clonal Characterisation of a Progenitor Cell Sub-Population in Normal Human Articular Cartilage S. Agarwal, ed. *PLoS ONE*. **5**(10), p.e13246.

Wilson, A.J., Murphy, W.A., Hardy, D.C. and Totty, W.G. 1988. Transient osteoporosis: transient bone marrow edema? *Radiology*. **167**(3), pp.757–760.

Winter, A., Breit, S., Parsch, D., et al. 2003. Cartilage-like gene expression in differentiated human stem cell spheroids: a comparison of bone marrow-derived and adipose tissue-derived stromal cells. *Arthritis and rheumatism*. **48**(2), pp.418–29.

Wluka, A.E., Lombard, C.B. and Cicuttini, F.M. 2013. Tackling obesity in knee osteoarthritis. *Nature Reviews Rheumatology*. **9**(4), pp.225–235.

Woolhead, G., Gooberman-Hill, R., Dieppe, P. and Hawker, G. 2010. Night pain in hip and knee osteoarthritis: A focus group study. *Arthritis Care & Research*. **62**(7), pp.944–949.

van der Woude, J.A.D., Nair, S.C., Custers, R.J.H., et al. 2016. Knee Joint Distraction Compared to Total Knee Arthroplasty for Treatment of End Stage Osteoarthritis: Simulating Long-Term Outcomes and Cost-Effectiveness C. Zhao, ed. *PLOS ONE*. **11**(5), p.e0155524.

Wysolmerski, J.J. 2013. Osteocytes remove and replace perilacunar mineral during reproductive cycles. *Bone*. **54**(2), pp.230–236.

Wysolmerski, J.J. 2012. Osteocytic osteolysis: time for a second look? *BoneKEy Reports*. **1**, p.229.

Xiao, Z., Zhang, S., Mahlios, J., et al. 2006. Cilia-like Structures and Polycystin-1 in Osteoblasts/Osteocytes and Associated Abnormalities in Skeletogenesis and Runx2 Expression. *Journal of Biological Chemistry*. **281**(41), pp.30884–30895.

Xiong, J., Piemontese, M., Onal, M., et al. 2015. Osteocytes, not Osteoblasts or Lining Cells, are the Main Source of the RANKL Required for Osteoclast Formation in Remodeling Bone. *PloS one*. **10**(9), p.e0138189.

Xu, L., Hayashi, D., Roemer, F.W., Felson, D.T. and Guermazi, A. 2012. Magnetic Resonance Imaging of Subchondral Bone Marrow Lesions in Association with Osteoarthritis. *Seminars in Arthritis and Rheumatism*. **42**(2), pp.105–118.

Yamamoto, T. and Bullough, P.G. 2000. The role of subchondral insufficiency fracture in rapid destruction of the hip joint: A preliminary report. *Arthritis & Rheumatism*. **43**(11), pp.2423–2427.

Yoshiko, Y., Wang, H., Minamizaki, T., et al. 2007. Mineralized tissue cells are a principal source of FGF23. *Bone*. **40**(6), pp.1565–1573.

You, L.-D., Weinbaum, S., Cowin, S.C. and Schaffler, M.B. 2004. Ultrastructure of the osteocyte process and its pericellular matrix. *The Anatomical Record*. **278A**(2), pp.505–513.

Yu, B., Zhang, X. and Li, X. 2014. Exosomes derived from mesenchymal stem cells. *International Journal of Molecular Sciences*. **15**(3), pp.4142–4157.

Zaidi, M. 2007. Skeletal remodeling in health and disease. *Nature Medicine*. **13**(7), pp.791–801.

Zanetti, M., Bruder, E., Romero, J. and Hodler, J. 2000. Bone Marrow Edema Pattern in Osteoarthritic Knees: Correlation between MR Imaging and Histologic Findings. *Radiology*. **215**(3), pp.835–840.

Zarei, A., Hulley, P.A., Sabokbar, A. and Javaid, M.K. 2017. Co-expression of DKK-1 and Sclerostin in Subchondral Bone of the Proximal Femoral Heads from Osteoarthritic Hips. *Calcified Tissue International*. **100**(6), pp.609–618.

Zhang, F., Tsai, S., Kato, K., et al. 2009. Transforming Growth Factor-β Promotes Recruitment of Bone Marrow Cells and Bone Marrow-derived Mesenchymal Stem Cells through Stimulation of MCP-1 Production in Vascular Smooth Muscle Cells. *Journal of Biological Chemistry*. **284**(26), pp.17564–17574.

Zhang, K., Barragan-Adjemian, C., Ye, L., et al. 2006. E11/gp38 selective expression in osteocytes: regulation by mechanical strain and role in dendrite elongation. *Molecular and cellular biology*. **26**(12), pp.4539–52.

Zhang, W., Moskowitz, R.W., Nuki, G., et al. 2008. OARSI recommendations for the management of hip and knee osteoarthritis, Part II: OARSI evidence-based, expert consensus guidelines. *Osteoarthritis and Cartilage*. **16**(2), pp.137–162.

Zhang, W., Ouyang, H., Dass, C.R. and Xu, J. 2016. Current research on pharmacologic and regenerative therapies for osteoarthritis. *Bone research*. **4**, p.15040.

Zhang, W., Ouyang, H., Dass, C.R. and Xu, J. 2016. Current research on pharmacologic and regenerative therapies for osteoarthritis. *Bone Research*. **4**.

Zhen, G., Wen, C., Jia, X., et al. 2013. Inhibition of TGF-β signaling in mesenchymal stem cells of subchondral bone attenuates osteoarthritis. *Nature medicine*. **19**(6), pp.704–12.

Zhou, S., Greenberger, J.S., Epperly, M.W., et al. 2008. Age-related intrinsic changes in human bone-marrow-derived mesenchymal stem cells and their differentiation to osteoblasts. *Aging Cell*. **7**(3), pp.335–343.